ADVANCES IN NOVEL NATURAL PRODUCT PESTICIDES
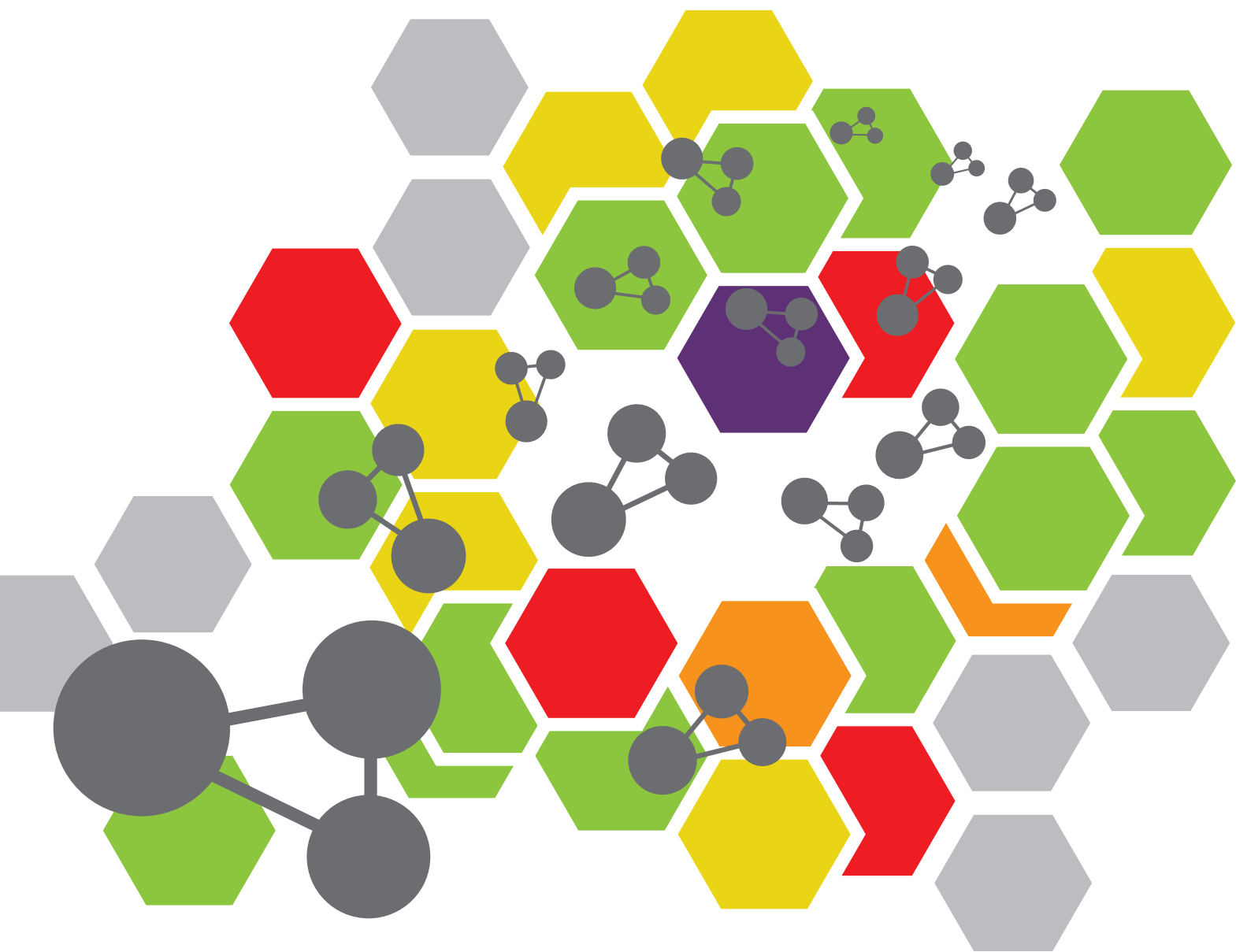
EDITED BY: Pei Li, Hu Li, Jiwen Zhang, Nannan Liu and Feng Liu

frontiers Research Topics

About Frontiers

Frontiers is more than just an open-access publisher of scholarly articles: it is a pioneering approach to the world of academia, radically improving the way scholarly research is managed. The grand vision of Frontiers is a world where all people have an equal opportunity to seek, share and generate knowledge. Frontiers provides immediate and permanent online open access to all its publications, but this alone is not enough to realize our grand goals.

Frontiers Journal Series

The Frontiers Journal Series is a multi-tier and interdisciplinary set of open-access, online journals, promising a paradigm shift from the current review, selection and dissemination processes in academic publishing. All Frontiers journals are driven by researchers for researchers; therefore, they constitute a service to the scholarly community. At the same time, the Frontiers Journal Series operates on a revolutionary invention, the tiered publishing system, initially addressing specific communities of scholars, and gradually climbing up to broader public understanding, thus serving the interests of the lay society, too.

Dedication to Quality

Each Frontiers article is a landmark of the highest quality, thanks to genuinely collaborative interactions between authors and review editors, who include some of the world's best academicians. Research must be certified by peers before entering a stream of knowledge that may eventually reach the public - and shape society; therefore, Frontiers only applies the most rigorous and unbiased reviews.
Frontiers revolutionizes research publishing by freely delivering the most outstanding research, evaluated with no bias from both the academic and social point of view. By applying the most advanced information technologies, Frontiers is catapulting scholarly publishing into a new generation.

What are Frontiers Research Topics?

Frontiers Research Topics are very popular trademarks of the Frontiers Journals Series: they are collections of at least ten articles, all centered on a particular subject. With their unique mix of varied contributions from Original Research to Review Articles, Frontiers Research Topics unify the most influential researchers, the latest key findings and historical advances in a hot research area! Find out more on how to host your own Frontiers Research Topic or contribute to one as an author by contacting the Frontiers Editorial Office: frontiersin.org/about/contact

ADVANCES IN NOVEL NATURAL PRODUCT PESTICIDES

Topic Editors:
Pei Li, Kaili University, China
Hu Li, Guizhou University, China
Jiwen Zhang, Northwest A&F University, China
Nannan Liu, Auburn University, United States
Feng Liu, University of California, San Diego, United States

Table of Contents

Editorial: Advances in novel natural product pesticides

Pei Li[1]*, Hu Li[2], Jiwen Zhang[3], Nannan Liu[4] and Feng Liu[5]

[1]Qiandongnan Engineering and Technology Research Center for Comprehensive Utilization of National Medicine, Kaili University, Kaili, China, [2]State Key Laboratory Breeding Base of Green Pesticide and Agricultural Bioengineering, Key Laboratory of Green Pesticide and Agricultural Bioengineering, Ministry of Education, Research and Development Center for Fine Chemicals, Guizhou University, Guiyang, China, [3]Key Laboratory of Botanical Pesticide R&D in Shaanxi Province, Northwest A&F University, Yangling, China, [4]Department of Entomology and Plant Pathology, Auburn University, Auburn, AL, United States, [5]Division of Biological Sciences, Cell and Developmental Biology Section University of California, San Diego, CA, United States

Editorial on the Research Topic
Advances in novel natural product pesticides

Plant pests and diseases pose a serious threat to agricultural production and cause huge economic losses each year (Rosegrant and Cline, 2003; Neeraja et al., 2010; Opara, 2013; Bhattacharjee and Dey, 2014; Liu and Wang, 2021). Use of pesticides is a standard approach to plant protection, however, the frequent use of conventional chemical pesticides has led to many problems such as resistance in bacterial/fungal/pest populations, environmental contamination, and risks to human health (Guo et al., 1998; Lin et al., 2010; Patel et al., 2014). With the improvement of human living standards and health, the demand for high-quality and safe agricultural products as food necessitates limitations on the use of traditional chemical pesticides and poses a challenge to the control of plant pests and diseases. Therefore, use of natural products to control plant pests and diseases is an innovative strategy for sustainable agricultural development because they are generally safer than traditional chemical pesticides due to their rapid environmental biodegradation and low toxicity to natural enemies, humans, and other mammals (Cantrell et al., 2012; Souto et al., 2021). Thus, natural products can be used either directly for pest control or as models for the development of novel synthetic analogs with promising biological and physicochemical properties.

This Research Topic presents a collection of original research and review articles on the synthesis of novel analogs of natural product pesticides, the toxicology/bioactivity of novel natural products and analogs, and the mechanism of action of novel natural product pesticides. Overall, 23 contributions including 5 reviews and 18 original research articles comprise this Research Topic.

A mini-review paper by Quan et al. shows that *Camellia* seed cake contains a large number of tea polyphenols and saponins, showing anti-melanin, hypoglycemic, antibacterial, and insecticidal activitiesy. Lintz et al. briefly review the anti-rust

peptides (ARPs) targeting different rust species, showing studies on ARP properties and activities mainly through *in vitro* assays, sometimes *in planta* assays, but with no explicit mode of action against rust fungi established so far. Terpenoids, one of the most prominent families among various categories of natural products, attract immense attention due to their promising physiological activities. The review by Xiao et al. summarizes recent advances toward the total synthesis of terpenoids by cobalt-mediated asymmetric catalysis, which may help direct future synthetic efforts toward natural pesticides such as celangulin, azadirachtin, etc. Abscisic acid (ABA) is an important plant endogenous hormone and plant stress resistance factor that participates in the regulation of various physiological processes in plants. Research progress on ABA analogues, including mechanism of action, signaling pathways, and ABA functional analogs, is reviewed by Liu et al.

Development of new botanical pesticides using plant active components has become an important direction. Original research by Cai et al. demonstrates that the active compounds alantolactone, dehydrocostus lactone, and costunolide from the root of *Aucklandia lappa* Decne (Radix Aucklandiae) have different inhibitory effects on *Botrytis cinerea*, *Sclerotinia sclerotiorum*, *Colletotrichum gloeosporioides*, *Fusarium oxysporum*, *Alternaria alternata*, *Fusarium graminearum*, and *Didymella glomerata*. Yi et al. report that 2,4-di-tert-butylphenol, *N*-acetyl-5-methoxytryptamine, and *p*-hydroxybenzoic acid isolated from *Paenibacillus polymyxa* Y-1 fermentation broth have excellent *in vitro* antibacterial activity against *Xanthomonas oryzae* pv. *oryzicola* and *Xanthomonas oryzae* pv. *oryzae*. Meanwhile, the work of Ren et al. demonstrates that plant essential oils and their combinations with synthetic pesticides possess good bioactivity against tobacco beetle (*Lasioderma serricorne* [F.]) adults, demonstrating that plant essential oils could be developed as environmentally friendly insect control agents. The work of Li et al. indicates that diamide and neonicotinoid mixtures as a corn seed treatment could be effective for control of fall armyworm (*Spodoptera frugiperda*) larvae over a relative long period without compromising plant growth and development. *Eucommia ulmoides* Oliv. (Duzhong), a valued traditional herbal medicine in China, is effective against a variety of plant pathogens. Lu et al. report that proteome and transcriptome association analyses and RT-qPCR results suggest that the response of *F. oxysporum* to *E. ulmoides* is likely related to the endoplasmic reticulum pathway.

Structural optimization of natural products is becoming one of the most effective ways to develop novel pesticides. In this Research Topic, several series of novel active compounds are reported by Tian et al., Shu et al., Xie et al., Pan et al., Lei et al., Liu et al., Luo et al., and Zhang et al. Original research by Tian et al.

documents a series of novel α-aminophosphonate derivatives containing a hydrazone moiety possessing good *in vivo* antiviral activity against tobacco mosaic virus (TMV). Shu et al. synthesized a series of novel galactoside derivatives containing an 1,3,4-thiadiazole moiety, and their bioassays indicate that the target compounds had good *in vitro* antifungal activity against *Gibberella zeae*, *Botryosphaeria dothidea*, *Phytophthora infestans*, *Thanatephorus cucumeris*, and *Phompsis* sp. as well as *in vitro* antibacterial activity against *Xanthomonas axonopodis* pv. *citri* and *X. oryzae* py. *oryzae*. Two series of sulfonic acid esters with significant *in vitro* antibacterial activity against *Pseudomonas syringae* pv. *actinidiae* and moderate insecticidal activity against *Spodoptera frugiperda* are reported by Xie et al. Pan et al. prepared a series of novel pyrimidine derivatives bearing an 1,3,4-thiadiazole skeleton, and their bioassays show moderate to good *in vitro* antifungal activity against *B. cinerea*, *Phomopsis* sp., and *B. dothidea*. Liu et al. prepared a series of novel 1,2,4-triazolo[4,3-*c*]trifluoromethylpyrimidine derivatives bearing a thioether moiety. Their bioassays show that most compounds exhibit obvious *in vitro* inhibitory activity against *B. cinerea*, *P. infestans*, and *Pyricularia oryzae* (*P. oryzae*). A series of novel pyrazolecarbamide derivatives bearing a sulfonate fragment were synthesized by Lei et al, with good *in vitro* antifungal activity against *Colletotrichum camelliae*, *Pestalotiopsis theae*, *G. zeae*, and *Rhizoctonia solani*, as well as moderate to good *in vivo* antiviral activity against TMV. Luo et al. report that chalcone derivatives containing an 1,2,4-oxadiazole moiety have good nematocidal activity against *Bursaphelenchus xylophilus*, *Aphelenchoides bessey,*. and *Ditylenchus dipsaci*, and antiviral activity against TMV, pepper mild mottle virus (PMMoV), and tomato spotted wilt virus (TSWV). Using piperine as the lead structure, Zhang et al. synthesized a series of piperine derivatives containing a linear bisamide moiety, with good insecticidal activity against *Plutella xylostella*.

This Research Topic includes some research on the postharvest protection of fruit. Qu et al. show that melatonin can enhance the postharvest disease resistance of blueberry fruits by mediating the jasmonic acid (JA) signaling pathway and the phenylpropane pathway. Meanwhile, in the study of Li et al., *Penicillium spinulosum*, *Phoma herbarum*, *Nemania bipapillata*, and *Aspergillus oryzae* were first isolated from dragon fruits with postharvest disease. Their bioassays reveal that some of the tested chemical pesticides and plant extracts have potent inhibitory activity against *Alternaria alternata* and *Fusarium proliferatum*. In addition, Yan et al. report that ethylene and 1-MCP can reduce the harvested time of kiwifruit to reach the "edible window" and prolong the "edible window" of kiwifruit.

We hope this Research Topic will attract attention to this area of researcher and inspire further investigation toward the development of novel natural product pesticides.

Author contributions

All authors listed, have made substantial, direct and intellectual contribution to the work, and approved it for publication.

Funding

Acknowledgments

Conflict of interest

The authors declare that the research was conducted in the absence of any commercial or financial relationships that could be construed as a potential conflict of interest.

Publisher's note

All claims expressed in this article are solely those of the authors and do not necessarily represent those of their affiliated organizations, or those of the publisher, the editors and the reviewers. Any product that may be evaluated in this article, or claim that may be made by its manufacturer, is not guaranteed or endorsed by the publisher.

References

Bhattacharjee, R., and Dey, U. (2014). An overview of fungal and bacterial biopesticides to control plant Pathogens/Diseases. *Afr. J. Microbiol. Res.* 8 (17), 1479–1762. doi: 10.5897/AJMR2013.6356

Cantrell, C. L., Dayan, F. E., and Duke, S. O. (2012). Natural products as sources for new pesticides. *J. Nat. Prod.* 75 (6), 1231–1242. doi: 10.1021/np300024u

Guo, F., Zhang, Z. Q., and Zhao, Z. (1998). Pesticide resistance of *Tetranychus cinnabarinus* (Acari: Tetranychidae) in China: A review. *Syst. Appl. Acarol.* 3 (1), 3–7. doi: 10.11158/saa.3.1.1

Lin, Y. J., He, Z. L., Rosskopf, E. N., Conn, K. L., Powell, C. A., and Lazarovits, G. (2010). Nylon membrane bag assay for determination of the effect of chemicals on soilborne plant pathogens in soil. *Plant Dis.* 94, 201–206. doi: 10.1094/PDIS-94-2-0201

Liu, J., and Wang, X. W. (2021). Plant diseases and pests detection based on deep learning: A review. *Plant Methods* 17, 22. doi: 10.1186/s13007-021-00722-9

Neeraja, C., Anil, K., Purushotham, P., Suma, K., Sarma, P., Moerschbacher, B. M., et al. (2010). Biotechnological approaches to develop bacterial chitinases as a bioshield against fungal diseases of plants. *Crit. Rev. Biotechnol.* 30 (3), 231–241. doi: 10.3109/07388551.2010.487258

Opara, U. L. (2013). Perspective: The evolving dimensions and perspectives on food security – what are the implications for postharvest technology research, policy and practice? *Int. J. Postharvest. Technol. Innov.* 3 (3), 324–332. doi: 10.1504/IJPTI.2013.059340

Patel, N., Desai, P., Patel, N., Jha, A., and Gautam, H. K. (2014). Agronanotechnology for plant fungal disease management: A review. *Int. J. Curr. Microbiol. App. Sci.* 3, 71–84.

Rosegrant, M. W., and Cline, S. R. (2003). Global food security: Challenges and policies. *Science* 302 (5652), 1917–1919. doi: 10.1126/science.1092958

Souto, A. L., Sylvestre, M., Tölke, E. D., Tavares, J. F., Barbosa-Filho, J. M., and Cebrián-Torrejón, G. (2021). Plant-derived pesticides as an alternative to pest management and sustainable agricultural production: Prospects, applications and challenges. *Molecules* 26 (16), 4835. doi: 10.3390/molecules26164835

Behavioral Response, Fumigation Activity, and Contact Activity of Plant Essential Oils Against Tobacco Beetle (*Lasioderma serricorne* (F.)) Adults

Yanling Ren[1,2†], Tao Wang[1,2*†], Yingjie Jiang[2], Ding Chen[3], Wenyu Zuo[4], Jianjun Guo[1] and Daochao Jin[1*]

[1]Guizhou Provincial Key Laboratory for Agricultural Pest Management of the Mountainous Region, Institute of Entomology, Scientific Observing and Experimental Station of Crop Pest in Guiyang, Ministry of Agriculture, Guizhou University, Guiyang, China, [2]Guizhou Light Industry Technical College, Guiyang, China, [3]China Tobacco Guizhou Import and Export Co., Ltd., Guiyang, China, [4]Guizhou Tobacco Redrying Co., Ltd., Guiyang Redrying Factory, Guiyang, China

Tobacco beetle (*Lasioderma serricorne* (F.)) is one of the main storage pests that harm tobacco leaves. The current control methods mainly include physical control, chemical control, and biological control, but they all have their own disadvantages. In this study, 22 kinds of plant essential oils in grapefruit, peppermint, juniper, eucalyptus, myrrh, lemon grass, geranium, tea tree, cypress, citronella, patchouli, benzoin, rosemary, cinnamon, clary sage, bergamot, mastic, ginger, rose hydrosol, cedar, thyme, and basil, respectively, are selected to explore their behavioral responses against *L. serricorne* adults using a glass Y-tube olfactometer. The behavioral responses results show that 17 kinds of essential oils in eucalyptus, basil, grapefruit, cypress, mastic, peppermint, patchouli, juniper, geranium, thyme, benzoin, lemon grass, cinnamon, ginger, rosemary, clary sage, and citronella can avoid *L. serricorne* adults, while five kinds of essential oils in tea tree, rose hydrosol, myrrh, bergamot, and cedar can attract *L. serricorne* adults. Especially, essential oils in eucalyptus and grapefruit can avoid *L. serricorne* adults at 1 µl/L with the repellent rates of 94.67 and 94.56%, respectively. Meanwhile, 17 kinds of essential oils which can avoid *L. serricorne* adults are selected to determine their fumigation activity against *L. serricorne* adults using the Erlenmeyer flask test method, and bioassay results show that after 72 h of treatment, five kinds of plant essential oils in rosemary, eucalyptus, basil, citronella, and geranium show excellent fumigation activity against *L. serricorne* adults with the mortality rates of 100.00, 95.29, 95.29, 94.12, and 91.76%, respectively, and their LD_{50} of the contact activity against *L. serricorne* adults determined using the leaf-dipping method are 3.60, 3.49, 8.90, 6.70, and 7.80 µl/L, respectively. Our results show that plant essential oils could be developed as environmentally friendly insect control agents.

Keywords: plant essential oils, behavioral response, fumigation activity, contact activity, *Lasioderma serricorne* (F.)

INTRODUCTION

Cigarette beetle (*Lasioderma serricorne* (F.)), a worldwide storage pest, caused harm to stored goods in China, United States, India, and other countries (Shaymaa et al., 2019). The control of *L. serricorne* is great significance to reduce the loss rate of stored goods. At present, methods such as control atmosphere (Cao et al., 2015; Chaitanyam et al., 2017; Kumar et al., 2017; Xu et al., 2017; Sun et al., 2020), control temperature (Makhijani and Gurney, 1995; Yu et al., 2011; Li et al., 2018), and installation of barrier nets (Chen et al., 2013) in physical control methods, phosphine fumigation (Peng et al., 2015; Fukazawa and Takahashi, 2017; Wu et al., 2017), and pesticide methods (Xiong et al., 2014; Tang et al., 2015; Li et al., 2021) in chemical control methods, and natural enemies (such as *Beauveria bassiana* and *Anisopteromalus calandrae*) in biological control methods (Kaelin et al., 1994; Kaelin et al., 1999; Guo et al., 2021; Khanum and Javed, 2021) are more popular control methods. However, physical control is more effective inside the warehouse but has little effect on the *L. serricorne* outside the warehouse; the current application range and types of biological control are not extensive; chemical control methods will inevitably produce residues and lead to *L. serricorne* resistance (Rajendran and Narasimhan, 1994; Zettler and Keevr, 1994; Savvidou et al., 2003; Silva et al., 2017). Therefore, the development of novel and eco-friendly control agents and methods is essential for the control of *L. serricorne*.

Over the past few decades, the world has been studying to find alternatives to biological control, especially plant essential oils. At present, the use of plant extracts has made significant progress in the prevention and control of pests. Since the 1980s, research on plant essential oils against *L. serricorne*, such as the lure or avoidance (Işikber et al., 2009; Guarino et al., 2021), fumigation activity (Işikber et al., 2009; Boukaew et al., 2017), contact activity (Huang and Ho, 1998; Huang et al., 2002; Naveen et al., 2021), has been carried out. Ramadan et al. (2020) studied the avoidance of *L. serricorne* by carvacrol, citronella, geraniol, nootkatone, and *N,N*-diethyl-meta-toluamide. Kamal et al. (2019) studied the avoidance of *L. serricorne* by extracts of sponge gourd (*Luffa aegyptiaca*), ajwain/caraway seeds (*Carum copticum*), and turmeric (*Curcuma longa*). The lure effect of *Capsicum* spp. dried fruit odorants against *L. serricorne* was studied by Guarino et al., which showed that *Capsicum annuum* and *Capsicum frutescens* have an attractive effect on *L. serricorne* (Guarino et al., 2021). In 2016, Lü and Liu found that the citronellal and citral had attractive activities against *L. serricorne* at a low concentration and had repellent activity against *L. serricorne* at higher concentration. Meanwhile, some reported literatures also showed that some plant essential oils, such as *Anethum graveolens*, *Azadirachta indica*, *Eucalyptus globulus*, *Mentha piperita*, and *Artemisia dubia*, revealed good fumigation and contact activity against *L. serricorne* (Khemira et al., 2012; Karakoc et al., 2018; Cheng et al., 2019; Naveena et al., 2021; Yang et al., 2021).

In this study, 22 kinds of plant essential oils were selected: grapefruit, peppermint, juniper, eucalyptus, myrrh, lemon grass, geranium, tea tree, cypress, citronella, patchouli, benzoin, rosemary, cinnamon, clary sage, bergamot, mastic, ginger, rose hydrosol, cedar, thyme, and basil, respectively, and for the first time their behavioral response, fumigation activity, and contact activity against *L. serricorne* adults was studied.

MATERIAL AND METHODS

Insect Collection and Rearing

Samples (*L. serricorne*) were collected from the Guizhou Tobacco Redrying Co., Ltd., Guiyang Redrying Factory, and then placed in the Department of Guizhou Light Industrial Technical College for breeding with corn:tobacco foam:beer yeast = 90:5:5 as food. After that, *L. serricorne* were raised in an artificial intelligence climate box (LAC-450HPY-2, Shanghai Longyue Co., Ltd.) at a temperature, relative humidity, and photoperiod of 25 ± 1°C, 75 ± 5%, and 14L: 10D, respectively.

Behavioral Response Test

The behavioral responses of 22 kinds of plant essential oils (99% purity), provided by Beijing Maosi Trading Company (Beijing, China), against *L. serricorne* adults were determined using a glass Y-tube olfactometer (Yancheng Xinmingte Glass Instrument Co., Ltd., Yancheng, China) (Li et al., 2014). Each 1 μl plant essential oil was dripped in a 1 L pre-washed bottle and acetone (1 μl) served as the negative control. After turning on the air pump for 5 min, 50 two-day-old *L. serricorne* adults pre-starved for 8 h were placed in the middle of the straight arm of the Y-type olfactometer. Three replicates were conducted for each treatment. After 5 min of treatment, the repellent rate of each plant essential oil is calculated using the following formula, where N_c represents the number of insects in the blank arm and N_t represents the number of insects in the treatment arm.

$$Repellent\ rate\ (\%) = \frac{N_c - N_t}{N_c + N_t} \times 100.$$

Fumigant Activity Test

The fumigation activities against *L. serricorne* adults of 17 kinds of essential oils which can avoid *L. serricorne* adults were studied using the Erlenmeyer flask test method (Wu et al., 2015). Each plant essential oil (15 μl) was dripped into a rectangular filter paper (1.5 cm × 4.0 cm), then the filter paper was hung vertically in the middle of a 1 L pre-washed bottle which contained 10 g Flue-cured tobacco leaves (Yunyan 85) and 30 two-day-old *L. serricorne* adults inside. Acetone (15 μl) served as the negative control. Each treatment was conducted three times. After 48 and 72 h of treatment, the mortality rate is determined, and the corrected mortality rate is calculated using the Abbott's formula.

$$Mortality\ rate\ (\%) = \frac{Number\ of\ dead\ insects}{Number\ of\ test\ insects} \times 100,$$

$$Corrected\ mortality\ rate\ (\%) = \frac{\begin{array}{c}Mortality\ rate\ of\ treatment\ group\\ -Mortality\ rate\ of\ control\ group\end{array}}{1 - Mortality\ rate\ of\ control\ group} \times 100.$$
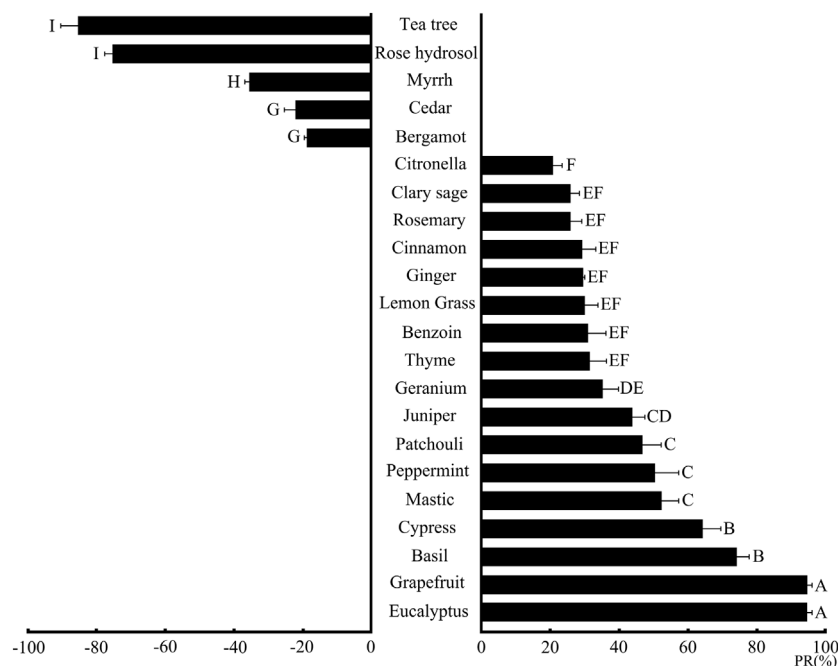
FIGURE 1 | Behavioral response of 22 plant essential oils against *L. serricorne* adults. Different uppercase letters represented in the figure indicate a significant difference through LSD among different plant essential oils against *L. serricorne* adults. PR (%), repellent rate (Mean ± SE).

TABLE 1 | Fumigation activity of 17 kinds of plant essential oils against *L. serricorne* adults at 15 µl/L.

Essential oil	Fumigation activity (mean ± SE) (%)[a]	
	48 h	**72 h**
Rosemary	40.00 ± 1.92 C	100.00 A
Eucalyptus	53.33 ± 1.92 B	95.29 ± 3.11 A
Basil	25.56 ± 1.11 D	95.29 ± 11.77 A
Citronella	74.44 ± 4.84 A	94.12 ± 2.35 A
Geranium	77.78 ± 2.94 A	91.76 ± 31.13 A
Thyme	40.00 ± 3.85 C	76.47 ± 3.11 B
Clary sage	27.78 ± 1.11 D	71.76 ± 4.08 B
Cinnamon	31.11 ± 1.11 D	51.76 ± 1.18 C
Juniper	11.11 ± 1.11 E	47.06 ± 5.39 C
Grapefruit	8.89 ± 1.11 EF	36.47 ± 3.53 D
Ginger	11.11 ± 1.11 E	22.35 ± 2.04 E
Patchouli	0 G	21.17 ± 2.35 E
Peppermint	0 G	18.82 ± 2.03 E
Benzoin	0 G	9.41 ± 2.35 F
Lemon grass	3.33 ± 1.92 FG	7.05 ± 1.18 F
Mastic	11.11 ± 1.11 E	5.88 ± 1.18 F
Cypress	0 G	5.88 ± 1.18 F

[a]*Different uppercase letters indicate the fumigation activity against* L. serricorne *adults of the plant essential oils with a significant difference through LSD.*

Contact Activity Test

The plant essential oils with good fumigation activity were selected to study their contact activity against *L. serricorne* adults using the leaf-dipping method (Yuan et al., 2018). Five concentration gradients of each essential oil were diluted with acetone (200 ml). Flue-cured tobacco leaves (Yunyan 85) with the

same growth condition were dipped into each concentration gradients of each essential oil for 30 s, and then dried in the air. After that, the Flue-cured tobacco leaves (Yunyan 85) were placed in a box (19.5 cm × 13.4 cm × 4.0 cm). 20 two-day-old *L. serricorne* adults were transferred to the box. Acetone served as the negative control, Pirimiphos-methyl (Actellic 50 EC®, Syngenta AG, Cape Town, South Africa) and Chlorantraniliprole (Zhengzhou Salongda Weixin Pesticide Co., Ltd., Henan, China) were selected as positive controls according to the research studies reported by Wang et al. (2011) and Han et al. (2014). Three replicates were conducted for each treatment. After 72 h of treatment, the mortality rate is determined and corrected using the Abbott's formula.

Statistical Analysis

All data represented in this study are analyzed using SPSS version 23 software (IBM, NY, United States). The toxic regression equation and LD_{50} values are analyzed by the Probit model from SPSS. The *p* value lower than 0.05, analyzed by statistical significance, is considered to be significant.

RESULTS AND DISCUSSION

Behavioral Response

In this study, a total of 22 kinds of plant essential oils are selected to explore their behavioral responses against *L. serricorne* adults. Our results (**Figure 1**) show that 17 kinds of plant essential oils in eucalyptus, basil, grapefruit, cypress, mastic, peppermint,

TABLE 2 | Contact activity of five kinds of plant essential oils against *L. serricorne* adults.

Essential oil	Contact activity (mean ± SE) (%)[a]							
	0.5 µl/L	1 µl/L	2.5 µl/L	5 µl/L	10 µl/L	15 µl/L	20 µl/L	40 µl/L
Rosemary	5.35 ± 1.79 E	10.71 ± 1.79 D	39.28 ± 1.79 C	69.64 ± 1.79 B	100.00 A	-	-	-
Eucalyptus	7.14 ± 3.57 E	42.86 ± 1.79 D	-	71.43 ± 1.79 C	89.29 ± 0.03 B	100.00 A	-	-
Basil	-	10.71 ± 1.79 D	-	41.07 ± 3.09 C	51.78 ± 6.19 B	80.36 ± 1.79 A	89.29 ± 0.01 A	-
Citronella	-	7.14 ± 1.79 D	-	48.21 ± 3.57 C	58.93 ± 3.57 C	-	73.21 ± 5.36 B	92.86 ± 1.79 A
Geranium	-	12.5 ± 3.57 E	-	41.07 ± 3.09 D	64.28 ± 1.79 C	82.14 ± 3.57 B	94.64 ± 3.09 A	-

[a]*Different uppercase letters indicate the contact activity against* L. serricorne *adults of the plant essential oils with a significant difference through LSD.*

TABLE 3 | The LD_{50} values of the contact activity against *L. serricorne* adults of the tested plant essential oils.

Treatment	Toxic regression equation	Chi-Square	LD_{50} (mean ±95% confidence limit) (µl/L)
Rosemary	y = -1.639 + 0.456x	0.23	3.60 (1.26–83.63)
Eucalyptus	y = -0.812 + 0.233x	1.04	3.49 (-10.18–14.68)
Basil	y = -1.094 + 0.123x	0.39	8.90 (-16.40–22.12)
Citronella	y = -1.372 + 0.721x	0.36	6.70 (0.01–35.58)
Geranium	y = -1.072 + 0.138x	0.39	7.80 (-12.20–16.82)
Pirimiphos-methyl	y = -0.651 + 0.042x	3.15	15.45 (-7.05–34.27)
Chlorantraniliprole	y = -2.033 + 0.003x	3.91	249.77 (305.02–689.48)

patchouli, juniper, geranium, thyme, benzoin, lemon grass, cinnamon, ginger, rosemary, clary sage, and citronella can avoid *L. serricorne* adults with the repellent rates of 20.79–94.67%. Especially, essential oils in eucalyptus and grapefruit are found to be the most successful plant essential oils that caused the maximum repellent rate (94.67 and 94.56%, respectively) against *L. serricorne* adults over the whole exposure period followed by basil (74.15%) and cypress (64.31%). Similar results reported by Song et al. (2018) showed that eucalyptus essential oil (500 µl) can avoid *L. serricorne* adults up to 67%, whereas Tampe et al. (2020) reported that eucalyptus essential oil (500 ng) was attractive for both sexes of *Aegorhinus superciliosus*. Meanwhile, **Figure 1** also shows that five kinds of essential oils in tea tree, myrrh, bergamot, rose hydrosol, and cedar can attract *L. serricorne* adults with the repellent rates of −18.56– −84.98%; among them, the tea tree essential oil has the most attractive effect on *L. serricorne* with a repellent rate of −84.98% followed by rose hydrosol (−74.85%). Buteler et al. (2019) identified the behaviour effect of tea tree essential oil on *Acromyrmex* spp. ants, and the results showed that the tea tree essential oil (10 ml/L) can 69% avoid *Acromyrmex* spp. Ants at 30 min. Diaz–Montano and Trumble (2013) reported that tea tree essential oil (2000 µl) showed a significant repellency on potato psyllid (*Bactericera cockerelli*) adults.

Fumigant Activity

Base on the behavioral responses of the plant essential oils against *L. serricorne* adults, 17 kinds of plant essential oils, which can avoid *L. serricorne* adults, are selected to study their fumigation activity against *L. serricorne* adults at 15 µl/L. **Table 1** shows that,

after 48 and 72 h of treatment, some of the plant essential oils exhibit good fumigation activity against *L. serricorne* adults at 15 µl/L. Among of them, after 72 h of treatment, rosemary essential oil shows the best fumigation activity against *L. serricorne* adults with a 100.00% mortality rate. Yang et al. (2020) selected 28 kinds of essential oils to evaluate their fumigation activity against maize weevils (*Sitophilus zeamais*), the results showed that essential oils in cinnamon (LD_{50} = 0.04 mg/cm²), ylang ylang (LD_{50} = 0.032 mg/cm²), and tea tree (LD_{50} = 0.15 mg/cm²) revealed superior fumigation activity against maize weevils. Meanwhile, Trivedi et al. (2017) reported that the LD_{50} values of fumigation activity obtained for 24, 48 and 72 h for rosemary essential oil against the stored grain pest *Callosobruchus chinensis* were 3.282, 4.261, and 1.509 mg/L, respectively. In addition, Çetin and Güdek (2020) found that rosemary essential oil exhibited perfect fumigation activity against fifth instar larvae of the date moth *Ectomyelois ceratoniae* with the mortality rate of 100.00% at 90 µl/L after 30 days of exposure.

Contact Activity

Five kinds of plant essential oils, rosemary, eucalyptus, basil, citronella, and geranium, are selected to study their contact activity against *L. serricorne* adults. **Table 2** shows that, after 72 h of treatment, plant essential oils in rosemary, eucalyptus, basil, citronella, and geranium exhibit good contact activity against *L. serricorne* adults, with the mortality rates of 5.35%–100.00%, 7.14%–100.00%, 10.71%–89.29%, 7.14%–92.86%, and 12.5%–94.64%, respectively. Especially, two kinds of plant essential oils in rosemary and eucalyptus revealed a

100% mortality rate against *L. serricorne* adults at 10 and 15 μl/L, respectively. Meanwhile, **Table 3** shows that the LD_{50} of the contact activity against *L. serricorne* adults of plant essential oils in rosemary, geranium, citronella, basil, and eucalyptus are 3.60, 3.49, 8.90, 6.70, and 7.80 μl/L, respectively, which are even better than those of Pirimiphos-methyl (15.45 μl/L) and Chlorantraniliprole (249.77 μl/L). In recent years, many research studies on the essential oils against *L. serricorne* have been performed, for example, Liang et al. (2021) found that *Elsholtzia densa* essential oil possesses obvious contact activity (LD_{50} = 24.29 mg/L) against *L. serricorne*. Meanwhile, Zhou et al. (2018) reported that the *Artemisia lavandulaefolia* (Compositae) essential oil also exhibited good contact toxicity (LD_{50} = 13.51 μg/L) to control *L. serricorne*.

CONCLUSION

In this study, 22 kinds of plant essential oils are selected to study their behavioral response, fumigant activity, and contact activity against *L. serricorne* adults. Our results show that five plant essential oils can attract *L. serricorne* adults, whereas 17 plant essential oils can avoid *L. serricorne* adults. Meanwhile, rosemary essential oil shows the best fumigation activity against *L. serricorne* adults, and eucalyptus essential oil shows the best contact activity against *L. serricorne* adults, supporting the interest of industrial use of plant essential oils, such as rosemary and geranium essential oils, as environmentally friendly insect control agents.

REFERENCES

Boukaew, S., Prasertsan, P., and Sattayasamitsathit, S. (2017). Evaluation of Antifungal Activity of Essential Oils against Aflatoxigenic *Aspergillus flavus* and Their Allelopathic Activity from Fumigation to Protect maize Seeds during Storage. *Ind. Crops Prod.* 97, 558–566. doi:10.1016/j.indcrop.2017.01.005

Buteler, M., Alma, A. M., Herrera, M. L., Gorosito, N. B., and Fernández, P. C. (2019). Novel Organic Repellent for Leaf-Cutting Ants: tea Tree Oil and its Potential Use as a Management Tool. *Int. J. Pest Manage.* 67 (1), 1–9. doi:10.1080/09670874.2019.1657201

Cao, Y., Yang, W. J., Meng, Y. L., Liu, Y., Xiong, Z. L., Zeng, L., et al. (2015). Toxicity of CO_2 to *Oryzaephilus Surnamensis* and Content and Utilization of its Energy Substances. *J. Northwest A&F Univ.* 43 (11), 123–128. doi:10.13207/j.cnki.jnwafu.2015.11.018

Çetin, H., and Güdek, M. (2020). Effect of Essential Oil from the Leaves of Rosemary Used in the Control of *Callosobruchus Maculatus* (F.) on the Hydration Coefficient, Cookability, Taste and Color of the Edible Chickpea. *J. Essent. Oil Bearing Plants* 23 (2), 301–310. doi:10.1080/0972060X.2020.1748522

Chaitanya, N., Swamy, S. V. S. G., and Madhumathi, T. (2017). Effect of Modified Atmosphere on Cigarette Beetle *Lasioderma Serricorne* (F.) in Stored Turmeric. *Ind. Jour. Entomol.* 79 (2), 202–207. doi:10.5958/0974-8172.2017.00040.2

Chen, S. J., Mao, J. J., Gu, L., and Peng, X. L. (2013). Tobacco Beetle Control Mode Based on the Control Technology. *Acad. Periodical Farm Prod. Process.* 6, 69–72.

Cheng, F., Zhang, Y. W., Shao, M. K., Zhang, R., Liu, S. J., Kong, W. B., et al. (2019). Repellent Activities of Essential Oil Extracts from Five *Artemisia* Species against *Lasioderma Serricorne* and *Liposcelis Bostrychophila*. *Tob. Sci. Techn.* 52 (11), 17–22. doi:10.16135/j.issn1002-0861.2018.0507

DATA AVAILABILITY STATEMENT

The original contributions presented in the study are included in the article/Supplementary Material; further inquiries can be directed to the corresponding authors.

AUTHOR CONTRIBUTIONS

Conceptualization, YR and TW; methodology, DJ; software, YJ; validation, YR, TW, and DJ; formal analysis, YJ and DC; investigation, DC, WZ, and YJ; resources, YR; data curation, TW; writing—original draft preparation, TW; writing—review and editing, YR; visualization, YR; supervision, DJ; project administration, TW; and funding acquisition, YR. All authors contributed to the article and approved the submitted version.

FUNDING

Diaz-Montano, J., and Trumble, J. T. (2013). Behavioral Responses of the Potato Psyllid (Hemiptera: Triozidae) to Volatiles from Dimethyl Disulfide and Plant Essential Oils. *J. Insect Behav.* 26, 336–351. doi:10.1007/s10905-012-9350-8

Fukazawa, N., and Takahashi, R. (2017). Effect of Time and Concentration on Mortality of the Cigarette Beetle, *Lasioderma Serricorne* (F.), Fumigated with Phosphine. *Beiträge zur Tabakforschung Int.* 27 (6), 97–101. doi:10.1515/cttr-2017-0010

Guarino, S., Basile, S., Arif, M. A., Manachini, B., and Peri, E. (2021). Odorants of *Capsicum* Spp. Dried Fruits as Candidate Attractants for *Lasioderma Serricorne* F. (Coleoptera: Anobiidae). *Insects* 12 (61), 61–69. doi:10.3390/insects12010061

Guo, J. H., Lv, J. H., Wang, G. Y., Guo, Y. F., Guo, C., Song, J. Z., et al. (2021). A Feasibility Study on Controlling *Lasioderma Serricorne* Larvae with *Anisopteromalus Calandrae* Based on Artificial Inoculation. *Tob. Sci. Techn.* 54 (32), 24–29. doi:10.16135/j.issn1002-0861.2020.0341

Han, Z. M., Meng, Z. N., Zhou, Z. J., Su, W. L., and Xiong, M. R. (2014). Indoor Poisonous Effects of Six Insecticides on the Larva of Tobacco Moth *Ephestia Elutella* (Hübner). *J. Anhui Agric. Univ.* 41 (1), 87–91. doi:10.13610/j.cnki.1672-352x.2014.01.010

Huang, Y., Ho, S.-H., Lee, H.-C., and Yap, Y.-L. (2002). Insecticidal Properties of Eugenol, Isoeugenol and Methyleugenol and Their Effects on Nutrition of *Sitophilus Zeamais* Motsch. (Coleoptera: Curculionidae) and *Tribolium castaneum* (Herbst) (Coleoptera: Tenebrionidae). *J. Stored Prod. Res.* 38, 403–412. doi:10.1016/S0022-474X(01)00042-X

Huang, Y., and Ho, S. H. (1998). Toxicity and Antifeedant Activities of Cinnamaldehyde against the Grain Storage Insects, Tribolium castaneum (Herbst) and Sitophilus Zeamais Motsch. *J. Stored Prod. Res.* 34, 11–17. doi:10.1016/S0022-474X(97)00038-6

Işıkber, A. A., Özder, N., and Sağlam, Ö. (2009). Susceptibility of Eggs of *Tribolium confusum, Ephestia Kuehniella* and *Plodia Interpunctella* to Four Essential Oil Vapors. *Phytoparasitica* 37, 231–239. doi:10.1007/s12600-009-0035-6

Kaelin, P., Morel, P., and Gadani, F. (1994). Isolation of Bacillus Thuringiensis from Stored Tobacco and Lasioderma Serricorne (F.). *Appl. Environ. Microbiol.* 60 (1), 19–25. doi:10.1128/AEM.60.1.19-25.1994

Kaelin, P., Zaugg, L., Albertini, A. M., and Gadani, F. (1999). Activity of *Bacillus Thuringiensis* Isolates on *Lasioderma Serricorne* (F.) (Coleoptera: Anobiidae). *J. Stored Prod. Res.* 35, 145–158. doi:10.1016/S0022-474X(98)00040-X

Kamal, W., Ahmad, S., Saeed, M., Rehman, A., Zada, H., Latif, A., et al. (2019). Repellency Evaluation of Botanical Extracts against *Lasioderma Serricorne* (Anobiidae: Coleoptera) under Laboratory Condition. *J. Entomol. Zoolog. Stud.* 7 (1), 479–481. Available at: https://www.researchgate.net/publication/336915924.

Karakoç, Ö. C., Alkan, M., Şimşek, Ş., Gökçe, A., and Çam, H. (2018). Fumigant Activity of Some Plant Essential Oils and Their Consustent against to Stegobium Paniceum and Lasioderma Serricorne (Coleoptera:Anobidae). *Bitki Koruma Bülteni/Plant Prot. Bull.* 58 (3), 9–10. doi:10.16955/bitkorb. 370866

Khanum, T. A., and Javed, S. (2021). Pathogenicity of Pakistani Isolates of *Steinernema Bifurcatum* and *S. Affine* (Rhabditida: Steinernematidae) in Management of Stored Grain Pests *Lasioderma Serricorne* and *Tribolium castaneum* (Coleoptera: Ptinidae, Tenebrionidae). *Egypt. J. Biol. Pest Control.* 31, 73. doi:10.1186/s41938-021-00418-1

Khemira, S., Mediouni-Ben Jemâa, J., and Khouja, M. L. (2013). Assessment of Fumigant Activity of Two eucalyptus Essential Oils against the Cigarette Beetle *Lasioderma Serricorne* F. (Coleoptera: Anobiidae). *Acta Hortic.* 997 (997), 201–205. doi:10.17660/ActaHortic.2013.997.24

Kumar, R., Reddy, C. N., Lakshmi, K. V., Radhika, P., Ash, R., Keshavulu, K., et al. (2017). Modified Atmosphere with Effect of Elevated Levels of Co2 against Cigarette Beetle (Lasioderma Serricorne Fabricius) in Cured Turmeric Rhizomes (Curcuma Longa Linnaeus) during Storage. *Int.J.Curr.Microbiol.App.Sci* 6 (6), 1538–1546. doi:10.20546/ijcmas.2017. 606.181

Li, C. H., Xu, Q., Cai, J. W., Wang, Z. Y., Li, J. W., and Xiong, Y. N. (2021). Research Progress in the Control of Tobacco Beetle. *Jiangsu Agric. Sci.* 49 (7), 33–43. doi:10.15889/j.issn.1002-1302.2021.07.006

Li, M., Li, X.-J., Lü, J.-H., and Huo, M.-F. (2018). The Effect of Acclimation on Heat Tolerance of *Lasioderma Serricorne* (Fabricius) (Coleoptera: Anobiidae). *J. Therm. Biol.* 71, 153–157. doi:10.1016/j.jtherbio.2017.11.007

Li, W. Z., Fan, Y. Y., An, J. J., Wang, Q., Guo, X. R., Luo, M. H., et al. (2014). Screening of Plant-Derived Repellents against Tobacco Beetle, *Lasioderma Serricorne* (Fabricius). *Acta Tabacaria Sinica* 20 (5), 93–97. doi:10.3969/j. issn.1004-5708.2014.05.015

Liang, J., Shao, Y., Wu, H., An, Y., Wang, J., Zhang, J., et al. (2021). Chemical Constituents of the Essential Oil Extracted from *Elsholtzia Densa* and Their Insecticidal Activity against *Tribolium castaneum* and *Lasioderma Serricorne*. *Foods* 10 (10), 2304. doi:10.3390/foods10102304

Lü, J., and Liu, S. (2016). The Behavioral Response of *Lasioderma Serricorne* (Coleoptera: Anobiidae) to Citronellal, Citral, and Rutin. *SpringerPlus* 5 (798), 1–7. doi:10.1186/s40064-016-2553-2

Makhijani, A., and Gurney, K. (1995). *Mending the Ozone Hole: Science, Technology, and Policy*. Cambridge: The Massachusetts Institute of Technology Press.

Naveen, M., Jayaraj, J., Chinniah, C., Mini, M., Vellaikumar, S., and Shanthi, M. (2021). Insecticidal Property of Methanolic Leaf Extract of Sweet Basil, *Ocimum Basilicum* (L.) against Cigarette Beetle, *Lasioderma Serricorne* (Fab.) (Coleoptera: Anobiidae). *J. Entomol. Zool. Stud.* 9 (1), 259–262. doi:10. 22271/j.ento.2021.v9.i1d.8155

Naveena, K., Sridhar, R. P., and Roseleen, S. S. J. (2021). Management of Cigarette Beetle, *Lasioderma Serricorne* (F.) (Coleoptera: Anobiidae) Infesting Stored Turmeric, *Curcuma Longa* (L.) with Phyto-Fumigation. *J. Entomol. Zool. Stud.* 9 (1), 725–728. doi:10.22271/j.ento.2021.v9.i1j.8232

Peng, T., Liu, S. W., Tan, L., Yu, X. J., and Guo, N. M. (2015). Killing Effect of Mixed Fumigation of Phosphineand Carbon Dioxide on Eggs of *Lasioderma Serricorne* F. *Agric. Sci. Techn.* 16 (12), 2730–2732. doi:10.16175/j.cnki.1009-4229.2015. 12.031

Rajendran, S., and Narasimhan, K. S. (1994). Phosphine Resistance in the Cigarette beetleLasioderma serricorne(Coleoptera: Anobiidae) and Overcoming Control Failures during Fumigation of Stored Tobacco. *Int. J. Pest Manage.* 40, 207–210. doi:10.1080/09670879409371883

Ramadan, G. R. M., Abdelgaleil, S. A. M., Shawir, M. S., El-bakary, A. S., Zhu, K. Y., and Phillips, T. W. (2020). Terpenoids, DEET and Short Chain Fatty Acids as Toxicants and Repellents for Rhyzopertha dominica (Coleoptera: Bostrichidae) and Lasioderma Serricorne (Coleoptera: Ptinidae). *J. Stored Prod. Res.* 87 (101610), 101610–101618. doi:10.1016/j.jspr.2020.101610

Savvidou, N., Mills, K., and Pennington, A. (2003). *Phosphine Resistance in Lasioderma Serricorne (Fabricius) (Coleoptera: Anobiidae) Advances in Stored Product Protection International Working Conference on Stored Product Protection*. Editors P. F. A. Credland, D. M. Armitage, C. H. Bell, P. M. Cogan, and E. Highley (Wallingford, UK: CAB International), 702–712.

Shaymaa, H. A., Samar, M. S., and Hind, I. A. (2019). Review of Cigarette Beetle *Lasioderma Serricorne* (F.)(Coleoptera Anobiidae). *J. Res. Ecol.* 7 (2), 2641–2646. Available at: http://ecologyresearch.info/documents/EC0698.pdf.

Silva, S. M., Haddi, K., Viteri-Jumbo, L. O., and Oliveira, E. E. (2017). Progeny of the maize Weevil, Sitophilus Zeamais , Is Affected by Parental Exposure to Clove and Cinnamon Essential Oils. *Entomol. Exp. Appl.* 163 (2), 220–228. doi:10.1111/eea.12559

Song, J.-H., Md, A. A., 압, 둘., Choi, E.-D., Choi, D.-S., and Seo, H.-J. (2018). Screening of Essential Oil Repellents against the Organic Pear Pest Holotrichia Parallela (Coleoptera: Scarabaeidae)*. *Korean J. Org. Agric.* 26 (2), 259–268. doi:10.11625/KJOA.2018.26.2.259

Sun, J. F., Yang, F. Y., and Li, Z. (2020). The Application Research on Killing *Lasioderma Serricorne* by CO_2. *Hubei Agric. Sci.* 59 (3), 87–90. doi:10.14088/j. cnki.issn0439-8114.2020.03.017

Tampe, J., Pacheco, B., Bardehle, L., Fuentes, E., Salas, L., and Quiroz, A. (2020). Attractant Effect of Eucalyptus Globulus (Labill) and Foeniculum Vulgare (Mill.) Essential Oils on Aegorhinus Superciliosus (Guérin) (Coleoptera: Curculionidae). *J. Soil Sci. Plant Nutr.* 20, 775–783. doi:10.1007/s42729-019-00164-2

Tang, J., Ban, G. X., Luo, Q. Q., Yao, F., Jiang, T., Li, Z. H., et al. (2015). Control Effects of Twelve Insecticides against *Lasioderma Serricorne* (Fabricius) Indoors. *J. Anhui Agric. Univ.* 42 (2), 252–256. doi:10.13610/j.cnki.1672-352x.20150302.021

Trivedi, A., Nayak, N., and Kumar, J. (2017). Fumigant Toxicity Study of Different Essential Oils against Stored Grain Pest. *J. Pharmacognosy Phytochemistry* 6 (4), 1708–1711. Available at: https://www.researchgate. net/publication/322204227.

Wang, X. F., Ren, G. W., Wang, X. W., Chen, D., and Ma, Q. (2011). Toxicity of Several Pesticides to *Lasioderma Serricorna* (Fabricius). *Chin. Tob. Sci.* 32 (4), 84–86. doi:10.3969/j.issn.1007-5119.2011.04.019

Wu, C. C., Huang, P., Xue, Z. L., Chen, D. X., and He, L. X. (2017). Effects of Aluminium Phosphide and Methyl Bromide on Storage Pests of Tangerine Peel with Fumigation and Heat Treatment. *Biol. Disaster Sci.* 40 (4), 280–283. doi:10. 3969/j.issn.2095-3704.2017.04.61

Wu, Y., Zhang, W. J., Li, Z. H., Zheng, L. S., Wang, P. J., and Wei, J. Y. (2015). Toxic Activities of *Platycladus Orientalis* against *Lasioderma Serricorne* and *Tribolium castaneum* in Stored Tobacco. *Tob. Sci. Techn.* 48 (10), 31–56. doi:10.16135/j.issn1002-0861.20151005

Xiong, M. R., Su, W. L., Xiao, Y., Wu, G. B., Wei, L. S., Jiang, T., et al. (2014). Control Effect of Three Organophosphorus Insecticides on *Lasioderma Serricorne*. *Hunan Agric. Sci.* 21, 46–49. doi:10.16498/j.cnki.hnnykx.2014. 21.011

Xu, K. K., Ding, T. B., Yan, Y., Li, C., and Yang, W. J. (2017). Expression Analysis of Glutathione S-Transferase Genes in *Lasioderma Serricorne* (Coleoptera: Anobiidae) Subjected to CO_2-enriched Atmosphere. *J. Zhejiang Univ. (Agric. Life Sci.)* 43 (5), 599–607. doi:10.3785/j.issn. 1008-9209.2017.02.261

Yang, Y., Isman, M. B., and Tak, J.-H. (2020). Insecticidal Activity of 28 Essential Oils and a Commercial Product Containing *Cinnamomum cassia* Bark Essential Oil against *Sitophilus Zeamais* Motschulsky. *Insects* 11 (8), 474. doi:10.3390/insects11080474

Yang, Y. Y., Shao, Y. Z., Shi, M. N., Xu, J., and Liang, J. Y. (2021). Toxic Activities of Essential Oil Extracted from *Ajania Salicifolid* against *Lasioderma Serricorne* and *Tribolium castaneum*. *Tob. Sci. Techn.* 54 (2), 30–43. doi:10.16135/j. issn1002-0861.2020.0108

Yu, C., Subramanyam, B., Flinn, P. W., and Gwirtz, J. A. (2011). Susceptibility of *Lasioderma Serricorne* (Coleoptera: Anobiidae) Life Stages to Elevated

Temperatures Used during Structural Heat Treatments. *Jnl. Econ. Entom.* 104 (1), 317–324. doi:10.1603/ec10067

Yuan, M., Ou, H. D., Yang, M. F., Yang, H., Jin, X., and Zhou, F. J. (2018). Sensitivity of *Ephestia Elutella* to Five Insecticides. *J. Mountain Agric. Biol.* 37 (5), 36–40. doi:10.15958/j.cnki.sdnyswxb.2018.05.008

Zettler, L. J., and Keever, D. W. (1994). Phosphine Resistance in Cigarette Beetle (Coleoptera: Anobiidae) Associated with Tobacco Storage in the Southeastern United States. *J. Economical Entomol.* 87 (3), 546–550. doi:10.1093/jee/87.3.546

Zhou, J., Zou, K., Zhang, W., Guo, S., Liu, H., Sun, J., et al. (2018). Efficacy of Compounds Isolated from the Essential Oil of *Artemisia Lavandulaefolia* in Control of the Cigarette Beetle, *Lasioderma Serricorne*. *Molecules* 23 (2), 343. doi:10.3390/molecules23020343

Publisher's Note: All claims expressed in this article are solely those of the authors and do not necessarily represent those of their affiliated organizations, or those of the publisher, the editors and the reviewers. Any product that may be evaluated in this article, or claim that may be made by its manufacturer, is not guaranteed or endorsed by the publisher.

Active Metabolites From the Endophyte *Paenibacillus polymyxa* Y-1 of *Dendrobium nobile* for the Control of Rice Bacterial Diseases

Wenshi Yi[1,2], Chao Chen[1] and Xiuhai Gan[1]*

[1]*State Key Laboratory Breeding Base of Green Pesticide and Agricultural Bioengineering, Key Laboratory of Green Pesticide and Agricultural Bioengineering, Ministry of Education, Guizhou University, Guiyang, China,* [2]*School of Chemistry and Materials Science, Guizhou Education University, Guiyang, China*

Microbial bactericides have been a research hotspot in recent years. In order to find new microbial fungicides for preventing and treating rice bacterial diseases, *Paenibacillus polymyxa* Y-1 (*P. polymyxa* Y-1) was isolated from *Dendrobium nobile* in this study, and the optimal medium was selected by a single-factor experiment, and then eight metabolites were isolated from *P. polymyxa* Y-1 fermentation broth by bioactivity tracking separation. The bioassay results showed that 2,4-di-tert-butylphenol, N-acetyl-5-methoxytryptamine, and P-hydroxybenzoic acid have good antibacterial activity against *Xanthomonas oryzae* pv. *Oryzicola* (*Xoo*) and *Xanthomonas oryzae* pv. *oryzae* (*Xoc*), with 50% effective concentration values of 49.45 µg/ml, 64.22 µg/ml, and 16.32 µg/ml to *Xoo*, and 34.33 µg/ml, 71.17 µg/ml, and 15.58 µg/ml to *Xoc*, respectively, compared with zhongshengmycin (0.42 and 0.82 µg/ml, respectively) and bismerthiazol (85.64 and 92.49 µg/ml, respectively). *In vivo* experiments found that 2,4-di-tert-butylphenol (35.9 and 35.4%, respectively), N-acetyl-5-methoxytryptamine (42.9 and 36.7%, respectively), and P-hydroxybenzoic acid (40.6 and 36.8%, respectively) demonstrated excellent protective and curative activity against rice bacterial leaf blight, which were better than that of zhongshengmycin (38.4 and 34.4%, respectively). In addition, after 2,4-di-tert-butylphenol, N-acetyl-5-methoxytryptamine, and P-hydroxybenzoic acid acted on rice, SOD, POD, and CAD defense enzymes increased under the same condition. In conclusion, these results indicated that the activity and mechanism research of new microbial pesticides were helpful for the prevention and control of rice bacterial diseases.

Keywords: *Dendrobium nobile*, *Paenibacillus polymyxa* Y-1, active metabolites, rice bacterial diseases, antibacterial activity

1 INTRODUCTION

Plant bacterial diseases caused by microorganisms lead to tremendous economic losses to crops all over the world every year. Rice bacterial leaf blight (BLB) is caused by *Xanthomonas oryzae* pv. *oryzae* (*Xoo*) and results in reduced rice quality and yield with up to 40–80% loss (Cao et al., 2020; Zou et al., 2021). Traditional bactericides such as long-term use of bismerthiazol and thiodiazole copper will lead to drug resistance of pathogenic bacteria, which will affect the safety of the environment and plants, while microbial bactericides such as zhongshengmycin and shenqinmycin

have low field control effects (Wang et al., 2019; Wang et al., 2021). Therefore, it is essential to discover new, highly active microbial antibacterial drugs.

Dendrobium nobile (*D. nobile*), a medicinal and edible plant, is native to China and belongs to the Orchidaceae family, which is rich in endophytic bacteria (Cai et al., 2015). Among them, *Paenibacillus polymyxa* (*P. polymyxa*) is an important endophytic bacterium from *D. nobile*, which can produce a variety of active metabolites, such as polymyxins (Niu et al., 2013; Mülner et al., 2021), paenibacillin (Huang and Yousef, 2015; Campbell et al., 2021), fusaricidins (Mikkola et al., 2017; Mülner et al., 2021), cytokinins (Liu et al., 2020), auxins (Sadhana and Tabacchioni, 2009), chitinase (Belén et al., 2020), and hydrolase(Sadhana and Tabacchioni, 2009). These metabolites can promote plant growth, improve plant nutrient utilization, and induce plant systemic resistance.

In previous work, three pairs of fusaricidin compounds were isolated from *P. polymyxa* Y-1. *In vitro* and *in vivo* activity studies found that fusaricidin compounds exhibited good antifungal activity against *Pestalotiopsis*. The mechanism study showed that fusaricidin compounds could inhibit amino acid biosynthesis and energy generation of *Pestalotiopsis* (Yang et al., 2018). In this study, the optimum nutrient medium was selected by a single factor experiment, and then eight metabolites were isolated from *P. polymyxa* Y-1 by bioactivity tracking separation. 2,4-Di-tert-butylphenol, N-acetyl-5-methoxytryptamine, and P-hydroxybenzoic acid exhibited good antibacterial activity to *Xoo* and *Xoc*. In addition, the *in vivo* activities of 2,4-di-tert-butylphenol, N-acetyl-5-methoxytryptamine, and P-hydroxybenzoic acid were investigated. It lays a foundation for the mechanism research of new microbial bactericides.

2 MATERIALS AND METHODS

2.1 Samples, Strains, and Culture Condition
D. nobile samples were obtained from Chishui City, Guizhou Province, China. In previous work, *P. polymyxa* Y-1 has been isolated from *D. nobile* (Yang et al., 2018). *Xoo* and *Xoc* strains came from the State Key Laboratory Breeding Base of Green Pesticide and Agricultural Bioengineering, Ministry of Education, Guizhou University, China. *P. polymyxa* Y-1 was cultured at 28°C with nutrient broth (NB) medium and stored at −80°C in Luria-Bertani culture medium with 30% (v/v) glycerol. The *Xoo* and *Xoc* strains were cultured at 28°C with NB medium and stored at 4°C with nutrient agar medium.

2.2 Single-Factor Experiment
Single factors such as carbon source, nitrogen source, concentration, temperature, pH value, and time were selected to study their effects on the bacteriostatic ability of *P. polymyxa* Y-1 fermentation broth. Using 10 g/L peptone, 0.4 g/L $MgSO_4$ and 2 g/L KH_2PO_4 as basal medium (PH = 7), 30 g/L lactose, glucose, maltose, fructose, glycerol, and starch carbon sources were respectively added to prepare different carbon sources culture medium (200 ml), and then *P. polymyxa* Y-1 strain (10 ml) was inoculated. Using 20 g/L glycerol, 0.4 g/L $MgSO_4$, and 2 g/L KH_2PO_4 as basal medium (PH = 7), 10 g/L

peptone, tryptone, beef extract, yeast powder, and urea nitrogen sources were respectively added to prepare different nitrogen sources culture medium (200 ml), and then *P. polymyxa* Y-1 strain (10 ml) was inoculated. Using 0.4 g/L $MgSO_4$ and 2 g/L KH_2PO_4 as the basal medium (PH = 7), carbon source and nitrogen source were respectively added to prepare concentrations of 50, 40, 30, 20, and 10 g/L nutrient medium (200 ml), and then *P. polymyxa* Y-1 strain (10 ml) was inoculated. The effect of pH value showed the pH value was adjusted to 5.0, 5.5, 6.0, 6.5, 7.0, 7.5, and 8.0 with 1 mol/L HCL and NaOH in the basal medium (200 ml), and then *P. polymyxa* Y-1 strain (10 ml) was inoculated. The temperature effect showed that *P. polymyxa* Y-1 was cultured on a shaking table at 25, 26, 27, 28, 29, and 30°C, respectively. The time effect showed that *P. polymyxa* Y-1 was incubated on a shaker for 48, 72, 96, 120, 144, 168, 192, and 216 h, respectively. The paper disk method was used to detect the antibacterial activity of the *P. polymyxa* Y-1 fermentation broth to *Xoo* and *Xoc*. The experiments were all performed three times and in triplicate (Miao et al., 2012).

2.3 Antibacterial Activity Experiments
The paper disk method was used to detect the antibacterial activity of the *P. polymyxa* Y-1 fermentation broth to *Xoo* and *Xoc*. The turbidimetric method was used to evaluate the *in vitro* antibacterial activities of the metabolites from *P. polymyxa* Y-1 to *Xoo* or *Xoc* (Dalgaard et al., 1994; Happy, 2017). The protective and curative activities of active metabolites against BLB were measured in potted rice by Schaad's method (Li et al., 2018). Zhongshengmycin (12% wettable powder) was used as positive controls. SPSS 17.0 software was used to calculate 50% effective concentration (EC_{50}) values of the active metabolites. These experiments were all performed three times and in triplicate.

2.4 Extraction, Isolation, and Structural Identification of Metabolites From *P. polymyxa* Y-1
The metabolites were separated from the *P. Polymyxa* Y-1 fermentation broth by biological activity tracking separation, the separation process is shown in **Figure 1**. The fermentation broth was centrifuged to take the supernatant, which was placed on an Amberlite XAD-16 column and eluted with water–methanol, the eluant polarity was gradually reduced, the ratios of pure water to methanol were 100:0 (A), 75:25 (B), 50:50 (C), 20:80 (D), and 0:100 (E) in turn. The same polarity sections were combined and concentrated into a yellow solid. The solid of B (18.3 g) segment was redissolved in 1 L pure water, filtered through a 0.22 μm microporous membrane filter, and loaded onto a Sephadex LH-20 column. The column was eluted with 20% (B1), and 50% (B2) methanol in turn at a rate of 6 s per drop. Approximately, 50 ml from each of the eluant was collected, and the same segments were enriched and concentrated. The B1 (292.4 mg) sub-fractions was placed on a Phenomenex Gemini C^{18} (00G-4435-N0) and eluted with 0.1% trifluoroacetic acid (TFA) water–acetonitrile to obtain Y1 (32.5 mg). The B2 (167.8 mg) sub-fractions was placed in SKP-10-1800 reverse-phase resin and eluted with methanol to obtain Y2 (24.7 mg). The solid of C (876 mg) segment was redissolved in pure water (600 ml), filtered using a 0.22 μm microporous membrane

FIGURE 1 | Metabolites extraction, separation, and purification flow chart of *P. polymyxa* Y-1.
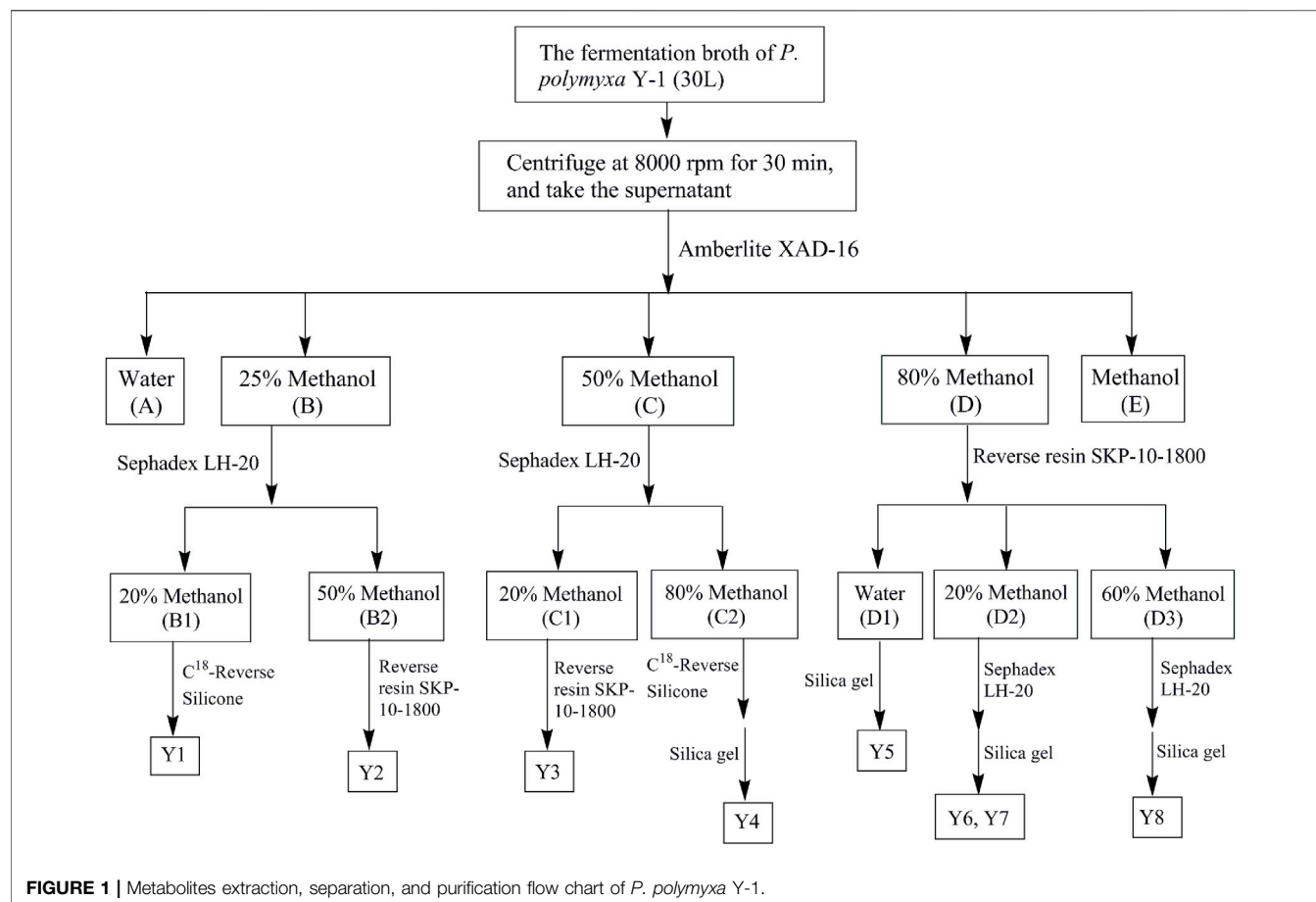
filter, and loaded onto a Sephadex LH-20 column. The column was eluted with 20% (C1) and 80% (C2) methanol in turn at a rate of 6 s per drop. The C1 (187.4 mg) sub-fractions were placed in SKP-10-1800 reverse-phase resin and eluted with water–methanol to obtain Y3 (40.5 mg). The C2 (123.4 mg) sub-fractions were placed on a Phenomenex Gemini C^{18} (00G-4435-N0) and eluted with 0.1% TFA water–acetonitrile to obtain Y4 (26.7 mg). The solid of D (10.2 g) segment was redissolved in 800 ml pure water, filtered using a 0.22 μm microporous membrane filter, and loaded onto a SKP-10-1800 reverse-phase resin. The column was eluted with water (D1), 20% (D2) and 60% (D3) methanol in turn at a rate of 6 s per drop. The D1 (198.5 mg) sub-fractions was placed in a silica gel column and eluted with dichloromethane–methanol to obtain Y5 (26.3 mg). The D2 (273.4 mg) and D3 (123.8 mg) sub-fractions were respectively placed on a Sephadex LH-20 column and eluted with water–methanol to obtain Y6 (18.2 mg), Y7 (32.9 mg), and Y8 (16.5 mg). The structures were identified by using ^{1}H NMR, ^{13}C NMR and high resolution mass spectrometry.

2.5 Defensive Enzyme Activity Detection

The protective activities of active metabolites against BLB were determined in potted rice by Schaad's method, and then the samples were harvested on the 1st, 3rd, 5th, and 7th days. The activities of superoxide dismutase (SOD), peroxidase (POD), and cinnamyl alcohol dehydrogenase (CAD) were measured,

according to the instructions of the enzyme assay reagent kits (Beijing Solarbao Life Sciences, China). These experiments were all performed three times and in triplicate.

3 RESULTS AND DISCUSSION

3.1 Antibacterial Activity Assay of *P. polymyxa* Y-1 Supernatant

The *in vitro* antibacterial activity of the *P. polymyxa* Y-1 fermentation broth against *Xoo* and *Xoc* was determined by the paper disk method, and the bioassay results showed that the bacteriostatic rates of *P. polymyxa* Y-1 fermentation broth against *Xoo* and *Xoc* were 34.29 and 30.16%, respectively (**Supplementary Figure S1**).

3.2 Single Factor Experiment Assay

The bacteriostatic rates of *P. polymyxa* Y-1 fermentation broth under different culture conditions were maintained to determine the optimal culture conditions.

3.2.1 Effects of Different Carbon Sources on the Resistance of *P. polymyxa* Y-1

As shown in **Figure 2A**, when glycerol, starch, fructose, maltose, glucose, and lactose were the carbon sources of the nutrient
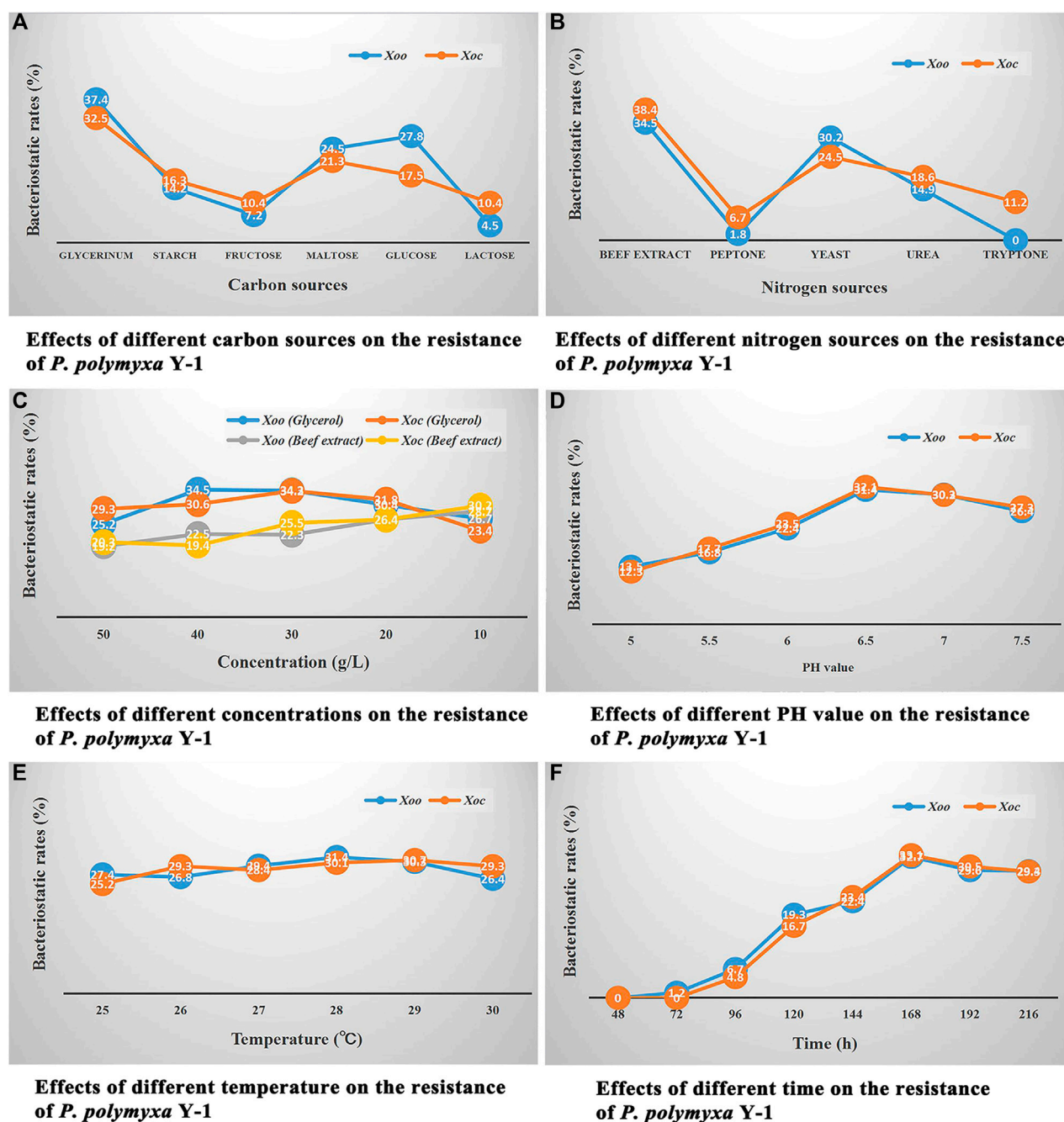
FIGURE 2 | Single factor experiment assay. **(A)** Effects of different carbon sources on the resistance of *P. polymyxa* Y-1. **(B)** Effects of different nitrogen sources on the resistance of *P. polymyxa* Y-1. **(C)** Effects of different concentrations on the resistance of *P. polymyxa* Y-1. **(D)** Effects of different pH on the resistance of *P. polymyxa* Y-1. **(E)** Effects of different temperature on the resistance of *P. polymyxa* Y-1. **(F)** Effects of different time on the resistance of *P. polymyxa* Y-1.

medium, different nutrient medium were used to culture *P. polymyxa* Y-1, the *in vitro* bacteriostatic rates of its fermentation broth against *Xoo* were 37.4, 14.2, 7.2, 24.5, 27.8, and 4.5%, respectively, the *in vitro* bacteriostatic rates against *Xoc*

were 32.5, 16.3, 10.4, 21.3, 17.5, and 10.4%, respectively. The results showed that glycerol was the best carbon source, and the *in vitro* bacteriostatic rates of the *P. polymyxa* Y-1 fermentation broth to *Xoo* and *Xoc* were 37.4 and 32.5%, respectively.
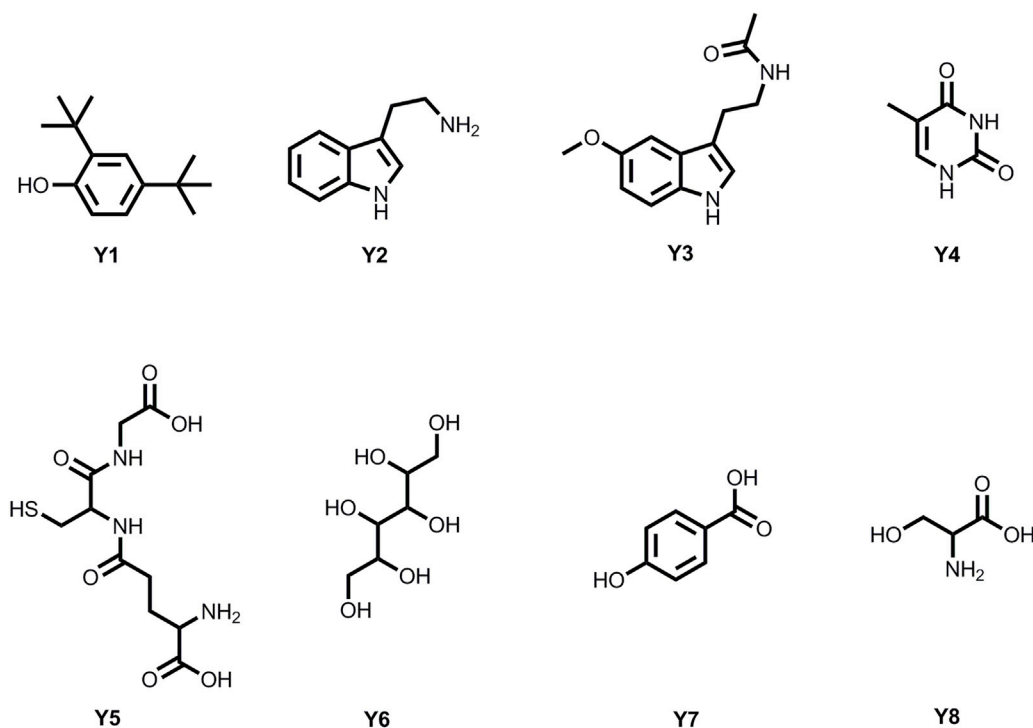
FIGURE 3 | Chemical structures of eight metabolites.

3.2.2 Effects of Different Nitrogen Sources on the Resistance of *P. polymyxa* Y-1

As shown in **Figure 2B**, when beef extract, peptone, yeast, urea, and tryptone were the nitrogen sources of the nutrient medium, different nutrient medium were used to culture *P. polymyxa* Y-1, the *in vitro* bacteriostatic rates of its fermentation broth against *Xoo* were 34.5, 1.8, 30.2, 14.9, 0%, respectively, the *in vitro* bacteriostatic rates against *Xoc* were 38.4, 6.7, 24.5, 18.6, 11.2%, respectively. The results showed that the beef extract was the best nitrogen source, the *in vitro* bacteriostatic rates of the *P. polymyxa* Y-1 fermentation broth to *Xoo* and *Xoc* were 34.5 and 38.4%, respectively.

3.2.3 Effects of Different Concentrations on the Resistance of *P. polymyxa* Y-1

As shown in **Figure 2C**, when the concentration of the beef extract was fixed and the concentration of glycerol was 50, 40, 30, 20, and 10 g/L, respectively, the nutrient medium with different carbon sources were used to culture *P. polymyxa* Y-1, the *in vitro* bacteriostatic rates of its fermentation broth against *Xoo* were 25.2, 34.5, 34.3, 30.4, and 26.7%, respectively, the *in vitro* bacteriostatic rates against *Xoc* were 29.3, 30.6, 34.2, 31.8, and 23.4%, respectively. When the concentration of glycerol was fixed and the concentration of the beef extract were 50, 40, 30, 20, and 10 g/L, respectively, the nutrient medium with different nitrogen sources were used to culture *P. polymyxa* Y-1, the *in vitro* bacteriostatic rates of its fermentation broth against *Xoo* were

19.2, 22.5, 22.3, 26.4, and 28.7%, respectively, the *in vitro* bacteriostatic rates against *Xoc* were 20.3, 19.4, 25.5, 26.4, and 30.2%, respectively. The results showed that the optimal concentration of glycerol was 30 g/L, and the *in vitro* bacteriostatic rates of *P. polymyxa* Y-1 fermentation broth against *Xoo* and *Xoc* were 34.3 and 34.2%, respectively. The optimal concentration of the beef extract was 10 g/L, and the *in vitro* bacteriostatic rates of *P. polymyxa* Y-1 fermentation broth against *Xoo* and *Xoc* were 28.7 and 30.2%, respectively.

3.2.4 Effects of Different pH Values on the Resistance of *P. polymyxa* Y-1

As shown in **Figure 2D**, when the pH values were adjusted to 5.0, 5.5, 6.0, 6.5, 7.0, and 7.5, respectively, different nutrient medium were used to culture *P. polymyxa* Y-1, the *in vitro* bacteriostatic rates of its fermentation broth against *Xoo* were 13.5, 16.8, 22.4, 31.4, 30.3, and 26.4%, respectively, the *in vitro* bacteriostatic rates against *Xoc* were 12.3, 17.7, 23.5, 32.1, 30.2, and 27.3%, respectively. The results showed that the optimum pH value was 6.5, and the *in vitro* bacteriostatic rates of the *P. polymyxa* Y-1 fermentation broth against *Xoo* and *Xoc* were 31.4 and 32.1%, respectively.

3.2.5 Effects of Different Temperatures on the Resistance of *P. polymyxa* Y-1

As shown in **Figure 2E**, when the culture temperature were 25, 26, 27, 28, 29, and 30°C, respectively, the *in vitro* bacteriostatic rates of *P. polymyxa* Y-1 fermentation broth against *Xoo* were

TABLE 1 | *In vitro* antibacterial activity of metabolites and positive control drugs against *Xoo* and *Xoc*.

Serial number	Metabolite	*Xoo* (Ininbition rate %)		*Xoc* (Ininbition rate %)	
		100 μg/ml	200 μg/ml	100 μg/ml	200 μg/ml
1	2,4-di-tert-butylphenol (Y1)	72.31 ± 4.06	82.57 ± 2.45	75.24 ± 3.17	80.14 ± 1.29
2	3-(2-aminoethyl) indole (Y2)	12.17 ± 1.26	22.54 ± 4.23	15.62 ± 2.67	27.45 ± 1.74
3	N-acetyl-5-methoxytryptamine (Y3)	32.43 ± 4.25	51.81 ± 2.30	40.37 ± 6.12	50.12 ± 3.44
4	2,4-dihydroxy-5- methylpyrimidin (Y4)	4.81 ± 0.51	16.54 ± 1.94	3.24 ± 0.22	8.42 ± 0.70
5	Glutathione (Y5)	21.37 ± 0.22	35.42 ± 1.61	12.35 ± 0.44	32.41 ± 1.12
6	Mannitol (Y6)	5.41 ± 0.73	6.22 ± 0.91	4.92 ± 0.50	5.47 ± 0.60
7	P-hydroxybenzoic acid (Y7)	95.46 ± 5.32	96.72 ± 3.81	96.54 ± 4.47	98.13 ± 3.53
8	Serine (Y8)	22.16 ± 1.91	32.23 ± 4.26	12.11 ± 2.40	22.54 ± 1.43
9	Zhongshengmycin	100 ± 5.21	100 ± 3.18	100 ± 2.37	100 ± 3.24
10	Bismerthiazol	60.21 ± 2.78	76.48 ± 1.64	59.16 ± 3.72	79.24 ± 2.53

TABLE 2 | EC_{50} values of the 2,4-di-tert-butylphenol, N-acetyl-5-methoxytryptamine, P-hydroxybenzoic acid, zhongshengmycin, and bismerthiazol against *Xoo* and *Xoc*.

Serial number	Metabolite	*Xoo* EC_{50} (μg/ml)	*Xoc* EC_{50} (μg/ml)
1	2,4-di-tert-butylphenol (Y1)	49.45 ± 0.07	34.33 ± 0.12
2	N-acetyl-5-methoxytryptamine (Y3)	64.22 ± 2.16	71.17 ± 1.37
3	P-hydroxybenzoic acid (Y7)	16.32 ± 0.04	15.58 ± 0.06
4	Zhongshengmycin	0.42 ± 0.08	0.82 ± 0.05
5	Bismerthiazol	85.64 ± 3.24	92.49 ± 3.72

TABLE 3 | Protective activity of 2,4-di-tert-butylphenol, N-acetyl-5-methoxytryptamine, P-hydroxybenzoic acid, and zhongshengmycin against BLB at different concentrations (greenhouse conditions).

Treatment	Protection activity (200 μg/ml)		Curative activity (200 μg/ml)	
	Infection index (%)	Control efficiency (%)	Infection index (%)	Control efficiency (%)
2,4-di-tert-butylphenol (Y1)	50.2 ± 2.1	35.9 ± 1.6	50.6 ± 3.4	35.4 ± 2.7
N-acetyl-5-methoxytryptamine (Y3)	44.7 ± 1.5	42.9 ± 1.7	49.6 ± 1.4	36.7 ± 1.7
P-hydroxybenzoic acid (Y7)	46.5 ± 2.7	40.6 ± 1.6	49.5 ± 2.5	36.8 ± 1.9
Zhongshengmycin	48.2 ± 1.2	38.4 ± 1.7	51.4 ± 2.1	34.4 ± 2.4
CK	78.3 ± 1.4	/	78.3 ± 1.4	/

27.4, 26.8, 29.4, 31.4, 30.3, and 26.4%, respectively, the *in vitro* bacteriostatic rates against *Xoc* were 25.2, 29.3, 28.4, 30.1, 30.7, and 29.3%, respectively. The results showed that the optimum temperature was 28°C, and the *in vitro* bacteriostatic rates of the *P. polymyxa* Y-1 fermentation broth against *Xoo* and *Xoc* were 31.4 and 30.1%, respectively.

3.2.6 Effects of Different Time on the Resistance of *P. polymyxa* Y-1

As shown in **Figure 2F**, When the culture time were 48, 72, 96, 120, 144, 168, 192, and 216 h, respectively, the *in vitro* bacteriostatic rates of *P. polymyxa* Y-1 fermentation broth against *Xoo* were 0, 1.2, 6.7, 19.3, 22.4, 32.7, 29.6, and 29.4%, respectively, the *in vitro* bacteriostatic rates against *Xoc* were 0, 0, 4.8, 16.7, 23.4, 33.1, 30.5, and 29.3%, respectively. The results showed that the optimum time was 168 h, and the *in vitro* bacteriostatic rates of the *P. polymyxa* Y-1 fermentation broth against *Xoo* and *Xoc* were 32.7 and 33.1%, respectively.

3.3 Structure Identification of Metabolites

Eight metabolites were isolated from *P. polymyxa* Y-1 fermentation broth with bioactivity tracking separation (**Figure 3**); the structures of the metabolites were confirmed by using ^{1}H NMR, ^{13}C NMR, and HRMS data (**Supplementary Material**).

3.3.1 2,4-Di-tert-butylphenol (Y1)

Light yellow solid; m.p. 53–56°C. ^{1}H NMR (500 MHz, CD$_3$OD) δ 7.17 (d, *J* = 2.44 Hz, 1H), 6.94 (dd, *J* = 8.30, 2.50°Hz, 1H), 6.58 (d, *J* = 8.29°Hz, 1H), 1.34 (s, 9H), 1.21 (s, 9H); ^{13}C NMR (125 MHz, CD$_3$OD) δ 153.4, 140.9, 134.8, 123.0, 122.9, 115.3, 34.4, 33.7, 31.0, 28.9. HRMS (ESI): calculated for $C_{14}H_{21}O$ [M-H]$^-$: 205.15979, found: 205.16041 (Seema et al., 2014).

3.3.2 3-(2-Aminoethyl) Indole (Y2)

Light yellow powder; m.p. 113–116°C. ^{1}H NMR (400 MHz, DMSO-d_6) δ 10.81 (s, 1H), 7.52 (d, *J* = 7.83°Hz, 1H), 7.34 (d, *J* = 8.07°Hz, 1H), 7.13 (d, *J* = 1.83°Hz, 1H), 7.08–7.04 (m, 1H),
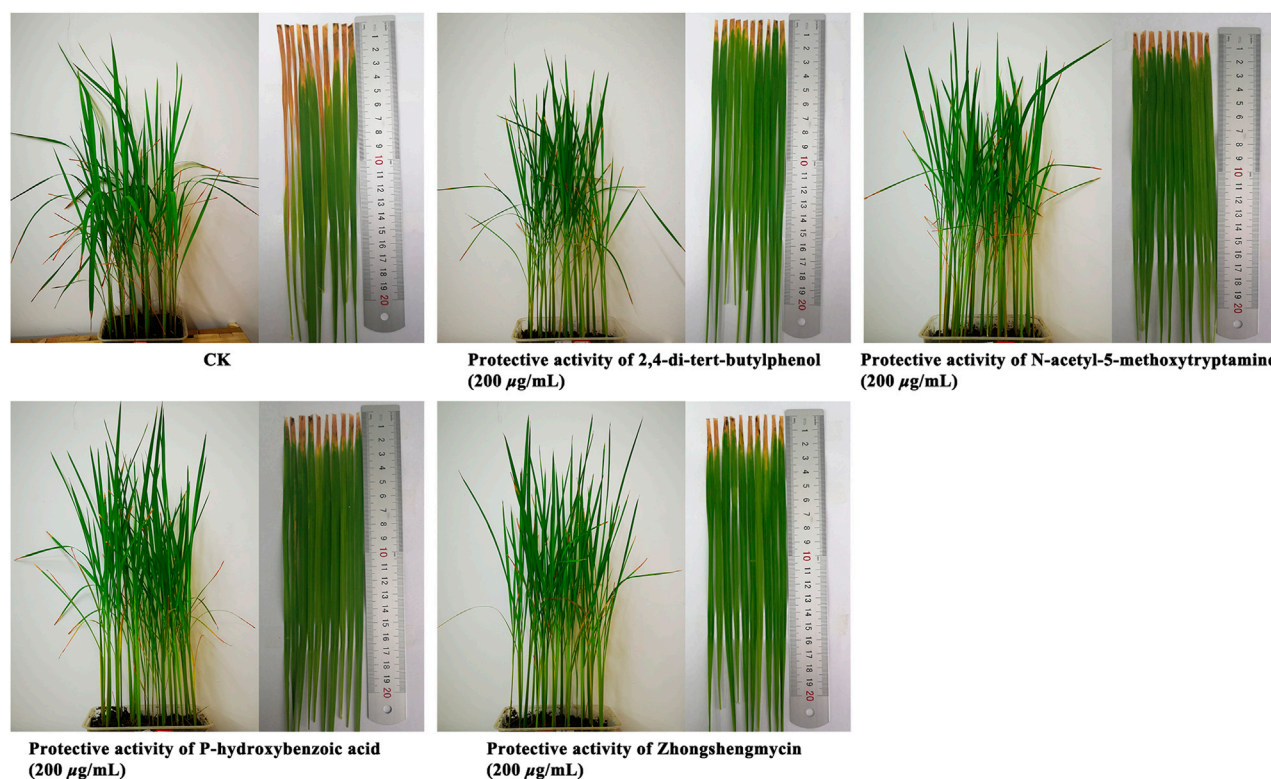
FIGURE 4 | Protective activity of 2,4-di-tert-butylphenol, N-acetyl-5-methoxytryptamine, P-hydroxybenzoic acid against BLB at concentrations of 200 µg/ml.

6.99–6.95 (m, 1H), 2.84–2.74 (m, 4H), 1.57 (s, 2H). ^{13}C NMR (101 MHz, DMSO-d_6) δ 136.7, 127.8, 123.0, 121.3, 118.8, 118.6, 113.1, 111.8, 43.2, 30.1. HRMS (ESI): calculated for $C_{10}H_{11}N_2$ [M-H]$^-$: 159.09277, found: 159.09279 (Güngőr et al., 1994).

3.3.3 N-Acetyl-5-Methoxytryptamine (Y3)
White crystal powder; m.p. 116–118°C. ^{1}H NMR (400 MHz, DMSO-d_6) δ 10.64 (s, 1H), 7.94 (t, J = 5.24°Hz, 1H), 7.23 (d, J = 8.73°Hz, 1H), 7.10 (d, J = 2.17°Hz, 1H), 7.02 (d, J = 2.34°Hz, 1H), 6.72 (dd, J = 8.73, 2.40°Hz, 1H), 3.76 (s, 3H), 3.31 (dd, J = 16.00, 8.00°Hz, 2H), 2.78 (t, J = 7.41°Hz, 2H), 1.81 (s, 3H); ^{13}C NMR (101 MHz, DMSO-d_6) δ 169.5, 153.4, 131.8, 128.0, 123.7, 112.4, 112.2, 111.5, 100.6, 55.8, 39.9, 25.7, 23.2. HRMS (ESI): calculated for $C_{13}H_{15}N_2O_2$ [M-H]$^-$: 231.11390, found: 231.11430 (Hwang and Lee, 1999).

3.3.4 2,4-Dihydroxy-5-Methylpyrimidine (Y4)
Light yellow powder; m.p. 316–317°C. ^{1}H NMR (500 MHz, DMSO-d_6) δ 11.02 (s, 1H), 10.60 (s, 1H), 7.25 (s, 1H), 1.72 (d, J = 1.1°Hz, 3H). ^{13}C NMR (125 MHz, DMSO-d_6) δ 165.5, 152.0, 138.3, 108.2, 12.3. HRMS (ESI): calculated for $C_5H_7N_2O_2$ [M + H]$^+$: 127.05020, found: 127.01517 (Cadet et al., 1975).

3.3.5 Glutathione (Y5)
Yellow powder; m.p. 192–195°C. ^{1}H NMR (400 MHz, D$_2$O) δ 4.60 (t, J = 6.09°Hz, 1H), 4.00 (s, 2H), 3.86 (t, J = 6.37°Hz, 1H), 3.02–2.92 (m, 2H), 2.61–2.56 (m, 2H), 2.20 (dd, J = 16.00, 8.00°Hz,

2H); ^{13}C NMR (101 MHz, D$_2$O) δ 174.9, 173.6, 173.6, 172.4, 55.6, 53.8, 41.6, 31.2, 26.0, 25.4. HRMS (ESI): calculated for $C_{10}H_{16}N_3O_6S$ [M-H]$^-$: 306.07653, found: 306.07667 (Fujiwara et al., 1977).

3.3.6 Mannitol (Y6)
White crystal powder; m.p. 167–170°C. ^{1}H NMR (400 MHz, DMSO-d_6) δ 4.41 (d, J = 5.48°Hz, 2H), 4.32 (t, J = 5.69°Hz, 2H), 4.13 (d, J = 7.05°Hz, 2H), 3.64–3.59 (m, 2H), 3.55 (t, J = 7.50°Hz, 2H), 3.49–3.43 (m, 2H), 3 41–3.35 (m, 2H); ^{13}C NMR (101 MHz, DMSO-d_6) δ 71.8, 70.1, 64.3. HRMS (ESI): calculated for $C_6H_{13}O_6$ [M-H]$^-$: 181.07176, found: 181.07159 (Tarczynski et al., 1992).

3.3.7 P-Hydroxybenzoic Acid (Y7)
Light yellow crystal; m.p. 213–215°C. ^{1}H NMR (400 MHz, CD$_3$OD) δ 7.84 (d, J = 8.62°Hz, 2H) 6.78 (d, J = 8.72°Hz, 2H). ^{13}C NMR (101 MHz, CD$_3$OD) δ 168.7, 162.0, 131.6, 121.3, 114.7. HRMS (ESI): calculated for $C_7H_5O_3$ [M-H]$^-$: 137.02442, found: 137.02449 (Hsieha et al., 2005).

3.3.8 Serine (Y8)
White powder; m.p. 239–241°C. ^{1}H NMR (400 MHz, D$_2$O) δ 4.06–3.96 (m, 2H) 3.91–3.88 (m, 1H). ^{13}C NMR (101 MHz, D$_2$O) δ 172.4, 60.2, 55.4. HRMS (ESI): calculated for $C_3H_6NO_3$ [M-H]$^-$: 104.03532, found: 104.03470 (Pogliani and Ziessow, 1981).
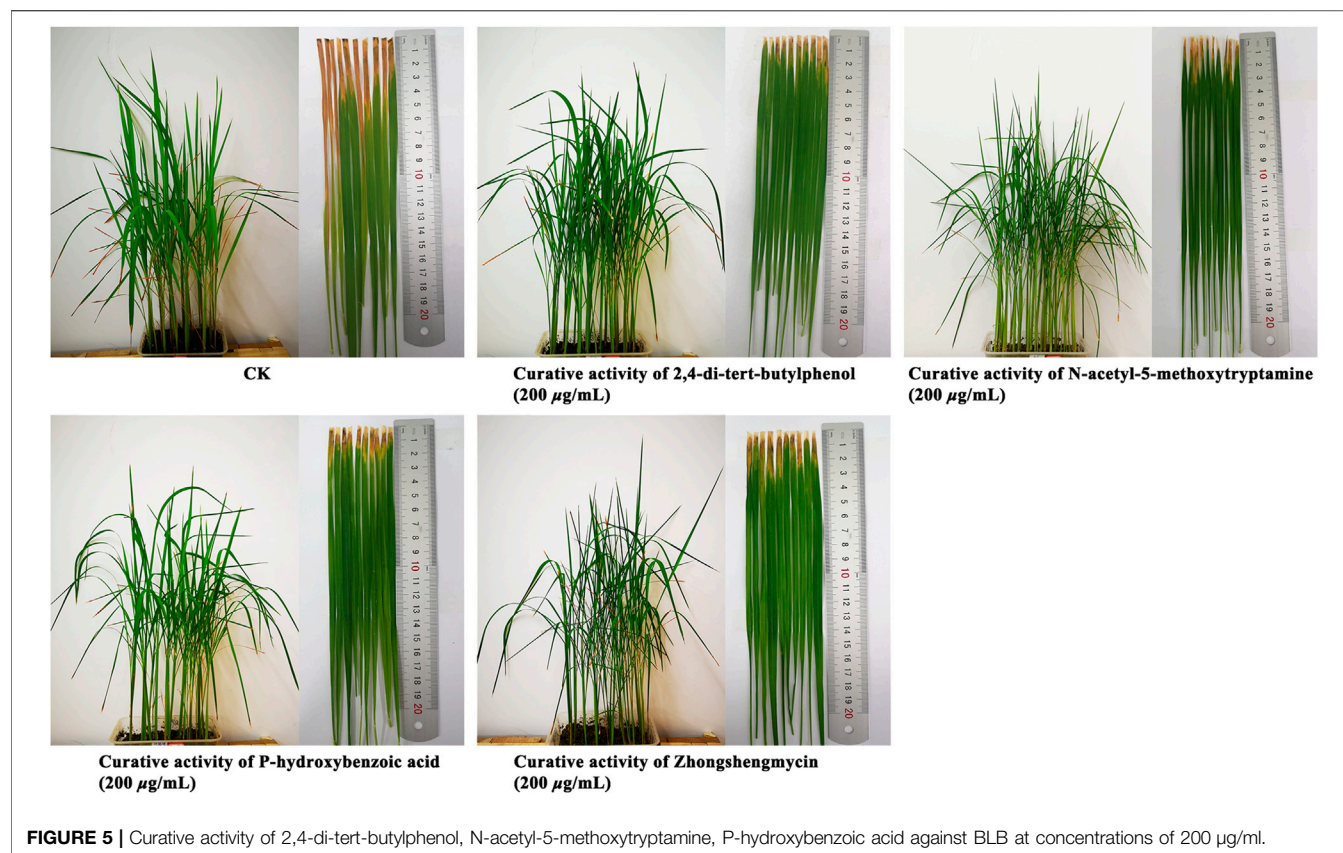
FIGURE 5 | Curative activity of 2,4-di-tert-butylphenol, N-acetyl-5-methoxytryptamine, P-hydroxybenzoic acid against BLB at concentrations of 200 μg/ml.

3.4 *In vitro* Antibacterial Activity Assays of Metabolites

The *in vitro* bacteriostatic rates of the eight metabolites and two positive control drugs against *Xoo* and *Xoc* were determined by the turbidimeter tests, and the results are shown in **Table 1**. The result showed that when the concentrations of the metabolites were 200 and 100 μg/ml, 2,4-di-tert-butylphenol (82.57 and 72.31%, 80.14 and 75.24%, respectively), N-acetyl-5-methoxytryptamine (51.81 and 32.43%, 50.12 and 40.37%, respectively) and P-hydroxybenzoic acid (96.72 and 95.46%, 98.13 and 96.54%, respectively) exhibited excellent *in vitro* antibacterial activities to *Xoo* and *Xoc*, which was better than bismerthiazol (76.48 and 60.21%, 79.24 and 59.16%, respectively) and lower than zhongshengmycin (100%).

The EC_{50} values of 2,4-di-tert-butylphenol, P-hydroxybenzoic acid, and N-acetyl-5-methoxytryptamine are shown in **Table 2**. 2,4-di-tert-butylphenol, N-acetyl-5-methoxytryptamine, and P-hydroxybenzoic acid exhibited good antibacterial activity to *Xoo*, with EC_{50} values of 49.45 μg/ml, 64.22 μg/ml, and 16.32 μg/ml, respectively, which were better than bismerthiazol (85.64 μg/ml) and lower than zhongshengmycin (0.42 μg/ml). Meanwhile, 2,4-di-tert-butylphenol, N-acetyl-5-methoxytryptamine, and P-hydroxybenzoic acid also showed good antibacterial activity

to *Xoc*, with EC_{50} values of 34.33 μg/ml, 71.17 μg/ml, and 15.58 μg/ml, respectively, which were better than bismerthiazol (92.49 μg/ml) and lower than zhongshengmycin (0.82 μg/ml). The results showed that 2,4-di-tert-butylphenol, N-acetyl-5-methoxytryptamine, and P-hydroxybenzoic acid had better bacteriostatic rates and could be used as new antibacterial agents.

3.5 *In vivo* Antibacterial Activity Assay

The *In vivo* antibacterial activities of 2,4-di-tert-butylphenol, N-acetyl-5-methoxytryptamine, and P-hydroxybenzoic acid are shown in **Table 3** and **Figure 4**. Under the greenhouse conditions, when the concentration was 200 μg/ml, the protective activity of 2,4-di-tert-butylphenol (35.9%) was lower than that of positive control drugs, zhongshengmycin (38.4%), the protective activity of N-acetyl-5-methoxytryptamine (42.9%) and P-hydroxybenzoic acid (40.6%) against BLB were better than that of zhongshengmycin (38.4%). As shown in **Table 3** and **Figure 5**, when the concentration was 200 μg/ml, the curtive activity of 2,4-di-tert-butylphenol (35.4%), N-acetyl-5-methoxytryptamine (36.7%), and P-hydroxybenzoic acid (36.8%) against BLB were similar to that of zhongshengmycin (34.4%). The results indicated that 2,4-di-
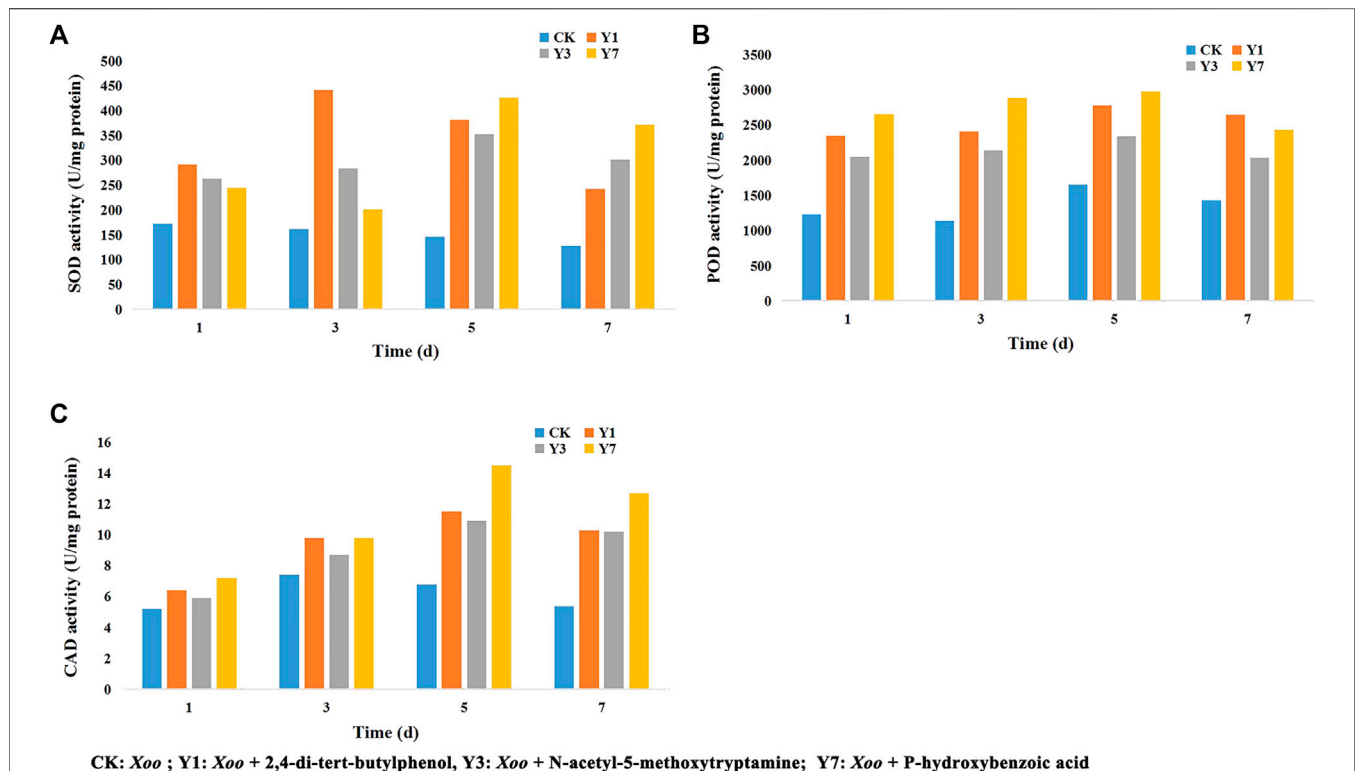
FIGURE 6 | Effects of 2,4-di-tert-butylphenol, N-acetyl-5-methoxytryptamine, and P-hydroxybenzoic acid on SOD **(A)**, POD **(B)**, and CAD **(C)** activities in rice leaves.

tert-butylphenol, N-acetyl-5-methoxytryptamine, and P-hydroxybenzoic acid significantly reduced the occurrence of BLB disease.

3.6 Defensive Enzyme Activities

As shown in **Figure 6**, the CK group was inoculated with *Xoo* after Tween water protection, the Y1 group was inoculated with *Xoo* after 2,4-di-tert-butylphenol protection, the Y3 group was inoculated with *Xoo* after N-acetyl-5-methoxytryptamine protection, and the Y7 group was inoculated with *Xoo* after P-hydroxybenzoic acid protection. The SOD activity was significantly increased in the Y1 treatment group and reached the maximum value on the 3rd day, higher than that of the CK group, and then the activity decreased. The SOD activity increased in the Y3 and Y7 treatment groups and reached the maximum on the 5th day, which was higher than that of the CK group. The POD activity was significantly increased in the Y1, Y3, and Y7 treatment groups and reached the maximum value on the 5th day, which was higher than that of the CK group, then POD activity decreases. The CAD activity was significantly increased in the Y1, Y3, and Y7 treatment group and reached the maximum value on the 3rd day, higher than that of the CK group, and then the activity decreased. These results suggest that 2,4-di-tert-butylphenol, N-acetyl-5-methoxytryptamine, and P-hydroxybenzoic acid could enhance the disease resistance of rice by inducing an enzymatic defense response.

4 CONCLUSION

In this study, a series of studies were carried out on the fermentation conditions of *P. polymyxa* Y-1, the extraction, isolation, and structural identification of active metabolites, as well as their biological activities. The optimum nitrogen source, carbon source, concentration, temperature, time, and pH value were selected by a single factor experiment. Then eight metabolites were isolated from the fermentation broth of *P. polymyxa* Y-1 by biological activity tracking separation. 2,4-di-tert-butylphenol, N-acetyl-5-methoxytryptamine, P-hydroxybenzoic acid all exhibited good *in vitro* anti-*Xoo* and -*Xoc* activities. The protection experiments of rice plants showed that 2,4-di-tert-butylphenol, N-acetyl-5-methoxytryptamine, and P-hydroxybenzoic acid could protect rice against BLB at 200 µg/ml. Defensive enzyme activity experiments also found that 2,4-di-tert-butylphenol, N-acetyl-5-methoxytryptamine, and P-hydroxybenzoic acid could enhance the disease resistance of rice by inducing an enzymatic defense response. These results will provide important insights into the study of novel microbial pesticides for the treatment of rice bacterial diseases, especially in terms of fermentation conditions, *in vitro* and *in vivo* activities, and mechanisms of action.

DATA AVAILABILITY STATEMENT

The original contributions presented in the study are included in the article/**Supplementary Material**, and further inquiries can be directed to the corresponding author.

AUTHOR CONTRIBUTIONS

XG and WY: conceived and designed the research, XG and WY: wrote the manuscript, and CC: analyzed the data.

FUNDING

ACKNOWLEDGMENTS

SUPPLEMENTARY MATERIAL

The Supplementary Material for this article can be found online at: https://www.frontiersin.org/articles/10.3389/fchem.2022.879724/full#supplementary-material

REFERENCES

Belén, C. R., Nadia, D. R. V., Cecilia, M. M. T., Carlos, H. A. A., Misael, M. B., María, S. V. M., et al. (2020). *Paenibacillus Polymyxa* NMA1017 as a Potential Biocontrol Agent of Phytophthora Tropicalis, Causal Agent of Cacao Black Pod Rot in Chiapas, Mexico. *Antonie. Van. Leeuwenhoek.* 114, 55–68. doi:10.1007/s10482-020-01498-z

Cadet, J., Ulrich, J., and Teoule, R. (1975). Isomerization and New Specific Synthesis of Thymine Glycol. *Tetrahedron* 31, 2057–2061. doi:10.1016/0040-4020(75)80195-5

Cai, H., Hao, Y. T., Xue, J., and Luo, W. J. (2015). *Chinese Pharmacopoeia*. first ed. Beijing: China Medical Science and Technology Press, 92–93.

Campbell, E. P., Hussein, W. E., Huang, E., and Yousef, A. E. (2021). Enhancing Titre and Production Stability of Paenibacillin from *Paenibacillus Polymyxa* by Sequential Drug Resistance Screening. *J. Appl. Microbiol.* 131, 2876–2885. doi:10.1111/jam.15165

Cao, J., Chu, C., Zhang, M., He, L., Qin, L., Li, X., et al. (2020). Different Cell Wall-Degradation Ability Leads to Tissue-Specificity between Xanthomonas Oryzae Pv. Oryzae and Xanthomonas Oryzae Pv. Oryzicola. *Pathogens* 9, 187. doi:10.3390/pathogens9030187

Dalgaard, P., Ross, T., Kamperman, L., Neumeyer, K., and McMeekin, T. A. (1994). Estimation of Bacterial Growth Rates from Turbidimetric and Viable Count Data. *Int. J. Food Microbiol.* 23, 391–404. doi:10.1016/0168-1605(94)90165-1

Dharni, S., Sanchita, G., Maurya, A., Samad, A., Srivastava, S. K., Sharma, A., et al. (2014). Purification, Characterization, and *In Vitro* Activity of 2,4-Di-Tert-Butylphenol from Pseudomonas Monteilii PsF84: Conformational and Molecular Docking Studies. *J. Agric. Food Chem.* 62, 6138–6146. doi:10.1021/jf5001138

Fujiwara, S., Formicka-Kozlowska, G., and Kozlowski, H. (1977). Conformational Study of Glutathione by NMR. *Bcsj* 50, 3131–3135. doi:10.1246/bcsj.50.3131

Güngör, T., Malabre, P., and Teulon, J. M. (1994). New Synthesis of 1-Substituted 3-(2-Aminoethyl)indoles. *Synth. Commun.* 24, 2247–2256. doi:10.1080/00397919408019049

Hsieh, T.-J., Su, C.-C., Chen, C.-Y., Liou, C.-H., and Lu, L.-H. (2005). Using Experimental Studies and Theoretical Calculations to Analyze the Molecular Mechanism of Coumarin, *P*-Hydroxybenzoic Acid, and Cinnamic Acid. *J. Mol. Struct.* 741, 193–199. doi:10.1016/j.molstruc.2005.02.009

Huang, E., and Yousef, A. E. (2015). Biosynthesis of Paenibacillin, a Lantibiotic with N-Terminal Acetylation, by *Paenibacillus Polymyxa*. *Microbiol. Res.* 181, 15–21. doi:10.1016/j.micres.2015.08.001

Hwangyy, K.-J., and Lee, T.-S. (1999). A Practical Synthesis of N-Acetyl-5-Methoxy-Tryptamine (Melatonin). *Synth. Commun.* 29, 2099–2104. doi:10.1080/00397919908086203

Li, P., Hu, D., Xie, D., Chen, J., Jin, L., and Song, B. (2018). Design, Synthesis, and Evaluation of New Sulfone Derivatives Containing a 1,3,4-Oxadiazole Moiety as Active Antibacterial Agents. *J. Agric. Food Chem.* 66, 3093–3100. doi:10.1021/acs.jafc.7b06061

Liu, H., Wang, J., Sun, H. M., Han, X. B., Peng, Y. L., Liu, J., et al. (2020). Transcriptome Profiles Reveal the Growth-Promoting Mechanisms of Paenibacillus Polymyxa YC0136 on Tobacco (Nicotiana Tabacum L.). *Front. Microbiol.* 4, 584174. doi:10.3389/fmicb.2020.584174

Miao, L., Wang, X., Jiang, W., Yang, S., Zhou, H., Zhai, Y., et al. (2012). Optimization of the Culture Condition for an Antitumor Bacterium *Serratia Proteamacula* 657 and Identification of the Active Compounds. *World J. Microbiol. Biotechnol.* 29, 855–863. doi:10.1007/s11274-012-1240-x

Mikkola, R., Andersson, M. A., Grigoriev, P., Heinonen, M., and Salkinoja-Salonen, M. S. (2017). The Toxic Mode of Action of Cyclic Lipodepsipeptide Fusaricidins, Produced by Paenibacillus Polymyxa , toward Mammalian Cells. *J. Appl. Microbiol.* 123, 436–449. doi:10.1111/jam.13498

Mülner, P., Schwarz, E., Dietel, K., Herfort, S., Jähne, J., Lasch, P., et al. (2021). Fusaricidins, Polymyxins and Volatiles Produced by *Paenibacillus Polymyxa* Strains DSM 32871 and M1. *Pathogens* 10, 1485. doi:10.3390/pathogens10111485

Niu, B., Vater, J., Rueckert, C., Blom, J., Lehmann, M., Ru, J. J., et al. (2013). Polymyxin P Is the Active Principle in Suppressing Phytopathogenic *Erwinia Spp.* By the Biocontrol Rhizobacterium *Paenibacillus Polymyxa* M-1. *BMC. Microbiol.* 13. doi:10.1186/1471-2180-13-137

Nursyam, H. (2017). Antibacterial Activity of Metabolites Products of *Vibrio Alginolyticus* Isolated from Sponge *Haliclona* Sp. Against *Staphylococcus Aureus*. *Ital. J. Food Saf.* 6, 18–22. doi:10.4081/ijfs.2017.6237

Pogliani, L., and Ziessow, D. (1981). 1H and13C NMR Study of Tri-L-serine in Aqueous Solution. *Org. Magn. Reson.* 17, 214–216. doi:10.1002/mrc.1270170317

Sadhana, L., and Tabacchioni, S. (2009). Ecology and Biotechnological Potential of *Paenibacillus Polymyxa*: a Minireview. *Indian J. Microbiol.* 49, 2–10. doi:10.1007/s12088-009-0008-y

Tarczynski, M. C., Jensen, R. G., and Bohnert, H. J. (1992). Expression of a Bacterial *mtlD* Gene in Transgenic Tobacco Leads to Production and Accumulation of Mannitol. *Proc. Natl. Acad. Sci.* 89, 2600–2604. doi:10.1073/pnas.89.7.2600

Wang, Q., Zhang, C., Long, Y., Wu, X., Su, Y., Lei, Y., et al. (2021). Bioactivity and Control Efficacy of the Novel Antibiotic Tetramycin against Various Kiwifruit Diseases. *Antibiotics* 10, 289. doi:10.3390/antibiotics10030289

Wang, S. B., Gan, X. H., Wang, Y. J., Li, S. Y., Yi, C. F., Chen, J. X., et al. (2019). Novel 1,3,4-oxadiazole Derivatives Containing a Cinnamic Acid Moiety as Potential Bactericide for rice Bacterial Diseases. *Int. J. Mol. Sci.* 20, 1–17. doi:10.3390/ijms20051020

Yang, A., Zeng, S., Yu, L., He, M., Yang, Y., Zhao, X., et al. (2018). Characterization and Antifungal Activity against *Pestalotiopsis* of a Fusaricidin-type Compound Produced by *Paenibacillus Polymyxa* Y-1. *Pestic. Biochem. Physiol.* 147, 67–74. doi:10.1016/j.pestbp.2017.08.012

Zou, L. F., Zhang, C. P., Li, Y. L., Yang, X. F., Wang, Y. Y., Yan, Y. C., et al. (2021). An Improved, Versatile and Efficient Modular Plasmid Assembly System for Expression Analyses of Genes in Xanthomonas Oryzae. *Mol. Plant Pathol.* 22, 480–492. doi:10.1111/mpp.13033

Conflict of Interest: The authors declare that the research was conducted in the absence of any commercial or financial relationships that could be construed as a potential conflict of interest.

Antimicrobial Effects and Active Compounds of the Root of *Aucklandia Lappa* Decne (Radix Aucklandiae)

Xuewei Cai[†], Chunping Yang[†], Guangwei Qin[†], Min Zhang, Yan Bi, Xiaoyan Qiu, Liya Lu and Huabao Chen *

College of Agronomy, Sichuan Agricultural University, Chengdu, China

The development of new biological fungicides using plant metabolites has become an important direction for pesticide development, and previous studies found that Radix Aucklandiae had a certain inhibitory effect on plant pathogens. In this study, we systematically studied the antimicrobial activity of extracts of Radix Aucklandiae, and the active compounds were isolated, purified and structurally identified. Ethanol extracts of Radix Aucklandiae had different inhibitory effects on seven common plant-pathogenic fungi, with EC_{50} (concentration for 50% of maximal effect) values ranging from 114.18 mg/L to 414.08 mg/L. The extract at concentration of 1,000 mg/L had a significant control effect on strawberry grey mould and wheat powdery mildew of more than 90%. Three active compounds were isolated and purified from the extract, which were identified as alantolactone, dehydrocostus lactone and costunolide. All three compounds showed significant inhibitory effects on *Botrytis cinerea*, and the MIC (minimal inhibitory concentration) values were 15.63 mg/L, 3.91 mg/L and 15.63 mg/L. Dehydrocostus lactone also showed obvious inhibitory effect on *Fusarium graminearum* with an MIC value of 62.25 mg/L. The extract of Radix Aucklandiae has high antimicrobial activity against some common plant-pathogenic fungi, and the work lays a foundation for the development of extracts of Radix Aucklandiae as botanical fungicides.

Keywords: Radix Aucklandiae, antimicrobial activity, alantolactone, dehydrocostus lactone, costunolide

INTRODUCTION

Plant-pathogenic fungi can cause a decline in crop yield and quality directly or indirectly and secrete a variety of toxins and harmful metabolites (Guo et al., 2021). Therefore, it is necessary to control fungal diseases in agricultural production. At present, chemical fungicides are widely used to control plant diseases. However, chemical fungicide abuse has had a serious negative impact on human health and environmental safety, especially leading to prominent "3R" (Resistance, resurgence, and Residue) problems (Ju, 2011). Therefore, it is urgent to develop environmentally friendly fungicides. Botanical fungicides are pesticides used to control plant diseases with the advantages of high efficiency, low or no toxicity, easy degradation, high selectivity and a low risk of inducing drug resistance (Bhandari et al., 2021). Therefore, the development of new botanical fungicides is a hot spot in the development of new environmentally friendly pesticides. At present, many plant extracts have been proven to have antimicrobial activity. For example, extracts of *Sophora flavescens* have inhibitory effect on *Gibberella zeae*, *Glomerella cingulata* and *Botrytis cinerea* (Li et al., 2006).

Extracts of *Syzygium aromaticum* (L.) have inhibitory effect on *Colletotrichum gloeosporioides* and *Fusarium oxysporum* f. sp. *cubense* (He et al., 2006).

Radix Aucklandiae (Chinese trade name: Muxiang) is the dried root of *Aucklandia lappa* Dence. (a perennial herb of the genus *Saussurea*, family Compositae), which is cultivated in Yunnan and Sichuan Provinces (Shu et al., 2015). It is widely used in clinical medicine because of its anti-inflammatory, anti-ulcer, hepatoprotective, cholagogic, antitumour and other functions (Bocca et al., 2004; Lai et al., 2008; Wang et al., 2008; He et al., 2011; Butturini et al., 2014; Sun et al., 2015). In addition, it has also been proven that Radix Aucklandiae has antimicrobial activity in agricultural production. The water extract of Radix Aucklandiae has inhibitory effect on *Botrytis cinerea* and *Alternaria alternata* (Hasi et al., 2009). Its ethanol extract also can inhibit *Penicillium italicum* Wehmer, *Verticillium dahlia*, *Fusarium oxysporium*, *Rhizoctonia solani* Kuhn and *Gloeosporium piperatum* (Hu et al., 2009; Liu et al., 2011; Wang et al., 2012; Jin et al., 2019). However, the antimicrobial activity compounds of Radix Aucklandiae is not clear and has not been systematically explored at present.

The inhibitory effect of extracts of Radix Aucklandiae on common plant-pathogenic fungi was systematically studied based on the above, and active compounds of extracts of Radix Aucklandiae were isolated, purified and identified, which laid a foundation for the further development and utilization of the extract as a fungicide.

MATERIALS AND METHODS

Materials
Radix Aucklandiae was purchased from Bozhou Huakai Electronic Commerce Co., Ltd. The 11 common pathogens including *F. graminearum*, *Blumeria graminis* (*Bgt*), *B. cinerea*, *C. gloeosporioides*, *Sclerotinia sclerotiorum*, *F. oxysporum*, *Fusarium lateritium*, *A. alternata*, *Pythium aphanidermatum*, *D. glomerata* and *Phytophthora infestans* were preserved and provided by the College of Agronomy of Sichuan Agricultural University. The wheat (Triticum aestivum L.) variety Chuannong 30, which is mildew and is grown at the College of Agronomy of Sichuan Agricultural University.

Preparation of Extracts of Radix Aucklandiae
Plant extracts were prepared by solvent extraction (Zhang and Wang, 2011; Chen et al., 2012). Radix Aucklandiae was dried in an electrothermal constant temperature blast drying oven at 55°C, crushed into dry powder with a tissue grinder and stored in a sealed fresh-storage bag away from light. Dry powder (2 kg) was extracted by soaking in 5 times volume ethanol while avoiding light. The extract was filtered out, and the same amount of ethanol was added after 3 days. The extract was filtered out after 2 days, and the two parts of the filtrate were combined. The filtrate was concentrated to paste at 50–60°C by a rotary evaporator and stored in a refrigerator at 4°C for later use.

Toxicity Determination of Extracts of Radix Aucklandiae
The toxicity was determined by the mycelium growth rate (Wang et al., 2014). The paste extract was dissolved in dimethyl sulfoxide (DMSO) and then prepared into 1,000 mg/L, 500 mg/L, 250 mg/L, 125 mg/L, 62.5 mg/L, and 31.25 mg/L solutions with double distilled water (contain 0.1% Tween 80). The solution (1 ml) was mixed with Potato Dextrose Agar (PDA) medium (containing 1% streptomycin sulfate) (9 ml) and then poured into a sterile Petri dish (9 cm in diameter) to make a medium-filled plate. After the medium was solidified, an agar block (with a diameter of 0.5 cm) containing pathogenic fungi to be tested was placed in each medium plane, and the side of the agar block containing fungi was placed onto the surface of the medium. Each concentration was tested using three biological replicates. Double distilled water (containing 0.1% Tween 80 and 2% DMSO) was used as the negative control. Pathogenic fungi were cultured at 25°C. The diameter of colony growth was measured by the cross method after 2–7 days, and the inhibition rate of mycelium growth was calculated. Then, the toxicity regression equation and EC_{50} value of the extract were obtained according to the probit analysis method for toxicity.

$$\textbf{Colony growth diameter (mm) = Average of measured diameters}$$
$$\textbf{−5 (diameter of agar block)}$$

$$\textbf{Mycelium growth inhibition rate (\%)} = \frac{\textbf{CK − PT}}{\textbf{CK}} \times \textbf{100}$$

where CK is the negative control colony growth diameter, and PT is the colony growth diameter under extract solution treatment.

Bioassay of Extracts of Radix Aucklandiae *In Vivo*
Control Effect on Wheat Powdery Mildew
The paste extract was dissolved in DMSO and then prepared into 1,000 mg/L, 500 mg/L and 250 mg/L solutions with double distilled water (contain 0.1% Tween 80). Wheat seeds were planted in a glass tube (4 cm in diameter), and the tube was sealed with parafilm. Seeds were cultured to the three-leaf stage at 20 ± 1°C and 60–70% humidity with a 16:8 h light/dark photoperiod. Then, wheat leaves were sprayed with 250 mg/L, 500 mg/L and 1,000 mg/L extract solutions with three replications at each concentration. Leaves were also sprayed with 100 mg/L prothioconazole as a positive control and with double distilled water (contain 2% DMSO and 0.1% Tween 80) as a negative control. Fresh spores of *Bgt* were inoculated onto the plants by shaking over the foliage of the wheat seedlings (Xie et al., 2021). The protective activity was determined by spray application of the extract solution first followed by inoculation with the pathogenic fungi 24 h later; the curative activity was determined by inoculation with the pathogenic fungi first followed by spray application of the extract solution 24 h later. Protective activity and curative activity were reflected by relative disease control efficiency (RDCE). The methods for detecting the protective and curative activities of the subsequent experiment were the same. Wheat was further cultured after treatment, and

the disease incidence was investigated 7, 9 and 11 days after treatment. The disease was divided into six grades according to the percentage of lesion area to leaf area (Grade 0: 0%; Grade 1: less than 5%; Grade 3: 6–10%; Grade 5: 11–20%; Grade 7: 21–50%; Grade 9: more than 51%) (Liu et al., 2000). Then disease index and RDCE was calculated using the following formula:

$$\text{Disease index} = \frac{\Sigma \left(\begin{array}{c} \text{Number of diseased leaves/plants per grade} \\ \times \text{ Corresponding grade} \end{array} \right)}{\text{Total number of diseased leaves} \times 9}$$

$$\text{RDCE}(\%) = \left(\frac{\text{CK} - \text{PT}}{\text{PT}} \right) \times 100$$

Where, CK is DI of sterile water-treatment; PT is DI of medicament treatment.

Control Effect on Wheat Head Blight

Wheat seeds were planted in pots (15 cm in diameter) and cultured to the earing and flowering stage at 26 ± 2°C and 65–75% humidity in the greenhouse. Then, wheat leaves were sprayed with 400 mg/L and 4,000 mg/L extract solutions with three replications at each concentration. Leaves were also sprayed with 100 mg/L tebuconazole as a positive control and with double distilled water (contain 2% DMSO and 0.1% Tween 80) as a negative control. A spore suspension of *F. graminearum* (10 μL) was injected into wheat panicles with a microinjector. Spores were observed and counted on a haemocytometer under an optical microscope (4 × 10). The method for adjusting the spore suspension in the later experiment was the same. It is advisable to adjust the spore concentration to 80–100 spores per field. Wheat was further cultured after treatment, and the disease incidence was investigated 7, 9 and 12 days after treatment. The disease was divided into five grades according to the percentage of dry ear area to ear area (Grade 0: 0%; Grade 1: less than 25%; Grade 3: 26–50%; Grade 5: 51–75%; Grade 7: more than 76%) (Zhu et al., 2007). Then the disease index and the RDCE was calculated using the formula in 4.2.1.

Control Effect on Strawberry Grey Mould

Fresh strawberry fruits of uniform size were selected, soaked in 75% ethanol for 2 min, washed with double distilled water and then dried. Then, fruits were sprayed with 500 mg/L and 1,000 mg/L extract solutions with three replications at each concentration. Leaves were also sprayed with 100 mg/L pyraclostrobin as a positive control and with double distilled water (contain 2% DMSO and 0.1% Tween 80) as a negative control. The equator of the strawberry was pricked with a sterile needle of a 1 ml injector, a 2 mm wound was formed, and then a suspension of *B. cinerea* was evenly spread on the fruit surface (Han et al., 2019). The fruit was placed in a culture plate and stored at 25°C and 95% humidity after treatment. The disease incidence was investigated 3, 5 and 7 days after treatment. The disease was divided into six grades according to the percentage of lesion area to fruit surface area (Grade 0: 0.0%; Grade 1: less than 5.0%; Grade 2: 5.1–15.0%; Grade 3: 15.1–30.0%; Grade 4: 30.1–50.0%; Grade 5: more than 50.1%) (Han et al., 2019),

and then the disease index and the RDCE were calculated using the formula in 4.2.1.

Control Effect on Citrus Anthracnose

Fruits of Jincheng orange with consistent appearance and no mechanical damage were selected, soaked in 75% ethanol for 2 min, washed with double distilled water and then dried. Then, the fruits were sprayed with 2000 mg/L and 4,000 mg/L extract solutions. Three biological replicates were performed at each concentration with 10 fruits per treatment. Leaves were also sprayed with 86 mg/L pyraclostrobin as a positive control and with double distilled water (contain 2% DMSO and 0.1% Tween 80) as a negative control. *C. gloeosporioides* was inoculated by needle puncture. The depth of the pinhole was 2 mm, and a spore suspension (10 μL) was dropped at the pinhole (Tian et al., 2019). The fruits were cultured at 28°C and 95% relative humidity after treatment. The diameters of the lesions were measured by the cross method, and the mycelium growth inhibition rate 7 days after treatment was calculated using the formula in 2.3.

Data Processing and Analysis

The inhibition results of different concentrations of extracts of Radix Aucklandiae against different pathogenic fungi were recorded, and the data were statistically analysed with SPSS Statistics 23.

Isolation, Purification and Structure Identification of Active Compounds From Radix Aucklandiae

Macroporous Resin Isolation

D101 macroporous resin was soaked in absolute ethanol for 24 h. Then, it was loaded into the chromatography column after the resin was fully swollen. The resin was rinsed repeatedly with absolute ethanol until the supernatant was free of white turbidity and then rinsed with distilled water until no ethanol was available. The paste extract of Radix Aucklandiae was evenly dispersed in double distilled water. Then, the treated solution (10 L) was adsorbed statically with D101 macroporous resin (2 kg) for 48 h. Then, resin was loaded into the chromatographic column. The resin was eluted with distilled water (3 times the volume of the column), and the eluent was discarded. Then, the resin was eluted with 70% ethanol (5 times the volume of the column). The eluent was collected and concentrated under pressure to obtain the crude extract of Radix Aucklandiae.

Chromatography Isolation

The crude extract was evenly dispersed in double distilled water. The aqueous solution was extracted with petroleum ether at the same volume 4 times. The organic phase was concentrated under reduced pressure at 45°C to obtain petroleum ether extract. The extract was isolated by normal-phase silica gel chromatography and then eluted with different petroleum ether and ethyl acetate mixtures (50:0, 10:1 and 1:1 by volume). Three fractions (Fr. H1-H3) were isolated and antimicrobial active fractions were traced and selected by the spore germination method using *B. cinerea* as an indicator pathogen. After further silica gel column

TABLE 1 | Toxicity test results of extracts of Radix Aucklandiae against several plant-pathogenic fungi.

Plant-pathogenic fungi	Toxicity regression equation	Correlation coefficient	EC_{50}(mg/L)	Confidence intervals (mg/L)
F. graminearum	y = 1.0107x+5.4036	0.9839	398.74	210–750
B. cinerea	y = 3.6591x+8.4484	0.9800	114.18	90–140
C. gloeosporioides	y = 0.7907x+5.4735	0.9786	251.87	80–800
S. sclerotiorum	y = 3.8796x+8.2840	0.9927	142.40	120–170
F. oxysporum	y = 1.7997x+5.9428	0.8997	299.34	230–400
F. lateritium	y = 0.7094x+5.1638	0.9081	587.69	310–1,120
A. alternata	y = 2.0376x+6.0220	0.9503	315.07	250–400
P. aphanidermatum	y = 1.3650x+5.645	0.9018	757.71	530–1,090
D. glomerata	y = 1.6341x+5.6257	0.8786	414.08	260–670
P. infestans	y = 1.0780x+5.2852	0.9804	543.82	350–830

chromatography isolation, the fraction Fr.H1-1 was obtained by eluting Fr.H1 with petroleum ether: acetone (15:1 by volume) as the eluent. In addition, the fractions Fr. H2-1 and Fr. H3-1 were obtained by eluting Fr.H2 and Fr. H3 with petroleum ether and ethyl acetate mixtures (15:1, 20:1 and 1:1 by volume) as the eluent.

Preparation of High-Performance Liquid Chromatography (HPLC)

Fractions (Fr. H1-1, Fr. H2-1 and Fr. H3-1) were further isolated through a Phenomenex C18 column (250 × 10 mm, Phenomenex, Aschaffenburg, Germany) and UV detector. Fr. H1-1 was eluted with 30% acetonitrile (containing 0.1% formic acid) to obtain compounds numbered Compound **1** (20 mg), Compound **2** (20 mg) and Compound **3** (5 mg). Fr. H2-1 was eluted with 35% acetonitrile (containing 0.1% formic acid) to obtain compounds numbered Compound **4** (20 mg) and Compound **5** (20 mg). Fr. H3-1 was eluted with 35% acetonitrile (containing 0.1% formic acid) to obtain compounds numbered Compound **6** (20 mg) and Compound **7** (20 mg). The antimicrobial active compound was traced and selected by the spore germination method using *B. cinerea* as indicator pathogen.

Compound Structure Identification

The purity was determined by HPLC. The mass spectrum, ^{1}H-NMR (nuclear magnetic resonance) and ^{13}C-NMR spectra of the compounds with higher purity were determined (the ^{1}H-NMR spectra were 400 MHz; the ^{13}C-NMR spectra were 100 MHz; and the solvent was CDCl$_3$). The chemical structure of the compound was identified according to spectroscopic data.

Compound Activity Identification

The MIC against the pathogen spores was determined by the microtiter method (Yang et al., 2012). The pure compound was prepared with DMSO in mother liquor at 2000 mg/L. Then, mother liquor was diluted with double distilled water to nine concentrations: 1,000 mg/L, 500 mg/L, 250 mg/L, 125 mg/L, 62.25 mg/L, 31.125 mg/L, 15.625 mg/L, 7.8125 mg/L, 3.906 mg/L, 1.953 mg/L. Compound solutions of different concentrations (5 μL) and PDA (45 μL) were added to each well of a 96-well plate and fully mixed. Spore suspension (10 μL) was added to each well after standing for 10 min, and DMSO solution (10 μL) was added as a negative control. Three biological replicates were performed per treatment. The degree of conidial germination in all wells was observed to determine the MIC value after cultivation at 28°C for 48 h.

RESULTS

Toxicity Determination of Extracts of Radix Aucklandiae

The extract of Radix Aucklandiae showed different degrees of inhibition on the mycelial growth of 10 different plant-pathogenic fungi (**Table 1**). Among them, the inhibitory effects of the extract on *B. cinerea*, *S. sclerotiorum*, *C. gloeosporioides*, *F. oxysporum*, *A. alternata*, *F. graminearum* and *D. glomerata* were significant, and the EC_{50} values were 114.18 mg/L, 142.40 mg/L, 251.87 mg/L, 299.34 mg/L, 315.07 mg/L, 398.74 mg/L and 414.08 mg/L, respectively. The extract had a poor inhibitory effect on *P. infestans*, *F. lateritium* and *P. aphanidermatum*, and the EC_{50} values were in the range of 500–1,000 mg/L.

Bioassay of Extracts of Radix Aucklandiae *In Vivo*

Control Effect on Wheat Powdery Mildew

The different concentrations of extracts of Radix Aucklandiae had different effects on the control of wheat powdery mildew (**Table 2**). With the increase in the concentration of the extract, the control effect on wheat powdery mildew was higher, and the protective activity was better than the curative activity. When the extract concentrations were 1,000 mg/L, the RDCEs of protective and curative acivities were higher than that of the control agent (100 mg/L propiconazole).

Statistical significance was determined using one-way ANOVA. Different lowercase letters in the footnote in the same column showed significant difference in the relative disease control efficiency of different treatment at each time points ($p < 0.05$).

Control Effect on Wheat Head Blight

Different concentrations of extracts of Radix Aucklandiae had different degrees of control effects on wheat head blight (**Table 3**). The higher the concentration, the better the control effect, and the protective activity was better than the curative activity, but the

TABLE 2 | RDCE of extracts of Radix Aucklandiae on wheat powdery mildew.

Treatment	Concentration (mg/L)	Protective activity			Curative activity		
		7d (%)	9d (%)	11d (%)	7d (%)	9d (%)	11d (%)
Extracts of Radix Aucklandiae	1,000	96.86ab	91.69b	90.53b	90.53b	78.28b	57.11c
	500	86.15c	84.29c	83.42c	83.42c	70.85c	55.81c
	250	61.19d	57.89d	56.07d	56.07d	35.04d	32.56d
Prothioconazole	100	92.31b	84.53c	80.32c	88.62bc	76.35b	70.46b

TABLE 3 | RDCE of extracts of Radix Aucklandiae on wheat head blight.

Treatment	Concentration (mg/L)	Protective activity			Curative activity		
		7d (%)	9d (%)	12d (%)	7d (%)	9d (%)	12d (%)
Extracts of Radix Aucklandiae	400	37.51c	11.96c	4.76c	34.38c	27.30c	2.38c
	4,000	56.26b	51.98b	11.90b	40.63b	36.39b	11.90b
Tebuconazole	86	71.88a	81.99a	88.10a	54.56a	87.50a	80.95a

TABLE 4 | RDCE of extracts of Radix Aucklandiae on strawberry grey mould *in vivo*.

Treatment	Concentration (mg/L)	Protective activity			Curative activity		
		3d (%)	5d (%)	7d (%)	3d (%)	5d (%)	7d (%)
Extracts of Radix Aucklandiae	1,000	100.00a	100.00a	100.00a	100.00a	100.00a	100.00a
	500	100.00a	85.71b	77.78b	100.00a	75.00b	63.64b
Pyraclostrobin	100	100.00a	100.00a	100.00a	100.00a	100.00a	100.00a

control effect of the extract was lower than that of the control agent (86 mg/L Tebuconazole). When the concentration of extracts was 4,000 mg/L, the protective and curative activities of wheat head blight were the best. The RDCEs of the protective activities were 56.26%, 51.98 and 11.90%, and of curative activities were 40.63, 36.39, 11.90% at 7, 9 and 12 days after treatment, respectively.

Statistical significance was determined using one-way ANOVA. Different lowercase letters in the footnote in the same column showed significant difference in the relative disease control efficiency of different treatment at each time points ($p < 0.05$).

Control Effect on Strawberry Grey Mould
Different concentrations of extracts of Radix Aucklandiae had different degrees of control effects on strawberry grey mould (**Table 4**). When the concentration of the extract was 500 mg/L, it had obvious protective and curative activitys on strawberry gray mold. The RDCEs of the protective activities were 100.00, 85.71 and 77.78%, and those of the curative activities were 100.00, 75.00, 63.64% at 3, 5 and 7 days after treatment, respectively. When concentration of extract was 1,000 mg/L, the RDCE of protective and curative activities reached 100%, which can achieve the control effect of the control agent (100 mg/L pyraclostrobin).

Statistical significance was determined using one-way ANOVA. Different lowercase letters in the footnote in the same column

showed significant difference in the relative disease control efficiency of different treatment at each time points ($p < 0.05$).

Control Effect on Citrus Anthracnose
Different concentrations of extracts of Radix Aucklandiae had different degrees of control effects on citrus anthracnose (**Table 5**). The higher the concentration, the better the control effect, and the protective activity was better than the therapeutic effect, but the control effect of the extract was lower than that of the control agent (86 mg/L Tebuconazole). When the concentration of the extract was 4,000 mg/L, the protective and curative activities on citrus anthracnose were the best. The inhibitory rate for the protective activity was 67.65%, and that of the protective activity was 57.5% at 7 days after treatment.

CK is negative control. Statistical significance was determined using one-way ANOVA. Different lowercase letters in the footnote in the same column showed significant difference in the inhibitory rate ($p < 0.05$).

Chemical Structure Identification of Active Compounds From Radix Aucklandiae
Compound 2
Compound **2** was obtained as white amorphous powder. Its molecular formula was determined to be $C_{15}H_{20}O_2$ based on the HRESIMS data (m/z 233.1540 $[M + H]^+$), indicating six

TABLE 5 | Control effect of extracts of Radix Aucklandiae on citrus anthracnose *in vivo* at 7 days after treatment.

Treatment	Concentration (mg/L)	Protective activity		Curative activity	
		Average diameters of lesions (cm)	Inhibitory rate (%)	Average diameters of lesions (cm)	Inhibitory rate (%)
Extracts of Radix Aucklandiae	4,000	0.55	67.65b	0.68	57.50b
	2000	0.80	52.94c	0.93	38.54c
	1,000	1.12	34.31d	1.17	27.08d
Tebuconazole	86	0.52	69.61a	0.54	66.15a
CK	-	1.70	-	1.60	-

TABLE 6 | ^{1}H and ^{13}C-NMR data of Compound 2, Compound 5 and Compound 6 ($CDCl_3$, δ in ppm, J in Hz).

No.	Compound 2[a]		Compound 5[a]		Compound 6[a]	
	δ_H	δ_C	δ_H	δ_C	δ_H	δ_C
1	4.83 (m)	127.1	2.89 (m)	47.7	2.03 (m)	41.9
2	2.08 (m)	28.1	1.89 (m)	32.7	2.07 (m)	16.9
3	1.81 (m)	41.1	2.51 (m)	30.4	2.43 (m)	32.8
4	-	140.2	-	151.4	2.23 (m)	37.7
5	4.72 (d, 9.9)	127.4	2.89 (m)	52.1	-	149.2
6	4.55 (dd, 8.8, 9.8)	82.0	3.96 (t, 9.2)	85.4	5.14 (d, 4.1)	118.9
7	2.55 (m)	50.5	2.89 (m)	45.2	3.56 (m)	39.6
8	1.70 (m)	26.3	2.15 (m); 1.41 (m)	31.1	4.81 (dt, 3.0, 6.5)	76.6
9	1.46 (m)	39,5	2.51 (m); 2.23 (m)	36.4	2.55 (m)	42.8
10	-	137.1	-	149.4	-	140.0
11	-	141.6	-	139.9	-	32.8
12	-	170.6	-	170.4	-	170.6
13	6.24 (d, 3.4); 5.51 (d, 3.4)	119.8	6.21 (d,3.3); 5.48 (d,3.3)	120.3	6.18 (d,1.8); 5.61 (d, 1.8)	121.8
14	1.40 (s)	16.2	5.26 (d, 1.3); 5.06 (d, 1.3)	109.7	1.08 (d, 7.6)	28.7
15	1.68 (d, 1.3)	17.4	4.89 (s); 4.81 (s)	112.7	1.18 (s)	22.7

[a]Recorded at 400 MHz, for ^{1}H and 100 MHz, for [13]C.

FIGURE 1 | Chemical structural of costunolide.

FIGURE 2 | Chemical structural of dehydrocostus lactone.

degrees of unsaturation. The ^{1}H-NMR data (**Table 6**) showed four olefinic protons at δ_H 6.24 (1H, d, J = 3.6 Hz), 5.51 (1H, d, J = 3.2 Hz), 4.83 (1H, m) and 4.72 (1H, d, J = 9.9 Hz); one oxygen-bearing methine signal at δ_H 4.55 (1H, dd, 8.8, 9.8), a methine signal at δ_H 2.55 (1H, m), and two methyl proton signal at δH 1.68 (3H, d, J = 1.3 Hz), 1.40 (3H, s). The ^{13}C-NMR spectrum (**Table 6**) contained fifteen carbon signals, which were assigned to one lactone carbonyl carbon (δc 170.6), six olefinic carbons (δ_C 141.4, 140.0, 136.9, 127.2, 127.0, 119.6), one
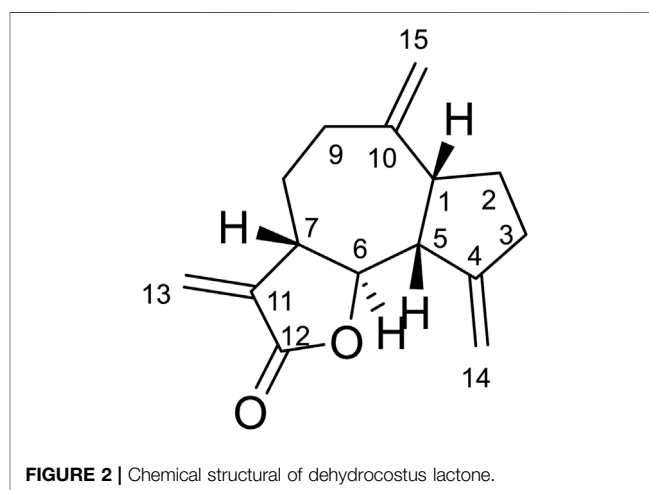
oxy-methine carbon (δ_C 81.9), one methine carbon (δ_C 50.3), four methylenes (δ_C 40.9, 39.4, 28.0, 26.1), and two methyl carbons (δc 17.3, 16.0). These spectral data were elucidated to the published data of Costunolide (Kaur et al., 2017; Chacon-Morales et al., 2020). Therefore, compound **2** was identified as costunolide and its molecular formula is shown in **Figure 1**. MS diagrams and ^{1}H-NMR and ^{13}C-NMR spectra were shown in Figures S1, S2 and S3, respectively.
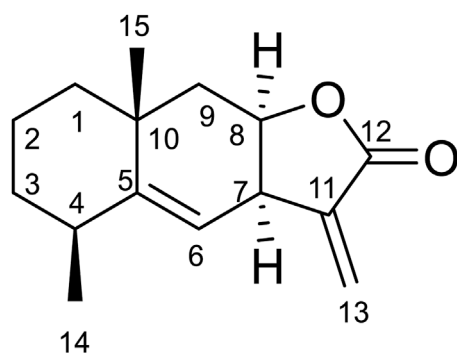
FIGURE 3 | Chemical structural of alantolactone.

Compound 5

Compound **5** was obtained as white amorphous powder. Its molecular formula was determined to be $C_{15}H_{20}O_2$ based on the ESIMS data (m/z 233.1 [M + H]$^+$), indicating six degrees of unsaturation. The ^{1}H-NMR data (**Table 6**) showed three olefinic protons [δ_H 6.18 (1H, d, J = 1.9 Hz), 5.61 (1H, d, J = 1.6 Hz), 5.14 (1H, d, J = 4.1 Hz)]; one oxygen-bearing methine signal at δ_H 4.81 (1H, dt, 3.0, 6.5), three methine signals at δ_H 3.56 (1H, m), 2.43 (1H, m), and two methyl proton signal at δ_H 1.18 (3H, s), 1.08 (3H, d, J = 7.6 Hz),. The ^{13}C-NMR spectrum (**Table 6**) contained fifteen carbon signals, which were assigned to one lactone carbonyl carbon (δc 170.6), four olefinic carbons (δc 149.2, 140.0, 121.8, 118.9), one oxy-methine carbon (δc 76.6), two methine carbons (δ_C 39.6, 37.7), four methylenes (δ_C 42.8, 41.9, 32.8, 16.9), and two methyl carbons (δ_C 28.7, 22.7). These spectral data were elucidated to the published data of Alantolactone (Neves et al., 1999; Yuuya et al., 1999). Therefore, compound **5** was identified as dehydrocostus lactone and its molecular formula is shown in **Figure 2**. MS diagrams and ^{1}H-NMR and ^{13}C-NMR spectra were shown in **Supplementary Figures S4–S6**, respectively.
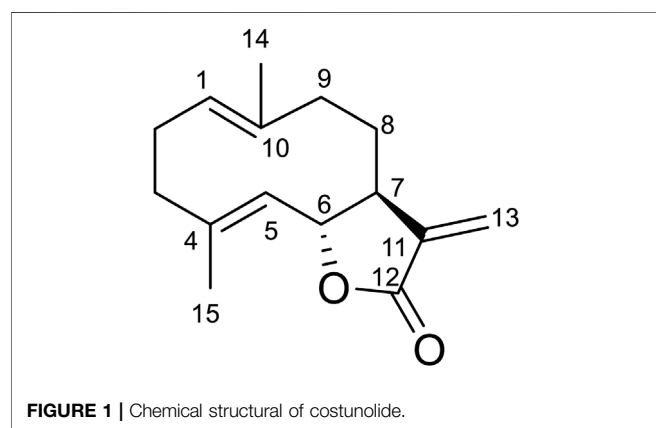
Compound 6

Compound **6** was obtained as white amorphous powder. Its molecular formula was determined to be $C_{15}H_{20}O_2$ based on the ESIMS data (m/z 233.1 [M + H]$^+$), indicating six degrees of unsaturation. The ^{1}H-NMR data (**Table 6**) showed three olefinic protons [δ_H 6.18 (1H, d, J = 1.9 Hz), 5.61 (1H, d, J = 1.6 Hz), 5.14 (1H, d, J = 4.1 Hz)]; one oxygen-bearing methine signal at δ_H 4.81 (1H, dt, 3.0, 6.5), three methine signals at δ_H 3.56 (1H, m), 2.43

(1H, m), and two methyl proton signal at δ_H 1.18 (3H, s), 1.08 (3H, d, J = 7.6 Hz),. The ^{13}C-NMR spectrum (**Table 6**) contained fifteen carbon signals, which were assigned to one lactone carbonyl carbon (δ_C 170.6), four olefinic carbons (δ_C 149.2, 140.0, 121.8, 118.9), one oxy-methine carbon (δ_C 76.6), two methine carbons (δ_C 39.6, 37.7), four methylenes (δ_C 42.8, 41.9, 32.8, 16.9), and two methyl carbons (δ_C 28.7, 22.7). These spectral data were elucidated to the published data of Alantolactone (Ming et al., 1989; Dereli et al., 2020). Therefore, compound **6** was identified as alantolactone and its molecular formula is shown in **Figure 3**. MS diagrams and ^{1}H-NMR and ^{13}C-NMR spectra were shown in **Supplementary Figures S7–S9**, respectively.

Antifungal Activity of Active Compoundsactive Ingredients

Alantolactone, dehydrocostus lactone and costunolide isolated from extracts of Radix Aucklandiae had inhibitory effects on the spore germination of *F. graminearum*, *B. cinerea*, *C. gloeosporioides* and *F. oxysporum* (**Table 7**). The MIC values of alantolactone against *B. cinerea* and *F. graminearum* were 15.63 mg/L and 250 mg/L, and those against *C. gloeosporioides* and *F. oxysporum* were both more than 1,000 mg/L. The MIC values of dehydrocostus lactone against *F. graminearum*, *B. cinerea*, *C. gloeosporioides* and *F. oxysporum* were 3.91 mg/L, 62.25 mg/L, 125 mg/L, 250 mg/L, respectively. The MIC values of costunolide against *B. cinerea* and *F. graminearum* were 15.625 mg/L and 1,000 mg/L, and those against *C. gloeosporioides* and *F. oxysporum* were both more than 1,000 mg/L.

DISCUSSION

Radix Aucklandiae is the dried root of *Aucklandia lappa* Dence. (Genus *Saussurea*, family Compositae). There are a few reports about the antimicrobial activity of the extract in medicine and agriculture. Research has reported that the extract has antimicrobial activity against *Helicobacter pylori* and *Streptococcus* in medicine (Yu et al., 2007; Han et al., 2011). The extract also has antimicrobial activity against *B. cinerea*, *A. alternata*, *Penicillium italicum* Wehmer, *Verticillium dahliae* and *F. oxysporum* (Hasi et al., 2009; Hu et al., 2009; Wang et al., 2012; Jin et al., 2019). In this study, extracts of Radix Aucklandiae had significant inhibitory effects on *B. cinerea*, *S. sclerotiorum* and *C. gloeosporioides*, and had obvious control effects on wheat

TABLE 7 | MIC values of active compounds of Radix Aucklandiae against four plant-pathogenic fungi.

Treatments	MIC value (mg/L)			
	F. graminearum	*B. cinerea*	*C. gloeosporioides*	*F. oxysporum*
Alantolactone	250	15.63	>1,000	>1,000
Dehydrocostus lactone	62.25	3.91	250	125
Costunolide	1,000	15.625	>1,000	>1,000
Pyraclostrobin	40	2	1.25	2.5

powdery mildew, wheat head blight, strawberry grey mould and citrus anthracnose. Therefore, the extract has potential development and application value as a botanical fungicide.

The chemical composition of Radix Aucklandiae is diverse. At present, there have been many reports on the chemical composition of extracts of Radix Aucklandiae. For example, more than 200 compounds, such as sesquiterpene lactones, monoterpenes, phenylpropanoids, lignans, flavonoids and volatile oils, have been isolated from Radix Aucklandiae (Mao et al., 2017). In this study, three active compounds were isolated and purified from Radix Aucklandiae, and identified as alantolactone, dehydrocostus lactone and costunolide, which are all terpenoids.

At present, the biological activities of these three compounds have mainly been reported in the context of medicine and are less known in agriculture. In medicine, it was found that these compounds had antimicrobial, antitumor, anti-inflammatory, hepatoprotective and other pharmacological effects. These compounds can inhibit *Fusarium solani* (Mart.) Sacc., *Mycobacterium tuberculosis* and *Staphylococcus aureus* in the human body (Wahab et al., 1979; Cantrell et al., 1999; O'Shea et al., 2009). In agriculture, recent research has also shown that alantolactone has a significant inhibitory effect on *Phytophthora nicotianae* (Feng et al., 2018). Dehydrocostus lactone and costunolide have inhibitory effects on *Cunninghamella echinulata*, *Colletotrichum acutatum*, *B. cinerea* and *F. oxysporum* (Barrero et al., 2000; Wedge et al., 2000). In this study, alantolactone, dehydrocostus lactone and costunolide all had different degrees of inhibitory effects on *F. graminearum*, *B. cinerea*, *C. gloeosporioides* and *F. oxysporum*. Alantolactone have inhibitory effects on *F. graminearum* and *B. cinerea*, and costunolide have inhibitory effects on *B. cinerea*, while dehydrocostus lactone has inhibitory effects on four plant-pathogenic fungi. Among them, dehydrocostus lactone showed the best control effect on plant fungous diseases.

Dehydrocostus lactone is a guaiane-type sesquiterpene isolated from Radix Aucklandiae. Dehydrocostus lactone is mainly extracted by solvent extraction, microwave-assisted extraction, ultrasonic-assisted extraction, and separated and purified by column chromatography (He et al., 2009; He et al., 2010). There are still difficulties in large-scale extraction. At present, the research on the structural modification and derivation of dehydrocostus lactone mainly focuses on Michael addition reaction at C-13 site and some oxidation reactions (Qian et al., 2012). The erivatives played an important role in tumor therapy. However, whether dehydrocostus lactone can be used as a lead compound in agricultural disease control remains to be verified. This study laid a foundation for the further development and utilization of extracts of Radix Aucklandiae as botanical fungicides.

DATA AVAILABILITY STATEMENT

The raw data supporting the conclusions of this article will be made available by the authors, without undue reservation.

AUTHOR CONTRIBUTIONS

XC, CY and GQ: Experimental design and the draft writing; MZ and HC: Experimental guidance and article modification; YB, XQ and LL: Participating in part experimental processes.

FUNDING

SUPPLEMENTARY MATERIAL

The Supplementary Material for this article can be found online at: https://www.frontiersin.org/articles/10.3389/fchem.2022.872480/full#supplementary-material

REFERENCES

Barrero, A. F., Oltra, J. E., Álvarez, M., Raslan, D. S., Saúde, D. A., and Akssira, M. (2000). New Sources and Antifungal Activity of Sesquiterpene Lactones. *Fitoterapia* 71 (1), 60–64. doi:10.1016/s0367-326x(99)00122-7

Bhandari, S., Yadav, P. K., and T Sarhan, A. (2021). Botanical Fungicides; Current Status, Fungicidal Properties and Challenges for Wide Scale Adoption: A Review. *Review.food.agr.* 2 (2), 63–68. doi:10.26480/rfna.02.2021.63.68

Bocca, C., Gabriel, L., Bozzo, F., and Miglietta, A. (2004). A Sesquiterpene Lactone, Costunolide, Interacts with Microtubule Protein and Inhibits the Growth of MCF-7 Cells. *Chemico-Biological Interactions* 147 (1), 79–86. doi:10.1016/j.cbi.2003.10.008

Butturini, E., Di Paola, R., Suzuki, H., Paterniti, I., Ahmad, A., Mariotto, S., et al. (2014). Costunolide and Dehydrocostuslactone, Two Natural Sesquiterpene Lactones, Ameliorate the Inflammatory Process Associated to Experimental Pleurisy in Mice. *Eur. J. Pharmacol.* 730 (1), 107–115. doi:10.1016/j.ejphar.2014.02.031

Cantrell, C. L., Abate, L., Fronczek, F. R., Franzblau, S. G., Quijano, L., and Fischer, N. H. (1999). Antimycobacterial Eudesmanolides from *Inula Helenium* and *Rudbeckia Subtomentosa*. *Planta Med.* 65 (4), 351–355. doi:10.1055/s-1999-14001

Chacón-Morales, P. A., Dugarte, C. S., and Amaro-Luis, J. M. (2020). Helenin from Stevia Lucida. The First Report of This Natural Eudesmanolide Mixture in Eupatorieae Tribe. *Nat. Product. Res.* 35, 4139–4142. doi:10.1080/14786419.2020.1739677

Chen, X., Pan, R., and Gai, Y. (2012). Antimicrobial Activities in Methanol Extracts of 31 Plant Species against *Peronophythora Litchii* and *Colletotrichum Gloeosporioides*. *Guangdong Agric. Sci.* 39 (3), 1–3. doi:10.16768/j.issn.1004-874x.2012.03.045

Feng, C., Zhan, H., Cui, M., Xu, C., Wang, X., and Chen, D. (2018). Chemical Identification of Tobacco Root Exudates and Their Effect on *Phytophthora Nicotianae*. *J. Anhui Agric. Sci.* 46 (17), 148–152. doi:10.13989/j.cnki.0517-6611.2018.17.044

Guo, Y., Chen, J., Ren, D., Du, B., Wu, L., Zhang, Y., et al. (2021). Synthesis of Osthol-Based Botanical Fungicides and Their Antifungal Application in Crop protection. *Bioorg. Med. Chem.* 40, 116184. doi:10.1016/j.bmc.2021.116184

Güragaç Dereli, F. T., Ilhan, M., and Küpeli Akkol, E. (2020). Identification of the Main Active Antidepressant Constituents in A Traditional Turkish Medicinal Plant, Centaurea Kurdica Reichardt. *J. Ethnopharmacology* 249, 112373. doi:10.1016/j.jep.2019.112373

Han, Y., Chen, C., Li, J., and Yan, Z. (2019). Effects of Tea Tree Oil Treatment on Grey Mold Disease in Postharvest Strawberry Fruit. *J. Xinjiang Agric. Univ.* 42 (4), 249–260. doi:10.16021/j.cnki.1007-8622.2011.06.013

Han, Y., Zhang, Y., Liu, X., Tan, H., Du, X., and Yang, Y. (2011). *Helicobacter pylori* Eradication with Extractive of 20 Species of Medicinal Plants. *Med. J. Natl. Defending Forces Northwest China* 32 (6), 413–415.

Hasi, G., Ai, Q., Wei, Y., Wu, Z., and Zhang, X. (2009). Antimicrobial Activity of Chinese Herbal Medicine Extracts against Two Postharvest Pathogenic Fungi from Vegetables. *J. Beijing Agric. Coll.* 24 (01), 20–23. doi:10.13473/j.cnki.issn.1002-3186.2009.01.009

He, Y., Hu, H., Fu, C., Huo, Y., Zhang, J., and Xu, L. (2011). Mechanism of Acetic Ether from Vlaimiria Souliei on Pyloric-Ligation Ulcet Model. *J. Chengdu Univ. TCM* 34 (3), 72–74.

He, Y., Zhan, R., and Zhao, Y. (2006). Inhibtion Effects of *Syzygium Aromaticum* (L.) Extracts against *Colletotrichum Gloeosporioides* and *Fusarium Oxysporum* f.sp.*Cubense*. *J. Sichuan Agric. Univ.* 24 (4), 394–397+404.

He, Z., Fu, D., Wang, H., Yang, S., and Tan, W. (2009). Study on Microwave Extraction of Costunolide and Dehydrocostuslactone from Radix Valdimiriae. *Appl. Chem. Industry* 38 (6), 878–879.

He, Z., Li, Y., Fu, D., Zhou, S., and Tan, W. (2010). Study on Ultrasonic Power Extraction of Costunolide and Dehydrocostuslactone from Radix Valdimiriae. *J. Anhui Agric. Sci.* 38 (35), 20040–20042.

Hu, M., Chen, G., and Du, G. (2009). Inhibition of 20 Kinds of Chinese Herbs Extracts against a Rot-Causing Fungus in Postharvest Citrus Fruits. *Tianjin Agric. Sci.* 15 (2), 56–58.

Jin, L., Yin, H., Wan, P., Huang, W., Xu, D., and Huang, N. (2019). Antimicrobial Activity of 25 Kinds of Chinese Herbal Extract against *Verticillium Dahlia*. *Plant Prot.* 45 (2), 234–237+246.

Ju, X. (2011). Connotation and Denotation of Chemical and Biological Pesticides. *Agrochemicals* 50 (2), 153–154. doi:10.16820/j.cnki.1006-0413.2011.02.024

Kaur, R., Chahal, K. K., and Bhardwaj, U. (2017). Sesquiterpenolides from Inula Racemosa and Their Chemical Transformations. *Asian J. Chem.* 29 (3), 568–570. doi:10.14233/ajchem.2017.20254

Lai, X., Meng, B., Jang, Z., Song, Y., and Wu, Q. (2008). Effects of Radix Vladimiriae on Experimental Gastric Ulcer in Rats. *Prog. Mod. Biomeicine* 8 (1), 34–36. doi:10.13241/j.cnki.pmb.2008.01.019

Li, L., Ji, M., and Su, Z. (2006). Research Advances in Use of the Agricultural Fungicide. *Sophora flavescensAgrochemicals* 45 (9), 581–583. doi:10.1016/j.meatsci.2005.08.008

Liu, J., Xue, G., Wang, X., Song, M., Wang, L., and Fan, H. (2011). Study on the Antibacterial Activity of Ten Ultrasound Extracts from Medicinal Plants. *Hubei Agric. Sci.* 50 (9), 1809–1811. doi:10.14088/j.cnki.issn0439-8114.2011.09.034

Liu, N., Wu, X., Gu, B., and Zhu, Q. (2000). *GB/T 17980-22-2000 Pesticide-Guidelines for the Field Eficacy Trials (1)-Fungicides against Cereal Powdery Mildew*. Bejjing: Standards Press of China, 90–93p.

Mao, J., Wang, G., Yi, M., Huang, Y., and Chen, M. (2017). Research Progress on Chemical Constituents in *Vladimiriae Radix* and Their Pharmacological Activities. *Chin. Traditional Herbal Drugs* 48 (22), 4797–4803.

Neves, M., Morais, R., Gafner, S., Stoeckli-Evans, H., and Hostettmann, K. (1999). New Sesquiterpene Lactones from the Portuguese Liverwort *Targionia Lorbeeriana*. *Phytochemistry* 50 (6), 967–972. doi:10.1016/s0031-9422(98)00648-7

O'Shea, S., Lucey, B., and Cotter, L. (2009). *In Vitro* activity of *Inula Helenium* against Clinical *Staphylococcus aureus* Strains Including MRSA. *Br. J. Biomed. Sci.* 66 (4), 186–189. doi:10.1080/09674845.2009.11730271

Qian, W., Xu, Y., Wang, C., Mu, X., Zhang, Q., and Zhang, Z. (20121874). Researching Progress of Aucklandiae Radix about its Chemical Compositions and Structural Modification. *Nat. Product. Res. Develop.* 24 (12), 1857–1865. doi:10.16333/j.1001-6880.2012.12.034

Shum, K. C., Chen, F., Li, S. L., Wang, J., But, P. P., and Shaw, P. C. (2015). Authentication of Radix Aucklandiae and its Substitutes by GC-MS and Hierarchical Clustering Analysis. *J. Sep. Sci.* 30 (18), 3233–3239. doi:10.1002/jssc.200700232

Sun, W., Zhang, X., Huang, Z., Chen, T., Kang, C., Gao, J., et al. (2015). The Protective Activity of Dehydrocostus Lactone on Liver Injury in Laboratory Rats. *World Chin. Med.* 10 (3), 399–401. doi:10.3969/j.issn.1673-7202.2015.03.025

Tian, L., Peng, R., Yao, S., Deng, L., and Zeng, K. (2019). *Pichia Membranaefaciens* Combined with Chitosan Treatment Induces Resistance to Anthracnose in Citrus Fruit. *Food Sci.* 40 (7), 228–237. doi:10.7506/spkx1002-6630-20180913-120

Wahab, S., Lal, B., Jacob, Z., Pandey, V. C., and Srivastava, O. P. (1979). Studies on a Strain of *Fusarium Solani* (Mart.) Sacc. Isolated from a Case of Mycotic Keratitis. *Mycopathologia* 68 (1), 31–38. doi:10.1007/bf00490388

Wang, L., Liu, J., Wang, D., Li, J., and Fan, H. (2012). Inhibition Effect of Four Plants Compound Fungicides against *Fusarium Oxysporum*. *China Vegetables* 1 (16), 80–85.

Wang, L., Zhao, F., He, E., Wang, S., Xu, B., and Liu, K. (2008). Effects of Eighteen Sesquiterpenes from *Saussurea Lappa* on the Proliferation of Six Human Cancer Cell Lines. *Nat. Prod. Res. Deo* 20 (5), 808–812. doi:10.16333/j.1001-6880.2008.05.022

Wang, M., Shen, H., and Zhou, X. (2014). *Laboratory Guide for Chemical Protection of Plant*. Beijing: Peking University Press, 113–115p.

Wedge, D. E., Galindo, J. C. G., and Macı´as, F. A. (2000). Fungicidal Activity of Natural and Synthetic Sesquiterpene Lactone Analogs. *Phytochemistry* 53 (7), 747–757. doi:10.1016/s0031-9422(00)00008-x

Wei Ming, C., Mayer, R., Zimmermann, H., and Rücker, G. (1989). A Non-oxidized Melampolide and Other Germacranolides from *Aristolochia Yunnanensis*. *Phytochemistry* 28 (11), 3233–3234. doi:10.1016/0031-9422(89)80315-2

Xie, D., Cai, X., Yang, C., Xie, L., Qin, G., Zhang, M., et al. (2021). Studies on the Control Effect of *Bacillus Subtilis* on Wheat Powdery Mildew. *Pest Manag. Sci.* 77 (10), 4375–4382. doi:10.1002/ps.6471

Yang, X., Wang, M., Shen, R., and Liu, F. (2012). Microtiter Method to Test the Sensitivity of *Botrytis Cinerea* to Fungicides. *Scientia Agricultura Sinica* 45 (15), 3075–3082. doi:10.3864/j.issn.0578-1752.2012.15.008

Yu, H.-H., Lee, J.-S., Lee, K.-H., Kim, K.-Y., and You, Y.-O. (2007). Saussurea Lappa Inhibits the Growth, Acid Production, Adhesion, and Water-Insoluble Glucan Synthesis of Streptococcus Mutans. *J. Ethnopharmacology* 111 (2), 413–417. doi:10.1016/j.jep.2006.12.008

Yuuya, S., Hagiwara, H., Suzuki, T., Ando, M., Yamada, A., Suda, K., et al. (1999). Guaianolides as Immunomodulators. Synthesis and Biological Activities of Dehydrocostus Lactone, Mokko Lactone, Eremanthin, and Their Derivatives. *J. Nat. Prod.* 62 (1), 22–30. doi:10.1021/np980092u

Zhang, T., and Wang, G. (2011). Research Advances in Extraction of Antimicrobial Activity Components from the Plant Materials. *Guangdong Agric. Sci.* 38 (13), 59–62. doi:10.16768/j.issn.1004-874x.2011.13.006

Zhu, C., Zhou, M., Shen, Y., Wu, X., Zhang, W., Zhang, W., et al. (2007). *NY/T 1464.15_2007 Guidelines on Efficacy of Pesticides Part 15: Fungicides against fusarium Head Blight of Wheat*. Bejjing: Standards Press of China, 1–4p.

Synthesis and Bioactivities of Novel Galactoside Derivatives Containing 1,3,4-Thiadiazole Moiety

Yafei Shu, Meihang Chen*, Daowang Lu, Zengyan Zhou, Jianhong Yu, Xiaoling Hu, Jiaqin Yang, Aiqin Li, Jianglong Liu and Hairong Luo

Colleges of Material and Chemistry Engineering, Tongren University, Tongren, China

A series of novel galactoside derivatives containing 1,3,4-thiadiazole moiety were synthesized, and the structure of them was verified by spectroscopy of NMR and HRMS, and antifungal and antibacterial activities of them were screened. The results showed that the newly synthesized compounds had good antifungal activities. Among them, III16, III17, and III19 exhibited satisfactory activities against *Phytophthora infestans (P. infestans)*, with EC$_{50}$ values of 5.87, 4.98, and 6.17 μg/ml, respectively, which were similar to those of dimethomorph (5.52 μg/ml). Meanwhile, the title compounds also possessed certain antibacterial activities.

Keywords: galactoside, thiadiazole, aromatic amide, synthesis, bioactivity

INTRODUCTION

Galactoside and its derivatives are widely found in litchi, laver, seaweed, and snails (Choucry et al., 2021; Kumar, 2020) and had anticancer (Tacke et al., 2017; Oueslati et al., 2020), antiviral (Cai et al., 2006; Abu-Zaied et al., 2021), and antibacterial (Upadhyay et al., 2010) activities. In addition, it was found that novel galactoside derivatives containing a pyrimidine moiety possessed good antifungal activities against *Gibberella zeae* (*G. zeae*), *Botryosphaeria dothidea* (*B. dothidea*), *Phytophthora infestans* (*P. infestans*), *Thanatephorus cucumeris* (*T. cucumeris*), and *Phompsis* sp in the preliminary working of our group (Chen M. H. et al., 2021; Chen et al., 2022). Moreover, it has been reported that glycosylation can improve the properties of active lead compounds, such as solubility, stability, and bioactivity (Wu et al., 2014; Gurung et al., 2017).

It is known that nitrogen-containing heterocyclic compounds have not only a broad spectrum of biological activity and diversity of structure changes but also low toxicity to most warm-blooded animals, birds, fish, and bees (Mermer et al., 2021). 1,3,4-Thiadiazole derivatives, important nitrogen-containing heterocyclic compounds, showed a wide range of bioactivities, such as antifungal (Bhinge et al., 2015; Chudzik et al., 2019), antibacterial (Wu et al., 2021), anticancer (Abas et al., 2021; Avvaru et al., 2021), and antiviral (Yu et al., 2017) activities. In our previous working, 1,3,4-thiadiazole derivatives of glucosides showed good antibacterial and antifungal activities (Chen M. et al., 2021).

In order to find novel structure and effective biological activity of galactoside derivatives, 19 novel galactoside derivatives containing 1,3,4-thiadiazole moiety were synthesized by five reactions and were designed under the guidance of the active substructure splicing method by retaining a part of 1,3,4-thiadiazole and replacing the original glucoside with galactoside on the basis of our previous working (**Figure 1**). Then, the newly synthesized title compounds are tested for antibacterial and antifungal activities.
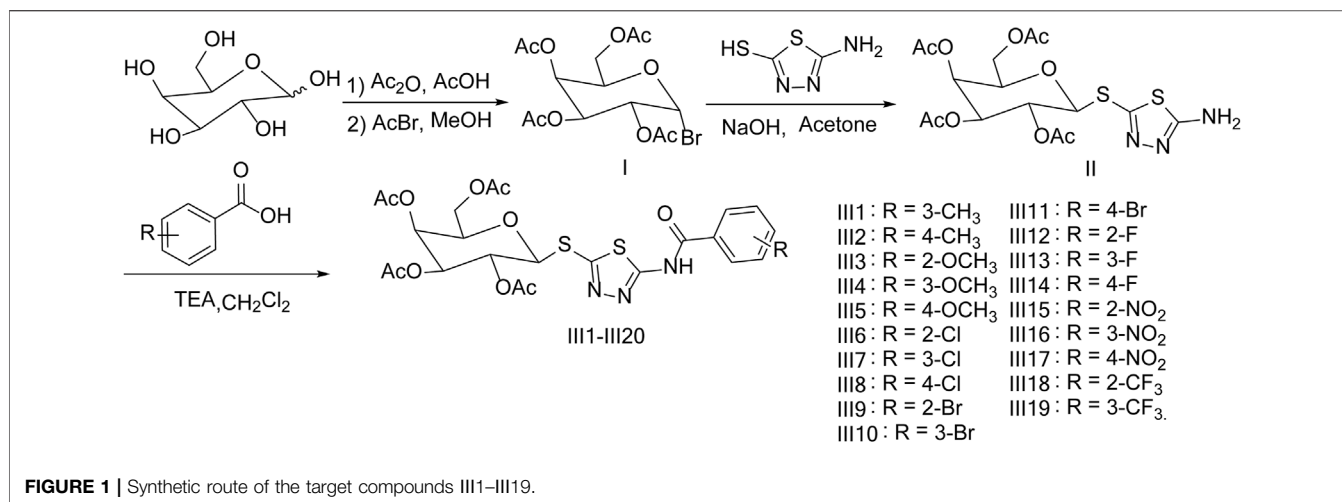
FIGURE 1 | Synthetic route of the target compounds III1–III19.

EXPERIMENTAL

Materials and Instruments

All solvents and reagents were purchased from commercial suppliers and met the standards. ^{1}H NMR and ^{13}C NMR spectra were obtained using Bruker DPX 400 MHz and Bruker DPX 600 MHz spectrometers (Bruker, Germany) in DMSO-d6 or CDCl3 solution. High-resolution mass spectrometry (HRMS) of the title compounds was performed using an Agilent Technologies mass spectrometer (Agilent Technologies, United States).

Chemistry

General Synthesis Procedures for Intermediate II
Intermediate I was synthesized by referring to the method of the literature (Kamat et al., 2007; Chen M. et al., 2021). The crude product of intermediate I is used directly for the next step of the reaction. To 2-amino-5-mercapto-1,3,4-thiadiazole (1.33 g, 10.0 mmol), 50 ml acetone and 40% sodium hydroxide solution (10 ml) were added successively into a 100-ml two-necked bottle. Then, a solution of intermediate I (4.11 g, 10.0 mmol) in acetone (5 ml) was added and maintained under stirring for about 30 min (Scattolin et al., 2020; Chen M. et al., 2021). After the reaction was completed, the mixture was concentrated, and 30 ml of water was added and extracted with dichloromethane (3 × 20 ml), and the organic layer was concentrated and recrystallized with ethyl acetate to afford the intermediate II (3.9 g, yield: 84%) as a white solid. ^{1}H NMR (600 MHz, DMSO-d6) δ 7.48 (s, 2H, NH$_2$), 5.33 (s, 1H, H-1´), 5.30–5.21 (m, 2H, H-2´, H-3´), 5.05 (t, J = 9.9 Hz, 1H, H-4´), 4.33 (t, J = 6.2 Hz, 1H, H-5´), 4.13–4.00 (m, 2H, H-6´, H-6´´), 2.14 (s, 3H, CH$_3$), 2.07 (s, 3H, CH$_3$), 2.02 (s, 3H, CH$_3$), and 1.93 (s, 3H, CH$_3$).

General Synthesis Procedures for Title Compounds III1–III19
Substituted benzoic acid (2.4 mmol) was added to 4 ml thionyl chloride in batches with magnetic stirring and refluxed for 2.0 h

(monitored by TLC). The solvent was removed under negative pressure; dichloromethane (2 ml) was added into the residue to give a light yellow solution, which was added dropwise into a mixture of the intermediate II (0.93 g, 2.0 mmol), 15 ml dichloromethane, and triethylamine (0.24 g, 2.4 mmol) (Chen M. et al., 2021). After the reaction was completed, 10 ml water was added into the mixture and divided, and the organic layer was concentrated to the crude product. The crude product was recrystallized with isopropanol to afford the title compounds III1–III19. The characterization details of the title compounds III2–III19 are presented in the **Supplemental Material**.

(2R,3S,4S,5R,6S)-2-(acetoxymethyl)-6-((5-(3-methylbenzamido)-1,3,4-thiadiazol-2-l)thio)tetrahydro-2H-pyran-3,4,5-triyltriacetate (III1): white solid, yield 75.0%, m.p. 159–161°C; 1H NMR (400 MHz, CDCl$_3$) δ 12.33 (s, 1H, NH), 8.01 (s, 1H, Ar-H), 7.95 (d, J = 7.3 Hz, 1H, Ar-H), 7.55–7.37 (m, 2H, Ar-H), 5.48 (d, J = 2.9 Hz, 1H, H-3´), 5.38 (t, J = 10.0 Hz, 1H, H-1´), 5.11 (dd, J = 10.0, 3.3 Hz, 1H, H-2´), 5.03 (d, J = 10.1 Hz, 1H, H-4´), 4.20 (d, J = 7.6 Hz, 2H, H-5´, H-6´), 3.99 (t, J = 6.4 Hz, 1H, H-6´´), 2.48 (s, 3H, CH$_3$), 2.20 (s, 3H, CH$_3$), 2.10 (s, 6H, 2×CH$_3$), and 2.00 (s, 3H, CH$_3$). ^{13}C NMR (150 MHz, CDCl$_3$) δ 172.48, 170.58, 170.45, 169.89, 169.80, 154.72, 138.62, 134.24, 131.59, 129.35, 129.11, 126.02, 83.10, 74.70, 71.16, 68.06, 67.32, 62.39, 40.41, 40.27, 40.13, 39.99, 39.85, 39.71, 39.57, 21.35, 20.90, and 20.78; HRMS [M+H]$^+$ calculated for C$_{24}$H$_{27}$N$_3$O$_{10}$S$_2$: m/z 582.1216, found 582.1210.

Antifungal Activity *In Vitro*

The antifungal activity of the title compounds III1–III19 against *G. zeae, B. dothidea, Phompsis* sp., *P. infestans,* and *T. cucumeris in vitro* were tested by a mycelia growth method at 50 μg/ml (Maddila et al., 2016; Chen M. H. et al., 2021; Chen M. et al., 2021; Chen et al., 2022). Dimethomorph was used as a positive control, and DMSO was used as a negative control, and each treatment was operated in three replicates. Subsequently, the title compounds III16, III17, and III19 were further evaluated for their corresponding antifungal EC$_{50}$ values with three replicates and used dimethomorph as the positive controls.

TABLE 1 | Reaction conditions for intermediate II were optimized.

Entry	Catalyst	Solvent	Temperature/°C	Yield[a] (%)
1	$NaHCO_3$	CH_2Cl_2	r.m.	18
2	Na_2CO_3	CH_2Cl_2	r.m.	30
3	NaOH	CH_2Cl_2	r.m.	72
3	Et_3N	CH_2Cl_2	r.m.	55
4	NaOH	THF	r.m.	66
5	NaOH	$CHCl_3$	r.m.	70
6	NaOH	CH_3CN	r.m.	66
7	NaOH	$(CH_3)_2CO$	r.m.	82
8	NaOH	$(CH_3)_2CO$	0°C	72
9	NaOH	$(CH_3)_2CO$	50°C	78
10	NaOH	$(CH_3)_2CO$	Reflux	81

Antibacterial Activity *In Vitro*

The antibacterial activity of the title compounds III1–III19 against *Xcc* and *Xoo in vitro* was tested using the turbidimeter test at 200 and 100 µg/ml (Dalgaard et al., 1994; Yu et al., 2017; Chen M. H. et al., 2021; Chen et al., 2022). Thiodiazole-copper was used as a positive control, and DMF was used as a negative control, and each treatment was operated in three replicates.

RESULT AND DISCUSSION

Synthesis

The method of the synthesis for title compounds was listed as follows: Intermediate I was synthesized by galactose acetylation and bromination, and then intermediate I reacted with 2-amino-5-mercapto-1,3,4-thiadiazole to give intermediate II; substituted benzoic acids were chlorinated by thionyl chloride and reacted with intermediate II to

TABLE 3 | EC$_{50}$ value of antifungal activity for part of compounds against *P. infestans*.

Compound	Toxic regression equation	R	EC$_{50}$ (µg/ml)
III16	y = 0.63x + 4.51	0.96	5.87 ± 1.5
III17	y = 0.61x + 4.57	0.99	4.98 ± 2.1
III19	y = 0.67x + 4.47	0.98	6.17 ± 1.8
Dimethomorph	y = 0.94x + 4.30	0.99	5.52 ± 1.2[a]

[a]*Refer to the previous articles of our group (Chen M. et al., 2021).*

produce the title compounds III1–III19. Moreover, to optimize the reaction conditions of the key intermediate II, the influence of catalyst, temperature, and solvent were tested and are listed in **Table 1**. The results indicated that the catalyst, solvent, and temperature had a pronounced effect on the yield, and a maximum yield of 82% was achieved when sodium hydroxide was used as a catalyst and acetone as a solvent for 0.5 h at room temperature.

Antifungal Activity *In Vitro*

The antifungal activity of the title compounds III1–III19 against *G. zeae, B. dothidea, P. infestans, Phompsis* sp., and *T. cucumeris* are listed in **Table 2**. **Table 2** indicated that III1–III19 showed good antifungal activities, with the inhibition rates of 21.5%–63.4%, 21.6%–66.0%, 23.6%–80.1%, 32.5%–58.1%, and 33.4%–68.4% at 50 µg/ml, respectively. Among them, III16, III17, and III19 exhibited satisfactory *in vitro* antifungal activities against *P. infestans*, with the inhibition rates of 80.1, 79.7, and 79.3%, respectively, which were equal to those of dimethomorph (78.2%). Based on the aforementioned results, the EC$_{50}$ values of III16, III17, and III19 were tested and are shown in **Table 3**. **Table 3** indicated that III16, III17, and III19 showed good

TABLE 2 | Antifungal activity of compounds III1–III19 *in vitro* (50 µg/ml).

Compound	Inhibition rate (%)				
	G. zeae	*B. dothidea*	*P. infestans*	*Phompsis* sp.	*T. cucumeris*
III1	28.8 ± 1.3	24.5 ± 2.0	23.6 ± 2.8	49.2 ± 2.6	45.2 ± 1.7
III2	34.5 ± 1.6	32.0 ± 1.0	28.1 ± 1.7	36.3 ± 3.4	33.4 ± 1.4
III3	37.6 ± 2.0	31.0 ± 1.8	25.6 ± 2.0	32.5 ± 1.5	56.3 ± 2.1
III4	45.4 ± 2.6	25.8 ± 1.2	24.7 ± 1.5	36.2 ± 1.8	42.6 ± 1.7
III5	40.1 ± 2.1	26.8 ± 2.6	25.3 ± 2.6	47.5 ± 1.9	47.5 ± 1.8
III6	36.2 ± 1.1	21.6 ± 2.8	56.4 ± 1.4	34.2 ± 2.1	43.4 ± 1.5
III7	47.0 ± 1.3	33.2 ± 2.3	56.7 ± 3.2	55.6 ± 1.4	46.3 ± 1.5
III8	34.2 ± 1.6	48.5 ± 2.1	56.1 ± 1.2	35.2 ± 2.4	35.7 ± 2.4
III9	38.6 ± 1.5	54.8 ± 1.7	59.8 ± 2.1	33.5 ± 2.2	45.6 ± 1.8
III10	43.0 ± 1.3	51.6 ± 2.0	57.5 ± 3.0	37.3 ± 2.3	55.4 ± 1.4
III11	45.4 ± 0.8	50.7 ± 1.2	57.6 ± 2.7	45.1 ± 1.9	43.0 ± 1.2
III12	63.4 ± 1.0	50.5 ± 2.3	73.5 ± 2.1	34.5 ± 2.1	59.7 ± 2.2
III13	53.8 ± 1.2	46.4 ± 1.6	73.1 ± 1.6	48.1 ± 1.3	68.3 ± 1.8
III14	52.3 ± 1.8	66.4 ± 1.2	77.5 ± 2.1	42.6 ± 1.2	56.5 ± 2.1
III15	61.0 ± 2.4	65.3 ± 2.6	75.1 ± 2.2	45.2 ± 1.5	56.3 ± 1.3
III16	52.2 ± 2.1	66.0 ± 2.5	80.1 ± 1.3	58.1 ± 1.4	56.5 ± 1.6
III17	45.2 ± 1.6	54.3 ± 2.4	79.7 ± 1.2	43.2 ± 1.5	58.7 ± 1.0
III18	55.4 ± 2.0	55.2 ± 2.0	78.0 ± 2.3	44.5 ± 2.2	65.3 ± 2.0
III19	57.2 ± 1.6	54.7 ± 2.5	79.3 ± 2.1	48.2 ± 1.4	68.4 ± 1.9
Dimethomorph	74.3 ± 2.0[a]	72.3 ± 1.6[a]	78.2 ± 1.1[a]	69.3 ± 1.6[a]	68.3 ± 1.6[a]

[a]*Refer to the previous articles of our group (Chen M. et al., 2021).*

TABLE 4 | Antibacterial activity of compounds (III1–III19) *in vitro*.

Compound	*Xoo*		*Xcc*	
	200 µg/ml	100 µg/ml	200 µg/ml	100 µg/ml
III1	47.6 ± 2.5	29.1 ± 1.6	45.4 ± 1.4	28.5 ± 1.2
III2	43.5 ± 1.2	23.1 ± 1.3	42.2 ± 2.3	29.2 ± 1.5
III3	46.7 ± 1.2	25.4 ± 2.0	44.3 ± 2.1	24.1 ± 1.3
III4	45.5 ± 1.1	23.1 ± 1.2	48.0 ± 2.3	29.2 ± 1.4
III5	35.3 ± 2.0	18.3 ± 2.4	42.1 ± 1.5	24.7 ± 2.1
III6	41.5 ± 2.3	21.5 ± 3.1	45.1 ± 2.1	24.8 ± 1.4
III7	36.2 ± 2.8	19.2 ± 3.0	57.7 ± 1.3	36.1 ± 1.7
III8	45.4 ± 2.3	26.5 ± 2.1	53.5 ± 2.1	34.8 ± 2.5
III9	37.3 ± 1.8	19.1 ± 1.0	55.0 ± 1.8	27.0 ± 1.4
III10	43.4 ± 2.6	24.3 ± 1.2	53.1 ± 1.4	26.2 ± 1.2
III11	44.2 ± 1.5	27.5 ± 2.7	40.0 ± 1.7	19.8 ± 2.0
III12	52.6 ± 2.4	26.8 ± 1.8	41.2 ± 1.0	20.4 ± 1.4
III13	56.2 ± 1.1	26.5 ± 3.1	48.1 ± 2.5	25.7 ± 2.5
III14	57.6 ± 2.0	29.0 ± 1.0	45.2 ± 1.1	21.2 ± 1.6
III15	64.2 ± 1.2	30.3 ± 1.4	54.1 ± 2.9	26.0 ± 1.7
III16	58.6 ± 1.2	23.2 ± 2.1	55.1 ± 1.8	27.8 ± 1.1
III17	62.8 ± 1.1	34.5 ± 0.9	57.0 ± 2.2	28.9 ± 2.0
III18	54.2 ± 1.2	33.0 ± 1.3	49.0 ± 1.0	29.4 ± 2.7
III19	53.0 ± 1.4	36.2 ± 2.2	45.4 ± 2.6	23.8 ± 2.5
Thiodiazole-copper	70.1 ± 2.3[a]	43.6 ± 1.5[a]	80.2 ± 1.5[a]	46.1 ± 1.3[a]

[a]*Refer to the previous articles of our group (Chen et al., 2022).*

antifungal activities against *P. infestans,* with EC$_{50}$ values of 5.87, 4.98, and 6.17 µg/ml, respectively, which were similar to those of dimethomorph (5.52 µg/ml) (Chen et al., 2022), and which were comparable to those of the previously found inhibitory activity of glucosides derivatives containing 4-fluorobenzamido-1,3,4-thiadiazole against *P. infestans* (3.43 µg/ml) (Chen M. et al., 2021).

Antibacterial Activity *In Vivo*

Moreover, the antibacterial activities of the title compounds against *Xcc* and *Xoo* were tested at 200 and 100 µg/ml and are listed in **Table 4**. **Table 4** indicated that the title compounds III1–III19 exhibited certain antibacterial activities against *Xoo* and *Xcc* at 200 and 100 µg/ml, with the inhibition rates of 31.5%–64.2% and 40.8%–57.7% and 18.3%–36.2% and 19.8%–36.1%, respectively, which were lower than those of thiodiazole-copper (70.1, 43.6, and 46.1%), and which were comparable to that of the previously found novel glucoside derivatives containing 1,3,4-thiadiazole moiety with antibacterial activity (Chen M. et al., 2021). Based on the aforementioned results, it was demonstrated that the antifungal and antibacterial activities of compounds replacing the original glucoside with galactoside did not show any improvement, that is, the configuration of the third on the six-member sugar ring has little influence on the antifungal and antibacterial activities.

CONCLUSION

A total of 19 novel galactoside derivatives containing 1,3,4-thiadiazole moiety were designed under the guidance of the active substructure splicing method and synthesized by five reactions. The bioactivity results indicated that the title compounds exhibited good antibacterial and antifungal activities, while some of them showed excellent antifungal activities. Therefore, it was demonstrated that the galactoside derivatives containing 1,3,4-thiadiazole moiety can be used to develop potential agrochemicals in the future.

DATA AVAILABILITY STATEMENT

The original contributions presented in the study are included in the article/**Supplementary Material**, further inquiries can be directed to the corresponding author.

AUTHOR CONTRIBUTIONS

YS and MC performed the synthesis and bioactivity of all compounds. DL and HL contributed to the original manuscript. ZZ, AL, and JL analyzed the results. JHY, XH, and JQY drafted the version of the manuscript.

FUNDING

SUPPLEMENTARY MATERIAL

The Supplementary Material for this article can be found online at: https://www.frontiersin.org/articles/10.3389/fchem.2022.910710/full#supplementary-material

REFERENCES

Abas, M., Bahadur, A., Ashraf, Z., Iqbal, S., Rajoka, M. S. R., Rashid, S. G., et al. (2021). Designing Novel Anticancer Sulfonamide Based 2,5-Disubstituted-1,3,4-Thiadiazole Derivatives as Potential Carbonic Anhydrase Inhibitor. *J. Mol. Struct.* 1246, 131145. doi:10.1016/j.molstruc.2021.131145

Abu-Zaied, M. A., Elgemeie, G. H., and Mahmoud, N. M. (2021). Anti-covid-19 Drug Analogues: Synthesis of Novel Pyrimidine Thioglycosides as Antiviral Agents against SARS-COV-2 and Avian Influenza H5N1 Viruses. *ACS Omega* 6 (26), 16890–16904. doi:10.1021/acsomega.1c01501

Avvaru, S. P., Noolvi, M. N., More, U. A., Chakraborty, S., Dash, A., Aminabhavi, T. M., et al. (2021). Synthesis and Anticancer Activity of Thiadiazole Containing Thiourea, Benzothiazole and Imidazo[2,1-B][1,3,4]thiadiazole Scaffolds. *Mc* 17, 750–765. doi:10.2174/1573406416666200519085626

Bhinge, S. D., Chature, V., and Sonawane, L. V. (2015). Synthesis of Some Novel 1,3,4-thiadiazole Derivatives and Biological Screening for Anti-microbial, Antifungal and Anthelmintic Activity. *Pharm. Chem. J.* 49, 367–372. doi:10.1007/s11094-015-1287-8

Cai, S.-Q., Wang, R., Yang, X., Shang, M., Ma, C., and Shoyama, Y. (2006). Antiviral Flavonoid-TypeC-Glycosides from the Flowers of Trollius Chinensis. *Chem. Biodivers.* 3, 343–348. doi:10.1002/cbdv.200690037

Chen, M. H., Lu, D. W., Zhang, X., Chen, M. Y., and Luo, H. R. (2021). Synthesis and Biological Activities of Novel S-β-D-Glucopyranoside Derivatives of 1,2,4-triazole. *Phosphorus Sulfur*, 1–6. doi:10.1080/10426507.2021.1901704

Chen M., M., Zhang, X., Lu, D., Luo, H., Zhou, Z., Qin, X., et al. (2021). Synthesis and Bioactivities of Novel 1,3,4-thiadiazole Derivatives of Glucosides. *Front. Chem.* 9, 645876. doi:10.3389/fchem.2021.645876

Chen, M., Zhang, X., Luo, H., Zhou, Z., Chen, M., Wu, W., et al. (2022). Synthesis and Antifungal and Antibacterial Evaluation of Novel Pyrimidine Derivatives with Glycoside Scaffolds. *Chem. Pap.* 76, 1321–1328. doi:10.1007/s11696-021-01907-1

Chudzik, B., Bonio, K., Dabrowski, W., Pietrzak, D., Niewiadomy, A., Olender, A., et al. (2019). Synergistic Antifungal Interactions of Amphotericin B with 4-(5-Methyl-1,3,4-Thiadiazole-2-Yl) Benzene-1,3-Diol. *Sci. Rep.* 9, 12945–12959. doi:10.1038/s41598-019-49425-1

Dalgaard, P., Ross, T., Kamperman, L., Neumeyer, K., and Mcmeekin, T. A. (1994). Estimation of Bacterial Growth Rates from Turbidimetric and Viable Count Data. *Int. J. Food Microbiol.* 23, 391–404. doi:10.1016/0168-1605(94)90165-1

Gurung, R. B., Gong, S. Y., Dhakal, D., Le, T. T., Jung, N. R., Jung, H. J., et al. (2017). Synthesis of Curcumin Glycosides with Enhanced Anticancer Properties Using One-Pot Multienzyme Glycosylation Technique. *J. Microbiol. Biotechnol.* 27, 1639–1648. doi:10.4014/jmb.1701.01054

Kamat, M. N., Rath, N. P., and Demchenko, A. V. (2007). Versatile Synthesis and Mechanism of Activation of S-Benzoxazolyl Glycosides. *J. Org. Chem.* 72 (18), 6938–6946. doi:10.1021/jo0711844

Maddila, S., Gorle, S., Sampath, C., and Lavanya, P. (2016). Synthesis and Anti-inflammatory Activity of Some New 1,3,4-thiadiazoles Containing Pyrazole and Pyrrole Nucleus. *J. Saudi Chem. Soc.* 20, S306–S312. doi:10.1016/j.jscs.2012.11.007

Mermer, A., Keles, T., and Sirin, Y. (2021). Recent Studies of Nitrogen Containing Heterocyclic Compounds as Novel Antiviral Agents: a Review. *Bioorg. Chem.* doi:10.1016/j.bioorg.2021.105076

Oueslati, M. H., Tahar, L. B., and Harrath, A. H. (2020). Catalytic, Antioxidant and Anticancer Activities of Gold Nanoparticles Synthesized by Kaempferol Glucoside from *lotus Leguminosae*. *Arabian J. Chem.* 13, 3112–3122. (in press). doi:10.1016/j.arabjc.2018.09.003

Scattolin, T., Bortolamiol, E., Rizzolio, F., Demitri, N., and Visentin, F. (2020). Allyl Palladium Complexes Bearing Carbohydrate-based N-heterocyclic Carbenes: Anticancer Agents for Selective and Potent In Vitro Cytotoxicity. *Appl. Organomet. Chem.* 34, 5876. doi:10.1002/aoc.5876

Tacke, M., Zhu, X., Werner, C., Schmidt, C., Sanchez-Sanz, G., Ott, I., et al. (2017). In Vitro and In Vivo Investigations into the Carbene Gold Chloride and Thioglucoside Anticancer Drug Candidates NHC-AuCl and NHC-AuSR. *Lett. Drug Des. Discov.* 14 (2), 125–134. doi:10.2174/1570180813666160826100158

Upadhyay, N. K., Yogendra Kumar, M. S., and Gupta, A. (2010). Antioxidant, Cytoprotective and Antibacterial Effects of Sea Buckthorn (*Hippophae Rhamnoides l.*) Leaves. *Food Chem. Toxicol.* 48, 3443–3448. doi:10.1016/j.fct.2010.09.019

Wu, M., Han, G., Meng, C., Wang, Z., Liu, Y., and Wang, Q. (2014). Design, Synthesis, and Anti-tobacco Mosaic Virus (TMV) Activity of Glycoconjugates of Phenanthroindolizidines Alkaloids. *Mol. Divers.* 18, 25–37. doi:10.1007/s11030-013-9484-4

Wu, S., Shi, J., Chen, J., Hu, D., Zang, L., and Song, B. (2021). Synthesis, Antibacterial Activity, and Mechanisms of Novel 6-Sulfonyl-1,2,4-Triazolo [3,4-*B*][1,3,4]thiadiazole Derivatives. *J. Agric. Food Chem.* 69 (16), 4645–4654. doi:10.1021/acs.jafc.1c01204

Yu, L., Gan, X., Zhou, D., He, F., Zeng, S., and Hu, D. (2017). Synthesis and Antiviral Activity of Novel 1,4-Pentadien-3-One Derivatives Containing a 1,3,4-thiadiazole Moiety. *Molecules* 22 (4), 658. doi:10.3390/molecules22040658

Discovery of Novel α-Aminophosphonates with Hydrazone as Potential Antiviral Agents Combined With Active Fragment and Molecular Docking

Jia Tian[1†], Renjing Ji[1†], Huan Wang[1], Siyu Li[1] and Guoping Zhang[1,2]*

[1]*Chemistry and Material Science College, Huaibei Normal University, Huaibei, China,* [2]*Key Laboratory of Green and Precise Synthetic Chemistry and Applications, Ministry of Education, Huaibei Normal University, Huaibei, China*

A series of novel α-aminophosphonate derivatives containing hydrazone were designed and synthesized based on active fragments. Bioassay results demonstrated that title compounds possessed good activities against tobacco mosaic virus. Among them, compounds 6a, 6g, 6i, and 6j were equivalent to the commercial antiviral agents like *dufulin*. On structure optimization-based molecular docking, compound 6k was synthesized and displayed excellent activity with values of 65.1% curative activity, 74.3% protective activity, and 94.3% inactivation activity, which were significantly superior to the commercial antiviral agents *dufulin* and *ningnanmycin*. Therefore, this study indicated that new lead compounds could be developed by adopting a joint strategy with active fragments and molecular docking.

Keywords: α-aminophosphonate, hydrazone, synthesis, antiviral, docking

1 INTRODUCTION

Tobacco mosaic virus (TMV) is one of the most widely studied plant viruses that can cause deformation and stunting of the leaves, flowers, and fruits of infected plants (Ritzenthaler, 2005). Plant diseases caused by tobacco mosaic virus (TMV) are difficult to control because TMV is absolutely parasitic, and transmissibility to host cells and plants may completely suppress immune system (Bos, 1982). Although several commercial antiviral agents against TMV have been used, efficient and practical varieties are few. The widely used antiviral agent ribavirin only gave less than 50% anti-TMV effect at 500 μg/ml (Hansen and Stace Smith, 1989). The developing novel structure, remarkable effect, and environmentally friendly anti-TMV agents are needed urgently. At present, the main representative research groups are Wang Qingmin's group and Song Baoan's group on domestic development of anti-plant virus agents. In 2019–2021, Song Baoan's group mainly designed and synthesized antiviral compounds based on active fragments through *in vitro* activity screening by microscale thermophoresis (MST) (He et al., 2019; Zan et al., 2020; Liu et al., 2021; Zhang et al., 2021). During the same period, Wang Qingming's group mainly designed and synthesized new and efficient antiviral lead compounds based on natural products through traditional *in vivo* activity screening by using the half leaf dry spot method (Li et al., 2019; Hao et al., 2020a; Chen et al., 2020; Li et al., 2021). Then, the primary action mechanism of antiviral agents was studied by the *vivo* interaction of viral coat protein and drug molecules. These results indicated that viral coat protein was a key target protein for antiviral agents. Therefore, molecular docking could accelerate the development of antiviral agents.

FIGURE 1 | Structure of *dufulin*.
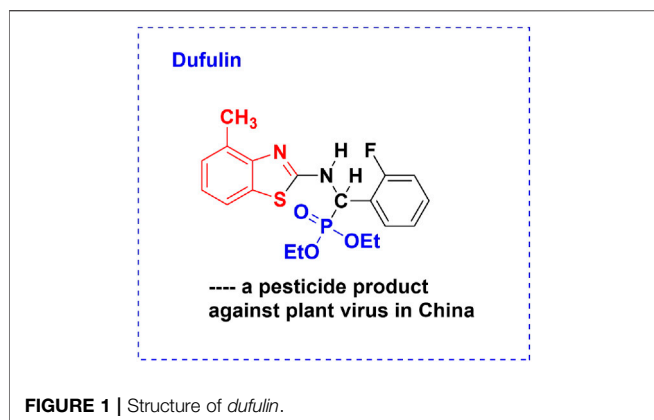
α-Aminophosphonates are considered to be structural analogs of α-amino acids. Compounds bearing the α-aminophosphonate moiety play an important role in biochemical and medicinal chemistry such as antitumor activity (Liu et al., 2010; Ye et al., 2014; Fang et al., 2016; Ewies et al., 2019; Zhang et al., 2020), antivirus activity (Zhang et al., 2010; Zhang and Liu, 2016; Zhang et al., 2017; Lan et al., 2017; Poola et al., 2020; Zhou et al., 2021), antimicrobial activity (He et al., 2015), and antibacterial activity (Dake et al., 2011; Hellal et al., 2017). In recent years, Song and coworkers (Chen et al., 2009; Yang et al., 2011; Zhang et al., 2016) reported that many α-aminophosphonates with anti-TMV and anti-CMV activity were synthesized via substructural splicing. Among them, dufulin (**Figure 1**), a new commercially registered plant antiviral product, was developed, which belongs to the α-aminophosphonate family (Song et al., 2006). In addition, it has been highly effective in preventing infection caused by rice viruses and tobacco mosaic virus and, as a result, has obtained a national invention patent in the People's Republic of China. It was registered by the Ministry of Agriculture of China (LS 20071280, 20071282, and 20130359) and was subsequently industrialized for large-scale field application. It has been widely used to prevent and control rice, vegetable, and tobacco viral diseases in China. This may provide some useful information for the future design of novel structural aminophosphonates.

Hydrazone derivatives are biologically interesting compounds known for their antiviral (Massarani et al., 1970; Wang et al., 2019), anticancer (Mehlika et al., 2012), insecticidal (Liu et al., 2010b), and antimicrobial (Martin et al., 2021) effects. Among them, hydrazones with promising antiviral activity have attracted our attention. In order to discover new molecules with antiviral effects, we sought to incorporate the active substructural unit hydrazone into the backbone structure of α-aminophosphonate. Based on the aforementioned facts, we designed and synthesized the title compounds by a joint strategy with active fragments and molecular docking (**Figure 2**). This article describes the syntheses and bioactivities of the designed compounds. The structure–activity relationships of these phosphonate–hydrazone analogs are examined in comparison with their parent aminophosphonate analogs to further the design of more effective antiviral compounds.

2 MATERIALS AND METHODS

2.1 Chemicals
All reagents were purchased from commercial suppliers and used without further purification.

2.2 Instruments
^{1}H NMR and ^{13}C NMR spectra of the compounds were obtained using a Bruker DPX 400 MHz (Bruker, Germany) and Bruker DPX 600 MHzin CDCl3 or DMSO-*d*6 solution. HRMS was performed with a Thermo Scientific Q Exactive (Thermo Scientific, United States). Infrared (IR) spectra were recorded on a Bruker VECTOR 22 spectrometer using KBr disks. The melting points of the compounds were measured using WRX-4 equipment.

2.3 General Procedures
2.3.1 Procedures for the Synthesis of Intermediates (4a–4h)
Aromatic aldehyde containing a hydroxyl group (1, 100 mmol) was added to a vial containing acetonitrile (50 ml) and potassium carbonate (100 mmol), and then ethyl bromoacetate (2, 110 mmol) was added in the reaction vessel. After the mixture was stirred and refluxed for 12 h, the solvent was removed *in vacuo*. The reaction mixture was poured into water (100 ml) and extracted with dichloromethane (50 ml×3). The dichloromethane solution was dried with anhydrous Na_2SO_4 and evaporated in a vacuum. The residue was recrystallized from acetonitrile to obtain the intermediates (3a~3 h). A solution of intermediates 3 (80 mmol) and 2-amino-4-methylbenzothiazole (80 mmol) in toluene (50 ml) was refluxed for 3 h. Then, diethyl phosphite (120 mmol) was added to the reaction solution and refluxed for 6–12 h. The crude product was afforded through removing the solvent and recrystallized from acetonitrile to obtain the intermediates (4a~4 h). Characterization data of the intermediate 4a are given as follows, and the data of other compounds are listed in **Supplementary Material S1**.

4a: Yield 78%, m. p. 128–130°C; ^{1}H NMR (600 MHz, DMSO) δ 8.89 (dd, J = 9.6, 2.9 Hz, 1H), 7.43 (dd, J = 14.9, 7.5 Hz, 3H), 7.01 (d, J = 7.3 Hz, 1H), 6.96–6.84 (m, 3H), 5.58 (dd, *J* = 21.0, 9.6 Hz, 1H), 4.73 (s, 2H), 4.12 (q, J = 7.1 Hz, 2H), 4.08–3.96 (m, 2H), 3.94–3.86 (m, 1H), 3.84–3.76 (m, 1H), 2.41 (s, 3H), 1.16 (t, J = 7.1 Hz, 3H), 1.13 (t, J = 7.0 Hz, 3H), 1.03 (t, J = 7.0 Hz, 3H). ^{13}C NMR (151 MHz, DMSO) δ 169.13 (s), 164.99 (d, J = 9.7 Hz), 157.67 (s), 150.92 (s), 130.76 (s), 129.91 (d, J = 5.7 Hz), 129.01 (s), 128.00 (s), 126.68 (s), 121.69 (s), 118.86 (s), 114.75 (s), 65.13 (s), 63.07 (d, J = 6.7 Hz), 62.86 (d, J = 6.8 Hz), 61.09 (s), 54.84 (s), 53.81 (s), 18.41 (s), 16.72 (d, J = 5.4 Hz), 16.53 (d, J = 5.4 Hz), 14.48 (s). IR (thin film, cm^{-1}): 3233.5 (s), 2982.6 (s), 2928.9 (s), 1753.3 (s), 1587.9 (s), 1534.9 (s), 1446.3 (s), 1197.7 (s), 1053.1 (s), 1018.7 (s), 976.1 (s). HRMS (ESI) m/z for ($C_{23}H_{29}N_2O_6PS$ [M + H]$^+$ cacld. 493.1557, found 493.1553.

2.3.2 Procedures for the Synthesis of Intermediate 5a
The intermediate 4a (60 mmol) was added to the reaction flask with ethyl alcohol (50 ml), and then hydrazine hydrate (70 mmol) was added to the reaction mixture. After the mixture was stirred
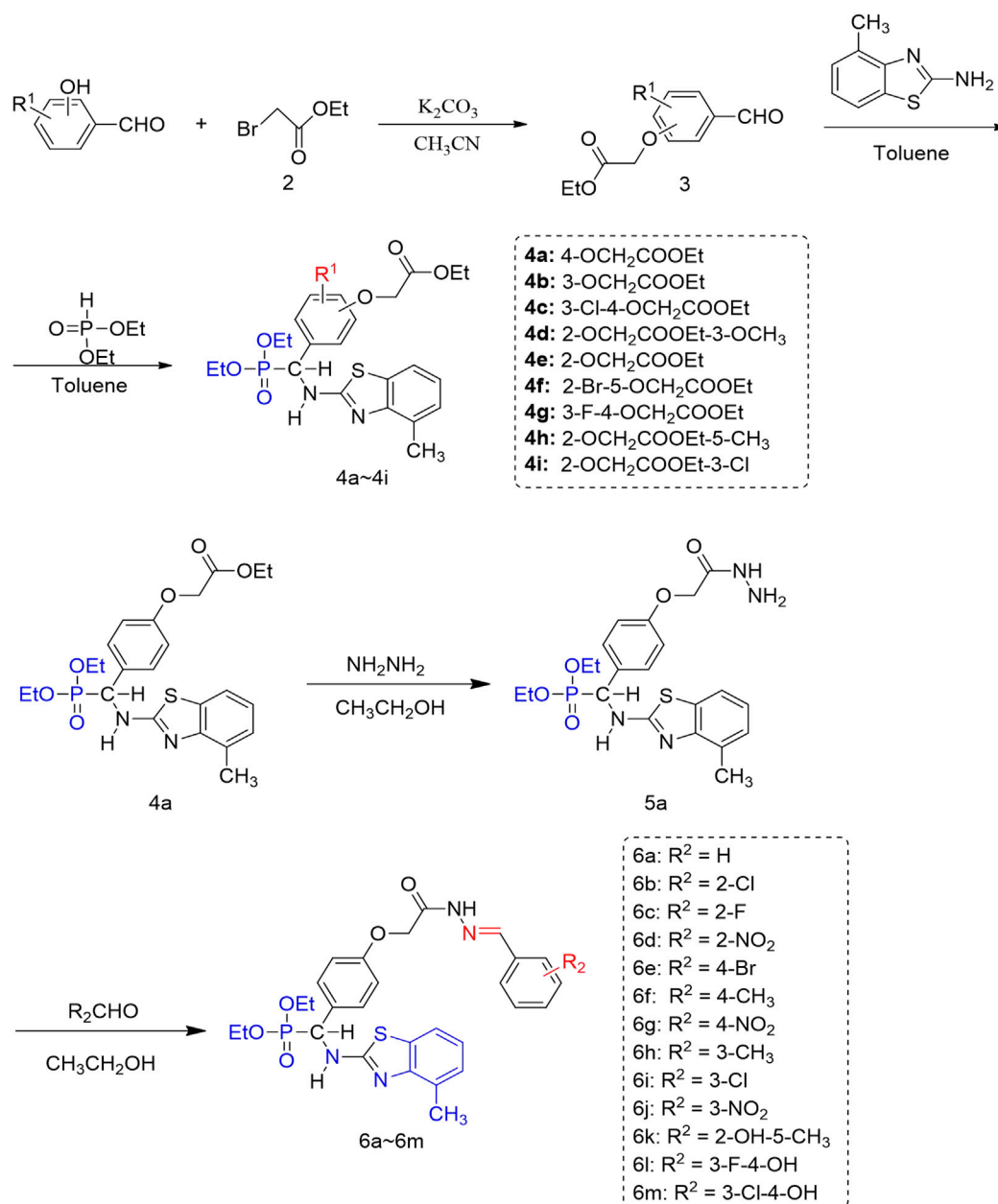
FIGURE 2 | Synthetic routes of novel α-aminophosphonate derivatives with hydrazone.

and refluxed for 12 h, ethyl alcohol was evaporated under reduced pressure to afford the crude product. The residue was purified by recrystallization affording acyl-hydrazine (5a) using alcohol. Characterization data of the intermediate 5a are given as follows.

5a: Yield 71%, m. p. 126–128°C; ^{1}H NMR (600 MHz, DMSO-d_6) δ: 9.29 (s, 1H), 8.92–8.85 (m, 1H), 7.49–7.38 (m, 3H), 7.01 (d, J = 7.4 Hz, 1H), 6.96–6.87 (m, 3H), 5.57 (dd, J = 21.0, 9.5 Hz, 1H), 4.44 (s, 2H), 4.32 (s, 2H), 4.08–3.95 (m, 2H), 3.93–3.87 (m, 1H), 3.83–3.77 (m, 1H), 2.40 (s, 3H), 1.13 (t, J = 7.0 Hz, 3H), 1.04 (t, J = 7.0 Hz, 3H); ^{13}C NMR (151 MHz, DMSO-d_6) δ: 167.03 (s), 165.00 (d, J = 9.8 Hz), 157.87 (s), 150.92 (s), 130.76 (s), 129.87 (d, J = 5.6 Hz), 128.94 (s), 127.99 (s),

126.68 (s), 121.69 (s), 118.87 (s), 114.88 (s), 66.74 (s), 63.07 (d, J = 6.7 Hz), 62.87 (d, J = 6.7 Hz), 56.50 (s), 54.89 (s), 53.86 (s), 19.03 (s), 18.41 (s), 16.73 (d, J = 5.2 Hz), 16.55 (d, J = 5.4 Hz). IR (thin film, cm^{-1}): 3231.8 (s), 3037.2 (s), 2984.6 (s), 1671.9 (s), 1590.3 (s), 1536.9 (s), 1510.7 (s), 1446.6 (s), 1239.3 (s), 1050.8 (s), 1024.6 (s), 973.9 (s). HRMS (ESI) m/z for ($C_{21}H_{27}N_4O_5PS$ [M + H]$^+$ cacld. 479.1513, found. 479.1509.

2.3.3 Procedures for the Synthesis of Title Compounds (6a~6 m)

The intermediate 5a (2.0 mmol) and aldehyde (2.0 mmol) were added to 5 ml of alcohol. The mixture was stirred at 80°C for 6 h.

The resulting mixture was concentrated under reduced pressure to give the crude product. A total of 5 ml of water was added to the crude product and stirred for 0.5 h. The crude product was purified by column chromatography using hexane/EtOAc (1:2, v/v) or recrystallization with alcohol. The data for the title compound 6a are shown as follows, and the data of other compounds are listed in **Supplementary Material S1**.

6a: Yield 86%, m. p. 184–186°C; ^{1}H NMR (400 MHz, DMSO-d_6) δ: 11.56 (trans), 11.51 (cis) (s, 1H, CONH), 8.90 (d, J = 9.6 Hz, 1H, NH-Hetero), 8.30 (cis), 7.97(trans) (s, 1H, CH = N), 7.74–7.60 (m, 2H, Ar-H), 7.47–7.36 (m, 6H, Ar-H), 7.07–6.84 (m, 4H, Ar-H), 5.58 (dd, J = 21.0, 9.6 Hz, 1H, CHP), 5.10 (trans), 4.63(cis) (s, 2H, COCH$_2$O), 4.10–3.96 (m, 2H, CH$_2$OP), 3.95–3.87 (m, 1H, CHOP), 3.86–3.75 (m, 1H, CHOP), 2.41 (s, 3H, CH$_3$-Hetero), 1.13 (t, J = 7.0 Hz, 3H, CH$_3$), 1.04 (t, J = 7.0 Hz, 3H, CH$_3$). trans:cis=(0.61:0.39); ^{13}C NMR (151 MHz, DMSO-d_6) δ: 169.03 (s), 164.61 (d, J = 9.6 Hz), 164.25 (s), 157.89 (s), 157.43 (s), 150.55 (s), 148.04 (s), 143.86 (s), 134.18 (s), 134.04 (s), 130.37 (s), 130.24 (s), 130.01 (s), 129.56 (d, J = 5.3 Hz), 129.44 (d, J = 5.3 Hz), 128.88 (d, J = 4.6 Hz), 128.72 (s), 128.12 (s), 127.60 (s), 127.21 (s), 127.00 (s), 126.28 (s), 121.28 (s), 118.47 (s), 114.54 (s), 114.35 (s), 66.63 (s), 64.84 (s), 62.66 (d, J = 6.9 Hz), 62.46 (d, J = 6.5 Hz), 54.48 (s), 53.45 (s), 18.04 (s), 16.34 (d, J = 5.2 Hz), 16.16 (d, J = 5.3 Hz). IR (thin film, cm^{-1}): 3273.9 (s), 3106.5 (s), 2979.7 (s), 2914.9 (s), 1695.5 (s), 1612.8 (s), 1586.6 (s), 1534.4 (s), 1511.5 (s), 1430.5 (s), 1229.8 (s), 1047.5 (s), 1023.7 (s); HRMS (ESI) m/z for (C$_{28}$H$_{31}$N$_4$O$_5$PS [M + H]$^+$ cacld. 567.1826, found. 567.1824.

2.3.4 Evaluation of Phytotoxic Activities Against Tobacco and Anti-TMV Activity

Phytotoxic activities against tobacco and anti-TMV activity were assessed according to the aforementioned method (Ji et al., 2019; Wang et al., 2012). Tobacco mosaic virus (TMV) was purified. The biological activity of the compounds against TMV was evaluated by using a half-leaf method.

2.4 Molecular Docking

Molecular docking with AutoDock 4.0 (Huey et al., 2007; Trott and Olson, 2010) between compound 6a and TMV-CP was performed. The X-ray crystal structure of TMV-CP used for the computation was downloaded from RCSB (Bhyravbhatla et al., 1998). Most of the parameters for the docking calculation were set to the default values. Each docked structure was scored by the built-in scoring function and was clustered by 1 Å of RMSD criteria. Finally, the enzyme ligand complex structures were selected according to the criteria for autodocking score.

3 RESULTS AND DISCUSSION

3.1 Synthesis and Spectroscopy

The synthetic route of the target compounds (6a~6 m) is shown in **Figure 2**. 4-hydroxybenzaldehyde 1) reacted with ethyl bromoacetate, 2) in acetonitrile to give aldehyde with an ester group, and 3) compound 3 condensed with 2-amino-4-methylbenzothiazole via a Schiff base condensation to give the intermediate of imine, which was followed by phosphine

hydrogenation with diethyl phosphite to afford the compound 4. Compound 4 continued to react with hydrazine hydrate in alcohol to give the intermediate compound 5. Title compound 6 was smoothly prepared by the reaction of an aromatic aldehyde with the corresponding hydrazides. The chemical structures of these compounds were identified by NMR, IR, and HRMS (**Supplementary Material**). In ^{1}H NMR of the title compounds, the CH-P proton appeared at δ 5.58–5.63 as dd, the NH-Ar proton appeared at δ 8.89–8.93 as double, and the CH = N proton of cis-isomer appeared at the higher magnetic field (8.17–8.70) than trans-isomer (7.85–8.34), the ratio of which was 3:2. In the ^{13}C NMR spectra of compound 6, the typical carbon resonance at δ169 was indicative of a carbonyl group (C=O). The IR spectra of compound C showed bands at 1684–1701 cm^{-1} for C=O stretching.

3.2 Phytotoxic Activities and Antivirus Activities

First, the data on phytotoxic activity against tobacco indicated that compounds 6a–6k at 500 μg·mL$^-$ showed no toxicity. Then, the tested concentration of the compounds at 500 μg/ml was chosen, and the biological activities against TMV were evaluated. The results of anti-TMV activity are shown in **Table1**. The intermediates (4a~4h) exhibited lower antiviral activities against TMV in vivo. Among them, the intermediate 4a displayed moderate activities, with values of 33.2% curative activity, 45.7% protective activity, and 78.7% inactivation activity. The intermediate 5a exhibited higher activities than compound 4a, especially in curative activity. The title compounds 6a, 6g, 6i, and 6j derived from α-aminophosphonate possessed good activities, which were similar to those controls of ningnanmycin and dufulin. Compound 6k exhibited excellent activity, with the values of 65.1% curative activity, 74.3% protective activity, and 94.3% inactivation activity, which were significantly greater than those of controls. Compounds 6b, 6f, and 6h possessed slightly lower activity than these controls. Other compounds showed lower activities. The antiviral activity results of the intermediates 4a~4i and intermediate 5a suggest that the structure of α-aminophosphonate with benzothiazole is critical for the activity, and generally, in addition, the R$_2$ substituted phenyl series of the title compounds influenced the antiviral activity for the derivatives (6a~6 m). The R$_2$ substitutions at the ortho-position of the phenyl ring connected to the hydrazone moiety (6b, 6c, and 6d) showed weaker curative activity than the R$_2$ = H of the phenyl ring. As for the para-substituted derivatives, it is clear to see that the order of the curative activity against TMV was NO$_2$-substituted (6g) > CH$_3$-substituted (6f) > Br-substituted (6e). When the R$_2$ group was at the meta-position of the phenyl ring, the compounds (6h~6j) exhibited relatively similar curative activities to compound 6a (R$_2$ = H). Fortunately, 2-OH-5-CH$_3$-substituted compound **6k** showed the best curative activity (65.1%) against TMV, which was significantly better than that of ningnanmycin (53.3%). Considering the prior discussion, we found that the antiviral activities of our designed compounds could be increased by the introduction of 2-OH and 5-CH$_3$ on benzene rings. The results further suggested that small differences of substituted position on the phenyl ring could lead to large differences in the overall activities, which implies further possibilities for lead compound development.

TABLE 1 | Antiviral activity of the compounds (4a~6m) against TMV at 500 μg/mL[a].

Compound	Curative activity[a] (%)	Protective activity[a] (%)	Inactivation activity[a] (%)
4a	33.2 ± 2.6	45.7 ± 2.1	78.7 ± 2.2
4b	21.2 ± 3.1	35.6 ± 2.7	48.6 ± 1.8
4c	26.3 ± 3.3	37.1 ± 2.6	52.2 ± 2.4
4d	0	9.1 ± 3.4	0
4e	0	0	0
4f	23.6 ± 2.8	43.3 ± 2.1	57.4 ± 2.3
4g	27.5 ± 3.2	44.1 ± 1.6	67.6 ± 2.1
4 h	22.2 ± 2.4	34.6 ± 1.9	51.3 ± 2.8
5a	50.3 ± 1.6	49.7 ± 1.9	83.1 ± 2.6
6a	51.3 ± 1.4	54.1 ± 1.7	90.3 ± 1.3
6b	47.6 ± 2.1	35.8 ± 3.3	49.3 ± 2.7
6c	41.6 ± 1.9	34.8 ± 3.5	51.3 ± 3.1
6d	39.1 ± 2.8	53.3 ± 1.4	77.6 ± 1.9
6e	29.3 ± 3.6	32.5 ± 2.7	45.3 ± 2.4
6f	48.6 ± 2.3	31.3 ± 3.1	43.1 ± 2.9
6g	56.7 ± 1.3	38.5 ± 2.9	49.3 ± 2.6
6 h	48.1 ± 2.1	45.0 ± 2.3	77.3 ± 2.3
6i	54.2 ± 1.8	56.6 ± 1.3	81.5 ± 1.7
6j	55.5 ± 1.8	60.0 ± 1.2	88.7 ± 2.7
6k	65.1 ± 1.2	74.3 ± 1.5	94.3 ± 1.1
6L	32.2 ± 3.3	35.4 ± 3.7	60.1 ± 1.8
6 m	31.4 ± 2.9	33.7 ± 3.4	57.3 ± 2.1
Dufulin [b]	50.3 ± 2.6	54.3 ± 1.9	87.6 ± 2.2
Ningnanmycin [c]	53.3 ± 2.3	58.3 ± 1.7	92.3 ± 1.4

[a]Average of three replicates.
[b]Dufulin was also used as the control.
[c]Ningnanmycin was used as the control.

FIGURE 3 | 3D mode of the interaction of compound 6a and receptor TMV-CP analyzed by AutoDock 4.0 software. Conventional hydrogen bond, carbon–hydrogen bond, and alkyl, as well as Pi–alkyl, are shown by green, light green, and pink, respectively.
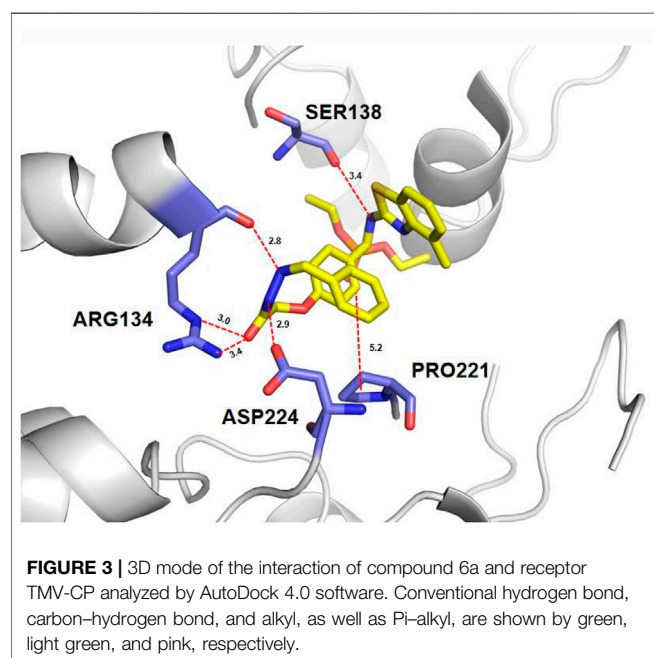
3.3 Molecular Modeling Analysis

TMV-CP is an important protein involved in plant virus infections and is being studied as a potential protein target to develop effective antivirus agents (Hao et al., 2020b; Kang et al., 2020). In order to gain more understanding of the structure–activity relationships and further structure

optimization, molecular docking was performed on the binding mode of compound 6a into the binding pocket of TMV-CP using AutoDock 4.0 software. The 3D binding models of compound 6a with TMV-CP are shown in **Figure 3**. Results showed that the benzothiazole ring of 6a fit into the binding pocket, surrounded by the amino acid residues of SER138. Detailed analysis of the binding mode showed that the hydrazone of 6a was surrounded by the amino acid residues of ARG134 and ASP224. These docking results suggested that the benzothiazole ring in the title compound was critical for the activity and the phenyl ring of hydrazone influenced the antiviral activity. On structure optimization-based molecular docking, compound 6k was synthesized and displayed excellent activity, with values of 65.1% curative activity, 74.3% protective activity, and 94.3% inactivation activity, which were significantly superior to the commercial antiviral agents *dufulin* and *ningnanmycin*. Therefore, molecular docking could accelerate the development of lead compounds.

4 CONCLUSION

A series of *α*-aminophosphonate-hydrazone derivatives were synthesized and evaluated for antiviral activities. Some derivatives showed good inhibitory activity. The SARS analysis showed that the volume and position of the substituted groups at the phenyl ring of hydrazones had significant influences on inhibitory activity. The docking studies showed that compound **6a** was well bound to the TMV-CP via one hydrogen bond with SER 138, ARG 134, and ASP

224. This also indicated that the structures of benzothiazole and hydrazone play a key role in the activity of the title compound. Among them, compound 6k displayed excellent activity, with values of 65.1% curative activity, 74.3% protective activity, and 94.3% inactivation activity. Therefore, the basic motif of compound 6k can be used as a lead compound for further development.

DATA AVAILABILITY STATEMENT

The original contributions presented in the study are included in the article/**Supplementary Material**, further inquiries can be directed to the corresponding author.

AUTHOR CONTRIBUTIONS

All authors have contributed to the work, have read the manuscript, and have agreed to be listed as authors. The submitted manuscript has not been published elsewhere nor is it currently under review by another publication. GZ designed the project and wrote the manuscript; JT and RJ performed the experiments; and HW and SL analyzed the data.

SUPPLEMENTARY MATERIAL

The Supplementary Material for this article can be found online at: https://www.frontiersin.org/articles/10.3389/fchem.2022.911453/full#supplementary-material

REFERENCES

Altıntop, M. D., Özdemir, A., Turan-Zitouni, G., Ilgın, S., Atlı, Ö., İşcan, G., et al. (2012). Synthesis and Biological Evaluation of Some Hydrazone Derivatives as New Anticandidal and Anticancer Agents. *Eur. J. Med. Chem.* 58, 299–307. doi:10.1016/j.ejmech.2012.10.011

Bhyravbhatla, B., Watowich, S. J., and Caspar, D. L. D. (1998). Refined Atomic Model of the Four-Layer Aggregate of the Tobacco Mosaic Virus Coat Protein at 2.4-Å Resolution. *Biophysical J.* 74, 604–615. doi:10.1016/s0006-3495(98)77819-1

Bos, L. (1982). Crop Losses Caused by Viruses. *Crop Prot.* 1, 263–282. doi:10.1016/0261-2194(82)90002-3

Chen, L., Hao, Y., Song, H., Liu, Y., Li, Y., Zhang, J., et al. (2020). Design, Synthesis, Characterization, and Biological Activities of Novel Spirooxindole Analogues Containing Hydantoin, Thiohydantoin, Urea, and Thiourea Moieties. *J. Agric. Food Chem.* 68, 10618–10625. doi:10.1021/acs.jafc.0c04488

Chen, M.-H., Chen, Z., Song, B.-A., Bhadury, P. S., Yang, S., Cai, X.-J., et al. (2009). Synthesis and Antiviral Activities of Chiral Thiourea Derivatives Containing an α-Aminophosphonate Moiety. *J. Agric. Food Chem.* 57, 1383–1388. doi:10.1021/jf803215t

Dake, S. A., Raut, D. S., Kharat, K. R., Mhaske, R. S., Deshmukh, S. U., and Pawar, R. P. (2011). Ionic Liquid Promoted Synthesis, Antibacterial and *In Vitro* Antiproliferative Activity of Novel α-aminophosphonate Derivatives. *Bioorg. Med. Chem. Lett.* 21 (8), 2527–2532. doi:10.1016/j.bmcl.2011.02.039

Ewies, E. F., El-Hussieny, M., El-Sayed, N. F., and Fouad, M. A. (2019). Design, Synthesis and Biological Evaluation of Novel α-aminophosphonate Oxadiazoles via Optimized Iron Triflate Catalyzed Reaction as Apoptotic Inducers. *Eur. J. Med. Chem.* 180 (15), 310–320. doi:10.1016/j.ejmech.2019.07.029

Fang, Y.-L., Wu, Z.-L., Xiao, M.-W., Tang, Y.-T., Li, K.-M., Ye, J., et al. (2016). One-Pot Three-Component Synthesis of Novel Diethyl((2-Oxo-1,2-Dihydroquinolin-3-Yl)(arylamino)methyl)phosphonate as Potential Anticancer Agents. *Ijms* 17 (5), 653–667. doi:10.3390/ijms17050653

Hansen, A. J., and Stace Smith, R. (1989). Antiviral Chemicals for Plant Disease Control. *Crit. Rev. Plant Sci.* 8, 45–88. doi:10.1080/07352688909382270

Hao, Y., Guo, J., Wang, Z., Liu, Y., Li, Y., Ma, D., et al. (2020b). Discovery of Tryptanthrins as Novel Antiviral and Anti-phytopathogenic-fungus Agents. *J. Agric. Food Chem.* 68, 5586–5595. doi:10.1021/acs.jafc.0c02101

Hao, Y., Wang, K., Wang, Z., Liu, Y., Ma, D., and Wang, Q. (2020a). Luotonin A and its Derivatives as Novel Antiviral and Antiphytopathogenic Fungus Agents. *J. Agric. Food Chem.* 68, 8764–8773. doi:10.1021/acs.jafc.0c04278

He, F., Shi, J., Wang, Y., Wang, S., Chen, J., Gan, X., et al. (2019). Synthesis, Antiviral Activity, and Mechanisms of Purine Nucleoside Derivatives Containing a Sulfonamide Moiety. *J. Agric. Food Chem.* 67 (31), 8459–8467. doi:10.1021/acs.jafc.9b02681

He, S., Ouyang, X., Huang, X., Hu, W., Dai, W., Tian, X., et al. (2015). Synthesis of Derivatives of Artesunate α-Aminophosphonate and Their Antimicrobial Activities. *Lddd* 12, 408–416. doi:10.2174/1570180812666141125004502

Hellal, A., Chafaa, S., Chafai, N., and Touafri, L. (2017). Synthesis, Antibacterial Screening and DFT Studies of Series of α-amino-phosphonates Derivatives from Aminophenols. *J. Mol. Struct.* 1134, 217–225. doi:10.1016/j.molstruc.2016.12.079

Huey, R., Morris, G. M., Olson, A. J., and Goodsell, D. S. (2007). A Semiempirical Free Energy Force Field with Charge-Based Desolvation. *J. Comput. Chem.* 28, 1145–1152. doi:10.1002/jcc.20634

Ji, R. J., Shi, W. M., Tian, D. Y., Zhang, G. P., and Wang, H. (2019). Facile Synthesis of Novel Dithioacetal-Naphthalene Derivatives as Potential Activators for Plant Resistance Induction. *RSC Adv.* 9, 32375–32381. doi:10.1039/c9ra06843k

Kang, J., Gao, Y., Zhang, M., Ding, X., Wang, Z., Ma, D., et al. (2020). Streptindole and its Derivatives as Novel Antiviral and Anti-phytopathogenic Fungus Agents. *J. Agric. Food Chem.* 68, 7839–7849. doi:10.1021/acs.jafc.0c03994

Krátký, M., Štěpánková, Š., Konečná, K., Svrčková, K., Maixnerová, J., Švarcová, M., et al. (2021). Novel Aminoguanidine Hydrazone Analogues: from Potential Antimicrobial Agents to Potent Cholinesterase Inhibitors. *Pharmaceuticals* 14, 1229–1259. doi:10.3390/ph14121229

Lan, X., Xie, D., Yin, L., Wang, Z., Chen, J., Zhang, A., et al. (2017). Novel α,β-unsaturated Amide Derivatives Bearing α-amino Phosphonate Moiety as Potential Antiviral Agents. *Bioorg. Med. Chem. Lett.* 27 (18), 4270–4273. doi:10.1016/j.bmcl.2017.08.048

Li, L., Zou, J., Xu, C., You, S., Deng, Z., Chen, G., et al. (2021). Preparation and Anti-tobacco Mosaic Virus Activities of Crocetin Diesters. *J. Agric. Food Chem.* 69 (45), 13637–13643. doi:10.1021/acs.jafc.1c03884

Li, L., Zou, J., You, S., Deng, Z., Liu, Y., and Wang, Q. (2019). Natural Product Cerbinal and its Analogues Cyclopenta[c]pyridines: Synthesis and Discovery as Novel Pest Control Agents. *J. Agric. Food Chem.* 67, 10498–10504. doi:10.1021/acs.jafc.9b03699

Liu, J.-Z., Song, B.-A., Fan, H.-T., Bhadury, P. S., Wan, W.-T., Yang, S., et al. (2010a). Synthesis and *In Vitro* Study of Pseudo-peptide Thioureas Containing α-aminophosphonate Moiety as Potential Antitumor Agents. *Eur. J. Med. Chem.* 45 (11), 5108–5112. doi:10.1016/j.ejmech.2010.08.021

Liu, M., Wang, Y., Wangyang, W.-z., Liu, F., Cui, Y.-l., Duan, Y.-s., et al. (2010b). Design, Synthesis, and Insecticidal Activities of Phthalamides Containing a Hydrazone Substructure. *J. Agric. Food Chem.* 58, 6858–6863. doi:10.1021/jf1000919

Liu, Y., Chen, J., Xie, D., Song, B., and Hu, D. (2021). First Report on Anti-TSWV Activities of Quinazolinone Derivatives Containing a Dithioacetal Moiety. *J. Agric. Food Chem.* 69, 12135–12142. doi:10.1021/acs.jafc.1c03171

Massarani, E., Nardi, D., Pozzi, R., and Degen, L. (1970). Arylglyoxal N,N-disubstituted Hydrazones with Antiviral and Antifungal Activity. *J. Med. Chem.* 13 (1), 157–159. doi:10.1021/jm00295a052

Poola, S., Nagaripati, S., Tellamekala, S., Chintha, V., Kotha, P., Yagani, J. R., et al. (2020). Green Synthesis, Antibacterial, Antiviral and Molecular Docking Studies of α-aminophosphonates. *Synth. Commun.* 50, 2655–2672. doi:10.1080/00397911.2020.1753079

Ritzenthaler, C. (2005). Resistance to Plant Viruses: Old Issue, News Answers? *Curr. Opin. Biotechnol.* 16, 118–122. doi:10.1016/j.copbio.2005.02.009

Song, B. A., Zhang, G. P., Hu, D. Y., Pang, L., Yang, S., Liu, G., et al. (2006). N-Substituted Benzothiazoline-1-Substituted Phenyl -O,O- Dialkyl -α- Amino Phosphonate Derivatives and Their Preparation Method and Application. CN 1291993C.

Trott, O., and Olson, A. J. (2009). AutoDock Vina: Improving the Speed and Accuracy of Docking with a New Scoring Function, Efficient Optimization, and Multithreading. *J. Comput. Chem.* 31, NA. doi:10.1002/jcc.21334

Wang, Y., Xu, F., Luo, D., Guo, S., He, F., Dai, A., et al. (2019). Synthesis of Anthranilic Diamide Derivatives Containing Moieties of Trifluoromethylpyridine and Hydrazone as Potential Anti-viral Agents for Plants. *J. Agric. Food Chem.* 67, 13344–13352. doi:10.1021/acs.jafc.9b05441

Wang, Z., Wei, P., Xizhi, X., Liu, Y., Wang, L., and Wang, Q. (2012). Design, Synthesis, and Antiviral Activity Evaluation of Phenanthrene-Based Antofine Derivatives. *J. Agric. Food Chem.* 60, 8544–8551. doi:10.1021/jf302746m

Yang, X., Song, B., Jin, L., Wei, X., Bhadury, S. P., Li, X., et al. (2011). Synthesis and Antiviral Bioactivities of Novel Chiral Bis-thiourea-type Derivatives Containing α-aminophosphonate Moiety. *Sci. China Chem.* 54 (1), 103–109. doi:10.1007/s11426-010-4129-5

Ye, M.-Y., Yao, G.-Y., Pan, Y.-M., Liao, Z.-X., Zhang, Y., and Wang, H.-S. (2014). Synthesis and Antitumor Activities of Novel α-aminophosphonate Derivatives Containing an Alizarin Moiety. *Eur. J. Med. Chem.* 83 (18), 116–128. doi:10.1016/j.ejmech.2014.02.067

Zan, N., Xie, D., Li, M., Jiang, D., and Song, B. (2020). Design, Synthesis, and Anti-ToCV Activity of Novel Pyrimidine Derivatives Bearing a Dithioacetal Moiety that Targets ToCV Coat Protein. *J. Agric. Food Chem.* 68, 6280–6285. doi:10.1021/acs.jafc.0c00987

Zhang, B., Hu, X.-T., Gu, J., Yang, Y.-S., Duan, Y.-T., and Zhu, H.-L. (2020). Discovery of Novel Sulfonamide-Containing Aminophosphonate Derivatives as Selective COX-2 Inhibitors and Anti-tumor Candidates. *Bioorg. Chem.* 105, 104390–110400. doi:10.1016/j.bioorg.2020.104390

Zhang, G.-P., and Liu, M. (2016). Novel Biphenyl Derivatives with ?-Aminophosphonate Moiety: Design, Synthesis and Antivirus Activity. *Lddd* 13, 706–714. doi:10.2174/1570180813666160125222813

Zhang, G.-P., Pan, J.-K., Zhang, J., Wu, Z.-X., Liu, D.-Y., and Zhao, L. (2017). Design, Synthesis, Antiviral Activities of Novel Phosphonate Derivatives Containing Quinazoline Based on Chalone Motif. *J. Heterocycl. Chem.* 54, 2548–2555. doi:10.1002/jhet.2849

Zhang, G., Hao, G., Pan, J., Zhang, J., Hu, D., and Song, B. (2016). Asymmetric Synthesis and Bioselective Activities of α-Amino-phosphonates Based on the Dufulin Motif. *J. Agric. Food Chem.* 64, 4207–4213. doi:10.1021/acs.jafc.6b01256

Zhang, J., He, F., Chen, J., Wang, Y., Yang, Y., Hu, D., et al. (2021). Purine Nucleoside Derivatives Containing a Sulfa Ethylamine Moiety: Design, Synthesis, Antiviral Activity, and Mechanism. *J. Agric. Food Chem.* 69, 5575–5582. doi:10.1021/acs.jafc.0c06612

Zhang, X., Qu, Y., Fan, X., Bores, C., Feng, D., Andrei, G., et al. (2010). Solvent-free Synthesis of Pyrimidine Nucleoside-Aminophosphonate Hybrids and Their Biological Activity Evaluation. *Nucleosides, Nucleotides Nucleic Acids* 29, 616–627. doi:10.1080/15257770.2010.496281

Zhou, X., Ye, Y., Liu, S., Shao, W., Liu, L., Yang, S., et al. (2021). Design, Synthesis and Anti-TMV Activity of Novel α-aminophosphonate Derivatives Containing a Chalcone Moiety that Induce Resistance against Plant Disease and Target the TMV Coat Protein. *Pesticide Biochem. Physiology* 172, 104749. doi:10.1016/j.pestbp.2020.104749

Applications of Chinese *Camellia oleifera* and its By-Products: A Review

Wenxuan Quan[1,2], Anping Wang[1], Chao Gao[2] and Chaochan Li[1]*

[1]*Guizhou Provincial Key Laboratory for Information Systems of Mountainous Areas and Protection of Ecological Environment, Guizhou Normal University, Guiyang, China, [2]Key Laboratory of Forest Cultivation in Plateau Mountain of Guizhou Province, Institute for Forest Resources and Environment of Guizhou, Guizhou University, Guiyang, China*

Camellia oleifera is a woody oil tree species unique to China that has been cultivated and used in China for more than 2,300 years. Most biological research on *C. oleifera* in recent years has focused on the development of new varieties and breeding. Novel genomic information has been generated for *C. oleifera*, including a high-quality reference genome at the chromosome level. Camellia seeds are used to process high-quality edible oil; they are also often used in medicine, health foods, and daily chemical products and have shown promise for the treatment and prevention of diseases. *C. oleifera* by-products, such as camellia seed cake, saponin, and fruit shell are widely used in the daily chemical, dyeing, papermaking, chemical fibre, textile, and pesticide industries. *C. oleifera* shell can also be used to prepare activated carbon electrodes, which have high electrochemical performance when used as the negative electrode of lithium-ion batteries. *C. oleifera* is an economically valuable plant with diverse uses, and accelerating the utilization of its by-products will greatly enhance its industrial value.

Keywords: camellia oil, by-products, medical value, activated carbon, applications

INTRODUCTION

Edible oil is an important food for humans that provides essential fatty acids and promotes the absorption of fat-soluble vitamins (Soussanaet 2014; Khatri and Jain, 2017). China is the world's largest consumer and second-largest producer of edible oil (Cassiday 2019; Bai et al., 2021), and the demand for edible oil in China continues to increase with the continued growth of the economy and improvement in living standards.

Edible vegetable oils in China include rapeseed oil, soybean oil, peanut oil, cottonseed oil, sunflower oil, sesame oil, camellia oil, and linseed oil (Bai et al., 2021). Vegetable oils are rich in nutrients and provide various health benefits: camellia oil in particular shows antibacterial activity against *Escherichia coli* (Yang et al., 2018).

Camellia oleifera Abel. is one of the four major sources of the world's edible oil, along with *Olea europaea* L., *Elaeis guineensis* Jacq., and *Cocos nucifera* L. (Ma et al., 2011). It is a perennial shrub or small arbour that grows in warm and humid hills and mountains and is mainly distributed in the southern provinces (regions) of China (**Figure 1**), including Zhejiang, Jiangxi, Henan, Hunan, and Guangxi Provinces; it also occurs in Thailand (Suealek et al., 2019). The varieties mainly include ordinary *Camellia oleifera*, *Camellia yuhsiensis* Hu, *Camellia chekangoleosa* Hu, *Camellia meiocarpa* Hu, Camellia vietnamensis T. C. Huang ex Hu, and *Camellia reticulata* Lindl (Liu et al., 2018a). Zhou et al. indicated that the germplasms of *C oleifera* possess high genetic diversity, as geographic isolation has affected the degree of genetic differentiation among populations (Zhou et al., 2015).

FIGURE 1 | Distribution **(A,B)** of *C. oleifera* and images of the flowers and fruits **(C,D)** of *C. oleifera* plants.
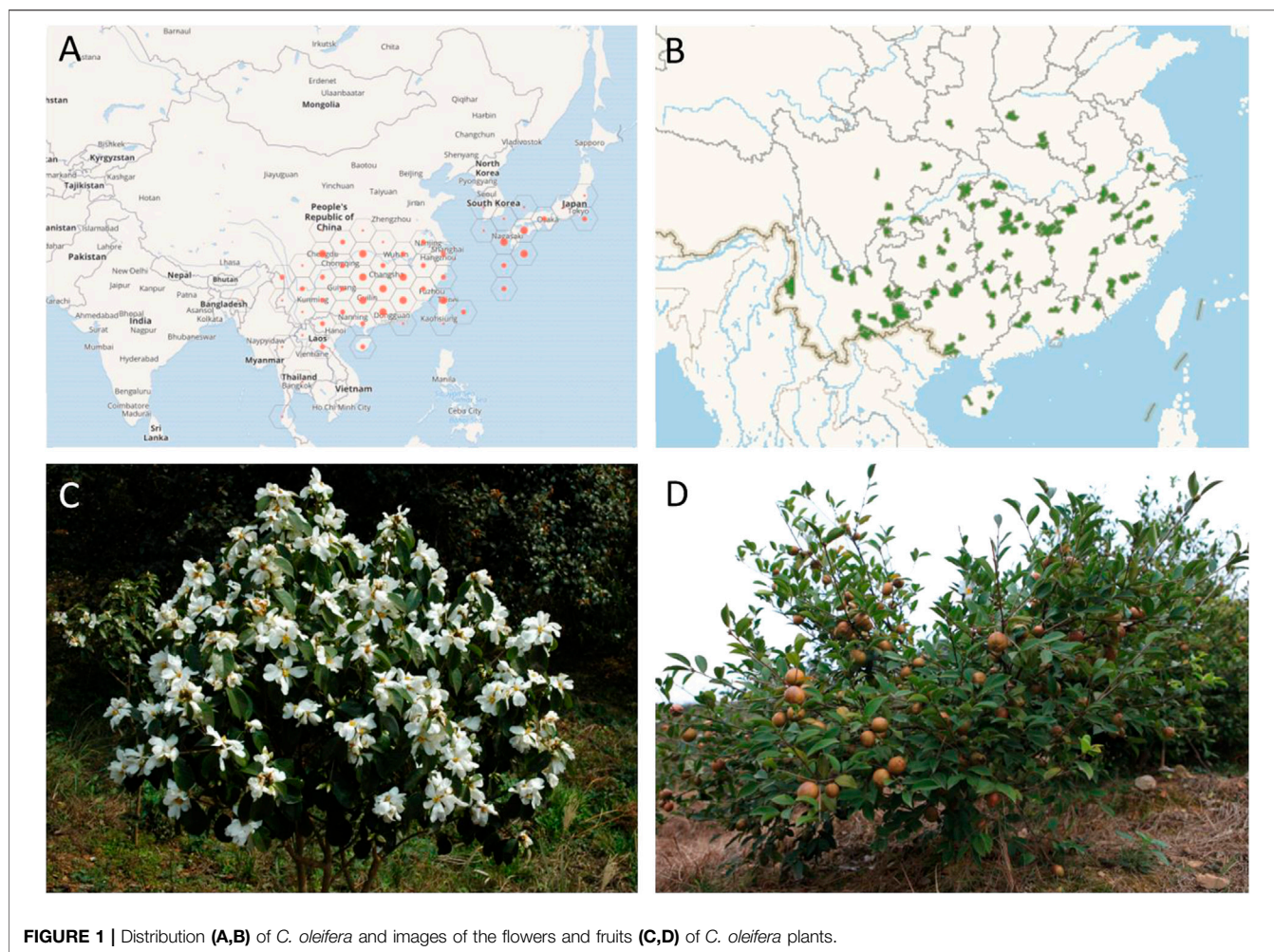
C. oleifera trees are evergreen and highly adaptable. The benefits of planting *C. oleifera* can be reaped for as long as a century. The total output value of the Chinese camellia industry was 116 billion yuan in 2019, and the plantation area of *C. oleifera* was 4.5 million hm^2; the camellia industry is a source of income for a total of 1.73 million people.

Figure 1A,B were obtained from the Global Biodiversity Information Facility (https://www.gbif.org/) and Map Bio of China (http://map.especies.cn/), respectively.

C. oleifera is an economically important tree species with high utilization value. The main product derived from *C. oleifera* is camellia oil, and other by-products include tea shell and tea meal. Tea meal can be further processed into tea saponin, and tea shell has been used to make furfural, xylitol, tannin extract, activated carbon, and culture medium (Robards et al., 2009).

RESEARCH ON THE BIOLOGY OF *C. OLEIFERA*

C. oleifera is a woody oil plant that is highly resistant to various types of stress. However, genetic and genomic information for this species is lacking (Yang et al., 2017). The large polyploid genome of *C. oleifera* makes genomic analyses rather challenging and hinders further molecular genetic improvement. Recently, an abundance of genomic information has been generated for *C. oleifera*. The published genome of *Camellia lanceoleosa* provides an important reference for analyzing the formation and regulation of important traits such as self-incompatibility and lipid synthesis (Gong et al., 2022). Construction of a high-quality reference genome at the chromosome level of *C. oleifera* has demonstrated that the alleles regulating the synthesis of *C. oleifera* have been under artificial selection, and this genome resource could provide new insights with implications for the genetic improvement of *C. oleifera* varieties (Lin et al., 2022). In addition, a high-quality, chromosome-level genome of *Camellia chekiangoleosa* has been published, and this has provided new insights into the adaptive evolution and oil metabolism of Camellia (Shen et al., 2022).

Wang et al. (2018) found that the total nitrogen content and dry weight accumulation of the seedlings are highest when NO_3^- and NH_4^+ (ratio 1:1) are applied. Liu et al. (2019b) found that a total of 797 miRNAs are significantly differentially expressed in the flowers and fruits of *C. oleifera*. miR156, miR390, and miR395

FIGURE 2 | Diagram illustrating the various industrial uses of *C. oleifera*.

regulate the expression of carbohydrate accumulation genes, and miR477 plays a key role in fatty acid synthesis. miR156 contributes to the expression of genes regulating glycolysis and nutrient transformation.

The high rate of flower and fruit drop in *C. oleifera*, especially under extreme climate conditions, affects *C. oleifera* yields. Hu et al. (2021) studied the relationship between ethylene and fruit abscission and found that the CoACO genes (*CoACO1* and *CoACO2*) regulate fruit abscission.

C. oleifera is highly tolerant of drought. An understanding of the molecular mechanism of drought tolerance is important. Dong et al. (2017) identified several 76,585 unigenes under drought stress using transcriptome technology and obtained functional annotations for 52,531 of the unigenes.

Other studies have examined the high-affinity Pi transporter gene and have characterized *rbcL* and *rbcS* genes from *C. oleifera* (Chen et al., 2015; Zhou et al., 2020). These findings are useful for identifying promising cultivars (**Figure 2**)

CAMELLIA OIL AND THE COMPOSITION OF ITS MAIN FATTY ACIDS

The oil content of the dry seeds of new cultivars and wild *C. oleifera* is approximately 47%; the dry seeds also possess volatile aroma components (Jia et al., 2021). The content of unsaturated fatty acids of *C. oleifera* oil is as high as 90%; oleic acid makes up more than 80% of these unsaturated fatty acids, and linoleic acid comprises 7–13% (Ma et al., 2011; Yang et al., 2016). Variation in the composition of

unsaturated fatty acids mainly stems from differences in genotype and extraction method (Zeng et al., 2019a) (**Table 1**). Fatty acids can be extracted using the petroleum ether, hydrolytic, or potassium hydroxide/methanol extraction methods. The fatty acid composition of camellia oil is mainly determined using gas chromatography or gas chromatography–mass spectrometry.

Oleic acid provides various health benefits (Farooqui 2013); olive oil is approximately 59–75% oleic acid (Newmark 1997), and palm oil contains 43% oleic acid (Waterman and Lockwood 2007). The main characteristic feature of camellia oil is its high oleic acid content compared with other woody edible oils.

C. OLEIFERA PRODUCTS

Medicinal Research on Camellia Oil

Camellia oil contains tocopherol, sterol, squalene, vitamin E, and flavonoids (Lee and Yen 2006; Robards 2009; Cao et al., 2017; Wang et al., 2017; Zeng and Endo 2019b), and these compounds are thought to aid weight loss and reduce the risks of cardiovascular and cerebrovascular diseases.

Camellia oil also contains large amounts of functional nutrients, such as squalene, plant sterols (e.g., β-sitosterol and campesterol), polyphenols (e.g., phenolic acid), tocopherols (α-, γ-, and δ-tocopherols), carotenoids (e.g., lycopene), β-carotene, and lutein (Wang et al., 2017; Wang et al., 2018; Yang et al., 2018). These active substances can delay the degradation of unsaturated fatty acids in camellia oil (Zhou et al., 2019), provide various health benefits (Luan

TABLE 1 | Fatty acid composition of camellia oil according to studies using different extraction methods.

No.	Analytical Method	Main Fatty Acids (% of the Total Fatty Acids)	References
1	Petroleum ether extraction and gas chromatography (GC)	82–84% unsaturated fatty acids (UFA),68–77% monounsaturated fatty acids (MUFA), 7–14% polyunsaturated fatty acids (PUFA).	Ma et al. (2011)
2	gas chromatography–mass spectrometry (GC–MS)	90% UFA, 66.54–83.24% oleic acid, 8.15–9.70% palmitic acid, 5.64–7.96% linoleic acid.	Yuan et al. (2012)
3	GC–MS	87.45–90.17% UFA, 77.08–82.78% MUFA, 5.17–11.27% PUFA.	Yang et al. (2016)
4	Hydrolytic extraction and GC	10–10.4% SFA, 89.55–90.00% UFA, 79.35–81.60% MUFA, 8.40–10.20% PUFA.	Cao et al. (2017)
5	GC	12.65–12.40% SFA, 79.16–81.05% MUFA, 8.19–8.04% PUFA.	Zhang et al. (2019)
6	Methanol extraction and GC–MS	87.85–91.44% UFA, 80.53– 86.18% oleic acid, 6.72–9.26% palmitic acid, 4.19–8.95% linoleic acid, 0.84–1.65% stearic acid, 0.09–0.26% eicosenoic acid	Liu et al. (2021)

TABLE 2 | Specific medicinal uses of camellia oil.

No.	Materials	Experimental Model	Specific Medicinal Use	References
1	Camellia seed	Male Wistar rats	Repair nonalcoholic fatty liver disease	Yeh et al. (2019)
2	Camellia oil	Male Sprague-Dawley rats	Repair oxidative damage in the stomach and intestine	Cheng et al. (2014)
3	Camellia oil	Male BALB/c mice	Ameliorate ethanol-induced acute gastric mucosal injury	Tu et al. (2017)
4	Camellia oil	Four-week-old male BALB/c mice	Repair gastrointestinal mucosal damage	Wang et al. (2019a)
5	Camellia oil	Human Int-407 cells; Female Sprague-Dawley rats	Mitigate Alzheimer's disease (AD)	Weng et al. (2020)
6	Camellia oil	Hamsters	Reduce fat	Suealeket al. (2019)
7	Camellia oil	Female ovariectomized mice	Reduce fat	Tung et al. (2019)
8	Camellia seed	Five human cancer cell lines	Anticancer: saponin OSC6 is a potential therapeutic agent for the treatment of cancer	Zong et al. (2016)
9	Camellia seed	Male ICR mice	Anticancer: a new glycoprotein (COG2a) has anticancer action.	Li et al. (2019)
10	Camellia seed	Wistar rats	Hepatoprotective effects	Ko et al. (2019)
11	Camellia oil	Male Sprague-Dawley rats	Alleviates colitis	Lee et al. (2018)
12	Camellia oil	2,2-diphenyl-1-picrylhydrazyl (DPPH) scavenging activity and Trolox equivalent antioxidant capacity	Free radical scavenging: two compounds isolated exhibit antioxidant activity.	Lee and Yen, (2006)

et al., 2020), and show antioxidant, anti-inflammatory, and antibacterial activity (Zhu et al., 2019). These compounds can also lower cholesterol, blood sugar, and blood lipids, relieve constipation, and reduce liver and gastrointestinal damage (**Table 2**).

Camellia oil can be used as a nutritional supplement and be further refined and processed into an advanced skin care product. Recently, the seed extract of camellia oil has been shown to reduce liver fat in rats (Yang et al., 2019).

The Main Nutrient Components of *Camellia* By-Products

Residues such as camellia seed cake, saponin, and fruit shells are widely used in the daily chemical, dyeing, papermaking, chemical fibre, textile, and pesticide industries (Liu et al., 2018b). Previous studies have shown that polysaccharides extracted from fruit shells have hypoglycemic effects (Zhang and Li, 2015; Gao et al., 2020).

The seeds remaining after oil extraction are by-products referred to as camellia seed cake (Xiao et al., 2017). Oil makes up approximately 5%–6% of the seed cake, and the remaining seed cake after extraction can be used to extract 4% of high-quality saponin (Zhu et al., 2018). Recent studies have shown that seed cakes contain large amounts of polyphenols and new saponins with antimelanogenic and hypoglycemic activity (Zhang et al., 2012; Zhang and Li 2018; Hong et al., 2019). For example, kaempferol extracted from seed cakes shows excellent scavenging activity of 2,2-diphenyl-1-picrylhydrazyl (DPPH) radical (Zheng et al., 2019), saponins show anticancer activity (Di et al., 2017; Wang et al., 2019a), and polysaccharides show hypoglycemic activity (Zhang and Li 2018; Zhu et al., 2018; Jin et al., 2019).

Saponin from *C. oleifera* is a natural plant pesticide that shows potential to be used for the control of insect and fungal pests (Zhang et al., 2014). Contact toxicity tests and gastric toxicity tests have shown that saponin is an effective insecticide against *Ectropis obliqua* (Cui et al., 2019).

FIGURE 3 | Structural characteristics **(A)** and morphological changes at different stages **(B)** of *C. oleifera* fruit.
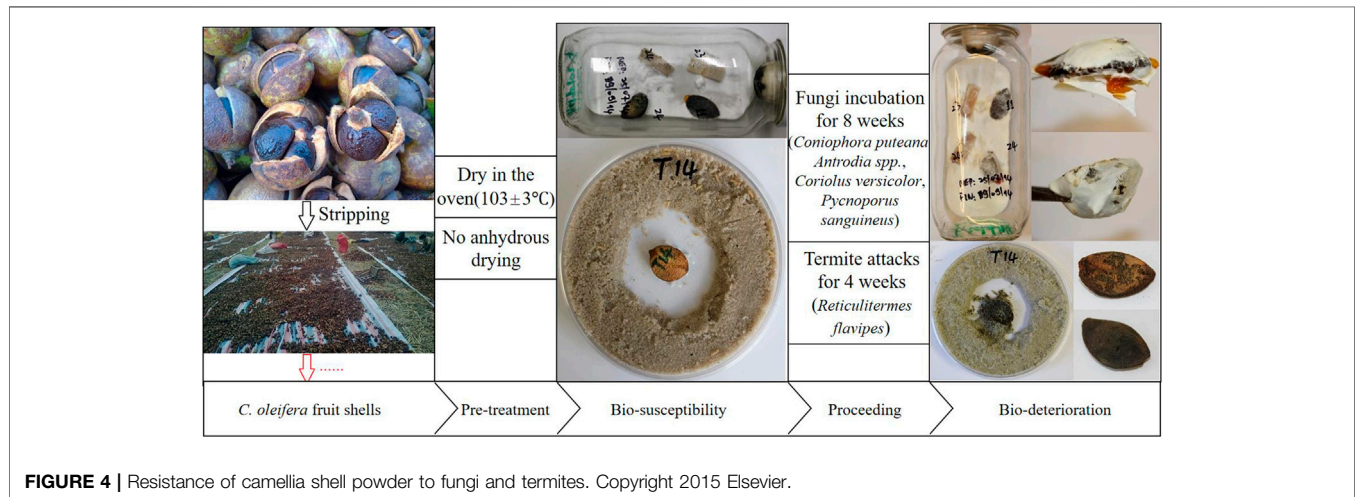
FIGURE 4 | Resistance of camellia shell powder to fungi and termites. Copyright 2015 Elsevier.

Saponin mixtures can also be used as a potential plant insecticide to control *Rhizoctonia* damping-off in vegetable seedlings (Kuo et al., 2010).

UTILIZATION OF *C. OLEIFERA* SHELL

Morphological Changes of Camellia Shell

C. oleifera shell is mainly composed of cellulose, hemicellulose, and lignin; it is generally used as waste given its low utilization efficiency (Hu et al., 2015). Approximately 54% of *C. oleifera* fruits are shells (Zhu et al., 2013; Zhao et al., 2017). Camellia shell is thus a rich biomass resource; the shells contain rich quantities

of lignin and are an ideal raw material for preparing activated carbon (Hu et al., 2018). Hu et al. (2018) and Wang et al. (2019b, 2021) showed that mature camellia shell is composed of stone cells, spiral vessels, and parenchyma, and the latter two are the main cell types (**Figure 3**).

Functions and Applications of Camellia Shell

The high-quality by-products of *C. oleifera* shell have been used in many industries. Camellia shell contains tannins, furfural, bioactive phenolic compounds (Zhang et al., 2013), and saponins (Chen et al., 2013; Xiong et al., 2018; Yu and Yong

FIGURE 5 | Porous carbon microspheres made from camellia shells by KOH chemical activation. Copyright 2016 Elsevier.
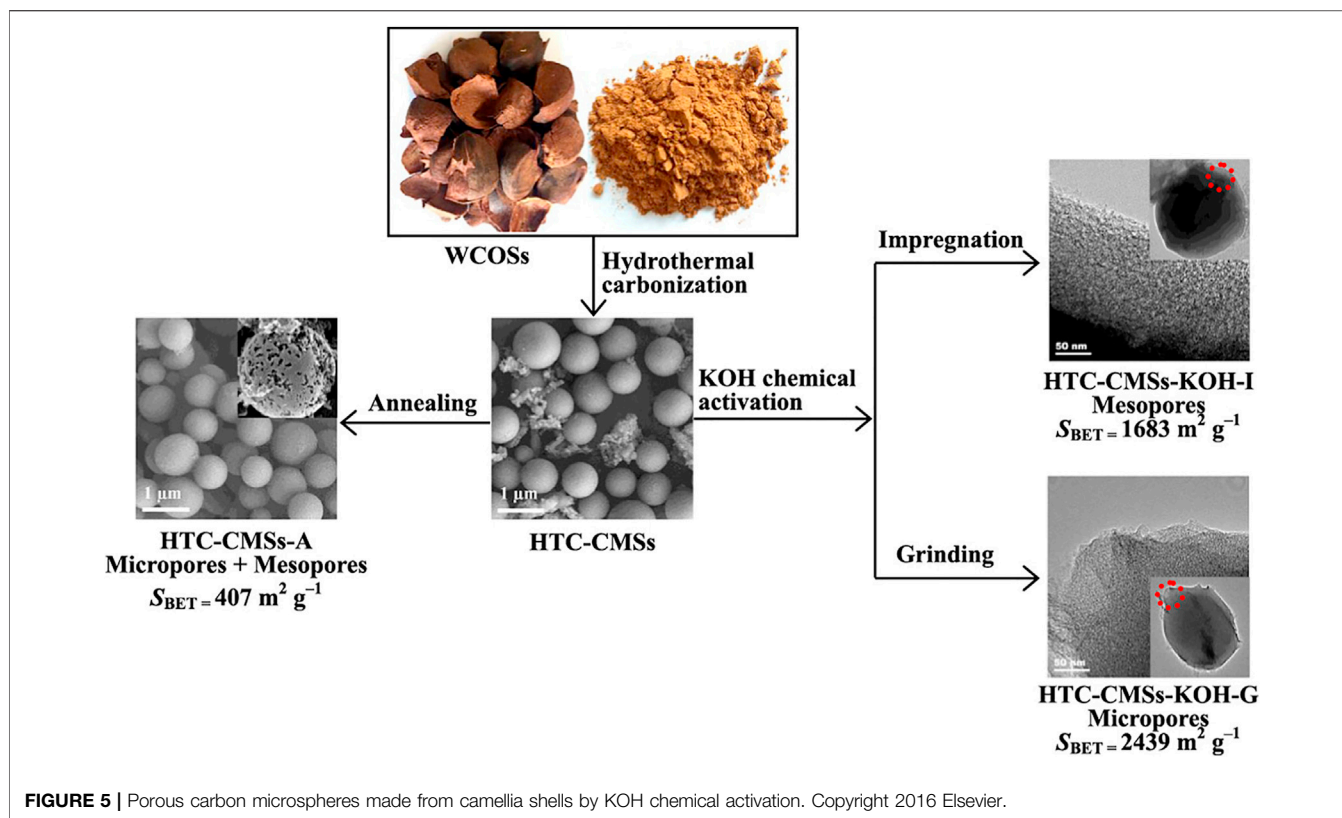
2018), which are used to make tannins, furfural, activated carbon, and other chemical raw materials. Zhu et al. (2013) used camellia shell to produce ethanol, vanillin, and xylooligosaccharides; camellia shell can also be used as a natural colourant for pigment printing on cotton fabrics (Nakpathom et al., 2017).

Previous studies have examined the ability of camellia shell extract to inhibit tyrosinase activity *in vitro* as well as the melanin inhibition of a cosmetic formula containing the extract in 30 female subjects. Camellia shell extract has been used as a skin whitening agent in cosmetic products (Liu et al., 2019a). Hu et al. (2015) investigated the resistance of camellia shell to fungi and termites; the shells appeared to be toxic to fungi and termites but did not completely eradicate them (**Figure 4**). This indicates that Camellia shell has the potential to be used as a green pesticide.

Application of Camellia Shell as High-Quality Activated Carbon

Activated carbon is widely used, and its most notable features are its large surface area, porosity, highly adsorptive internal porous structure, and low cost (Sakaray and Ramirez, 2014). *C. oleifera* shell is composed of cellulose, hemicellulose, and lignin, and highly developed mesoporous activated carbon can be formed through various technologies. The advantages of Camellia shell activated carbon mainly include its high yield and low cost, as well as the fact that it provides a guaranteed source of raw materials; Camellia shell activated carbon also shows high electrical conductivity and can be used as electrodes. Activated carbon

has been obtained from many other plant materials, and these activated carbons, such as macadamia nut shell (Wang et al., 2002), *Terminalia catappa* shell (Inbaraj and Sulochana, 2006), peanut shell (Wu et al., 2013), durian fruit shell (Tey et al., 2016), baobab fruit shell (Vunain et al., 2017), *Aegle marmelos* Correa fruit shell (Sivarajasekar et al., 2018), and *Swietenia macrophylla* fruit shell (Hossain et al., 2021), show high application prospects.

Camellia shell activated carbon is a porous carbon material generated through the carbonization and activation process and an economically important chemical product. It shows high selective adsorption and is widely used in decolorization and water purification. Camellia shell activated carbon has more functions compared with the conventional activated carbon, and Camellia shell activated carbon products with different adsorption characteristics can be prepared using various methods (Sun et al., 2011; Guo et al., 2016, 2018; Fan et al., 2017; Nie et al., 2019). *C. oleifera* shell can be used to synthesize zirconium dioxide biochar and improve the removal of fluorine in water (Lei et al., 2019).

Activated carbon produced by the steam method has many micropores, which is suitable for adsorbing small molecular impurities. The activated carbon produced by the phosphoric acid method has many mesopores and is suitable for adsorbing macromolecular impurities. The phosphoric acid method has become the main method used in the industrial production of activated carbon from husks because it generates fewer pollutants compared with other methods. *C. oleifera* shell carbon can remove hexavalent chromium and methylene blue from water

by adsorption (Ma et al., 2019); the shell has similar burning properties to ordinary wood (Tan et al., 2020). It can also rapidly remove phenolic pollutants in water (**Figure 5**) (Li et al., 2016).

Activated carbon electrodes can be prepared from *C. oleifera* shell, and this is a particularly efficient method for using camellia resources. Zhang et al. (2012) used *C. oleifera* shell to prepare activated carbon electrodes using the $ZnCl_2$ activation method. Ma et al. (2019) made a porous carbon material synthesized from *C. oleifera* shells *via* K_2CO_3 impregnation and pyrolysis, and this material has excellent electrochemical properties when it is used as the anode of Li-ion batteries. Porous carbon with a three-dimensional porous architecture, large surface area, and electrochemical-active oxygen functionalities has been prepared using the microwave-assisted carbonization/activation method (Liang et al., 2018).

CONCLUSION AND PROSPECTS

In this review, recent research on *C. oleifera* was summarized, including physiological and ecological research on *C. oleifera* trees, as well as research on the quality and function of camellia oil and the various uses of camellia by-products. The camellia industry has a long industrial chain, and the results of recent research have promoted the development of the entire industrial chain.

C. oleifera oil is a high-end edible oil with high medicinal value. The unsaturated fatty acid content of *C. oleifera* oil is greater than 80%. The oil can be used as a nutritional supplement and can also be further refined into an advanced skin care product. Camellia oil can aid weight loss and reduce the risk of cardiovascular and cerebrovascular diseases.

Camellia seed cake has high medicinal value and can be used to develop several products. The seed cake contains a large number of tea polyphenols and saponins, which show anti-melanin, hypoglycemic, antibacterial, and insecticidal activity.

Camellia shells can be used to prepare high-quality activated carbon and electrodes. The shell activated carbon is a porous carbon material generated through the carbonization and activation process that is widely used in decolourization and water purification. The shell is a residue produced during the production process and is not effectively utilized; making full use of this waste to prepare high value-added products should thus be a major focus of future research.

AUTHOR CONTRIBUTIONS

CL conceived the structure of the manuscript. WQ, CG, and AW collected materials and data. WQ wrote the manuscript. CL revised and approved the manuscript.

FUNDING

REFERENCES

Bai, Y., Zhai, Y., Ji, C., Zhang, T., Chen, W., Shen, X., et al. (2021). Environmental Sustainability Challenges of China's Edible Vegetable Oil Industry: from Farm to Factory. *Resour. Conservation Recycl.* 170, 105606. doi:10.1016/j.resconrec.2021.105606

Cao, Y., Yao, X., Ren, H., and Wang, K. (2017). Determination of Fatty Acid Composition and Metallic Element Content of Four Camellia Species Used for Edible Oil Extraction in China. *J. Consum. Prot. Food Saf.* 12, 165–169. doi:10.1007/s00003-017-1104-2

Cassiday, L. (2017). China's Evolving Edible Oils Industry. *Inform* 28, 6–9. doi:10.21748/inform.04.2017.06

Chen, L., Chen, J., and Xu, H. (2013). Sasanquasaponin from *Camellia Oleifera* Abel. Induces Cell Cycle Arrest and Apoptosis in Human Breast Cancer MCF-7 Cells. *Fitoterapia* 84, 123–129. doi:10.1016/j.fitote.2012.11.009

Chen, Y., Wang, B., Chen, J., Wang, X., Wang, R., Peng, S., et al. (2015). Identification of Rubisco rbcL and rbcS in *Camellia Oleifera* and Their Potential as Molecular Markers for Selection of High Tea Oil Cultivars. *Front. Plant Sci.* 06, 189. doi:10.3389/fpls.2015.00189

Cheng, Y.-T., Wu, S.-L., Ho, C.-Y., Huang, S.-M., Cheng, C.-L., and Yen, G.-C. (2014). Beneficial Effects of Camellia Oil (Camellia Oleifera Abel.) on Ketoprofen-Induced Gastrointestinal Mucosal Damage through Upregulation of HO-1 and VEGF. *J. Agric. Food Chem.* 62, 642–650. doi:10.1021/jf404614k

Cui, C., Yang, Y., Zhao, T., Zou, K., Peng, C., Cai, H., et al. (2019). Insecticidal Activity and Insecticidal Mechanism of Total Saponins from *Camellia Oleifera*. *Molecules* 24, 4518. doi:10.3390/molecules24244518

Di, T.-M., Yang, S. L., Yang, S.-L., Du, F.-Y., Zhao, L., Xia, T., et al. (2017). Cytotoxic and Hypoglycemic Activity of Triterpenoid Saponins from *Camellia*

Oleifera Abel. Seed Pomace. *Molecules* 22, 1562. doi:10.3390/molecules22101562

Dong, B., Wu, B., Hong, W., Li, X., Li, Z., Xue, L., et al. (2017). Transcriptome Analysis of the Tea Oil Camellia (*Camellia Oleifera*) Reveals Candidate Drought Stress Genes. *PLoS ONE* 12, e0181835. doi:10.1371/journal.pone.0181835

Fan, F., Zheng, Y., Huang, Y., Lu, Y., Wang, Z., Chen, B., et al. (2017). Preparation and Characterization of Biochars from Waste Camellia Oleifera Shells by Different Thermochemical Processes. *Energy Fuels* 31, 8146–8151. doi:10.1021/acs.energyfuels.7b00269

Farooqui, A. A. (2013). "Beneficial Effects of Extra Virgin Olive Oil (N-9 Fatty Acids) on Neurological Disorders," in *Phytochemicals, Signal Transduction, and Neurological Disorders* (New York, NY: Springer). doi:10.1007/978-1-4614-3804-5_2

Gao, C., Cai, C., Liu, J., Wang, Y., Chen, Y., Wang, L., et al. (2020). Extraction and Preliminary Purification of Polysaccharides from *Camellia Oleifera* Abel. Seed Cake Using a Thermoseparating Aqueous Two-phase System Based on EOPO Copolymer and Deep Eutectic Solvents. *Food Chem.* 313, 126164. doi:10.1016/j.foodchem.2020.126164

Gong, W., Xiao, S., Wang, L., Liao, Z., Chang, Y., Mo, W., et al. (2022). Chromosome-level Genome of Camellia Lanceoleosa Provides a Valuable Resource for Understanding Genome Evolution and Self-incompatibility. *Plant J.* 110, 881–898. doi:10.1111/tpj.15739

Guo, H., Bi, C., Zeng, C., Ma, W., Yan, L., Li, K., et al. (2018). *Camellia Oleifera* Seed Shell Carbon as an Efficient Renewable Bio-Adsorbent for the Adsorption Removal of Hexavalent Chromium and Methylene Blue from Aqueous Solution. *J. Mol. Liq.* 249, 629–636. doi:10.1016/j.molliq.2017.11.096

Guo, H., Yan, L., Song, D., and Li, K. (2016). Citric Acid modifiedCamellia Oleiferashell for Removal of Crystal Violet and Pb(II): Parameters Study

and Kinetic and Thermodynamic Profile. *Desalination Water Treat.* 57, 15373–15383. doi:10.1080/19443994.2015.1072057

Hong, C., Chang, C., Zhang, H., Jin, Q., Wu, G., and Wang, X. (2019). Identification and Characterization of Polyphenols in Different Varieties of *Camellia Oleifera* Seed Cakes by UPLC-QTOF-MS. *Food Res. Int.* 126, 108614. doi:10.1016/j.foodres.2019.108614

Hossain, M., Goni, L. K. M. O., Muntaha, N., Jamal, M. S., Jamal, M. S., Sujan, S. M. A., et al. (2021). Box-Behnken Design-Based Optimization for Biodiesel Production from Waste Cooking Oil Using Mahogany (Swietenia Macrophylla) Fruit Shell Derived Activated Carbon as a Heterogeneous Base Catalyst. *Reac. Kinet. Mech. Cat.* 133, 117–138. doi:10.1007/s11144-021-01995-w

Hu, J., Chang, S., Peng, K., Hu, K., and Thévenon, M.-F. (2015). Bio-susceptibility of Shells of *Camellia Oleifera* Abel. Fruits to Fungi and Termites. *Int. Biodeterior. Biodegrad.* 104, 219–223. doi:10.1016/j.ibiod.2015.06.011

Hu, J., Shi, Y., Liu, Y., and Chang, S. (2018). Anatomical Structure of *Camellia Oleifera* Shell. *Protoplasma* 255, 1777–1784. doi:10.1007/s00709-018-1271-8

Hu, X., Yang, M., Gong, S., Li, H., Zhang, J., Sajjad, M., et al. (2021). Ethylene-regulated Immature Fruit Abscission Is Associated with Higher Expression of CoACO Genes in *Camellia Oleifera*. *R. Soc. Open Sci.* 8, 202340. doi:10.1098/rsos.202340

Inbaraj, B., and Sulochana, N. (2006). Mercury Adsorption on a Carbon Sorbent Derived from Fruit Shell of *Terminalia catappa*. *J. Hazard. Mater.* 133, 283–290. doi:10.1016/j.jhazmat.2005.10.025

Jia, X., Deng, Q., Yang, Y., Xiang, X., Zhou, X., Tan, C., et al. (2021). Unraveling of the Aroma-Active Compounds in Virgin Camellia Oil (*Camellia Oleifera* Abel) Using Gas Chromatography-Mass Spectrometry-Olfactometry, Aroma Recombination, and Omission Studies. *J. Agric. Food Chem.* 69, 9043–9055. doi:10.1021/acs.jafc.0c07321

Jin, R., Guo, Y., Xu, B., Wang, H., and Yuan, C. (2019). Physicochemical Properties of Polysaccharides Separated from *Camellia Oleifera* Abel Seed Cake and its Hypoglycemic Activity on Streptozotocin-Induced Diabetic Mice. *Int. J. Biol. Macromol.* 125, 1075–1083. doi:10.1016/j.ijbiomac.2018.12.059

Kang, S., Jian-chun, J., and Dan-dan, C. (2011). Preparation of Activated Carbon with Highly Developed Mesoporous Structure from *Camellia Oleifera* Shell through Water Vapor Gasification and Phosphoric Acid Modification. *Biomass Bioenergy* 35, 3643–3647. doi:10.1016/j.biombioe.2011.05.007

Khatri, P., and Jain, S. (2017). Environmental Life Cycle Assessment of Edible Oils: A Review of Current Knowledge and Future Research Challenges. *J. Clean. Prod.* 152, 63–76. doi:10.1016/j.jclepro.2017.03.096

Ko, J., Yeh, W. J., Huang, W. C., and Yang, H. Y. (2019). Camellia Oleifera Seed Extract Mildly Ameliorates Carbon Tetrachloride-Induced Hepatotoxicity in Rats by Suppressing Inflammation. *J. Food Sci.* 84, 1586–1591. doi:10.1111/1750-3841.14645

Kuo, P.-C., Lin, T.-C., Yang, C.-W., Lin, C.-L., Chen, G.-F., and Huang, J.-W. (2010). Bioactive Saponin from Tea Seed Pomace with Inhibitory Effects against Rhizoctonia Solani. *J. Agric. Food Chem.* 58, 8618–8622. doi:10.1021/jf1017115

Lee, C.-P., and Yen, G.-C. (2006). Antioxidant Activity and Bioactive Compounds of Tea Seed (*Camellia Oleifera* Abel.) Oil. *J. Agric. Food Chem.* 54, 779–784. doi:10.1021/jf052325a

Lee, W.-T., Tung, Y.-T., Wu, C.-C., Tu, P.-S., and Yen, G.-C. (2018). Camellia Oil (Camellia Oleifera Abel.) Modifies the Composition of Gut Microbiota and Alleviates Acetic Acid-Induced Colitis in Rats. *J. Agric. Food Chem.* 66, 7384–7392. doi:10.1021/acs.jafc.8b02166

Lei, Z., Wang, S., Fu, H., Gao, W., Wang, B., Zeng, J., et al. (2019). Thermal Pyrolysis Characteristics and Kinetics of Hemicellulose Isolated from *Camellia Oleifera* Shell. *Bioresour. Technol.* 282, 228–235. doi:10.1016/j.biortech.2019.02.131

Li, K., Liu, S., Shu, T., Yan, L., Guo, H., Dai, Y., et al. (2016). Fabrication of Carbon Microspheres with Controllable Porous Structure by Using Waste *Camellia Oleifera* Shells. *Mater. Chem. Phys.* 181, 518–528. doi:10.1016/j.matchemphys.2016.06.089

Li, T., Meng, X., Wu, C., Fan, G., Yang, J., and Pan, W. (2019). Anticancer Activity of a Novel Glycoprotein from *Camellia Oleifera* Abel Seeds against Hepatic Carcinoma *in vitro* and *in vivo*. *Int. J. Biol. Macromol.* 136, 284–295. doi:10.1016/j.ijbiomac.2019.06.054

Liang, J., Qu, T., Kun, X., Zhang, Y., Chen, S., Cao, Y.-C., et al. (2018). Microwave Assisted Synthesis of *Camellia Oleifera* Shell-Derived Porous Carbon with Rich Oxygen Functionalities and Superior Supercapacitor Performance. *Appl. Surf. Sci.* 436, 934–940. doi:10.1016/j.apsusc.2017.12.142

Lin, P., Wang, K., Wang, Y., Hu, Z., Yan, C., Huang, H., et al. (2022). The Genome of Oil-Camellia and Population Genomics Analysis Provide Insights into Seed Oil Domestication. *Genome Biol.* 23, 14. doi:10.1186/s13059-021-02599-2

Liu, C., Chen, L., Tang, W., Peng, S., Li, M., Deng, N., et al. (2018a). Predicting Potential Distribution and Evaluating Suitable Soil Condition of Oil Tea Camellia in China. *Forests* 9, 487. doi:10.3390/f9080487

Liu, L., Cheng, X. X., Cheng, X., Zhao, W., Wang, Y., Dong, X., et al. (2018b). Systematic Characterization of Volatile Organic Components and Pyrolyzates from *Camellia Oleifera* Seed Cake for Developing High Value-Added Products. *Arabian J. Chem.* 11, 802–814. doi:10.1016/j.arabjc.2017.12.031

Liu, L., Feng, S., Chen, T., Zhou, L., Yuan, M., Liao, J., et al. (2021). Quality Assessment of *Camellia Oleifera* Oil Cultivated in Southwest China. *Separations* 8, 144. doi:10.3390/separations8090144

Liu, W., Wang, M., Xu, S., Gao, C., and Liu, J. (2019a). Inhibitory Effects of Shell of *Camellia Oleifera* Abel Extract on Mushroom Tyrosinase and Human Skin Melanin. *J. Cosmet. Dermatol.* 18, 1955–1960. doi:10.1111/jocd.12921

Liu, X.-X., Luo, X.-F., Luo, K.-X., Liu, Y.-L., Pan, T., Li, Z.-Z., et al. (2019b). Small RNA Sequencing Reveals Dynamic microRNA Expression of Important Nutrient Metabolism during Development of *Camellia Oleifera* Fruit. *Int. J. Biol. Sci.* 15, 416–429. doi:10.7150/ijbs.26884

Luan, F., Zeng, J., Yang, Y., He, X., Wang, B., Gao, Y., et al. (2020). Recent Advances in *Camellia Oleifera* Abel: A Review of Nutritional Constituents, Biofunctional Properties, and Potential Industrial Applications. *J. Funct. Foods* 75, 104242. doi:10.1016/j.jff.2020.104242

Ma, B., Huang, Y., Nie, Z., Qiu, X., Su, D., Wang, G., et al. (2019). Facile Synthesis of *Camellia Oleifera* Shell-Derived Hard Carbon as an Anode Material for Lithium-Ion Batteries. *RSC Adv.* 9, 20424–20431. doi:10.1039/C9RA03345A

Ma, J., Ye, H., Rui, Y., Chen, G., and Zhang, N. (2011). Fatty Acid Composition of *Camellia Oleifera* Oil. *J. Verbr. Leb.* 6, 9–12. doi:10.1007/s00003-010-0581-3

Nakpathom, M., Somboon, B., Narumol, N., and Mongkholrattanasit, R. (2017). Fruit Shells of *Camellia Oleifera* Abel as Natural Colourants for Pigment Printing of Cotton Fabric. *Prt* 46, 56–63. doi:10.1108/PRT-01-2016-0010

Newmark, H. L. (1999). Squalene, Olive Oil, and Cancer Risk: Review and Hypothesis. *Ann. N. Y. Acad. Sci.* 889, 193–203. doi:10.1111/j.1749-6632.1999.tb08735.x

Nie, Z., Huang, Y., Ma, B., Qiu, X., Zhang, N., Xie, X., et al. (2019). Nitrogen-doped Carbon with Modulated Surface Chemistry and Porous Structure by a Stepwise Biomass Activation Process towards Enhanced Electrochemical Lithium-Ion Storage. *Sci. Rep.* 9, 15032. doi:10.1038/s41598-019-50330-w

Robards, K., Prenzler, P., Ryan, D., and Zhong, H. (2009). "Camellia Oil and Tea Oil," in *Gourmet and Health-Promoting Specialty Oils*. Editors Robert A. Moreau and Afaf Kamal-Eldin (AOCS Press), 313–343. doi:10.1016/B978-1-893997-97-4.50017-6

Sakaray, A., and Ramirez, D. (2014). "Manufacture and Physical Characterization of Wood-Derived Activated Carbon from South texas Mesquite for Environmental Applications," in *Environmental Sustainability Issues in the South Texas–Mexico Border Region*. Editors D. Ramirez, J. Ren, K. Jones, and H. Lamm (Dordrecht: Springer). doi:10.1007/978-94-007-7122-2_6

Shen, T. F., Huang, B., Xu, M., Zhou, P. Y., Ni, Z. X., Gong, C., et al. (2022). The Reference Genome of *Camellia Chekiangoleosa* Provides Insights into Camellia Evolution and Tea Oil Biosynthesis. *Hortic. Res.* 9, uhab083. doi:10.1038/hortres.2022.uhab08310.1093/hr/uhab083

Sivarajasekar, N., Mohanraj, N., Baskar, R., and Sivamani, S. ((2018)). Fixed-bed Adsorption of Ranitidine Hydrochloride onto Microwave Assisted-Activated Aegle Marmelos Correa Fruit Shell: Statistical Optimization and Breakthrough Modelling. *Arab. J. Sci. Eng.* 43, 2205–2215. doi:10.1007/s13369-017-2565-4

Soussana, J.-F. (2014). Research Priorities for Sustainable Agri-Food Systems and Life Cycle Assessment. *J. Clean. Prod.* 73, 19–23. doi:10.1016/j.jclepro.2014.02.061

Suealek, N., Yokoyama, W. H., Rojpibulstit, P., Holt, R. R., and Hackman, R. M. (2019). Thai Tea Seed (Camellia Oleifera) Oil Favorably Affects Plasma Lipid

Responses in Hamsters Fed High-Fat Diets. *Eur. J. Lipid Sci. Technol.* 121, 1800024. doi:10.1002/ejlt.201800024

Tan, M., Luo, L., Wu, Z., Huang, Z., Zhang, J., Huang, J., et al. (2020). Pelletization of *Camellia Oleifera* Abel. Shell after Storage: Energy Consumption and Pellet Properties. *Fuel Process. Technol.* 201, 106337. doi:10.1016/j.fuproc.2020. 106337

Tey, J. P., Careem, M. A., Yarmo, M. A., Arof, A. K., and Arof, A. K. (2016). Durian Shell-Based Activated Carbon Electrode for EDLCs. *Ionics* 22, 1209–1216. doi:10.1007/s11581-016-1640-2

Tu, P.-S., Tung, Y.-T., Lee, W.-T., and Yen, G.-C. (2017). Protective Effect of Camellia Oil (*Camellia Oleifera* Abel.) against Ethanol-Induced Acute Oxidative Injury of the Gastric Mucosa in Mice. *J. Agric. Food Chem.* 65, 4932–4941. doi:10.1021/acs.jafc.7b01135

Tung, Y.-T., Hsu, Y.-J., Chien, Y.-W., Huang, C.-C., Huang, W.-C., and Chiu, W.-C. (2019). Tea Seed Oil Prevents Obesity, Reduces Physical Fatigue, and Improves Exercise Performance in High-Fat-Diet-Induced Obese Ovariectomized Mice. *Molecules* 24, 980. doi:10.3390/molecules24050980

Vunain, E., Kenneth, D., and Biswick, T. (2017). Synthesis and Characterization of Low-Cost Activated Carbon Prepared from Malawian Baobab Fruit Shells by H3PO4 Activation for Removal of Cu(II) Ions: Equilibrium and Kinetics Studies. *Appl. Water Sci.* 7, 4301–4319. doi:10.1007/s13201-017-0573-x

Wang, D., Huo, R., Cui, C., Gao, Q., Zong, J., Wang, Y., et al. (2019a). Anticancer Activity and Mechanism of Total Saponins from the Residual Seed Cake of *Camellia Oleifera* Abel. In Hepatoma-22 Tumor-Bearing Mice. *Food Funct.* 10, 2480–2490. doi:10.1039/C9FO00069K

Wang, Q., Chang, S., Tan, Y., and Hu, J. (2019b). Mesopore Structure in *Camellia Oleifera* Shell. *Protoplasma* 256, 1145–1151. doi:10.1007/s00709-019-01371-5

Wang, Q., Hu, J., Yang, T., and Chang, S. (2021). Anatomy and Lignin Deposition of Stone Cell in *Camellia Oleifera* Shell during the Young Stage. *Protoplasma* 258, 361–370. doi:10.1007/s00709-020-01568-z

Wang, R., Chen, L., Chen, J., Chen, Y., Zhang, Z., Wang, X., et al. (2018). Different Nitrate and Ammonium Ratios Affect Growth and Physiological Characteristics of Camellia Oleifera Abel. Seedlings. *Forests* 9, 784. doi:10. 3390/f9120784

Wang, X., Zeng, Q., del Mar Contreras, M., and Wang, L. (2017). Profiling and Quantification of Phenolic Compounds in Camellia Seed Oils: Natural Tea Polyphenols in Vegetable Oil. *Food Res. Int.* 102, 184–194. doi:10.1016/j. foodres.2017.09.089

Wang, Z.-M., Kanoh, H., Kaneko, K., Lu, G. Q., and Do, D. (2002). Structural and Surface Property Changes of Macadamia Nut-Shell Char upon Activation and High Temperature Treatment. *Carbon* 40, 1231–1239. doi:10.1016/S0008-6223(01)00286-X

Waterman, E., and Lockwood, B. (2007). Active Components and Clinical Applications of Olive Oil. *Altern. Med. Rev.* 12, 331–342.

Weng, M.-H., Chen, S.-Y., Li, Z.-Y., and Yen, G.-C. (2020). Camellia Oil Alleviates the Progression of Alzheimer's Disease in Aluminum Chloride-Treated Rats. *Free Radic. Biol. Med.* 152, 411–421. doi:10.1016/j.freeradbiomed.2020.04.004

Wu, M., Guo, Q., and Fu, G. (2013). Preparation and Characteristics of Medicinal Activated Carbon Powders by CO2 Activation of Peanut Shells. *Powder Technol.* 247, 188–196. doi:10.1016/j.powtec.2013.07.013

Xiao, X., He, L., Chen, Y., Wu, L., Wang, L., and Liu, Z. (2017). Anti-inflammatory and Antioxidative Effects of *Camellia Oleifera* Abel Components. *Future Med. Chem.* 9, 2069–2079. doi:10.4155/fmc-2017-0109

Xiong, W., Fu, J.-P., Hu, J.-W., Wang, H.-B., Han, X.-D., and Wu, L. (2018). Secondary Metabolites from the Fruit Shells of *Camellia Oleifera*. *Chem. Nat. Compd.* 54, 1189–1191. doi:10.1007/s10600-018-2592-8

Yang, C., Liu, X., Chen, Z., Lin, Y., and Wang, S. (2016). Comparison of Oil Content and Fatty Acid Profile of Ten New *Camellia Oleifera* Cultivars. *J. Lipids* 2016, 3982486. doi:10.1155/2016/3982486

Yang, H.-Y., Yeh, W.-J., Ko, J., and Chen, J.-R. (2019). *Camellia Oleifera* Seed Extract Attenuated Abdominal and Hepatic Fat Accumulation in Rats Fed a High-Fat Diet. *Appl. Physiol. Nutr. Metab.* 44, 320–325. doi:10.1139/apnm-2018-0392

Yang, H., Zhou, H. Y., Yang, X. N., Zhan, J. J., Zhou, H., Wang, C., et al. (2017). Transcriptomic Analysis of *Camellia Oleifera* in Response to Drought Stress Using High Throughput RNA-Seq. *Russ. J. Plant Physiol.* 64, 728–737. doi:10. 1134/S1021443717050168

Yang, R., Zhang, L., Li, P., Yu, L., Mao, J., Wang, X., et al. (2018). A Review of Chemical Composition and Nutritional Properties of Minor Vegetable Oils in China. *Trends Food Sci. Technol.* 74, 26–32. doi:10.1016/j.tifs.2018.01.013

Yeh, W.-J., Ko, J., Huang, W.-C., Cheng, W.-Y., and Yang, H.-Y. (2019). Crude Extract of Camellia Oleifera Pomace Ameliorates the Progression of Non-alcoholic Fatty Liver Disease via Decreasing Fat Accumulation, Insulin Resistance and Inflammation. *Br. J. Nutr.* 123, 508–515. doi:10.1017/S0007114519003027

Yu, X.-L., and He, Y. (2018). Tea Saponins: Effective Natural Surfactants Beneficial for Soil Remediation, from Preparation to Application. *RSC Adv.* 8, 24312–24321. doi:10.1039/c8ra02859a

Yuan, J. J., Wang, C. Z., Chen, H. X., Ye, J. Z., and Zhou, H. (2012). Oil Content and Fatty Acid Composition Analysis of Different Varieties of Camellia Oleifera Seeds. *China Oils Fats* 37, 75–79. doi:10.3969/j.issn.1003-7969.2012. 01.019

Zeng, W., and Endo, Y. (2019a). Effects of Cultivars and Geography in China on the Lipid Characteristics of Camellia Oleifera Seeds. *J. Oleo Sci.* 68, 1051–1061. doi:10.5650/jos.ess19154

Zeng, W., and Endo, Y. ((2019b)). Lipid Characteristics of Camellia Seed Oil. *J. Oleo Sci.* 68, 649–658. doi:10.5650/jos.ess18234

Zhang, J., Gong, L., Sun, K., Jiang, J., and Zhang, X. (2012). Preparation of Activated Carbon from Waste *Camellia Oleifera* Shell for Supercapacitor Application. *J. Solid State Electrochem.* 16, 2179–2186. doi:10.1007/s10008-012-1639-1

Zhang, L. L., Wang, Y. M., Wu, D. M., Xu, M., and Chen, J. H. (2013). Comparisons of Antioxidant Activity and Total Phenolics of *Camellia Oleifera* Abel Fruit Hull from Different Regions of China. *J. Med. Plants Res.* 4, 1407e1413. doi:10. 5897/JMPR10.270

Zhang, S., and Li, X.-Z. (2015). Inhibition of α-glucosidase by Polysaccharides from the Fruit Hull of Camellia Oleifera Abel. *Carbohydr. Polym.* 115, 38–43. doi:10. 1016/j.carbpol.2014.08.059

Zhang, S., and Li, X. (2018). Hypoglycemic Activity *in vitro* of Polysaccharides from *Camellia Oleifera* Abel. Seed Cake. *Int. J. Biol. Macromol.* 115, 811–819. doi:10.1016/j.ijbiomac.2018.04.054

Zhang, S., Pan, Y. G., Zheng, L., Yang, Y., Zheng, X., Ai, B., et al. (2019). Application of Steam Explosion in Oil Extraction of Camellia Seed (Camellia Oleifera Abel.) and Evaluation of its Physicochemical Properties, Fatty Acid, and Antioxidant Activities. *Food Sci. Nutr.* 7, 1004–1016. doi:10. 1002/fsn3.924

Zhang, X.-F., Han, Y.-Y., Bao, G.-H., Ling, T.-J., Zhang, L., Gao, L.-P., et al. (2012). A New Saponin from Tea Seed Pomace (*Camellia Oleifera* Abel) and its Protective Effect on PC12 Cells. *Molecules* 17, 11721–11728. doi:10.3390/molecules171011721

Zhang, X.-F., Yang, S.-L., Han, Y.-Y., Zhao, L., Lu, G.-L., Xia, T., et al. (2014). Qualitative and Quantitative Analysis of Triterpene Saponins from Tea Seed Pomace (*Camellia Oleifera* Abel) and Their Activities against Bacteria and Fungi. *Molecules* 19, 7568–7580. doi:10.3390/molecules19067568

Zhao, K., Liu, S., Li, K., Hu, Z., Yuan, Y., Yan, L., et al. (2017). Fabrication of −SO3H Functionalized Aromatic Carbon Microspheres Directly from Waste Camellia Oleifera Shells and Their Application on Heterogeneous Acid Catalysis. *Mol. Catal.* 433, 193–201. doi:10.1016/j.mcat.2017.02.032

Zheng, L., Chen, L., Li, J., Liang, L., Fan, Y., Qiu, L., et al. (2019). Two Kaempferol Glycosides Separated from Camellia Oleifera Meal by High-Speed Countercurrent Chromatography and Their Possible Application for Antioxidation. *J. Food Sci.* 84, 2805–2811. doi:10.1111/1750-3841. 14765

Zhou, D., Shi, Q., Pan, J., Liu, M., Long, Y., and Ge, F. (2019). Effectively Improve the Quality of Camellia Oil by the Combination of Supercritical Fluid Extraction and Molecular Distillation (SFE-MD). *LWT* 110, 175–181. doi:10. 1016/j.lwt.2019.04.075

Zhou, J., Lu, M., Zhang, C., Qu, X., Liu, Y., Yang, J., et al. (2020). Isolation and Functional Characterisation of the PHT1 Gene Encoding a High-Affinity Phosphate Transporter in *Camellia Oleifera*. *J. Hortic. Sci. Biotechnol.* 95, 553–564. doi:10.1080/14620316.2019.1703562

Zhou, L.-Y., Wang, X.-N., Wang, L.-P., Chen, Y.-Z., and Jiang, X.-C. (2015). Genetic Diversity of Oil-Tea Camellia Germplasms Revealed by

ISSR Analysis. *Int. J. Biomath.* 08, 1550070. doi:10.1142/S1793524515500709

Zhu, C., Zhang, M., Tang, Q., Yang, Q., Li, J., He, X., et al. (2019). Structure and Activity of the Camellia Oleifera Sapogenin Derivatives on Growth and Biofilm Inhibition of *Staphylococcus aureus* and *Escherichia coli. J. Agric. Food Chem.* 67, 14143–14151. doi:10.1021/acs.jafc.9b03577

Zhu, J., Zhu, Y., Jiang, F., Xu, Y., Ouyang, J., and Yu, S. (2013). An Integrated Process to Produce Ethanol, Vanillin, and Xylooligosaccharides from *Camellia Oleifera* Shell. *Carbohydr. Res.* 382, 52–57. doi:10.1016/j.carres.2013.10.007

Zhu, W.-F., Wang, C.-L., Ye, F., Sun, H.-P., Ma, C.-Y., Liu, W.-Y., et al. (2018). Chemical Constituents of the Seed Cake ofCamellia Oleiferaand Their Antioxidant and Antimelanogenic Activities. *Chem. Biodivers.* 15, e1800137. doi:10.1002/cbdv.201800137

Zong, J., Wang, D., Jiao, W., Zhang, L., Bao, G., Ho, C.-T., et al. (2016). Oleiferasaponin C6 from the Seeds of *Camellia Oleifera* Abel.: A Novel Compound Inhibits Proliferation through Inducing Cell-Cycle Arrest and Apoptosis on Human Cancer Cell Lines *in vitro. RSC Adv.* 6, 91386–91393. doi:10.1039/C6RA14467E

Recent Research Progress: Discovery of Anti-Plant Virus Agents Based on Natural Scaffold

Jixiang Chen[1]*, Xin Luo[1], Yifang Chen[1], Yu Wang[1], Ju Peng[1,2] and Zhifu Xing[1]

[1]State Key Laboratory Breeding Base of Green Pesticide and Agricultural Bioengineering, Key Laboratory of Green Pesticide and Agricultural Bioengineering, Ministry of Education, Guizhou University, Guiyang, China, [2]Guizhou Rice Research Institute, Guizhou Academy of Agricultural Sciences, Guiyang, China

Plant virus diseases, also known as "plant cancers", cause serious harm to the agriculture of the world and huge economic losses every year. Antiviral agents are one of the most effective ways to control plant virus diseases. Ningnanmycin is currently the most successful anti-plant virus agent, but its field control effect is not ideal due to its instability. In recent years, great progress has been made in the research and development of antiviral agents, the mainstream research direction is to obtain antiviral agents or lead compounds based on structural modification of natural products. However, no antiviral agent has been able to completely inhibit plant viruses. Therefore, the development of highly effective antiviral agents still faces enormous challenges. Therefore, we reviewed the recent research progress of anti-plant virus agents based on natural products in the past decade, and discussed their structure-activity relationship (SAR) and mechanism of action. It is hoped that this review can provide new inspiration for the discovery and mechanism of action of novel antiviral agents.

Keywords: plant virus, natural products, antiviral agents, SAR, mechanism

1 INTRODUCTION

Plant viruses are a serious threat to the safe production of world agriculture, causing global economic losses as high as $60 billion every year (Bos, 2000; Barna et al., 2003; Zhao et al., 2017a). Tobacco mosaic virus (TMV), tomato spotted wilt virus (TSWV), tomato yellow leaf curl virus (TYLCV), cucumber mosaic virus (CMV), potato virus Y (PVY) are the top five most important plant viruses of the world according to science/economic importance (Scholthof et al., 2011). TMV is one of the oldest known plant viruses and ranks first among the top 10 plant viruses, causing economic losses in excess of $100 million per year. The host range of TMV exceeds 400 species, and TMV may alter the metabolism and impair the defense system of hosts (Silverman et al., 2005; Scholthof et al., 2011; Sharma et al., 2021). After the plant virus invades the host, the substances required for the life process are completely dependent on the host, and its replication may be combined with the metabolism of the host, making it difficult to prevent and control the viral diseases (Rodrigues et al., 2016; Wang D. et al., 2021). There is no antiviral agent that can completely inhibit plant viruses, and the development of high-efficiency antiviral agents still faces huge challenges (Gan et al., 2021).

Natural products have long been regarded as a source of inspiration for drug design, providing many unknown chemical scaffolds and pharmacophores (Eschenbrenner-Lux et al., 2014). In addition, natural products readily interact with biological targets, thereby
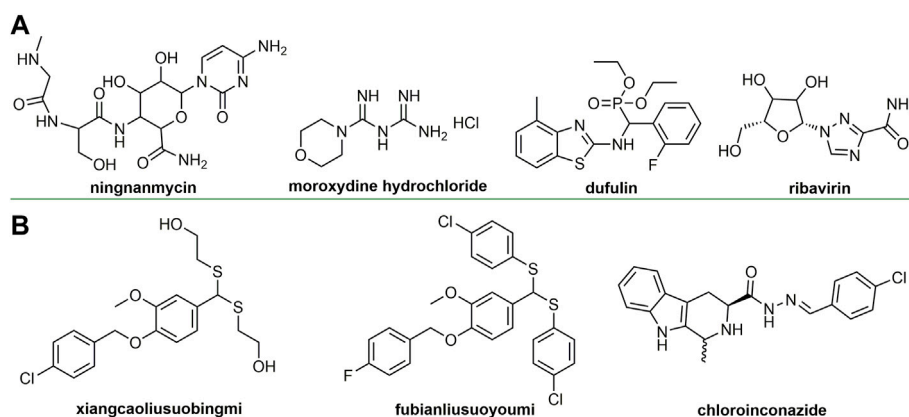
FIGURE 1 | Chemical structures of commercialized **(A)** or under development antiviral agents **(B)**.

exhibiting specific biological activities (Lowe, 2014; Bauer and Brönstrup, 2014). Identifying natural product structure and studying biological activity are of great significance for drug discovery (Chen and Song, 2021; Della-Felice et al., 2022). The discovery of anti-plant virus agents based on natural products is an important research direction in the prevention and control of plant virus diseases and has always attracted much attention (Eckert et al., 2003; Carli et al., 2012; Katayama et al., 2013; Wang et al., 2015). Ningnamycin (**Figure 1A**), isolated from *Strepcomces noursei* var *xichangensisn* for the first time, has broad-spectrum and excellent antiviral activity and is currently the most successful antiviral agent, playing a huge role in the control of plant virus diseases (Han et al., 2014). Ningnanmycin promotes the accumulation of pathogen-related proteins (PRs), a marker of systemic acquired resistance (SAR), by inhibiting the polymerization process of TMV coat protein (TMV-CP) (Han et al., 2014). In addition, ningnamycin can activate redox and metabolic processes in CMV-infected tobacco (Gao et al., 2019).

In recent years, great progress has been made in the research and development of anti-plant virus agents (Carli et al., 2010; Li and Song, 2017; Park et al., 2021). The discovery of some new antiviral agents based on natural products (**Figure 1B**) not only reflects the important role of natural products in the discovery of antiviral agents, but also provides great help for the control of plant viruses. Special natural molecular scaffolds can serve as bridges for the derivatization of antiviral agents (Jassbi et al., 2017; Chen J. et al., 2020), which can provide innovative solutions for the discovery of novel antiviral agents. We wish to analyze the research progress of chemical antiviral agents based on natural scaffold. However, most of these references come from China in recent 10 years. From the perspective of natural products, we reviewed the latest research progress of anti-plant virus chemical active compounds in recent years and discussed their anti-viral activity, structure-activity relationship and mechanism of action, aiming to provide new insights for the discovery of new anti-viral agents.

2 ANTIVIRAL ACTIVE COMPOUNDS

2.1 Acids
2.2.1 Fatty Acids or Carboxylic Acids
Some natural fatty acids or carboxylic acids have good anti-plant virus activity (Katayama et al., 2013; Deshoux et al., 2020). For example, compound **1** (**Figure 2**), isolated from cottonseed sludge was able to increase the phenylalanine ammonia lyase (PAL) and peroxidase (POD) activities of tobacco, as well as the expression levels of *PR-1a* and *PR-5* genes. Its anti-plant virus activity may be related to the expression and activation of various defense-related genes in tobacco (Zhao et al., 2017b). Compound **2**, a derivative of the marine natural product essramycin, exhibited 62, 64, and 68% of TMV inactivating, curative, and protective activities at 500 mg/L, respectively. Compound **2** showed antiviral activity by inhibiting viral assembly and promoting aggregation of 20S disk proteins (Wang T. et al., 2020).

2.2.2 Ferulic Acid Derivatives
Ferulic acid is widely found in plants, and its derivatives have broad-spectrum biological activities (Sonar et al., 2019; Boulebd et al., 2022). Ferulic acid derivatives have good performance in antiviral activity. For example, compound **3** (**Figure 3**) has EC_{50} values of 135.5 and 178.6 mg/L for TMV and CMV. Compound **3** can significantly alter the levels of tobacco gene transcription and protein expression, and enhance the defense response of tobacco by inducing the accumulation of secondary metabolites in the biosynthetic pathway of tobacco phenylpropanoid, thereby inhibiting virus infection (Gan et al., 2021). At a concentration of 500 mg/L, the curative, protective and inactivating activities of compound **4** against TMV were 62.5, 61.8 and 83.5%, respectively. Compound **4** is not only able to cause the breaking and bending of TMV, but also has a strong binding force on TMV-CP (Wang Y. et al., 2020). The EC_{50} values for the curative and protective activity of compound **5** against CMV were 284.67 and 216.30 mg/L, respectively (Lan et al., 2017). The EC_{50} value of compound **6** for TMV inactivating activity was 36.59 mg/L (Wang et al., 2017). The derivatization of ferulic acid is mainly
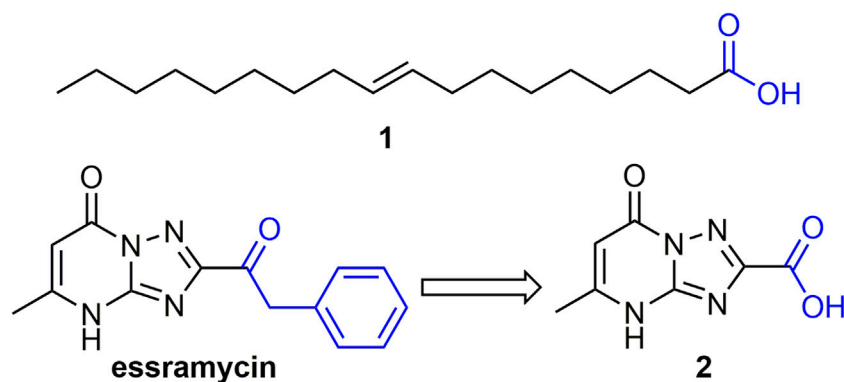
FIGURE 2 | Structures of representative fatty acids or carboxylic acids in antiviral activities.
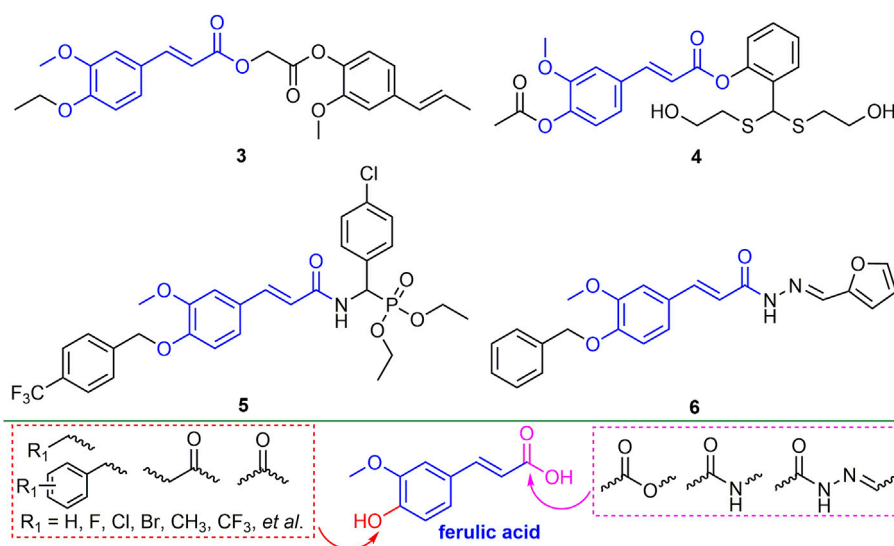
FIGURE 3 | Structures of representative ferulic acid derivatives in antiviral activities.

phenolic hydroxyl and carboxyl moieties. In the phenolic hydroxyl part, benzyl, alkyl, and carbonyl groups are mainly introduced for derivatization, and in the carboxyl part, new ferulic acid derivatives are synthesized mainly through esterification, amidation and acylhydrazone.

2.2 Ketones
2.2.1 Chalcone Derivatives
Chalcone derivatives showed good antiviral activity (Sinha, et al., 2019). For example, compound **7** (**Figure 4**) showed 55.6, 71.2 and 92.4% of curative, protective, and inactivating activities against TMV, respectively. Compound **7** induced plant tolerance to mosaic virus by enhancing tobacco defense enzyme activity, chlorophyll content, and photosynthesis (Gan et al., 2017a). Compounds **8** and **9** not only have good passivation activities (EC$_{50}$, 51.65 and 30.57 mg/L) for TMV, but also have a strong binding ability to TMV-CP (Gan et al., 2017b; Zhou et al., 2018). Compound **10** has good curative and protective activities

against TMV (57.6 and 59.9%), which may trigger the breakdown of TMV by directly interacting with TMV, while also inducing plant resistance (Zhou et al., 2021). The derivatization direction of chalcone is mainly two benzene rings. The benzene ring connected to the carbonyl group mainly introduces halogen, alkoxy, alkyl, and aryl ether, while the benzene ring connected to the double bond mainly introduces halogen, alkoxy, benzyl, aryl ether and ester groups.

2.2.2 Pentadienone Derivatives
There have been many reports on the antiviral activity of pentadienone derivatives. For example, compound **11** (**Figure 5**) has an EC$_{50}$ value of 52.9 mg/L for TMV inactivation activity and has a micromolar affinity for TMV-CP (Chen et al., 2015). At 500 mg/L, the *in vivo* curative activity of compound **12** against TMV and CMV was 48.2 and 59.84%, respectively, and the inactivation activity was 82.6 and 89.8%, respectively (Han et al., 2015). The EC$_{50}$ values of the protective
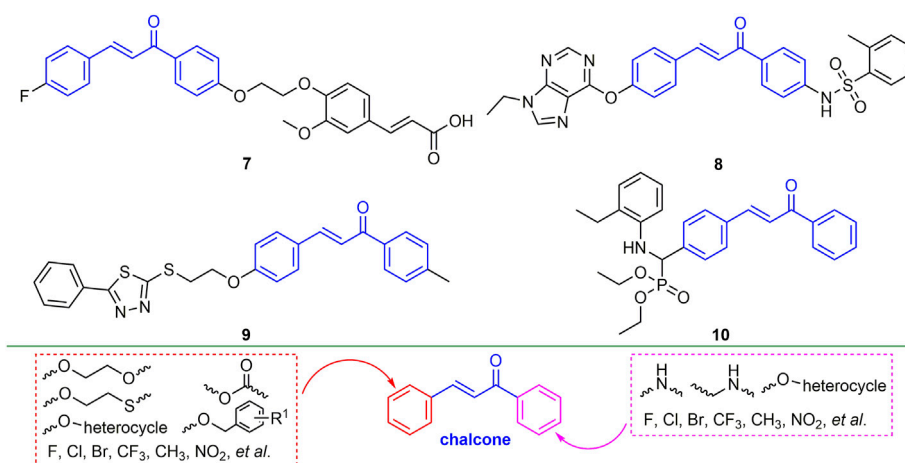
FIGURE 4 | Structures of representative chalcone derivatives in antiviral activities.
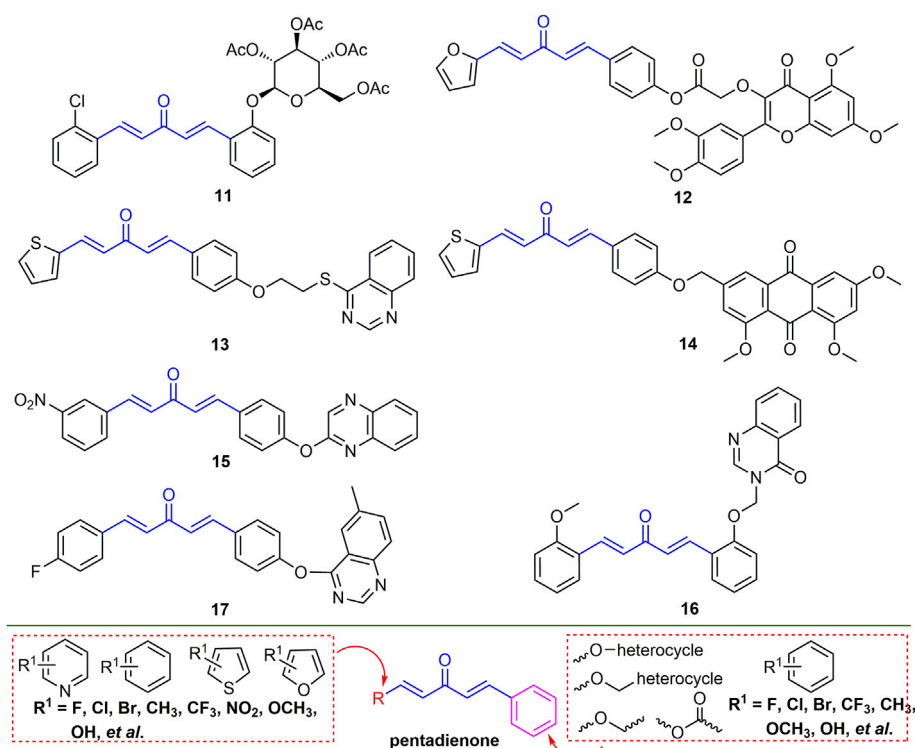
FIGURE 5 | Structures of representative pentadienone derivatives in antiviral activities.

activity against TMV and the curative activity against CMV of compound **13** were 124.3 and 365.5 mg/L, respectively (Long et al., 2015). At a concentration of 500 mg/L, the curative and protective activities of compound **14** against TMV were 52.6 and 55.4%, respectively (Wu et al., 2016). Compound **15** has a strong binding affinity to CMV-CP with a dissociation constant of 0.071 μM (Li et al., 2019). The EC$_{50}$ value of compound **16** for TMV curative activity was 132.2 mg/L (Ma et al., 2014). The

EC$_{50}$ values of compound **17** for the curative, protective and inactivating of TMV were 441.3, 364.6, 243.3 mg/L, and the EC$_{50}$ values for the curative, protective and inactivating activity of CMV were 533.6, 490.7 and 471.6 mg/L, respectively (Luo et al., 2013). The backbone structure of 1,4-pentadien-3-one was obtained by curcumin derivatization. The modification of the 1,4-pentadien-3-one structure is mainly at the terminal positions of the two olefinic bonds. If one of the positions is a benzene ring,
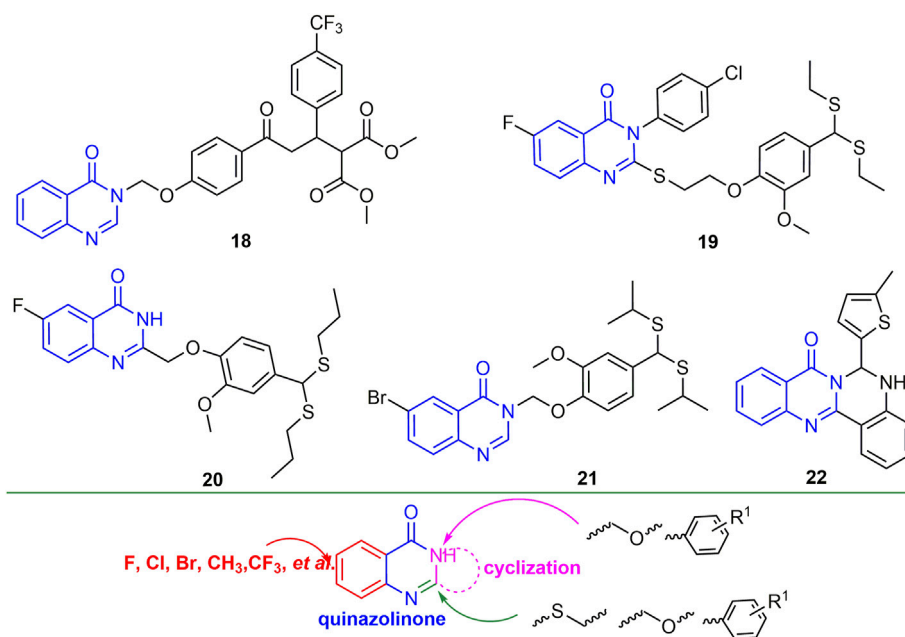
FIGURE 6 | Structures of representative quinazolinone derivatives in antiviral activities.
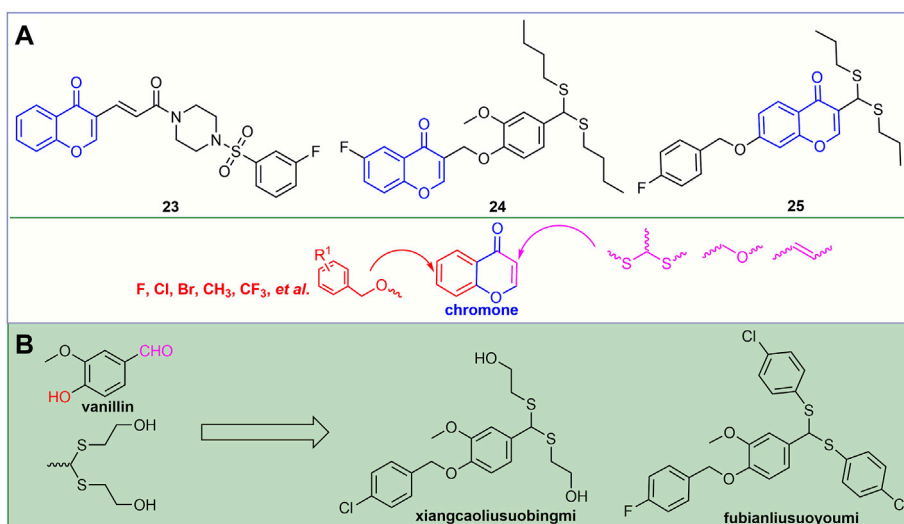
FIGURE 7 | Structures of representative chromone derivatives in antiviral activities **(A)**. Discovery of novel antiviral agents xiangcaoliusuobingmi and fubianliusuoyoumi **(B)**.

halogen, alkoxy, benzyl, and ester groups are mainly introduced into the benzene ring. And another position can be benzene ring, thiophene, furan, and pyridine ring, and mainly halogen is introduced in the ring.

2.2.3 Quinazolinone Derivatives

Quinazolinone is the backbone structure of many alkaloids, and its derivatives have good anti-plant virus activity. For example,

compound **18** (**Figure 6**) not only exhibited good curative activity against CMV (EC$_{50}$, 146.30 mg/L), but also had micromolar binding to CMV-CP (Chen L. et al., 2016). Compounds **19** and **20** have a strong binding ability to tomato chlorosis virus coat protein (ToCV-CP), and the relative expression of ToCV-CP gene in tomato was decreased by 93.3 and 81.0%, respectively (Ran et al., 2020; Zu et al., 2020). Compound **21** not only has good inactivating activity against TSWV (EC$_{50}$, 188 mg/L), but also has
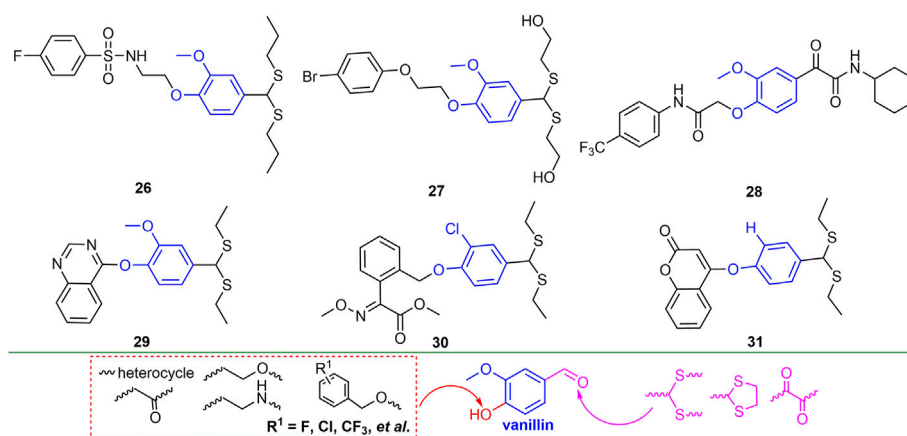
FIGURE 8 | Structures of representative vanillin derivatives in antiviral activities.

a strong binding force to TSWV coat protein (Liu et al., 2021). At 500 mg/L, the inactivating, curative and protective activities of compound **22** against TMV were 51, 43 and 54%, respectively. In addition, compound **22** may show excellent antiviral activity by preventing viral assembly (Hao et al., 2020). Halogen, CF_3, and alkyl are mainly introduced into the benzene ring of quinazolinone. The two- and 3-positions of quinazoline are mainly introduced into thioether, ether and benzene rings, while between the two- and 3-positions, new heterocycles can be obtained by cyclization.

2.2.4 Chromone Derivatives

Chromones, which are widely present in plants, have good antiviral activity. For example, compound **23** (**Figure 7A**) not only has good binding ability to ToCV-CP, but also reduces the relative expression of ToCV-CP gene by 67.2% (Jiang et al., 2021). The curative and protective EC_{50} values of compound **24** against TSWV were 124.2 and 109.3 gm/L, respectively. It may exert antiviral activity by blocking the binding of TSWV N to viral RNA (Zan et al., 2021). At a concentration of 500 mg/L, compound **25** exhibited good curative, protective and inactivating activities against TMV, which were 68.8, 58.8, and 86.0%, respectively. It may exert antiviral activity by disrupting the phenotype and integrity of TMV (Li et al., 2020). Halogen, CF_3, alkyl and benzyl are mainly introduced into the benzene ring of chromone. The second-flow acetal was mainly introduced at the 3-position of the chromone, and the oxygen-containing flexible chain and the olefinic bond were derivatized.

2.3 Vanillin Derivatives

Vanillin is a natural fragrance with a strong aroma and is widely used in the production of cosmetics and fragrances (Libardi et al., 2011; Kayaci and Uyar, 2011). For example, the discovery of novel antiviral agents xiangcaoliusuobingmi and fubianliusuoyoumi (**Figure 7B**) benefits from this. The EC_{50} values of xiangcaoliusuobingmi for the curative and protective activities against PVY were 217.6 and 205.7 mg/L, respectively, and the EC_{50} values for the curative and protective activities against CMV

were 206.3 and 186.2 mg/L, respectively (Zhang et al., 2017). In addition, it can regulate the expression of defense genes and increase the activity of defense enzymes to exert antiviral activity (Shi et al., 2018).

The EC_{50} for the curative, protective and inactivating activities of compound **26** (**Figure 8**) against TMV were 329.5, 269.2 and 48.1 mg/L (Yang Y. et al., 2020). The curative, protective and inactivating activities of compound **27** against TMV were 50.9, 58.9 and 81.8%, respectively. Compound **27** can not only destroy the morphology of TMV particles, but also has a strong binding effect with TMV-CP (Wang et al., 2019). At 500 mg/L, compound **28** exhibited 51.8 and 90.1% of the curative and inactivating activities against TMV, respectively, and it was able to hinder the self-assembly of TMV (Luo et al., 2020). Compound **29** inhibited ToCV infection in the host and decreased the expression level of ToCV-mCP gene (Yang H. et al., 2020). Compound **30** has good curative and protective activities against PVY, CMV and TMV, and can improve the resistance of tobacco to viruses (Chen et al., 2018).

The curative, protective and inactivating activities of compound **31** against TMV were 62.1, 54.5 and 94.2%, respectively, and it could disrupt the structure of TMV particles, thereby inhibiting virus infection (Zhao et al., 2020a; Zan et al., 2020). The modification sites of vanillin are mainly hydroxyl and aldehyde groups, and benzyl, alkoxy, imino, heterocyclic and carbonyl groups are mainly introduced into the hydroxyl part, while the aldehyde groups are mainly changed to dithioacetal and carbonyl. Among them, the antiviral activity was significantly improved after the aldehyde group was changed to dithioacetal, and the chain length and substituent of the acetal also significantly affected the antiviral activity of the compounds.

2.4 Indole Derivatives

Indole is the core backbone structure of many alkaloids and is widely used in the discovery of pesticides (Çokuğraş and Bodur, 2013; Ji et al., 2016; Rajasekharan et al., 2020; Dong et al., 2020). The inactivating, curative and protective activities of compound **33** against TMV were 54, 50, and 53%, respectively, and it may
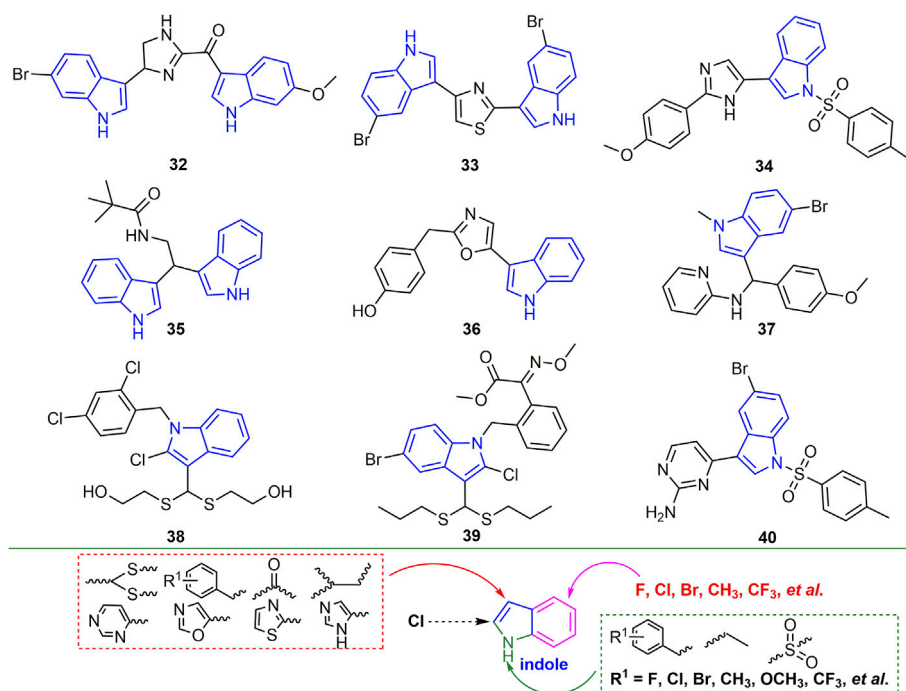
FIGURE 9 | Structures of representative indole derivatives in antiviral activities (l).

TABLE 1 | Antiviral activity of other representative indole derivatives.

Comp	Anti-TMV Activity				Mechanism	Ref
	Concentration (mg/L)	Curative (%)	Protective (%)	Inactivating (%)		
35	500	50	53	54	—	Ji et al. (2018)
37	500	56	52	55	—	Liu et al. (2019)
38	500	65	66	68	Possibly inhibiting viral assembly by cross-linking TMV-CP.	Lu et al. (2019)
39	500	55.1	57.2	80.3	Not only destroys the TMV particle morphology, but also has a strong interaction with TMV-CP.	Wei et al. (2020)

exert antiviral activity by preventing the movement of the virus in plants (**Figure 9**) (Guo et al., 2019). Compound **35** may show good anti-TMV activity by inhibiting the assembly of viral particles and the aggregation of 20S CP (Kang et al., 2020). The antiviral activity of compound **39** against TMV, CMV, and PVY was associated with an increase in chlorophyll content and defense-related enzyme activity (Wei et al., 2019). Antiviral activity of other representative indole derivatives is shown in **Table 1**. Halogen, alkyl and CF₃ are mainly introduced into the benzene ring of indole. Benzyl, alkyl and sulfonyl groups are mainly introduced on the N atom. At the 3-position, heterocycle, benzene ring, dithioacetal, carbonyl and alkyl are mainly introduced for derivatization.

The inactivating, curative, and protective activities of the marine natural product debromohamacanthin A (**Figure 10A**)

against TMV were 53, 51 and 56%, respectively. The inactivating, curative, and protective activities of its derivative **41** against TMV were 60, 59, and 63%, respectively, and the antiviral activity of the compound was improved through structural optimization (Wang T. et al., 2021). In addition, compound **41** can bind to TMV-CP and interfere with the assembly process of TMV-CP and RNA, thus showing antiviral resistance. The inactivating, curative, and protective activities of compound **42** (**Figure 10B**) against TMV were 51.2, 49.0, and 53.6%, respectively (Wang et al., 2022). The functional groups containing CF₂, indole or cyano favored the antiviral activity of 3,3-helix cyclic indole derivatives. At 500 mg/L, the curative, protective, and inactivating activities of compound **43** against TMV were 47, 50, and 51%, respectively (Chen L. et al., 2020). At
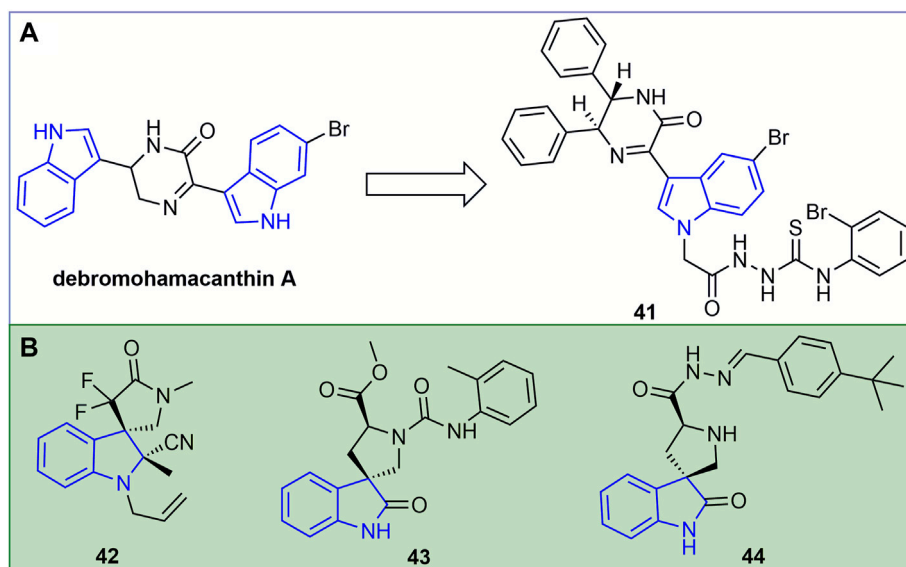
FIGURE 10 | Structures of representative of debromohamacanthin A derivatives in antiviral activities **(A)**. Structures of representative of indole spirocycles derivatives in antiviral activities **(B)**.
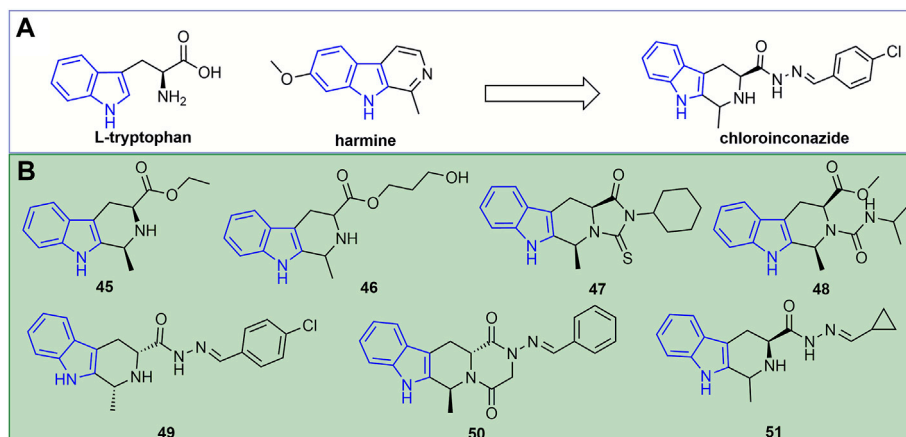
FIGURE 11 | Discovery of a novel antiviral agent chloroinconazide **(A)**. Structures of representative indole derivatives in antiviral activities **(B)**.

500 mg/L, the inactivating, curative, and protective activities of compound **44** were 58, 55.2, and 49.7%, respectively (Chen M. et al., 2016).

A novel antiviral agent, chloroinconazide (**Figure 11A**), was discovered based on the natural product harmine. Its inactivating, curative, and protective activities at 500 mg/L against TMV were 70.4, 71.5, and 64.2%, respectively (Liu et al., 2014). Chloroinconazide can also activate reactive oxygen species and antioxidant levels, induce an increase in salicylic acid content and the expression of its response gene *PR2* (Lv et al., 2021). Furthermore, it can attenuate the virulence of TMV by directly changing the morphological structure of the virion and increasing the activity of antioxidant enzymes, thereby

reducing the production of TMV-induced reactive oxygen species (ROS) during plant infection (Lv et al., 2020).

At 500 mg/L, the inactivating, curative, and protective activities of compound **46** (**Figure 11B**) against TMV were 50.4, 43.9, and 47.9% (Song H. et al., 2014). The *in vitro* antiviral activity of compound **47** against TMV was 48.2% (Song H.-j. et al., 2014). The anti-TMV inactivating, curative, and protective activities of compound **48** were 59, 63 and 60% at 500 mg/L, respectively (Huang et al., 2018). Compound **49** showed excellent inactivating, curative, and protective activities against TMV with EC_{50} values of 127, 156, and 108 mg/L, respectively (Wang and Song, 2020c). Compound **50** not only retarded TMV proliferation, but also had a
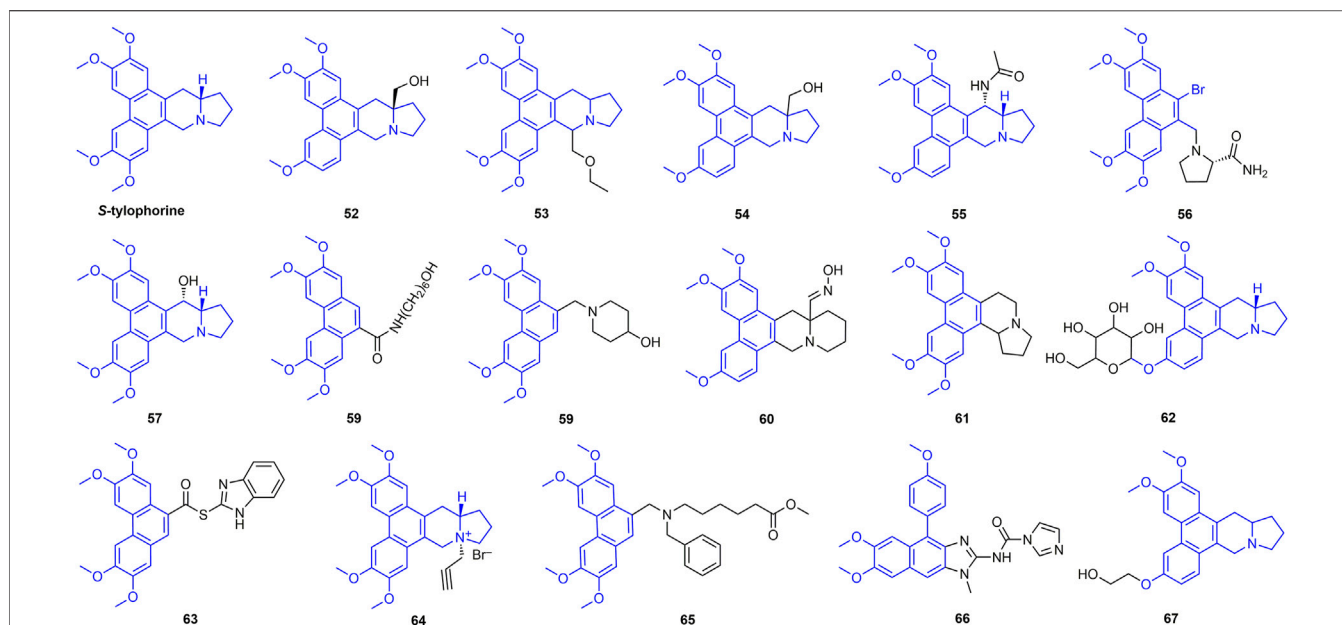
FIGURE 12 | Structures of representative tylophorine analogues in antiviral activities.

TABLE 2 | Antiviral activity of other representative tylophorine analogues.

Comp	Anti-TMV Activity (500 mg/L)				Ref
	Concentration (mg/L)	Curative (%)	Protective (%)	Inactivating (%)	
55	500	69.6	72.7	72.2	Wang et al. (2012a)
56	500	36.6	39.5	42.1	Wang et al. (2012b)
57	500	67.9	63.7	57.8	Wang et al. (2012c)
58	500	81	84	-	Wang et al. (2010b)
59	500	37.4	70.8	71.1	Wang et al. (2014a)
60	500	65.8	69.2	70.3	Su et al. (2021)
61	500	58.6	54.1	55.8	Su et al. (2014b)
62	500	68.1	69.3	63.2	Wu et al. (2014)
63	500	56	53	57	Yu et al. (2016)
64	500	82.1	77.6	76.6	Han et al. (2018)
65	500	49.4	55.3	52.6	Wang et al. (2014b)
66	500	66	71	68	Li et al. (2018)
67	500	44	42.3	40.5	Wu et al. (2013)

concentration-dependent effect on tobacco growth and biomass accumulation (Zhang X. et al., 2021). The inactivating, curative, and protective activities of compound **51** against TMV were 49, 50 and 52%, respectively (Xie et al., 2020).

2.5 Tylophorine Derivatives

Tylophorine has good antiviral activity, and there have been many reports on the antiviral activity of its derivatives (**Figure 12**) (Wang et al., 2010a). For example, the inactivating, curative, and protective activities of compound **52** against TMV were 78.1, 80.1 and 88.4%, respectively. The planarity of the molecule and the rigidity of the D-ring also have a strong effect on the activity, suggesting that the three-dimensional conformation is also very important for enhanced

biological activity (Su et al., 2016). At 500 mg/L, the inactivating, curative, and protective activities of compound **53** against TMV were 67.7, 65.3, and 65.9%, respectively, and its EC$_{50}$ value was 296 mg/L (Yan et al., 2021). The inactivating, curative and protective activities of compound **54** against TMV were 75.3, 76.2 and 68.4% at 500 mg/L, respectively. The methoxy group on the phenanthrene unit significantly affects the antiviral activity of the compounds (Su et al., 2014a). Antiviral activity of other representative tylophorine analogues is shown in **Table 2**.

2.6 Purine Nucleoside Derivatives

Purine nucleosides have excellent antiviral activity, and the curative and protective activities of its derivative **68** (**Figure 13**) against PVY and CMV were 52.5, 60.0, 60.2%, respectively. The excellent antiviral activity of compound **68** is
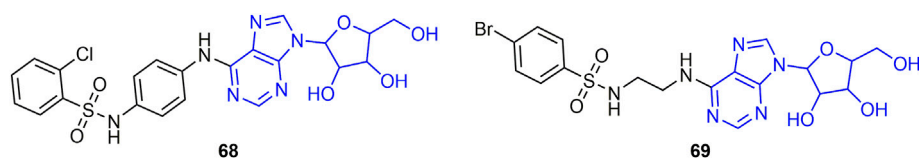
FIGURE 13 | Structures of representative purine nucleoside derivatives in antiviral activities.
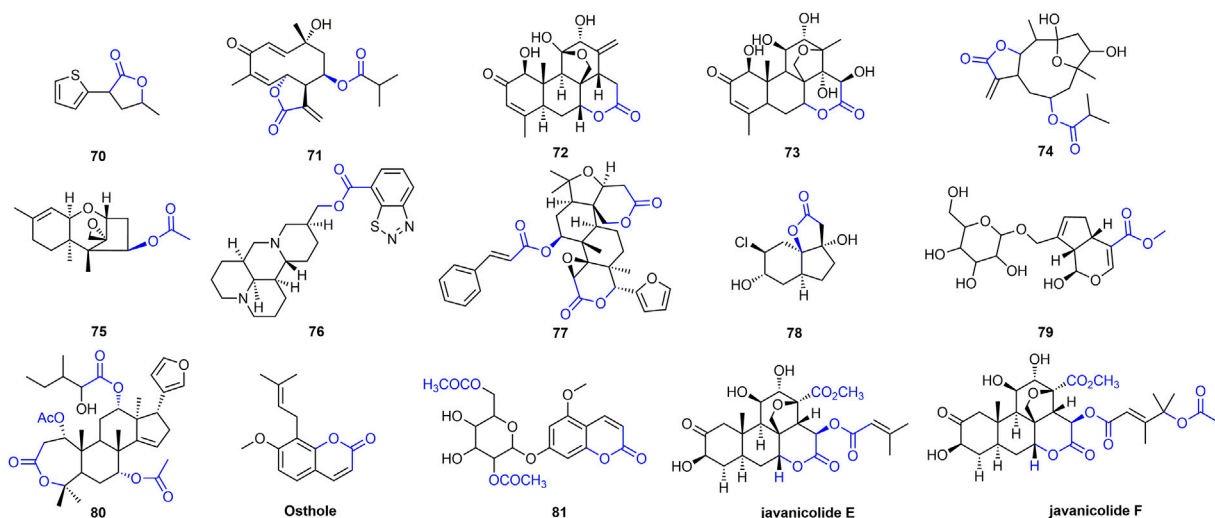
FIGURE 14 | Structures of representative ester or lactide derivatives in antiviral activities.

TABLE 3 | Antiviral activity of other representative ester or lactone derivatives.

Comp	Anti-TMV Activity				Mechanism	Ref
	Concentration (mg/L)	Curative (%)	Protective (%)	Inactivating (%)		
75	—	—	—	—	Compound **75** can delay transmission of pepper mottle virus (PepMoV) in host plants and protect host plants from PepMoV infection	(Ryu et al., 2017)
76	500	72.3	75.7	76.9	—	(Ni et al., 2017)
77	500	41.7	29.3	65.7	—	(Huang et al., 2020)
78	500	-	-	98	—	(Zhu et al., 2019)
79	500	45.8	39.4	42.9	—	(Xia et al., 2018)
80	500	—	—	—	Can inhibit the accumulation of TMV CP *in vitro*	(Ge et al., 2012)
81	—	—	—	—	Inhibiting viral replication	(Zhang et al., 2018)
Osthole	500	70.2	61.9	—	The epidermal protein levels of TMV were significantly reduced, and its replication might be inhibited	(Chen et al., 2020c)
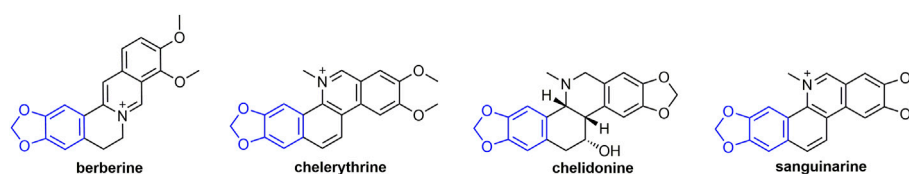
FIGURE 15 | Structures of representative berberine analogs in antiviral activities.

related to its immune-inducing effect, which can regulate the activities of defense-related enzymes, defense-related genes, and photosynthesis-related proteins in plants (He et al., 2019). The EC_{50} values of the protective activity of compound **69** against CMV and PVY were 137 and 209 mg/L, respectively. The EC_{50} value of compound **69** for the inactivating activity of TMV was 48 mg/L. Compound **69** may further damage the viral structure TMV virus by binding to the coat protein of the virus, thus weakening its infectivity and infectivity (Zhang J. et al., 2021).

2.7 Esters or Lactones Derivatives

Esters or lactones have made great progress in the study of antiviral activity, which has attracted the attention of researchers (Olivon et al., 2015; Eriksson et al., 2008; Hellwig et al., 2003). At 500 mg/L, the inactivating, curative, and protective activities of compound **70** (**Figure 14**) were 52, 57, and 56%, respectively (Lu et al., 2014). The curative activity of compound **71** against TMV was 62.86% at 100 mg/L, and it could inhibit TMV infection by interfering with the expression of TMV-CP (Zhao et al., 2017c). Compound **72** inhibits the expression of tobacco TMV-CP with an IC_{50} value of 5.56 μM (Tan et al., 2018; Yan et al., 2010). Compound **73** has obvious inhibitory activity against TMV infection and replication with IC_{50} of 13.98 and 7.13 mg/L, respectively (Shen et al., 2008). Compound **74** inhibited gene expression of TSWV by more than 85%. Compound **74** activates the JA pathway, promotes PAL activity, induces systemic resistance, inhibits gene expression of TSWV, and defends against TSWV infection (Zhao et al., 2020b). Antiviral activity of other representative ester or lactone derivatives are shown in **Table 3**.

2.8 Berberine Analogs

The protective activity of berberine (**Figure 15**) against TMV was 62.8%. Berberine induces an immune response to TMV in tobacco and associated with systemic resistance through activation of salicylic acid signaling (Guo et al., 2020). At 500 mg/L, chelerythrine had obvious inactivation, proliferation inhibition, and protection effects on TMV, and the inhibition ratio were 72.67, 77.52, and 59.34%, respectively. (Guo et al., 2021).

3 CONCLUSION

In recent years, great progress has been made in the research and development of antiviral agents. The discovery of some new

antiviral agents has provided more options for the prevention and control of plant virus diseases. These new antiviral agents are expected to become pillar products in the future. These novel antiviral agents are obtained by structural modification of natural products as lead compounds. In the past 10 years, some important natural products or backbone structures based on natural products in the research and development of anti-plant virus agents are mainly acids (fatty acids, carboxylic acids, and ferulic acids), ketones (chalcones, pentadienones, quinazolinones, and chromones), vanilloids, indoles, silmenines, purine nucleosides, esters or lactones, and berberine analogs. Among them, the derivatives based on vanillin and indole show great application prospects. For example, xiangcaoliusuobingmi and fubianliusuoyoumi are novel antiviral agents based on vanillin, and chloroinconazide is a novel antiviral agent based on indole. Currently, the discovery methods of anti-plant viral agents mainly include natural product isolation, natural product-based structural modification, protein-based structural design, and computational-based structural optimization. The research on the mechanism of action of antiviral agents mainly focuses on the relationship between drugs and RNA, proteins, and pathways, and the in-depth mechanism of action in living host plants needs to be further explored. The design of new scaffolds and lead compounds inspired by natural products has played an important role in the development of antiviral agents and has been demonstrated in practice. With the continuous discovery of new natural products, more anti-plant virus agents based on natural products will be discovered and applied in the future.

AUTHOR CONTRIBUTIONS

JC: conceived and designed the research, JC and XL: wrote the manuscript, YC, YW, JP, and ZX: analyzed and interpreted the data.

REFERENCES

Barna, B., Fodor, J., Pogány, M., and Király, Z. (2003). Role of Reactive Oxygen Species and Antioxidants in Plant Disease Resistance. *Pest. Manag. Sci.* 59, 459–464. doi:10.1002/ps.706

Bauer, A., and Brönstrup, M. (2014). Industrial Natural Product Chemistry for Drug Discovery and Development. *Nat. Prod. Rep.* 31, 35–60. doi:10.1039/c3np70058e

Bos, L. (2000). 100 Years of Virology: From Vitalism via Molecular Biology to Genetic Engineering. *Trends Microbiol.* 8, 82–87. doi:10.1016/s0966-842x(99)01678-9

Boulebd, H., Mechler, A., Thi Hoa, N., and Vo, Q. V. (2022). Insights on the Kinetics and Mechanisms of the Peroxyl Radical Scavenging Capacity of Caftaric Acid: the Important Role of the Acid-Base Equilibrium. *New J. Chem.* 46, 7403–7409. doi:10.1039/d2nj00377e

Chen, J.-x., and Song, B.-a. (2021). Natural Nematicidal Active Compounds: Recent Research Progress and Outlook. *J. Integr. Agric.* 20, 2015–2031. doi:10.1016/s2095-3119(21)63617-1

Chen, J., Li, Q. X., and Song, B. (2020a). Chemical Nematicides: Recent Research Progress and Outlook. *J. Agric. Food Chem.* 68, 12175–12188. doi:10.1021/acs.jafc.0c02871

Chen, J., Shi, J., Yu, L., Liu, D., Gan, X., Song, B., et al. (2018). Design, Synthesis, Antiviral Bioactivity, and Defense Mechanisms of Novel Dithioacetal Derivatives Bearing a Strobilurin Moiety. *J. Agric. Food Chem.* 66, 5335–5345. doi:10.1021/acs.jafc.8b01297

Chen, L., Hao, Y., Song, H., Liu, Y., Li, Y., Zhang, J., et al. (2020b). Design, Synthesis, Characterization, and Biological Activities of Novel Spirooxindole Analogues Containing Hydantoin, Thiohydantoin, Urea, and Thiourea Moieties. *J. Agric. Food Chem.* 68, 10618–10625. doi:10.1021/acs.jafc.0c04488

Chen, L., Xie, J., Song, H., Liu, Y., Gu, Y., Wang, L., et al. (2016a). Design, Synthesis, and Biological Activities of Spirooxindoles Containing Acylhydrazone Fragment Derivatives Based on the Biosynthesis of Alkaloids Derived from Tryptophan. *J. Agric. Food Chem.* 64, 6508–6516. doi:10.1021/acs.jafc.6b02683

Chen, M., Hu, D., Li, X., Yang, S., Zhang, W., Li, P., et al. (2015). Antiviral Activity and Interaction Mechanisms Study of Novel Glucopyranoside Derivatives. *Bioorg. Med. Chem. Lett.* 25, 3840–3844. doi:10.1016/j.bmcl.2015.07.068

Chen, M., Li, P., Hu, D., Zeng, S., Li, T., Jin, L., et al. (2016b). Synthesis, Antiviral Activity, 3D-QSAR, and Interaction Mechanisms Study of Novel Malonate Derivatives Containing Quinazolin-4(3h)-One Moiety. *Bioorg. Med. Chem. Lett.* 26, 168–173. doi:10.1016/j.bmcl.2015.11.006

Chen, Y. H., Guo, D. S., Lu, M. H., Yue, J. Y., Liu, Y., Shang, C. M., et al. (2020c). Inhibitory Effect of Osthole from *Cnidium Monnieri* on Tobacco Mosaic Virus (TMV) Infection in Nicotiana Glutinosa. *Molecules* 25, 65. doi:10.3390/molecules25010065

Çokuğraş, A. N., and Bodur, E. (2013). Comparative Effects of Two Plant Growth Regulators; Indole-3-Acetic Acid and Chlorogenic Acid on Human and Horse Serum Butyrylcholinesterase. *Pestic. Biochem. Physiol.* 77, 24–33. doi:10.1016/S0048-3575(03)00071-3

Cooper, B., Eckert, D., Andon, N. L., Yates, J. R., and Haynes, P. A. (2003). Investigative Proteomics: Identification of an Unknown Plant Virus from Infected Plants Using Mass Spectrometry. *J. Am. Soc. Mass Spectrom.* 14, 736–741. doi:10.1016/S1044-0305(03)00125-9

Della-Felice, F., Bartolomeu, A. A., and Pilli, R. A. (2022). The Phosphate Ester Group in Secondary Metabolites. *Nat. Prod. Rep.* doi:10.1039/d1np00078k

Deshoux, M., Masson, V., Arafah, K., Voisin, S., Guschinskaya, N., van Munster, M., et al. (2020). Cuticular Structure Proteomics in the Pea Aphid *Acyrthosiphon Pisum* Reveals New Plant Virus Receptor Candidates at the Tip of Maxillary Stylets. *J. Proteome Res.* 19, 1319–1337. doi:10.1021/acs.jproteome.9b00851

Dong, J., Huang, S. S., Hao, Y. N., Wang, Z. W., Liu, Y. X., Li, Y. Q., et al. (2020). Marine-natural-products for Biocides Development: First Discovery of Meridianin Alkaloids as Antiviral and Anti-phytopathogenic-fungus Agents. *Pest Manag. Sci.* 76, 3369–3376. doi:10.1002/ps.5690

Eriksson, U., Peterson, L. W., Kashemirov, B. A., Hilfinger, J. M., Drach, J. C., Borysko, K. Z., et al. (2008). Serine Peptide Phosphoester Prodrugs of Cyclic Cidofovir: Synthesis, Transport, and Antiviral Activity. *Mol. Pharm.* 5, 598–609. doi:10.1021/mp8000099

Eschenbrenner-Lux, V., Küchler, P., Ziegler, S., Kumar, K., and Waldmann, H. (2014). An Enantioselective Inverse-Electron-Demand Imino Diels-Alder Reaction. *Angew. Chem. Int. Ed.* 53, 2134–2137. doi:10.1002/anie.201309022

Gan, X., Hu, D., Chen, Z., Wang, Y., and Song, B. (2017b). Synthesis and Antiviral Evaluation of Novel 1,3,4-Oxadiazole/thiadiazole-Chalcone Conjugates. *Bioorg. Med. Chem. Lett.* 27, 4298–4301. doi:10.1016/j.bmcl.2017.08.038

Gan, X., Hu, D., Wang, Y., Yu, L., and Song, B. (2017a). Novel Trans-ferulic Acid Derivatives Containing a Chalcone Moiety as Potential Activator for Plant Resistance Induction. *J. Agric. Food Chem.* 65, 4367–4377. doi:10.1021/acs.jafc.7b00958

Gan, X., Wang, Z., and Hu, D. (2021). Synthesis of Novel Antiviral Ferulic Acid-Eugenol and Isoeugenol Hybrids Using Various Link Reactions. *J. Agric. Food Chem.* 69, 13724–13733. doi:10.1021/acs.jafc.1c05521

Gao, D., Wang, D., Chen, K., Huang, M., Xie, X., and Li, X. (2019). Activation of Biochemical Factors in CMV-Infected Tobacco by Ningnanmycin. *Pesticide Biochem. Physiology* 156, 116–122. doi:10.1016/j.pestbp.2019.02.012

Ge, Y.-h., Liu, K.-x., Zhang, J.-x., Mu, S.-z., and Hao, X.-j. (2012). The Limonoids and Their Antitobacco Mosaic Virus (TMV) Activities from *Munronia Unifoliolata Oliv.* *J. Agric. Food Chem.* 60, 4289–4295. doi:10.1021/jf205362d

Guo, J., Hao, Y., Ji, X., Wang, Z., Liu, Y., Ma, D., et al. (2019). Optimization, Structure-Activity Relationship, and Mode of Action of Nortopsentin Analogues Containing Thiazole and Oxazole Moieties. *J. Agric. Food Chem.* 67, 10018–10031. doi:10.1021/acs.jafc.9b04093

Guo, W., Lu, X., Liu, B., Yan, H., and Feng, J. (2021). Anti-TMV Activity and Mode of Action of Three Alkaloids Isolated from Chelidonium Majus. *Pest Manag. Sci.* 77, 510–517. doi:10.1002/ps.6049

Guo, W., Yan, H., Ren, X., Tang, R., Sun, Y., Wang, Y., et al. (2020). Berberine Induces Resistance against *Tobacco Mosaic Virus* in Tobacco. *Pest Manag. Sci.* 76, 1804–1813. doi:10.1002/ps.5709

Han, G., Chen, L., Wang, Q., Wu, M., Liu, Y., and Wang, Q. (2018). Design, Synthesis, and Antitobacco Mosaic Virus Activity of Water-Soluble Chiral Quaternary Ammonium Salts of Phenanthroindolizidines Alkaloids. *J. Agric. Food Chem.* 66, 780–788. doi:10.1021/acs.jafc.7b03418

Han, Y., Ding, Y., Xie, D., Hu, D., Li, P., Li, X., et al. (2015). Design, Synthesis, and Antiviral Activity of Novel Rutin Derivatives Containing 1, 4-Pentadien-3-One Moiety. *Eur. J. Med. Chem.* 92, 732–737. doi:10.1016/j.ejmech.2015.01.017

Han, Y., Luo, Y., Qin, S., Xi, L., Wan, B., and Du, L. (2014). Induction of Systemic Resistance against Tobacco Mosaic Virus by Ningnanmycin in Tobacco. *Pesticide Biochem. Physiology* 111, 14–18. doi:10.1016/j.pestbp.2014.04.008

Hao, Y., Wang, K., Wang, Z., Liu, Y., Ma, D., and Wang, Q. (2020). Luotonin A and its Derivatives as Novel Antiviral and Antiphytopathogenic Fungus Agents. *J. Agric. Food Chem.* 68, 8764–8773. doi:10.1021/acs.jafc.0c04278

He, F., Shi, J., Wang, Y., Wang, S., Chen, J., Gan, X., et al. (2019). Synthesis, Antiviral Activity, and Mechanisms of Purine Nucleoside Derivatives Containing a Sulfonamide Moiety. *J. Agric. Food Chem.* 67, 8459–8467. doi:10.1021/acs.jafc.9b02681

Hellwig, V., Mayer-Bartschmid, A., Müller, H., Greif, G., Kleymann, G., Zitzmann, W., et al. (2003). Pochonins A−F, New Antiviral and Antiparasitic Resorcylic Acid Lactones from Pochonia Chlamydosporia Var. Catenulata. *J. Nat. Prod.* 66, 829–837. doi:10.1021/np020556v

Huang, X., Li, T., Shan, X., Lu, R., Hao, M., Lv, M., et al. (2020). High Value-Added Use of Citrus Industrial Wastes in Agriculture: Semisynthesis and Anti-tobacco Mosaic Virus/Insecticidal Activities of Ester Derivatives of Limonin Modified in the B Ring. *J. Agric. Food Chem.* 68, 12241–12251. doi:10.1021/acs.jafc.0c05588

Huang, Y., Guo, Z., Song, H., Liu, Y., Wang, L., and Wang, Q. (2018). Design, Synthesis, and Biological Activity of β-Carboline Analogues Containing Hydantoin, Thiohydantoin, and Urea Moieties. *J. Agric. Food Chem.* 66, 8253–8261. doi:10.1021/acs.jafc.8b03087

Jassbi, A. R., Zare, S., Asadollahi, M., and Schuman, M. C. (2017). Ecological Roles and Biological Activities of Specialized Metabolites from the Genus Nicotiana. *Chem. Rev.* 117, 12227–12280. doi:10.1021/acs.chemrev.7b00001

Ji, X., Guo, J., Liu, Y., Lu, A., Wang, Z., Li, Y., et al. (2018). Marine-Natural-Product Development: First Discovery of Nortopsentin Alkaloids as Novel Antiviral, Anti-phytopathogenic-fungus, and Insecticidal Agents. *J. Agric. Food Chem.* 66, 4062–4072. doi:10.1021/acs.jafc.8b00507

Ji, X., Wang, Z., Dong, J., Liu, Y., Lu, A., and Wang, Q. (2016). Discovery of Topsentin Alkaloids and Their Derivatives as Novel Antiviral and Anti-phytopathogenic Fungus Agents. *J. Agric. Food Chem.* 64, 9143–9151. doi:10.1021/acs.jafc.6b04020

Jiang, D., Chen, J., Zan, N., Li, C., Hu, D., and Song, B. (2021). Discovery of Novel Chromone Derivatives Containing a Sulfonamide Moiety as Anti-ToCV Agents through the Tomato Chlorosis Virus Coat Protein-Oriented Screening Method. *J. Agric. Food Chem.* 69, 12126–12134. doi:10.1021/acs.jafc.1c02467

Kang, J., Gao, Y., Zhang, M., Ding, X., Wang, Z., Ma, D., et al. (2020). Streptindole and its Derivatives as Novel Antiviral and Anti-phytopathogenic Fungus Agents. *J. Agric. Food Chem.* 68, 7839–7849. doi:10.1021/acs.jafc.0c03994

Katayama, S., Ohno, F., Yamauchi, Y., Kato, M., Makabe, H., and Nakamura, S. (2013). Enzymatic Synthesis of Novel Phenol Acid Rutinosides Using Rutinase and Their Antiviral Activity In Vitro. *J. Agric. Food Chem.* 61, 9617–9622. doi:10.1021/jf4021703

Kayaci, F., and Uyar, T. (2011). Solid Inclusion Complexes of Vanillin with Cyclodextrins: Their Formation, Characterization, and High-Temperature Stability. *J. Agric. Food Chem.* 59, 11772–11778. doi:10.1021/jf202915c

Lan, X., Xie, D., Yin, L., Wang, Z., Chen, J., Zhang, A., et al. (2017). Novel α,β-unsaturated Amide Derivatives Bearing α-amino Phosphonate Moiety as Potential Antiviral Agents. *Bioorg. Med. Chem. Lett.* 27, 4270–4273. doi:10.1016/j.bmcl.2017.08.048

Li, G., Guo, J., Wang, Z., Liu, Y., Song, H., and Wang, Q. (2018). Marine Natural Products for Drug Discovery: First Discovery of Kealiinines A-C and Their Derivatives as Novel Antiviral and Antiphytopathogenic Fungus Agents. *J. Agric. Food Chem.* 66, 7310–7318. doi:10.1021/acs.jafc.8b02238

Li, M., Zan, N., Huang, M., Jiang, D., Hu, D., and Song, B. (2020). Design, Synthesis and Anti-TMV Activities of Novel Chromone Derivatives Containing Dithioacetal Moiety. *Bioorg. Med. Chem. Lett.* 30, 126945. doi:10.1016/j.bmcl.2019.126945

Li, X.-y., and Song, B.-a. (2017). Progress in the Development and Application of Plant-Based Antiviral Agents. *J. Integr. Agric.* 16, 2772–2783. doi:10.1016/s2095-3119(17)61788-x

Li, X., Wang, Y., Chen, K., Gao, D., Wang, D., and Xue, W. (2019). Cucumber Mosaic Virus Coat Protein: The Potential Target of 1, 4-Pentadien-3-One Derivatives. *Pesticide Biochem. Physiology* 155, 45–50. doi:10.1016/j.pestbp.2019.01.004

Libardi, S. H., Borges, J. C., Skibsted, L. H., and Cardoso, D. R. (2011). Deactivation of Ferrylmyoglobin by Vanillin as Affected by Vanillin Binding to β-Lactoglobulin. *J. Agric. Food Chem.* 59, 6202–6208. doi:10.1021/jf1047173

Liu, B., Li, R., Li, Y., Li, S., Yu, J., Zhao, B., et al. (2019). Discovery of Pimprinine Alkaloids as Novel Agents against a Plant Virus. *J. Agric. Food Chem.* 67, 1795–1806. doi:10.1021/acs.jafc.8b06175

Liu, Y., Chen, J., Xie, D., Song, B., and Hu, D. (2021). First Report on Anti-TSWV Activities of Quinazolinone Derivatives Containing a Dithioacetal Moiety. *J. Agric. Food Chem.* 69, 12135–12142. doi:10.1021/acs.jafc.1c03171

Liu, Y., Song, H., Huang, Y., Li, J., Zhao, S., Song, Y., et al. (2014). Design, Synthesis, and Antiviral, Fungicidal, and Insecticidal Activities of Tetrahydro-β-Carboline-3-Carbohydrazide Derivatives. *J. Agric. Food Chem.* 62, 9987–9999. doi:10.1021/jf503794g

Long, C., Li, P., Chen, M., Dong, L., Hu, D., and Song, B. (2015). Synthesis, Anti-tobacco Mosaic Virus and Cucumber Mosaic Virus Activity, and 3D-QSAR Study of Novel 1,4-Pentadien-3-One Derivatives Containing 4-Thioquinazoline Moiety. *Eur. J. Med. Chem.* 102, 639–647. doi:10.1016/j.ejmech.2015.08.029

Lowe, D. B. (2014). Combichem All over Again. *Nat. Chem.* 6, 851–852. doi:10.1038/nchem.2074

Lu, A., Wang, J., Liu, T., Han, J., Li, Y., Su, M., et al. (2014). Small Changes Result in Large Differences: Discovery of (−)-Incrustoporin Derivatives as Novel Antiviral and Antifungal Agents. *J. Agric. Food Chem.* 62, 8799–8807. doi:10.1021/jf503060k

Lu, A., Wang, T., Hui, H., Wei, X., Cui, W., Zhou, C., et al. (2019). Natural Products for Drug Discovery: Discovery of Gramines as Novel Agents against a Plant Virus. *J. Agric. Food Chem.* 67, 2148–2156. doi:10.1021/acs.jafc.8b06859

Luo, D., Guo, S., He, F., Chen, S., Dai, A., Zhang, R., et al. (2020). Design, Synthesis, and Bioactivity of α-Ketoamide Derivatives Containing a Vanillin Skeleton for Crop Diseases. *J. Agric. Food Chem.* 68, 7226–7234. doi:10.1021/acs.jafc.0c00724

Luo, H., Liu, J., Jin, L., Hu, D., Chen, Z., Yang, S., et al. (2013). Synthesis and Antiviral Bioactivity of Novel (1E, 4E)-1-Aryl-5-(2-(quinazolin-4-Yloxy) phenyl)-1,4-Pentadien-3-One Derivatives. *Eur. J. Med. Chem.* 63, 662–669. doi:10.1016/j.ejmech.2013.02.035

Lv, X., Xiang, S., Wang, X., Wu, L., Liu, C., Yuan, M., et al. (2020). Synthetic Chloroinconazide Compound Exhibits Highly Efficient Antiviral Activity against Tobacco Mosaic Virus. *Pest Manag. Sci.* 76, 3636–3648. doi:10.1002/ps.5910

Lv, X., Yuan, M., Pei, Y., Liu, C., Wang, X., Wu, L., et al. (2021). The Enhancement of Antiviral Activity of Chloroinconazide by Aglinate-Based Nanogel and its Plant Growth Promotion Effect. *J. Agric. Food Chem.* 69, 4992–5002. doi:10.1021/acs.jafc.1c00941

Ma, J., Li, P., Li, X., Shi, Q., Wan, Z., Hu, D., et al. (2014). Synthesis and Antiviral Bioactivity of Novel 3-((2-((1e,4e)-3-Oxo-5-Arylpenta-1,4-Dien-1-Yl) phenoxy)methyl)-4(3h)-Quinazolinone Derivatives. *J. Agric. Food Chem.* 62, 8928–8934. doi:10.1021/jf502162y

Ni, W., Li, C., Liu, Y., Song, H., Wang, L., Song, H., et al. (2017). Various Bioactivity and Relationship of Structure-Activity of Matrine Analogues. *J. Agric. Food Chem.* 65, 2039–2047. doi:10.1021/acs.jafc.6b05474

Olivon, F., Palenzuela, H., Girard-Valenciennes, E., Neyts, J., Pannecouque, C., Roussi, F., et al. (2015). Antiviral Activity of Flexibilane and Tigliane Diterpenoids fromStillingia Lineata. *J. Nat. Prod.* 78, 1119–1128. doi:10.1021/acs.jnatprod.5b00116

Park, J., Wen, A. M., Gao, H., Shin, M. D., Simon, D. I., Wang, Y., et al. (2021). Designing S100A9-Targeted Plant Virus Nanoparticles to Target Deep Vein Thrombosis. *Biomacromolecules* 22, 25822594. doi:10.1021/acs.biomac.1c00303

Rajasekharan, S. K., Kim, S., Kim, J.-C., and Lee, J. (2020). Nematicidal Activity of 5-iodoindole against Root-Knot Nematodes. *Pesticide Biochem. Physiology* 163, 76–83. doi:10.1016/j.pestbp.2019.10.012

Ran, L., Yang, H., Luo, L., Huang, M., and Hu, D. (2020). Discovery of Potent and Novel Quinazolinone Sulfide Inhibitors with Anti-tocv Activity. *J. Agric. Food Chem.* 68, 5302–5308. doi:10.1021/acs.jafc.0c00686

Rodrigues, T., Reker, D., Schneider, P., and Schneider, G. (2016). Counting on Natural Products for Drug Design. *Nat. Chem.* 8, 531–541. doi:10.1038/nchem.2479

Ryu, S. M., Lee, H. M., Song, E. G., Seo, Y. H., Lee, J., Guo, Y., et al. (2017). Antiviral Activities of Trichothecenes Isolated from *Trichoderma Albolutescens* against Pepper Mottle Virus. *J. Agric. Food Chem.* 65, 4273–4279. doi:10.1021/acs.jafc.7b01028

Scholthof, K.-B. G., Adkins, S., Czosnek, H., Palukaitis, P., Jacquot, E., Hohn, T., et al. (2011). Top 10 Plant Viruses in Molecular Plant Pathology. *Mol. Plant Pathol.* 12, 938–954. doi:10.1111/j.1364-3703.2011.00752.x

Sharma, J., Bhardwaj, V. K., Das, P., and Purohit, R. (2021). Plant-Based Analogues Identified as Potential Inhibitor against Tobacco Mosaic Virus: A Biosimulation Approach. *Pesticide Biochem. Physiology* 175, 104858. doi:10.1016/j.pestbp.2021.104858

Shen, J.-G., Zhang, Z.-K., Wu, Z.-J., Ouyang, M.-A., Xie, L.-H., and Lin, Q.-Y. (2008). Antiphytoviral Activity of Bruceine-D fromBrucea Javanica Seeds. *Pest. Manag. Sci.* 64, 191–196. doi:10.1002/ps.1465

Shi, J., Yu, L., and Song, B. (2018). Proteomics Analysis of Xiangcaoliusuobingmi-Treated *Capsicum Annuum* L. Infected with Cucumber Mosaic Virus. *Pesticide Biochem. Physiology* 149, 113–122. doi:10.1016/j.pestbp.2018.06.008

Silverman, F. P., Petracek, P. D., Heiman, D. F., Fledderman, C. M., and Warrior, P. (2005). Salicylate Activity. 3. Structure Relationship to Systemic Acquired Resistance. *J. Agric. Food Chem.* 53, 9775–9780. doi:10.1021/jf051383t

Sinha, S., Manju, S. L., and Doble, M. (2019). Chalcone-Thiazole Hybrids: Rational Design, Synthesis, and Lead Identification against 5-Lipoxygenase. *ACS Med. Chem. Lett.* 10, 1415–1422. doi:10.1021/acs.jpca.8b0678710.1021/acsmedchemlett.9b00193

Sonar, V. P., Fois, B., Distinto, S., Maccioni, E., Meleddu, R., Cottiglia, F., et al. (2019). Ferulic Acid Esters and Withanolides: In Search of Withania Somnifera GABAA Receptor Modulators. *J. Nat. Prod.* 82, 1250–1257. doi:10.1021/acs.jnatprod.8b01023

Song, H.-j., Liu, Y.-x., Liu, Y.-x., Huang, Y.-q., Li, Y.-q., and Wang, Q.-m. (2014b). Design, Synthesis, Anti-TMV, Fungicidal, and Insecticidal Activity Evaluation of 1,2,3,4-Tetrahydro-β-Carboline-3-Carboxylic Acid Derivatives Based on Virus Inhibitors of Plant Sources. *Bioorg. Med. Chem. Lett.* 24, 5228–5233. doi:10.1016/j.bmcl.2014.09.063

Song, H., Liu, Y., Liu, Y., Wang, L., and Wang, Q. (2014a). Synthesis and Antiviral and Fungicidal Activity Evaluation of β-Carboline, Dihydro-β-Carboline,

Tetrahydro-β-Carboline Alkaloids, and Their Derivatives. *J. Agric. Food Chem.* 62, 1010–1018. doi:10.1021/jf404840x

Su, B., Cai, C., Deng, M., Liang, D., Wang, L., and Wang, Q. (2014a). Design, Synthesis, Antiviral Activity, and Sars of 13a-Substituted Phenanthroindolizidine Alkaloid Derivatives. *Bioorg. Med. Chem. Lett.* 24, 2881–2884. doi:10.1016/j.bmcl.2014.04.101

Su, B., Cai, C., Deng, M., and Wang, Q. (2016). Spatial Configuration and Three-Dimensional Conformation Directed Design, Synthesis, Antiviral Activity, and Structure-Activity Relationships of Phenanthroindolizidine Analogues. *J. Agric. Food Chem.* 64, 2039–2045. doi:10.1021/acs.jafc.5b06112

Su, B., Cai, C., Li, Y., and Wang, Q. (2021). Design, Synthesis, Antivirus Activity, and Sars of Phenanthroquinolizidine Alkaloid Derivatives. *ACS Agric. Sci. Technol.* 1, 222–229. doi:10.1021/acsagscitech.1c00032

Su, B., Chen, F., Wang, L., and Wang, Q. (2014b). Design, Synthesis, Antiviral Activity, and Structure-Activity Relationships (Sars) of Two Types of Structurally Novel Phenanthroindo/Quinolizidine Analogues. *J. Agric. Food Chem.* 62, 1233–1239. doi:10.1021/jf405562r

Tan, Q.-W., Ni, J.-C., Zheng, L.-P., Fang, P.-H., Shi, J.-T., and Chen, Q.-J. (2018). Anti-Tobacco Mosaic Virus Quassinoids from *Ailanthus Altissima* (Mill.) Swingle. *J. Agric. Food Chem.* 66, 7347–7357. doi:10.1021/acs.jafc.8b01280

Wang, D., Liu, B., Ma, Z., Feng, J., and Yan, H. (2021a). Reticine A, a New Potent Natural Elicitor: Isolation from the Fruit Peel of Citrus Reticulate and Induction of Systemic Resistance against Tobacco Mosaic Virus and Other Plant Fungal Diseases. *Pest Manag. Sci.* 77, 354–364. doi:10.1002/ps.6025

Wang, H., and Song, H. (2020c). Synthesis of Four Optical Isomers of Antiviral Agent NK0209 and Determination of Their Configurations and Activities against a Plant Virus. *J. Agric. Food Chem.* 68, 2631–2638. doi:10.1021/acs.jafc.9b07694

Wang, J., Yu, G., Li, Y., Shen, L., Qian, Y., Yang, J., et al. (2015). Inhibitory Effects of Sulfated Lentinan with Different Degree of Sulfation against Tobacco Mosaic Virus (TMV) in Tobacco Seedlings. *Pesticide Biochem. Physiology* 122, 38–43. doi:10.1016/j.pestbp.2014.12.027

Wang, K., Hu, Y., Liu, Y., Mi, N., Fan, Z., Liu, Y., et al. (2010b). Design, Synthesis, and Antiviral Evaluation of Phenanthrene-Based Tylophorine Derivatives as Potential Antiviral Agents. *J. Agric. Food Chem.* 58, 12337–12342. doi:10.1021/jf103440s

Wang, K., Su, B., Wang, Z., Wu, M., Li, Z., Hu, Y., et al. (2010a). Synthesis and Antiviral Activities of Phenanthroindolizidine Alkaloids and Their Derivatives. *J. Agric. Food Chem.* 58, 2703–2709. doi:10.1021/jf902543r

Wang, Q., Song, H., and Wang, Q. (2022). Studies on the Biological Activity of Gem-Difluorinated 3,3′-spirocyclic Indole Derivatives. *Chin. Chem. Lett.* 33, 859–862. doi:10.1016/j.cclet.2021.08.005

Wang, T., Li, L., Zhou, Y., Lu, A., Li, H., Chen, J., et al. (2021b). Structural Simplification of Marine Natural Products: Discovery of Hamacanthin Derivatives Containing Indole and Piperazinone as Novel Antiviral and Anti-phytopathogenic-fungus Agents. *J. Agric. Food Chem.* 69, 10093–10103. doi:10.1021/acs.jafc.1c04098

Wang, T., Yang, S., Li, H., Lu, A., Wang, Z., Yao, Y., et al. (2020a). Discovery, Structural Optimization, and Mode of Action of Essramycin Alkaloid and its Derivatives as Anti-tobacco Mosaic Virus and Anti-phytopathogenic Fungus Agents. *J. Agric. Food Chem.* 68, 471–484. doi:10.1021/acs.jafc.9b06006

Wang, Y., He, F., Wu, S., Luo, Y., Wu, R., Hu, D., et al. (2020b). Design, Synthesis, Anti-TMV Activity, and Preliminary Mechanism of Cinnamic Acid Derivatives Containing Dithioacetal Moiety. *Pesticide Biochem. Physiology* 164, 115–121. doi:10.1016/j.pestbp.2020.01.002

Wang, Y., Zhang, J., He, F., Gan, X., Song, B., and Hu, D. (2019). Design, Synthesis, Bioactivity and Mechanism of Dithioacetal Derivatives Containing Dioxyether Moiety. *Bioorg. Med. Chem. Lett.* 29, 2218–2223. doi:10.1016/j.bmcl.2019.06.030

Wang, Z., Feng, A., Cui, M., Liu, Y., Wang, L., and Wang, Q. (2014a). Design, Synthesis, Anti-tobacco Mosaic Virus (TMV) Activity, and Sars of 7-Methoxycryptopleurine Derivatives. *Chem. Biol. Drug. Des.* 84, 531–542. doi:10.1111/cbdd.12340

Wang, Z., Wang, L., Ma, S., Liu, Y., Wang, L., and Wang, Q. (2012a). Design, Synthesis, Antiviral Activity, and Sars of 14-Aminophenanthroindolizidines. *J. Agric. Food Chem.* 60, 5825–5831. doi:10.1021/jf3013376

Wang, Z., Wei, P., Liu, Y., and Wang, Q. (2014b). D and E Rings May Not Be Indispensable for Antofine: Discovery of Phenanthrene and Alkylamine Chain Containing Antofine Derivatives as Novel Antiviral Agents against Tobacco Mosaic Virus (TMV) Based on Interaction of Antofine and TMV RNA. *J. Agric. Food Chem.* 62, 10393–10404. doi:10.1021/jf5028894

Wang, Z., Wei, P., Wang, L., and Wang, Q. (2012c). Design, Synthesis, and Anti-tobacco Mosaic Virus (TMV) Activity of Phenanthroindolizidines and Their Analogues. *J. Agric. Food Chem.* 60, 10212–10219. doi:10.1021/jf303550a

Wang, Z., Wei, P., Xizhi, X., Liu, Y., Wang, L., and Wang, Q. (2012b). Design, Synthesis, and Antiviral Activity Evaluation of Phenanthrene-Based Antofine Derivatives. *J. Agric. Food Chem.* 60, 8544–8551. doi:10.1021/jf302746m

Wang, Z., Xie, D., Gan, X., Zeng, S., Zhang, A., Yin, L., et al. (2017). Synthesis, Antiviral Activity, and Molecular Docking Study of Trans-ferulic Acid Derivatives Containing Acylhydrazone Moiety. *Bioorg. Med. Chem. Lett.* 27, 4096–4100. doi:10.1016/j.bmcl.2017.07.038

Wei, C., Zhang, J., Shi, J., Gan, X., Hu, D., and Song, B. (2019). Synthesis, Antiviral Activity, and Induction of Plant Resistance of Indole Analogues Bearing Dithioacetal Moiety. *J. Agric. Food Chem.* 67, 13882–13891. doi:10.1021/acs.jafc.9b05357

Wei, C., Zhao, L., Sun, Z., Hu, D., and Song, B. (2020). Discovery of Novel Indole Derivatives Containing Dithioacetal as Potential Antiviral Agents for Plants. *Pesticide Biochem. Physiology* 166, 104568. doi:10.1016/j.pestbp.2020.104568

Wu, J., Zhu, Y.-Y., Zhao, Y.-H., Shan, W.-L., Hu, D.-Y., Chen, J.-X., et al. (2016). Synthesis and Antiviral Activities of Novel 1,4-Pentadien-3-One Derivatives Bearing an Emodin Moiety. *Chin. Chem. Lett.* 27, 948–952. doi:10.1016/j.cclet.2016.01.051

Wu, M., Han, G., Meng, C., Wang, Z., Liu, Y., and Wang, Q. (2014). Design, Synthesis, and Anti-tobacco Mosaic Virus (TMV) Activity of Glycoconjugates of Phenanthroindolizidines Alkaloids. *Mol. Divers* 18, 25–37. doi:10.1007/s11030-013-9484-4

Wu, M., Han, G., Wang, Z., Liu, Y., and Wang, Q. (2013). Synthesis and Antiviral Activities of Antofine Analogues with Different C-6 Substituent Groups. *J. Agric. Food Chem.* 61, 1030–1035. doi:10.1021/jf304905k

Xia, Q., Dong, J., Li, L., Wang, Q., Liu, Y., and Wang, Q. (2018). Discovery of Glycosylated Genipin Derivatives as Novel Antiviral, Insecticidal, and Fungicidal Agents. *J. Agric. Food Chem.* 66, 1341–1348. doi:10.1021/acs.jafc.7b05861

Xie, J., Xu, W., Song, H., Liu, Y., Zhang, J., and Wang, Q. (2020). Synthesis and Antiviral/Fungicidal/Insecticidal Activities Study of Novel Chiral Indole Diketopiperazine Derivatives Containing Acylhydrazone Moiety. *J. Agric. Food Chem.* 68, 5555–5571. doi:10.1021/acs.jafc.0c00875

Yan, C., Dong, J., Liu, Y., Li, Y., and Wang, Q. (2021). Target-Directed Design, Synthesis, Antiviral Activity, and Sars of 9-Substituted Phenanthroindolizidine Alkaloid Derivatives. *J. Agric. Food Chem.* 69, 7565–7571. doi:10.1021/acs.jafc.1c02276

Yan, X.-H., Chen, J., Di, Y.-T., Fang, X., Dong, J.-H., Sang, P., et al. (2010). Anti-Tobacco Mosaic Virus (TMV) Quassinoids from *Brucea Javanica* (L.) Merr. *J. Agric. Food Chem.* 58, 1572–1577. doi:10.1021/jf903434h

Yang, H., Zu, G., Liu, Y., Xie, D., Gan, X., and Song, B. (2020b). Tomato Chlorosis Virus Minor Coat Protein as A Novel Target to Screen Antiviral Drugs. *J. Agric. Food Chem.* 68, 3425–3433. doi:10.1021/acs.jafc.9b08215

Yang, Y., Zhang, J., Li, X., He, F., Wu, R., Hu, D., et al. (2020a). Discovery of Dithioacetal Derivatives Containing Sulfonamide Moiety of Novel Antiviral Agents by TMV Coat Protein as A Potential Target. *ACS Omega* 5, 22596–22602. doi:10.1021/acsomega.0c03306

Yu, X., Wei, P., Wang, Z., Liu, Y., Wang, L., and Wang, Q. (2016). Design, Synthesis, Antiviral Activity and Mode of Action of Phenanthrene-containingN-Heterocyclic Compounds Inspired by the Phenanthroindolizidine Alkaloid Antofine. *Pest. Manag. Sci.* 72, 371–378. doi:10.1002/ps.4008

Zan, N., Li, J., He, H., Hu, D., and Song, B. (2021). Discovery of Novel Chromone Derivatives as Potential Anti-TSWV Agents. *J. Agric. Food Chem.* 69, 10819–10829. doi:10.1021/acs.jafc.1c03626

Zan, N., Xie, D., Li, M., Jiang, D., and Song, B. (2020). Design, Synthesis, and Anti-tocv Activity of Novel Pyrimidine Derivatives Bearing a Dithioacetal Moiety that Targets ToCV Coat Protein. *J. Agric. Food Chem.* 68, 6280–6285. doi:10.1021/acs.jafc.0c00987

Zhang, J., He, F., Chen, J., Wang, Y., Yang, Y., Hu, D., et al. (2021b). Purine Nucleoside Derivatives Containing a Sulfa Ethylamine Moiety: Design, Synthesis, Antiviral Activity, and Mechanism. *J. Agric. Food Chem.* 69, 5575–5582. doi:10.1021/acs.jafc.0c06612

Zhang, J., Zhao, L., Zhu, C., Wu, Z., Zhang, G., Gan, X., et al. (2017). Facile Synthesis of Novel Vanillin Derivatives Incorporating a Bis(2-Hydroxyethyl) dithhioacetal Moiety as Antiviral Agents. *J. Agric. Food Chem.* 65, 4582–4588. doi:10.1021/acs.jafc.7b01035

Zhang, X., Huang, W., Lu, X., Liu, S., Feng, H., Yang, W., et al. (2021a). Identification of Carbazole Alkaloid Derivatives with Acylhydrazone as Novel Anti-TMV Agents with the Guidance of a Digital Fluorescence Visual Screening. *J. Agric. Food Chem.* 69, 7458–7466. doi:10.1021/acs.jafc.1c00897

Zhang, X., Zhou, Y., Wei, Z., Shen, J., Wang, L., Ma, Z., et al. (2018). Antiphytoviral Toxins of *Actinidia Chinensis* Root Bark (ACRB) Extract: Laboratory and Semi-field Trials. *Pest. Manag. Sci.* 74, 1630–1636. doi:10.1002/ps.4854

Zhao, L., Chen, Y., Wu, K., Yan, H., Hao, X., and Wu, Y. (2017a). Application of Fatty Acids as Antiviral Agents against Tobacco Mosaic Virus. *Pesticide Biochem. Physiology* 139, 87–91. doi:10.1016/j.pestbp.2017.05.005

Zhao, L., Dong, J., Hu, Z., Li, S., Su, X., Zhang, J., et al. (2017c). Anti-TMV Activity and Functional Mechanisms of Two Sesquiterpenoids Isolated from Tithonia Diversifolia. *Pesticide Biochem. Physiology* 140, 24–29. doi:10.1016/j.pestbp.2017.05.009

Zhao, L., Feng, C., Wu, K., Chen, W., Chen, Y., Hao, X., et al. (2017b). Advances and Prospects in Biogenic Substances against Plant Virus: A Review. *Pesticide Biochem. Physiology* 135, 15–26. doi:10.1016/j.pestbp.2016.07.003

Zhao, L., Hu, Z., Li, S., Zhang, L., YuZhang, P. J., Zhang, J., et al. (2020b). Tagitinin A from *Tithonia* Diversifolia Provides Resistance to Tomato Spotted Wilt Orthotospovirus by Inducing Systemic Resistance. *Pesticide Biochem. Physiology* 169, 104654. doi:10.1016/j.pestbp.2020.104654

Zhao, L., Zhang, J., Liu, T., Mou, H., Wei, C., Hu, D., et al. (2020a). Design, Synthesis, and Antiviral Activities of Coumarin Derivatives Containing Dithioacetal Structures. *J. Agric. Food Chem.* 68, 975–981. doi:10.1021/acs.jafc.9b06861

Zhou, D., Xie, D., He, F., Song, B., and Hu, D. (2018). Antiviral Properties and Interaction of Novel Chalcone Derivatives Containing a Purine and Benzenesulfonamide Moiety. *Bioorg. Med. Chem. Lett.* 28, 2091–2097. doi:10.1016/j.bmcl.2018.04.042

Zhou, X., Ye, Y., Liu, S., Shao, W., Liu, L., Yang, S., et al. (2021). Design, Synthesis and Anti-TMV Activity of Novel α-aminophosphonate Derivatives Containing a Chalcone Moiety that Induce Resistance against Plant Disease and Target the TMV Coat Protein. *Pesticide Biochem. Physiology* 172, 104749. doi:10.1016/j.pestbp.2020.104749

Zhu, Y. J., Wu, Q. F., Fan, Z. J., Huo, J. Q., Zhang, J. L., Zhao, B., et al. (2019). Synthesis, Bioactivity and Mode of Action of 5 A 5 B 6 C Tricyclic Spirolactones as Novel Antiviral Lead Compounds. *Pest. Manag. Sci.* 75, 292–301. doi:10.1002/ps.5115

Zu, G., Gan, X., Xie, D., Yang, H., Zhang, A., Li, S., et al. (2020). Design, Synthesis, and Anti-ToCV Activity of Novel 4(3*H*)-Quinazolinone Derivatives Bearing Dithioacetal Moiety. *J. Agric. Food Chem.* 68, 5539–5544. doi:10.1021/acs.jafc.0c00086

Check for updates

Synthesis and Bioactivities of Novel Piperonylic Acid Derivatives Containing a Sulfonic Acid Ester Moiety

Dandan Xie [1,2]*, Xin Hu [3], Xiaoli Ren [1,2] and Zaiping Yang [4]

[1]State Key Laboratory Breeding Base of Green Pesticide and Agricultural Bioengineering, Ministry of Education, Guizhou University, Huaxi District, Guiyang, China, [2]Key Laboratory of Green Pesticide and Agricultural Bioengineering, Ministry of Education, Guizhou University, Huaxi District, Guiyang, China, [3]School of Biological Sciences, Guizhou Education University, Wudang District, Guiyang, China, [4]School of Biologi and Engineering, Guizhou Medical University, Huaxi District, Guiyang, China

The crop loss caused by bacteria has increased year by year due to the lack of effective control agents. In order to develop efficient, broad-spectrum, and structurally simple agricultural bactericide, the structure of piperonylic acid was modified and a series of novel piperonylic acid derivatives containing a sulfonic acid ester moiety was synthesized. Bioassay results indicated the compounds exhibited significantly antibacterial activities. Among them, compound **41** exhibited excellent antibacterial activities against *Pseudomonas syringae pv. Actinidiae* (Psa), with inhibitory value 99 and 85% at 100 μg/ml and 50 μg/ml, respectively, which was higher than that of thiodiazole-copper (84 and 77%) and bismerthiazol (96 and 78%). In addition, some compounds also showed moderate insecticidal activity against *Spodoptera frugiperda.* The abovementioned results confirm the broadening of the application of piperonylic acid, with reliable support for the development of novel agrochemical bactericide.

Keywords: piperonylic acid, sulfonic acid esters, synthesis, antibacterial activities, insecticidal activity

1 INTRODUCTION

Crop diseases caused by bacteria are considered as the second largest disease in agriculture, second only to fungal diseases, and cause major agricultural losses every year (Abdullahiab et al., 2020; Wang et al., 2021). Although there are some agents widely used to control bacterial diseases, such as bismerthiazol, streptomycin, and copper compounds (Chen M. H. et al., 2021), due to long-term and large-scale use for many years, it not only caused resistance in bacteria but also caused serious environmental problems. Pests were also an important culprit in reducing crop yields. In addition to fed directly on crops, pests also transmitted many viruses and bacteria during migration and feeding. Therefore, it was very necessary to develop an efficient and broad-spectrum agricultural bactericide (Wang et al., 2022).

Due to its characteristics of unique mechanism of action, novel scaffolds, and easy derivation, the natural products have always been a valuable source for lead compounds discovery in agricultural chemistry. Piperonylic acid is an aromatic acid mainly found in black pepper (Moreira et al., 2021). Lots of research results revealed members of the piperonylic acid family had a range of biological activities and were further developed into a commercial drug and widely used in the field of medicine, such as oxolinic acid (Yamazawa et al., 2021; Boycov et al., 2022; Quan et al., 2022), kakuol (Jang et al., 2020; Matsumoto et al., 2020; Sui et al., 2020), and miloxacin (Horie and Nakazawa, 1992; Ueno

GRAPHICAL ABSTRACT |
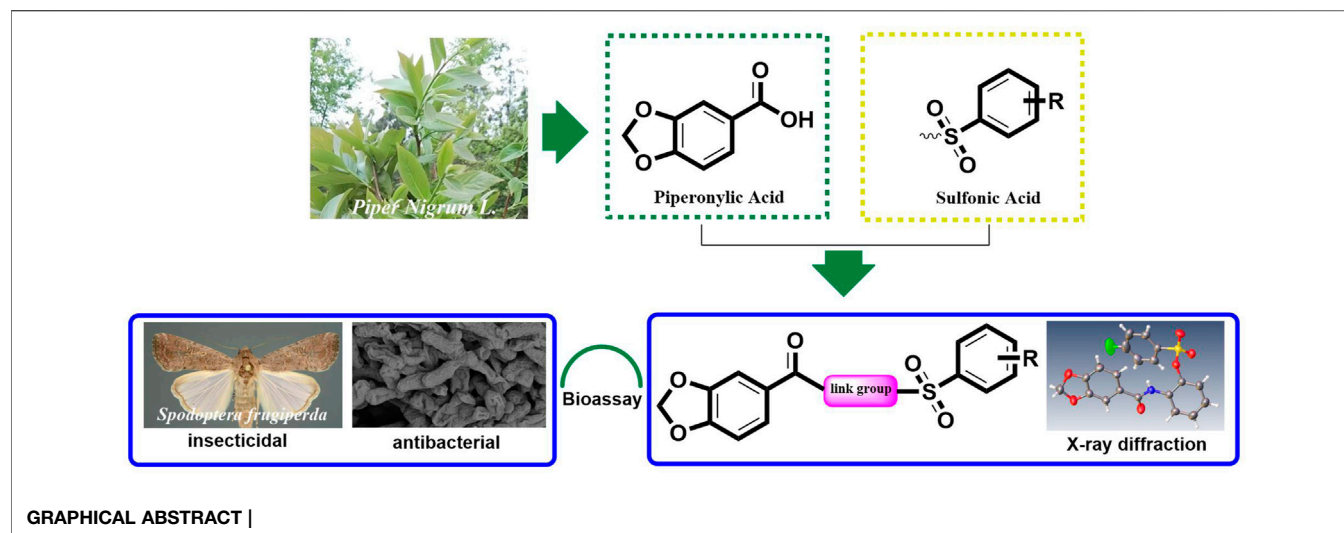
and Aoki, 1996; Ueno et al., 2001). In addition, piperonylic acid derivatives also showed good activity against bacteria (Umadevi et al., 2013). Sulfonic acid groups are widely used in the field of medicine mainly in the form of sulfonate derivatives. Such as apatinib mesylate (Guo Q. et al., 2020; Chen M. et al., 2021; Kou et al., 2021; Zheng et al., 2021), donafenib tosylate (Wang et al., 2017), and dabrafenib mesylate (Carlos et al., 2015; Liu et al., 2019; Rai et al., 2020) that have been widely used to treat cancer, gemifloxacin mesylate for antibacterial (Chai et al., 2019), and pradefovir mesylate for antiviral (Tuerkova and Zdrazil, 2020). However, many research results revealed that sulfonic acid ester derivatives also had very extensive and excellent biological activities, especially the antibacterial activity was impressive. Guo et al. (2019) and Guo T. et al. (2020) had reported that by splicing a sulfonic acid ester moiety into the backbone of 1,4-pentadien-3-one and chalcone, respectively, the two series of derivatives obtained showed excellent inhibitory activities against bacteria such as *Xanthomonas axonopodis pv. citri* (*Xac*),

Ralstonia solanacearum (*Rs*), and *Xanthomonas oryzae pv. oryzae* (*Xoo*). Inspired by the results of these studies, the present work aims to incorporate a sulfonic acid ester moiety into the piperonylic acid backbone to synthesize a series of novel derivatives, and further evaluate their antibacterial and insecticidal activity, and hope to obtain piperonylic acid derivatives with good antibacterial activities.

2 EXPERIMENTAL

2.1 Chemistry

All starting materials and reagents were commercially available and used without further purification, except as indicated. The ^{1}H NMR and ^{13}C NMR spectra were recorded on a Bruker DPX 400 MHz (Bruker BioSpin GmbH, Rheinstetten, Germany) NMR spectrometer with $CDCl_3$ as the solvent. The following abbreviations were used to explain the multiplicities: s, singlet;

4a: R= -4-FPh; **4b**: R= -CH$_2$-Ph; **4c**: R= -2,5-2ClPh; **4d**: R= -2-BrPh; **4e**: R= -3,5-2FPh; **4f**: R= -4-CH$_3$OPh;
4g: R=-2-ClPh; **4h**: R= -2-Naphthalene; **4i**: R= -2,4,6-3CH$_3$Ph; **4j**: R= -4-ClPh; **4k**: R= -4-CF$_3$Ph; **4l**: R= -Ph;
4m: R= -2-FPh; **4n**: R= -4-tBuPh; **4o**: R= -4-BrPh; **4p**: R= -2,5-2FPh; **4q**: R= -3-NO$_2$Ph; **4r**: R= -3-FPh;
4s: R= -2,4-2FPh; **4t**: R= -3-CF$_3$Ph; **4u**: R= -2-CF$_3$Ph; **4v**: R= -3-BrPh; **4w**: R= -3-ClPh; **4x**= -4-CH$_3$Ph
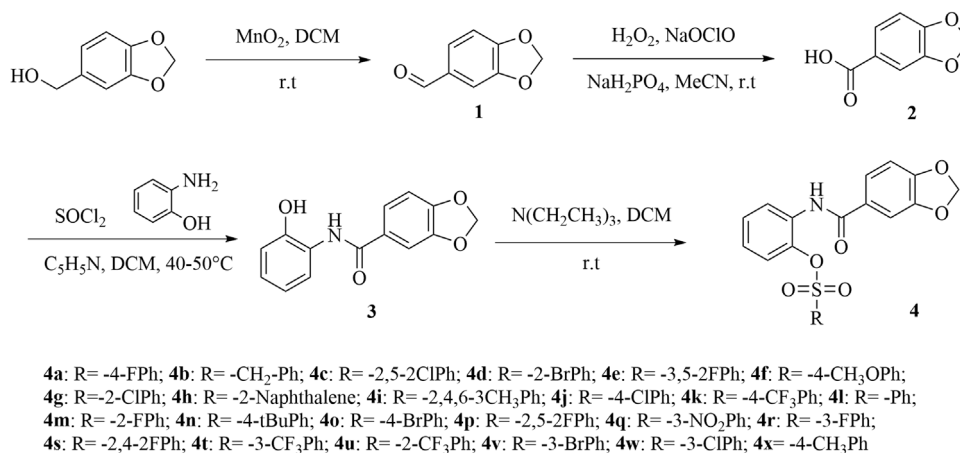
SCHEME 1 | The synthetic route of title compounds 4a-4x.

d, doublet; t, triplet; m, multiplet; and br, broadened. The melting points were determined on a WRX-4 microscope melting point apparatus (YiCe Apparatus & Equipment co., LTD, Shanghai, China). High-resolution mass spectrometry (HRMS) was conducted using a Thermo Scientific Q Exactive (Thermo Fisher Scientific, Massachusetts, America). The X-ray crystallographic data were determined on a D8 Quest X-ray diffractometer (Bruker BioSpin GmbH, Rheinstetten, German).

2.1.1 General Procedures for Preparing Compounds

The synthetic route for the final compounds **4a–4x** were depicted in **Scheme 1**. Intermediates **1–2** were synthesized according to a previously reported method (Dam and Madsen, 2009; Zazeri et al., 2020). Intermediate **3** was prepared according to literature method (Joseph et al., 2019). Target compounds **4a–4x** were synthesized by condensation of different sulfonyl chloride which contained different substituent group and intermediate **3** at room temperature condition. Intermediate **2** equivalent of triethylamine was added to the system as a catalyst to neutralize the HCl generated by the reaction so that the reaction can proceed smoothly. After approximately about 4 h, the solvent was removed, and the residue was purified by flash chromatography on silica gel with petroleum *n*-hexane/ ethyl acetate (volume ratio 5:1) to obtain the pure product.

2.1.1.1 N-(2-((4-fluorophenyl)sulfonyl)phenyl)benzo[d][1,3] dioxole-5-carboxamide (4a)

Light yellow powder, yield 82%. m.p 133.4–134.7°C. ^{1}H NMR (400 MHz, CDCl$_3$) δ 8.32 (dd, J = 8.3, 1.6 Hz, 1H, Ph-H), 8.26 (s, 1H, -NH-), 7.87 (dd, J = 9.0, 4.9 Hz, 2H, Ph-H), 7.40 (dd, J = 8.1, 1.9 Hz, 1H, Ph-H), 7.36–7.29 (m, 2H, Ph-H), 7.21–7.10 (m, 2H, Ph-H), 7.06–7.02 (m, 1.6 Hz, 1H, Ph-H), 6.94–6.87 (m, 2H, Ph-H), 6.09 (s, 2H, -OCH$_2$O-). ^{13}C NMR (100 MHz, CDCl$_3$) δ 164.4, 151.0, 148.3, 139.2, 131.5, 131.4, 128.2, 124.5, 123.3, 122.9, 122.0, 117.1, 116.8, 108.3, 107.7, 102.0. HRMS (ESI): calculated for C$_{20}$H$_{14}$FNO$_6$S [M + Na]$^+$: 438.0526, found: 438.0418.

2.1.1.2 2-(Benzo[d][1,3]dioxole-5-carboxamido)phenyl Phenyl Methanesulfonate (4b)

Light yellow powder, yield 80%. m.p 127.5–128.5°C. ^{1}H NMR (400 MHz, CDCl$_3$) δ 7.48 (dd, J = 7.8, 1.8 Hz, 1H, -NH-), 7.29 (s, 2H, Ph-H), 7.13–7.01 (m, 6H, Ph-H), 6.95 (dd, J = 8.2, 1.5 Hz, 1H, Ph-H), 6.83 (d, J = 8.7 Hz, 1H, Ph-H), 6.07 (s, 2H, -OCH$_2$O-), 4.65 (s, 2H, -CH$_2$-PH). ^{13}C NMR (100 MHz, CDCl$_3$) δ 164.6, 150.8, 148.1, 138.0, 131.8, 130.9, 129.6, 129.2, 128.4, 128.2, 126.8, 124.6, 123.3, 123.0, 122.1, 108.2, 107.8, 101.8, 57.8. HRMS (ESI): calculated for C$_{21}$H$_{17}$NO$_6$S [M + Na]$^+$: 434.0777, found: 434.0667.

2.1.1.3 2-(Benzo[d][1,3]dioxole-5-carboxamido)phenyl 2,5-Dichlorobenzenesulfonate (4c)

Light yellow powder, yield 83%. m.p 149.7–152.7°C. ^{1}H NMR (400 MHz, CDCl$_3$) δ 8.67 (s, 1H, -NH-), 8.30–7.76 (m, 2H, Ph-H), 7.69–7.33 (m, 2H, Ph-H, Ph-H), 7.21–6.74 (m, 6H, Ph-H), 6.08 (s, 2H, -OCH$_2$O-). ^{13}C NMR (100 MHz, CDCl$_3$) δ 166.4 151.3, 148.8, 127.2, 125.7, 122.4, 122.3, 120.6, 119.8, 108.3, 107.9,

102.1. HRMS (ESI): calculated for C$_{20}$H$_{13}$Cl$_2$NO$_6$S [M + Na]$^+$: 487.9732, found: 487.9705.

2.1.1.4 2-(Benzo[d][1,3]dioxole-5-carboxamido)phenyl 2-Bromobenzenesulfonate (4d)

Light yellow powder, yield 85%. m.p 130.5–132.5°C. ^{1}H NMR (400 MHz, CDCl$_3$) δ 8.58 (s, 1H, -NH-), 8.37 (dd, J = 8.3, 1.6 Hz, 1H, Ph-H), 8.11–8.04 (m, 1H, Ph-H), 7.78 (d, J = 7.5 Hz, 1H, Ph-H), 7.56–7.46 (m, 3H, Ph-H), 7.41 (d, J = 1.8 Hz, 1H, Ph-H), 7.31–7.29 (m, 1H, Ph-H), 7.16–6.98 (m, 2H, Ph-H), 6.90 (d, J = 8.1 Hz, 1H, Ph-H), 6.08 (s, 2H, -OCH$_2$O-). ^{13}C NMR (100 MHz, CDCl$_3$) δ 164.7, 151.0, 148.2, 138.8, 135.9, 135.6, 132.6, 128.2, 128.0, 124.5, 123.3, 122.8, 122.3, 121.3, 108.2, 108.0, 101.9. HRMS (ESI): calculated for C$_{20}$H$_{14}$BrNO$_6$S [M + Na]$^+$: 497.9617, found: 497.9614.

2.1.1.5 2-(Benzo[d][1,3]dioxole-5-carboxamido)phenyl 3,5-Difluorobenzenesulfonate (4e)

Light yellow powder, yield 81.5%. m.p 152.7–153.8°C. ^{1}H NMR (400 MHz, CDCl$_3$) δ 8.32 (dd, J = 8.3, 1.6 Hz, 1H, Ph-H), 8.17 (s, 1H, -NH-), 7.46–7.31 (m, 5H, Ph-H), 7.17–6.82 (m, 4H, Ph-H), 6.09 (s, 2H, -OCH$_2$O-). ^{13}C NMR (100 MHz, CDCl$_3$) δ 164.4, 161.6, 151.1, 148.4, 139.1, 131.2, 128.5, 128.1, 124.8, 123.6, 122.6, 121.9, 112.3, 112.0, 110.6, 108.3, 107.7, 102.0. HRMS (ESI): calculated for C$_{20}$H$_{13}$F$_2$NO$_6$S [M + Na]$^+$: 456.0324, found: 456.0319.

2.1.1.6 2-(Benzo[d][1,3]dioxole-5-carboxamido)phenyl 4-Methoxybenzenesulfonate (4f)

Light yellow powder, yield 89%. m.p 94.3–95.2°C. ^{1}H NMR (400 MHz, CDCl$_3$) δ 8.34 (s, 1H, -NH-), 8.32 (d, J = 2.0 Hz, 1H, Ph-H), 7.75 (d, J = 9.0 Hz, 2H, Ph-H), 7.39 (dd, J = 8.1, 1.9 Hz, 1H, Ph-H), 7.34–7.28 (m, 2H, Ph-H), 7.01 (dd, J = 7.5, 1.6 Hz, 1H, Ph-H), 6.95–6.87 (m, 4H, Ph-H), 6.08 (s, 2H, -OCH$_2$O-), 3.86 (s, 3H, -OCH$_3$). ^{13}C NMR (100 MHz, CDCl$_3$) δ 164.6, 164.4, 150.9, 139.3, 130.8, 127.9, 125.7, 124.4, 123.1, 122.9, 122.0, 114.7, 108.2, 107.8, 101.9, 55.8. HRMS (ESI): calculated for C$_{21}$H$_{17}$NO$_7$S [M + Na]$^+$: 450.0618, found: 450.0619.

2.1.1.7 2-(Benzo[d][1,3]dioxole-5-carboxamido)phenyl 2-Chlorobenzenesulfonate (4g)

Light yellow powder, yield 88%. m.p 101.8–103.6°C. ^{1}H NMR (400 MHz, CDCl$_3$) δ 8.53 (s, 1H, -NH-), 8.40 (dd, J = 8.3, 1.6 Hz, 1H, Ph-H), 7.93–7.90 (m, 1H, Ph-H), 7.73–7.67 (m, 1H, Ph-H), 7.49 (dd, J = 8.1, 1.9 Hz, 1H, Ph-H), 7.42 (d, J = 1.8 Hz, 1H, Ph-H), 7.36–7.29 (m, 2H, Ph-H), 7.24–7.16 (m, 1H, Ph-H), 7.09–7.05 (m, 1H, Ph-H), 6.91 (d, J = 8.2 Hz, 1H, Ph-H), 6.08 (s, 2H, -OCH$_2$O-). ^{13}C NMR (100 MHz, CDCl$_3$) δ 164.6, 160.8, 158.2, 151.0, 148.2, 138.4, 137.5, 137.4, 131.5, 131.4, 128.4, 128.2, 124.8, 124.5, 123.0, 122.8, 122.2, 117.7, 117.5, 108.2, 107.9, 101.9. HRMS (ESI): calculated for C$_{20}$H$_{14}$ClNO$_6$S [M + Na]$^+$: 454.0210, found: 424.0146.

2.1.1.8 2-(Benzo[d][1,3]dioxole-5-carboxamido)phenyl Naphthalene-2-sulfonate (4h)

Light yellow powder, yield 83%. m.p 145.6–147.1°C. ^{1}H NMR (400 MHz, CDCl$_3$) δ 8.44 (s, 1H, Ph-H), 8.32 (dd, J = 8.3, 1.4 Hz,

1H, Ph-H), 8.22 (s, 1H, -NH-), 7.90 (q, *J* = 8.4 Hz, 3H, Ph-H), 7.75–7.58 (m, 3H, Ph-H), 7.32–7.27 (m, 1H, Ph-H), 7.24–7.16 (m, 2H, Ph-H), 6.77 (d, *J* = 8.1 Hz, 1H, -OCH₂O-). ¹³C NMR (100 MHz, CDCl₃) δ 164.3, 150.8, 148.1, 139.3, 135.6, 131.8, 131.6, 131.4, 130.5, 129.9, 129.5, 128.1, 128.0, 124.4, 123.1, 123.0, 122.4, 121.7, 108.1, 107.7, 101.8. HRMS (ESI): calculated for $C_{24}H_{17}Cl_2NO_6S$ [M + Na]⁺: 470.0777, found: 470.6777.

2.1.1.9 2-(Benzo[d][1,3]dioxole-5-carboxamido)phenyl 2,4,6-Trimethylbenzenesulfonate (4i)

Light yellow powder, yield 84%. m.p 130.5–131.6°C. ¹H NMR (400 MHz, CDCl₃) δ 8.60 (s, 1H, -NH-), 8.38 (dd, *J* = 8.3, 1.6 Hz, 1H, Ph-H), 7.47 (dd, *J* = 8.1, 1.8 Hz, 1H, Ph-H), 7.41 (d, *J* = 1.9 Hz, 1H, Ph-H), 7.29 (d, *J* = 1.4 Hz, 1H, Ph-H), 7.02–6.84 (m, 4H, Ph-H), 6.67 (dd, *J* = 8.2, 1.5 Hz, 1H, Ph-H), 6.07 (s, 2H, -OCH₂O-), 2.56 (s, 6H, -2CH₃), 2.34 (s, 3H, -CH₃). ¹³C NMR (100 MHz, CDCl₃) δ 164.6, 150.9, 148.2, 144.7, 140.7, 139.1, 132.1, 132.0, 129.8, 128.7, 127.8, 124.3, 123.2, 122.5, 122.0, 108.2, 107.9, 101.8, 22.9, 21.2. HRMS (ESI): calculated for $C_{23}H_{21}NO_6S$ [M + Na]⁺: 462.0982, found: 462.0977.

2.1.1.10 2-(Benzo[d][1,3]dioxole-5-carboxamido)phenyl 4-Chlorobenzenesulfonate (4j)

Light yellow powder, yield 85%. m.p 134.6–137.0°C. ¹H NMR (400 MHz, CDCl₃) δ 8.31 (dd, *J* = 8.3, 1.6 Hz, 1H, Ph-H), 8.19 (s, 1H, -NH-), 7.77 (d, *J* = 8.6 Hz, 2H, Ph-H), 7.44 (d, *J* = 8.6 Hz, 2H, Ph-H), 7.37 (dd, *J* = 8.1, 1.9 Hz, 1H, Ph-H), 7.33–7.29 (m, 2H, Ph-H), 7.13–7.02 (m, 1H, Ph-H), 6.95 (dd, *J* = 8.2, 1.5 Hz, 1H, Ph-H), 6.90 (d, *J* = 8.1 Hz, 1H, Ph-H), 6.09 (s, 2H, -2CH₃). ¹³C NMR (100 MHz, CDCl₃) δ 164.3, 151.1, 148.3, 141.8, 139.2, 133.1, 131.3, 129.9, 129.8, 128.2, 124.6, 123.3, 122.9, 121.9, 108.3, 107.7, 102.0. HRMS (ESI): calculated for $C_{20}H_{14}ClNO_6S$ [M + Na]⁺: 454.0122, found: 454.0119.

2.1.1.11 2-(Benzo[d][1,3]dioxole-5-carboxamido)phenyl 4-(Trifluoromethyl)benzenesulfonate (4k)

Light yellow powder, yield 82.3%. m.p 120.8–122.5°C. ¹H NMR (400 MHz, CDCl₃) δ 8.31 (dd, *J* = 8.3, 1.6 Hz, 1H, Ph-H), 8.17 (s, 1H, -NH-), 8.05–7.66 (m, 4H, Ph-H), 7.46–7.29 (m, 3H, Ph-H), 7.10–6.86 (m, 3H, Ph-H), 6.09 (s, 2H, -OCH₂O-). ¹³C NMR (100 MHz, CDCl₃) δ 164.2, 151.1, 148.3, 139.2, 138.3, 131.2, 129.0, 128.4, 128.1, 126.6, 126.7, 124.7, 123.6, 122.8, 121.9, 108.2, 107.7, 102.0. HRMS (ESI): calculated for $C_{21}H_{14}F_3NO_6S$ [M + Na]⁺: 488.0386, found: 488.0386.

2.1.1.12 2-(Benzo[d][1,3]dioxole-5-carboxamido)phenyl Benzenesulfonate (4l)

Light yellow powder, yield 86.2%. m.p 140.0–140.9°C. ¹H NMR (400 MHz, CDCl₃) δ 8.34 (dd, *J* = 8.3, 1.6 Hz, 1H, Ph-H), 8.31 (s, 1H, -NH-), 7.86 (dd, *J* = 8.5, 1.3 Hz, 2H, Ph-H), 7.69–7.65 (m, 1H, Ph-H), 7.52–7.48 (m, 2H, Ph-H), 7.40–7.37 (m, 1H, Ph-H), 7.35–7.28 (m, 2H, Ph-H), 7.04–7.02 (m, 1H, Ph-H), 6.95–6.86 (m, 2H, Ph-H), 6.08 (s, 2H, -OCH₂O-). ¹³C NMR (100 MHz, CDCl₃) δ 164.4, 151.0, 148.2, 139.2, 134.9, 131.4, 129.5, 128.4, 128.0, 124.4, 123.0, 122.9, 122.0, 108.2, 107.8, 101.9. HRMS (ESI): calculated for $C_{20}H_{15}NO_6S$ [M + Na]⁺: 420.0512, found: 420.0511.

2.1.1.13 2-(Benzo[d][1,3]dioxole-5-carboxamido)phenyl 2-Fluorobenzenesulfonate (4m)

Light yellow powder, yield 80%. m.p 93.7–94.7°C. ¹H NMR (400 MHz, CDCl₃) δ 8.58 (s, 1H, -NH-), 8.37 (dd, *J* = 8.3, 1.6 Hz, 1H, Ph-H), 8.05 (dd, *J* = 8.0, 1.6 Hz, 1H, Ph-H), 7.62–7.54 (m, 2H, Ph-H), 7.49 (dd, *J* = 8.1, 1.8 Hz, 1H, Ph-H), 7.41 (d, *J* = 1.8 Hz, 1H, Ph-H), 7.36–7.27 (m, 2H, Ph-H), 7.14–7.02 (m, 2H, Ph-H), 6.91 (d, *J* = 8.1 Hz, 1H, Ph-H), 6.08 (s, 2H, Ph-H). ¹³C NMR (100 MHz, CDCl₃) δ 164.7, 151.0, 138.7, 135.7, 132.4, 131.6, 128.2, 127.4, 124.5, 123.2, 122.8, 122.2, 108.2, 108.0, 101.9. HRMS (ESI): Calculated for $C_{20}H_{14}FNO_6S$ [M + K]⁺: 454.0163, found: 454.0120.

2.1.1.13 2-(Benzo[d][1,3]dioxole-5-carboxamido)phenyl 4-(tert-butyl) Benzenesulfonate (4n)

Light yellow powder, yield 82%. m.p 107.7–109.3°C. ¹H NMR (400 MHz, CDCl₃) δ 8.36 (dd, *J* = 8.3, 1.6 Hz, 1H, Ph-H), 8.33 (s, 1H, -NH-), 7.64 (dd, *J* = 111.7, 8.7 Hz, 4H, Ph-H), 7.39 (dd, *J* = 8.1, 1.9 Hz, 1H, Ph-H), 7.33–7.27 (m, 2H, Ph-H), 7.06–6.96 (m, 2H, Ph-H), 6.90 (d, *J* = 8.1 Hz, 1H, Ph-H), 6.08 (s, 2H, -OCH₂O-), 1.31 (s, 9H, -CH₃ × 3). ¹³C NMR (100 MHz, CDCl₃) δ 164.2, 159.2, 150.9, 148.2, 139.2, 131.5, 128.4, 128.3, 128.0, 126.5, 124.3, 123.0, 122.8, 122.0, 108.2, 107.8, 101.9, 35.4, 30.9. HRMS (ESI): calculated for $C_{24}H_{23}Cl_2NO_6S$ [M + Na]⁺: 476.1144, found: 476.1138.

2.1.1.14 2-(Benzo[d][1,3]dioxole-5-carboxamido)phenyl 4-Bromobenzenesulfonate (4o)

Light yellow powder, yield 83%. m.p 122.2–125.1°C. ¹H NMR (400 MHz, CDCl₃) δ 8.31 (dd, *J* = 8.3, 1.6 Hz, 1H, Ph-H), 8.17 (s, 1H, -NH-), 7.73–7.58 (m, 4H, Ph-H), 7.43–7.30 (m, 3H, Ph-H), 7.06 (td, *J* = 7.9, 1.6 Hz, 1H, Ph-H), 6.96 (dd, *J* = 8.2, 1.5 Hz, 1H, Ph-H), 6.90 (d, *J* = 8.1 Hz, 1H, Ph-H), 6.09 (s, 2H, -OCH₂O-). ¹³C NMR (100 MHz, 7.30 (m, 3H) δ 164.3, 151.1, 148.3, 139.2, 133.6, 132.9, 131.2, 130.5, 129.8, 128.2, 124.6, 123.3, 122.9, 121.9, 108.3, 107.7, 102.0. HRMS (ESI): calculated for $C_{20}H_{14}BrNO_6S$ [M + Na]⁺: 497.9617, found: 497.9612.

2.1.1.15 2-(Benzo[d][1,3]dioxole-5-carboxamido)phenyl 2,5-Difluorobenzenesulfonate (4p)

Light yellow powder, yield 88%. m.p 109.9–121.6°C. ¹H NMR (400 MHz, CDCl₃) δ 8.45 (s, 1H, -NH-), 8.39 (dd, *J* = 8.3, 1.6 Hz, 1H, Ph-H), 7.66–7.57 (m, 1H, Ph-H), 7.48 (dd, *J* = 8.1, 1.9 Hz, 1H, Ph-H), 7.44–7.30 (m, 3H, Ph-H), 7.24–7.17 (m, 2H, Ph-H), 7.10 (ddd, *J* = 8.2, 7.4, 1.6 Hz, 1H, Ph-H), 6.92 (d, *J* = 8.1 Hz, 1H, Ph-H), 6.08 (s, 2H, -OCH₂O-). ¹³C NMR (100 MHz, CDCl₃) δ 164.6, 151.1, 148.3, 138.4, 131.4, 128.5, 124.6, 123.2, 122.7, 122.1, 118.2, 108.3, 107.8, 101.9. HRMS (ESI): calculated for $C_{20}H_{13}F_2NO_6S$ [M + Na]⁺: 456.0323, found: 456.0322.

2.1.1.16 2-(Benzo[d][1,3]dioxole-5-carboxamido)phenyl 3-Nitrobenzenesulfonate (4q)

Light yellow powder, yield 81%. m.p 116.2–127.1°C. ¹H NMR (400 MHz, CDCl₃) δ 8.44 (s, 1H, -NH-), 8.24 (dd, *J* = 8.3, 1.6 Hz, 1H, Ph-H), 7.86 (dd, *J* = 7.8, 1.5 Hz, 1H, Ph-H), 7.74 (td, *J* = 7.7, 1.5 Hz, 1H, Ph-H), 7.66 (td, *J* = 7.7, 1.4 Hz, 1H, Ph-H), 7.53 (dd,
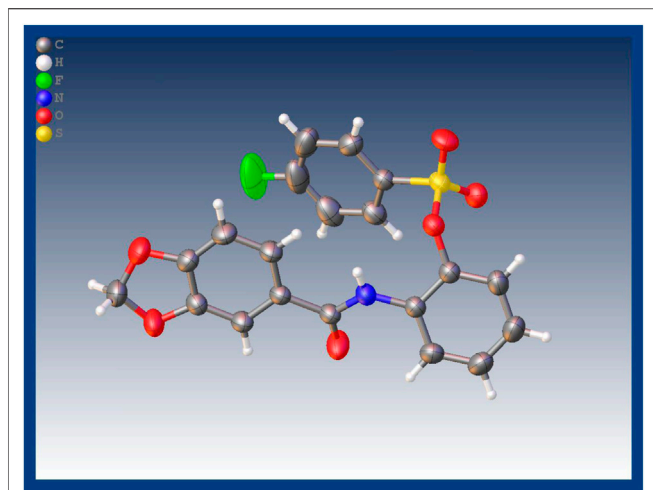
FIGURE 1 | X-ray crystal structure of compound **4a**.

$J = 7.9$, 1.4 Hz, 1H, Ph-H), 7.43–7.29 (m, 3H, Ph-H), 7.21 (d, $J = $ 1.9 Hz, 1H, Ph-H), 7.15 (ddd, $J = 8.3$, 7.5, 1.6 Hz, 1H, Ph-H), 6.86 (d, $J = 8.1$ Hz, 1H, Ph-H), 6.07 (s, 2H, -OCH$_2$O-). ^{13}C NMR (100 MHz, CDCl$_3$) δ 164.6, 151.0, 148.0, 138.9, 135.7, 132.5, 132.1, 131.0, 128.4, 128.2, 127.8, 124.9, 124.7, 123.6, 123.2, 122.4, 108.1, 108.0, 101.9. HRMS (ESI): calculated for C$_{20}$H$_{14}$Cl$_2$N$_2$O$_8$S [M + Na]$^+$: 465.0363, found: 465.0362.

2.1.1.17 2-(Benzo[d][1,3]dioxole-5-carboxamido)phenyl 3-Fluorobenzenesulfonate (4r)

Light yellow powder, yield 86.6%. m.p 160.0–162.1°C. ^{1}H NMR (400 MHz, CDCl$_3$) δ 8.33 (dd, $J = 8.3$, 1.6 Hz, 1H, Ph-H), 8.23 (s, 1H, -NH-), 7.67–7.62 (m, 1H, Ph-H), 7.59 (ddd, $J = 7.7$, 2.6, 1.7 Hz, 1H, Ph-H), 7.50 (td, $J = 8.1$, 5.1 Hz, 1H, Ph-H), 7.41–7.31 (m, 4H, Ph-H), 7.05 (ddd, $J = 8.9$, 7.4, 1.6 Hz, 1H, Ph-H), 6.96 (dd, $J = 8.2$, 1.5 Hz, 1H, Ph-H), 6.91 (d, $J = 8.1$ Hz, 1H, Ph-H), 6.09 (s, 2H, -OCH$_2$O-). ^{13}C NMR (100 MHz, CDCl$_3$) δ 164.4, 151.0, 148.3, 139.1, 131.4, 131.3, 128.3, 128.2, 124.6, 124.3, 123.3, 122.8, 122.4, 122.2, 121.9, 116.0, 115.7, 108.3, 107.7, 101.9. HRMS (ESI): calculated for C$_{20}$H$_{14}$FNO$_6$S [M + Na]$^+$: 438.0418, found: 438.0419.

2.1.1.18 2-(Benzo[d][1,3]dioxole-5-carboxamido)phenyl 2,4-Difluorobenzenesulfonate (4s)

Light yellow powder, yield 83.2%. m.p 95.6–98.4°C. ^{1}H NMR (400 MHz, CDCl$_3$) δ 8.46 (s, 1H, -NH-), 8.38 (dd, $J = 8.3$, 1.6 Hz, 1H, Ph-H), 7.97–7.87 (m, 1H, Ph-H), 7.49 (dd, $J = 8.1$, 1.9 Hz, 1H, Ph-H), 7.41 (d, $J = 1.9$ Hz, 1H, Ph-H), 7.35–7.29 (m, 1H, Ph-H), 7.21–7.14 (m, 1H, Ph-H), 7.12–6.87 (m, 4H, Ph-H), 6.09 (s, 2H, -OCH$_2$O-). ^{13}C NMR (100 MHz, CDCl$_3$) δ 164.6, 151.0, 148.3, 138.5, 133.4, 133.3, 131.4, 128.4, 124.6, 123.3, 122.8, 122.1, 112.7, 108.3, 107.8, 106.3, 101.9. HRMS (ESI): calculated for C$_{20}$H$_{13}$F$_2$NO$_6$S [M + Na]$^+$: 456.0324, found: 456.0326.

2.1.1.19 2-(Benzo[d][1,3]dioxole-5-carboxamido)phenyl 3-(Trifluoromethyl)benzenesulfonate (4t)

Light yellow powder, yield 84%. m.p 120.9–123.6°C. ^{1}H NMR (400 MHz, CDCl$_3$) δ 8.33 (dd, $J = 8.3$, 1.6 Hz, 1H, Ph-H), 8.23 (s,

1H, -NH-), 8.14 (s, 1H, Ph-H), 8.06–7.90 (m, 2H, Ph-H), 7.67 (t, $J = 7.9$ Hz, 1H, Ph-H), 7.43–7.31 (m, 3H, Ph-H), 7.06 (ddd, $J = $ 9.1, 7.4, 1.6 Hz, 1H, Ph-H), 6.94 (dd, $J = 8.3$, 1.5 Hz, 1H, Ph-H), 6.90 (d, $J = 8.1$ Hz, 1H, Ph-H), 6.08 (s, 2H, -OCH$_2$O-). ^{13}C NMR (100 MHz, CDCl$_3$) δ 164.3, 151.1, 148.3, 139.0, 135.9, 131.6, 131.2, 130.4, 128.4, 128.1, 125.5, 124.6, 123.5, 122.7, 121.9, 108.3, 107.7, 102.0. HRMS (ESI): calculated for C$_{21}$H$_{14}$F$_3$NO$_6$S [M + Na]$^+$: 488.0386, found: 488.0396.

2.1.1.20 2-(Benzo[d][1,3]dioxole-5-carboxamido)phenyl 2-(Trifluoromethyl)benzenesulfonate (4u)

Light yellow powder, yield 87%. m.p 101.3–105.4°C. ^{1}H NMR (400 MHz, CDCl$_3$) δ 8.36 (s, 1H, -NH-), 8.34 (d, $J = 4.1$ Hz, 1H, Ph-H), 8.13 (d, $J = 7.9$ Hz, 1H, Ph-H), 7.90 (d, $J = 8.3$ Hz, 1H, Ph-H), 7.85–7.69 (m, 2H, Ph-H), 7.42 (dd, $J = 8.1$, 1.8 Hz, 1H, Ph-H), 7.35 (d, $J = 1.9$ Hz, 1H, Ph-H), 7.33–7.28 (m, 1H, Ph-H), 7.08–7.04 (m, 2H, Ph-H), 6.90 (d, $J = 8.1$ Hz, 1H, Ph-H), 6.08 (s, 2H, -OCH$_2$O-). ^{13}C NMR (100 MHz, CDCl$_3$) δ 148.2, 138.8, 134.8, 132.9, 132.6, 131.4, 128.3, 124.5, 123.2, 123.0, 122.1, 108.2, 107.8, 101.9. HRMS (ESI): calculated for C$_{21}$H$_{14}$F$_3$NO$_6$S [M + Na]$^+$: 488.0386, found: 488.0388.

2.1.1.21 2-(Benzo[d][1,3]dioxole-5-carboxamido)phenyl 3-Bromobenzenesulfonate (4v)

Light yellow powder, yield 84%. m.p 158.0–158.5°C. ^{1}H NMR (400 MHz, CDCl$_3$) δ 8.34 (dd, $J = 8.3$, 1.6 Hz, 1H, Ph-H), 8.20 (s, 1H, -NH-), 8.04 (t, $J = 1.9$ Hz, 1H, Ph-H), 7.80–7.71 (m, 2H, Ph-H), 7.44–7.30 (m, 4H, Ph-H), 7.09–7.05 (m, 1H, Ph-H), 6.98 (dd, $J = $ 8.2, 1.6 Hz, 1H, Ph-H), 6.91 (d, $J = 8.1$ Hz, 1H, Ph-H), 6.09 (s, 2H, -OCH$_2$O-). ^{13}C NMR (100 MHz, CDCl$_3$) δ 151.1, 148.4, 139.1, 137.9, 136.4, 131.3, 131.1, 130.9, 128.3, 128.2, 127.0, 124.6, 123.5, 123.3, 122.8, 121.9, 108.3, 107.8, 101.9. HRMS (ESI): calculated for C$_{20}$H$_{14}$BrNO$_6$S [M + Na]$^+$: 497.9617, found: 497.9619.
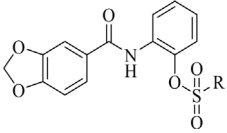
2.1.1.22 2-(Benzo[d][1,3]dioxole-5-carboxamido)phenyl 3-Chlorobenzenesulfonate (4w)

Light yellow powder, yield 86%. m.p 148.4–150.1°C. ^{1}H NMR (400 MHz, CDCl$_3$) δ 8.33 (dd, $J = 8.2$, 1.6 Hz, 1H, Ph-H), 8.20 (s, 1H, -NH-), 7.88 (t, $J = 1.9$ Hz, 1H, Ph-H), 7.74–7.67 (m, 1H, Ph-H), 7.61 (dd, $J = 2.1$, 1.0 Hz, 1H, Ph-H), 7.44 (t, $J = 8.0$ Hz, 1H, Ph-H), 7.39–7.30 (m, 3H, Ph-H), 7.07 (ddd, $J = 9.0$, 7.4, 1.6 Hz, 1H, Ph-H), 6.98 (dd, $J = 8.2$, 1.5 Hz, 1H, Ph-H), 6.91 (d, $J = 8.1$ Hz, 1H, Ph-H), 6.08 (s, 2H, -OCH$_2$O-). ^{13}C NMR (100 MHz, CDCl$_3$) δ 164.3, 151.1, 148.3, 139.1, 136.3, 135.9, 135.0, 131.3, 130.7, 128.3, 126.5, 124.6, 123.3, 122.8, 121.9, 108.3, 107.8, 101.9. HRMS (ESI): calculated for C$_{20}$H$_{14}$ClNO$_6$S [M + Na]$^+$: 454.0168, found: 454.0121.

2.1.1.23 2-(Benzo[d][1,3]dioxole-5-carboxamido)phenyl 4-Methylbenzenesulfonate (4x)

Light yellow powder, yield 85%. m.p 130.0–131.1°C. ^{1}H NMR (400 MHz, CDCl$_3$) δ 8.33 (dd, $J = 8.3$, 1.6 Hz, 1H, Ph-H), 8.28 (s, 1H, -NH-), 7.72 (d, $J = 8.4$ Hz, 2H, Ph-H), 7.38 (dd, $J = 8.1$, 1.8 Hz, 1H, Ph-H), 7.32–7.27 (m, 3H, Ph-H), 7.26 (s, 1H, Ph-H), 7.02 (td, $J = 7.8$, 7.4, 1.6 Hz, 1H, Ph-H), 6.94 (dd, $J = 8.2$, 1.5 Hz, 1H, Ph-H), 6.90 (d, $J = 8.1$ Hz, 1H, Ph-H), 6.08 (s, 2H, -OCH$_2$O-), 2.42 (s, 3H, -CH$_3$). ^{13}C NMR (100 MHz, CDCl$_3$) δ 164.3, 150.9, 148.2,

TABLE 1 | *In vitro* antibacterial activities of the target compounds **4a**–**4x**.

Compound	R	*Pseudomonas syringae pv. actinidiae (Psa)*		*Xanthomonas oryzae pv. oryzae (Xoo)*	
		100 µg/ml	50 µg/ml	100 µg/ml	50 µg/ml
4a	-4-FPh	76 ± 1.3	68 ± 2.7	52 ± 0.6	45 ± 0.9%
4b	-CH$_2$-Ph	77 ± 1.2	73 ± 1.2	42 ± 2.2	38 ± 2.3%
4c	-2,5-2ClPh	80 ± 0.8	75 ± 1.4	59 ± 1.1	52 ± 1.1%
4d	-2-BrPh	96 ± 1.5	80 ± 1.6	38 ± 1.3	30 ± 0.8%
4e	-3,5-2BrPh	83 ± 1.8	77 ± 2.4	87 ± 2.8	76 ± 1.5%
4f	-4-CH$_3$OPh	87 ± 0.7	80 ± 1.0	67 ± 3.6	51 ± 0.9%
4g	-2-ClPh	82 ± 1.0	80 ± 1.7	37 ± 1.7	61 ± 0.8%
4h	-2-Naphthalene	93 ± 2.1	80 ± 1.4	35 ± 0.5	17 ± 1.2%
4i	-2,4,6-3CH$_3$Ph	82 ± 1.1	75 ± 2.2	61 ± 1.9	44 ± 1.1%
4j	-4-ClPh	90 ± 1.7	71 ± 1.3	76 ± 0.8	43 ± 2.4%
4k	-4-CF$_3$Ph	88 ± 1.8	72 ± 2.0	53 ± 1.7	39 ± 1.2%
4l	-Ph	99 ± 2.0	85 ± 1.3	47 ± 2.7	18 ± 1.6%
4m	-2-FPh	94 ± 3.0	78 ± 0.6	45 ± 0.6	13 ± 2.9%
4n	-4-tBu Ph	88 ± 2.3	79 ± 3.0	38 ± 1.6	36 ± 1.8%
4o	-4-BrPh	99 ± 1.4	81 ± 2.1	59 ± 3.4	54 ± 2.7%
4p	-2,5-2FPh	94 ± 1.0	78 ± 1.3	54 ± 2.3	44 ± 1.3%
4q	-3-NO$_2$Ph	81 ± 1.1	78 ± 2.6	62 ± 1.8	32 ± 2.5%
4r	-3-FPh	86 ± 1.4	79 ± 2.9	61 ± 2.0	30 ± 1.3%
4s	-2,4-2FPh	91 ± 2.3	89 ± 0.8	64 ± 2.0	42 ± 2.4%
4t	-3-CF$_3$Ph	87 ± 2.1	78 ± 0.9	47 ± 1.4	9 ± 1.5%
4u	-2-CF$_3$Ph	81 ± 1.6	78 ± 1.4	44 ± 2.8	12 ± 0.3%
4v	-3-BrPh	99 ± 1.1	81 ± 1.6	64 ± 1.8	47 ± 0.4%
4w	-3-FPh	79 ± 1.6	75 ± 2.4	54 ± 2.9	30 ± 2.3%
4x	-4-CH$_3$Ph	83 ± 1.4	78 ± 1.3	29 ± 1.0	8 ± 1.5%
—	Piperonylic acid	59 ± 2.1	47 ± 1.1	21 ± 1.9	13 ± 1.7%
—	Bismerthiazol	96 ± 3.1	78 ± 2.1	55 ± 2.2	53 ± 2.3%
—	Thiodiazole-copper	84 ± 1.8	77 ± 3.1	60 ± 1.9	59 ± 0.6%

146.3, 139.2, 131.6, 131.4, 130.1, 128.4, 128.0, 124.4, 123.0, 122.9, 122.0, 108.2, 107.8, 101.9, 21.8. HRMS (ESI): calculated for $C_{21}H_{17}NO_6S$ [M + Na]$^+$: 434.0669, found: 434.0673.

2.2 Antimicrobial Assay

The antimicrobial activity of the derivatives (**4a**–**4x**) was tested using the turbidimeter test, the commercial agricultural bactericide bismerthiazol, thiodiazole-copper and lead compound piperonylic acid used as control. The test compounds were dissolved in 150 µL of dimethylformamide (DMF) and diluted with 0.1% (v/v) Tween-20 to prepare two concentrations of 100 and 50 µg/ml. One milliliter of the liquid sample was added to the 40 ml non-toxic nutrient broth medium (NB: 1.5 g of beef extract, 2.5 g of peptone, 0.5 g of yeast powder, 5.0 g of glucose, and 500 ml of distilled water, pH 7.0–7.2). Then, 40 µL of NB medium containing bacteria was added to 5 ml of solvent NB containing the test compounds or thiodiazole–copper. The inoculated test tubes were incubated at 30 ± 1°C with continuous shaking at 180 rpm for 48 h. The culture growth was monitored spectrophotometrically by measuring the optical density at 600 nm (OD$_{600}$) and expressed as corrected turbidity. The relative inhibition rates Inhibition (%) were calculated as the following equation, where C_{tur} was the corrected turbidity value of bacterial growth on untreated NB and T_{tur} was the corrected turbidity value of bacterial growth on treated NB.

$$Inhibition\,(\%) = (C_{tur} - T_{tur})/C_{tur} \times 100\%.$$

2.3 Insecticidal Activity Assay

Divide 20 second-instar larvae of *Spodoptera frugiperda* into 20 small cups and starve for 3–4 h. Cut the fresh corn leaves into small leaf discs of 1 cm × 1 cm with scissors, and then soak them in each test solution for 5 s, and then air dry them naturally. Then put them in a cup with *Spodoptera frugiperda* and keep it under the conditions of temperature of 25 ± 1°C, relative humidity of 60~70%, and a light-dark cycle of L: D = 14 h: 10 h. Feed normal fresh corn leaf discs after 12 h and record the number of dead insects at 12, 24, and 36 h.

3 RESULTS AND DISCUSSION

3.1 Chemistry

The synthetic route for the target compounds **4a**–**4x** was shown in **Scheme 1**. Intermediates **2–3** were prepared according to previously reported procedures, and the yield of all compounds was satisfactory, usually higher than 80%. In the syntheses target compounds of **4a**–**4x**, the yield when using inorganic base, such as K$_2$CO$_3$ or KHCO$_3$ as catalyst was usually only approximately 30%. When inorganic base was
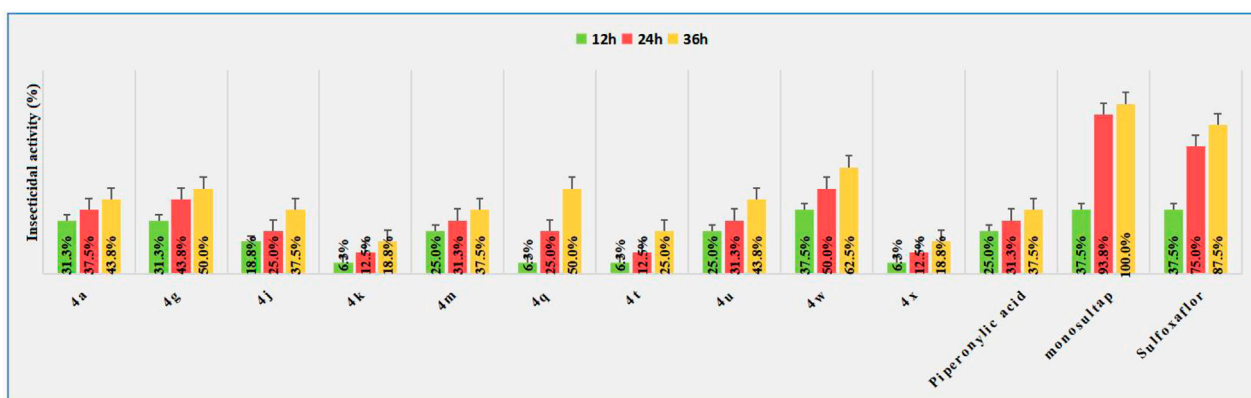
FIGURE 2 | Insecticidal activity against *Spodoptera frugiperda* of title compounds.

replaced with organic base triethylamine as the catalyst, the yield was considerably greater usually more than 80%. It was worth noting that when the intermediates **3** were synthesized using acid and 2-amino phenol the carboxyl group might have reacted with hydroxyl group to form an ester, or it may have reacted with the amino group to form an amide. These two structures of isomers were difficult to confirm through HRMS or NMR. In order to get the exact structure of the target compound, we used X-ray to confirm the structure of compound **4a**, and the results are show in **Figure 1** (CCDC 2131244). Crystal data of **4a** indicated that target compounds were in the form of carbonamide instead of carbonate.

3.2 *In Vitro* Antibacterial Activity

Antibacterial activities of target compounds **4a–4x** against agriculturally important pathogenic bacteria *Psa* and *Xoo* were determined *in vitro via* the turbidimetric method, using the commercialized bismerthiazol, thiodiazole-copper, and piperonylic acid as a control agent. The bactericide which was used to make the bioassay was provided by Guizhou Tea Institute, and the results of the bioassay against *Psa* and *Xoo* are shown in **Table 1** and indicated that most of the title compounds exhibited good to excellent activities *in vitro*. Compounds **4l, 4o,** and **4v** showed excellent activities against *Psa* at 100 µg/ml with inhibition rates of 99%, which were higher than those of thiodiazole-copper (84%), bismerthiazol (96%), and lead compound piperonylic acid (59%), respectively. In particular, even at a concentration as low as 50 µg/ml, compound **4l** was found to still possess a pronounced anti-Pas efficacy of 85%. Moreover, compounds **4e, 4f,** and **4j** exhibited higher activities (i.e., 87, 67 and 76%, respectively) against *Xoo* than that of thiodiazole-copper (60%), bismerthiazol (55%), and piperonylic acid (21%) at 100 µg/ml even at a concentration as low as 50 µg/ml, compound **4e** was found to still possess a pronounced anti-*Xoo* effifcacy of 76%, which was significantly higher than that of control agent. It is worth mentioning that whether for *Psa* or *Xoo*, the activities of almost all target compounds were significantly higher than that of the lead compound piperonylic acid. This indicated that

incorporation of a sulfonic acid ester moiety into the piperonylic acid backbone could significantly improve its antibacterial activity.

3.3 Insecticidal Activity Assay Against *Spodoptera frugiperda*

In view of the literature which reported that piperonylic acid has certain insecticidal activities, we also evaluated the activity of some title compounds against *Spodoptera frugiperda* at 50 µg/ml, The *Spodoptera frugiperda* used in the biological tests were collected from fields in Luodian County, Guizhou Province, China, and bred in a greenhouse. The pesticidal results are shown in **Figure 2**. Although most compounds exhibited certain insecticidal effect on *Spodoptera frugiperda*, such as the lethal rate of compound **4g**, **4q**, and **4w** on to the second instar larvae of the insect reached 50.0, 50.0 and 62.5% at the 36 h, respectively, which was significantly higher than the lead structure piperonylic acid (37.5%), but still lower than the commercial insecticide monosultap (100%) and sulfoxaflor (87.5%).

4 CONCLUSION

In summary, in order to seek new efficiency, broad-spectrum, and structure simple agricultural bactericide, a series of novel piperonylic acid derivatives containing a sulfonic acid ester moiety was synthesized. The structures of the title compounds were verified by ^{1}H NMR, ^{13}C NMR, and HRMS. The bioassay results revealed that these compounds showed good inhibition activity against *Xoo* and *Psa*, and some compounds even exhibited higher antibacterial activity than those of commercial bactericide which are widely used. The title compounds showed weaker activity against |*Spodoptera frugiperda* compared with commercial pesticides. Thus, we recommend these newly designed and synthesized scaffolds should be used as a bactericide lead compound rather than an insecticide lead compound for further optimization and research.

DATA AVAILABILITY STATEMENT

The original contributions presented in the study are included in the article/**Supplementary Material**; further inquiries can be directed to the corresponding author.

AUTHOR CONTRIBUTIONS

DX and XH contributed to the synthesis, purification, and characterization of all compounds and prepared the original manuscript. XH and ZY performed the biological activity research. DX and XR analyzed the experimental results and drafted the first and second version of the manuscript. All authors discussed, edited, and approved the final version.

REFERENCES

Abdullahiab, A., Khairulmazmibce, A., Yasmeen, S., Ismail, I. S., Norhayu, A., Sulaiman, M. R., et al. (2020). Phytochemical Profiling and Antimicrobial Activity of Ginger (*Zingiber Officinale*) Essential Oils against Important Phytopathogens. *Arab. J. Chem.* 13, 8012–8025. doi:10.1016/j.arabjc.2020.09.031

Boycov, D. E., Manin, A. N., Drozd, K. V., Churakov, A. V., and Perlovich, G. L. (2022). Thermal Method Usage Features for Multicomponent Crystal Screening. *CrystEngComm* 24, 2280–2290. doi:10.1039/d1ce01717a

Carlos, G., Anforth, R., Clements, A., Menzies, A. M., Carlino, M. S., Chou, S., et al. (2015). Cutaneous Toxic Effects of bRAF Inhibitors Alone and in Combination with MEK Inhibitors for Metastatic Melanoma. *JAMA Dermatol* 151, 1103–1109. doi:10.1001/jamadermatol.2015.1745

Chai, F., Zhao, X., Gao, H., Zhao, Y., Huang, H., and Gao, Z. (2019). Effective Removal of Antibacterial Drugs from Aqueous Solutions Using Porous Metal-Organic Frameworks. *J. Inorg. Organomet. Polym.* 29, 1305–1313. doi:10.1007/s10904-019-01094-3

Chen, M. H., Zhang, X., Lu, D. W., Luo, H. R., Zhou, Z. Y., Qi, X. F., et al. (2021). Synthesis and Bioactivities of Novel 1,3,4-thiadiazole Derivatives of Glucosides. *Front. Chem.* 9, 1–8. doi:10.3389/fchem.2021.645876

Chen, M., Wu, S., He, Z., Cheng, Z., Duan, S., Jiang, H., et al. (2021). Apatinib Combined with Concurrent Chemoradiotherapy in Patients with Subglottic Small Cell Carcinoma: a Case Report. *J. Int. Med. Res.* 49, 030006052110161. doi:10.1177/03000605211016146

Dam, J. H., and Madsen, R. (2009). Convergent Synthesis of Pancratistatin from Piperonal and Xylose. *Eur. J. Org. Chem.* 2009, 4666–4673. doi:10.1002/ejoc.200900719

Guo, Q., Sun, Y., Kong, E., Rao, L., Chen, J., Wu, Q., et al. (2020). Apatinib Combined with Chemotherapy or Concurrent Chemo-Brachytherapy in Patients with Recurrent or Advanced Cervical Cancer. *Medicine* 99, e19372. doi:10.1097/md.0000000000019372

Guo, T., Xia, R., Chen, M., He, J., Su, S., Liu, L., et al. (2019). Biological Activity Evaluation and Action Mechanism of Chalcone Derivatives Containing Thiophene Sulfonate. *RSC Adv.* 9, 24942–24950. doi:10.1039/c9ra05349b

Guo, T., Xia, R., Chen, M., Su, S., He, J., He, M., et al. (2020). Biological Activity Evaluation and Action Mechanism of 1,4-Pentadien-3-One Derivatives Containing Thiophene Sulfonate. *Phosphorus, Sulfur, Silicon Relat. Elem.* 195, 123–130. doi:10.1080/10426507.2019.1655418

Horie, M., and Nakazawa, H. (1992). Determination of Miloxacin and its Metabolite in Fish by High Performance Liquid Chromatography with Fluorescence and UV Detection. *J. Liq. Chromatogr.* 15, 2057–2070. doi:10.1080/10826079208016325

Jang, S., Park, S. H., and Kim, H. K. (2020). Simultaneous Determination of 6 Antiallergic Components in Asarum Sieboldii Using High-Performance Liquid Chromatography. *Nat. Prod. Commun.* 15, 1–10. doi:10.1177/1934578x20966191

ACKNOWLEDGMENTS

SUPPLEMENTARY MATERIAL

The Supplementary Material for this article can be found online at: https://www.frontiersin.org/articles/10.3389/fchem.2022.913003/full#supplementary-material

Joseph, J., Dixit, S. R., and Pujar, G. V. (2019). Design, Synthesis and *In-Vitro* Evaluation of Aryl Amides as Potent Inhibitors against Mycobacterium tuberculosis. *J. Pharm. Sci. Res.* 11, 3166–3173. http://www.jpsr.pharmainfo.in/Documents/Volumes/vol11issue09/jpsr11091913.pdf.

Kou, S.-B., Lin, Z.-Y., Wang, B.-L., Shi, J.-H., and Liu, Y.-X. (2021). Evaluation of the Interaction of Novel Tyrosine Kinase Inhibitor Apatinib Mesylate with Bovine Serum Albumin Using Spectroscopies and Theoretical Calculation Approaches. *J. Biomol. Struct. Dyn.* 39, 4795–4806. doi:10.1080/07391102.2020.1782767

Liu, C., Zhang, J., and You, G. (2019). Interaction of Anticancer Drugs with Human Organic Anion Transporter hOAT4. *J. Oncol.* 2019, 1951786. doi:10.1155/2019/1951786

Matsumoto, T., Takiyama, M., Sanechika, S., Nakayama, A., Aoki, K., Ohbuchi, K., et al. (2020). *In Vivo* pharmacokinetic Analysis Utilizing Non-targeted and Targeted Mass Spectrometry and *In Vitro* Assay against Transient Receptor Potential Channels of Maobushisaishinto and its Constituent Asiasari Radix. *Molecules* 25, 4283. doi:10.3390/molecules25184283

Moreira, K. G., do Prado, T. P., Mendes, N. F., de Medeiros Bezerra, R., Jara, C. P., Melo Lima, M. H., et al. (2021). Accelerative Action of Topical Piperonylic Acid on Mice Full Thickness Wound by Modulating Inflammation and Collagen Deposition. *PLoS One* 16, e0259134. doi:10.1371/journal.pone.0259134

Quan, X., Xu, X., and Yan, B. (2022). Facile Fabrication of Tb3+-Functionalized COF Mixed-Matrix Membrane as a Highly Sensitive Platform for the Sequential Detection of Oxolinic Acid and Nitrobenzene. *J. Hazard. Mater.* 427, 127869. doi:10.1016/j.jhazmat.2021.127869

Rai, S. K., Gunnam, A., Mannava, M. K. C., and Nangia, A. K. (2020). Improving the Dissolution Rate of the Anticancer Drug Dabrafenib. *Cryst. Growth & Des.* 20, 1035–1046. doi:10.1021/acs.cgd.9b01365

Sui, G., Xu, D., Luo, T., Guo, H., Sheng, G., Yin, D., et al. (2020). Design, Synthesis and Antifungal Activity of Amide and Imine Derivatives Containing a Kakuol Moiety. *Bioorg. Med. Chem. Lett.* 30, 126774. doi:10.1016/j.bmcl.2019.126774

Tuerkova, A., and Zdrazil, B. (2020). An Integrative Drug Repurposing Pipeline Using KNIME and Programmatic Data Access: a Case Study on COVID-19 Data. *ChemRxiv* 6, 1–32. doi:10.26434/chemrxiv.12678488

Ueno, R., and Aoki, T. (1996). High-performance Liquid Chromatographic Method for the Rapid and Simultaneous Determination of Sulfamonomethoxine, Miloxacin and Oxolinic Acid in Serum and Muscle of Cultured Fish. *J. Chromatogr. B Biomed. Sci. Appl.* 682, 179–181. doi:10.1016/0378-4347(96)00078-3

Ueno, R., Okada, Y., and Tatsuno, T. (2001). Pharmacokinetics and Metabolism of Miloxacin in Cultured Eel. *Aquaculture* 193, 11–24. doi:10.1016/s0044-8486(00)00475-0

Umadevi, P., Deepti, K., and Venugopal, D. V. R. (2013). Synthesis, Anticancer and Antibacterial Activities of Piperine Analogs. *Med. Chem. Res.* 22, 5466–5471. doi:10.1007/s00044-013-0541-4

Wang, J., Lü, B. H., Dai, X. J., Zhang, Y. F., Chen, X. Y., and Zhong, D. F. (2017). Simultaneous Determination of Donafenib and its N-Oxide Metabolite in Human Plasma by Liquid Chromatography-Tandem Mass Spectrometry.

Yao Xue Xue Bao 52, 443–448. (In Chinese). doi:10.16438/j.0513-4870.2016-0954

Wang, X., Wang, X., Zhou, B., Long, J., and Li, P. (2021). Design, Synthesis, and Evaluation of New 4(3 H)-quinazolinone Derivatives Containing a Pyrazole Carboxamide Moiety. *J. Heterocycl. Chem.* 58, 2109–2116. doi:10.1002/jhet.4334

Wang, Y., Zhou, R., Sun, N., He, M., Wu, Y., and Xue, W. (2022). Synthesis and Antibacterial Activity of Novel 1,4-pentadien-3-one Derivatives Bearing a Benzothiazole Moiety. *J. Heterocycl. Chem* 59, 533–542. doi:10.1002/jhet.4399

Yamazawa, T., Kobayashi, T., Kurebayashi, N., Konishi, M., Noguchi, S., Inoue, T., et al. (2021). A Novel RyR1-Selective Inhibitor Prevents and Rescues Sudden Death in Mouse Models of Malignant Hyperthermia and Heat Stroke. *Nat. Commun.* 12, 4293. doi:10.1038/s41467-021-24644-1

Zazeri, G., Povinelli, A. P. R., Le Duff, C. S., Tang, B., Cornelio, M. L., and Jones, A. M. (2020). Synthesis and Spectroscopic Analysis of Piperine- and Piperlongumine-Inspired Natural Product Scaffolds and Their Molecular Docking with IL-1β and NF-Kb Proteins. *Molecules* 25, 2841–2848. doi:10.3390/molecules25122841

Zheng, Q., Ma, Y., Shen, F., Wang, Q., Song, X., Jiang, W., et al. (2021). Case of Bullous Pemphigoid Induced by Apatinib Mesylate. *Br. J. Clin. Pharmacol.* 87, 2158–2159. doi:10.1111/bcp.14583

Seed Treatment with Diamide and Neonicotinoid Mixtures for Controlling Fall Armyworm on Corn: Toxicity Evaluation, Effects on Plant Growth and Residuality

Hongbo Li[1][*][†], Lei Feng[2][†], Junhong Fu[2][†], Ying Zhang[1], Wenyuan Huang[1], Tingting Duan[1], Yang Hu[1] and Jichun Xing[2][*]

[1]Institute of Plant Protection, Guizhou Academy of Agricultural Sciences, Guiyang, China, [2]Guizhou Provincial Key Laboratory for Agricultural Pest Management of the Mountainous Region, School of Agriculture, Institute of Entomology, Guizhou University, Guiyang, China

The diamides, chlorantraniliprole (CHL) and cyantraniliprole (CYA), have been used as seed treatment agents against the fall armyworm (FAW), *Spodoptera frugiperda* in China. However, large-scale application of these two insecticides is prohibited because of their high cost. The neonicotinoid insecticides, clothianidin (CLO) and thiamethoxam (THI), are cheaper and widely used. In this study, we tested the efficacy of CHL + CLO and CYA + THI as seed treatment agents against FAW larvae both in laboratory and field conditions. Laboratory experiments showed that the two binary mixtures (both 240 g.a.i.100 kg^{-1} corn seeds) caused FAW mortality exceeded 84.00% at 14 days after seedling emergence (DAE). The mortality of the binary mixtures were similar to either CHL (300 g.a.i.100 kg^{-1} corn seeds) or CYA (144 g a.i.100 kg^{-1} corn seeds), but higher than CLO (120 g.a.i.100 Kg^{-1} corn seeds) or THI (180 g a.i.100 kg^{-1} corn seeds). Two independent field experiments showed that both binary mixtures resulted in above 68.00% control efficacy at 14 DAE, suggesting that these insecticidal combinations could effectively control FAW over a relative long period. In addition, both binary mixtures showed no negative effects on the growth and development of corn seedlings. The residues of binary mixtures in corn leave were also lower at 28 DAE as compared to residues in CHL or CYA alone. Most importantly, the costs of CHL + CLO were reduced up to 50% and CYA + THI up to 20% when compared to singly used chemical. Totally, our results indicated that CHL + CLO and CYA + THI had the same control efficacy as CHL or CYA alone, but with much lower cost.

Keywords: *Spodoptera frugiperda*, diamide, neonicotinoid, seed treatment, combined toxicity

INTRODUCTION

Corn is a globally-important food crop, that is, consumed by approximately 4.5 billion people worldwide (Shiferaw et al., 2011). In the field, corn yield is reduced by multiple insect pests, including *Spodoptera frugiperda* Smith (Lepidoptera: Noctuidae). *S. frugiperda*, also known as the Fall Armyworm (FAW), is a native corn pest in tropical and subtropical areas of North America

(Martinelli et al., 2006). In recent years, the FAW has invaded Africa and Asia. This pest is highly destructive due to its wide host range, robust migration ability, high fecundity and resistance to insecticides (Guo et al., 2019). In China, FAW was first found in Yunnan province in December 2018 (Sun et al., 2021); it quickly spread throughout 26 provinces and damaged approximately $65.53 \times 10^4 \, hm^2$ corn (Jiang et al., 2019). The FAW is now well-established in winter corn grown in southern China and is a dominant corn pest due to its migratory ability (Qi et al., 2020; Jiang et al., 2021).

Spraying chemical insecticides remains as the most effective measure for controlling this pest. However, there are several factors reducing the efficacy of insecticide spraying against FAW. For example, the efficacy of insecticidal sprays is largely effected by weather and subject to dilution by rain and wind (Zheng et al., 2006; Ranabhat and Wang, 2020). The efficacy of insecticides is also impacted by larval behavior; this is especially relevant for FAW since larvae hide inside the maize whorl, which reduces their exposure to insecticides (Muraro et al., 2020). A further barrier is the labor shortage, which can delay spray applications and reduce efficacy. Finally, the overuse of chemical insecticides contaminates the environment and has impacts on mammals and nontarget arthropods (Lahm et al., 2007).

Seed treatment with systemic insecticides has been used to control pests on many crops (Taylor et al., 2001). In general, treating seeds with chemicals requires less insecticide than spray application and reduces environmental contamination and exposure of nontarget organisms (Schemeer et al., 1990; Nault et al., 2004). Consequently, seed treatment is popular in integrated pest management programs (Zhang et al., 2011). Previous studies demonstrated that seed treatment with carbofuran or thiamethoxam (THI) was ineffective for controlling early larval stages of FAW on corn (Azevedo et al., 2004). Chlorantraniliprole (CHL) and cyantraniliprole (CYA) are anthranilic diamides that target insect ryanodine receptors and disrupt the functioning of calcium channels (Lahm et al., 2007). These two compounds control insect pests by directly killing individuals and inhibiting their feeding, development and reproduction (Huang et al., 2016; Lutz et al., 2018). Previous studies demonstrated that these insecticides showed excellent control efficacy, particularly when used for lepidopteran pests such as FAW (Wang et al., 2019a; Pes et al., 2020). Recently, CHL and CYA were labeled as seed treatments for the control of FAW larvae (Muraro et al., 2020; Pes et al., 2020) because of their low LogPow (octanol/water partition coefficient) and high solubility in water (Selby et al., 2017).; unfortunately, the cost of CHL and CYA is much more expensive than traditional insecticides.

The combined application of two different insecticides could improve control of target pests (Thrash et al., 2013; Carscallen et al., 2019; Muraro et al., 2020). The dual application of anthranilic diamides with other insecticides for FAW control is under-investigated but clearly needed to reduce the cost of control. Thus, the objective of this study was to compare the efficacy of corn seed treatments with CHL, CYA, clothianidin (CLO), THI and the binary mixture of CHL + CLO and CYA + THI for control of FAW larvae in laboratory and field conditions. A recent study suggested that the application of selected insecticides as seed treatments inhibited crop growth because of prolonged, high residue level (Abdu-Allah and Hashem, 2017). Thus, we also evaluated the effects of the above-mentioned chemicals on growth of corn plants and determined insecticide residue levels.

MATERIALS AND METHODS

Insects
FAW populations for laboratory experiments were collected in 2019 from corn fields located at the Guizhou Academy of Agricultural Sciences in Guizhou province, China. The larvae were reared on a corn-based artificial dietat $25 \pm 1°C$ and 70% relative humidity (RH) with a 16:8 h (L:D) photoperiod (Wang et al., 2019b). Third instar larvae were used in the laboratory experiments.

Corn Seeds and Insecticides
Corn seeds of the cultivar Jinyu 818 were provided by Guizhou Jinlong Technology Co., Ltd. Insecticides were sourced from the following companies: chlorantraniliprole (CHL, 50% FSC), DuPont Crop Protection (United States); cyantraniliprole + thiamethoxam (CYA + THI, 60% FSC) and cyantraniliprole (CYA, 40% FSC), Syngenta AG (Switzerland); chlorantraniliprole + clothianidin (CHL + CLO, 40% FSC), Guangdong Kairuifeng Technology Co., Ltd. (China); clothianidin (CLO, 20% FSC), Hebei Lishijie Technology Co. (China); and thiamethoxam (THI, 30% FSC), Bayer Crop Science LP, Monheim (Germany).

Laboratory Experiments
Laboratory experiments were conducted from May to July in 2021 and consisted of the following seven treatments (concentrations in g a.i.100 kg^{-1}corn seeds): 1) CHL, 300; 2) CYA, 144; 3) CHL 60 + CLO 180; 4) CYA 120 + THI 120; 5) CLO, 120; 6) THI, 180; and 7) untreated control. The concentration of each insecticide was chosen based on recommended field rates.

One day prior to sowing, seeds and pesticides were placed in plastic bags, sealed, shaken until insecticides coated the seed surface, and allowed to dry overnight. Fifty corn seeds were sown in individual containers $(30 \times 20 \times 20 \, cm)$ containing sand (40%), clay (40%) and organic matter (20%) at 25°C, 70% RH and a 14:10 (L:D) photoperiod. Water was provided during seed emergence and growth as necessary, and the emergence rate of seeds in each treatment was recorded. At 3, 7, 14, 21, 28 days after seedling emergence (DAE), twenty newly-molted 3rd instar larvae were collected, starved for 2 h, and then transferred to corn plants. Finally, the plants together with FAW larvae were placed in nylon cages to prevent escaping. Each potting container was considered as one replication, and each treatment had four replications. Larval mortality was recorded after 3 days transferring, and larvae were considered dead if there was no response to stimulation with a moist brush.

Field Experiments

Two identical field experiments were conducted to evaluate the efficacy of six insecticidal formulations for FAW larval control on corn seedlings in Luodian county (106.63°E, 25.62°N), Guizhou province, in July and September of 2021. In the two field experiments, 28 plots were arranged in a randomized complete block design with seven treatments and four replications. Insecticide-treated corn seeds were sown on 23 June and 23 August 2021. Each plot was 30 m² (5 × 6 m) and consisted of 10 rows separated by 60 cm of uncultivated ground. The emergence rate of corn seeds was recorded by counting the number of emerged plants in each plot. A five-point sampling method where each point consisted of 10 plants was used to record the number of FAW larvae on corn in each plot at 7, 14, 21, and 28 DAE. The damage rate caused by FAW and the control efficacy of tested insecticides were calculated by the following formulas:

$$\text{Percentage of corn seedlings with FAW damage (\%)}$$
$$= \frac{\#\text{corn plant with FAW damage}}{\#\text{investigated corn plants}} \times 100\% \quad (1)$$

$$\text{Control efficacy (\%)} =$$
$$\frac{\#\text{FAW in untreated plot} - \#\text{FAW in treated plot}}{\#\text{FAW in treated plot}} \times 100\% \quad (2)$$

Effect of Insecticides on Fall Armyworm Emergence and Corn Growth

The emergence rate of corn seeds treated with the six insecticidal formulations were recorded at 7 DAE in both laboratory and field experiments. The impact of the six insecticides on corn grown was evaluated by random selection of 20 plants in each plot at 14 DAE. Plant height, root length, and above-ground and underground fresh weight were measured in July and September of 2021.

Determination of Residual Insecticides in Corn Leaves

Corn leaves were randomly selected from field plots at 3, 7, 14, 21, and 28 DAE in July 2021 and stored at −20°C until needed for analysis. Homogenized corn leaves (5.0 ± 0.1 g) were weighed in 50 ml Teflon centrifuge tubes, and water (5 ml) and 10 ml acetonitrile with 1% (v/v) methanol (HOAc) were added to samples. Sample tubes were shaken vigorously for 10 min, allowed to stand for 30 min, and NaCl (3 g) and MgSO₄ (4 g) were added. Tubes were capped, mixed for 1 min and centrifuged for 5 min at 3216 × g. The upper acetonitrile layer (1.5 ml) was transferred into 2.0 ml tubes containing 50 mg octadecylsilane (C₁₈), 15 mg graphitized carbon black (GCB) and 150 mg MgSO₄. The tubes were vortexed for 30 s and centrifuged for 5 min at 2233 × g. The resulting supernatants were subjected to ultrafiltration (0.22 μm nylon filter) and then loaded into auto-sampler vials for UHPLC-MS/MS analysis.

Chromatographic separation of CLO, THI, CHL, CYA, and J9Z38 (metabolite of CYA) was performed using a Dionex Ultimate 3000 UHPLC system and a Syncronis C₁₈ column

(100 mm × 2.1 mm, 1.9 μm) (Thermo Fisher Scientific, United States) at 40°C with a 5 μl injection volume. The mobile phases consisted of solution A (H₂O containing 0.1% v/v formic acid) and solution B (methanol); the flow rate was 0.25 ml·min⁻¹. The elution program was: 25% solvent B from 0 to 1.0 min; 25%–85% solvent B from 1.0 to 1.5 min; 85% solvent B from 1.5 to 6 min; 85%–25% solvent B from 6 to 6.5 min; and 25% solvent B for 1.5 min. Qualitative and quantitative analysis of CLO, THI, CHL, CYA, and J9Z38 were obtained with a triple-quadrupole mass spectrometer (TSQ Vantage) equipped with an ESI interface (Thermo, San Jose, CA, United States). Nitrogen was used as the sheath and auxiliary gas at 30 and 10 PSI, respectively. The vaporizer and capillary temperatures were both 330°C, and the spray voltage was 3.2 kV. The pressure of argon in the collision cell was 1.5 mTorr. The MS/MS conditions were optimized to acquire satisfactory sensitivity and resolution using the parameters listed in **Supplementary Table S1**. First-order kinetic and bi-exponential models were used to analyze the dissipation curves of CLO, THI, CHL, CYA, and J9Z38. Analysis of t kinetics was performed in KinGUIIv2.1 (BASF Corporation) as follows:

$$C = C_0 e^{-kt} \quad (3)$$
$$T_{1/2} = \ln 2/K \quad (4)$$

Statistical Analysis

Data associated with mortality were arcsine-transformed before statistical analysis. One-way ANOVA was used to determine statistical significance among treatments, followed by a Tukey's HSD method. Results were considered significant at $p < 0.05$. Statistical analyses were performed in DPS v. 17.0 (Tang and Zhang, 2013).

RESULTS

Efficacy of Insecticidal Seed Treatments in Laboratory Experiments

In laboratory experiments, the percentage of corn seedlings damaged by FAW in CHL + CLO, CYA + THI, CHL, and CYA ranged from 15.35 to 45.13% at 3–28 DAE, and these levels were significantly lower than the untreated control where damage was 52.03%–86.70% (**Figure 1**). The percentage of corn seedlings with FAW damage in CLO or THI alone was generally either slightly lower or not significantly different from the untreated control (**Figures 1A–E**).

The corrected mortality of FAW larvae fed on corn plants treated with the six insecticides declined as days after seed emergence increased (**Table 1**). At DAE 3, 7, and 14, CHL, CYA, CHL + CLO and CYA + THI treatments resulted in similar levels of mortality and ranged from 72.00% to 94.44%; furthermore, FAW mortality in these four treatments was significantly higher than in larvae exposed to CLO and THI treatments. At 21 or 28 DAE, mortality in the CHL, CYA, CHL + CLO and CYA + THI treatments ranged from 60.00% to 72.97% and remained significantly higher than mortality in the CLO or THI treatments.
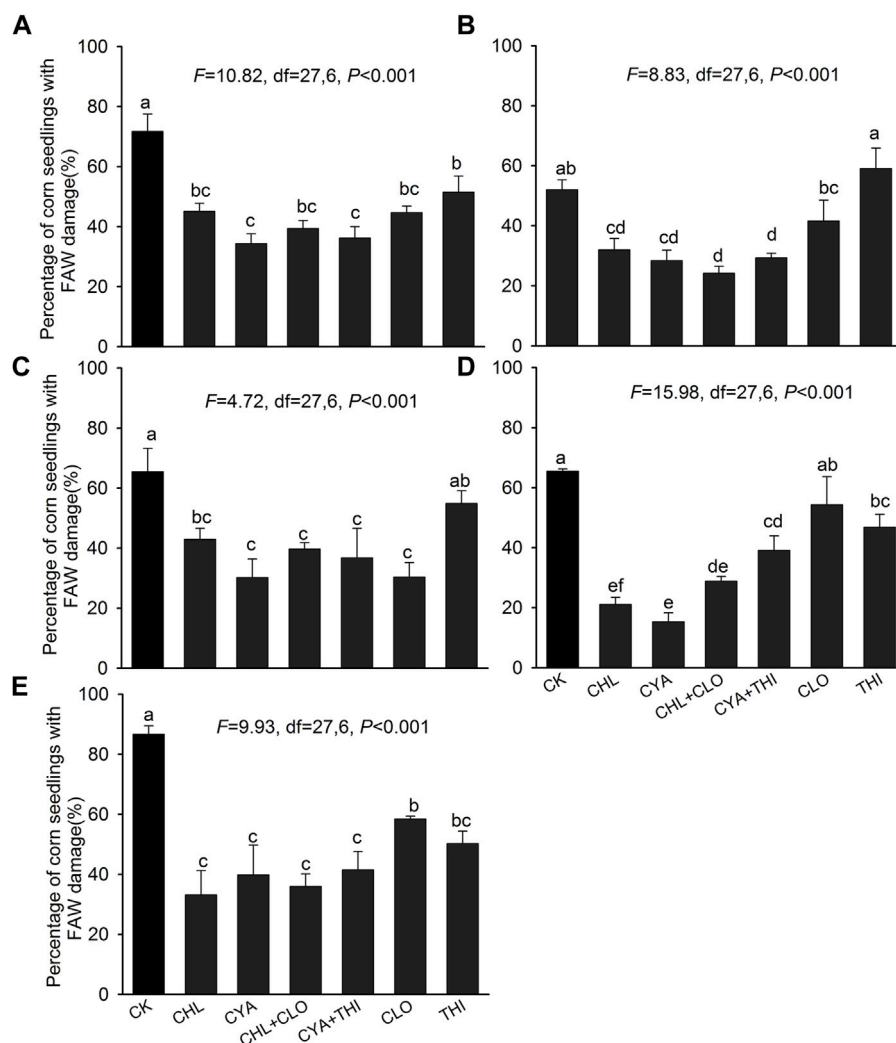
FIGURE 1 | Percentage of corn seedlings damaged by FAW in laboratory experiments corn where seeds were treated with chlorantraniliprole (CHL), cyantraniliprole (CYA), clothianidin (CLO), thiamethoxam (THI), CHL + CLO and CYA + THI; CK is the untreated control. Damage is shown on corn seedlings subjected to FAW larvae at 3 panel **(A)**, 7 **(B)**, 14 **(C)**, 21 **(D)**, and 28 **(E)** days after emergence (DAE). Columns labeled with different letters indicate significant differences among treatments with Tukey's HSD test at $p < 0.05$.

TABLE 1 | The corrected mortality (±SE) of FAW larvae fed on corn plants subjected to insecticidal seed treatments in laboratory experiments.

Treatments	Dosage (ga.i.100 kg⁻¹seeds)	Corrected mortality (%)				
		3 DAE	**7 DAE**	**14 DAE**	**21 DAE**	**28 DAE**
CHL	300	88.89 ± 2.27a	78.08 ± 2.24b	72.00 ± 1.33b	63.51 ± 1.35a	61.43 ± 2.74a
CYA	144	90.28 ± 3.21a	89.04 ± 2.24a	78.67 ± 5.33ab	66.22 ± 1.35a	60.00 ± 6.17a
CHL + CLO	240	94.44 ± 1.39a	90.41 ± 2.62a	89.33 ± 4.87a	71.62 ± 2.59a	64.29 ± 5.89a
CYA + TH	240	94.44 ± 2.27a	93.15 ± 1.37a	84.00 ± 2.18ab	72.97 ± 6.62a	61.43 ± 2.74a
CLO	120	65.28 ± 4.74b	58.90 ± 1.58c	54.67 ± 1.54c	35.14 ± 6.24b	17.14 ± 1.65b
THI	180	58.33 ± 3.59b	43.84 ± 4.11d	41.33 ± 3.77d	40.54 ± 2.21b	18.57 ± 1.43b
F	-	14.12	50.47	14.14	14.84	25.72
df	-	23.5	23.5	23.5	23.5	23.5
p	-	<0.001	<0.001	<0.001	<0.001	<0.001

Values followed by different letters indicate significant differences among treatments with Tukey's HSD test at p < 0.05.
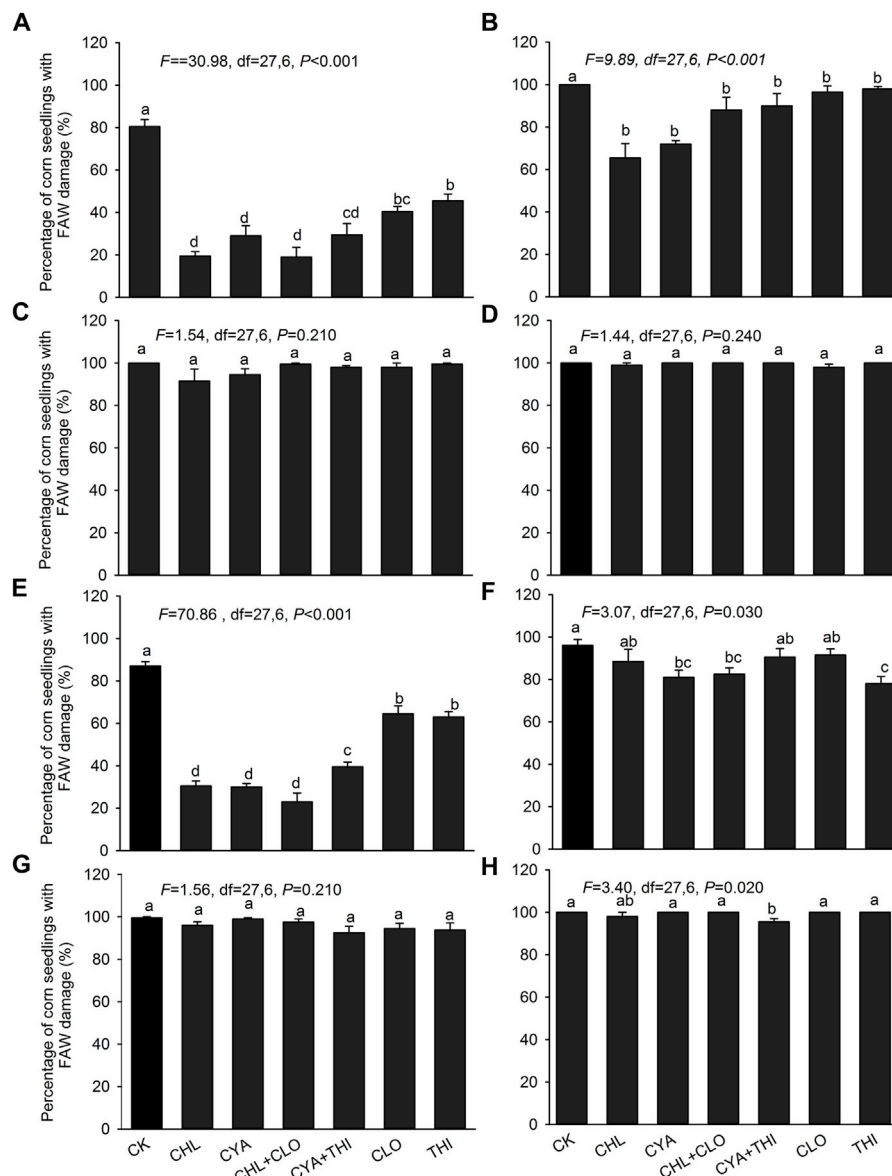
FIGURE 2 | Percentage of corn seedlings damaged by FAW in field experiments corn where seeds were treated with chlorantraniliprole (CHL), cyantraniliprole (CYA), clothianidin (CLO), thiamethoxam (THI), CHL + CLO and CYA + THI; CK is the untreated control. Damage rates (±SE) caused by FAW larvae are shown for July 2021 at 7 panel **(A)**, 14 **(B)**, 21 **(C)** and 28 **(D)** DAE. Damage rates in September 2021 are shown for 7 panel **(E)**, 14 **(F)**, 21 **(G)** and 28 **(H)** DAE. Columns labeled with different letters indicate significant differences among treatments with Tukey's HSD test at $p < 0.05$.

Efficacy of Insecticidal Seed Treatments in Field Experiments

In July 2021, the percentage of corn seedlings damaged by FAW in insecticide-treated field plots ranged from 19.50% to 63.00% at 7 DAE, which was significantly lower than the control (80.00%) (**Figure 2A**). At 14 DAE, the value in insecticide-treated plots showed a substantial increase but were still significantly lower than the untreated control (**Figure 2B**). At 21 and 28 DAE, the value in treated plots were not significantly different from the control (**Figures 2C,D**). The percentage of corn seedlings with

FAW damage in September 2021 at all four sampling times were similar to results in July (**Figures 2E–H**).

In July, CHL, CYA, CHL + CLO and CYA + THI treatments resulted in 79.84%–87.88% control efficacy at 7 DAE, which were significantly higher than those in the CLO and THI treatments (**Table 2**). Furthermore, control efficacy in the CYA + THI treatment was higher than in corn treated with CYA alone. At 14 DAE, control efficacy in the CHL, CYA, CHL + CLO and CYA + THI treatments were higher than CLO and THI treatments; however, the efficacy of the CHL, CYA, CHL + CLO and CYA +

TABLE 2 | Control efficacy (mean ± SE) of six insecticidal seed treatments for control of FAW on corn in the field.

Experimental time	Treatments	Dosage (ga.i.100 kg^{-1}seeds)	Control efficacy (%)			
			7 DAE	14 DAE	21 DAE	28 DAE
July	CHL	300	84.15 ± 2.82ab	76.42 ± 2.22ab	55.79 ± 4.37ab	40.94 ± 2.45b
	CYA	144	79.84 ± 3.45b	68.93 ± 3.82b	49.54 ± 4.76bc	14.09 ± 7.02d
	CHL + CLO	240	87.88 ± 1.83a	77.94 ± 3.25a	48.61 ± 1.71bc	32.21 ± 4.57b
	CYA + THI	240	86.71 ± 1.92a	71.46 + 1.51ab	44.68 ± 2.34c	19.46 ± 1.10cd
	CLO	120	65.97 ± 2.20c	57.09 ± 4.14d	57.87 ± 1.39a	31.54 ± 4.17bc
	THI	180	72.49 ± 2.20c	62.35 ± 1.99cd	58.33 ± 2.17a	53.69 ± 2.29a
	F	-	14.68	7.27	3.36	12.34
	df	-	23.5	23.5	23.5	23.5
	p	-	<0.001	<0.001	0.03	<0.001
September	CHL	300	84.43 ± 1.09a	74.79 ± 3.12a	61.23 ± 5.64ab	66.79 ± 4.20a
	CYA	144	87.00 ± 1.92a	70.15 ± 1.67a	62.28 ± 2.90a	63.38 ± 1.78a
	CHL + CLO	240	85.53 ± 1.85a	68.33 ± 0.74a	57.56 ± 2.91ab	66.43 ± 3.46a
	CYA + THI	240	87.73 ± 0.92a	72.31 ± 1.06a	50.00 ± 5.56b	64.63 ± 1.56a
	CLO	120	41.94 ± 3.63b	58.54 ± 2.79b	51.02 ± 2.13ab	59.43 ± 3.60a
	THI	180	42.67 ± 2.21b	61.19 ± 2.43b	57.8 ± 2.51ab	62.84 ± 2.61a
	F	-	113.42	8.77	3.73	0.80
	df	-	23.5	23.5	23.5	23.5
	p	-	<0.001	<0.001	0.02	0.56

Values with different letters indicate significant differences with Tukey's HSD test at p < 0.05.

FIGURE 3 | The emergence rate (±SE) of corn seeds after treatment with chlorantraniliprole (CHL), cyantraniliprole (CYA), clothianidin (CLO), thiamethoxam (THI), CHL + CLO and CYA + THI; CK is the untreated control. Panels: **(A)** emergence rate of corn seeds in laboratory experiments; **(B)** and **(C)** emergence rate of corn seeds in field experiments in July and September 2021, respectively. Columns labeled with the same letter were not significantly different using Tukey's HSD test at *p* < 0.05.

THI treatments decreased dramatically at 21 and 28 DAE (**Table 2**). In September, CHL, CYA, CHL + CLO and CYA + THI treatments resulted in control efficacy ranging from 84.43% to 87.73% and 68.33%–74.79% at 7 and 14 DAE, respectively, and the values were significantly higher than those in the CLO and THI treatments. Similar to results obtained in July, the efficacy in CHL, CYA, CHL + CLO and CYA + THI treatments decreased at 21 and 28 DAE and were not significantly different from the CLO and THI treatments (**Table 2**).

Effect of Insecticides on Emergence Rates and Corn Growth

The emergence rate of corn treated with the six different insecticide formulations exceeded 90% in both laboratory and field experiments

with no significant differences between treatments (**Figure 3**). In July 2021, corn seedlings in field plots treated with CHL + CLO and CYA + THI were significantly taller than seedlings in other treatments (**Figure 4A**). Root length and fresh weight of above-ground tissue were generally higher in seedlings treated with CHL + CLO and CYA + THI as compared to the other four treatments, although these differences were not always significant (**Figures 4B,C**). The underground fresh weights in CHL + CLO and CYA + THI treatments were significantly higher than those in CLO treatment and control (**Figure 4D**). In September, data points for plant height and fresh weight of above-ground and underground tissues were similar to those recorded in July for all treatments (**Figures 4E,G,H**). Unlike July, the root length data in September was not significantly different among treatments (**Figure 4F**).
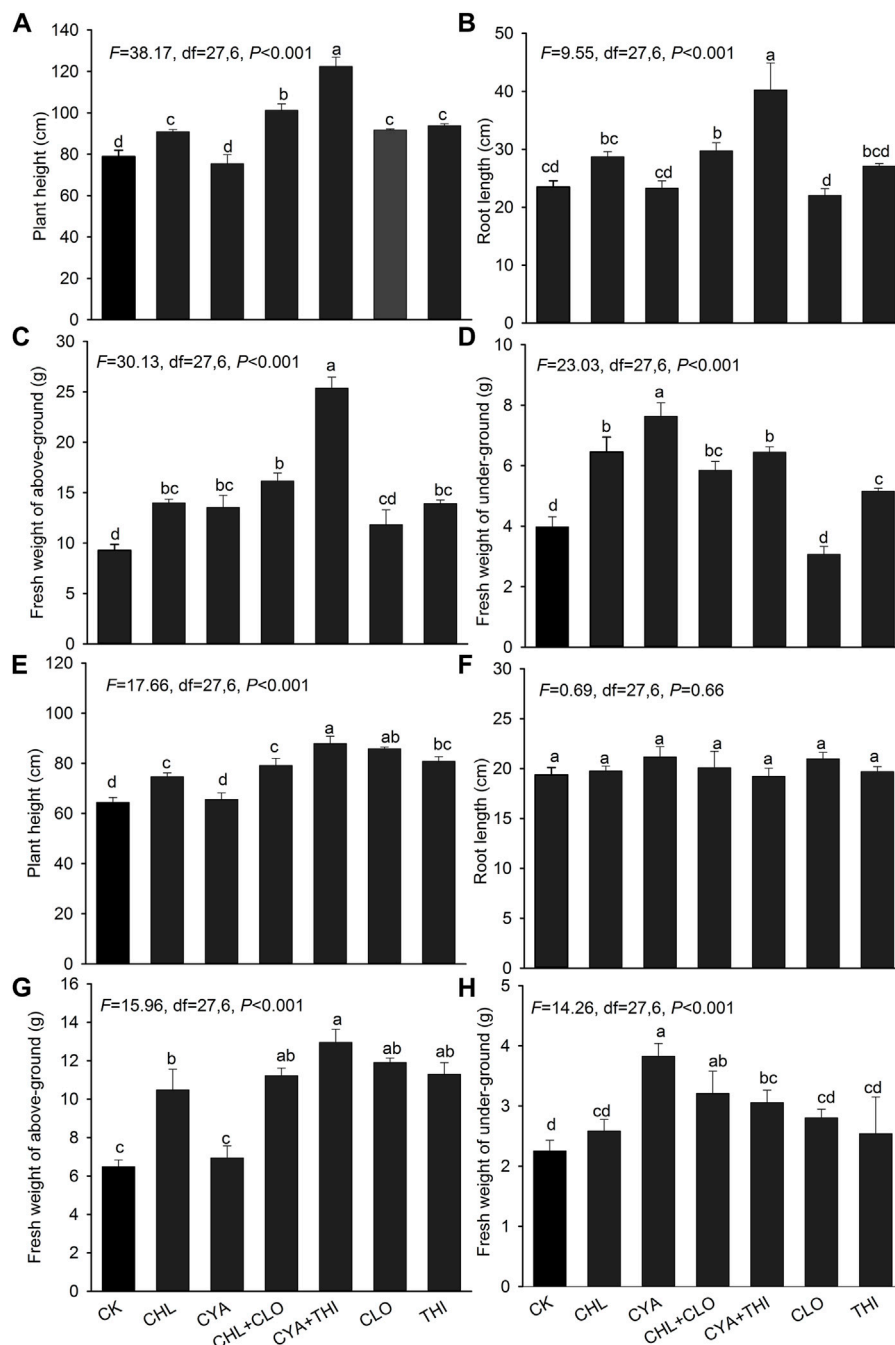
FIGURE 4 | The mean plant height, root length, and fresh weight above-ground and underground of corn seedlings treated with CHL, CYA, CLO, THI, CHL + CLO and CYA + THI in the July **(A–D)** and September **(E–H)** of 2021. Columns labeled with the same letter were not significantly different using Tukey's HSD test at $p < 0.05$.

Insecticide Residues in Treated Corn Plants

Residues levels of the six insecticidal formulations and their metabolites gradually decreased in corn plants throughout the sampling period (**Figure 5**). For example, in the CHL + CLO treatment, the CHL residues declined from 0.29 mg·kg^{-1} at 3 DAE to 0.02 mg·kg^{-1} at 28 DAE, while the CLO residues declined from 11.44 mg·kg^{-1} at 3 DAE to 0.12 at 28 DAE (**Figure 5E**). The half-life ($t_{1/2}$) of CHL in corn plants treated

with CHL + CLO was 2.32 days, which was shorter than that in the CHL treatment alone (4.35 days) (**Supplementary Table S2**). The half-life of CLO in CHL + CLO treated corn plants was 2.26 days, which was similar to that in the CLO treatment alone (2.15 days) (**Figure 5A**, **Supplementary Table S2**).

In the CYA + THI treatment, residues of CYA and its metabolite J9Z38 degraded from 1.58 to 0.04 mg·kg^{-1} and
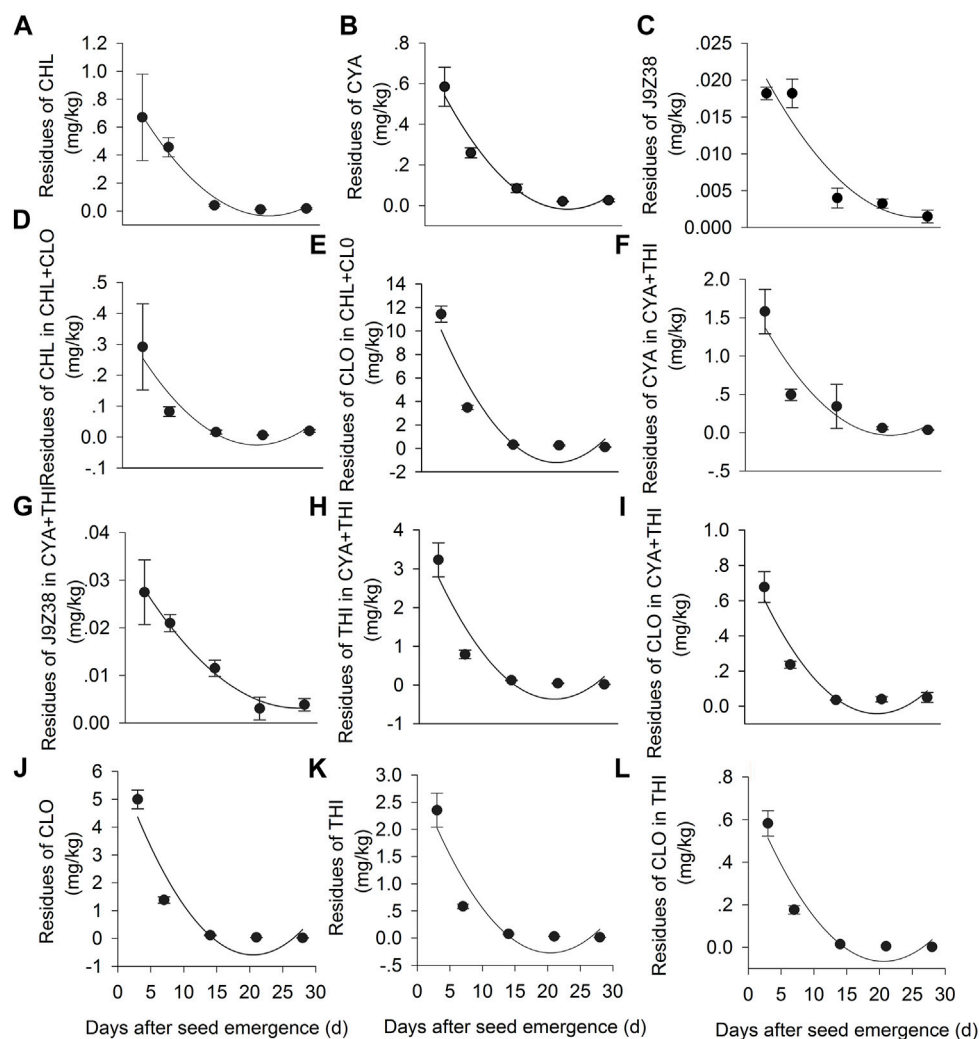
FIGURE 5 | Dynamic changes in the concentrations of insecticides and their metabolites in CHL, CYA, CHL + CLO, CYA + THI, CLO, THI treated leaves in July corn plants. Panels: **(A)** CHL residue in CHL treated leaves; **(B)** CYA residues in CYA treated leaves; **(C)** J9Z38 residues in CYA treatedleaves; **(D)** CHL residues in CHL + CLO treated leaves; **(E)** CLO residues in CHL + CLO treatedleaves; **(F)** CYA residues in CYA + THI treated leaves; **(G)** J9Z38 residues in CYA + THI treatedleaves; **(H)** THI residues in CYA + THI treated leaves; **(I)** CLO residue in CYA + THI treated leaves; **(J)** CLO residue in CLO treated leaves; **(K)** THI residues in THI treated leaves; **(L)** CLO residues in THI treated leaves. Fitted regression lines are from the equation $C_t = C_0 e^{-bt}$, and showed in **Supplementary Table S2**.

0.03–0.00 mg·kg⁻¹, respectively, during 3–28 DAE period (**Figures 5F,G**). Residues of THI and its metabolite (CLO) degraded from 3.23 to 0.02 mg·kg⁻¹ and 0.68 to 0.03 mg·kg⁻¹, respectively, during the same period (**Figures 5H,I**). The estimated half-life of the CYA, J9Z38, THI and CLO in CYA + THI combination were 3.07, 7.76, 1.99 and 2.67 days, respectively, most of which were low when compared to the CYA or THI treatment alone (**Figures 5B,C,K,L, Supplementary Table S2**).

Comparison of the Cost of the Insecticides

As shown in **Supplementary Table S3**, the cost of both CHL + CLO and CYA + THI were below 50.00 $ ha⁻¹, which lead to reduced cost of 42.52 $ ha⁻¹ and 11.34 $ ha⁻¹ when compared to CHL (85.04 $ ha⁻¹) and CYA (56.69 $ ha⁻¹), respectively.

DISCUSSION

The diamide insecticides kill insect pests by targeting their ryanodine receptor channels (RyRs) that cause muscle contraction and death (Lahm et al., 2007), while the neonicotinoid insecticides kill insect pests by targeting their nicotinic acetylcholine receptors (nAChRs) (Matsuda et al., 2020). In previous laboratory studies, the diamide insecticides such as CHL and CYA were highly toxic to FAW larvae with LC₅₀ values of 0.01 and 0.25 μg ml⁻¹, respectively (Bolzan et al., 2019; Zhou et al., 2020). These two insecticides were recently labeled as a seed treatment for controlling FAW and exhibited a high level of control efficacy against this species (Zhang P. et al., 2016; Pes et al., 2020). Neonicotinoid insecticides such as CLO and THI have been widely used as seed treatments in multiple crops and

exhibit good activity against a broad range of pests including aphids (Zhang P. et al., 2016; Zhang Z. et al., 2016), whiteflies (Zhang et al., 2011), and thrips (Reisig et al., 2012; Ding et al., 2018). To the best of our knowledge, there are no prior studies assessing the efficacy of diamides in combination with neonicotinoids for FAW larval control as seed treatments.

CHL + CLO, CYA + THI, CHL, and CYA were effective at reducing percentage of corn seedlings with FAW damage in the laboratory. The percentage of corn seedlings with FAW damage was similar among the four treatments, suggesting that CHL + CLO and CYA + THI were comparable to CHL and CYA treatment alone. Prior studies reported that CHL can rapidly inhibit the feeding of some lepidopteran pests. For example, the feeding behavior of *Trichoplusia ni*, *Plutella xylostella* and *Helicoverpa zea* ended within 30 min after exposure to CHL, and damage decreased by 90%–99% (Hannig et al., 2009). Therefore, diamides alone or in combination with neonicotinoid insecticides reduce damage by causing early mortality, inhibiting feeding, and disrupting larval development, which is similar to results reported elsewhere (Hannig et al., 2009; Carscallen et al., 2019).

The percentage of corn seedlings with FAW damage in our two field experiments was generally higher than in the laboratory, which may be attributed to one or more of the following reasons, Firstly, 3rd instar larvae were used in the lab studies, and this life stage is relatively stable and uniform. Secondly, the high damage rate in the field is likely related to FAW behavior and environmental conditions; for example, FAW adults randomly deposit eggs on corn and the newly-hatched larvae are disseminated by wind, thus increasing range and the damage rate of corn. Therefore, damage rates may not be a suitable index for evaluating the efficacy of insecticides when applied as seed treatments in the field. Recently, an injury score rating was used to evaluate the control efficacy of seed coatings by measuring the feeding area in some lepidopteran species (Carscallen et al., 2019; Wu et al., 2020). It is unclear whether this index is suitable for FAW and further study is needed.

Our lab experiments showed that application of CHL + CLO and CYA + THI to corn resulted in high FAW mortality (84.00%–94.44%) at 14 DAE, which indicates that the combined application of insecticides was an effective control strategy. Our results were similar to those reported for application of CHL and CYA alone in one study (Wu et al., 2020), but were much higher than results reported by Thrash et al. (2013). These disparate outcomes may be caused by variability in plant hosts, FAW populations and insecticide doses. The effectiveness of diamide insecticides alone or in combination with neonicotinoids has also been reported for *Mythimna unipuncta* (Carscallen et al., 2019). Furthermore, as corn plants grew larger in the present study, the corrected mortality of FAW larvae in all treatments decreased; this is likely due to the decline in insecticidal residues and increase in body size of larvae over time. We also observed that the CLO and THI treatments caused mortality from 41% to 65.28% at 14 DAE, which indicates that these two insecticides are somewhat effective in controlling FAW larvae. These data are consistent with previous results reported for *Agrotis ipsilon* (Zhang et al., 2019), *Ostrinia nubilalis*, and *Plodia interpunctella* (Yue et al., 2003).

To validate findings in the laboratory, we conducted two field experiments in July and September of 2021, respectively. Our results showed that CHL + CLO and CYA + THI treatments resulted in control efficacy of 79.84%–87.88% at 7 DAE and 68.93%–77.94% at 14 DAE. These results were similar to the use of diamides alone and were consistent with laboratory results. Thus, CHL + CLO and CYA + THI treatments exhibited control efficacy equivalent to CHL and CYA treatment alone; however, it is important to mention that the dosage of diamides in the combined treatments was lower than the usage of CHL and CYA alone. These results suggest that synergistic action are present when the diaminde and neonicotinoid insecticides are simultaneously used. The snyergistic effect may be caused by the following two reasons: firstly, neonicotinoid insecticides block the metabolic systems of FAW that would break down diaminde molecules; secondly, neonicotinoid insecticides interfere with the detoxication of diamindes insecticides through their action on polysubstrate monooxygenases (PSMOs) and other enzyme systems (Bernard and Philogène, 1993). Most importantly, application of CHL + CLO and CYA + THI reduce the control cost when they are used to manage FAW larvae. For example, the control cost of CHL + CLO is 42.52 \$ per hectare, which reduced 42.52 \$ when compared to CHL (85.04 \$ ha^{-1}). Similarly, control cost of CYA + THI is 45.35 \$ per hectare, which reduced 11.34 \$ per hectare when compared to CYA (56.69 \$ ha^{-1}). Therefore, this strategy is helpful for large-scale application of these insecticides as seed treatments.

Moreover, the control efficacy of the four treatments in field experiments was lower than laboratory studies, which may be attributed to the rapid degradation of insecticide residues in field-grown corn. Weather conditions, application time, insecticide characteristics, and translocation within plants can influence the persistence of insecticides and may impact efficacy (Pfeil, 2014; Teló et al., 2015). Reduced control efficacy in the field can be impacted by: 1) environmental factors such as UV irradiation and rain (Lim et al., 1990; Lanka et al., 2014); 2) translocation to plant tissues where active ingredients may be diluted (Zhang et al., 2019); and 3) insecticide resistance. In addition, we observed that the control efficacy at 21 DAE or later was lower in summer months as compared to autumn. This may be caused by higher soil temperatures or elevated moisture levels during seedling emergence in summer, which may influence microbial activity and further contribute to insecticide degradation (Zhang et al., 2019).

To evaluate the effects of CHL + CLO and CYA + THI as seed treatments in corn, we measured growth indicators and evaluated residue concentrations and dynamics. Firstly, the emergence rates of corn seeds treated with CHL + CLO and CYA + THI were not different from other treatments and the untreated control both in laboratory and field experiments, which suggests that the combined insecticides had no adverse effects on emergence. Secondly, the CHL + CLO and CYA + THI treatments had stimulatory effects on measured parameters. Our results were different from those reported by Abdu-Allah and Hashem (2017) and Huang et al. (2015) but consistent with studies showing that

neonicotinoid seed treatments could promote seed germination and increase primary root length, weight, and height of corn seedlings (Horii et al., 2007; Duan et al., 2012; Zhang et al., 2015). The stimulation of growth parameters may be the result of improved activity of antioxidants and stress-related enzymes such as guaiacol peroxidase and glucose-6-phosphate dehydrogenase (Ding et al., 2018). Previous studies have shown that insecticides, especially neonicotinoids, cause a decline in natural enemies and pollinators (Moser and Obrycki, 2009; Bredeson and Lundgren, 2018). Therefore, further studies are needed to explore the effects of CHL + CLO and CYA + THI on nontarget insects in the corn field. Finally, we observed that insecticide residues in the CHL + CLO and CYA + THI treatments gradually declined, and the half-life of the combined residues was relatively low when compared that of individual, single applications. Collectively, our results suggest that CHL + CLO and CYA + THI are relatively safe insecticides when applied to seeds and had no negative effect on corn growth.

CONCLUSION

In summary, our results indicate that the application of CHL + CLO and CYA + THI as a corn seed treatment effectively controls FAW larvae on seedlings up to 14 DAE without compromising plant growth and development. Thus, CHL + CLO and CYA + THI are effective, environmentally-friendly insecticidal formulations that reduce the cost associated with single applications of CHL and CYA.

REFERENCES

Abdu-Allah, G. A. M., and Hashem, M. M. (2017). Efficiency and Side Effects of Three Neonicotinoid Insecticides Used as Faba Bean Seed Treatments for Controlling Cowpea Aphid. *Egypt. Sci. J. Pestic.* 3, 20–27. Available at: https://www.researchgate.net/publication/318701413.

Azevedo, R. D., Grutzmacher, A. D., Loeck, A. E., Silva, F. F. D., Storch, G., and Herpich, M. I. (2004). Effect of Seed Treatment and Leaf Spray of Insecticides in Different Water Volumes, on the Control of *Spodoptera frugiperda* (J.E. Smith, 1797) (Lepidoptera: Noctuidae), in Lowland Corn and Sorghum Crops. *R.Bras. Agrociência.* 10, 71–77. Available at: https://www.researchgate.net/publication/242633987.

Bernard, C. B., and Philogène, B. J. R. (1993). Insecticide Synergists: Role, Importance, and Perspectives. *J. Toxicol. Environ. Health* 38, 199–223. doi:10.1080/15287399309531712

Bolzan, A., Padovez, F. E., Nascimento, A. R., Kaiser, I. S., Lira, E. C., Amaral, F. S., et al. (2019). Selection and Characterization of the Inheritance of Resistance ofSpodoptera frugiperda(Lepidoptera: Noctuidae) to Chlorantraniliprole and Cross-resistance to Other Diamide Insecticides. *Pest. Manag. Sci.* 75, 2682–2689. doi:10.1002/ps.5376

Bredeson, M. M., and Lundgren, J. G. (2018). Thiamethoxam Seed Treatments Reduce Foliar Predator and Pollinator Populations in Sunflowers (*Helianthus Annuus*), and Extra-floral Nectaries as a Route of Exposure for Seed Treatments to Affect the Predator, *Coleomegilla maculata* (Coleoptera: Coccinellidae). *Crop Prot.* 106, 86–92. doi:10.1016/j.cropro.2017.12.019

Carscallen, G. E., Kher, S. V., and Evenden, M. L. (2019). Efficacy of Chlorantraniliprole Seed Treatments against Armyworm (*Mythimna unipuncta* [Lepidoptera: Noctuidae]) Larvae on Corn (Zea mays). *J. Econ. Entomol.* 112, 188–195. doi:10.1093/jee/toy338

DATA AVAILABILITY STATEMENT

The raw data supporting the conclusions of this article will be made available by the authors, without undue reservation.

AUTHOR CONTRIBUTIONS

LF: methodology, software, data curation, and analysis. JF: data curation. YZ: residues data analysis; WH: residues determination. TD: UHPLC-MS/MS equipment. YH: draft manuscript review and editing. JX: supervision. HL: writing—review and editing, funding acquisition. All authors have read and agreed to the published version of the manuscript.

FUNDING

SUPPLEMENTARY MATERIAL

The Supplementary Material for this article can be found online at: https://www.frontiersin.org/articles/10.3389/fchem.2022.925171/full#supplementary-material

Ding, J., Li, H., Zhang, Z., Lin, J., Liu, F., and Mu, W. (2018). Thiamethoxam, Clothianidin, and Imidacloprid Seed Treatments Effectively Control Thrips on Corn under Field Conditions. *J. Insect Sci.* 18 (6), 19. doi:10.1093/jisesa/iey128

Duan, Q., Zhao, G. L., Jiang, X. Y., Wang, C., Bao, J., Liu, X. D., et al. (2012). Effects of Imidacloprid Seed Dressing on the Seed Activity and the Seedling Growth of Maize. *J. Maize Sci.* 20, 63–69. doi:10.13597/j.cnki.maize.science.2012.06.015

Guo, J. F., He, K. L., and Wang, Z. Y. (2019). Biological Characteristics, Trend of Fall Armyworm *Spodoptera frugiperda*, and the Strategy for Management of the Pest. *Chin. J. Appl. Entomol.* 56, 361–369. doi:10.7679/j.issn.2095-1353.2019.045

Hannig, G. T., Ziegler, M., and Marçon, P. G. (2009). Feeding Cessation Effects of Chlorantraniliprole, a New Anthranilic Diamide Insecticide, in Comparison with Several Insecticides in Distinct Chemical Classes and Mode-Of-Action Groups. *Pest. Manag. Sci.* 65, 969–974. doi:10.1002/ps.1781

Horii, A., Mccue, P., and Shetty, K. (2007). Enhancement of Seed Vigour Following Insecticide and Phenolic Elicitor Treatment. *Bioresour. Technol.* 98, 623–632. doi:10.1016/j.biortech.2006.02.028

Huang, L., Lu, M., Han, G., Du, Y., and Wang, J. (2016). Sublethal Effects of Chlorantraniliprole on Development, Reproduction and Vitellogenin Gene (CsVg) Expression in the Rice Stem borer,Chilo Suppressalis. *Pest. Manag. Sci.* 72, 2280–2286. doi:10.1002/ps.4271

Huang, L., Zhao, C.-l., Huang, F., Bai, R.-e., Lü, Y.-b., Yan, F.-m., et al. (2015). Effects of Imidacloprid and Thiamethoxam as Seed Treatments on the Early Seedling Characteristics and Aphid-Resistance of Oilseed Rape. *J. Integr. Agric.* 14, 2581–2589. doi:10.1016/S2095-3119(15)61140-6

Jiang, Y. Y., Liu, J., Wu, Q. L., Ciren, Z. G., and Zeng, J. (2021). Investigation on Winter Breeding and Overwintering Areas of *Spodoptera frugiperda* in China. *Plant Prot.* 47, 212–217. doi:10.16688/j.zwbh.2020432

Jiang, Y. Y., Liu, J., Xie, M. C., Li, Y. H., Yang, J. J., Zhang, M. L., et al. (2019). Observation on Law of Diffusion Damage of *Spodoptera frugiperda* in China in 2019. *Plant Prot.* 6, 10–19. doi:10.16688/j.zwbh.2019539

Lahm, G. P., Stevenson, T. M., Selby, T. P., Freudenberger, J. H., Cordova, D., Flexner, L., et al. (2007). Rynaxypyr: a New Insecticidal Anthranilic Diamide that Acts as a Potent and Selective Ryanodine Receptor Activator. *Bioorg. Med. Chem. Lett.* 17 (22), 6274–6279. doi:10.1016/j.bmcl.2007.09.012

Lanka, S. K., Stout, M. J., Beuzelin, J. M., and Ottea, J. A. (2014). Activity of Chlorantraniliprole and Thiamethoxam Seed Treatments on Life Stages of the Rice Water Weevil as Affected by the Distribution of Insecticides in Rice Plants. *Pest. Manag. Sci.* 70, 338–344. doi:10.1002/ps.3570

Lim, L. O., Scherer, S. J., Shuler, K. D., and Toth, J. P. (1990). Disposition of Cyromazine in Plants under Environmental Conditions. *J. Agric. Food Chem.* 38, 860–864. doi:10.1021/jf00093a057

Lutz, A. L., Bertolaccini, I., Scotta, R. R., Curis, M. C., Favaro, M. A., Fernandez, L. N., et al. (2018). Lethal and Sublethal Effects of Chlorantraniliprole on *Spodoptera cosmioides* (Lepidoptera: Noctuidae). *Pest. Manag. Sci.* 74, 2817–2821. doi:10.1002/ps.5070

Martinelli, S., Barata, R. M., Zucchi, M. I., DeCastroSilva-Filho, M., Omoto, C., and Celso, O. (2006). Molecular Variability of *Spodoptera frugiperda* (Lepidoptera: Noctuidae) Populations Associated to Maize and Cotton Crops in Brazil. *J. Econ. Entomol.* 99, 519–526. doi:10.1603/0022-0493-99.2.51910.1093/jee/99.2.519

Matsuda, K., Ihara, M., and Sattelle, D. B. (2020). Neonicotinoid Insecticides: Molecular Targets, Resistance, and Toxicity. *Annu. Rev. Pharmacol. Toxicol.* 60, 241–255. doi:10.1146/annurev-pharmtox-010918-021747

Moser, S. E., and Obrycki, J. J. (2009). Non-target Effects of Neonicotinoid Seed Treatments; Mortality of Coccinellid Larvae Related to Zoophytophagy. *Biol. Control* 51, 487–492. doi:10.1016/j.biocontrol.2009.09.001

Muraro, D. S., Stacke, R. F., Cossa, G. E., Godoy, D. N., Garlet, C. G., Valmorbida, I., et al. (2020). Performance of Seed Treatments Applied on Bt and Non-Bt Maize against Fall Armyworm (Lepidoptera: Noctuidae). *Environ. Entomol.* 49, 1137–1144. doi:10.1093/ee/nvaa088

Nault, B. A., Taylor, A. G., Urwiler, M., Rabaey, T., and Hutchison, W. D. (2004). Neonicotinoid Seed Treatments for Managing Potato Leafhopper Infestations in Snap Bean. *Crop Prot.* 23, 147–154. doi:10.1016/j.cropro.2003.08.002

Pes, M. P., Melo, A. A., Stacke, R. S., Zanella, R., Perini, C. R., Silva, F. M. A., et al. (2020). Translocation of Chlorantraniliprole and Cyantraniliprole Applied to Corn as Seed Treatment and Foliar Spraying to Control *Spodoptera frugiperda* (Lepidoptera: Noctuidae). *PLoS One* 15, e0229151. doi:10.1371/journal.pone.0229151

Pfeil, R. (2014). Pesticide Residues: Pyrethroids. *Encycl. Food Saf.* 3, 31–34. doi:10.1016/b978-0-12-378612-8.00239-0

Qi, G. J., Huang, D. C., Wang, L., Zhang, Y. P., Xiao, H. X., Shi, Q. X., et al. (2020). The Occurrence Characteristic in Winter and Year Round Breeding Region of the Fall Armyworm, *Spodoptera frugiperda* (J.E Smith) in Guangdong Province. *J. Environ. Entomol.* 42, 573–582. doi:10.3969/j.issn.1674-0858.2020.03.8

Ranabhat, S., and Wang, C. (2020). Effect of Moisture on Efficacy of Selected Insecticide Dusts against the Common Bed Bug, *Cimex lectularius* (Hemiptera: Cimicidae). *J. Environ. Entomol.* 113, 1933–1939. doi:10.1093/jee/toaa122

Reisig, D. D., Herbert, D. A., and Malone, S. (2012). Impact of Neonicotinoid Seed Treatments on Thrips (Thysanoptera: Thripidae) and Soybean Yield in Virginia and North Carolina. *Jnl. Econ. Entom.* 105, 884–889. doi:10.1603/ec11429

Schemeer, H. E., Bluett, D. J., Meredith, R., and Heatherington, P. J. (1990). "Field Evaluation of Imidacloprid as an Insecticidal Seed Treatment in Sugar Beet and Cereals with Particular Reference to Virus Vector Control," in Proc Brighton Crop Prot Conf, Pest and Dis, BCPC, Alton, Hants, UK, 29–36. 0144-1612.

Selby, T. P., Lahm, G. P., and Stevenson, T. M. (2017). A Retrospective Look at Anthranilic Diamide Insecticides: Discovery and Lead Optimization to Chlorantraniliprole and Cyantraniliprole. *Pest. Manag. Sci.* 73, 658–665. doi:10.1002/ps.4308

Shiferaw, B., Prasanna, B. M., Hellin, J., and Bänziger, M. (2011). Crops that Feed the World 6. Past Successes and Future Challenges to the Role Played by Maize in Global Food Security. *Food Sec.* 3, 307–327. doi:10.1007/s12571-011-0140-5

Sun, X.-X., Hu, C.-X., Jia, H.-R., Wu, Q.-L., Shen, X.-J., Zhao, S.-Y., et al. (2021). Case Study on the First Immigration of Fall Armyworm, *Spodoptera frugiperda* Invading into China. *J. Integr. Agric.* 20, 664–672. doi:10.1016/s2095-3119(19)62839-x

Tang, Q.-Y., and Zhang, C.-X. (2013). Data Processing System (DPS) Software with Experimental Design, Statistical Analysis and Data Mining Developed for Use in Entomological Research. *Insect Sci.* 20, 254–260. doi:10.1111/j.1744-7917.2012.01519.x

Taylor, A. G., Eckenrode, C. J., and Straub, R. W. (2001). Seed Coating Technologies and Treatments for Onion: Challenges and Progress. *HortSci* 36, 199–205. doi:10.21273/hortsci.36.2.199

Teló, G. M., Senseman, S. A., Marchesan, E., Camargo, E. R., Jones, T., and McCauley, G. (2015). Residues of Thiamethoxam and Chlorantraniliprole in Rice Grain. *J. Agric. Food Chem.* 63, 2119–2126. doi:10.1021/jf5042504

Thrash, B., Adamczyk, J. J., Lorenz, G., Scott, A. W., Armstrong, J. S., Pfannenstiel, R., et al. (2013). Laboratory Evaluations of Lepidopteran-Active Soybean Seed Treatments on Survivorship of Fall Armyworm (Lepidoptera: Noctuidae) Larvae. *Fla. Entomol.* 96, 724–728. doi:10.1653/024.096.0304

Wang, S. Y., Zhu, Q. Z., Tan, Y. T., Ma, Q. L., Wang, R. F., Zhang, M. F., et al. (2019). Artificial Diets and Rearing Technique of *Spodoptera frugiperda* (J. E. Smith) in Laboratory. *J. Environ. Entomol.* 41, 742–747. doi:10.3969/j.issn.1674-0858.2019.04.8

Wang, Y. Q., Ma, Q. L., Tan, Y. T., Zheng, Q., Yan, W. J., Yang, S., et al. (2019). The Toxicity and Field Efficacy of Chlorantraniliprole against *Spodoptera frugiperda*. *J. Environ. Entomol.* 42, 782–788. doi:10.3969/j.issn.1674-0858.2019.04.14

Wu, C., Xiong, T., Yin, Y., Zhong, G., and Feng, X. (2020). The Effect of Prevention and Control against *Spodoptera frugiperda* by Corn Seeds Pelleting. *J. Environ. Entomol.* 42, 1314–1321. doi:10.3969/j.issn.1674-0858.2020.06.4

Yue, B., Wilde, G. E., and Arthur, F. (2003). Evaluation of Thiamethoxam and Imidacloprid as Seed Treatments to Control European Corn Borer and Indianmeal Moth (Lepidoptera: Pyralidae) Larvae. *J. Econ. Entomol.* 96, 503–509. doi:10.1603/0022-0493-96.2.50310.1093/jee/96.2.503

Zhang, L., Greenberg, S. M., Zhang, Y., and Liu, T.-X. (2011). Effectiveness of Thiamethoxam and Imidacloprid Seed Treatments against *Bemisia tabaci* (Hemiptera: Aleyrodidae) on Cotton. *Pest. Manag. Sci.* 67, 226–232. doi:10.1002/ps.2056

Zhang, P., Zhang, X., Zhao, Y., Ren, Y., Mu, W., and Liu, F. (2015). Efficacy of Granular Applications of Clothianidin and Nitenpyram against Aphis Gossypii (Glover) and Apolygus Lucorum (Meyer-Dür) in Cotton Fields in China. *Crop Prot.* 78, 27–34. doi:10.1016/j.cropro.2015.08.012

Zhang, P., Zhang, X., Zhao, Y., Wei, Y., Mu, W., and Liu, F. (2016a). Effects of Imidacloprid and Clothianidin Seed Treatments on Wheat Aphids and Their Natural Enemies on Winter Wheat. *Pest. Manag. Sci.* 72, 1141–1149. doi:10.1002/ps.4090

Zhang, Z., Xu, C., Ding, J., Zhao, Y., Lin, J., Liu, F., et al. (2019). Cyantraniliprole Seed Treatment Efficiency against Agrotis Ipsilon (Lepidoptera: Noctuidae) and Residue Concentrations in Corn Plants and Soil. *Pest. Manag. Sci.* 75, 1464–1472. doi:10.1002/ps.5269

Zhang, Z., Zhang, X., Wang, Y., Zhao, Y., Lin, J., Liu, F., et al. (2016b). Nitenpyram, Dinotefuran, and Thiamethoxam Used as Seed Treatments Act as Efficient Controls against Aphis Gossypii via High Residues in Cotton Leaves. *J. Agric. Food Chem.* 64, 9276–9285. doi:10.1021/acs.jafc.6b03430

Zheng, C. G., Li, G. H., Lu, X. J., Tang, L., and Chen, Q. J. (2006). Effects of Environmental Factors on Control Efficiency of SeNPV Pesticides. *J. Environ. Entomol.* 28, 66–70. doi:10.1001/j.issn.6155(2006)02-066-05

Zhou, Z. X., Tang, J. H., Lü, B. Q., and Lu, H. (2020). Indoor Toxicity and Field Efficacy of Four Kinds of Insecticide against *Spodoptera frugiperda* in Hainan. *Chin. J. Trop. Agric.* 40, 6–12. doi:10.12008/j.issn.1009-2196.2020

Check for updates

Novel Pyrimidine Derivatives Bearing a 1,3,4-Thiadiazole Skeleton: Design, Synthesis, and Antifungal Activity

Nianjuan Pan[†], Chunyi Liu[†], Ruirui Wu, Qiang Fei and Wenneng Wu *

Food and Pharmaceutical Engineering Institute, Guiyang University, Guiyang, China

In this study, twenty novel pyrimidine derivatives bearing a 1,3,4-thiadiazole skeleton were designed and synthesized. Then their antifungal activity against *Botrytis cinereal* (*B. cinereal*), *Botryosphaeria dothidea* (*B. dothidea*), and *Phomopsis* sp. were determined using the poison plate technique. Biological test results showed that compound **6h** revealed lower EC_{50} values (25.9 and 50.8 μg/ml) on *Phompsis* sp. than those of pyrimethanil (32.1 and 62.8 μg/ml).

Keywords: 4-thiadiazole, pyrimidine, design, synthesis, antifungal activity

1 INTRODUCTION

Due to their structure, which is similar to their alkaloid-like structure in living organisms, nitrogen-containing heterocyclic compounds have the characteristics of high target specificity and good environmental compatibility and have become the mainstream research field for the creation of new pesticides (Li et al., 2017; He et al., 2019). Among them, 1,3,4-thiadiazoles containing both N and S elements in the heterocyclic structure are important and lead molecules for designing biologically active compounds with various biological activities (Hu et al., 2014). For the past years, a large number of studies have shown that 1,3,4-thiadiazole and their derivatives had various biological activities including herbicidal (Sun et al., 2013), bactericidal (Li et al., 2015; Zhang et al., 2019; Wu Q. et al., 2020; Wu et al., 2021), fungicidal (Zou et al., 2002; Zine et al., 2016; Wu W. et al., 2020), antiviral (Wu et al., 2016a; Gan et al., 2017), insecticidal (Dai et al., 2016; Lv et al., 2018), anticancer (Chen et al., 2019), and so on. In the field of medicine and pesticides, especially in the field of fungicides, the products that have been successfully developed at present are thiabendazole, thiabendron copper, thiazole zinc, and thiazole.

Meanwhile, in the agricultural field, pyrimidine derivatives also have good biological activities such as antiviral (Wu, et al., 2015; Zan et al., 2020), insecticidal (Liu, et al., 2017; Wu, et al., 2019; Chen, et al., 2021; Liu, et al., 2021; Sun, et al., 2021), fungicidal (Guan et al., 2017; Yan et al., 2020; Yang, et al., 2020), bactericidal (Li et al., 2020), herbicidal (Chen et al., 2019; Li et al., 2020), and anticancer (Guo et al., 2020) properties. In the last few decades, some pyrimidine derivatives have been commercialized as pesticides for controlling plant diseases and insect pests. Therefore, pyrimidine was considered an active substructure to develop promising pesticides in recent years.

Based on the biological activity of 1,3,4-thiadiazole and the pyrimidine ring, in order to find new pyrimidine lead compounds with good biological activity, this work adopts the active substructure splicing method to design and synthesize a series of novel pyrimidine derivatives containing a 1,3,4-thiadiazole moiety (**Figure 1**), which were evaluated *in vitro* with regard to their antifungal activity against *Botrytis cinereal* (*B. cinereal*), *Botryosphaeria dothidea* (*B. dothidea*), and *Phomopsis* sp.

FIGURE 1 | Design of the target compounds.

6a: R$_1$ = H, R$_2$ = 2-CH$_3$
6b: R$_1$ = H, R$_2$ = 2-F
6c: R$_1$ = H, R$_2$ = 4-F
6d: R$_1$ = H, R$_2$ = 2-Cl
6e: R$_1$ = H, R$_2$ = 3-Cl
6f: R$_1$ = H, R$_2$ = 4-Cl
6g: R$_1$ = H, R$_2$ = 2-CN
6h: R$_1$ = H, R$_2$ = 4-CF$_3$
6i: R$_1$ = H, R$_2$ = 3,4-diCl
6j: R$_1$ = CH$_3$, R$_2$ = 2-CH$_3$

6k: R$_1$ = CH$_3$, R$_2$ = 4-F
6l: R$_1$ = CH$_3$, R$_2$ = 2-Cl
6m: R$_1$ = CH$_3$, R$_2$ = 3-Cl
6n: R$_1$ = CH$_3$, R$_2$ = 4-Cl
6o: R$_1$ = CH$_3$, R$_2$ = 2-CN
6p: R$_1$ = CH$_3$, R$_2$ = 2-CF$_3$
6q: R$_1$ = CH$_3$, R$_2$ = 4-CF$_3$
6r: R$_1$ = CH$_3$, R$_2$ = 2,3-diCl
6s: R$_1$ = CH$_3$, R$_2$ = 2,4-diCl
6t: R$_1$ = CH$_3$, R$_2$ = 3,4-diCl
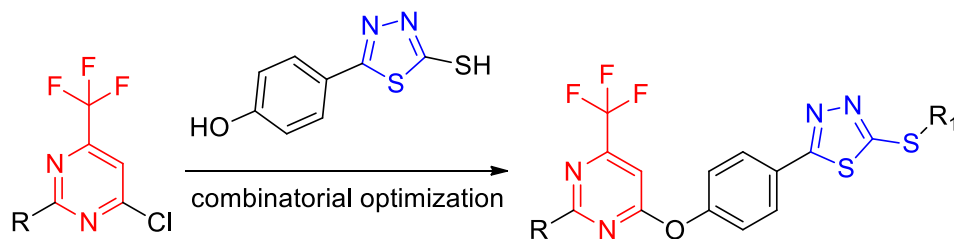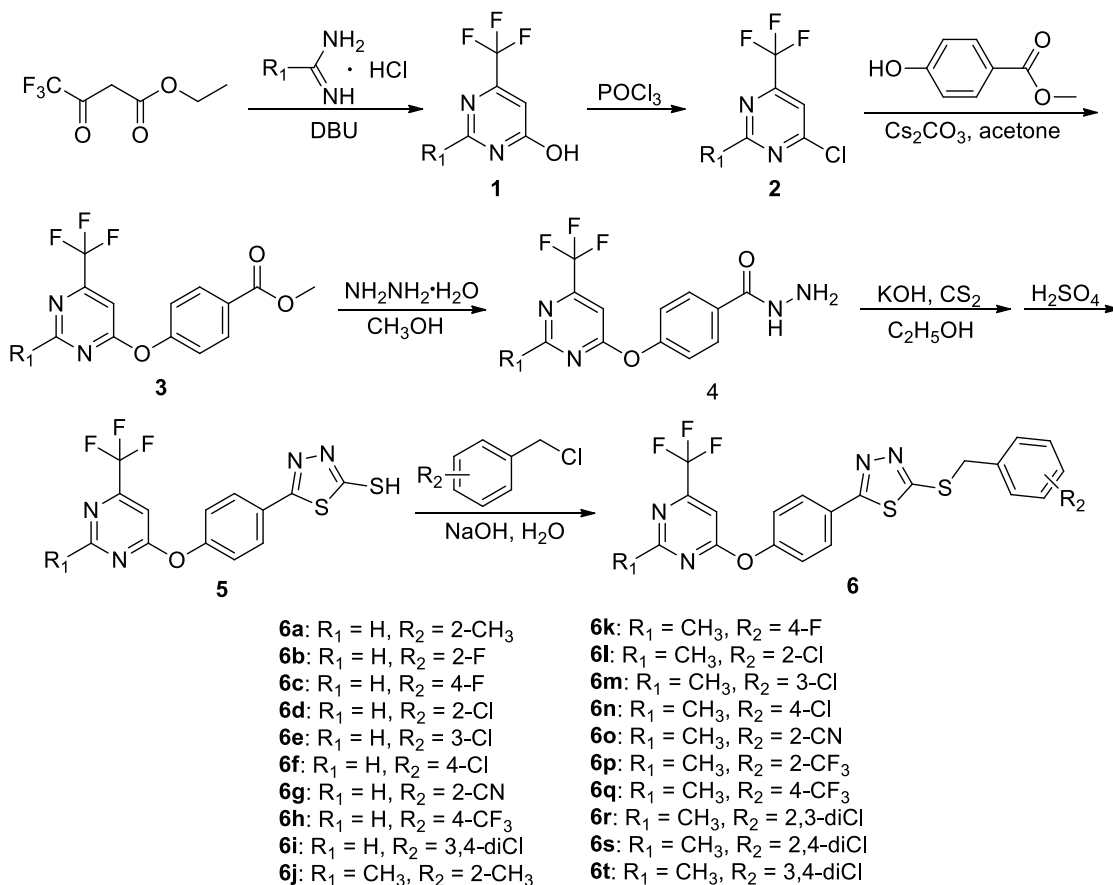
SCHEME 1 | Synthetic process and experimental method of the target compounds **6a–6t**.

2 MATERIALS AND METHODS

2.1 Chemistry

Melting points (m.p.) were obtained using a microscope apparatus (XT-4, Beijing Tech Instrument Co., China). Nuclear magnetic resonance (^{1}H NMR and ^{13}C NMR) was determined on a Bruker NMR spectrometer (Bruker, Germany). High-resolution mass spectrometry (HRMS) was performed on a Thermo Scientific Q Exactive Plus instrument (Thermo Fisher Scientific, United States).

2.2 The Preparation Procedure of Intermediates 1–5

Intermediates **1** and **2** were obtained by referring to the previously reported methods (Wu W. et al., 2020).

To a 100-ml three round-bottom flask, intermediate **2** (0.01 mol), ethyl 4-hydroxybenzoate (0.012 mol), Cs$_2$CO$_3$ (0.02 mol), and acetone (50 ml) were added. After reacting for 2–4 h at room temperature, the solvent was vacuum evaporated. The residues were recrystallized from ethanol to give pure intermediate **3**.

TABLE 1 | Inhibition rates of compounds **6a–6t** against *B. cinereal*, *B. dothidea*, and *Phomopsis* sp. at 50 μg/ml.

Compounds	Inhibition rate (%)		
	B. dothidea	**Phomopsis sp.**	**B. cinerea**
6a	41.8 ± 2.1	50.6 ± 2.2	73.2 ± 1.8
6b	63.0 ± 1.3	83.2 ± 1.3	78.7 ± 1.3
6c	75.6 ± 1.1	89.6 ± 1.8	85.1 ± 2.5
6d	57.4 ± 1.5	74.6 ± 1.4	71.1 ± 1.9
6e	65.9 ± 1.3	79.4 ± 2.1	79.2 ± 2.3
6f	72.4 ± 2.6	84.5 ± 1.2	84.9 ± 2.4
6g	80.0 ± 1.9	88.7 ± 2.2	86.1 ± 3.2
6h	82.6 ± 2.6	89.2 ± 1.9	90.7 ± 2.6
6i	70.8 ± 1.1	84.6 ± 1.2	85.4 ± 1.1
6j	36.2 ± 3.0	42.9 ± 2.1	65.3 ± 1.4
6k	59.0 ± 1.0	71.6 ± 1.8	74.0 ± 1.8
6l	51.5 ± 1.2	64.5 ± 1.7	65.7 ± 1.2
6m	57.4 ± 1.7	71.9 ± 1.3	73.3 ± 1.2
6n	65.4 ± 2.3	78.4 ± 1.4	80.4 ± 2.4
6o	73.7 ± 3.3	76.7 ± 1.0	78.8 ± 2.6
6p	68.4 ± 1.8	80.3 ± 1.5	81.8 ± 1.2
6q	75.7 ± 1.9	86.8 ± 1.9	88.3 ± 0.9
6r	58.2 ± 1.5	69.0 ± 1.7	66.5 ± 1.3
6s	75.6 ± 1.6	82.4 ± 1.4	83.9 ± 2.2
6t	65.7 ± 1.7	78.0 ± 1.3	80.8 ± 1.5
Pyrimethanil	84.4 ± 2.1	85.1 ± 1.4	82.8 ± 1.4

TABLE 2 | EC$_{50}$ values of the title compounds against *B. dothidea*, *Phomopsis* sp., and *B. cinereal*.

Compounds	EC$_{50}$ (μg/ml)		
	B. dothidea	**Phomopsis sp.**	**B. cinerea**
6c	—	25.4 ± 2.3	63.2 ± 1.2
6f	—	37.5 ± 1.7	67.6 ± 1.5
6g	67.8 ± 1.3	28.8 ± 2.6	57.5 ± 1.3
6h	63.6 ± 1.8	25.9 ± 1.4	50.8 ± 2.7
6i	—	34.8 ± 1.9	64.1 ± 2.9
6q	—	32.6 ± 1.5	59.9 ± 1.1
6s	—	—	68.8 ± 2.4
Pyrimethanil	57.6 ± 1.8	32.1 ± 2.0	62.8 ± 1.7

To a solution of intermediate **3** (20 mmol) in 40 ml absolute methanol, 80% hydrazine hydrate (60 mmol) was added dropwise. After reacting for 5–7 h under reflux conditions, the reaction was quenched to room temperature. The white solids precipitated from the reaction solution were filtrated and recrystallized from ethanol to give pure intermediate **4**.

To a mixture of intermediate **4** (30 mmol), KOH (45 mmol), and ethanol (500 ml), carbon disulfide (36 mmol) was added dropwise. The white precipitates were filtered, dried under vacuum, and then added to 30 ml precooled concentrated H$_2$SO$_4$. After stirring for 2 h at 0°C, the mixture was poured into 1,000 ml ice water and neutralized with sodium bicarbonate saturated solution (Wu et al., 2016a; Wu et al., 2016b). The filtrate was acidified with 5% hydrochloric acid, and the produced solid was filtered and recrystallized from ethanol to give the key intermediate **5**.

2.3 Preparation Procedure of the Target Compounds 6a–6t

Intermediate **5** (2 mmol), NaOH (2.2 mmol) dissolved in 15 ml water, and substituted benzyl chloride (2.1 mmol) were added in a 100-ml three round-bottom flask and stirred at room temperature for 2–4 h (**Scheme 1**). Upon completion of reaction, the residues were filtered and recrystallized from ethanol to produce the pure target compounds **6a–6t**. The physical properties, NMR, and HRMS for title compounds are reported in **Supplementary Data S1**, and the spectral data of **6a** are shown below. 2-((2-methylbenzyl)thio)-5-(4-((6-(trifluoromethyl)pyrimidin-4-yl)oxy)phenyl)-1,3,4-thiadiazole (**6a**). White solid; yield 65.24%; m. p. 104–107°C; ^{1}H NMR (600 MHz, DMSO-d_6, ppm) δ: 8.99 (s, 1H, pyrimidine-H),

8.04–8.02 (m, 2H, phenyl-H), 7.86 (s, 1H, pyrimidine-H), 7.50–7.48 (m, 4H, phenyl-H), 7.42 (d, 1H, *J* = 5.4 Hz, phenyl-H), 7.23–7.17 (m, 3H, phenyl-H), 4.65 (s, 2H, -SCH$_2$-), 2.41 (s, 3H, pyrimidine-CH$_3$); ^{13}C NMR (150 MHz, DMSO-d_6, ppm) δ: 170.32, 167.66, 165.34, 159.73, 156.22 (q, *J* = 35.1 Hz), 154.29, 137.37, 134.12, 130.98, 130.59, 129.74, 128.65, 127.66, 126.62, 123.27, 121.80 (q, *J* = 272.7 Hz), 116.13, 107.07, 36.66, 19.26; HRMS (ESI) calcd for C$_{21}$H$_{15}$ON$_4$S$_2$F$_3$ [M+Na]$^+$: 483.05249, found: 483.05316.

2.4 *In vitro* Antifungal Activity Test

The *in vitro* antifungal activity was determined according to the mycelial growth rate method (Zhang et al., 2018; Wang et al., 2019; Wu Q. et al., 2020). Each target compound (5 mg) was dissolved in DMSO (1 ml) and added to 9 ml H$_2$O and 90 ml potato dextrose agar (PDA) medium to prepare 9 dishes of mixed PDA plates with a concentration of 50 μg/ml. After that, a 0.4-cm diameter of each test fungus was put onto the middle of mixed PDA plates and fostered in an incubator at 28°C for 3–4 days. After the mycelia diameter of the untreated PDA plate reached 5–6 cm, the inhibition rates *I* (%) are calculated using the following formula, where C (cm) and T (cm) represent the fungi diameters of the untreated and treated PDA plates, respectively.

$$\text{Inhibition rate } I \ (\%) = (C - T)/(C - 0.4) \times 100$$

3 RESULTS AND DISCUSSION

3.1 Chemistry

In the ^{1}H NMR data of compound **6a**, a singlet appears at 4.65 ppm and indicates the presence of the -SCH$_2$- group. The CH proton of the 6-trifluoromethylpyrimidine ring appeared as two singlets at 8.99 and 7.86 ppm. Meanwhile, in the ^{13}C NMR data of compound **6a**, two signals at 170.32 and 167.66 ppm indicated the presence of C proton in the 1,3,4-thiadiazole group. One quartet at 156.22 ppm indicated the presence of -CF$_3$ in the pyrimidine fragment. In addition, compound **6a** was confirmed correctly by combining HRMS data with the [M + Na]$^+$ peaks.

3.2 *In vitro* Antifungal Activity

As shown in **Table 1**, compounds **6c**, **6g**, and **6h** exhibited higher *in vitro* antifungal activity against *Phomopsis* sp., and the inhibition rates were 89.6%, 88.7%, and 89.2%, respectively,

compared to that of pyrimethanil (85.1%). Meanwhile, **Table 1** shows that the inhibitory activity values of compounds **6g**, **6h**, and **6q** against *B. cinerea* were 86.1%, 90.7%, and 88.3%, respectively, which were superior to that of pyrimethanil (82.8%). In addition, compound **6h** possessed similar bioactivity against *B. dothidea* (82.6%) to that of pyrimethanil (84.4%).

Table 2 shows that compounds **6c**, **6g**, and **6h** had the EC_{50} values of 25.4, 28.8, and 25.9 µg/ml, respectively, which were better than that of pyrimethanil (32.1 µg/ml). Meanwhile, compounds **6g** (EC_{50} = 57.5 µg/ml) and **6h** (EC_{50} = 50.8 µg/ml) exhibited better *in vitro* bioactivity on *B. cinerea* than pyrimethanil (62.8 µg/ml). Meanwhile, compounds **6g** (EC_{50} = 67.8 µg/ml) and **6h** (EC_{50} = 63.6 µg/ml) exhibited lower *in vitro* bioactivity against *B. dothidea* than pyrimethanil (57.6 µg/ml).

Further structure–activity relationship analysis indicated that more than 80% of the title compounds showed excellent antifungal activity against *Phomopsis* sp. and *B. cinerea*. Meanwhile, changing R_1 (H or CH_3) did not significantly improve the antifungal activity of the compound. Only against *Phomopsis* sp., the number of compounds (R_1 = H) with activity higher than 80% is twice that of compounds (R_1 = CH_3). In addition, the introduction of strong electron withdraw groups (CN and CF_3) into R_2 was able to enhance the activity of the compounds, while the introduction of an alkyl group (CH_3) cannot obviously improve the antifungal activity of the compounds.

4 CONCLUSION

In conclusion, 20 novel 1,3,4-thiadiazole derivatives bearing a pyrimidine skeleton were synthesized and assessed for all compounds with regard to *in vitro* antifungal activities. Results of bioassays of the synthesized compounds showed excellent

antifungal activity compared to that of pyrimethanil. Therefore, 1,3,4-thiadiazole derivatives bearing a pyrimidine skeleton can be used as candidate leading structures for discovering new fungicidal agents.

DATA AVAILABILITY STATEMENT

The original contributions presented in the study are included in the article/**Supplementary Material**; further inquiries can be directed to the corresponding author.

AUTHOR CONTRIBUTIONS

FUNDING

SUPPLEMENTARY MATERIAL

The Supplementary Material for this article can be found online at: https://www.frontiersin.org/articles/10.3389/fchem.2022.922813/full#supplementary-material

REFERENCES

Chen, S., Zhang, Y., Liu, Y., and Wang, Q. (2021). Highly Efficient Synthesis and Acaricidal and Insecticidal Activities of Novel Oxazolines with *N*-Heterocyclic Substituents. *J. Agric. Food Chem.* 69, 3601–3606. doi:10.1021/acs.jafc.0c05558

Chen, Z., Li, D., Xu, N., Fang, J., Yu, Y., Hou, W., et al. (2019). Novel 1,3,4-Selenadiazole-Containing Kidney-type Glutaminase Inhibitors Showed Improved Cellular Uptake and Antitumor Activity. *J. Med. Chem.* 62, 589–603. doi:10.1021/acs.jmedchem.8b01198

Dai, H., Li, G., Chen, J., Shi, Y., Ge, S., Fan, C., et al. (2016). Synthesis and Biological Activities of Novel 1,3,4-Thiadiazole-Containing Pyrazole Oxime Derivatives. *Bioorg. Med. Chem. Lett.* 26, 3818–3821. doi:10.1016/j.bmcl.2016.04.094

Gan, X., Hu, D., Chen, Z., Wang, Y., and Song, B. (2017). Synthesis and Antiviral Evaluation of Novel 1,3,4-Oxadiazole/thiadiazole-Chalcone Conjugates. *Bioorg. Med. Chem. Lett.* 27, 4298–4301. doi:10.1016/j.bmcl.2017.08.038

Guan, A., Wang, M., Yang, J., Wang, L., Xie, Y., Lan, J., et al. (2017). Discovery of a New Fungicide Candidate through Lead Optimization of Pyrimidinamine Derivatives and its Activity against Cucumber Downy Mildew. *J. Agric. Food Chem.* 65, 10829–10835. doi:10.1021/acs.jafc.7b03898

Guo, W., Xing, Y., Zhang, Q., Xie, J., Huang, D., Gu, H., et al. (2020). Synthesis and Biological Evaluation of B-Cell Lymphoma 6 Inhibitors of *N*-Phenyl-4-Pyrimidinamine Derivatives Bearing Potent Activities against Tumor Growth. *J. Med. Chem.* 63, 676–695. doi:10.1021/acs.jmedchem.9b01618

He, W., Liu, D., Gan, X., Zhang, J., Liu, Z., Yi, C., et al. (2019). Synthesis and Biological Activity of Novel 1,3,4-Thiadiazolo[3,2-A]pyrimidinone Mesoionic Derivatives. *Chin. J. Org. Chem.* 39, 2287–2294. doi:10.6023/cjoc201903023

Hu, Y., Li, C.-Y., Wang, X.-M., Yang, Y.-H., and Zhu, H.-L. (2014). 1,3,4-Thiadiazole: Synthesis, Reactions, and Applications in Medicinal, Agricultural, and Materials Chemistry. *Chem. Rev.* 114, 5572–5610. doi:10.1021/cr400131u

Li, J.-h., Wang, Y., Wu, Y.-p., Li, R.-h., Liang, S., Zhang, J., et al. (2021). Synthesis, Herbicidal Activity Study and Molecular Docking of Novel Pyrimidine Thiourea. *Pesticide Biochem. Physiology* 172, 104766. doi:10.1016/j.pestbp.2020.104766

Li, P., Shi, L., Gao, M.-N., Yang, X., Xue, W., Jin, L.-H., et al. (2015). Antibacterial Activities against Rice Bacterial Leaf Blight and Tomato Bacterial Wilt of 2-Mercapto-5-Substituted-1,3,4-Oxadiazole/thiadiazole Derivatives. *Bioorg. Med. Chem. Lett.* 25, 481–484. doi:10.1016/j.bmcl.2014.12.038

Li, Q., Pang, K., Zhao, J., Liu, X., and Weng, J. (2017). Synthesis and Biological Activity of Novel 1,3,4-thiadiazole Thioether Derivatives Containing Pyrimidine Moiety. *Chin. J. Org. Chem.* 37, 1009–1015. doi:10.6023/cjoc201610026

Liu, X.-H., Wang, Q., Sun, Z.-H., Wedge, D. E., Becnel, J. J., Estep, A. S., et al. (2017). Synthesis and Insecticidal Activity of Novel Pyrimidine Derivatives Containing Urea Pharmacophore againstAedes Aegypti. *Pest. Manag. Sci.* 73, 953–959. doi:10.1002/ps.4370

Liu, X.-H., Wen, Y.-H., Cheng, L., Xu, T.-M., and Wu, N.-J. (2021). Design, Synthesis, and Pesticidal Activities of Pyrimidin-4-Amine Derivatives Bearing a 5-(Trifluoromethyl)-1,2,4-Oxadiazole Moiety. *J. Agric. Food Chem.* 69, 6968–6980. doi:10.1021/acs.jafc.1c00236

Lv, M., Liu, G., Jia, M., and Xu, H. (2018). Synthesis of Matrinic Amide Derivatives Containing 1,3,4-thiadiazole Scaffold as Insecticidal/acaricidal Agents. *Bioorg. Chem.* 81, 88–92. doi:10.1016/j.bioorg.2018.07.034

Sun, C., Zhang, S., Qian, P., Li, Y., Ren, W., Deng, H., et al. (2021). Synthesis and Fungicidal Activity of Novel Benzimidazole Derivatives Bearing Pyrimidine-thioether Moiety against Botrytis Cinerea. *Pest. Manag. Sci.* 77, 5529–5536. doi:10.1002/ps.6593

Sun, Z., Huang, W., Gong, Y., Lan, J., Liu, X., Weng, J., et al. (2013). Synthesis and Herbicidal Activity of New 1,3,4-thiadizols Sulfourea Derivative. *Chin. J. Org. Chem.* 33, 2612–2617. doi:10.6023/cjoc201306028

Wang, X., Fu, X., Yan, J., Wang, A., Wang, M., Chen, M., et al. (2019). Design and Synthesis of Novel 2-(6-Thioxo-1,3,5-Thiadiazinan-3-Yl)-N′-Phenylacethydrazide Derivatives as Potential Fungicides. *Mol. Divers.* 23, 573–583. doi:10.1007/s11030-018-9891-7

Wu, N., Cheng, L., Wang, J., Yu, J., Xing, J., Xu, T., et al. (2019). Synthesis and Insecticidal Activity of Novel 4-arylamino Pyrimidine Derivatives. *Chin. J. Org. Chem.* 39, 852–860. doi:10.6023/cjoc201807044

Wu, Q., Cai, H., Yuan, T., Li, S., Gan, X., and Song, B. (2020). Novel Vanillin Derivatives Containing a 1,3,4-thiadiazole Moiety as Potential Antibacterial Agents. *Bioorg. Med. Chem. Lett.* 30, 127113. doi:10.1016/j.bmcl.2020.127113

Wu, W.-N., Gao, M.-N., Tu, H., and Ouyang, G.-P. (2016a). Synthesis and Antibacterial Activity of Novel Substituted Purine Derivatives. *J. Heterocycl. Chem.* 53, 2042–2048. doi:10.1002/jhet.2527

Wu, W.-N., Tai, A.-Q., Chen, Q., and Ouyang, G.-P. (2016b). Synthesis and Antiviral Bioactivity of Novel 2-substituted Methlthio-5-(4-Amino-2-Methylpyrimidin-5-Yl)-1,3,4-Thiadiazole Derivatives. *J. Heterocycl. Chem.* 53, 626–632. doi:10.1002/jhet.2435

Wu, W., Chen, M., Fei, Q., Ge, Y., Zhu, Y., Chen, H., et al. (2020). Synthesis and Bioactivities Study of Novel Pyridylpyrazol Amide Derivatives Containing Pyrimidine Motifs. *Front. Chem.* 8, 522. doi:10.3389/fchem.2020.00522

Wu, W., Chen, Q., Tai, A., Jiang, G., and Ouyang, G. (2015). Synthesis and Antiviral Activity of 2-substituted Methylthio-5-(4-Amino-2-Methylpyrimidin-5-Yl)-1,3,4-Oxadiazole Derivatives. *Bioorg. Med. Chem. Lett.* 25, 2243–2246. doi:10.1016/j.bmcl.2015.02.069

Wu, Z., Shi, J., Chen, J., Hu, D., and Song, B. (2021). Design, Synthesis, Antibacterial Activity, and Mechanisms of Novel 1,3,4-thiadiazole Derivatives Containing an Amide Moiety. *J. Agric. Food Chem.* 69 (31), 8660–8670. doi:10.1021/acs.jafc.1c01626

Yan, Y., Cheng, W., Xiao, T., Zhang, G., Zhang, T., Lu, T., et al. (2020). Discovery of Novel 2,4,6-trisubstituted Pyrimidine Derivatives as Succinate Dehydrogenase Inhibitors. *Chin. J. Org. Chem.* 40, 4237–4248. doi:10.6023/cjoc202005057

Yang, J., Guan, A., Li, Z., Zhang, P., and Liu, C. (2020). Design, Synthesis, and Structure-Activity Relationship of Novel Spiropyrimidinamines as Fungicides against Pseudoperonospora Cubensis. *J. Agric. Food Chem.* 68, 6485–6492. doi:10.1021/acs.jafc.9b07055

Zan, N., Xie, D., Li, M., Jiang, D., and Song, B. (2020). Design, Synthesis, and Anti-ToCV Activity of Novel Pyrimidine Derivatives Bearing a Dithioacetal Moiety that Targets ToCV Coat Protein. *J. Agric. Food Chem.* 68, 6280–6285. doi:10.1021/acs.jafc.0c00987

Zhang, M., Xu, W., Wei, K., Liu, H., Yang, Q., Liu, Q., et al. (2019). Synthesis and Evaluation of 1,3,4-Thiadiazole Derivatives Containing Cyclopentylpropionamide as Potential Antibacterial Agent. *J. Heterocycl. Chem.* 56, 1966–1977. doi:10.1002/jhet.3576

Zhang, Z.-J., Zeng, Y., Jiang, Z.-Y., Shu, B.-S., Sethuraman, V., and Zhong, G.-H. (2018). Design, Synthesis, Fungicidal Property and QSAR Studies of Novel β-carbolines Containing Urea, Benzoylthiourea and Benzoylurea for the Control of Rice Sheath Blight. *Pest. Manag. Sci.* 74, 1736–1746. doi:10.1002/ps.4873

Zine, H., Rifai, L. A., Faize, M., Bentiss, F., Guesmi, S., Laachir, A., et al. (2016). Induced Resistance in Tomato Plants against Verticillium Wilt by the Binuclear Nickel Coordination Complex of the Ligand 2,5-Bis(pyridin-2-Yl)-1,3,4-Thiadiazole. *J. Agric. Food Chem.* 64, 2661–2667. doi:10.1021/acs.jafc.6b00151

Zou, X.-J., Lai, L.-H., Jin, G.-Y., and Zhang, Z.-X. (2002). Synthesis, Fungicidal Activity, and 3D-QSAR of Pyridazinone-Substituted 1,3,4-oxadiazoles and 1,3,4-thiadiazoles. *J. Agric. Food Chem.* 50, 3757–3760. doi:10.1021/jf0201677

Research of Synergistic Substances on Tobacco Beetle [*Lasioderma serricorne* (Fabricius) (Coleoptera: Anobiidae)] Adults Attractants

Yanling Ren[1,2†], Tao Wang[1,2*†], Yingjie Jiang[2], Pengchao Chen[2], Jian Tang[2], Juan Wang[2], Daochao Jin[1*] and Jianjun Guo[1]

[1]Guizhou Provincial Key Laboratory for Agricultural Pest Management of the Mountainous Region, Institute of Entomology, Scientific Observing and Experimental Station of Crop Pest in Guiyang, Ministry of Agriculture, Guizhou University, Guiyang, China, [2]Guizhou Light Industry Technical College, Guiyang, China

In this study, four kinds of chemical substances (2,3,5,6-tetramethylpyrazine, β-ionone, citronellal, and paeonol), three kinds of plant essential oils (tea tree essential oil, lavender essential oil, and myrrh essential oil), and their combinations were selected to explore their synergistic effects on tobacco beetle [*Lasioderma serricorne* (Fabricius) (Coleoptera: Anobiidae)] adults by the behavioral test and laboratory simulation test. Behavioral test results showed that some of the combinations revealed a synergistic effect on tobacco beetle adults, especially the sexual attractant +2,3,5,6-tetramethylpyrazine + β-ionone + citronellal + paeonol (SABCD, one portion of sexual attractant, and 1 mg/L synergistic substances) combination and the food attractant +2,3,5,6-tetramethylpyrazine + paeonol (FAD, 1 ml of food attractant and 1 mg/L synergistic substances) combination showed the best behavioral effect on tobacco beetle adults with average dwell times of 120.97 and 126.74 s, respectively, compared to those of other combinations. Meanwhile, SABCD had the highest selection rate [89.47%, about 1.5 times that of the sexual attractant (S)] on tobacco beetle adults compared with those of other combinations. In addition, laboratory simulation test results showed that the SABCD combination had the highest average selection rate (37.31%, about 2 times that of S) on tobacco beetle adults at 1 mg/L. However, our results showed that there was no significant difference in the indoor simulation results of food attractant synergistic substances. Our results will provide guidance for the development of new pesticides for tobacco beetle adults.

Keywords: chemical substances, plant essential oils, behavioral response, synergistic substances, tobacco beetle adults, laboratory simulation test

INTRODUCTION

Insects are divided into pests and beneficial insects. Beneficial insects need to be developed and utilized, and pests need to be controlled. At present, the control methods for pests are mainly physical control methods (Lü et al., 2022; Sang et al., 2022), biological control methods (Cheng et al., 2022; Hu et al., 2022), and chemical control methods (Bi et al., 2022; Chi et al., 2022). The commonly used pesticides in chemical control methods cause pest resistance and environmental pollution (McCaffery, 1998; Saglam et al., 2015; Tang et al., 2022), and some pesticides are banned in

many countries currently (Scholler et al., 2018). However, the products of sex attractants (Ikeda et al., 1980; Cao et al., 2020) and food attractants (Cai et al., 2018; Lu et al., 2020) rely on insect sex pheromones (Miao, 1989; Aziz et al., 1992) and plant essential oils or volatiles with attractive effects on insects (Light et al., 2001; Oliver and Mannion., 2001; Cai et al., 2018), respectively. Therefore, humans and the environment are very good and is a very popular chemical control method at present. Sex attractants rely on the principle that insects release sex pheromones to attract the opposite sex to come to mate and reproduce offspring (Miao, 1989; Li et al., 2012). Te sex attractants have been developed since the 1960s (Butenandt and Hecker, 1961; Regnier and Law, 1968) and have achieved good results in many pest control and monitoring applications, such as the *Cydia pomonella* sex attractant (Xiang et al., 2021), the *Spodoptera frugiperda* sex attractant (Huang et al., 2022), and the *Conogethes punctiferalis* sex attractant agent (Chen et al., 2022). Food attractants rely on the principle that herbivorous insects need to feed on plants to obtain the ability or rely on plants to synthesize some scarce substances (Knolhoff and Heckel, 2014; Cai et al., 2018), thereby attracting pests to achieve the goal of pest control. The food attractants of fruit fly pests (Shelly, 2010; Shelly et al., 2014; Gregg et al., 2016), Lepidoptera pests (Sutherland et al., 1977; Knight et al., 2015; Gregg et al., 2016), thrips pests (Niassy et al., 2011; Broughton and Harrison, 2012; Davidson et al., 2015; Mfuti et al., 2016), and beetle pests (Jackson et al., 2005; Ranger et al., 2011; Chen et al., 2014) are greatly developed and applied.

Attractants are widely used in the monitoring and control of pests. But most of the single attractants can only target male insects (Li et al., 2012) and the effect of a single attractant is not as good as the combination of different compounds (Lampman and Metcalf, 1988; Landolt et al., 2014; Knight et al., 2015). Therefore, the attractants composed of a large number of chemical substances and have attracting effects on insects are more meaningful for pest control. For example, *Bactrocera dorsalis* (Hendel) food attractants are composed of eugenol, matrix, and toxicant (Jang et al., 2013), and the bollworm food attractant contains 2-phenylethanol, phenylacetaldehyde, and volatiles found primarily in leaves (Gregg et al., 2010). The food attractants of *Diabrotica* spp. are composed of 1,2,4-trimethoxybenzene, indole, and *trans*-cinnamaldehyde (Lampman and Metcalf, 1987), and the M99 and G04-7 attractants of *Monochamus alternatus* Hope are composed of α-pinene, β-pinene, acetaldehyde, and acetone (Chen et al., 2014). In addition, FJ-MA-02, PE, PA, A-3, and SC-1 attractants, etc., of *M. alternatus* are composed of different chemical substances (Chen et al., 2014).

Tobacco beetle [*Lasioderma serricorne* (Fabricius) (Coleoptera: Anobiidae)] is a worldwide storage pest that harms tobacco (Linnie, 1994; Lü and Ma, 2015; Edde, 2019). Its sex pheromone (4S,6S,7S)-4,6-dimethyl-7-hydroxynonan-3-one (serricomine) was first isolated from female tobacco beetles in the 1980s (Chuman et al., 1979) and is still the main component of most sex pheromone traps (Papadopoulou and Buchelos, 2002; Athanassiou et al., 2018). In addition, the sex pheromone had 4,6-dimethyl-7-hydroxy-3-nonanon and 2,6-diethyl-3,5-dimethyl-2,3-dihydropyran (Mao et al., 1992), which are also slowly applied in the control of tobacco beetle. Studies on the synergistic substances

of tobacco beetle sex attractants include the following: Du (2006) studied the synergistic effects of Hangbaiju, Coriander, Gongju, and Brazilian flue-cured tobacco on sexual attractants, and the combined effect of Hangbaiju and pheromone was the most effective (; Xiong (2008) studied the synergistic effect of the combination of *Angelica sinensis*, citronella, fennel, alfalfa, and green tea on sex attractants; and Guarino et al. (2022) studied the synergistic effect of β-ionone on tobacco beetle sex pheromone, and the best-combined effect was about 1.5 times that of sex attractant alone. However, apart from plant essential oils and plant volatiles about tobacco beetle food attractants, there are currently no specific attractant products (Lu and Liu, 2016; Cao et al., 2019; Guarino et al., 2021).

Therefore, in this study, using the chemical substances and plant essential oils with good attracting effects on tobacco beetle adults reported in the previous studies (Lü and Liu, 2016; Cao et al., 2019; Guarino et al., 2021; Zhong et al., 2021; Ren et al., 2022) as research materials, we explore their synergistic effects of four kinds of chemical substances (2,3,5,6-tetramethylpyrazine, β-ionone, citronellal, and paeonol), three kinds of plant essential oils (tea tree essential oil, lavender essential oil, and myrrh essential oil), and their combinations on tobacco beetle adults by the behavioral test and laboratory simulation test.

MATERIAL AND METHODS

Test Insects
Tobacco beetle adults were obtained from the Institute of Entomology of Guizhou University and reared at the Guizhou Engineering Research Center for Mountain Featured Fruits and Products of Guizhou Light Industry and Technical College. The feeding feed was composed of corn residue, yeast powder, and tobacco leaf powder (15: 1: 0.75). The feeding equipment was an artificial intelligence climate box. The rearing conditions were as follows: photoperiod of 16L: 8D, relative humidity of 60 ± 5%, and temperature of 28 ± 1°C. About 12 h before the experiment, tobacco beetle adults that had emerged within a week were selected and placed in a 100 ml transparent packing box.

Test Materials
Sexual attractant (S), food attractant (F), and sticky cardboard were purchased from Henan LoveTree Technology Development Co. Ltd. (Henan, China). 2,3,5,6-Tetramethylpyrazine (A) was purchased from Shanghai Aladdin Biochemical Technology Co, Ltd. (Shanghai, China). β-Ionone (B) was purchased from Shanghai Macklin Biochemical Co., Ltd. (Shanghai, China). Citronellal (C) and paeonol (D) were purchased from Shanghai Macklin Biochemical Co., Ltd. (Shanghai, China). Tea tree essential oil (E), lavender essential oil (G), and myrrh essential oil (H) were purchased from Beijing Maosi Trading Company (Beijing, China). The combinations of the test materials are shown in **Table 1**.

Behavioral Test of Attractants
About 50 μL of 1 mg/L (chemical substances) or 1 μL/L (plant essential oils) of the substance (dilute with absolute ethanol) is taken and dripped onto a 2 cm × 4 cm filter paper strip. The amount

TABLE 1 | The combinations of the test materials.

| Full name	Abbreviation	Full name	Abbreviation
Sexual attractant	S	Food attractant	F
Sexual attractant +2,3,5,6-tetramethylpyrazine	SA	Food attractant +2,3,5,6-tetramethylpyrazine	FA
Sexual attractant +β-ionone	SB	Food attractant + β-ionone	FB
Sexual attractant + citronellal	SC	Food attractant + citronellal	FC
Sexual attractant + paeonol	SD	Food attractant + paeonol	FD
Sexual attractant +2,3,5,6-tetramethylpyrazine + β-ionone	SAB	Food attractant +2,3,5,6-tetramethylpyrazine + β-ionone	FAB
Sexual attractant +2,3,5,6-tetramethylpyrazine + citronellal	SAC	Food attractant +2,3,5,6-tetramethylpyrazine + citronellal	FAC
Sexual attractant +2,3,5,6-tetramethylpyrazine + paeonol	SAD	Food attractant +2,3,5,6-tetramethylpyrazine + paeonol	FAD
Sexual attractant + β-ionone + citronellal	SBC	Food attractant + β-ionone + citronellal	FBC
Sexual attractant + β-ionone + paeonol	SBD	Food attractant + β-ionone + paeonol	FBD
Sexual attractant + citronellal + paeonol	SCD	Food attractant + citronellal + paeonol	FCD
Sexual attractant +2,3,5,6-tetramethylpyrazine + β-ionone + citronellal	SABC	Food attractant +2,3,5,6-tetramethylpyrazine + β-ionone + citronellal	FABC
Sexual attractant +2,3,5,6-tetramethylpyrazine + β-ionone + paeonol	SABD	Food attractant +2,3,5,6-tetramethylpyrazine + β-ionone + paeonol	FABD
Sexual attractant + β-ionone + citronellal + paeonol	SBCD	Food attractant + β-ionone + citronellal + paeonol	FBCD
Sexual attractant +2,3,5,6-tetramethylpyrazine + β-ionone + citronellal + paeonol	SABCD	Food attractant +2,3,5,6-tetramethylpyrazine + β-ionone + citronellal + paeonol	FABCD
Sexual attractant + tea tree essential oil	SE	Food attractant + tea tree essential oil	FE
Sexual attractant + lavender essential oil	SG	Food attractant + lavender essential oil	FG
Sexual attractant + myrrh essential oil	SH	Food attractant + myrrh essential oil	FH
Sexual attractant + tea tree essential oil + lavender essential oil	SEG	Food attractant + tea tree essential oil + lavender essential oil	FEG
Sexual attractant + tea tree essential oil + myrrh essential oil	SEH	Food attractant + tea tree essential oil + myrrh essential oil	FEH
Sexual attractant + lavender essential oil + myrrh essential oil	SGH	Food attractant + lavender essential oil + myrrh essential oil	FGH
Sexual attractant + tea tree essential oil + lavender essential oil + myrrh essential oil	SEGH	Food attractant + tea tree essential oil + lavender essential oil + myrrh essential oil	FEGH
Sexual attractant +2,3,5,6-tetramethylpyrazine + β-ionone + citronellal + paeonol + tea tree essential oil + lavender essential oil + myrrh essential oil	SABCDGH	Food attractant +2,3,5,6-tetramethylpyrazine + β-ionone + citronellal + paeonol + tea tree essential oil + lavender essential oil + myrrh essential oil	FADEG

FIGURE 1 | The diagram for the behavioral test on tobacco beetle adults.
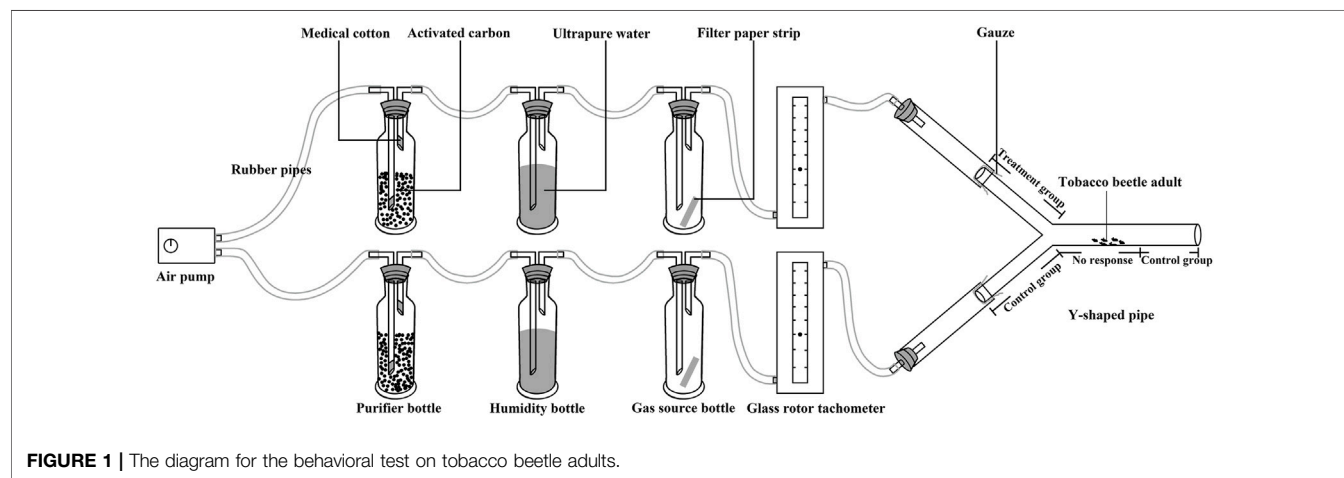
of sex attractant and food attractant in the experiment is 1 portion and 1 ml, respectively, for each trap required by the product instructions. The filter paper strip and attractant were put into the test source bottle and the filter paper strip was changed every 5 times. The gas source bottle and subsequent equipment from side to side were swapped every 20 times to reduce any risk of affecting the results of the experiment. After the behavioral test for each combination, the gas source bottle and all subsequent equipment pieces were first cleaned with alcohol 2–3 times, then cleaned with ultrapure water 2–3 times, and finally, dried at 70°C for 30 min.

The research method of the synergistic effect of four chemical substances and three plant essential oils, as well as their combinations on tobacco beetle sexual attractant and food attractant, is based on the study reported by Guarino et al. (2021), and the diagram for the behavioral test on tobacco beetle adults is shown in **Figure 1**. The temperature of the test room was controlled at 28 ± 1°C by an air conditioner. An air pump (Aco-5505, Guangdong Haili Group Co., Ltd., all instruments are connected by rubber pipes with inner and outer diameters of 6 and 9 mm, respectively) to generate

FIGURE 2 | The diagram for the laboratory simulation test on tobacco beetle adults.
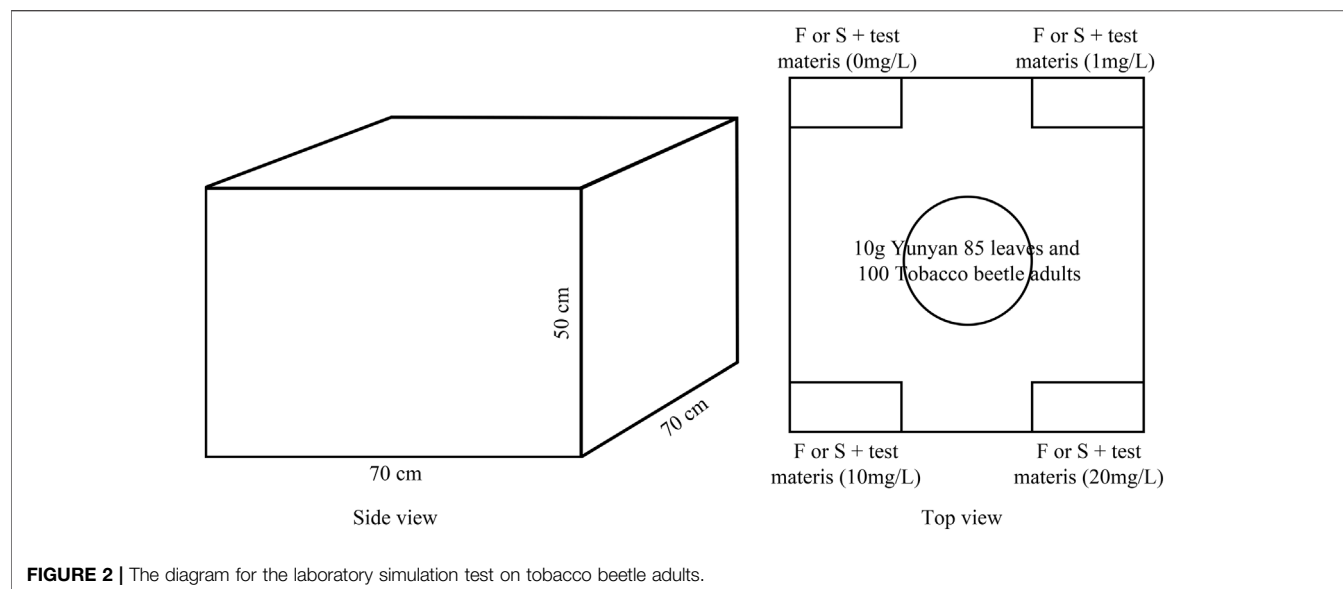
airflow. The airflow passes through 1,000 ml bottles filled with activated carbon to purify impurities and then passes through a 250 ml humidity bottle containing ultrapure water to increase air humidity. The airflow rate was adjusted through the airflow meter (flow rate: 500 ml/min); the airflow passed through the 250 ml gas source bottle to carry the smell and then entered the Y-shaped pipe (stem: 20 cm; arms: 15 cm at a 140 angle; stem internal diameter: 5.0 cm, arms internal diameter: 3.5 cm, placed in an evenly lit area). After 5 min of ventilation, one tobacco beetle adult was placed in the middle of the main stem (3–5 cm away from the Y-pipe connection).

The time when the tobacco beetle adult entered the experimental group (test arm) and the control group (the tobacco beetle entered the blank arm and the stem 5 cm away from the connection) was recorded and continued to observe for 300 s. The dwell time is calculated by the following formula:

$$\text{Average dwell time (s)} = \frac{\text{Test or control group insect active time}}{\text{Test group insects numbers} + \text{Control group insects numbers}},$$

TABLE 2 | The selection rates of sexual attractant (S) plus different chemical substances, plant essential oils, and their combinations.

Combination Abbreviations	Adults selection rate (%)		Male selection rate (%)		Female selection rate (%)	
	Test	Control	Test	Control	Test	Control
S	61.11	88.89	84.21	78.95	35.29	100.00
SA	52.94	70.59	87.50	50.00	22.22	88.89
SB	78.95	47.37	95.00	25.00	61.11	72.22
SC	33.33	88.89	58.82	82.35	94.74	63.16
SD	77.78	61.11	100.00	40.00	50.00	87.50
SAB	55.56	77.78	80.00	60.00	25.00	100.00
SAC	38.89	88.89	63.16	78.95	11.76	100.00
SAD	61.11	94.44	88.89	88.89	33.33	100.00
SBC	66.67	61.11	89.47	52.63	41.18	70.59
SBD	33.33	94.44	44.44	88.89	22.22	100.00
SCD	38.89	88.89	64.71	76.47	15.79	100.00
SABC	63.16	52.63	95.00	30.00	27.78	77.78
SABD	65.00	65.00	90.00	35.00	40.00	95.00
SBCD	68.43	78.95	90.00	70.00	44.44	88.89
SABCD	89.47	78.95	100.00	63.16	78.95	94.74
SE	30.77	69.23	58.33	41.67	23.53	94.12
SG	47.06	64.71	87.50	25.00	11.11	100.00
SH	60.00	60.00	94.12	29.41	15.38	100.00
SEG	61.11	58.33	100.00	30.00	12.50	93.75
SHE	69.44	66.67	95.00	65.00	37.50	68.75
SGH	73.68	73.68	80.00	55.00	66.67	94.44
SEGH	56.25	75.00	82.35	64.71	26.67	86.67
SABCDGH	73.68	68.42	100.00	40.00	44.44	100.00

FIGURE 3 | An average dwell time of male adults, female adults, and adults of tobacco beetle in the combination of chemical substances and sexual attractants. Different lowercase letters in the figure represent the average dwell time of male adults, female adults, and adults of tobacco beetles with a significant difference at $p <$ 0.05 in different combinations. Error bars shown in the figure represent mean ± SE.

Meanwhile, after the laboratory behavioral test, the tobacco beetle was placed in a 2 ml centrifuge tube, and then male and female identification was carried out using a stereoscopic microscope (SZ680, Chongqing Auto Optical Instrument Co., Ltd.). The abdomen was slightly squeezed with tweezers to expose the genitals. The genitals are simple in shape for females and are complex for males. Only sex attractant synergistic substance studies are conducted to identify males and females.

Laboratory Simulation Test

The blank rubber attractant core (Henan LoveTree Technology Development Co. Ltd., Henan, China) was immersed in absolute ethanol for 24 h, dried for 12 h, and then soaked in 20 ml of 0, 1, 10, and 20 mg/L (chemical substances) or 1 μL/L (plant essential oils) reagents (chemicals and plant essential oils) for 24 h. Finally,

it was taken out and placed on a sticky insect board during the experiment.

After the laboratory behavior test, the synergistic substances with the longest average dwell time were selected to be used in the laboratory simulation test. The experimental method referred to the research of Li et al. (2020) and the diagram for the laboratory simulation test on tobacco beetle adults is shown in **Figure 2**. The test materials were divided into four concentration gradients of 0, 1, 10, and 20 mg/L or μL/L, plus one sexual attractant or 1 ml of food attractant to form four test gas sources. The temperature of the test room was controlled at 28 ± 1°C by an air conditioner, and 10 g of Yunyan 85 leaves was placed in the middle of the wooden box with the length, width, and height of 70, 70, and 50 cm, respectively, to simulate the tobacco warehouse environment (the top of the wooden box was covered with gauze to prevent the escape of tobacco armor and
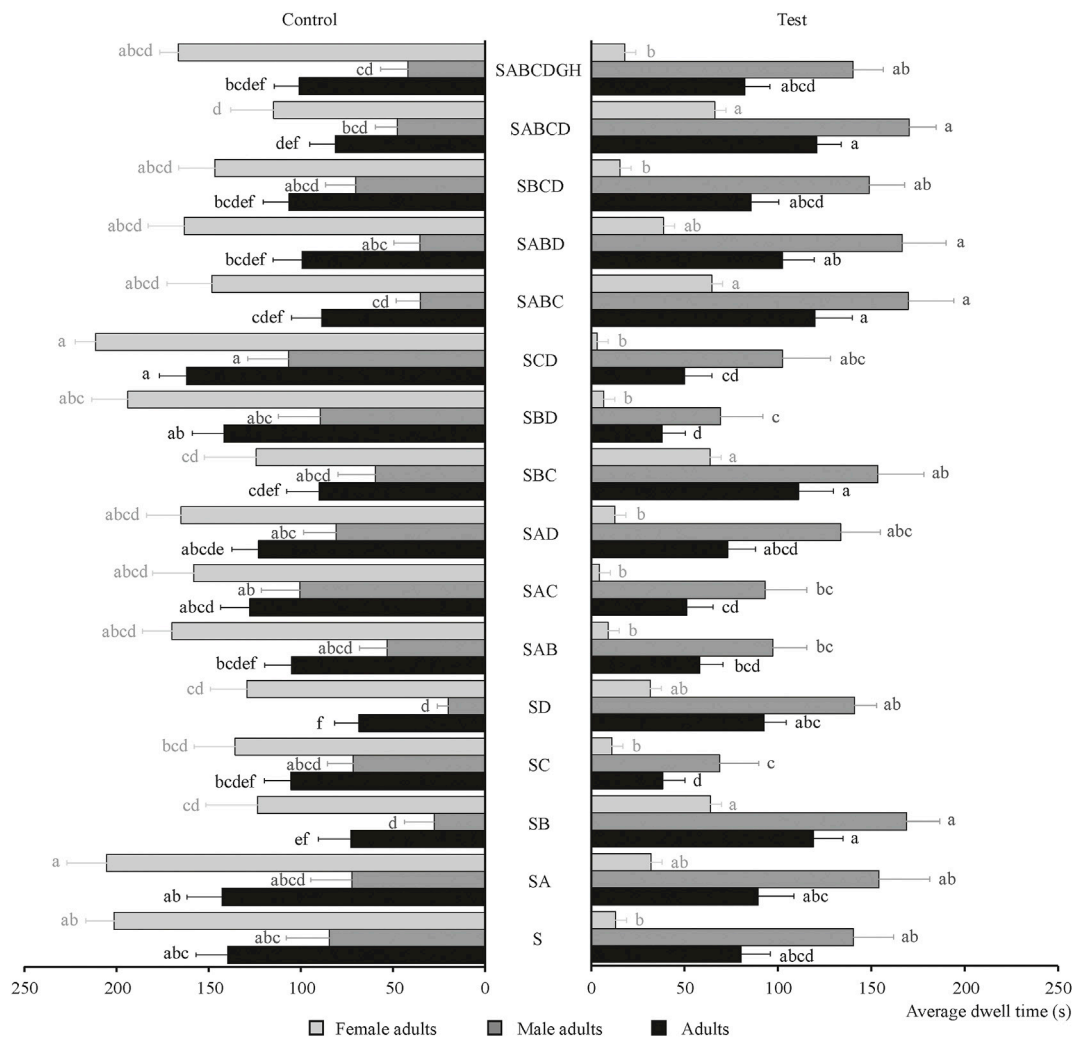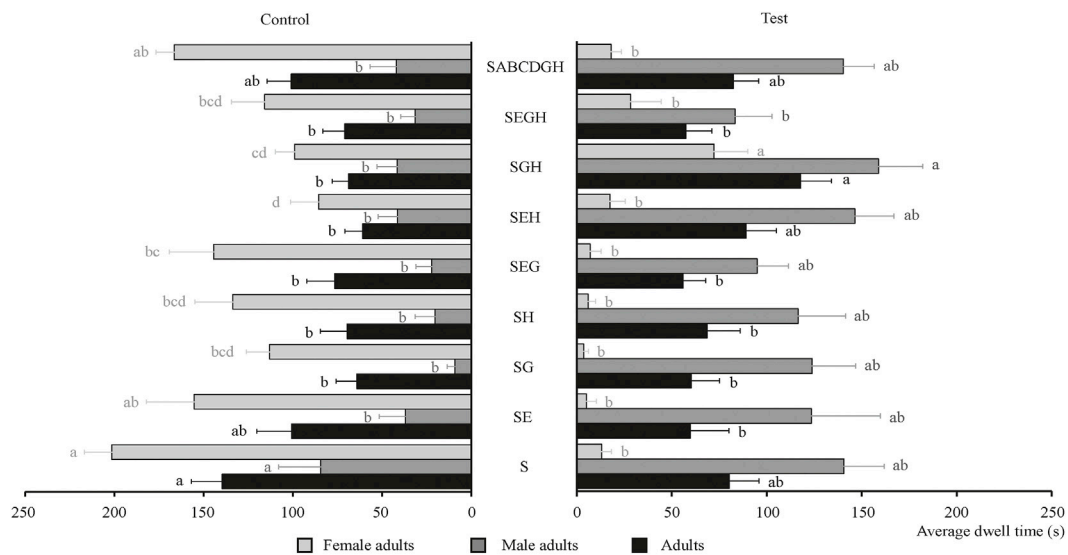
FIGURE 4 | Average dwell time of male adults, female adults, and adults of tobacco beetle in the combination of plant essential oils and sexual attractants. Different lowercase letters in the figure represent the average dwell time of male adults, female adults, and adults of tobacco beetle with a significant difference at $p < 0.05$ in different combinations. Error bars shown in the figure represent mean ± SE.
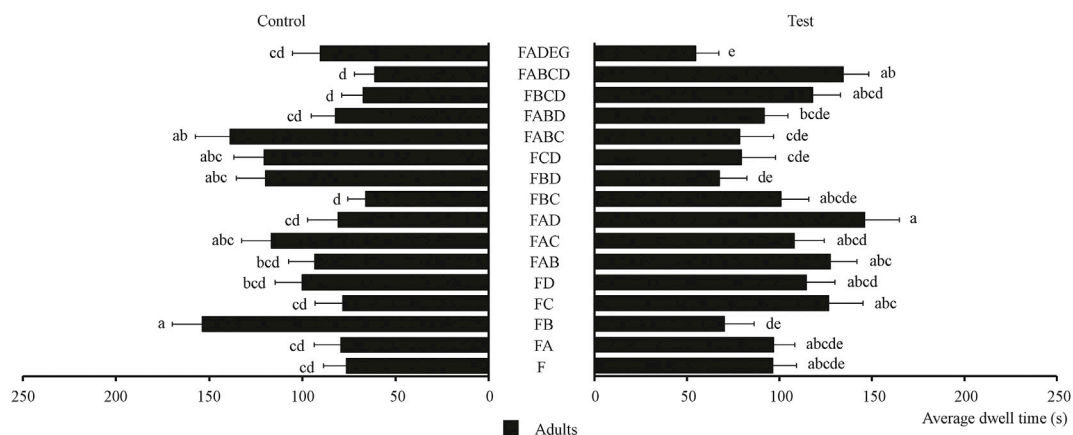
FIGURE 5 | Average dwell time of tobacco beetle adults in the combination of chemical substances and food attractants. Different lowercase letters in the figure represent the average dwell time of tobacco beetle adults with a significant difference at $p < 0.05$ in different combinations. Error bars shown in the figure represent mean ± SE.

ensure ventilation). The sticky insect boards were put down on the four corners of the wooden box, the test source was placed in the center of the sticky insect board, and 100 tobacco beetle adults were put in the bottom center point of the wooden box. After 24 h, the sticky insect board was collected, and the number of insects was recorded. After the laboratory simulation test, the wooden box was moved to the outdoor for 24 h ventilation. A total of 12 repetitions were performed, with each repetition moving the sticky insect boards clockwise. The selection rate is calculated by the following formula:

$$\text{Selection rate (\%)} = \frac{\text{Test or control group insects numbers}}{\text{Test group insects numbers} + \text{Control group insects numbers}} \times 100,$$

Statistical Analysis

Basic processing of data was performed using Microsoft Office Excel (version 2016). LSD test was conducted in SPSS (version 22), and the difference level was $p < 0.05$.

RESULTS

Behavioral Test of Sexual Attractants

The behavioral effects of four chemical substances and their combinations on the tobacco beetle sexual attractant were determined and shown in **Figure 3**. As shown in **Figure 3**, the

FIGURE 6 | Average dwell time of tobacco beetle adults in the combination of plant essential oils and food attractants. Different lowercase letters in the figure represent the average dwell time of tobacco beetle adults with a significant difference at $p < 0.05$ in different combinations. Error bars shown in the figure represent mean ± SE.
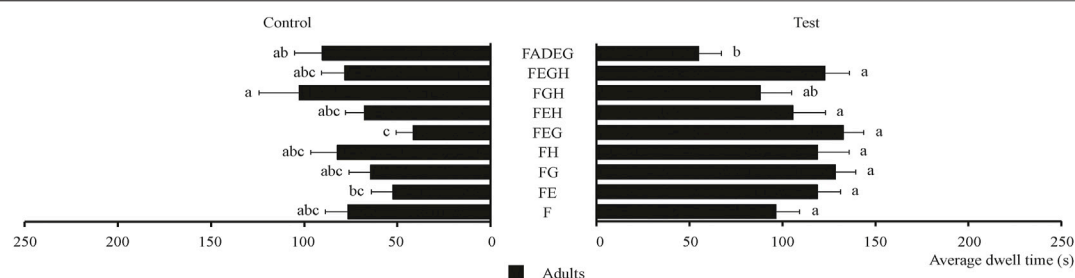
TABLE 3 | The selection rate of the food attractant (F) plus different chemical substances, plant essential oils, and their combinations.

Combination abbreviations	Adults' selection rate (%)	
	Test	**Control**
F	85.00	70.00
FA	80.00	75.00
FB	50.00	85.00
FC	73.68	68.42
FD	70.00	75.00
FAB	90.00	65.00
FAC	75.00	75.00
FAD	80.00	50.00
FBC	80.00	70.00
FBD	50.00	70.00
FCD	40.00	75.00
FABC	47.37	78.95
FABD	76.47	88.24
FBCD	81.08	59.46
FABCD	95.00	70.00
FE	100.00	55.56
FG	94.74	68.42
FH	84.21	57.89
FEG	95.00	50.00
FEH	75.00	65.00
FGH	61.76	41.18
FEGH	90.00	70.00
FADEG	52.94	70.59

chemical substance that had the best behavioral effect on sexual attractants is B; its average dwell time is 119.05 s, which is about 1.5 times that of S (80.33 s). Also, SABCD revealed a synergistic effect on tobacco beetle adults with the longest average dwell time of 120.97 s, which is about 1.5 times that of S. Meanwhile, the average dwell times of the SABCD combination for male and female adults were 170.25 and 66.22 s, respectively, which were 1.2 and 5.1 times than those of S (140.53 and 13.06 s, respectively), demonstrating that the SABCD combination also revealed a synergistic effect on male and female adults. Other substance combinations plus sexual attractants with synergistic effects are SA, SB, SD, SBC, SABC, SABD, and SBCD, while it is puzzling that the average dwell times of the combination of SC, SAB, SAC, SAD, SBD, and SCD were lower than those of S. The tobacco beetle adults remained in the experimental group of SD,

SB, SABCD, SABC, SBC, SABD, etc., more than the corresponding control group.

The behavioral effects of three plant essential oils and their combinations on the tobacco beetle food attractant were determined and shown in **Figure 4**. As shown in **Figure 4**, each of the three plant essential oils on the sexual attractant had no obvious synergistic effect on male adults, female adults, and adults of tobacco beetle compared with S. The longest average dwell time was with SGH combination, and its average dwell time (117.84 s) was about 1.5 times than that of S (80.33 s), demonstrating that SGH combination had a synergistic effect on tobacco beetle adults. The average dwell time (158.85 s) of male adults in the SGH combination was 1.1 times that of S (140.53 s); meanwhile, the average dwell time (72.28 s) of female adults in the SGH combination was about 5.5 times that of S (13.06 s), also demonstrating that the SGH combination had a synergistic effect on male and female adults. **Figure 3** also shows that the synergistic effects of SEH and SGH combinations are positive, and other plant essential oil combinations are all negative. The tobacco beetle adults remained in the experimental groups of SEH and SGH more than the corresponding control group, and SGH is about 1.7 times.

Behavioral Test of Food Attractants

The behavioral effect of four chemical substances and their combinations on food attractants were determined and the results are shown in **Figure 5**. **Figure 5** shows that the chemical substance that had the best behavioral effect on tobacco beetle adults is citronellal [average dwell time is 126.74 s, 1.3 times than F (80.33 s)]. Meanwhile, **Figure 5** also shows that the FAD combination showed the best synergistic effect on tobacco beetle adults with the longest average dwell time of 146.15 s, which was about 1.5 times that of F (96.45 s). Among these combinations, nine combinations (FA, FC, FD, FAB, FAC, FAD, FBC, FBCD, and FABCD) had synergistic effects on tobacco beetle adults, while six combinations (FB, FBD, FCD, FABC, and FABD) had no synergistic effect on tobacco beetle adults.

The behavioral effect of three plant essential oils and their combinations on food attractants was determined and the results are shown in **Figure 6**. As shown in **Figure 6**, all the combinations had no obvious synergistic effect on tobacco beetle adults compared with F. FEG had the highest average dwell time (132.75 s), which is about 1.4 times that of F (96.45 s).

Combination abbreviations	Average response rate (±SE) (%)	Concentration of synergistic substances (mg/L)	Average selection rate (±SE) (%)
SABCD	39.50 (±3.95)[a]	0	17.41 (±2.07)[c]
		1	37.31 (±1.91)[a]
		10	23.47 (±1.55)[b]
		20	21.81 (±1.63)[bc]
FAD	41.50 (±3.10)[a]	0	21.71 (±3.42)[a]
		1	32.28 (±3.40)[a]
		10	20.01 (±4.21)[a]
		20	26.00 (±4.78)[a]

The average response rate uses an independent-sample t-test. Different lowercase letters in the figure represent the average respones rate or average selection rate of tobacco beetle adults with a significant difference at p < 0.05 in different combinations.

Analysis of Selection Rate

From the characteristics of the sticky insect board, in reality, once the insects choose to enter the range of the sticky insect board, they cannot be re-selected. Therefore, according to the data record, we also analyzed the selection rate of S plus on different chemical substances, plant essential oils, and their combinations, respectively. As shown in **Table 2**, SABCD had the highest selection rate (89.47%) on tobacco beetle adults compared with those of S and other combinations. Meanwhile, the male selection rates of SD, SABCD, SEG, and SABCDGH combinations reached 100%, which was even better than those of S (84.21%) and other combinations. In addition, SC had the best female selection rate (94.74%) than those of S (35.29%) and other combinations.

Meanwhile, the selection rate of food attractants plus different chemical substances, plant essential oils, and their combinations, respectively, were also analyzed, and the results are shown in **Table 3**. As shown in **Table 3**, the adult selection rate of FE reached 100.00%, which was even better than F (85.00%) and other combinations. In addition, the average adult selection rate of the combination of synergistic substances and food attractants was higher than that of the combination of synergistic substances and sexual attractants (75.10% > 58.98%).

Laboratory Simulation Test

After the laboratory behavior test, the synergistic substances of SABCD and FAD were selected to be used in the laboratory simulation test, and the results are shown in **Table 4**. **Table 4** reveals that the average response rate of the FAD combination is 41.5%, which is equal to that of the SABCD combination (39.5%). Meanwhile, the SABCD combination had the highest average selection rate (37.31%) on tobacco beetle adults at 1 mg/L, which was 2.14 times the average selection rate at 0 mg/L, and with the increase of the concentration of the synergistic substance, the average selection rate has a tendency to decrease. In addition, **Table 4** also shows that the average selection rate of FAD had no significant change with the increase in the concentration of the synergistic substances.

DISCUSSION

In our study, the synergy of β-ionone and other substances was better (about 1.5–2 times) than that of single β-ionone for food/sex attractants; however, the synergistic effect of Hangbaiju on the tobacco nail attractant (Du, 2006), the synergistic effect of angelica + citronella on the tobacco nail attractant (Xiong, 2008), the synergistic effect of β-ionone on the tobacco nail attractant (Guarino et al., 2022), and their synergistic effect was not more than 1.5 times. But, judging from the research on attractants of other insects, the multiplier was far more than 2 times, and the number of *Mythimna separata* trapped by the combination of ethyl benzoate and armyworm sex pheromone was about 4–5 times that of armyworm sex pheromone (Yang et al., 2015). The combination of (Z)-8-dodecenyl acetate, (E)-8-dodecenyl acetate, and codlemone (95: 4: 10) was found to trap *Grapholita molesta* adults about 5–6 times more than the commercial sex attractants with the combination of (Z)-8-dodecenyl acetate, (E)- 8-dodecenyl acetate, and (Z)-8-dodecenol (95:4:1) (Liu et al., 2021).

In addition, some combinations had a very good lure effect on tobacco beetles, but after combining these best combinations, the effect was not as good as when it was not combined or the effect does not increase significantly. Similar results were also reported in other studies. Ataide et al. (2020) studied the behavioral response of different essential oils to tobacco beetle adults, but the synergistic effect of eucalyptol and euggenol combination was not better than a single one of them. Fornari et al. (2013) found that the average number of *Lobiopa insularis* was caught after 7 days of exposure to different food attractants, and the mixture of ripe strawberries and combination (dairy cattle feed, granulated sugar, and water) was not as large as their individual catches. Sathiyaseelan et al. (2022) found that rice bran and rice flour alone were more effective in attracting insects such as *Sitotroga cerealella*, *Rhyzopertha dominica*, *Tribolium* spp., *Sitophilus oryzae*, and *Oryzaephilus surinamensis* than their combinations. Therefore, it is very necessary to study the compounding of substances that have a good attraction to tobacco beetles.

CONCLUSION

In conclusion, the synergistic effects of four kinds of chemical substances, three kinds of plant essential oils, and their combinations on tobacco beetle adults were determined by the behavioral test and laboratory simulation test. Behavioral test results showed that the SABCD combination showed the best

synergistic effect and selection rate on tobacco beetle adults. Meanwhile, laboratory simulation test results showed that the SABCD combination had the highest average selection rate on tobacco beetle adults at 1 mg/L, demonstrating that the SABCD combination could be further used for the tobacco beetle adults' control. However, our results showed that there was no significant difference in the indoor simulation results of food attractant synergistic substances, providing guidance for controlling tobacco beetle adults.

DATA AVAILABILITY STATEMENT

The original contributions presented in the study are included in the article/Supplementary Material, further inquiries can be directed to the corresponding authors.

AUTHOR CONTRIBUTIONS

FUNDING

ACKNOWLEDGMENTS

REFERENCES

Ataide, J. O., Zago, H. B., Santos Júnior, H. J. G. d., Menini, L., and Carvalho, J. R. d. (2020). Acute Toxicity, Sublethal Effect and Changes in the Behavior of *Lasioderma Serricorne* Fabricius (Coleoptera: Anobiidae) Exposed to Major Components of Essential Oils. *Rsd* 9 (8), e170985581–20. doi:10.33448/rsd-v9i8.5581

Athanassiou, C., Bray, D. P., Hall, D. R., Phillips, C., and Vassilakos, T. N. (2018). Factors Affecting Field Performance of Pheromone Traps for Tobacco Beetle, *Lasioderma Serricorne*, and Tobacco Moth, *Ephestia Elutella*. *J. Pest Sci.* Vol. 91, 1381–1391. doi:10.1007/s10340-018-0987-8

Aziz, K. B., Aziz, A., and Kadir, S. A. (1992). *Pest Management and the Environment in 2000*. London: international Walling ford, 9–44.

Bi, J., Wen, M. M., Yu, L. J., Pan, D., and Dai, W. (2022). Research Progress of Ozone Application in the Control of Stored Grain Pests. *J. Henan Univ. Technol. Nat. Sci. Ed.* 43 (1), 131–138. doi:10.16433/j.1673-2383.2022.01.017

Broughton, S., and Harrison, J. (20122012). Evaluation of Monitoring Methods for Thrips and the Effect of Trap Colour and Semiochemicals on Sticky Trap Capture of Thrips (Thysanoptera) and Beneficial Insects (Syrphidae, Hemerobiidae) in Deciduous Fruit Trees in Western Australia. *Crop Prot.* 42 (1), 156–163. doi:10.1016/j.cropro.2012.05.004

Butenandt, A., and Hecker, E. (1961). Synthese des Bombykols, des Sexual-Lockstoffes des Seidenspinners, und seiner geometrischen Isomeren. *Angew. Chem.* 73 (11), 349–353. doi:10.1002/ange.19610731102

Cai, X. M., Li, Z. Q., Pan, H. S., and Lu, Y. H. (2018). Research and Application of Food-Based Attractants of Herbivorous Insect Pests. *Chin. J. Biol. Control* 34 (1), 8–35. doi:10.16409/j.cnki.2095-039x.2018.01.002

Cao, H. M., Hu, G. P., Du, X. M., Shi, X. P., and Hu, L. C. (2020). Application and Effect of Sex Pheromone Attractant for Mulberry Borer. *Appl. Eff. Sex Pheromone Attractant Mulberry Borer* 46 (6), 0757–0763. doi:10.13441/j.cnki.cykx.2020.06.013

Cao, Y., Benelli, G., Germinara, G. S., Maggi, F., Zhang, Y., Luo, S., et al. (2019). Innate Positive Chemotaxis to Paeonal from Highly Attractive Chinese Medicinal Herbs in the Cigarette Beetle, *Lasioderma Serricorne*. *Sci. Rep.* 9, 6995. doi:10.1038/s41598-019-43198-3

Chen, W. B., Yang, C., Huang, X. D., He, K. L., and Wang, Z. Y. (2022). Screening of the Sex Pheromones Formulation and Application for Population Dynamics Monitoring of *Conogethes Punctiferalis* (Guenée) in Huang-Huai-Hai Summer Corn Region in China. *Plant Prot.* 48 (1), 211–219. doi:10.16688/j.zwbh.2020585

Chen, Y. S., Li, F. X., and Wen, D. H. (2014). Review of Research on Attractant from Plants to *Monochamus Alternatus* Hope. *J. Henan Agric. Sci.* 43 (4), 5–10. doi:10.15933/j.cnki.1004-3268.2014.04.010

Cheng, J., Zhao, P., Li, J. Y., Li, Z., and Zhang, S. D. (2022). Progress on Pest Control of Deciduous Fruit Trees over the Past 60 Years in China. *J. Plant Prot.* 49 (01), 87–96. doi:10.13802/j.cnki.zwbhxb.2022.2022807

Chi, Y. Y., Lin, S. Y., Xu, S., and Chen, B. X. (2022). Tolfenpyrad against Common Pests in Cabbage Field: Application Effect Analysis. *Chin. Agric. Sci. Bull.* 38 (3), 110–115.

Chuman, T., Kohno, M., Kato, K., and Noguchi, M. (1979). 4.6-dimethyl-7-hydroxy-nonan-3-one, a Sex Pheromone of the Cigarette Beetle (*Lasioderma Serricorne* F.). *Tetrahedron Lett.* 20, 2361–2364. doi:10.1016/S0040-4039(01)93974-7

Davidson, M. M., Nielsen, M.-C., Butler, R. C., Castañé, C., Alomar, O., Riudavets, J., et al. (2015). Can Semiochemicals Attract Both Western Flower Thrips and Their Anthocorid Predators? *Entomol. Exp. Appl.* 155 (1), 54–63. doi:10.1111/eea.12284

Du, C. (2006). *Preliminary Research on Food Attractant against* Lasioderma Serricorne F. Hubei. Wuhan: Huazhong Agricultural University.

Edde, P. A. (2019). Biology, Ecology, and Control of *Lasioderma Serricorne* (F.) (Coleoptera: Anobiidae): a Review. *J. Econ. Entomology* 112, 1011–1031. doi:10.1093/jee/toy428

Fornari, R. A., Machota Junior, R., Bernardi, D., Botton, M., and Pastori, P. L. (2013). Evaluation of Damage, Food Attractants and Population Dynamics of Strawberry Sap Beetle. *Hortic. Bras.* 31, 380–385. doi:10.1590/S0102-05362013000300007

Gregg, P. C., Del Socorro, A. P., Hawes, A. J., and Binns, M. R. (2016). Developing Bisexual Attract-And-Kill for Polyphagous Insects: Ecological Rationale versus Pragmatics. *J. Chem. Ecol.* 42 (7), 666–675. doi:10.1007/s10886-016-0725-8

Gregg, P. C., Del Socorro, A. P., and Henderson, G. S. (2010). Development of a Synthetic Plant Volatile-Based Attracticide for Female Noctuid Moths. II. Bioassays of Synthetic Plant Volatiles as Attractants for the Adults of the Cotton bollworm, *Helicoverpa Armigera* (Hübner) (Lepidoptera: Noctuidae). *Aust. J. Entomology* 49 (1), 21–30. doi:10.1111/j.1440-6055.2009.00734.x

Guarino, S., Basile, S., Arif, M. A., Manachini, B., and Peri, E. (2021). Odorants of *Capsicum* Spp. Dried Fruits as Candidate Attractants for *Lasioderma Serricorne* F. (Coleoptera: Anobiidae). *Insects* 12 (61), 61–69. doi:10.3390/insects12010061

Guarino, S., Basile, S., Ranno, P., Suma, P., and Peri, E. (2022). Beta-ionone Increases Catches of *Lasioderma Serricorne* (F.) (Coleoptera: Anobiidae) in Traps Baited with Sex Pheromone. *J. Stored Prod. Res.* 96, 101948. doi:10.1016/j.jspr.2022.101948

Hu, F., Xu, T. T., Su, X. Y., Hu, B. J., and Bi, S. J. (2022). Control Efficacy of *Bacillus Thuringiensistiny* Microgranules on Maize Lepidopteran Pests. *Chin. J. Biol. Control.* online first. doi:10.16409/j.cnki.2095-039x.2022.01.002

Huang, M. L., Wang, X. J., Jin, H. L., and Lin, Y. X. (2022). Application Study of Sex Attractants in *Spodoptera Frugiperda* Population Monitoring. *J. Anhui Agric. Sci.* 50 (2), 151–153. doi:10.3969/j.issn.0517-6611.2022.05.040

Ikeda, T., Enda, N., Yamane, A., Oda, K., and Toyoda, T. (1980). Volatiles from Pine Logs as the Attractant for the Japanese Pine Sawyer *Monochamus Alternatus* Hope (Coleoptera: Cerambycidae). *J. Jpn. For. Soc.* 62 (4), 150–152. doi:10.11519/jjfs1953.62.4_150

Jackson, D. M., Sorensen, K. A., Sorenson, C. E., and Story, R. N. (2005). Monitoring Cucumber Beetles in Sweetpotato and Cucurbits with Kairomone-Baited Traps. *J. Econ. Entomology* 98 (1), 159–170. doi:10.1603/0022-0493-98.1.159

Jang, E. B., Ramsey, A., and Carvalho, L. A. (2013). Performance of Methyl Eugenol + Matrix + Toxicant Combinations under Field Conditions in Hawaii and California for Trapping *Bactrocera Dorsalis* (Diptera:Tephritidae). *Jnl. Econ. Entom.* 106 (2), 727–734. doi:10.1603/EC12371

Knight, A. L., Basoalto, E., Katalin, J., and El-Sayed, A. M. (2015). A Binary Host Plant Volatile Lure Combined with Acetic Acid to Monitor Codling Moth (Lepidoptera: Tortricidae). *Environ. Entomol.* 44 (5), 1434–1440. doi:10.1093/ee/nvv116

Knolhoff, L. M., and Heckel, D. G. (2014). Behavioral Assays for Studies of Host Plant Choice and Adaptation in Herbivorous Insects. *Annu. Rev. Entomol.* 59, 263–278. doi:10.1146/annurev-ento-011613-161945

Lampman, R. L., and Metcalf, R. L. (1987). Multicomponent Kairomonal Lures for Southern and Western Corn Rootworms (Coleoptera: Chrysomelidae: *Diabrotica* spp.). *J. Econ. Entomology* 80 (6), 1137–1142. doi:10.1093/ee/80.6.1137

Lampman, R. L., and Metcalf, R. L. (1988). The Comparative Response of *Diabrotica* Species (Coleoptera: Chrysomelidae) to Volatile Attractants1. *Environ. Entomol.* 17 (4), 644–648. doi:10.1093/ee/17.4.644

Landolt, P. J., Ohler, B., Lo, P., Cha, D., Davis, T. S., Suckling, D. M., et al. (2014). N-butyl Sulfide as an Attractant and Coattractant for Male and Female Codling Moth (Lepidoptera: Tortricidae). *Environ. Entomol.* 43 (2), 291–297. doi:10.1603/EN13178

Li, Q. Y., Li, J. L., Zhao, L. L., and Ma, R. Y. (20122012). Applications of Slow Release Technique of Sex Pherom One in Pest Control. *Chin. J. Biol. Control* 28 (4), 589–593. doi:10.16409/j.cnki.2095-039x.2012.04.022

Li, X. F., Li, J. Q., Cao, Y. Z., Yin, J., Zhang, S., Qin, J. H., et al. (2020). Screening and Evaluation of Semiochemical Mixtures Attracting *Holotrichiaoblita* (Coleoptera: Melolonthidae). *Acta Entomol. Sin.* 63 (4), 482–493. doi:10.16380/j.kcxb.2020.04.011

Light, D. M., Knight, A. L., Henrick, C. A., Rajapaska, D., Lingren, B., Dickens, J. C., et al. (2001). A Pear-Derived Kairomone with Pheromonal Potency that Attracts Male and Female Codling Moth, *Cydia Pomonella* (L.). *Naturwissenschaften* 88, 333–338. doi:10.1007/s001140100243

Linnie, M. J. (1994). Pest Control in Natural History Museums: a World Survey. *Mus. Manag. Curatorsh.* 6 (3), 43–58. doi:10.1016/0260-4779(87)90034-3

Liu, J., Zhou, T., Li, C., Li, R., Ye, X., and Tian, Z. (2021). Reverse Chemical Ecology Guides the Screening for *Grapholita Molesta* Pheromone Synergists. *Pest Manag. Sci.* 78 (2), 643–652. doi:10.1002/ps.6674

Lü, J. H., Zhang, Y. Q., and Kang, Y. L. (20222022). Advances in the Research and Application of Controlled Heat Treatment in Insect Pest Control. *Plant Prot.* 48 (1), 1–6. doi:10.16688/j.zwbh.2020569

Lü, J., and Liu, S. (2016). The Behavioral Response of *Lasioderma Serricorne* (Coleoptera: Anobiidae) to Citronellal, Citral, and Rutin. *SpringerPlus* 5, 798. doi:10.1186/s40064-016-2553-2

Lü, J., and Ma, D. (2015). Effect of Wheat Flour Packaging Materials on Infestation by *Lasioderma Serricorne* (F.). *J. Food Prot.* 78, 1052–1055. doi:10.4315/0362-028X.JFP-14-438

Lu, Y. F., Kan, H. L., Li, L. L., Zhuang, G. Y., and Wen, X. Y. (2020). Preliminary Evaluation of the Monitoring and Trapping Efficacy of Biological Food Attractant on Noctuidae Adults in Peanut Fields in Junan Country, Shandong Province. *Plant Prot.* 46 (2), 248–253. doi:10.16688/j.zwbh.2019056

Mao, R. Y., Song, J. Z., and Li, Y. (1992). Synthesis and Application of the Sex Pheromone of Female Cigarette Beetle. *Acta Tabacaria Sin.* 1 (1), 15–23. doi:10.1088/1004-423x/1/1/002

McCaffery, A. R. (1998). Resistance to Insecticides in *Heliothine Lepidoptera*: a Global View. *Phil. Trans. R. Soc. Lond. B* 353 (1376), 1735–1750. doi:10.1098/rstb.1998.0326

Mfuti, D. K., Subramanian, S., van Tol, R. W., Wiegers, G. L., De Kogel, W. J., Niassy, S., et al. (2016). Spatial Separation of Semiochemical Lurem- TR and Entomopathogenic Fungi to Enhance Their Compatibility and Infectivity in an Autoinoculation System for Thrips Management. *Pest. Manag. Sci.* 72 (1), 131–139. doi:10.1002/ps.3979

Miao, J. C. (1989). Test Method for Insect Pheromone Research. *J. Jiangsu For. Sci. Technol.* (01), 29–32. doi:10.16259/j.cnki.36-1342/s.1989.01.006

Niassy, S., Maniania, N. K., Subramanian, S., Gitonga, L. M., and Ekesi, S. (2011). Performance of a Semiochemical-Baited Autoinoculation Device Treated with Metarhizium Anisopliae for Control of Frankliniella Occidentalis on French Bean in Field Cages. *Entomologia Exp. Appl.* 142 (1), 97–103. doi:10.1111/j.1570-7458.2011.01203.x

Oliver, J. B., and Mannion, C. M. (2001). Ambrosia Beetle (Coleoptera: Scolytidae) Species Attacking Chestnut and Captured in Ethanol-Baited Traps in Middle Tennessee. *Environ. Entomol.* 30 (5), 909–918. doi:10.1603/0046-225X-30.5.909

Papadopoulou, S. C., and Buchelos, C. T. (2002). Comparison of Trapping Efficacy for *Lasioderma Serricorne* (F.) Adults with Electric, Pheromone, Food Attractant and Control-Adhesive Traps. *J. Stored Prod. Res.* 38, 375–383. doi:10.1016/S0022-474X(01)00039-X

Ranger, C. M., Reding, M. E., Gandhi, K. J. K., Oliver, J. B., Schultz, P. B., Cañas, L., et al. (20112011). Species Dependent Influence of (−)-α-Pinene on Attraction of Ambrosia Beetles (Coleoptera: Curculionidae: Scolytinae) to Ethanol-Baited Traps in Nursery Agroecosystems. *Jnl. Econ. Entom.* 104 (2), 574–579. doi:10.1603/ec10243

Regnier, F. E., and Law, J. H. (1968). Insect Pheromones. *J. Lipid Res.* 9 (5), 541–551. doi:10.1016/s0022-2275(20)42699-9

Ren, Y. L., Wang, T., Jiang, Y. J., Chen, D., Zuo, W. Y., Guo, J. J., et al. (2020). Behavioral Response, Fumigation Activity, and Contact Activity of Plant Essential oils Against Tobacco Beetle (*Lasioderma Serricorne* F.). Adults. *Front. Chem.* 10, 880608. doi:10.3389/fchem.2022.880608

Sağlam, Ö., Edde, P. A., and Phillips, T. W. (2015). Resistance of *Lasioderma serricorne* (Coleoptera: Anobiidae) to Fumigation with Phosphine. *J. Econ. Entomol.* 108, 2489–2495. doi:10.1093/jee/tov193

Sang, W., Gao, Q., Zhang, C. Y., Huang, Q. Y., and Lei, C. L. (2022). Research and Application of Physical Control of Agricultural Insect Pests in China. *J. Plant Prot.* 49 (1), 173–183. doi:10.13802/j.cnki.zwbhxb.2022.2022813

Sathiyaseelan, M., Jayarai, J., Shanthi, M., and Suijatha, K. (2022). Evaluation of Attractiveness and Volatile Profiling of Food Baits for Monitoring of Stored Product Pests in Paddy. *Ije* 49 (1), 221–226. doi:10.55362/IJE/2022/3507

Schöller, M., Prozell, S., Suma, P., and Russo, A. (2018). "Biological Control of Stored-Product Insects," in *Recent Advances in Stored Product Protection*. Editors C. Athanassiou and F. Arthur (Berlin, Heidelberg: Springer), 183–209. doi:10.1007/978-3-662-56125-6_9

Shelly, T. (2010). Effects of Methyl Eugenol and Raspberry Ketone/cue Lure on the Sexual Behavior of *Bactrocera* Species (Diptera: Tephritidae). *Appl. Entomol. Zool.* 45 (3), 349–361. doi:10.1303/aez.2010.349

Shelly, T., Epsky, N., Jang, E. B., Reyes-Flores, J., and Vargas, R. (2014). *Trapping and the Detection, Control, and Regulation of Tephritid Fruit Flies: Lures, Area-wide Programs, and Trade Implications.* Berlin: Springer Netherlands.

Sutherland, O. R. W., Wearing, C. H., and Hutchins, R. F. N. (1977). Production of ?-farnesene, an Attractant and Oviposition Stimulant for Codling Moth, by

Developing Fruit of Ten Varieties of Apple. *J. Chem. Ecol.* 3 (6), 625–631. doi:10.1007/BF00988062

Tang, H. R., Wang, L. J., Xu, H. L., Xie, Z. M., and Cai, J. (2022). Breeding for Resistance Strains in Flies: a Review. *Acta Lab. Anim. Sci. Sin.* 30 (01), 124–130. doi:10.3969/j.issn.1005-4847.2022.01.016

Xiang, H. M., Zheng, W. F., Li, S. P., Li, J. W., and Ma, R. Y. (2021). Research on Improvement of Monitoring Technology of *Cydia Pomonella* Based on Sex Pheromone. *Plant Quar.* 35 (5), 21–25. doi:10.19662/j.cnki.issn1005-2755.2021.05.002

Xiong, W. (2008). *Study on Filtration of Food Attractant and Their Mixed Ligand of Lasioderma Serricorne in Room.* Hubei: Huazhong Agricultural University.

Yang, G., Guo, P., Huo, L., and Ren, C. (2015). Optimization of the Irrigation Water Resources for Shijin Irrigation District in North China. *Agric. Water Manag.* 158 (16), 82–98. doi:10.13989/j.cnki.0517-6611.2015.16.034

Zhong, S. S., Gou, C. M., Ma, J. X., Sun, Q., and Huang, L. (2021). Attractive Activities of Different Aroma Components in Tobacco Leaves to *Lasioderma Serricorne*. *Tob. Sci. Technol.* 54 (4), 33–39. doi:10.16135/j.issn1002-0861.2020.0162

Publisher's Note: All claims expressed in this article are solely those of the authors and do not necessarily represent those of their affiliated organizations, or those of the publisher, the editors, and the reviewers. Any product that may be evaluated in this article, or claim that may be made by its manufacturer, is not guaranteed or endorsed by the publisher.

Check for updates

Synthesis, Antibacterial and Insecticidal Activities of Novel Capsaicin Derivatives Containing a Sulfonic Acid Esters Moiety

Dandan Xie[1]*, Zaiping Yang[2], Xin Hu[3] and Yin Wen[3]

[1]State Key Laboratory Breeding Base of Green Pesticide and Agricultural Bioengineering, Key Laboratory of Green Pesticide and Agricultural Bioengineering, Ministry of Education, Guizhou University, Guiyang, China, [2]School of Biology and Engineering, Guizhou Medical University, Guiyang, China, [3]School of Biological Sciences, Guizhou Education University, Guiyang, China

In order to develop an efficient and broad-spectrum bactericide, a series of novel capsaicin derivatives containing a sulfonic acid esters moiety was synthesized. The structure of these compounds were confirmed by nuclear magnetic resonance spectroscopy (NMR) and high-resolution mass spectrum (HRMS). The results of the bioactivities revealed that some target compounds exhibited remarkable antibacterial activity. Compound **3b** exhibited the highest activities against *Pseudomonas syringae* pv. *actinidiae* (Psa), *Xanthomonas oryzae* pv. *oryzae* (Xoo), and *Xanthomonas axonopodis* pv. *citri* (Xac), and the values were 86, 54, and 92% at 50 μg/ml, respectively, which were higher than were for thiodiazole copper (87, 34, and 77%) and bismerthiazol (87, 37 and 75%). Although some compounds also showed certain activity against *Spodoptera frugiperda*, it was weaker than the positive controls monosultap and mulfoxaflor. Thus, the bioassay results recommend that these newly designed and synthesized scaffolds should be used as a bactericide lead compound rather than an insecticide lead compound.

Keywords: sulfonic acid esters, synthesis, antibacterial activities, insecticidal activity, capsaicin derivatives

1 INTRODUCTION

Almost every crop is affected by bacterial diseases, resulting in significant quality and yield losses. Although there are some commercially available agricultural chemicals for bacterial disease control, frequent and long-term use of these result in problems in resistance in bacteria populations, environmental contamination, and human health. Therefore, there is still a need to develop novel, effective, and environmentally friendly bactericides (Chen et al., 2021; Li et al., 2021). The plants have established an excellent chemical defense system to selectively defend against pathogens through producing some chemicals with antimicrobial properties throughout their evolution. These secondary metabolites generally have antimicrobial activity against pathogens but are safe for the environment, animals, and humans. Thus, it could be imagined that these chemicals can be further developed into bactericides, as excellent lead structures (Morant et al., 2008a; Morant et al., 2008b; Xia et al., 2014).

Capsaicinoid is originally a kind of active ingredient extracted from the ripe fruit of the nightshade plant capsicum, with more than 19 compounds having similar structures such as capsaicin, hydrocapsaicin, mocapsaicin, and nordihydrocapsaicin (Mazourek et al., 2009; Huang et al., 2013). Due to these structures being highly similar, they has almost identical biological activities, such as insecticidal, bactericidal, analgesic, anticancer, antiviral, and other such activities (Lee et al., 2007; Snitker
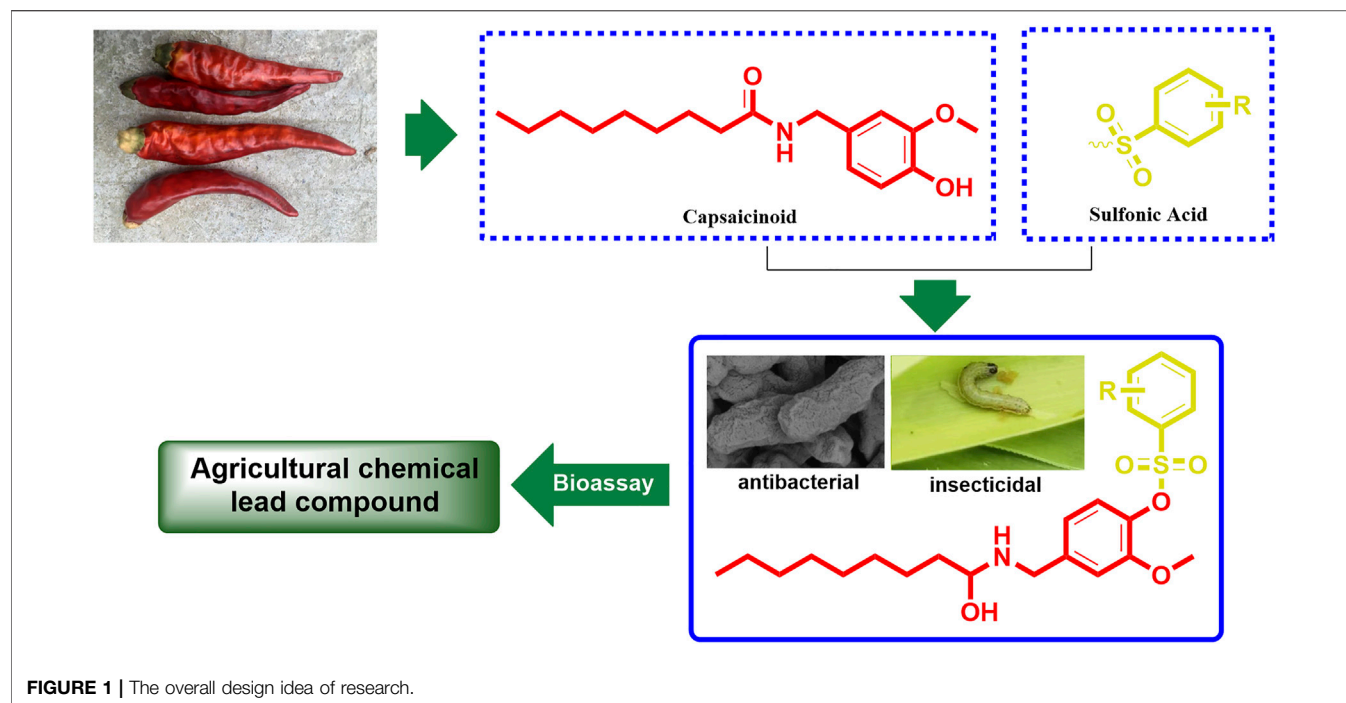
FIGURE 1 | The overall design idea of research.

et al., 2009; Díaz-Laviada, 2010; Liao et al., 2011). In particular, the bactericidal and insecticidal activities of capsaicinoid have been so impressive that capsaicinoid has even been developed into commercial bactericides and insecticides (Isaacs et al., 2004; Inoue et al., 2007; Claros Cuadrado et al., 2019). As a member of the capsaicinoid family, nonivamide is widely studied as a substitute of capsaicinoid in organic chemistry, analytical chemistry, and the biochemistry field, as it is easily synthesized than other capsaicinoid members (Anderson et al., 2014; Palo-Nieto et al., 2016). As the main functional group of covalent inhibitors drug, sulfonic acid groups play an important role in pharmaceutical chemistry. This is due to the sulfonic acid group easily forming covalent bonds with lysine, histidine, serine, and tyrosine of protein, which makes the parent compound better in acting on the protein target (Hatcher et al., 2018; Baggio et al., 2019; Bum-Erdene et al., 2020; Teng et al., 2020). In addition, sulfonic acid groups can also improve the physical and chemical properties of drug molecules (Guo et al., 2019; Guo et al., 2020). Inspired by the results of these studies, the present work aims to incorporate a sulfonic acid moiety into the nonivamide backbone to synthesize a series of novel derivatives and further evaluate their bactericidal and insecticidal activities (**Figure 1**), hoping to obtain capsaicinoid derivatives with higher activities than the existing commercial agricultural chemicals.

2 EXPERIMENTAL

2.1 Chemistry

All starting materials and reagents were commercially available and used without further purification, except as indicated. The ^{1}H-NMR and ^{13}C-NMR spectra were recorded on a Bruker DPX 400 MHz (Bruker BioSpin GmbH, Rheinstetten, Germany) NMR

spectrometer with $CDCl_3$ as the solvent. The following abbreviations were used to explain the multiplicities: s, singlet; d, doublet; t, triplet; m, multiplet; and br, broadened. The melting points were determined on a WRX-4 microscope melting point apparatus (YiCe Apparatus & Equipment Co., Ltd., Shanghai, China). High-resolution mass spectrometry (HRMS) was conducted using a Thermo Scientific Q Exactive (Thermo Fisher Scientific, Massachusetts, United States).

2.1.1 General Procedures for Preparing Compounds

The synthetic route for the title compounds **3a–3u** is depicted in **Scheme 1**. Intermediates **1–2** were synthesized according to a previous reported method (Anderson et al., 2014). Vanillylammonium chloride was dissolved in deionized water, and 10 wt% NaOH aqueous solution was added to the reaction system, slowly reaching pH = 12. Then, the white precipitate was filtered out, and sodium hydroxide solution added to the filtrate until reaching pH = 5. The intermediates **1** was precipitated from the system as a white solid. 0.12 mol of intermediates **1** and **3**–equivalent thionyl chloride was mixed and refluxed for 4 h. The excess thionyl chloride was removed by rotary evaporator, and the residue was dissolved by CH_2Cl_2. 0.1 mol vanillylamine was dissolved in 30 ml CH_2Cl_2, then a solution of acyl chloride/ CH_2Cl_2 mixture was added dropwise to the reaction mixture. After stirring at 40°C for 6 h, the reaction was stopped, and intermediates **2** was obtained through chromatography. Target compounds **3a–3u** were synthesized by condensation of different sulfonyl chloride, which contains different substituent groups and intermediates **2** at room temperature conditions. Two equivalents of triethylamine was added to the system as a catalyst to neutralize the HCl generated by the reaction such that the reaction can proceed smoothly. After about approximately 4 h, the solvent was
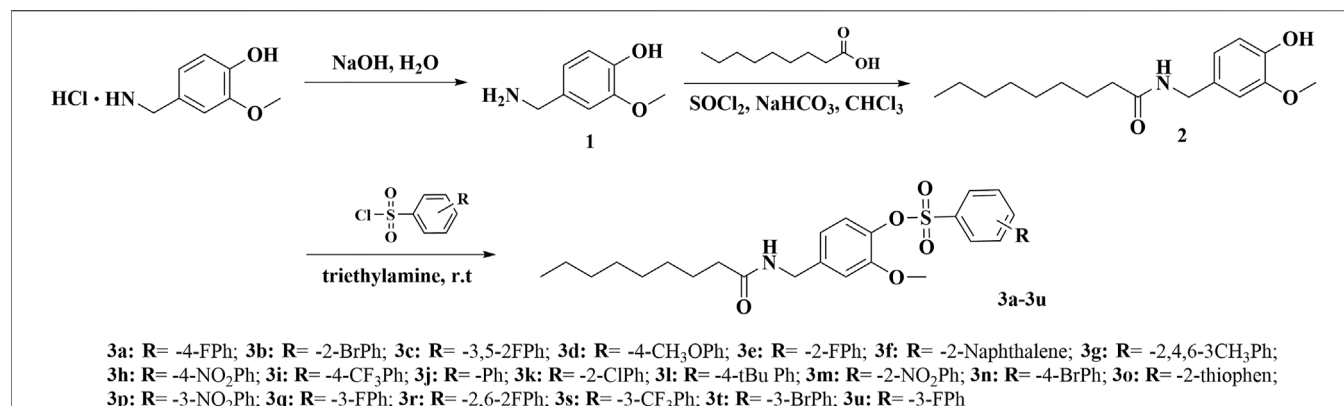
SCHEME 1 | Synthetic route of the target compounds **3a–3u**.

3a: R= -4-FPh; 3b: R= -2-BrPh; 3c: R= -3,5-2FPh; 3d: R= -4-CH₃OPh; 3e: R= -2-FPh; 3f: R= -2-Naphthalene; 3g: R= -2,4,6-3CH₃Ph; 3h: R= -4-NO₂Ph; 3i: R= -4-CF₃Ph; 3j: R= -Ph; 3k: R= -2-ClPh; 3l: R= -4tBu Ph; 3m: R= -2-NO₂Ph; 3n: R= -4-BrPh; 3o: R= -2-thiophen; 3p: R= -3-NO₂Ph; 3q: R= -3-FPh; 3r: R= -2,6-2FPh; 3s: R= -3-CF₃Ph; 3t: R= -3-BrPh; 3u: R= -3-FPh

removed, and the residue was purified by flash chromatography on silica gel with petroleum n-hexane/ethyl acetate (volume ratio 5:1) to obtain the pure product.

2.1.1.1 2-Methoxy-4-(Nonanamidomethyl)Phenyl 4-Fluorobenzenesulfonate (3a)

White powder, yield 81.0%. m.p. 36–37°C. ^{1}H-NMR (400 MHz, CDCl$_3$) δ 7.89–7.81 (m, 2H), 7.15 (d, J = 8.6 Hz, 2H), 7.06 (d, J = 8.0 Hz, 1H), 6.79–6.71 (m, 2H), 6.07 (t, J = 6.0 Hz, 1H), 4.34 (d, J = 6.0 Hz, 2H), 3.50 (s, 3H), 2.18 (t, J = 7.6 Hz, 2H), 1.61 (t, J = 7.3 Hz, 2H), 1.30–1.20 (m, 10H), and 0.85 (t, J = 6.7 Hz, 3H). ^{13}C-NMR (100 MHz, CDCl$_3$) δ 173.3, 164.6, 151.6, 139.3, 137.2, 132.1, 131.5, 131.4, 124.1, 119.6, 116.2, 116.0, 112.1, 55.5, 43.0, 36.7, 31.8, 29.3, 29.2, 25.8, 22.6, and 14.1. HRMS (ESI): calculated for C$_{23}$H$_{30}$FNO$_5$S [M+Na]$^+$: 474.1720, found: 474.1723.

2.1.1.2 2-Methoxy-4-(Nonanamidomethyl)Phenyl 2-Bromobenzenesulfonate (3b)

White powder, yield 83.0%. m.p. 65–66.5°C. ^{1}H-NMR (400 MHz, CDCl$_3$) δ 7.98–7.77 (m, 2H), 7.54–7.34 (m, 1H), 7.19 (t, J = 8.6 Hz, 1H), 7.05 (dd, J = 36.6, 8.1 Hz, 1H), 6.86–6.65 (m, 2H), 5.96 (q, J = 6.3 Hz, 1H), 4.37 (t, J = 6.3 Hz, 2H), 3.54 (s, 3H), 2.20 (m, 2H), 1.72–1.56 (m, 2H), 1.45–1.16 (m, 10H), and 0.87 (t, J = 6.7 Hz, 3H). ^{13}C-NMR (100 MHz, CDCl$_3$) δ 173.2, 151.6, 135.5, 134.6, 132.1, 131.5, 131.4, 124.1, 119.6, 116.2, 116.0, 112.1, 55.6, 55.5, 43.0, 36.7, 31.8, 29.3, 29.3, 29.2, 25.8, 22.6, and 14.1. HRMS (ESI): calculated for C$_{23}$H$_{30}$BrNO$_5$S [M+Na]$^+$: 534.0920, found: 534.0921.

2.1.1.3 2-Methoxy-4-(Nonanamidomethyl)Phenyl 3,5-Difluorobenzenesulfonate (3c)

White powder, yield 85.0%. m.p. 85.7–86.5°C. ^{1}H-NMR (400 MHz, CDCl$_3$) δ 7.62–7.35 (m, 2H), 7.16–7.05 (m, 2H), 6.91–6.67 (m, 2H), 5.85 (s, 1H), 4.40 (d, J = 6.0 Hz, 2H), 3.61 (s, 3H), 2.22 (t, J = 7.6 Hz, 2H), 1.66 (dd, J = 16.1, 8.8 Hz, 2H), 1.38–1.14 (m, 10H), and 0.87 (t, J = 6.8 Hz, 3H). ^{13}C-NMR (100 MHz, CDCl$_3$) δ 173.2, 161.2, 151.5, 139.6, 137.2, 124.0, 119.8, 112.3, 112.3, 109.6, 55.6, 43.1, 36.8, 31.8, 29.3, 29.2, 25.8, 22.6, and 14.1. HRMS (ESI): calculated for C$_{23}$H$_{29}$F$_2$NO$_5$S [M+Na]$^+$: 496.1627, found: 196.1633.

2.1.1.4 2-Methoxy-4-(Nonanamidomethyl)Phenyl 4-Methoxybenzenesulfonate (3d)

White powder, yield 81.0%. m.p. 78.9–80.2°C. ^{1}H-NMR (400 MHz, CDCl$_3$) δ 7.78 (d, J = 8.9 Hz, 2H), 7.06 (d, J = 8.7 Hz, 1H), 6.96 (d, J = 9.0 Hz, 2H), 6.76 (dd, J = 4.3, 2.4 Hz, 2H), 5.89 (s, 1H), 4.37 (d, J = 5.9 Hz, 2H), 3.88 (s, 3H), 3.56 (s, 3H), 2.21 (t, J = 7.6 Hz, 2H), 1.64 (p, J = 7.5 Hz, 2H), 1.38–1.18 (m, 10H), and 0.87 (t, J = 6.8 Hz, 3H). ^{13}C-NMR (100 MHz, CDCl$_3$) δ 173.2, 164.0, 151.9, 138.8, 137.6, 130.8, 127.5, 124.0, 119.6, 114.0, 112.1, 55.7, 55.6, 43.1, 36.8, 31.8, 29.3, 29.2, 25.8, 22.6, and 14.1. HRMS (ESI): calculated for C$_{24}$H$_{33}$NO$_6$S [M+Na]$^+$: 486.1921, found: 486.1927.

2.1.1.5 2-Methoxy-4-(Nonanamidomethyl)Phenyl 2-Fluorobenzenesulfonate (3e)

White powder, yield 84.0%. m.p. 54.3–56.6°C. ^{1}H-NMR (400 MHz, CDCl$_3$) δ 7.84–7.74 (m, 1H), 7.70–7.62 (m, 1H), 7.28 (t, J = 1.3 Hz, 1H), 7.24 (td, J = 7.6, 1.0 Hz, 1H), 7.11 (d, J = 8.0 Hz, 1H), 6.78 (d, J = 7.6 Hz, 2H), 5.93 (s, 1H), 4.37 (d, J = 5.9 Hz, 2H), 3.53 (s, 3H), 2.20 (t, J = 7.6 Hz, 2H), 1.64 (t, J = 7.4 Hz, 2H), 1.27 (d, J = 11.3 Hz, 10H), and 0.87 (t, J = 6.6 Hz, 3H). ^{13}C-NMR (100 MHz, CDCl$_3$) δ 173.1, 151.7, 139.1, 137.5, 136.4, 136.3, 131.2, 124.27, 124.0, 124.0, 119.7, 117.2, 117.0, 112.1, 55.6, 43.1, 36.8, 31.8, 29.3, 29.1, 25.8, 22.6, and 14.1. HRMS (ESI): calculated for C$_{23}$H$_{30}$FNO$_5$S [M+Na]$^+$: 474.1720, found: 474.1723.

2.1.1.6 2-Methoxy-4-(Nonanamidomethyl)Phenyl Naphthalene-1-Sulfonate (3f)

White powder, yield 82.0%. m.p. 52.5–54.0°C. ^{1}H-NMR (400 MHz, CDCl$_3$) δ 8.40 (d, J = 1.9 Hz, 1H), 8.02–7.84 (m, 4H), 7.75–7.61 (m, 2H), 7.09 (d, J = 8.2 Hz, 1H), 6.76 (dd, J = 8.2, 2.0 Hz, 1H), 6.72 (d, J = 2.0 Hz, 1H), 5.84 (s, 1H), 4.36 (d, J = 5.9 Hz, 2H), 3.39 (s, 3H), 2.25–2.14 (m, 2H), 1.62 (q, J = 7.1 Hz, 2H), 1.32–1.20 (m, 10H), and 0.86 (t, J = 6.8 Hz, 3H). ^{13}C-NMR (100 MHz, CDCl$_3$) δ 173.1, 151.8, 139.0, 137.6, 135.4, 133.2, 131.7, 130.3, 129.5, 129.4, 129.0, 127.9, 127.7, 124.1, 123.3, 119.6, 112.2, 55.5, 43.1, 36.8, 31.8, 29.3, 29.3, 29.1, 25.8, 22.6, and 14.1. HRMS (ESI): calculated for C$_{27}$H$_{33}$NO$_5$S [M+Na]$^+$: 506.2079, found: 506.1972.

2.1.1.7 2-Methoxy-4-(Nonanamidomethyl)Phenyl 2,4,6-Trimethylbenzenesulfonate (3g)

White powder, yield 85.0%. m.p. 62.5–64.0°C. ^{1}H-NMR (400 MHz, CDCl$_3$) δ 7.02–6.93 (m, 3H), 6.77 (d, J = 2.0 Hz, 1H), 6.73 (dd, J = 8.2, 2.0 Hz, 1H), 5.97 (t, J = 6.0 Hz, 1H), 4.36 (d, J = 5.8 Hz, 2H), 3.55 (s, 3H), 2.56 (s, 6H), 2.32 (s, 3H), 2.24–2.07 (m, 2H), 1.62 (q, J = 7.3 Hz, 2H), 1.46–1.21 (m, 10H), and 0.87 (t, J = 6.7 Hz, 3H). ^{13}C-NMR (100 MHz, CDCl$_3$) δ 173.2, 152.1, 143.5, 140.6, 138.6, 137.5, 131.6, 131.4, 123.8, 119.5, 112.2, 55.5, 43.1, 36.7, 31.8, 29.3, 29.2, 25.8, 22.8, 22.6, 21.1, and 14.1. HRMS (ESI): calculated for C$_{26}$H$_{37}$NO$_5$S [M+Na]$^+$: 498.2285, found: 498.2282.

2.1.1.8 2-Methoxy-4-(Nonanamidomethyl)phenyl 4-Nitrobenzenesulfonate (3h)

White powder, yield 80.0%. m.p. 65.0–67.0°C. ^{1}H-NMR (400 MHz, CDCl$_3$) δ 8.23 (dd, J = 109.8, 8.8 Hz, 4H), 7.15 (d, J = 8.2 Hz, 1H), 6.82 (dd, J = 8.3, 2.0 Hz, 1H), 6.79 (d, J = 2.0 Hz, 1H), 5.80 (s, 1H), 4.40 (d, J = 6.0 Hz, 2H), 3.53 (s, 3H), 2.26–2.16 (m, 2H), 1.65 (d, J = 3.2 Hz, 2H), 1.35–1.20 (m, 10H), and 0.87 (t, J = 6.8 Hz, 3H). ^{13}C-NMR (100 MHz, CDCl$_3$) δ 173.1, 151.4, 150.8, 142.0, 139.7, 137.1, 129.9, 124.1, 123.9, 119.8, 112.2, 55.5, 43.1, 36.8, 31.8, 29.3, 29.3, 29.2, 25.7, 22.6, and 14.1. HRMS (ESI): calculated for C$_{23}$H$_{30}$N$_2$O$_7$S [M+Na]$^+$: 501.1666, found: 501.1669.

2.1.1.9 2-Methoxy-4-(Nonanamidomethyl)phenyl 4-(Trifluoromethyl)Benzenesulfonate (3i)

White powder, yield 83.0%. m.p. 87.9–89.1°C. ^{1}H-NMR (400 MHz, CDCl$_3$) δ 7.90 (dd, J = 87.7, 8.3 Hz, 4H), 7.14 (d, J = 8.3 Hz, 1H), 6.81 (dd, J = 8.2, 2.0 Hz, 1H), 6.76 (d, J = 2.0 Hz, 1H), 5.82 (s, 1H), 4.39 (d, J = 6.0 Hz, 2H), 3.47 (s, 3H), 2.34–2.06 (m, 2H), 1.73–1.56 (m, 2H), 1.38–1.21 (m, 10H), and 0.87 (t, J = 6.8 Hz, 3H). ^{13}C-NMR (100 MHz, CDCl$_3$) δ 173.1, 151.5, 139.4, 137.2, 129.1, 125.9, 125.9, 125.8, 125.8, 124.2, 119.8, 112.1, 55.4, 43.1, 36.8, 31.8, 29.3, 29.3, 29.1, 25.8, 22.6, and 14.1. HRMS (ESI): calculated for C$_{24}$H$_{30}$F$_3$NO$_5$S [M+Na]$^+$: 524.1689, found: 524.1731.

2.1.1.10 2-Methoxy-4-(Nonanamidomethyl)Phenyl Benzenesulfonate (3j)

White powder, yield 82.0%. m.p. 71.2–72.7°C. ^{1}H-NMR (400 MHz, CDCl$_3$) δ 7.85 (dd, J = 8.4, 1.3 Hz, 2H), 7.71–7.60 (m, 1H), 7.51 (t, J = 7.9 Hz, 2H), 7.06 (d, J = 7.9 Hz, 1H), 6.87–6.67 (m, 2H), 6.05 (s, 1H), 4.36 (d, J = 5.9 Hz, 2H), 3.49 (s, 3H), 2.23–2.17 (m, 2H), 1.72–1.55 (m, 2H), 1.36–1.22 (m, 10H), and 0.87 (t, J = 6.8 Hz, 3H). ^{13}C-NMR (100 MHz, CDCl$_3$) δ 173.2, 151.8, 139.1, 137.4, 136.2, 134.0, 128.8, 128.5, 124.0, 119.6, 112.1, 55.5, 43.0, 36.7, 31.8, 29.3, 29.2, 25.8, 22.6, and 14.1. HRMS (ESI): calculated for C$_{23}$H$_{31}$NO$_5$S [M–H]$^+$: 433.1923, found: 432.1850.

2.1.1.11 2-Methoxy-4-(Nonanamidomethyl)Phenyl 2-Chlorobenzenesulfonate (3k)

White powder, yield 85.3%. m.p. 78.2–79.8°C. ^{1}H-NMR (400 MHz, CDCl$_3$) δ 7.97–7.78 (m, 2H), 7.50–7.33 (m, 1H), 7.19 (t, J = 8.6 Hz, 1H), 7.10 (d, J = 8.0 Hz, 1H), 7.01 (d, J = 8.1 Hz, 2H), 6.86–6.70 (m, 2H), 5.97 (s, 1H), 4.37 (t, J = 6.3 Hz, 2H), 3.54 (s, 3H), 2.20 (td, J = 7.6, 5.0 Hz, 2H), 1.75–1.55 (m, 2H), 1.35–1.18 (m, 10H), and 0.87 (t, J = 6.7 Hz, 3H). ^{13}C-NMR (100 MHz, CDCl$_3$) δ 173.2, 151.8, 139.2, 137.6, 134.7, 131.9, 126.6, 124.1, 119.6, 112.2, 55.6, 43.0, 36.7, 31.8, 29.3, 29.1, 25.8, 22.6, and 14.1. HRMS (ESI): calculated for C$_{23}$H$_{30}$ClNO$_5$S [M+Na]$^+$: 490.1425, found: 490.1429.

2.1.1.12 2-Methoxy-4-(Nonanamidomethyl)Phenyl 4-(Tert-Butyl)Benzenesulfonate (3l)

White powder, yield 83.0%. m.p. 81.2–83.0°C. ^{1}H-NMR (400 MHz, CDCl$_3$) δ 7.65 (dd, J = 105.8, 8.6 Hz, 4H), 7.11 (d, J = 8.1 Hz, 1H), 6.83–6.70 (m, 2H), 5.83 (s, 1H), 4.39 (d, J = 5.9 Hz, 2H), 3.49 (s, 3H), 2.21 (t, J = 7.6 Hz, 2H), 1.68–1.57 (m, 2H), 1.35 (s, 9H), 1.33–1.16 (m, 10H), and 0.87 (t, J = 6.8 Hz, 3H). ^{13}C-NMR (100 MHz, CDCl$_3$) δ 173.1, 158.0, 151.9, 138.8, 137.6, 133.2, 128.4, 125.8, 124.2, 119.6, 112.1, 55.5, 43.2, 36.8, 35.3, 31.8, 31.0, 29.3, 29.3, 29.2, 25.8, 22.6, and 14.1. HRMS (ESI): calculated for C$_{23}$H$_{30}$ClNO$_5$S [M+Na]$^+$: 512.2549, found: 512.2444.

2.1.1.13 2-Methoxy-4-(Nonanamidomethyl)Phenyl 2-Nitrobenzenesulfonate (3m)

White powder, yield 83.2%. m.p. 88.0–89.2°C. ^{1}H-NMR (400 MHz, CDCl$_3$) δ 8.03 (dd, J = 8.0, 1.4 Hz, 1H), 7.90–7.80 (m, 2H), 7.72 (ddd, J = 8.8, 7.3, 1.7 Hz, 1H), 7.09 (d, J = 8.0 Hz, 1H), 6.88–6.66 (m, 2H), 5.96 (s, 1H), 4.39 (d, J = 6.0 Hz, 2H), 3.54 (s, 3H), 2.26–2.18 (m, 2H), 1.63 (q, J = 7.1 Hz, 2H), 1.35–1.21 (m, 10H), and 0.91–0.84 (m, 3H). ^{13}C-NMR (100 MHz, CDCl$_3$) δ 173.2, 151.6, 139.6, 137.4, 134.9, 132.0, 131.6, 130.2, 124.7, 124.2, 119.8, 112.4, 55.6, 43.0, 36.7, 31.8, 29.3, 29.2, 25.8, 22.6, 14.2, and 14.1. HRMS (ESI): calculated for C$_{23}$H$_{30}$N$_2$O$_7$S [M+Na]$^+$: 501.1666, found: 501.1668.

2.1.1.14 2-Methoxy-4-(Nonanamidomethyl)Phenyl 4-Bromobenzenesulfonate (3n)

White powder, yield 80.1%. m.p. 79.1–80.8°C. ^{1}H-NMR (400 MHz, CDCl$_3$) δ 7.77–7.62 (m, 4H), 7.11 (d, J = 8.1 Hz, 1H), 6.85–6.70 (m, 2H), 5.80 (d, J = 7.3 Hz, 1H), 4.39 (d, J = 6.0 Hz, 2H), 3.54 (s, 3H), 2.33–2.16 (m, 2H), 1.65 (d, J = 2.9 Hz, 3H), 1.50–1.17 (m, 10H), and 1.00–0.75 (m, 3H). ^{13}C-NMR (100 MHz, CDCl$_3$) δ 173.1, 151.6, 139.2, 137.3, 135.2, 132.1, 130.0, 129.3, 124.1, 119.7, 112.1, 55.5, 43.1, 36.8, 31.8, 29.3, 29.2, 25.8, 22.6, and 14.1. HRMS (ESI): calculated for C$_{23}$H$_{30}$BrNO$_5$S [M+Na]$^+$: 534.0920, found: 534.0921.

2.1.1.15 2-Methoxy-4-(Nonanamidomethyl)Phenyl Thiophene-2-Sulfonate (3o)

White powder, yield 86.0%. m.p. 83.0–85.2°C. ^{1}H-NMR (400 MHz, CDCl$_3$) δ 7.72 (dd, J = 5.0, 1.4 Hz, 1H), 7.61 (dd, J = 3.8, 1.4 Hz, 1H), 7.18–7.01 (m, 2H), 6.79 (d, J = 7.1 Hz, 2H), 5.91 (s, 1H), 4.39 (d, J = 5.9 Hz, 2H), 3.60 (s, 3H), 2.22 (t, J = 7.6 Hz, 2H), 1.64 (q, J = 7.3 Hz, 2H), 1.39–1.18 (m, 10H), and 0.87 (t, J = 6.6 Hz, 3H). ^{13}C-NMR (100 MHz, CDCl$_3$) δ 173.2, 152.0, 139.2, 137.5, 135.6, 135.2, 134.3, 127.3, 124.0, 119.6, 112.2, 55.7, 43.1, 36.8, 31.8, 29.3, 29.2, 25.8, 22.6, and 14.1. HRMS (ESI): calculated for C$_{21}$H$_{29}$BrNO$_5$S$_2$ [M–H]$^+$: 439.1487, found: 438.1414.

2.1.1.16 2-Methoxy-4-(Nonanamidomethyl)Phenyl 3-Nitrobenzenesulfonate (3p)

White powder, yield 82.0%. m.p. 103.1–104.5°C. ^{1}H-NMR (400 MHz, CDCl$_3$) δ 8.77 (t, J = 2.0 Hz, 1H), 8.51 (ddd, J = 8.3, 2.2, 1.1 Hz, 1H), 8.24 (dt, J = 7.9, 1.4 Hz, 1H), 7.76 (t, J = 8.1 Hz, 1H), 7.20 (d, J = 8.2 Hz, 1H), 6.89–6.73 (m, 2H), 5.78 (s, 1H), 4.40 (d, J = 6.0 Hz, 2H), 3.55 (s, 3H), 2.29–2.13 (m, 2H), 1.71–1.62 (m, 2H), 1.34–1.23 (m, 10H), and 0.90–0.82 (m, 3H). ^{13}C-NMR (100 MHz, CDCl$_3$) δ 173.1, 151.3, 148.0, 139.7, 138.46, 137.0, 134.0, 130.1, 128.3, 124.2, 123.9, 120.0, 112.2, 55.6, 43.1, 36.8, 29.3, 29.2, 25.8, 22.6, and 14.1. HRMS (ESI): calculated for C$_{23}$H$_{30}$N$_2$O$_7$S [M+Na]$^+$: 501.1666, found: 501.1667.

2.1.1.17 2-Methoxy-4-(Nonanamidomethyl)Phenyl 3-Fluorobenzenesulfonate (3q)

White powder, yield 80.5%. m.p. 58.0–60.3°C. ^{1}H-NMR (400 MHz, CDCl$_3$) δ 7.68 (d, J = 7.9 Hz, 1H), 7.61 (ddd, J = 8.0, 2.5, 1.7 Hz, 1H), 7.51 (td, J = 8.1, 5.2 Hz, 1H), 7.39–7.34 (m, 1H), 7.11 (d, J = 8.0 Hz, 1H), 6.80 (d, J = 7.7 Hz, 2H), 5.80 (s, 1H), 4.39 (d, J = 5.9 Hz, 2H), 3.56 (s, 3H), 2.29–2.16 (m, 2H), 1.87–1.56 (m, 2H), 1.42–1.19 (m, 10H), and 0.87 (t, J = 6.8 Hz, 3H). ^{13}C-NMR (100 MHz, CDCl$_3$) δ 173.1, 151.7, 139.2, 137.3, 130.6, 124.1, 121.3, 119.7, 115.8, 112.1, 55.6, 43.1, 36.8, 31.8, 29.3, 29.2, 25.8, 22.7, and 14.1. HRMS (ESI): calculated for C$_{23}$H$_{30}$FNO$_5$S [M+Na]$^+$: 474.1721, found: 474.1721.

2.1.1.18 2-Methoxy-4-(Nonanamidomethyl)Phenyl 2,6-Difluorobenzenesulfonate (3r)

White powder, yield 82.0%. m.p. 38.2–39.1°C. ^{1}H-NMR (400 MHz, CDCl$_3$) δ 7.61 (tt, J = 8.5, 5.8 Hz, 1H), 7.17 (d, J = 8.8 Hz, 1H), 7.05 (t, J = 8.4 Hz, 2H), 6.81 (d, J = 6.8 Hz, 2H), 5.85 (s, 1H), 4.38 (d, J = 5.9 Hz, 2H), 3.55 (s, 3H), 2.29–2.17 (m, 2H), 1.78–1.58 (m, 2H), 1.37–1.19 (m, 10H), and 0.92–0.80 (m, 3H). ^{13}C-NMR (100 MHz, CDCl$_3$) δ 173.2, 151.5, 139.4, 137.4, 136.0, 124.2, 119.9, 113.0, 112.7, 112.2, 55.6, 43.1, 36.8, 31.8, 29.3, 29.2, 25.8, 22.7, and 14.1. HRMS (ESI): calculated for C$_{23}$H$_{29}$F$_2$NO$_5$S [M+Na]$^+$: 492.1627, found: 492.1626.

2.1.1.19 2-Methoxy-4-(Nonanamidomethyl)Phenyl 3-(Trifluoromethyl)Benzenesulfonate (3s)

White powder, yield 81.0%. m.p. 84.3–85.4°C. ^{1}H-NMR (400 MHz, CDCl$_3$) δ 8.17 (s, 1H), 8.06 (dt, J = 8.1, 1.4 Hz, 1H), 7.91 (d, J = 7.8 Hz, 1H), 7.67 (t, J = 7.9 Hz, 1H), 7.19 (d, J = 8.2 Hz, 1H), 6.82 (dd, J = 8.2, 2.0 Hz, 1H), 6.76 (s, 1H), 5.79 (s, 1H), 4.40 (s, 2H), 3.48 (s, 3H), 2.21 (t, J = 7.6 Hz, 2H), 1.83–1.48 (m, 2H), 1.39–1.23 (m, 10H), and 0.87 (t, J = 6.7 Hz, 3H). ^{13}C-NMR (100 MHz, CDCl$_3$) δ 173.1, 151.4, 139.5, 137.2, 129.5, 124.3, 119.8, 112.0, 55.3, 43.1, 36.8, 31.8, 29.3, 29.2, 25.8, 22.6, and 14.1. HRMS (ESI): calculated for C$_{24}$H$_{30}$F$_3$NO$_5$S [M+Na]$^+$: 524.1689, found: 524.1691.

2.1.1.20 2-Methoxy-4-(Nonanamidomethyl)Phenyl 3-Bromobenzenesulfonate (3t)

White powder, yield 86.2%. m.p. 57.5–59.5°C. ^{1}H-NMR (400 MHz, CDCl$_3$) δ 8.05 (t, J = 1.9 Hz, 1H), 7.78 (dt, J = 8.1, 2.0 Hz, 2H), 7.38 (t, J = 8.0 Hz, 1H), 7.13 (d, J = 8.1 Hz, 1H), 6.84–6.69 (m, 2H), 5.90 (s, 1H), 4.38 (d, J = 5.9 Hz, 2H), 3.55 (s, 3H), 2.32–2.16 (m, 2H), 1.65 (h, J = 7.4, 6.6 Hz, 2H), 1.40–1.20 (m, 10H), and 0.87 (t, J = 6.8 Hz, 3H). ^{13}C-NMR (100 MHz, CDCl$_3$) δ 173.2, 151.5, 139.3, 137.9, 137.2, 137.0, 131.4, 130.2, 127.1, 124.2, 122.6, 119.7, 112.1, 55.5, 43.1, 36.8, 31.8, 29.3, 29.2, 25.8, 22.7, and 14.1. HRMS (ESI): calculated for C$_{23}$H$_{30}$BrNO$_5$S [M+Na]$^+$: 534.0920, found: 534.0920.

2.1.1.21 2-Methoxy-4-(Nonanamidomethyl)Phenyl 3-Chlorobenzenesulfonate (3u)

White powder, yield 83.5%. m.p. 66.6–68.4°C. ^{1}H-NMR (400 MHz, CDCl$_3$) δ 7.90 (t, J = 1.9 Hz, 1H), 7.80–7.69 (m, 1H), 7.66–7.57 (m, 1H), 7.45 (t, J = 8.0 Hz, 1H), 7.13 (d, J = 8.1 Hz, 1H), 6.87–6.72 (m, 2H), 5.79 (s, 1H), 4.39 (d, J = 5.9 Hz, 2H), 3.55 (s, 3H), 2.40–2.01 (m, 2H), 1.79–1.52 (m, 2H), 1.35–1.21 (m, 10H), and 0.87 (t, J = 6.8 Hz, 3H). ^{13}C-NMR (100 MHz, CDCl$_3$) δ 173.1, 151.6, 139.3, 137.8, 137.3, 135.0, 134.1, 130.0, 128.6, 126.7, 124.2, 119.8, 112.1, 55.5, 43.1, 36.8, 31.8, 29.3, 29.2, 25.8, 22.7, and 14.1. HRMS (ESI): calculated for C$_{23}$H$_{30}$ClNO$_5$S [M+H]$^+$: 467.1553, found: 468.1604.

2.2 Antimicrobial Assay
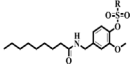
The bacteria which was used for the bioassay was provided by the Guizhou Tea Institute. The test method which was reported by Wang et al. (2021) was adopted, and the commercial agricultural bactericide bismerthiazol and thiodiazole copper were used as the positive control. Compounds were diluted to a concentration using a small amount of dimethyl sulfoxide (DMSO) and 0.1% Tween-20 (v/v). The bacteria were first grown in nutrient broth medium (NB), and then the medium containing the bacteria was added to solvent NB containing the test compounds. The inoculated test tubes were incubated at 30 ± 1°C under continuous shaking at 180 rpm for 48 h. The culture growth was monitored spectrophotometrically by measuring the optical density at 600 nm (OD$_{600}$) and expressed as corrected turbidity. The relative inhibition rates (%) were calculated according to the following equation, where C$_{tur}$ is the corrected turbidity value of bacterial growth in untreated NB, and T$_{tur}$ is the corrected turbidity value of bacterial growth in treated NB.

$$\text{Inhibition} \, (\%) \, = \, (\, C_{tur} \, - \, T_{tur} \,) \, / \, C_{tur} \, \times \, 100\%.$$

2.3 Insecticidal Activity Assay

Spodoptera frugiperda used in the biological tests were collected from the fields in Luodian County, Guizhou Province, China, and bred in a greenhouse. The specific test steps are as follows: 20 s instar larvae of *Spodoptera frugiperda* were divided into 20 small cups and starved for 3–4 h. Fresh corn leaves were cut into small leaf disks of 1 cm × 1 cm with scissors, and then soaked in each test solution for 5 s and air dried naturally. Then, they were put in the cups with *Spodoptera frugiperda* and kept under conditions of 25 ± 1°C, relative humidity of 60–70%, and a light-dark cycle of L: D = 14 h:10 h. Normal fresh corn leaf disks were given as feed after 12 h and the number of dead insects recorded at 12, 24, and 36 h.

TABLE 1 | The *in vitro* antibacterial activities of the target compounds **3a–3u**.

Compounds	R	*Pseudomonas syringae* pv. *actinidiae* (Psa)		*Xanthomonas oryzae* pv. *oryzae* (Xoo)		*Xanthomonas axonopodis* pv. *citri* (Xac)	
		100 μg/ml	50 μg/ml	100 μg/ml	50 μg/ml	100 μg/ml	50 μg/ml
3a	-4-FPh	100 ± 3.0	83 ± 2.3	98 ± 2.4	40 ± 1.3	99 ± 1.1	81 ± 1.0
3b	-2-BrPh	100 ± 1.4	86 ± 3.0	94 ± 2.8	54 ± 2.6	100 ± 1.6	92 ± 3.3
3c	-3,5-2FPh	98 ± 0.9	89 ± 2.7	84 ± 2.4	46 ± 1.7	98 ± 1.6	77 ± 1.1
3d	-4-CH₃OPh	100 ± 6.4	83 ± 3.9	90 ± 3.4	43 ± 2.7	98 ± 2.5	77 ± 2.1
3e	-2-FPh	100 ± 0.4	88 ± 2.9	61 ± 1.7	48 ± 2.2	99 ± 1.7	81 ± 1.3
3f	-2-Naphthalene	100 ± 2.2	74 ± 1.2	88 ± 3.9	52 ± 1.9	100 ± 1.6	71 ± 1.7
3g	-2,4,6-3CH₃Ph	100 ± 1.7	78 ± 1.6	92 ± 1.6	49 ± 2.3	96 ± 1.5	73 ± 2.7
3h	-4-NO₂Ph	100 ± 0.2	77 ± 2.2	59 ± 2.5	32 ± 2.3	100 ± 2.9	77 ± 3.4
3i	-4-CF₃Ph	97 ± 0.5	79 ± 2.8	83 ± 1.4	50 ± 1.7	95 ± 2.3	80 ± 1.3
3j	-Ph	100 ± 3.4	84 ± 2.0	76 ± 2.4	42 ± 1.3	99 ± 1.8	81 ± 1.6
3k	-2-FPh	100 ± 2.2	80 ± 2.4	81 ± 3.1	42 ± 2.2	99 ± 1.5	76 ± 3.0
3l	-4-tBu Ph	100 ± 7.1	78 ± 2.6	84 ± 2.4	56 ± 1.6	98 ± 2.5	79 ± 2.9
3m	-2-NO₂Ph	100 ± 1.3	79 ± 2.6	79 ± 1.5	39 ± 1.2	100 ± 2.2	81 ± 3.8
3n	-4-BrPh	100 ± 2.1	75 ± 2.2	82 ± 2.9	25 ± 1.5	99 ± 1.6	80 ± 1.9
3o	-2-Thiophene	100 ± 2.9	75 ± 2.3	86 ± 1.5	22 ± 1.4	105 ± 1.1	75 ± 2.1
3p	-3-NO₂Ph	100 ± 4.6	85 ± 2.7	66 ± 1.7	54 ± 2.8	100 ± 6.0	92 ± 3.6
3q	-3-FPh	98 ± 0.5	77 ± 1.9	67 ± 0.6	45 ± 1.0	99 ± 1.2	71 ± 1.9
3r	-2,6-2FPh	97 ± 0.4	71 ± 1.8	78 ± 2.3	33 ± 0.4	100 ± 4.0	65 ± 2.8
3s	-3-CF₃Ph	100 ± 0.8	84 ± 2.3	65 ± 1.3	37 ± 1.5	100 ± 3.4	80 ± 2.1
3t	-3-BrPh	100 ± 0.7	96 ± 2.5	79 ± 1.1	38 ± 1.7	100 ± 2.7	81 ± 2.1
3u	-3-ClPh	100 ± 2.7	93 ± 1.9	85 ± 2.3	34 ± 2.5	100 ± 3.3	88 ± 1.6
	Bismerthiazol	100 ± 2.9	87 ± 2.6	75.8 ± 2.6	34 ± 1.2	100 ± 5.2	77 ± 1.1
	Thiodiazole copper	100 ± 4.4	87 ± 3.4	79.4 ± 2.6	31 ± 1.8	100 ± 7.2	75 ± 2.5
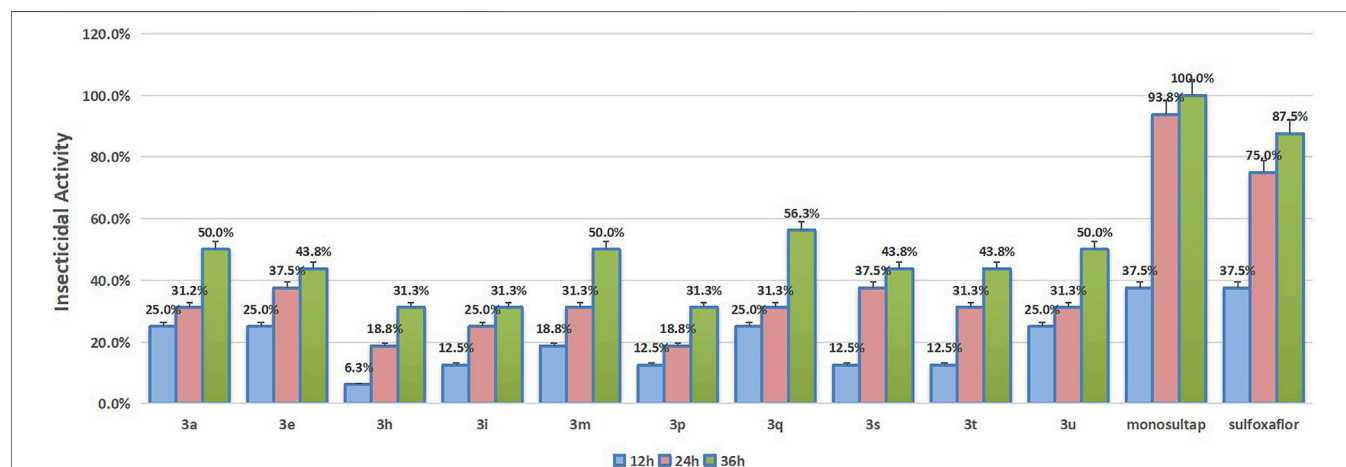
FIGURE 2 | The insecticidal activity against *Spodoptera frugiperda* of target compounds.

3 RESULTS AND DISCUSSION

3.1 Chemistry

The synthesis of intermediates **1** and **2** was achieved according to the method reported in the literature (Anderson et al., 2014). Target compounds were synthesized by condensation of different sulfonyl chloride which contained different substituent groups and intermediates **2** at room temperature conditions. HCl was produced as the byproduct in this reaction, and it was necessary to add an alkali to neutralize the HCl in the system to make the reaction proceed smoothly. Initially, we used Na_2CO_3 as the catalyst to be added to the system, but because Na_2CO_3 was difficult to dissolve in organic systems, the reaction was slow and the product yield was also very low. Therefore, we chose organic base triethylamine as the catalyst for the reaction, which made the reaction faster, and the yield was generally higher than 80%. The structures of all title compounds were confirmed by ^{1}H-NMR, ^{13}C-NMR, and HRMS. Due to these compounds having similar backbones, their ^{1}H-NMR spectra had something in common. For example, the proton signals of -OCH₃ of all compounds were

around 3.5 ppm, and the proton signals of acetyl were between 5.0 and 6.0 ppm. The proton signals of the alkyl chain in capsaicin were all below 4.0 ppm and were reflected in the NMR as four types of signals. These were the characteristics of the NMR spectra of these compounds.

3.2 *In vitro* Antibacterial Activity

As shown in **Table 1**, almost all title compounds exhibited antibacterial activities against *Pseudomonas syringae* pv. *actinidiae* (Psa), *Xanthomonas oryzae* pv. *oryzae* (Xoo), and *Xanthomonas axonopodis* pv. *citri* (Xac). Although many compounds exhibited comparable inhibition rates against Psa and Xac at a high concentration (100 μg/ml) as commercial bactericides, some compounds exhibited greater activity at a lower concentration (50 μg/ml). The inhibition rate of these compounds against Psa was in the range of 71–96% at 50 μg/ml. Among them, compounds **3c**, **3t**, and **3u** showed the highest activity with inhibition rates of 89, 96, and 93%, respectively, which were better than those of commercial bactericide bismerthiazol (87%) and thiodiazole copper (87%). The inhibition rate of these compounds against Xac was in the range of 71–92% at 50 μg/ml. Among them, compounds **3b** and **3p** showed the highest activity with inhibition rates of 92%, which were better than those of commercial bactericide bismerthiazol (77%) and thiodiazole copper (75%). The title compounds exhibited impressive inhibition activity against Xoo, especially compounds **3a**, **3b**, **3c**, **3d**, **3f**, **3g**, **3i**, and **3l**, and the bactericidal activity at the concentration of 100 and 50 μg/ml was higher than that in the commercial bactericide.

3.3 Insecticidal Activity Assay Against *Spodoptera frugiperda*

The results of the insecticidal activity against *Spodoptera frugiperda* of some compounds which were tested are shown in **Figure 2**. In general, although these compounds showed certain insecticidal activity against *Spodoptera frugiperda*, their activities were lower than those of the commercial insecticide monosultap and mulfoxaflor. Compounds **3a**, **3m**, **3q**, and **3u**, which showed the highest activity among these compounds, with lethal rates of 50, 50, 56.3, and 50% at 36 h, respectively, were still far lower than the positive controls monosultap (100% at 36 h) and mulfoxaflor (87.5% at 36 h). From the structure–activity relationship analysis, the group and its substitution position on the benzene ring of the title compounds affected insecticidal activity. When the nitro group was substituted at the 2-position of the benzene ring, the compound showed enhanced insecticidal activity. When the nitro group was substituted at the 3- or 4-position, the compound showed weak insecticidal activity.

4 CONCLUSION

In summary, in order to develop efficient and broad-spectrum agricultural chemicals, we diversified the structure of capsaicin and synthesized a series of novel capsaicin derivatives containing a sulfonic acid esters moiety. The structures of the compounds were confirmed through NMR and HRMS. The bioassay results revealed that the compounds exhibited obvious activities against *Pseudomonas syringae* pv. *actinidiae* (Psa), *Xanthomonas oryzae* pv. *oryzae* (Xoo), and *Xanthomonas axonopodis* pv. *citri* (Xac). A few of the compounds even exhibited higher activities than the commercial bactericides bismerthiazol and thiodiazole copper. Surprisingly, some compounds also showed some insecticidal activity against *Spodoptera frugiperda*, but the activity was far less than that of the commercial insecticides monosultap and mulfoxaflor. Therefore, further derivatives and optimization of the structure of the title compounds to improve their insecticidal activity are underway.

DATA AVAILABILITY STATEMENT

The original contributions presented in the study are included in the article/Supplementary Material; further inquiries can be directed to the corresponding author.

AUTHOR CONTRIBUTIONS

YW and WW contributed to the synthesis, purification, characterization of all compounds, and preparation of the original manuscript. XH and ZY performed the biological activity research. ZY and DX analyzed the experimental results. DX and XH drafted the first and second versions of the manuscript. All authors discussed, edited, and approved the final version.

REFERENCES

Anderson, M., Afewerki, S., Berglund, P., and Córdova, A. (2014). Total Synthesis of Capsaicin Analogues from Lignin-Derived Compounds by Combined Heterogeneous Metal, Organocatalytic and Enzymatic Cascades in One Pot. *Adv. Synth. Catal.* 356, 2113–2118. doi:10.1002/adsc.201301148

Baggio, C., Udompholkul, P., Gambini, L., Salem, A. F., Jossart, J., Perry, J. J. P., et al. (2019). Aryl-fluorosulfate-based Lysine Covalent Pan-Inhibitors of Apoptosis Protein (IAP) Antagonists with Cellular Efficacy. *J. Med. Chem.* 62, 9188–9200. doi:10.1021/acs.jmedchem.9b01108

Bum-Erdene, K., Liu, D., Gonzalez-Gutierrez, G., Ghozayel, M. K., Xu, D., and Meroueh, S. O. (2020). Small-molecule Covalent Bond Formation at Tyrosine Creates a Binding Site and Inhibits Activation of Ral GTPases. *Proc. Natl. Acad. Sci. U.S.A.* 117, 7131–7139. doi:10.1073/pnas.1913654117

Chen, M. H., Zhang, X., Lu, D. W., Luo, H. R., Zhou, Z. Y., Qi, X. F., et al. (2021). Synthesis and Bioactivities of Novel 1,3,4-thiadiazole Derivatives of Glucosides. *Front. Chem.* 9, 1–8. doi:10.3389/fchem.2021.645876

Claros Cuadrado, J. L., Pinillos, E. O., Tito, R., Mirones, C. S., and Gamarra Mendoza, N. N. (2019). Insecticidal Properties of Capsaicinoids and Glucosinolates Extracted from Capsicum Chinense and Tropaeolum Tuberosum. *Insects* 10, 132. doi:10.3390/insects10050132

Díaz-Laviada, I. (2010). Effect of Capsaicin on Prostate Cancer Cells. *Future Oncol.* 6, 1545–1550. doi:10.2217/fon.10.117

Guo, T., Xia, R., Chen, M., He, J., Su, S., Liu, L., et al. (2019). Biological Activity Evaluation and Action Mechanism of Chalcone Derivatives Containing Thiophene Sulfonate. *RSC Adv.* 9, 24942–24950. doi:10.1039/c9ra05349b

Guo, T., Xia, R., Chen, M., Su, S., He, J., He, M., et al. (2020). Biological Activity Evaluation and Action Mechanism of 1,4-Pentadien-3-One Derivatives Containing Thiophene Sulfonate. *Phosphorus, Sulfur, Silicon Relat. Elem.* 195, 123–130. doi:10.1080/10426507.2019.1655418

Hatcher, J. M., Wu, G., Zeng, C., Zhu, J., Meng, F., Patel, S., et al. (2018). SRPKIN-1: a Covalent SRPK1/2 Inhibitor that Potently Converts VEGF from Pro-angiogenic to Anti-angiogenic Isoform. *Cell Chem. Biol.* 25, 460–470. doi:10.1016/j.chembiol.2018.01.013

Huang, X.-F., Xue, J.-Y., Jiang, A.-Q., and Zhu, H.-L. (2013). Capsaicin and its Analogues: Structure-Activity Relationship Study. *Cmc* 20, 2661–2672. doi:10.2174/0929867311320210004

Inoue, N., Matsunaga, Y., Satoh, H., and Takahashi, M. (2007). Enhanced Energy Expenditure and Fat Oxidation in Humans with High Bmi Scores by the Ingestion of Novel and Non-pungent Capsaicin Analogues (Capsinoids). *Biosci. Biotechnol. Biochem.* 71, 380–389. doi:10.1271/bbb.60341

Isaacs, R., Mercader, R. J., and Wise, J. C. (2004). Activity of Conventional and Reduced-Risk Insecticides for Protection of Grapevines against the Rose Chafer, Macrodactylus Subspinosus (Coleoptera: Scarabaeidae). *J. Appl. Entomol.* 128, 371–376. doi:10.1111/j.1439-0418.2004.00861.x

Lee, I. O., Lee, K. H., Pyo, J. H., Kim, J. H., Choi, Y. J., and Lee, Y. C. (2007). Anti-inflammatory Effect of Capsaicin in helicobacter Pylori-Infected Gastric Epithelial Cells. *Helicobacter* 12, 510–517. doi:10.1111/j.1523-5378.2007.00521.x

Li, P., Yang, Y., Wang, X., and Wu, X. (2021). Recent Achievements on the Agricultural Applications of Thioether Derivatives: A 2010-2020 Decade in Review. *J. Heterocycl. Chem.* 58, 1225–1251. doi:10.1002/jhet.4234

Liao, H. T., Lee, H. J., Ho, Y. C., and Chiou, L. C. (2011). Capsaicin in the Periaqueductal Gray Induces Analgesia via Metabotropic Glutamate Receptor-mediated Endocannabinoid Retrograde Disinhibition. *Br. J. Pharmacol.* 163, 330–345. doi:10.1111/j.1476-5381.2011.01214.x

Mazourek, M., Pujar, A., Borovsky, Y., Paran, I., Mueller, L., and Jahn, M. M. (2009). A Dynamic Interface for Capsaicinoid Systems Biology. *Plant Physiol.* 150, 1806–1821. doi:10.1104/pp.109.136549

Morant, A. V., Bjarnholt, N., Kragh, M. E., Kjærgaard, C. H., Jørgensen, K., Paquette, S. M., et al. (2008). The β-Glucosidases Responsible for Bioactivation of Hydroxynitrile Glucosides in Lotus Japonicus. *Plant Physiol.* 147, 1072–1091. doi:10.1104/pp.107.109512

Morant, A. V., Jørgensen, K., Jørgensen, C., Paquette, S. M., Sánchez-Pérez, R., Møller, B. L., et al. (2008). β-Glucosidases as Detonators of Plant Chemical Defense. *Phytochemistry* 69, 1795–1813. doi:10.1016/j.phytochem.2008.03.006

Palo-Nieto, C., Afewerki, S., Anderson, M., Tai, C.-W., Berglund, P., and Córdova, A. (2016). Integrated Heterogeneous Metal/enzymatic Multiple Relay Catalysis for Eco-Friendly and Asymmetric Synthesis. *ACS Catal.* 6, 3932–3940. doi:10.1021/acscatal.6b01031

Snitker, S., Fujishima, Y., Shen, H., Ott, S., Pi-Sunyer, X., Furuhata, Y., et al. (2009). Effects of Novel Capsinoid Treatment on Fatness and Energy Metabolism in Humans: Possible Pharmacogenetic Implications. *Am. J. Clin. Nutr.* 89, 45–50. doi:10.3945/ajcn.2008.26561

Teng, M., Ficarro, S. B., Yoon, H., Che, J., Zhou, J., Fischer, E. S., et al. (2020). Rationally Designed Covalent BCL6 Inhibitor that Targets a Tyrosine Residue in the Homodimer Interface. *ACS Med. Chem. Lett.* 11, 1269–1273. doi:10.1021/acsmedchemlett.0c00111

Wang, X., Wang, X., Zhou, B., Long, J., and Li, P. (2021). Design, Synthesis, and Evaluation of New 4(3H)-quinazolinone Derivatives Containing a Pyrazole Carboxamide Moiety. *J. Heterocycl. Chem.* 58, 2109–2116. doi:10.1002/jhet.4334

Xia, Q., Wen, Y.-J., Wang, H., Li, Y.-F., and Xu, H.-H. (2014). β-Glucosidase Involvement in the Bioactivation of Glycosyl Conjugates in Plants: Synthesis and Metabolism of Four Glycosidic Bond Conjugates *In Vitro* and *In Vivo*. *J. Agric. Food Chem.* 62, 11037–11046. doi:10.1021/jf5034575

Check for updates

Total Synthesis of Natural Terpenoids Enabled by Cobalt Catalysis

Shu Xiao, Likun Ai, Qichang Liu, Baihui Yang, Jian Huang, Wei Xue* and Yang Chen*

State Key Laboratory Breeding Base of Green Pesticide and Agricultural Bioengineering, Key Laboratory of Green Pesticide and Agricultural Bioengineering, Ministry of Education, Research and Development Center for Fine Chemicals, Guizhou University, Guiyang, China

Transition metal catalysis plays an essential role in the total synthesis of natural products. Cobalt-mediated asymmetric catalysis has successfully been used as a primary or a secondary step in the total synthesis of natural products, especially terpenoids. Terpenoids represent one of the most prominent families among various categories of natural products, attracting immense attention due to their promising physiological activities. This review summarizes the recent advances toward the total synthesis of terpenoids by cobalt-mediated asymmetric catalysis, which may shed some light on their future synthetic efforts toward natural pesticides such as celanguline, azadirachtin, etc.

INTRODUCTION

Cobalt is a transition metal widely distributed on the earth. It has been used for organic synthesis in catalytic reactions for almost a century. Roelen (1938) achieved the hydroformylation alkene under $Co_2(CO)_8$-catalyzed conditions, which was a seminal work highlighting the impact of organometallic cobalt catalysts on selective organic transformations. It is worth mentioning that terpenoids are integral parts of natural products, widely distributed in plants, microbes, marine life, and some insects. The semi-synthesis and total synthesis of terpenoids gradually became one of the essential hotspots in the 20th century due to their various chemical structures and significant biological activities. In the following decades, great efforts have been made to explore novel strategies to synthesize the critical intermediates of terpenoids by catalyzing cobalt. Various studies have shown that cobalt catalysts expand the scope and range of organic methods, particularly in synthesizing small rings and enantioselective reactions. In this context, recent reviews summarized the enantioselective cobalt-catalyzed transformations (Pellissier and Clavier, 2014), catalytic activation of olefins using cobalt complex (Shigehisa, 2018), and metal-hydride hydrogen atom transfer (MHAT) reactions in natural product synthesis (Wu and Ma, 2021). However, there is a lack of a systematic and comprehensive summary of the application of cobalt catalysis in the total synthesis of terpenoids. Given the continuous progress in this research field, this review summarizes the total synthesis of terpenoids by asymmetric cobalt catalysis over the past few decades. It introduces aspects of hydration, hydrovinylation, hydroperoxidation, isomerization, and cycloaddition by cobalt-catalyzed. Partial functional group manipulation steps in the synthetic routes are omitted due to space limitations.

THE TOTAL SYNTHESIS OF TERPENOID ENABLED BY COBALT-CATALYZED

Hydration

Asymmetric hydration represents a powerful tool for converting alkenes into valuable and chiral building blocks for organic synthesis. It is a fundamental challenge for all hydration reactions to control the
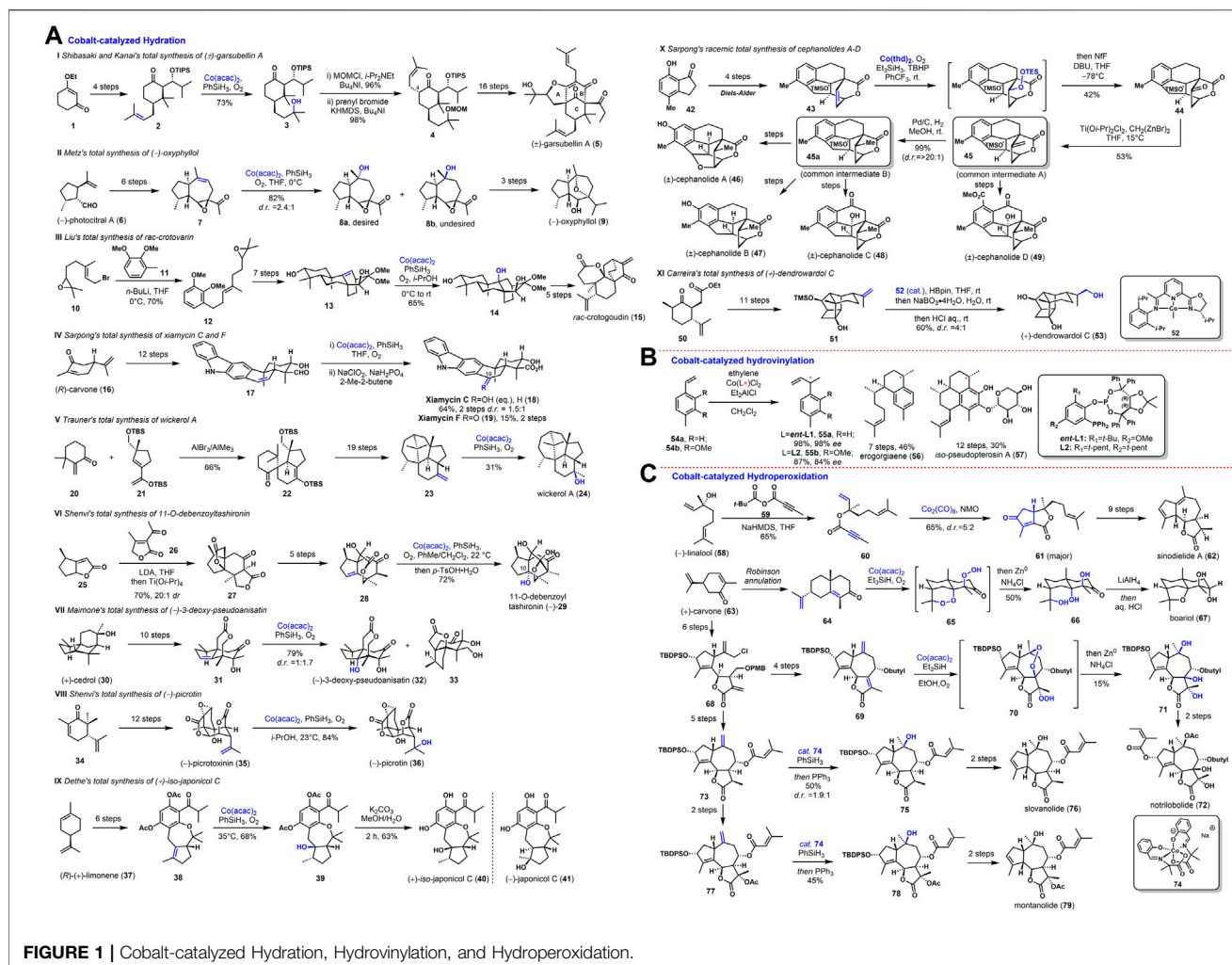
FIGURE 1 | Cobalt-catalyzed Hydration, Hydrovinylation, and Hydroperoxidation.

stereoselectivity of the alkene. We will systematically introduce applications of olefins hydration triggered through cobalt catalysis. One of the most widely employed cobalt radical reactions is the Mukaiyama hydration, a mild method to construct the C-O bonds across double bonds. Many reports show that cobalt-mediated Mukaiyama hydration of olefins has numerous applications due to its high regio- and chemoselectivity.

Shibasaki and Kanai (Kuramochi et al., 2005) achieved the first total synthesis of garsubellin A (5) using a cobalt-catalyzed Mukaiyama hydration. As shown in **Figure 1A-I**, isopropenyl ketone 2 was provided from commercially available cyclohexanone 1 in four steps. To complete the construction of the A-B rings in the later stage, the authors firstly protected the prenyl group under the conditions (Co(acac)$_2$, PhSiH$_3$, and O$_2$) to obtain tertiary alcohol 3, followed by treatment of 3 with MOMCl; a second prenyl group was introduced to C-4 at the axial position to give coupling compound 4. Later, (±)-garsubellin A (5) was prepared *via* a sixteen-step conversion from 4.

Metz (Zahel and Metz, 2013) finished the synthesis of (−)-oxyphyllol (9) by a regio- and diastereoselective Co

(II)-catalyzed hydration of olefin. As shown in **Figure 1A-II**, the total syntheses started from (−)-photocitral A (6). By a six-step conversion, the intermediate 7 was prepared. Under Co-catalyzed Mukaiyama hydration, a diastereomeric mixture of alcohol 8a and 8b was furnished with an 82% overall yield. (−)-Oxyphyllol (9) was then synthesized from 8a in three steps.

Liu (Song et al., 2015) applied Mukaiyama hydration in the total synthesis of atisane-type diterpenoids. As shown in **Figure 1A-III**, their synthesis started with 12, which could be accessed by coupling epoxy geranyl bromide 10 and 1,2-dimethoxy-3-methylbenzene 11. Afterward, a seven-step conversion furnished tetracyclic 13, followed by Mukaiyama hydration reaction with Co(acac)$_2$ as the catalyst to afford triol 14 in 65% yield. After five steps, the total synthesis of *rac*-crotovarin (15) was accomplished.

Sarpong (Pfaffenbach et al., 2019) synthesized indole sesquiterpenoids xiamycins A, C, F, H and oridamycin A. As shown in **Figure 1A-IV**, aldehyde 17 was prepared from (R)-carvone (16) after twelve steps as a common late-stage intermediate applied to synthesize several xiamycin congeners.

Mukaiyama hydration of 17 with $Co(acac)_2$ as the catalyst followed by Pinnick oxidation obtained a pair of diastereomers xiamycin C (18) and 19-*epi*-xiamycin C (*d.r.* = 1.5:1) in 64% yield over two steps, and xiamycin F (19) in 15% yield.

Trauner (Liu and Trauner, 2017) reported the synthesis of the antiviral diterpene, wickerol A (24). As shown in **Figure 1A-V**, with enone 20 and diene 21 as start material, tricyclic enol silyl ether 22 was constructed *via* Diels–Alder cycloaddition. Whereafter, tetracyclic compond 23 was obtained from 22 in nineteen steps. The authors finished the total synthesis of wickerol A (24) at the last step of the Mukaiyama hydration of olefin *via* $CpCo(CO)_2$ catalyst with a 31% yield.

Shenvi (Ohtawa et al., 2017) prepared neurotrophic sesquiterpenes, 11-*O*-debenzoyltashironin (29). As shown in **Figure 1A-VI**, The synthesis commenced with the construction of tetracycle 27, which was accessed through a cycloaddition between cyclopentanobutenolide 25 and butenolide 26. The seven-membered lactone 28 could be constructed in five steps containing a Dieckmann-type condensation from 27. The authors suspected that the stereochemistry of hydration products might be affected by steric shielding by the C10 alcohol. Thus, the authors applied Mukaiyama hydration *via* $Co(acac)_2$ catalyst in the last stage toward the total synthesis of 11-*O*-debenzoyltashironin (29), followed by hemiacetalization with *p*-TsOH·H_2O to transform the *trans*-hydrindane skeleton with tertiary alcocyclic in 72% yield.

Maimone (Hung et al., 2019) explored a terpene feed stock-based oxidative synthetic approach to synthesize the *Illicium* sesquiterpenes. As shown in **Figure 1A-VII**, the alkene 31 was prepared from (+)-cedrol (30) in ten steps. Under the presence of $Co(acac)_2$, $PhSiH_3$, and O_2, 31 could be converted to 3-deoxy-pseudoanisatin (32) and its epimer 33 in a 1:1.7 ratio with a 50% yield *via* a radical hydration reaction.

As shown in **Figure 1A-VIII**, Shenvi (Crossley et al., 2020) accomplished the total synthesis of (−)-picrotoxinin (35) from dimethyl-(*R*)-carvone 34 in 12 steps. Under Mukaiyama hydration conditions, $Co(acac)_2$ and $PhSiH_3$ in *i*-PrOH under O_2, (−)-picrotin (36) was isolated in one step and 84% yield.

Dethe (Dethe and Nirpal, 2021) described the enantiospecific total synthesis of japonicol C (41). The allyl alcohol 38 could be advanced to (*R*)-(+)-limonene (37) in six steps. As shown in **Figure 1A-IX**, treatment of 38 with $Co(acac)_2$, $PhSiH_3$, O_2, and THF, generated the stereospecific product 39 in 68% yield. Although it was an unsuccessful synthesis of japonicol C (41), it provided (+)-*iso*-japonicol C (40) after deacetylation of 39 in 63% yield. The authors speculated that the stereochemical outcome of the Mukaiyama reaction could be due to the Co-H hydride approaching from a less hindered side. To overcome the obstacle, they took advantage of $Pd(OH)_2$/C-catalyzed isomerization/hydrogenation to furnish (−)-japonicol C (41) from allyl alcohol 38.

As shown in **Figure 1A-X**, a divergent total synthesis of cephalotane-type nor-diterpenoids cephanolides A-D (46–49) was reported by Sarpong (Haider et al., 2021). Their synthesis commenced from the commercially available 7-hydroxy-4-methylindanone 42, which could be converted to bridge lactone 43 *via* a four-step sequence with intramolecular Diels–Alder cycloaddition as a critical step. The common intermediates 45 and 45a containing the A/B/C/D/E rings of cephanolides A-D were synthesized by Mukaiyama hydration under $Co(thd)_2$, O_2, Et_3SiH, and TBHP from 43. In addition, it is necessary to form 44 to use NfF and excess DBU, following converting ketone to an olefine 45 with $Ti(Oi-Pr)_2Cl_2$ and Nystedt reagents, followed by Pd catalytic hydrogenation reduction to get common intermediate B (45a). In a word, the cephanolide A (46) was successfully constructed using 42 as the starting material and 45 as common intermediate in overall 14 steps; cephanolide B (47, 10 steps), cephanolide C (48, 8 steps), and cephanolide D (49, 14 steps) were accessed through late-stage oxygenation from a commercially available indanone (42) and 45 as a comm intermediate A.

Carreira (Wolleb and Carreira, 2017) reported the asymmetric total synthesis of (+)-dendrowardol C (53). As shown in **Figure 1A-XI**, the fused tetracyclic carbon skeleton of 51 was prepared from known ester 50 in eleven steps. They initially tried to construct the primary alcohol 53 through hydroboration-oxidation reaction with the desired configuration. However, they always gave the 1:1 mixture of diastereomers. Towards this end, treatment of 51 with chiral Co^I (52) and HBpin, followed by oxidative and global deprotection, afforded the natural product (+)-dendrowardol C (53) in a diastereomeric ratio of 4:1 with 60% yield.

Hydrovinylation

Cobalt-catalyzed asymmetric hydrovinylation has the potential to control the *R/S* stereocentres of C–C bond formations. Moreover, the choice of the Co-catalyst enables diverse products. The method has been applied in the total synthesis of terpenoids. Co reacted as radical metal hydrides or hydrogen atom transfer (HAT) reagents, which prefer to add hydrogen to the less sterically hindered olefin position to form the most stable radical.

Schmalz (Movahhed et al., 2021) developed a new method of enantioselective cobalt-catalyzed hydrovinylation to introduce chiral olefins. As shown in **Figures 1B**, taking advantage of the novel method as the chirogenic step the asymmetric hydrovinylation of vinyl-arenes 54a/54b was performed utilizing $Co(L^*)Cl_2$ as a catalyst under the atmosphere of ethylene and Et_2AlCl, providing vinyl-arenes 55a/55b with remarkable efficiency and excellent enantioselectivity. The total synthesis of (+)-erogorgiaene (56) was achieved in only seven steps with a 46% overall yield from 4-methyl-styrene 54a. Moreover, the *iso*-pseudopterosin A (57) was prepared in 12 steps with a 30% overall yield from 54b, which proved to be equally anti-inflammatory as a mixture of natural pseudopterosins.

Hydroperoxidation

As shown in **Figure 1C**, Maimone (Hu et al., 2019) reported the synthesis of complex guaianolide sesquiterpenes. For sinodielide A (62), treatment of (−)-linalool (58) with NaHMDS and 59 was converted into ester 60, followed by underwent smooth Pauson-Khand reaction using dicobalt
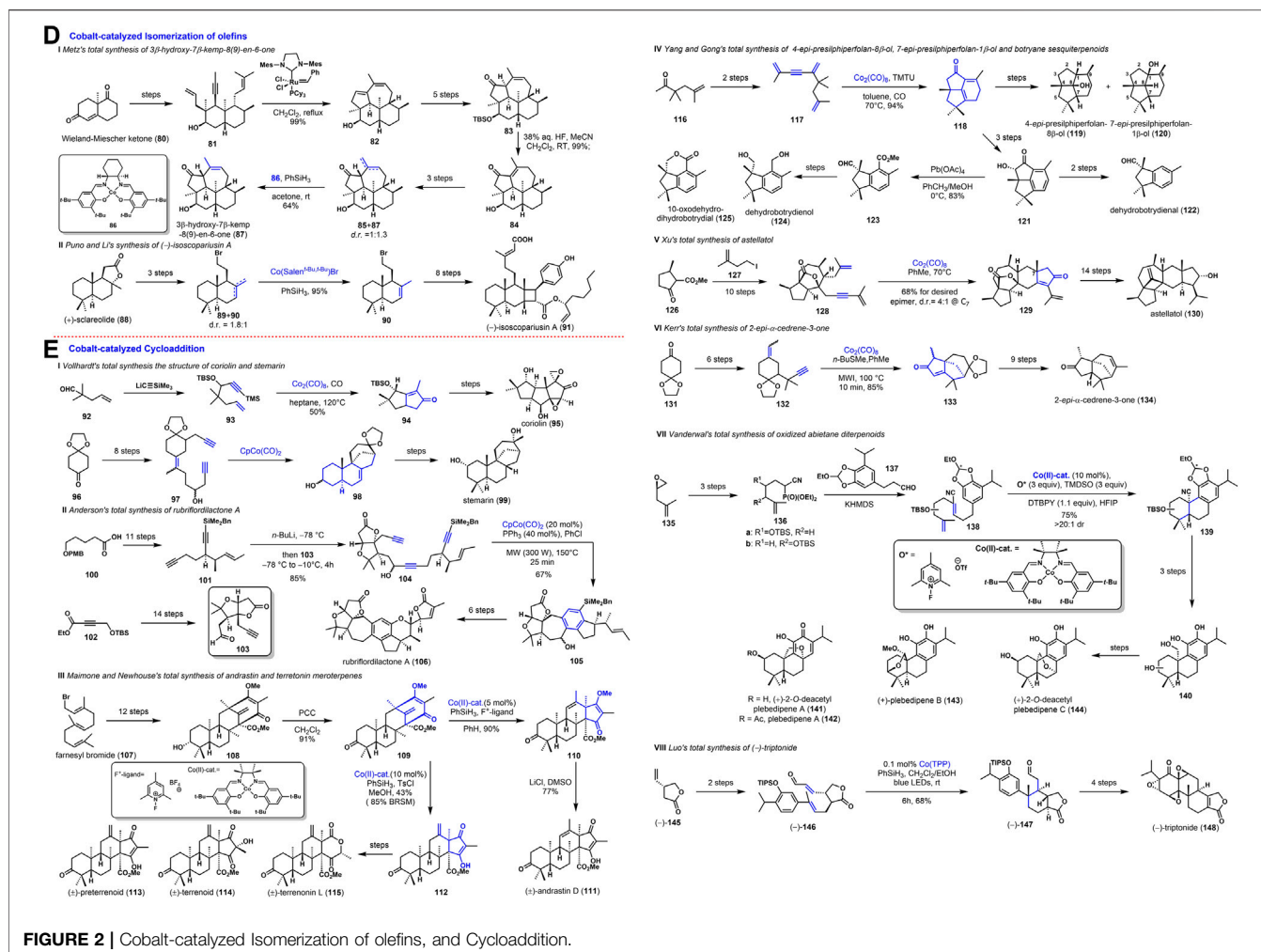
FIGURE 2 | Cobalt-catalyzed Isomerization of olefins, and Cycloaddition.

octacarbonyl (Co₂(CO)₈) gave bicyclic lactone 61. An additional nine steps gave 62, Wieland-Miescher Ketone analogue 64 was obtained by Robinson annulation starting with (+)-carvone (63). Then 64 was converted to triol 66 by a tandem cobalt-catalyzed hydroperoxidation via bis-peroxide intermediate 65, followed by Zinc powder reduction in a respectable 50% isolated yield. At the last step, boariol (67) was prepared using a stereoselective reduction with LiAlH₄ and etherification. With the same procedure and conversion, the total synthesis of notrilobolide (72) was achieved in the overall 14 steps from (+)-carvone (63) as starting material via trien 69 and triol 71 as critical intermediates. Notably, the total syntheses of slovanolide (76) and montanolide (79) via cobalt-catalyzed Mukaiyama-type hydration individually from common intermediate 73.

Isomerization of Olefins

The isomerization of double bonds has attracted attention during the last decade due to the growing importance of selectively shifting this synthetically essential functionality within a molecule. Cobalt complexes have also been utilized for the migration transposition of double bonds along a carbon chain. Hilt (Puenner et al., 2012) realized a transposition of a terminal alkene towards an internal alkene by cobalt catalyzed, and it was applied in a particular total synthesis of terpenoids later. As shown in **Figure 2D-I**, Metz (Wang et al., 2017) accomplished the first total synthesis of 3β-hydroxy-7β-kemp-8 (9)-en-6-one (87), which was isolated from the soldier defense secretion of the higher termites Nasutitermes octopolis. The Wieland-Miescher ketone 80 could be advanced to β-oriented alcohol 81 in multi-step transformation, giving rise to the requisite tetracyclic dienol 82 via Ru catalyzed domino metathesis. Following five steps of 82 generated the β, γ-unsaturated ketone 83. Later, desilylation and olefin isomerization with HF led to conjugated enone 84, which could be converted into the natural product in late continuous three steps. However, the byproduct of exocyclic olefin isomer 85 made the synthetic route more inefficient. Thus, they explored a cobalt-catalyzed isomerization strategy to install the β, γ-unsaturated ketone moiety from this tetracyclic compound 85 by hydrogen atom transfer with 86 as catalysis, provided the 3β-hydroxy-7β-kemp-8 (9)-en-6-one (87) in good yield.

Last year, Puno and Li (Yan et al., 2021) synthesized immunosuppressive meroditerpenoid, (−)-isoscopariusin A (91). As shown in **Figure 2D-II**, the synthesis commenced with the construction of mixed olefins 89 and 90 (*d.r.* = 1.8:1), which was accessed from (+)-sclareolide (88) *via* reduction, elimination and bromination. Inspired by Shenvi's protocol (Crossley et al., 2014) for olefin isomerization through Co(Salen$^{t-Bu,t-Bu}$)Br catalyzed, the exocyclic olefin 89 was converted to cycloolefin 90. Eventually, a following eight-step conversion achieved the total synthesis of (−)-isoscopariusin A (91) on a gram scale.

Cycloaddition

Cobalt catalyzed cycloaddition reaction has been used to construct polycyclic skeleton in total synthesis of terpenoids showed some case studies, such as [2+2+1] and [2+2+2] cycloaddition. The Pauson–Khand reaction is a metal-mediated [2+2+1] cycloaddition of an alkene, an alkyne, with carbon monoxide to construct an α, β-cyclopentenone skeleton.

Magnus (Exon and Magnus, 1983) employed intramolecular alkene-alkyne dicobaltocta-carbonyl mediated cyclopentenone cyclization to synthesize the antitumor sesquiterpene coriolin (95). The dicobalt octacarbonyl strategy for the stereoselective synthesis of hydroxylated bicyclo [3.3.0] enones provides a direct method of making many other natural and unnatural cyclopentanoid products. The unique ability of the [2+2+2] cycloaddition to form several new bonds within one step and thereby assemble smaller synthons to a bigger core structure predestinates this reaction to be applied to synthesize natural products. As shown in **Figure 2E-I**, Vollhardt (Germanas et al., 1991) employed a novel application of the cobalt-catalyzed cycloaddition to synthesize corioline (95) and stemarin (99). In the total synthesis of corioline (95), the cobalt-catalyzed Pauson–Khand reaction was used to construct the key intermediate 94. Moreover, cobalt mediated [2+2+2] cycloaddition reaction with CpCo(CO)$_2$ played an essential role in the total synthesis of stemarin (99), in which intermediates 98 were constructed with high efficiency and stereoselectivity.

Rubriflordilactones A and B from *Schisandra rubriflora* have attracted increasing attention because of their intriguing structures and promising anti-HIV activity. As shown in **Figure 2E-II**, Anderson (Goh et al., 2015) (Chaubet et al., 2017) completed the total synthesis of rubriflordilactone A (100) *via* a cobalt-catalyzed [2+2+2] cycloaddition as a pivotal step to close the key aromatic C-ring. This total synthesis takes 5-OPMB-pentanoic acid 100 as the starting material; Diyne 101 was prepared after a eleven-step sequence. Meanwhile, the cyclized precursor 104 was assembled with great facility *via* fragment coupling by 101 and bicyclic lactone alkyne 103, which was prepared from commercially available propargyl silicon 102 *via* fourteen steps. With an efficient cobalt-catalyzed [2+2+2] cycloaddition, the aromatic C-ring of intermediate 105 with pentacyclic core skeleton was constructed and followed a six-step transformation toward the total synthesis of rubriflordilactone A (106).

As shown in **Figure 2E-III**, in the total synthesis of andrastin and terretonin meroterpenes in 2017, Maimone and Newhouse

(Xu et al., 2017) employed a strategy of purely radical-based homoallyl-type rearrangement/HAT to forge protoaustinoid bicyclo [3.3.1] nonane nucleus. Cycloaddition substrate 109 could be conveniently prepared by PCC oxidation from tetracyclic block 108, which was obtained from commercially available farnesyl bromide 107 in twelve steps. As a common intermediate, 109 was converted to hydroxymethyl ether cyclopentenone 110 and iso-cyclopentenone 112 by cobalt-catalyzed intramolecular cycloaddition reaction under the action of 5% mol catalyst and 10% mol catalyst, respectively. After cyclopentenone isomerization, the total synthesis of (±)-andrastin D (111) was accomplished. On the other hand, (±)-preterrenoid (113), (±)-terrenoid (114), and (±)-terretonin L (115) were prepared by severe simple conversion processes.

As shown in **Figure 2E-IV**, Yang and Gong (Zhang et al., 2017) explored an approach of tandem Pauson–Khand and 6π-electrocyclization toward the total syntheses of 4-*epi*-presilphiperfolan-8β-ol (119) and 7-*epi*-presilphiperfolan-1β-ol (120). The preparation of cyclization precursor (117) was achieved from commercially available ketone (116) in a two-step. Under the condition of a catalytic amount of Co$_2$(CO)$_8$ and TMTU by the Pauson–Khand reaction, tricycle ketone 118 was obtained in excellent yield (94%). As a common intermediate, ketone 118 was transformed to 4-*epi*-presilphiperfolan-8β-ol (119) and 7-*epi*-presilphiperfolan-1β-ol (120) in a few steps reaction. Next year, Yang and Gong (Zhang et al., 2019) continued their previous work by the Co-TMTU-catalyzed tandem Pauson-Khand and 6π-electrocyclizationreactions, the total syntheses of three botryane sesquiterpenoids: dehydrobotrydienal (122), dehydrobotrydienol (124) and 10-oxodehydrodihydrobotrydial (125) were delivered from the common intermediate 118.

As shown in **Figure 2E-V**, in the synthetic studies towards astellatol (130), Xu (Zhao et al., 2018) used a cobalt-catalyzed Pauson-Khand cycloaddition to install the right-hand side scaffold of the sesterterpenoid. The cycloaddition precursor 128 could be advanced from chiral synthon 126 and the homoallylic iodide 127 as start materials in teen steps. Following [2+2+1], cycloaddition was carried out successfully with Co$_2$(CO)$_8$ in the toluene under the heating condition to give cyclopentenone 129. Finally, the authors accomplished the first and enantiospecific total synthesis of the rare sesterterpenoid, astellatol (130) in 25 steps (0.63% overall yield) from 126.

As shown in **Figure 2E-VI**, Kerr et al. (2018) accomplished the total synthesis of 2-*epi*-α-cedrene-3-one (134) *via* a cobalt-catalyzed Pauson-Khand reaction, which was isolated from the essential oil of *Juniperus thurifera*. Because the reaction required higher activation energy, the cycloaddition precursor 132 transformed to cyclopentenone 133 *via* a microwave-assisted, cobalt catalytic, Pauson-Khand reaction, which is used to construct the intriguing tricyclic core of the target molecule 134 following nine steps conversion.

As shown in **Figure 2E-VII**, Vanderwal (Vrubliauskas et al., 2021) systematically studied that Co-catalyzed MHAT-initiated (metal-catalyzed hydrogen atom transfer, MHAT) radical bicyclization was uniquely effective in synthesizing polycyclic terpenoids from polyene. The authors researched the utility of

these reactions in synthesizing three aromatic abietane diterpenoids. A known epoxide 135 as the starting material was transformed to phosphonate 136 with different cyanophosphonate reagents in three steps. Then the cyclization precursor 138 was prepared by HWE olefination with aldehyde 137. By a Co(II)-catalyzed tandem polyene cyclization, delivered 139 with excellent stereochemical control in 75% yield. The common intermediate 140 was prepared by continuous reduction and deprotection in three steps, following severe transformations prepared (+)-2-*O*-deacetyl plebedipene A (141), (±)-plebedipene B (143), (+)-2-*O*-deacetyl plebedipene C (144) and plebedipene A (142).

As shown in **Figure 2E-VIII**, Luo (Fang et al., 2022) described the total synthesis of (−)-triptonide (148) based on a Co(TPP)-catalyzed hydrogen atom transfer (MHAT)-initiated radical cyclization. Starting from (*R*)-(−)-Taniguchi lactone (145), fragment coupling was achieved through two-step reaction to obtain conjugated alkenal (146). By Cobalt-catalyzed in the presence of the photoredox catalyst and visible light, 146 was carried out to afford cycloadduct 147 smoothly. After the subsequent four steps transformation, (−)-triptonide (148) was produced.

CONCLUSION AND OUTLOOK

Cobalt-mediated asymmetric catalysis is a powerful method to functionalize olefins. The application of cobalt catalysts in [2+2+2] cycloaddition reactions of alkynes, alkenes, and nitriles to afford substituted benzenes, cyclohexadienes, and an extensive array of derivatives has been an active field of research over the last centuries. During the last decade, the heavier group congeners also significantly impacted this research field; especially cobalt catalysis is often the first choice when planning to include a cyclotrimerisation reaction in a synthetic sequence. Many reports have shown that cobalt-catalyzed could form C-C or C-X bonds. However, many of the already explored synthetic methods still represent an unsolved challenge for isolated natural products, as they remain inaccessible by the reported strategies. Such studies will benefit the detailed investigations of the mechanism of cobalt catalyzed and the application potential of natural products. The review may shed some light on future synthetic efforts on the cobalt-mediated total synthesis of terpenoids toward natural pesticides, such as celanguline, and azadirachtin.

AUTHOR CONTRIBUTIONS

SX: collected and organized all literature on the synthesis of terpenoid catalyzed by cobalt, and reviewed the total syntheses of terpenoid in some studies. LA: prepared some of the scheme, references, summary, and further prospects. QL: prepared "**Figure 1C**. BY: prepared "**Figure 2D**. JH: gave some valuable discussions on the total synthesis of terpenoid catalyzed by cobalt. WX: provided valuable discussions on the preparation of reaction schemes. YC: reviewed the abstract, introduction, and synthetic efforts towards the synthesis of terpenoid catalyzed by cobalt in recent decades, as well as summarizing all reaction schemes.

REFERENCES

Chaubet, G., Goh, S. S., Mohammad, M., Gockel, B., Cordonnier, M.-C. A., Baars, H., et al. (2017). Total Synthesis of the Schisandraceae Nortriterpenoid Rubriflordilactone A. *Chem. Eur. J.* 23, 14080–14089. doi:10.1002/chem.201703229

Crossley, S. W. M., Barabé, F., and Shenvi, R. A. (2014). Simple, Chemoselective, Catalytic Olefin Isomerization. *J. Am. Chem. Soc.* 136, 16788–16791. doi:10.1021/ja5105602

Crossley, S. W. M., Tong, G., Lambrecht, M. J., Burdge, H. E., and Shenvi, R. A. (2020). Synthesis of (−)-Picrotoxinin by Late-Stage Strong Bond Activation. *J. Am. Chem. Soc.* 142, 11376–11381. doi:10.1021/jacs.0c05042

Dethe, D. H., and Nirpal, A. K. (2021). Enantiospecific Total Synthesis of (−)-Japonicol C. *Org. Lett.* 23, 2648–2653. doi:10.1021/acs.orglett.1c00560

Exon, C., and Magnus, P. (1983). Stereoselectivity of Intramolecular Dicobalt Octacarbonyl Alkene-Alkyne Cyclizations: Short Synthesis of Dl-Coriolin. *J. Am. Chem. Soc.* 105, 2477–2478. doi:10.1021/ja00346a063

Fang, X., Zhang, N., Chen, S. C., Luo, T., Luo, T., Chen, S. C., et al. (2022). Scalable Total Synthesis of (−)-Triptonide: Serendipitous Discovery of a Visible-Light-Promoted Olefin Coupling Initiated by Metal-Catalyzed Hydrogen Atom Transfer (MHAT). *J. Am. Chem. Soc.* 144, 2292–2300. doi:10.1021/jacs.1c12525

Germanas, J., Aubert, C., and Vollhardt, K. P. C. (1991). One-step Construction of the Stemodane Framework via the Cobalt-Catalyzed Cyclization of Monocyclic Enynes: a Formal Total Synthesis of Stemodin. *J. Am. Chem. Soc.* 113, 4006–4008. doi:10.1021/ja00010a061

Goh, S. S., Chaubet, G., Gockel, B., Cordonnier, M.-C. A., Baars, H., Phillips, A. W., et al. (2015). Total Synthesis of (+)-Rubriflordilactone A. *Angew. Chem. Int. Ed.* 54, 12618–12621. doi:10.1002/anie.201506366

Haider, M., Sennari, G., Eggert, A., and Sarpong, R. (2021). Total Synthesis of the Cephalotaxus Norditerpenoids (±)-Cephanolides A-D. *J. Am. Chem. Soc.* 143, 2710–2715. doi:10.1021/jacs.1c00293

Hu, X., Musacchio, A. J., Shen, X., Tao, Y., and Maimone, T. J. (2019). Allylative Approaches to the Synthesis of Complex Guaianolide Sesquiterpenes from Apiaceae and Asteraceae. *J. Am. Chem. Soc.* 141, 14904–14915. doi:10.1021/jacs.9b08001

Hung, K., Condakes, M. L., Novaes, L. F. T., Harwood, S. J., Morikawa, T., Yang, Z., et al. (2019). Development of a Terpene Feedstock-Based Oxidative Synthetic Approach to the Illicium Sesquiterpenes. *J. Am. Chem. Soc.* 141, 3083–3099. doi:10.1021/jacs.8b12247

Kerr, W. J., McLaughlin, M., Paterson, L. C., and Pearson, C. M. (2018). Total Synthesis 2-Epi-α-Cedren-3-One via a Cobalt-Catalysed Pauson-Khand Reaction. *Tetrahedron* 74, 5062–5068. doi:10.1016/j.tet.2018.06.032

Kuramochi, A., Usuda, H., Yamatsugu, K., Kanai, M., and Shibasaki, M. (2005). Total Synthesis of (±)-Garsubellin A. *J. Am. Chem. Soc.* 127, 14200–14201. doi:10.1021/ja055301t

Liu, S.-A., and Trauner, D. (2017). Asymmetric Synthesis of the Antiviral Diterpene Wickerol A. *J. Am. Chem. Soc.* 139, 9491–9494. doi:10.1021/jacs.7b05046

Movahhed, S., Westphal, J., Kempa, A., Schumacher, C. E., Sperlich, J., Neudörfl, J. M., et al. (2021). Total Synthesis of (+)-Erogorgiaene and the Pseudopterosin A–F Aglycone via Enantioselective Cobalt-Catalyzed Hydrovinylation. *Chem. Eur. J.* 27, 11574–11579. doi:10.1002/chem.202101863

Ohtawa, M., Krambis, M. J., Cerne, R., Schkeryantz, J. M., Witkin, J. M., and Shenvi, R. A. (2017). Synthesis of (−)-11-O-Debenzoyltashironin: Neurotrophic Sesquiterpenes Cause Hyperexcitation. *J. Am. Chem. Soc.* 139, 9637–9644. doi:10.1021/jacs.7b04206

Pellissier, H., and Clavier, H. (2014). Enantioselective Cobalt-Catalyzed Transformations. *Chem. Rev.* 114, 2775–2823. doi:10.1021/cr4004055

Pfaffenbach, M., Bakanas, I., O'Connor, N. R., Herrick, J. L., and Sarpong, R. (2019). Total Syntheses of Xiamycins A, C, F, H and Oridamycin A and Preliminary Evaluation of Their Anti-Fungal Properties. *Angew. Chem. Int. Ed.* 58, 15304–15308. doi:10.1002/anie.201908399

Pünner, F., Schmidt, A., and Hilt, G. (2012). Up the Hill: Selective Double-Bond Isomerization of Terminal 1,3-dienes towards Z-1,3-Dienes or 2Z,4E-Dienes. *Angew. Chem. Int. Ed.* 51, 1270–1273. doi:10.1002/anie.201107512

Roelen, O. (1944). (to Chemische Verwertungsgesellschaft Oberhausen m.b.H.) German Patent DE 849548, 1938/1952; U.S. Patent 2327066, 1943. *Chem. Abstr.* 38, 3631.

Shigehisa, H. (2018). Studies on Catalytic Activation of Olefins Using Cobalt Complex. *Chem. Pharm. Bull.* 66, 339–346. doi:10.1248/cpb.c17-01006

Song, L., Zhu, G., Liu, Y., Liu, B., and Qin, S. (2015). Total Synthesis of Atisane-type Diterpenoids: Application of Diels-Alder Cycloadditions of Podocarpane-type Unmasked Ortho-Benzoquinones. *J. Am. Chem. Soc.* 137, 13706–13714. doi:10.1021/jacs.5b08958

Vrubliauskas, D., Gross, B. M., and Vanderwal, C. D. (2021). Stereocontrolled Radical Bicyclizations of Oxygenated Precursors Enable Short Syntheses of Oxidized Abietane Diterpenoids. *J. Am. Chem. Soc.* 143, 2944–2952. doi:10.1021/jacs.0c13300

Wang, Y., Jäger, A., Gruner, M., Lübken, T., and Metz, P. (2017). Enantioselective Total Synthesis of 3β-Hydroxy-7β-Kemp-8(9)-En-6-One, a Diterpene Isolated from Higher Termites. *Angew. Chem. Int. Ed.* 56, 15861–15865. doi:10.1002/anie.201708561

Wolleb, H., and Carreira, E. M. (2017). Total Synthesis of (+)-Dendrowardol C. *Angew. Chem. Int. Ed.* 56, 10890–10893. doi:10.1002/anie.201705809

Wu, J., and Ma, Z. (2021). Metal-hydride Hydrogen Atom Transfer (MHAT) Reactions in Natural Product Synthesis. *Org. Chem. Front.* 8, 7050–7076. doi:10.1039/d1qo01139a

Xu, G., Elkin, M., Tantillo, D. J., Newhouse, T. R., and Maimone, T. J. (2017). Traversing Biosynthetic Carbocation Landscapes in the Total Synthesis of Andrastin and Terretonin Meroterpenes. *Angew. Chem. Int. Ed.* 56, 12498–12502. doi:10.1002/anie.201705654

Yan, B. C., Zhou, M., Li, J., Li, X. N., He, S. J., Zuo, J. P., et al. (2021). (−)-Isoscopariusin A, a Naturally Occurring Immunosuppressive Meroditerpenoid: Structure Elucidation and Scalable Chemical Synthesis. *Angew. Chem. Int. Ed.* 60, 12859–12867. doi:10.1002/anie.202100288

Zahel, M., and Metz, P. (2013). A Concise Enantioselective Synthesis of the Guaiane Sesquiterpene (−)-oxyphyllol. *Beilstein J. Org. Chem.* 9, 20282025–20282032. doi:10.3762/bjoc.9.239

Zhang, Z., Li, Y., Zhao, D., He, Y., Gong, J., and Yang, Z. (2017). A Concise Synthesis of Presilphiperfolane Core through a Tandem TMTU-Co-Catalyzed Pauson-Khand Reaction and a 6π Electrocyclization Reaction (TMTU=Tetramethyl Thiourea). *Chem. Eur. J.* 23, 1258–1262. doi:10.1002/chem.201605438

Zhang, Z., Zhao, D., He, Y., Yang, Z., and Gong, J. (2019). Total Syntheses of Dehydrobotrydienal, Dehydrobotrydienol and 10-oxodehydrodihydrobotrydial. *Chin. Chem. Lett.* 30, 1503–1505. doi:10.1016/j.cclet.2019.03.033

Zhao, N., Yin, S., Xie, S., Yan, H., Ren, P., Chen, G., et al. (2018). Total Synthesis of Astellatol. *Angew. Chem. Int. Ed.* 57, 3386–3390. doi:10.1002/anie.201800167

Synthesis and Bioactivity of Novel Sulfonate Scaffold-Containing Pyrazolecarbamide Derivatives as Antifungal and Antiviral Agents

Zhi-Wei Lei[1,2]*, Jianmei Yao[2], Huifang Liu[2], Chiyu Ma[2] and Wen Yang[2]

[1]State Key Laboratory Breeding Base of Green Pesticide and Agricultural Bioengineering, Key Laboratory of Green Pesticide and Agricultural Bioengineering, Ministry of Education, Guizhou University, Guiyang, China, [2]Tea Research Institute, Guizhou Academy of Agricultural Sciences, Guiyang, China

Novel pyrazolecarbamide derivatives bearing a sulfonate fragment were synthesized to identify potential antifungal and antiviral agents. All the structures of the key intermediates and target compounds were confirmed by nuclear magnetic resonance (NMR) and high-resolution mass spectrometry (HRMS). The single-crystal X-ray diffraction of the compound **T22** showed that pyrazole carbamide is a sulfonate. The *in vitro* antifungal activities of the target compounds against Colletotrichum camelliae, Pestalotiopsis theae, Gibberella zeae, and Rhizoctonia solani were evaluated at 50 μg/ml. Among the four pathogens, the target compounds exhibited the highest antifungal activity against Rhizoctonia solani. The compound **T24** (EC_{50} = 0.45 mg/L) had higher antifungal activity than the commercial fungicide hymexazol (EC_{50} = 10.49 mg/L) against R. solani, almost similar to bixafen (EC_{50} = 0.25 mg/L). Additionally, the target compounds exhibited protective effects *in vivo* against TMV. Thus, this study reveals that pyrazolecarbamide derivatives bearing a sulfonate fragment exhibit potential antifungal and antiviral activities.

Keywords: pyrazolecarbamide, sulfonate, antifungal activity, antiviral activity, synthesis

INTRODUCTION

Phytopathogenic microorganisms, such as Rhizoctonia solani, Gibberella zeae, Pestalotiopsis theae, Colletotrichum camelliae, and tobacco mosaic virus (TMV) reduce the yield and quality of food and cash crops (Fisher et al., 2012). Chemical pesticides are still the most commonly used control measure for these diseases; however, the associated pesticide resistance and environmental hazards (Wei et al., 2020) impede their usage. Therefore, there is an urgent need to develop novel eco-friendly antifungal and antiviral agents agent with low toxicity and high efficiency.

Pyrazole and its derivatives have received considerable attention because of their diverse agrochemical and pharmaceutical applications. Most pyrazole derivatives exhibit a broad spectrum of biological activities, including antifungal (Kanungo and Joshi, 2014; Mu et al., 2016; Yan et al., 2018), insecticidal (Wu et al., 2012; Jiang et al., 2020), antibacterial (El Shehry et al., 2018; Wang et al., 2021), and other antimicrobial activities (Kasiotis et al., 2014; Saleh et al., 2020). Especially, pyrazole carboxamide derivatives, such as penthiopyrad, furametpyr, penflufen,

Graphical Abstract |
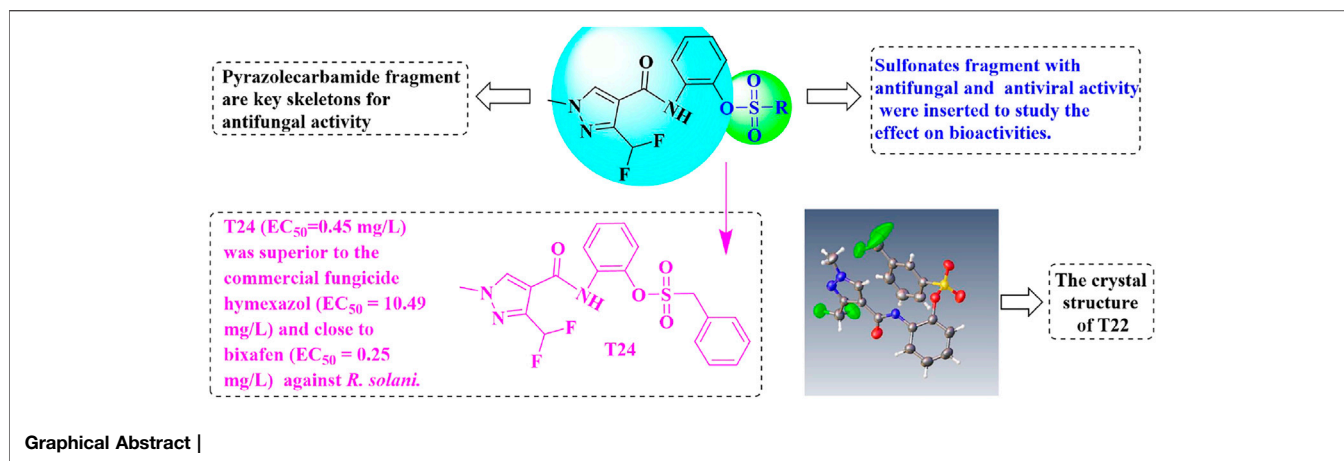
isopyrazam, and bixafen, which could inhibit the succinate dehydrogenase, have been developed and commercialized as fungicides (Si et al., 2019).

Sulfonates are also widely applied in agrochemical and medical industries because of their insecticidal (Sun et al., 2013; Wang et al., 2015), antifungal (Kang et al., 2019; Zhou et al., 2022), and antibacteria (Su et al., 2021) Moreover, the heterocyclic compounds containing aryl sulfonate moiety exhibit excellent antiviral activities (Zeng et al., 2010; Huang et al., 2015; Hadházi et al., 2017).

Therefore, we designed and synthesized a series of novel pyrazolecarbamide derivatives bearing a sulfonate moiety based on the active splicing principle and used the mycelial growth rate and half-leaf blight spot methods to evaluate their antifungal and antiviral activities.

MATERIALS AND METHODS

Chemistry

The ^{1}H and ^{13}C NMR spectra were recorded in CDCl$_3$ using 400 and 101 MHz spectrophotometers (Bruker BioSpin GmbH, Rheinstetten, Germany), respectively, while high-resolution mass spectrometry (HRMS) was performed using Thermo Scientific Q Exactive (Thermo Fisher Scientific, Massachusetts, America). The X-ray crystallographic data were collected and processed on a D8 Quest X-ray diffractometer (Bruker BioSpin GmbH, Rheinstetten, German). All solvents were dried using the standard methods and distilled before use.

3-(Difluoromethyl)-1-Methyl-1H-Pyrazole-4-Carboxylic Acid (4)

As shown in **Scheme 1**, the key intermediate **4** was synthesized using a previously published three-step procedure (Wang et al., 2020). White powder, yield 46%. m.p 201.1-201.9℃.^{1}H NMR (400 MHz, CDCl$_3$) δ 7.98 (s, 1H), 7.12 (t, J = 54.3 Hz, 1H), 4.02 (s, 3H). HRMS (ESI): calculated for C$_6$H$_6$F$_2$N$_2$O$_2$ [M + Na]$^+$: 199.02950, found: 199.02896.

2-(Difluoromethyl)-N-(2-Hydroxyphenyl)-1-Methyl-1H-Pyrazole-4-Carboxamide (6)

A mixture of 1-Ethyl-3-(3-dimethyllaminopropyl)carbodiimide hydrochloride (EDCI, 120 mmol), Intermediate **4** (100 mmol) and o-aminophenol (100 mmol), and dimethylaminopyridine (DMAP, 10 mmol) were dissolved in CH$_2$Cl$_2$ (500 ml) at −10℃ for 1 h. Thereafter, the mixture was stirred at room temperature for 8 h, and the key intermediate **6** was purified using column chromatography. Light yellow solid, yield 62%. m.p. 181.1-182.3℃ .^{1}H NMR (400 MHz, CDCl$_3$) δ 8.99 (s, 1H), 8.37 (s, 1H), 8.08 (s, 1H), 7.17 (td, J = 7.7, 1.6 Hz, 1H), 7.05 (ddd, J = 7.8, 6.0, 1.5 Hz, 2H), 6.91 (dd, J = 7.4,1.5 Hz, 1H), 6.88 (t, J = 54.1Hz, 1H), 3.97 (s, 3H). ^{13}C NMR (101 MHz, CDCl$_3$) δ 160.74, 149.12(t, J = 26.5 Hz), 136.77, 127.62, 125.42, 122.63, 120.51, 120.10, 115.5, 112.18, 110.40 (t, J = 235.3 Hz), 39.71. HRMS (ESI): calculated for C$_{12}$H$_{11}$F$_2$N$_3$O$_2$ [M + Na]$^+$: 290.07170, found: 290.07126.

General Procedure for the Preparation of the Target Compounds (T1-27)

Catalytic DMAP, arylsulfonyl chloride (1.1 mmol), and Et$_3$N (2 mmol) were added to a stirred CH$_3$CN (20 ml) solution of the key intermediate **6** (1 mmol), and the reaction was monitored at room temperature using TLC. Thereafter, the solvent was removed by rotary evaporation, and 10 ml of water was added to the residue, followed by extraction of the aqueous layer three times (30 ml × 3) using ethyl acetate. The organic layers were then combined and dried using anhydrous Na$_2$SO$_4$ and later concentrated under reduced pressure to form a crude product, purified using flash chromatography to obtain the target product.

2-(3-(Difluoromethyl)-1-Methyl-1H-Pyrazole-4-Carboxamido)Phenyl Benzenesulfonate (T1)

Gray powder, yield 72%. m.p. 138.3-139.6℃ .^{1}H NMR (400 MHz, CDCl$_3$) δ 8.33 (s, 1H), 8.27 (dd, J = 8.3, 1.6 Hz,
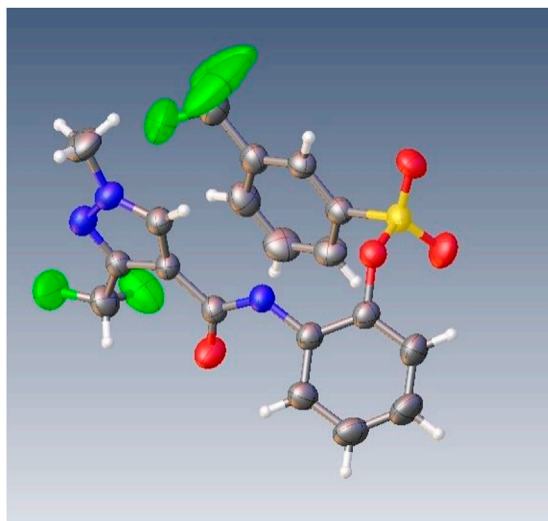
FIGURE 1 | The single-crystal X-ray diffraction of compound T22.
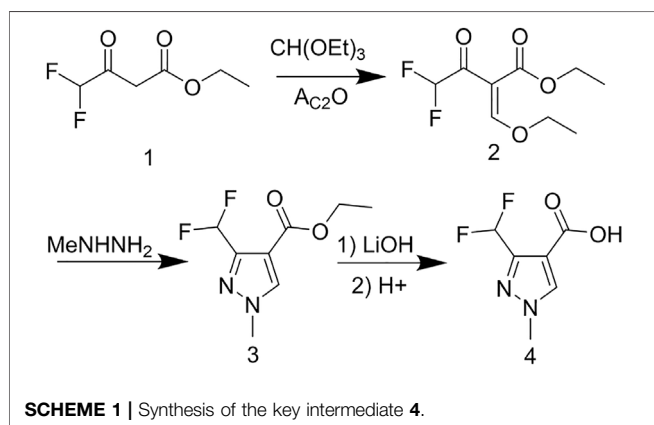
SCHEME 1 | Synthesis of the key intermediate **4**.

1H), 7.92 (s, 1H), 7.87–7.80 (m, 2H), 7.70–7.61 (m, 1H), 7.52–7.45 (m, 2H), 7.26 (dd, J = 15.7, 1.5 Hz, 1H), 7.08 (t, J = 54.1 Hz, 1H), 7.04–6.97 (m, 1H), 6.90 (dd, J = 8.2, 1.5 Hz, 1H), 4.00 (s, 3H).^{13}C NMR (101 MHz, CDCl₃) δ 159.33, 144.86(t, J = 26.5 Hz), 139.41, 134.99, 134.50, 133.41, 131.01, 129.44(×2), 128.65(×2), 128.01, 124.78, 123.27, 122.71, 116.68, 110.50 (t, J = 235.3 Hz), 39.92. HRMS (ESI): calculated for $C_{18}H_{15}F_2N_3O_4S[M + Na]^+$: 430.06490, found: 430.06531.

2-(3-(Difluoromethyl)-1-Methyl-1 H-Pyrazole-4-Carboxamido)Phenyl 4-Methylbenzenesulfonate (T2)

Light yellow power, yield 79%. m.p. 126.2-126.9℃ .^{1}H NMR (400 MHz, CDCl₃) δ 8.35 (s, 1H), 8.28 (dd, J = 8.3, 1.6 Hz, 1H), 7.92 (s, 1H), 7.76–7.64 (m, 2H), 7.31–7.21 (m, 4H), 7.09 (t, J = 54.1 Hz, 1H), 7.00 (td, J = 7.9, 1.6 Hz, 1H), 6.88 (dd, J = 8.2,

1.5 Hz, 1H), 4.00 (s, 3H), 2.42 (s, 3H).^{13}C NMR (101 MHz, CDCl₃) δ 159.35, 146.34, 145.05(t, J = 29.3 Hz), 139.50, 133.19, 131.54, 131.13, 130.07(×2), 128.72(×2), 127.94, 124.73, 123.20, 122.78, 116.82, 110.44(t, J = 235.8 Hz), 39.92, 21.87. HRMS (ESI): calculated for $C_{19}H_{17}F_2N_3O_4S$ [M + Na]⁺: 444.08055, found: 444.08109.
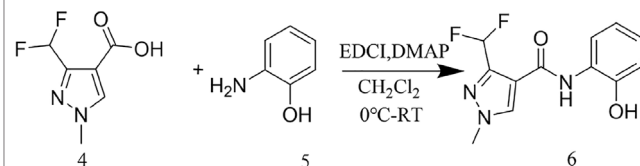
SCHEME 2 | Synthesis of the key intermediate **6**.

2-(3-(Difluoromethyl)-1-Methyl-1H-Pyrazole-4-Carboxamido)Phenyl 2-Fluorobenzenesulfonate (T3)

White powder, yield 78%. m.p. 123.9-124.5℃.^{1}H NMR (400 MHz, CDCl₃) δ 8.40 (s, 1H), 8.33 (dd, J = 8.3, 1.6 Hz, 1H), 7.96 (s, 1H), 7.89 (ddd, J = 8.3, 6.9, 1.8 Hz, 1H), 7.76–7.66 (m, 1H), 7.30 (qd, J = 7.7, 1.3 Hz, 3H), 7.26–7.19 (m, 2H), 7.12 (t, J = 54.0 Hz, 1H), 7.15 (dd, J = 8.2, 1.5 Hz, 1H), 7.10-7.02 (m, 1H), 4.02 (s, 3H).^{13}C NMR (101 MHz, CDCl₃) δ 160.92, 159.53, 158.34, 138.73, 137.67, 137.58, 132.71, 131.57, 131.09, 128.31, 125.00, 124.96, 124.88, 123.24, 122.66, 117.81, 117.60, 116.77, 112.53, 110.19, 39.97. HRMS (ESI): calculated for $C_{18}H_{14}F_3N_3O_4S$ [M + Na]⁺: 448.05548, found: 448.05454.

2-(3-(Difluoromethyl)-1-Methyl-1H-Pyrazole-4-Carboxamido)Phenyl 3-Fluorobenzenesulfonate (T4)

Gray powder, yield 76%. m.p. 119.3-120.9℃.^{1}H NMR (400 MHz, CDCl₃) δ 8.31–8.19 (m, 2H), 7.92 (s, 1H), 7.63–7.53 (m, 2H), 7.47 (td, J = 8.1, 5.2 Hz, 1H), 7.33 (tdd, J = 8.3, 2.5, 1.0 Hz, 1H), 7.30–7.27 (m, 1H), 7.05 (ddd, J = 8.7, 7.2, 1.5 Hz, 1H),7.02 (t, J = 54.1 Hz, 1H), 7.00 (dd, J = 8.2, 1.7 Hz, 1H), 3.99 (s, 3H).^{13}C NMR (101 MHz, CDCl₃) δ 163.61, 161.09, 159.26, 144.67, 144.40, 144.13, 139.44, 136.61, 136.53, 133.98, 131.37, 131.30, 130.85, 128.18, 124.96, 124.58, 124.54, 123.55, 122.56, 122.35, 122.14, 116.55, 116.08, 115.83, 113.16, 110.82, 108.49, 39.86. HRMS (ESI): calculated for $C_{18}H_{14}F_3N_3O_4S$ [M + Na]⁺:448.05548, found: 448.05454.

2-(3-(Difluoromethyl)-1-Methyl-1H-Pyrazole-4-Carboxamido) Phenyl 4-Fluorobenzenesulfonate (T5)

Light yellow powder, yield 69%. m.p. 165.2-165.9℃.^{1}H NMR (400 MHz, CDCl₃) δ 8.32–8.21 (m, 2H), 7.93 (s, 1H), 7.88–7.80
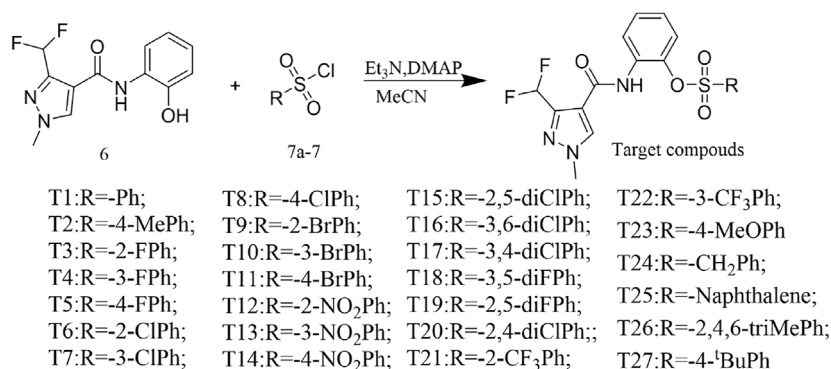
SCHEME 3 | Synthesis of the target compounds.

TABLE 1 | Inhibition rate *in vitro* of target compounds **T1-27** at 50 μg/ml.

Compounds	Inhibition Rate (%)			
	R. Solani (36 h)	C.camelliae (120 h)	P. Theae (120 h)	G.Zeae (120 h)
T1	29.37 ± 1.02 k	20.30 ± 1.22 kl	30.30 ± 0.42 ij	30.20 ± 1.33 j
T2	51.59 ± 1.31 e	41.09 ± 1.10 de	31.60 ± 1.69 hi	42.50 ± 1.23 d
T3	30.95 ± 1.19 k	26.90 ± 1.09 i	33.75 ± 0.19 fg	26.88 ± 2.09 k
T4	10.14 ± 0.24 q	11.74 ± 0.26o	12.04 ± 1.04 r	18.21 ± 1.04 no
T5	13.23 ± 0.97 op	16.20 ± 0.27 n	18.23 ± 1.08 p	19.69 ± 0.97 n
T6	44.97 ± 0.92 g	34.17 ± 0.12 f	40.02 ± 0.42 d	30.67 ± 0.62 j
T7	62.96 ± 1.27 d	12.90 ± 1.16o	32.16 ± 0.17 gh	36.16 ± 1.36 h
T8	61.38 ± 1.39 d	30.18 ± 1.09 h	29.08 ± 0.19 jk	41.38 ± 2.49 de
T9	23.02 ± 1.06 m	21.02 ± 0.76 k	20.19 ± 0.46o	25.02 ± 1.16 kl
T10	30.56 ± 1.42 k	20.66 ± 1.02 kl	28.51 ± 0.32 k	25.69 ± 1.02 kl
T11	36.77 ± 1.21 i	30.07 ± 0.41 h	33.71 ± 0.42 fg	38.27 ± 1.41 fg
T12	12.43 ± 1.01 p	19.73 ± 0.70 kl	17.40 ± 0.80 p	16.43 ± 1.21o
T13	13.46 ± 1.09 op	19.40 ± 1.17 lm	12.66 ± 0.19 r	10.26 ± 1.49 p
T14	20.45 ± 0.91 n	23.25 ± 0.78 j	22.05 ± 0.88 mn	22.45 ± 0.71 m
T15	24.34 ± 1.08 m	21.06 ± 0.98 k	23.04 ± 0.13 lm	26.64 ± 1.00 k
T16	48.15 ± 1.26 f	28.05 ± 0.16 i	33.18 ± 0.19 fgh	43.19 ± 0.26 d
T17	34.13 ± 1.10 j	24.03 ± 1.01 j	29.03 ± 1.00 jk	33.03 ± 0.16 i
T18	81.48 ± 1.06 c	40.40 ± 1.78 de	35.98 ± 0.76 e	40.08 ± 0.96 ef
T19	45.74 ± 1.02 g	35.04 ± 1.12 f	34.74 ± 0.92 ef	38.87 ± 0.46 f
T20	44.18 ± 1.00 g	40.01 ± 0.90 e	24.18 ± 0.10 l	36.58 ± 0.90 gh
T21	14.81 ± 0.98o	17.80 ± 0.68 mn	14.81 ± 0.78 q	24.73 ± 0.88 kl
T22	27.25 ± 0.93 l	23.15 ± 0.63 j	17.25 ± 0.13 p	26.35 ± 0.73 kl
T23	20.11 ± 0.95 n	20.71 ± 0.36 kl	13.05 ± 0.65 r	24.41 ± 0.65 l
T24	**100.00 ± 0.00 a**	45.31 ± 0.47 c	62.40 ± 0.51 c	48.00 ± 1.10 c
T25	29.37 ± 0.40 k	31.07 ± 0.69 gh	20.30 ± 0.16o	39.07 ± 0.64 f
T26	30.69 ± 0.73 k	32.19 ± 0.33 g	21.30 ± 0.44 no	32.64 ± 0.91 i
T27	40.21 ± 0.98 h	42.12 ± 1.84 d	20.20 ± 0.61˚	26.26 ± 0.68 kl
hymexazol	84.28 ± 0.96 b	54.91 ± 1.80 b	66.11 ± 3.20 b	67.33 ± 2.19 b
bixafen	**100.00 ± 0.00 a**	**79.49 ± 1.36 a**	**93.40 ± 1.77 a**	**100.00 ± 0.00 a**

Note: Data in the table are mean ± SD., Different lowercase letters in the same column indicate significant difference at p < 0.05 level by Duncan's new multiple range test.The meaning of bold is only to emphasize the good activity of the two compounds.

(m, 2H), 7.33–7.26 (m, 1H), 7.18–7.07 (m, 2H), 7.05 (ddd, J = 8.9, 7.4, 1.6 Hz, 1H),7.00 (t, J = 54.0 Hz, 1H), 6.98 (dd, J = 8.3, 1.6 Hz, 1H), 4.00 (s, 3H).^{13}C NMR (101 MHz, CDCl$_3$) δ 166.37(d, J = 259.6 Hz), 159.22, 144.15(t, J = 26.2 Hz), 144.18, 139.45, 134.24, 131.69, 131.59, 130.89, 130.69, 128.13, 124.92, 123.48, 122.78, 116.96, 116.73, 116.65, 110.90(t, J = 235.8 Hz), 105.41, 39.90. HRMS (ESI): calculated for C$_{18}$H$_{14}$F$_3$N$_3$O$_4$S [M + Na]$^+$:448.05548, found: 448.05454.

2-(3-(Difluoromethyl)-1-Methyl-1H-Pyrazole-4-Carboxamido)Phenyl 2-Chlorobenzenesulfonate (T6)

Gray powder, yield 70%. m.p. 116.3-117.2℃.^{1}H NMR (400 MHz, CDCl$_3$) δ 8.48 (s, 1H), 8.39–8.30 (m, 1H), 8.03 (dd, J = 8.0, 1.5 Hz, 1H), 7.97 (s, 1H), 7.67–7.57 (m, 2H), 7.44 (ddd, J = 8.0, 7.1, 1.6 Hz, 1H), 7.29 (ddd, J = 8.6, 5.6, 3.4 Hz, 1H), 7.11 (d, J = 54.1 Hz, 1H), 7.06–6.99 (m, 2H), 4.01 (s, 3H).^{13}C NMR

TABLE 2 | EC_{50} values of **T24** against R. solani.

Compound	Regression Equation	EC_{50} (mg/L)	R^2	95% confidence Interval (mg/L)
T24	y = 5.7941 + 1.3307x	0.45	0.9588	0.32-0.61
hymexazol	y = 3.9940 + 0.9853x	10.49	0.9949	6.35-17.33
bixafen	y = 5.7941 + 1.3307x	0.25	0.9976	0.13-0.47

TABLE 3 | Antiviral activity of the target compounds against TMV in vivo (500 mg/L).

Compound	Curative effect(%)	Protective effect(%)	Inactivation effect(%)
T1	30.9 ± 2.4 fg	40.1 ± 2.2 ghi	54.6 ± 3.2 jkl
T2	35.2 ± 1.6 f	43.1 ± 1.4 defghi	53.2 ± 1.3 jkl
T3	32.8 ± 3.2 fg	49.8 ± 2.3 b	63.3 ± 2.3 efgh
T4	40.8 ± 2.9 e	43.8 ± 2.6 cdefgh	62.6 ± 4.2 efghi
T5	42.4 ± 4.5 de	50.4 ± 1.5 b	59.5 ± 1.7 ghijk
T6	42.5 ± 2.0 de	42.4 ± 2.4 efghi	57.6 ± 2.5 hijk
T7	43.8 ± 1.7 de	43.5 ± 1.4 defghi	56.5 ± 3.0 ijk
T8	45.9 ± 2.5 cde	47.2 ± 3.0 bcde	62.8 ± 2.2 efghi
T9	35.2 ± 2.7 f	41.1 ± 3.2 ghi	50.5 ± 3.9 lmn
T10	32.2 ± 2.3 fg	42.5 ± 2.4 defghi	55.1 ± 3.4 hijk
T11	33.8 ± 4.0 f	49.8 ± 1.9 b	57.3 ± 3.5 jkl
T12	41.9 ± 2.0 de	50.2 ± 3.6 b	60.6 ± 2.4 fghij
T13	43.0 ± 3.7 de	45.4 ± 3.5 bcdefg	58.5 ± 4.7 hijk
T14	44.5 ± 3.1 de	43.0 ± 3.9 defghi	49.6 ± 4.5 lmn
T15	40.8 ± 0.7 e	49.5 ± 4.4 b	46.5 ± 3.7 no
T16	42.9 ± 3.1 de	48.0 ± 3.0 bcd	72.8 ± 4.9 bc
T17	41.5 ± 3.7 e	41.1 ± 4.2 ghi	67.6 ± 4.3 de
T18	54.2 ± 3.6 ab	49.1 ± 4.4 bc	70.2 ± 4.6 bcd
T19	46.9 ± 3.4 cd	40.1 ± 3.2 ghi	74.6 ± 4.2 b
T20	49.8 ± 3.9 bc	45.8 ± 4.6 bcdef	68.6 ± 3.9 cde
T21	28.4 ± 2.9 g	40.3 ± 1.5 fghi	65.3 ± 2.1 defg
T22	41.2 ± 2.0 e	32.4 ± 1.8 j	58.7 ± 3.8 hijk
T23	33.8 ± 1.7 f	38.6 ± 2.6 hi	66.3 ± 3.9 def
T24	35.9 ± 2.5 f	37.9 ± 3.1 i	42.8 ± 3.7o
T25	33.8 ± 1.7 f	45.6 ± 1.7 bcdefg	57.5 ± 1.9 hijk
T26	45.9 ± 2.5 cde	43.2 ± 2.8 defghi	49.8 ± 2.9 lmn
T27	30.9 ± 1.7 fg	40.2 ± 2.9 fghi	57.8 ± 2.1 hijk
Chitosan oligosaccharides	54.6 ± 2.7 a	57.6 ± 2.2 a	47.9 ± 1.5 mno
Ningnanmycin	55.3 ± 1.2 a	50.7 ± 1.1 b	98.1 ± 1.0 a

Note: Data in the table are mean ± SD., Different lowercase letters in the same column indicate significant difference at $p < 0.05$ level by Duncan's new multiple range test.

(101 MHz, $CDCl_3$) δ 159.59, 145.46(t, J = 26.5 Hz), 139.00, 135.92, 133.48, 133.15, 132.92, 132.54, 132.50, 131.21, 128.26, 127.52, 124.89, 123.48, 122.61, 116.70, 110.23 (t, J = 236.3 Hz), 39.96. HRMS (ESI): calculated for $C_{18}H_{14}ClF_2N_3O_4S$ [M + Na]$^+$: 464.02593, found: 464.02521.

## 2-(3-(Difluoromethyl)-1-Methyl-1H-Pyrazole-4-Carboxamido)Phenyl 3-Chlorobenzenesulfonate (T7)

Light yellow powder, yield 73%. m.p. 110.0-111.9°C.^{1}H NMR (400 MHz, $CDCl_3$) δ 8.24 (dd, J = 8.2, 1.4 Hz, 1H), 8.19 (s, 1H), 7.91 (s, 1H), 7.86 (t, J = 1.9 Hz, 1H), 7.63 (dt, J = 7.9, 1.4 Hz, 1H), 7.58 (ddd, J = 8.1, 2.1, 1.0 Hz, 1H), 7.41 (t, J = 8.0 Hz, 1H), 7.29 (ddd, J = 8.5, 6.6, 2.4 Hz, 1H), 7.11–7.02 (m, 2H), 7.01 (d, J = 54.1

Hz, 1H), 3.99 (s, 3H).^{13}C NMR (101 MHz, $CDCl_3$) δ 159.16, 144.30(t, J = 27.3 Hz), 139.40, 136.43, 135.79, 134.99, 134.11, 130.81, 130.70, 128.47, 128.22, 126.77, 124.98, 123.52, 122.72, 116.53, 110.90(t, J = 235.3 Hz), 39.88. HRMS (ESI): calculated for $C_{18}H_{14}ClF_2N_3O_4S$ [M + Na]$^+$: 464.02593, found: 464.02521.

2-(3-(Difluoromethyl)-1-Methyl-1 H-Pyrazole-4-Carboxamido)Phenyl 4-Chlorobenzenesulfonate (T8)

Light yellow powder, yield 79%. m.p. 185.6-185.9°C.^{1}H NMR (400 MHz, $CDCl_3$) δ 8.24 (dd, J = 8.2, 1.5 Hz, 2H), 8.22 (s, 1H), 7.93 (s, 1H), 7.77–7.69 (m, 2H), 7.44–7.36 (m, 2H), 7.29 (ddd, J = 8.6, 7.2, 1.8 Hz, 1H), 7.07 (td, J = 7.7, 1.5 Hz, 2H), 7.02 (dd, J = 8.2, 1.8 Hz, 1H), 6.98 (t, J = 54.1 Hz, 1H), 3.99 (s, 3H).^{13}C NMR

(101 MHz, CDCl$_3$) δ 159.15, 143.97(t, J = 26.7 Hz), 141.62, 139.54, 134.48, 133.37, 130.80, 130.04(×2), 129.75(×2), 128.15, 125.00, 123.59, 122.89, 116.64, 111.03(t, J = 234.7 Hz), 39.88. HRMS (ESI): calculated for C$_{18}$H$_{14}$ClF$_2$N$_3$O$_4$S [M + Na]$^+$: 464.02593, found: 464.02521.

2-(3-(Difluoromethyl)-1-Methyl-1H-Pyrazole-4-Carboxamido)Phenyl 2-Bromobenzenesulfonate (T9)

Gray powder, yield 69%. m.p. 133.9-134.2°C.^{1}H NMR (400 MHz, CDCl$_3$) δ 8.48 (s, 1H), 8.36–8.28 (m, 1H), 8.04 (dd, J = 7.8, 1.9 Hz, 1H), 7.98 (s, 1H), 7.81 (dd, J = 7.8, 1.4 Hz, 1H), 7.53 (td, J = 7.6, 1.9 Hz, 1H), 7.48 (td, J = 7.7, 1.4 Hz, 1H), 7.32–7.25 (m, 1H), 7.00 (t, J = 54.0 Hz, 1H), 7.04–6.98 (m, 2H), 4.00 (s, 3H).^{13}C NMR (101 MHz, CDCl$_3$) δ 159.59, 145.42(t, J = 25.8 Hz), 139.06, 136.05, 135.79, 134.98, 132.99, 132.79, 131.24, 128.23, 128.07, 124.89, 123.52, 122.66, 121.38, 116.82, 110.22(t, J = 235.6 Hz), 39.94. HRMS (ESI): calculated for C$_{18}$H$_{14}$BrF$_2$N$_3$O$_4$S [M + Na]$^+$: 507.97542, found: 507.97227.

2-(3-(Difluoromethyl)-1-Methyl-1H-Pyrazole-4-Carboxamido)Phenyl 3-Bromobenzenesulfonate (T10)

Light yellow powder, yield 80%. m.p. 128.4-128.5°C.^{1}H NMR (400 MHz, CDCl$_3$) δ 8.30–8.21 (m, 1H), 8.18 (s, 1H), 8.01 (t, J = 1.9 Hz, 1H), 7.91 (s, 1H), 7.73 (ddd, J = 8.1, 1.9, 1.0 Hz, 1H), 7.66 (ddd, J = 7.9, 1.8, 1.0 Hz, 1H), 7.33 (t, J = 8.0 Hz, 1H), 7.29 (td, J = 6.1, 3.3 Hz, 1H), 7.11–7.03 (m, 2H), 7.01 (t, J = 54.1 Hz, 1H), 3.99 (s, 3H).^{13}C NMR (101 MHz, CDCl$_3$) δ 159.13, 144.26 (t, J = 27.3 Hz), 139.35, 137.90, 136.47, 134.16, 131.24, 130.87, 130.75, 128.23, 127.18, 125.00, 123.50, 123.38, 122.78, 116.47, 110.91(t, J = 235.3 Hz), 39.91.HRMS (ESI): calculated for C$_{18}$H$_{14}$BrF$_2$N$_3$O$_4$S [M + Na]$^+$: 507.97542, found: 507.97227.

2-(3-(Difluoromethyl)-1-Methyl-1H-Pyrazole-4-Carboxamido)Phenyl 4-Bromobenzenesulfonate (T11)

Light yellow powder, yield 79%. m.p. 175.8-176.4°C.^{1}H NMR (400 MHz, CDCl$_3$) δ 8.23 (dd, J = 8.2, 1.5 Hz, 1H), 8.20 (s, 1H), 7.94 (s, 1H), 7.68–7.61 (m, 2H), 7.60–7.50 (m, 2H), 7.29 (ddd, J = 8.5, 7.0, 1.9 Hz, 1H), 7.07 (ddd, J = 8.6, 7.1, 1.5 Hz, 1H), 7.03 (dd, J = 8.2, 1.9 Hz, 1H), 6.97 (t, J = 54.1 Hz, 1H), 4.00 (s, 3H).^{13}C NMR (101 MHz, CDCl$_3$) δ 159.12, 143.91(t, J = 28.8 Hz), 139.54, 134.57, 133.94, 132.73(×2), 130.77, 130.26, 130.02(×2), 128.15, 125.02, 123.60, 122.92, 116.60, 111.06(t, J = 235.02 Hz), 39.89.HRMS (ESI): calculated for C$_{18}$H$_{14}$BrF$_2$N$_3$O$_4$S [M + Na]$^+$: 507.97542, found: 507.97227.

2-(3-(Difluoromethyl)-1-Methyl-1H-Pyrazole-4-Carboxamido)Phenyl 2-Nitrobenzenesulfonate (T12)

Light yellow powder, yield 83%. m.p. 146.0-147.8°C.^{1}H NMR (400 MHz, CDCl$_3$) δ 8.31 (s, 1H), 8.26 (dd, J = 8.3, 1.6 Hz, 1H), 7.92 (dd, J = 7.9, 1.4 Hz, 1H), 7.90 (d, J = 1.2 Hz, 1H), 7.81 (td, J = 7.8, 1.4 Hz, 1H), 7.69 (td, J = 7.8, 1.3 Hz, 1H), 7.66 (dd, J = 7.9, 1.3 Hz, 1H), 7.38 (dd, J = 8.3, 1.5 Hz, 1H), 7.34–7.28 (m, 1H), 7.13 (ddd, J = 8.3, 7.4, 1.6 Hz, 1H),7.11 (t, J = 54.1 Hz, 1H), 4.00 (s, 3H).^{13}C NMR (101 MHz, CDCl$_3$) δ 159.55, 148.37, 146.02(t, J = 25.3 Hz), 138.50, 136.28, 132.83, 132.35(×2), 130.76, 128.57, 128.06, 125.10, 124.90, 123.43, 123.06, 116.02(t, J = 2.7 Hz), 109.75(t, J = 236.8 Hz), 39.91. HRMS (ESI): calculated for C$_{18}$H$_{14}$F$_2$N$_4$O$_6$S [M + Na]$^+$: 475.04998, found: 475.04948.

2-(3-(Difluoromethyl)-1-Methyl-1H-Pyrazole-3-Carboxamido)Phenyl 4-Nitrobenzenesulfonate (T13)

Gray powder, yield 79%. m.p. 160.4-160.9°C.^{1}H NMR (400 MHz, CDCl$_3$) δ 8.70 (t, J = 2.0 Hz, 1H), 8.42 (ddd, J = 8.2, 2.2, 1.1 Hz, 1H), 8.14 (dd, J = 8.2, 1.6 Hz, 1H), 8.11 (d, J = 4.6 Hz, 1H), 7.99 (dt, J = 8.0, 1.3 Hz, 1H), 7.88 (s, 1H), 7.66 (t, J = 8.1 Hz, 1H), 7.32 (ddd, J = 8.3, 7.5, 1.5 Hz, 1H), 7.26 (dd, J = 8.3, 1.5 Hz, 1H), 7.14 (ddd, J = 8.5, 7.4, 1.6 Hz, 1H), 6.92 (t, J = 54.1 Hz, 1H), 3.98 (s, 3H).^{13}C NMR (101 MHz, CDCl$_3$) δ 158.87, 148.24, 143.29(t, J = 27.7 Hz),, 139.43, 136.92, 135.14, 134.01, 130.78, 130.38, 129.07, 128.44, 125.34, 123.96, 123.77, 122.79, 116.11, 111.46(t, J = 234.2 Hz), 39.83.HRMS (ESI): calculated for C$_{18}$H$_{14}$F$_2$N$_4$O$_6$S [M + Na]$^+$: 475.04998, found:475.04948.

2-(3-(Difluoromethyl)-1-Methyl-1H -Pyrazole-4-Carboxamido)Phenyl 4-Nitrobenzenesulfonate (T14)

Light yellow powder, yield 80%. m.p. 198.9-199.6°C.^{1}H NMR (400 MHz, CDCl$_3$) δ 8.24–8.17 (m, 2H), 8.15 (dd, J = 8.3, 1.6 Hz, 1H), 8.07 (s, 1H), 7.99–7.94 (m, 2H), 7.86 (s, 1H), 7.33 (td, J = 7.8, 1.6 Hz, 1H), 7.21 (dd, J = 8.3, 1.6 Hz, 1H), 7.14 (ddd, J = 8.5, 7.3, 1.6 Hz, 1H), 6.88 (t, J = 54.1 Hz, 1H), 3.98 (s, 3H).^{13}C NMR (101 MHz, CDCl$_3$) δ 158.82, 151.19, 144.20(t, J = 26.5 Hz), 140.75, 139.69, 135.60, 130.30, 130.00(×2), 128.42, 125.40, 124.41(×2), 124.16, 123.00, 116.31, 111.61(t, J = 234.7 Hz), 39.81. HRMS (ESI): calculated for C$_{18}$H$_{14}$F$_2$N$_4$O$_6$S [M + Na]$^+$: 475.04998, found:475.04948.

2-(3-(Difluoromethyl)-1-Methyl-1H -Pyrazole-4-Carboxamido)Phenyl 2,5-Dichlorobenzenesulfonate (T15)

Light yellow powder, yield 82%. m.p. 155.6-157.3°C.^{1}H NMR (400 MHz, CDCl$_3$) δ 8.40 (s, 1H), 8.35–8.27 (m, 1H), 8.01 (d, J = 2.4 Hz, 1H), 7.95 (s, 1H), 7.57 (dd, J = 8.6, 2.4 Hz, 1H), 7.52 (d, J = 8.5 Hz, 1H), 7.31 (ddd, J = 8.5, 5.4, 3.5 Hz, 1H), 7.10–7.03 (m, 2H), 7.06 (t, J = 54.1 Hz, 1H), 3.99 (s, 3H).^{13}C NMR (101 MHz, CDCl$_3$) δ 159.52, 145.01(t, J = 26.2 Hz), 138.96, 135.74, 134.44, 133.74, 133.54, 133.36, 132.06, 131.70, 131.01, 128.43, 125.11, 123.77, 122.47, 116.62, 110.43(t, J = 235.3 Hz), 39.93. HRMS (ESI): calculated for C$_{18}$H$_{13}$Cl$_2$F$_2$N$_3$O$_4$S [M + Na]$^+$: 497.98696, found: 497.98602.

2-(3-(Difluoromethyl)-1-Methyl-1H -Pyrazole-4-Carboxamido)Phenyl 3,5-Dichlorobenzenesulfonate (T16)

Gray powder, yield 78%. m.p. 128.9-129.5°C.^{1}H NMR (400 MHz, CDCl$_3$) δ 8.27–8.22 (m, 1H), 8.15 (s, 1H), 7.94 (s, 1H), 7.68 (d, J = 1.9 Hz, 2H), 7.56 (t, J = 1.9 Hz, 1H), 7.33 (ddd, J = 8.5, 5.7, 3.3 Hz, 1H), 7.15–7.12 (m, 2H), 7.06 (t, J = 54.0 Hz, 1H), 3.99 (s, 3H).^{13}C NMR (101 MHz, CDCl$_3$) δ 159.03, 143.78(t, J = 25.6 Hz), 139.33, 137.56, 136.50, 134.78, 134.76, 130.61, 128.44, 126.84(×2), 125.19, 123.82, 122.63, 116.40, 111.22(t, J = 234.9 Hz), 76.84, 39.89. HRMS (ESI): calculated for C$_{18}$H$_{13}$Cl$_2$F$_2$N$_3$O$_4$S [M + Na]$^+$: 497.98696, found: 497.98602.

2-(3-(Difluoromethyl)-1-Methyl-1H-Pyrazole-4-Carboxamido)Phenyl 3,4-Dichlorobenzenesulfonate (T17)

Gray powder, yield 79%. m.p. 173.4-174.4°C.^{1}H NMR (400 MHz, CDCl$_3$) δ 8.18 (dd, J = 8.2, 1.5 Hz, 1H), 8.11 (d, J = 4.1 Hz, 1H), 7.92 (d, J = 2.4 Hz, 2H), 7.56–7.43 (m, 2H), 7.32 (ddd, J = 8.5, 7.0, 1.9 Hz, 1H), 7.20–7.09 (m, 2H), 6.93 (t, J = 54.1 Hz, 1H), 3.99 (s, 3H).^{13}C NMR (101 MHz, CDCl$_3$) δ 158.92, 143.41(t, J = 28.3 Hz), 139.81, 139.59, 135.04, 134.65, 134.32, 131.42, 130.50, 130.29, 128.31, 127.52, 125.24, 123.89, 123.05, 116.33, 111.39(t, J = 234.8 Hz), 39.84.HRMS (ESI): calculated for C$_{18}$H$_{13}$Cl$_2$F$_2$N$_3$O$_4$S [M + Na]$^+$: 497.98696, found: 497.98602.

2-(3-(Difluoromethyl)-1-Methyl-1H-Pyrazole-4-Carboxamido)Phenyl 3,5-Difluorobenzenesulfonate (T18)

Gray powder, yield 86%. m.p. 143.1-144.0°C.^{1}H NMR (400 MHz, CDCl$_3$) δ 8.33–8.12 (m, 2H), 7.94 (s, 1H), 7.45–7.22 (m, 3H), 7.11–7.03 (m, 3H),7.00 (t, J = 54.0 Hz, 1H), 3.98 (s, 3H).^{13}C NMR (101 MHz, CDCl$_3$) δ 164.11, 164.00, 161.57, 161.45, 159.20, 144.23, 143.95, 143.68, 139.45, 137.91, 137.82, 137.73, 134.57, 130.68, 128.36, 125.15, 123.86, 122.38, 116.42, 113.44, 112.50, 112.41, 112.30, 112.21, 111.11, 110.83, 110.58, 110.33(t, J = 235.4 Hz), 39.84. HRMS (ESI): calculated for C$_{18}$H$_{13}$F$_4$N$_3$O$_4$S [M + Na]$^+$:466.04606, found: 466.04663.

2-(3-(Difluoromethyl)-1-Methyl-1 H-Pyrazole-4-Carboxamido)Phenyl 2,5-Difluorobenzenesulfonate (T19)

Light yellow powder, yield 80%. m.p. 141.4-141.6°C.^{1}H NMR (400 MHz, CDCl$_3$) δ 8.33 (s, 1H), 8.29 (dd, J = 8.2, 1.6 Hz, 1H), 7.95 (s, 1H), 7.58 (ddd, J = 7.0, 5.2, 3.2 Hz, 1H), 7.43–7.32 (m, 1H), 7.33–7.27 (m, 1H), 7.25–7.20 (m, 1H), 7.18 (dd, J = 8.1, 1.7 Hz, 2H), 7.09 (t, J = 54.1 Hz, 1H), 7.08 (dd, J = 15.6, 1.6 Hz, 2H), 3.99 (s, 3H).^{13}C NMR (101 MHz, CDCl$_3$) δ 159.50, 159.06, 156.94, 156.55, 154.39, 145.44, 145.18, 144.92, 138.78, 133.15, 130.87, 128.43, 125.06, 124.42, 124.34, 124.27, 124.19, 124.10, 124.04, 123.55, 122.51, 119.42, 119.34, 119.18, 119.10, 118.33, 118.06, 116.57, 112.73, 110.39, 108.05, 39.91. HRMS (ESI): calculated for C$_{18}$H$_{13}$F$_4$N$_3$O$_4$S [M + Na]$^+$: 466.04606, found: 466.04663.

2-(3-(Difluoromethyl)-1-Methyl-1 H-Pyrazole-4-Carboxamido)Phenyl 2,4-Difluorobenzenesulfonate (T20)

light yellow powder, yield 79%. m.p. 148.7-149.6°C.^{1}H NMR (400 MHz, CDCl$_3$) δ 8.36 (s, 1H), 8.30 (dd, J = 8.3, 1.6 Hz, 1H), 7.95 (s, 1H), 7.90 (ddd, J = 8.9, 7.8, 5.9 Hz, 1H), 7.30 (ddd, J = 8.5, 7.4, 1.6 Hz, 1H), 7.15 (dd, J = 8.3, 1.6 Hz, 1H), 7.10–7.05 (m, 1H),7.08 (t, J = 54.1 Hz, 1H), 7.04–6.95 (m, 2H), 4.00 (s, 3H).^{13}C NMR (101 MHz, CDCl$_3$) δ 159.46, 145.53, 138.87, 135.14, 133.40, 133.01, 132.81, 132.69, 130.97, 129.09, 129.00, 128.94, 128.76, 128.36, 124.93, 123.41, 123.01, 121.07, 116.49, 112.41, 110.07, 107.73, 39.90. HRMS (ESI): calculated for C$_{18}$H$_{13}$F$_4$N$_3$O$_4$S [M + Na]$^+$: 466.04606, found: 466.04663.

2-(3-(Difluoromethyl)-1-Methyl-1 H-Pyrazole-4-Carboxamido)Phenyl 2-(Trifluoromethyl)Benzenesulfonate (T21)

Gray powder, yield 69%. m.p. 120.6-121.2°C.^{1}H NMR (400 MHz, CDCl$_3$) δ 8.36 (s, 1H), 8.30 (dd, J = 8.3, 1.6 Hz, 1H), 7.95 (s, 1H), 7.90 (ddd, J = 8.9, 7.8, 5.9 Hz, 1H), 7.30 (ddd, J = 8.5, 7.4, 1.6 Hz, 1H), 7.15 (dd, J = 8.3, 1.6 Hz, 1H), 7.10–7.05 (m, 2H),7.09 (t, J = 54.1 Hz, 1H), 7.04–6.95 (m, 2H), 4.00 (s, 3H).^{13}C NMR (101 MHz, CDCl$_3$) δ 168.62, 166.13, 166.02, 162.04, 161.91, 159.48, 159.31, 145.37, 145.11, 144.85, 138.85, 133.57, 133.46, 133.26, 130.97, 128.36, 125.00, 123.51, 122.57, 119.62, 119.49, 116.67, 112.78, 112.75, 112.56, 112.53, 110.44, 108.10, 106.65, 106.41, 106.39, 106.15, 39.92.HRMS (ESI): calculated for C$_{19}$H$_{14}$F$_5$N$_3$O$_4$S [M + Na]$^+$: 498.05229, found: 498.05078.

2-(3-(Difluoromethyl)-1-Methyl-1 H-Pyrazole-3-Carboxamido)Phenyl 3-(Trifluoromethyl)Benzenesulfonate (T22)

Light yellow powder, yield 73%. m.p. 147.2-148.3°C.^{1}H NMR (400 MHz, CDCl$_3$) δ 8.27–8.15 (m, 2H), 8.12 (s, 1H), 7.92 (d, J = 7.8 Hz, 1H), 7.91 (s, 1H), 7.87 (d, J = 7.9 Hz, 1H), 7.62 (t, J = 7.9 Hz, 1H), 7.29 (ddd, J = 8.6, 5.8, 3.1 Hz, 1H), 7.13–7.03 (m, 2H), 6.96 (t, J = 54.1 Hz, 1H), 3.97 (s, 3H).^{13}C NMR (101 MHz, CDCl$_3$) δ 159.09, 144.17, 143.89, 143.62, 139.32, 136.04, 134.52, 132.64, 132.30, 131.96, 131.82, 131.63, 131.46, 131.43, 131.39, 131.36, 130.75, 130.30, 128.28, 125.69, 125.65, 125.62, 125.58, 125.02, 124.22, 123.59, 122.64, 121.50, 116.36, 113.43, 111.11, 108.78, 39.79.HRMS (ESI): calculated for C$_{19}$H$_{14}$F$_5$N$_3$O$_4$S [M + Na]$^+$: 498.05229, found: 498.05078.

2-(3-(Difluoromethyl)-1-Methyl-1 H-Pyrazole-4-Carboxamido)Phenyl 4-Methoxybenzenesulfonate (T23)

Gray powder, yield 83%. m.p. 130.0-131.1°C.^{1}H NMR (400 MHz, CDCl$_3$) δ 8.35 (s, 1H), 8.28 (dd, J = 8.2, 1.6 Hz, 1H), 7.91 (s, 1H), 7.78–7.70 (m, 2H), 7.30–7.23 (m, 1H), 7.09 (t, J = 54.0 Hz, 1H), 7.01 (td, J = 7.8, 1.6 Hz, 1H), 6.93-6.86 (m, 3H), 4.00 (s, 3H), 3.86 (s, 3H).^{13}C NMR (101 MHz, CDCl$_3$) δ 164.70, 159.36, 144.97(t, J = 25.8 Hz), 139.56, 133.27, 131.15, 131.02(×2), 127.90, 125.68, 124.72, 123.18, 122.93, 116.83, 114.64(×2), 110.48(t, J = 235.4 Hz), 55.93, 39.90.HRMS (ESI): calculated for C$_{19}$H$_{17}$F$_2$N$_3$O$_5$S [M + Na]$^+$: 460.07547, found: 460.07503.

2-(3-(Difluoromethyl)-1-Methyl-1 H-Pyrazole-4-Carboxamido)Phenyl Phenylmethanesulfonate (T24)

Light yellow powder, yield 83%. m.p. 123.4-124.2°C. ^{1}H NMR (400 MHz, CDCl$_3$) δ 8.35 (dd, J = 8.3, 1.6 Hz, 1H), 8.27 (s, 1H), 7.68 (s, 1H), 7.51–7.44 (m, 2H), 7.40 (dd, J = 5.0, 2.0 Hz, 3H), 7.31 (td, J = 7.9, 1.5 Hz, 1H), 7.20 (m, 1H),7.15 (t, J = 54.0 Hz, 1H), 7.09 (td, J = 7.8, 1.6 Hz, 1H), 7.02–6.97 (m, 1H), 4.65 (s, 2H), 3.97 (s, 3H). ^{13}C NMR (101 MHz, CDCl3) δ 159.54, 145.26(t, J = 25.8 Hz),138.25-132.95, 131.24, 131.09(×2), 129.67, 129.24, 128.23(×2), 126.88, 125.03, 123.19, 122.90,115.83,110.39 (t, J = 235.4 Hz), 57.29, 39.92. HRMS (ESI): calculated for C$_{19}$H$_{17}$F$_2$N$_3$O$_4$S [M + Na]$^+$:444.08055, found: 448.07975.

2-(3-(Difluoromethyl)-1-Methyl-1 H-Pyrazole-4-Carboxamido)Phenyl Naphthalene-2-Sulfonate (T25)

Light yellow powder, yield 80%. m.p. 158.7-159.5°C. ^{1}H NMR (400 MHz, CDCl$_3$) δ 8.43 (d, J = 1.9 Hz, 1H), 8.30–8.17 (m, 2H), 7.94–7.81 (m, 3H), 7.71 (ddd, J = 13.8, 8.5, 1.6 Hz, 2H), 7.65–7.58 (m, 2H), 7.31–7.21 (m, 1H), 7.04–6.99 (m, 2H), 6.98 (t, J = 54.1 Hz, 1H), 3.90 (s, 3H). ^{13}C NMR (101 MHz, CDCl$_3$) δ 159.11, 144.39(t, J = 25.7 Hz), 139.66, 135.70, 133.52, 131.91, 131.81, 130.94, 130.72, 129.89, 129.82, 129.55, 128.15, 128.01, 128.00, 124.87, 123.32, 123.04, 122.76, 116.48, 110.66 (t, J = 234.8 Hz, 1H), 39.76. HRMS (ESI): calculated for C$_{22}$H$_{17}$F$_2$N$_3$O$_4$S [M + Na]$^+$:480.08055, found: 448.08005.

2-(3-(Difluoromethyl)-1-Methyl-1 H-Pyrazole-4-Carboxamido)Phenyl 2,4,6-Trimethylbenzenesulfonate (T26)

White powder, yield 81%. m.p. 155.0-155.4°C. ^{1}H NMR (400 MHz, CDCl$_3$) δ 8.56 (s, 1H), 8.35 (dd, J = 8.3, 1.6 Hz, 1H), 7.95 (s, 1H), 7.28–7.23 (m, 1H), 7.15 (t, J = 54.1 Hz, 1H), 7.01 (s, 2H), 6.91 (td, J = 7.8, 1.6 Hz, 1H), 6.52 (dd, J = 8.2, 1.5 Hz, 1H), 4.01 (s, 3H), 2.55 (s, 6H), 2.35 (s, 3H). ^{13}C NMR (101 MHz, CDCl$_3$) δ 159.50, 145.40 (t, J = 25.3 Hz), 144.77, 140.77(×2), 139.25, 132.64, 132.05(×2), 131.52, 129.59, 127.78, 124.57, 123.25, 121.97, 116.80, 110.09 (t, J = 234.8Hz, 1H), 39.85, 22.85(×2), 21.23.HRMS (ESI): calculated for C$_{21}$H$_{21}$F$_2$N$_3$O$_4$S [M + Na]$^+$: 472.11185, found: 472.11150.

2-(3-(Difluoromethyl)-1-Methyl-1H -Pyrazole-4-Carboxamido)Phenyl 4-(Tert-butyl)Benzenesulfonate (T27)

Light yellow powder, yield 82%. m.p.149.7-150.5°C. ^{1}H NMR (400 MHz, CDCl$_3$) δ 8.41 (s, 1H), 8.31 (dd, J = 8.3, 1.6 Hz, 1H), 7.94 (s, 1H), 7.81–7.73 (m, 2H), 7.56–7.46 (m, 2H), 7.26 (td, J = 7.8, 1.5 Hz, 1H),7.11 (t, J = 54.1 Hz, 1H), 7.00 (td, J = 7.9, 1.6 Hz, 1H), 6.89 (dd, J = 8.2, 1.5 Hz, 1H), 4.00 (s, 3H), 1.32 (s, 9H). ^{13}C NMR (101 MHz, CDCl$_3$) δ 159.33, 159.29, 145.04(t, J = 25.2 Hz), 139.43, 133.31, 131.48, 131.22, 128.57(×2), 127.93,

126.46(×2), 124.66, 123.12, 122.75, 116.81, 110.45 (t, J = 236.3 Hz), 39.91, 35.54, 31.05(×3). HRMS (ESI): calculated for C$_{22}$H$_{23}$F$_2$N$_3$O$_4$S [M + Na]$^+$: 486.12750, found: 486.12686.

In Vitro Biological Evaluation

In Vitro Antifungal Assay

The test strains were Colletotrichum camelliae (C.camelliae), Pestalotiopsis theae (P. theae) provided by Guizhou Tea Research Institute, and Gibberella zeae (G. zeae), Rhizoctonia solani (R. solani) provided by Guizhou Institute of Plant Protection. In this study, the *in vitro* antifungal activity of the target compounds **T1-27** against four plant pathogens was screened by the mycelial growth rate method (Zhang et al., 2019). The tested compounds were dissolved in DMSO to prepare a 10 mg/ml stock solution before mixing with PDA. The PDA containing compounds at a concentration of 50 mg/L were then poured into sterilized Petri dishes for primary screening. Data Processing System (DPS, V9.50) was used for statistical analysis of test data, and Duncan's new multiple range method was used to test the significance of differences. The EC$_{50}$ values and 95% confidence limits were calculated after testing the inhibition rates, based on the above method. The inhibition rate of the potent compounds was further tested and the corresponding EC$_{50}$ values were calculated by using DPS. This test method is provided in the Supporting information.

In Vivo Antiviral Activities Assay

The *in vivo* antiviral activities of target compounds **T1-27** against TMV were tested by the half leaf blight spot method previously reported in the literature(Chen et al., 2021; Xie et al., 2018). TMV was propagated in Nicotiana tabacum cv. K326 by the Gooding method. Antiviral activities of the target compounds against TMV *in vivo* were at 500 mg/L. The commercial antiviral agents Ningnanmycin and Chitosan oligosaccharides were severed as the positive controls. Data is processed in the same way as that of antifungal activity.

RESULTS AND DISCUSSION

Chemistry

The reaction between the starting material, ethyl 4,4-difluoro-3-oxobutanoate **1**) and triethyl orthoformate in acetic anhydride at 140°C, yielded ethyl 2-(ethoxymethylene)-4,4-difluoro-3-oxobutanoate (compound **2**) (Sun and Zhou, 2015). Compound **2** was then treated with methylhydrazine to yield compound **3**, which was successively hydrolyzed with lithium hydroxide and hydrochloric acid to obtain a white solid of the key intermediate 3-(difluoromethyl)-1-methyl-1H-pyrazole-4-carboxylic acid (compound **4**) (**Scheme 1**). Thereafter, compound **6,** a light yellow solid, was formed by conjugating compound **4** with 2-aminophenol in CH$_2$Cl$_2$ using EDCI and DMAP (**Scheme 2**). Finally, different substituted moieties of arylsulfonyl chloride were reacted with compound **5** to yield

the target compounds (**Scheme 3**). The structures of all key intermediates and target compounds were confirmed *via* ^{1}H and ^{13}C NMR and HRMS, and their spectra data are shown in the **Supplementary Material**. The single-crystal X-ray diffraction of compound **T22** showed that the compound is a sulfonate and not a sulfonamide. **Figure 1** shows the crystal structure of **T22**, whose deposition number is CCDC 2168151.

In Vitro Biological Evaluation
In Vitro Antifungal Assay

The preliminary *in vitro* antifungal activities of the 27 target compounds are presented in **Tables 1**, **2**. Most of the target compounds exhibited some degree of antifungal activities against the four plant pathogens at 50 µg/ml (**Table 1**). Among the four plant pathogens, the target compounds, particularly **T24,** exhibited remarkable antifungal activity against R. solani. When R group was nitro group, the antifugal activity against R. solani was no more than 20%. It can be known from these data that the substituent on the benzene ring was a strong electron-withdrawing group, the antifungal activity was adversely affected. We also found that the activity of **T24** against R. solani was much higher than that of **T1** (**Table 1**). The only structural difference between these two compounds is the presence of an extra methylene group in **T24**, which is thought to enhance its antifungal activity. The compound **T24** (EC_{50} = 0.45 mg/L) was superior to the commercial fungicide hymexazol (EC_{50} = 10.49 mg/L), but closer to bixafen (EC_{50} = 0.25 mg/L) in its activity against R. solani (**Table 2**).

In Vivo Antiviral Activities of Compounds T1-27

The phenylsulfonyl fragment has been reported to increase the antiviral activity (Hadházi et al., 2017), we synthesised novel sulfonate scaffold-containing pyrazolecarbamide and evaluated their antiviral activities.The curative, protective, and inactivation effects of the 27 target compounds against TMV were evaluated using the half leaf blight spot method (Liu et al., 2021; Zhang et al., 2021), and the commercial agents, Ningnanmycin and Chitosan oligosaccharide, served as positive controls. Compound **T18** (54.2%) exhibited a close curative activity to ningnanmycin (55.3%) at 500 mg/ml. Additionally, most of the target compounds exhibited protective effects *in vivo*, and the protective effects of compounds **T5** (50.4%) and **T12** (50.2%) were similar to that of Ningnanmycin (50.7%). Although the target compounds had lower inactivation effects than ningnanmycin, most of them exhibited better inactivation activities than Chitosan oligosaccharides (**Table 3**).

CONCLUSION

In summary, 27 novel pyrazolecarbamide derivatives bearing a sulfonate fragment were synthesized and screened for their *in vitro* antifungal and *in vivo* antiviral activities against four plant pathogens (C. camelliae, P, theae, G. zeae, and R. solani). The structures of these compounds were identified using the single-crystal X-ray diffraction and spectral data obtained *via* ^{1}H and ^{13}C NMR and HRMS spectroscopy. The preliminary bioassay results showed that the target compounds exhibited certain inhibitory activities against the test fungi and TMV. Compound **T24** exhibited excellent antifungal activities against R. solani compared to the commercial fungicide hymexazol, almost similar to bixafen. Moreover, the target compounds displayed protective effects *in vivo* against TMV. Thus, our research group is conducting further structural optimization of the target compounds for wide-scale field application.

DATA AVAILABILITY STATEMENT

The original contributions presented in the study are included in the article/**Supplementary Material**, further inquiries can be directed to the corresponding author.

AUTHOR CONTRIBUTIONS

Z-WL and WY conceived and designed the paper. Z-WL and HL contributed to the synthesis, purification, characterization of all compounds. JY and CM performed the biological activity research. Z-WL wrote the manuscript. All authors have read and reviewed the manuscript.

ACKNOWLEDGMENTS

SUPPLEMENTARY MATERIAL

The Supplementary Material for this article can be found online at: https://www.frontiersin.org/articles/10.3389/fchem.2022.928842/full#supplementary-material

REFERENCES

Chen, M., Su, S., Zhou, Q., Tang, X., Liu, T., Peng, F., et al. (2021). Antibacterial and Antiviral Activities and Action Mechanism of Flavonoid Derivatives with a Benzimidazole Moiety. *J. Saudi Chem. Soc.* 25, 101194. doi:10.1016/j.jscs.2020.101194

El Shehry, M. F., Ghorab, M. M., Abbas, S. Y., Fayed, E. A., Shedid, S. A., and Ammar, Y. A. (2018). Quinoline Derivatives Bearing Pyrazole Moiety: Synthesis and Biological Evaluation as Possible Antibacterial and Antifungal Agents. *Eur. J. Med. Chem.* 143, 1463–1473. doi:10.1016/j.ejmech.2017.10.046

Fisher, M. C., Henk, D. A., Briggs, C. J., Brownstein, J. S., Madoff, L. C., McCraw, S. L., et al. (2012). Emerging Fungal Threats to Animal, Plant and Ecosystem Health. *Nature* 484, 186–194. doi:10.1038/nature10947

Hadházi, Á., Pascolutti, M., Bailly, B., Dyason, J. C., Borbás, A., Thomson, R. J., et al. (2017). A Sialosyl Sulfonate as a Potent Inhibitor of Influenza Virus Replication. *Org. Biomol. Chem.* 15, 5249–5253. doi:10.1039/C7OB00947J

Huang, T.-J., Chuang, H., Liang, Y.-C., Lin, H.-H., Horng, J.-C., Kuo, Y.-C., et al. (2015). Design, Synthesis, and Bioevaluation of Paeonol Derivatives as Potential Anti-HBV Agents. *Eur. J. Med. Chem.* 90, 428–435. doi:10.1016/j.ejmech.2014.11.050

Jiang, X., Wei, X., Lin, F., Zhang, Z., Yao, G., Yang, S., et al. (2020). Substrate-Controlled [5+1] Annulation of 5-Amino-1H -phenylpyrazoles with Alkenes: Divergent Synthesis of Multisubstituted 4,5-Dihydropyrazolo[1,5-A] quinazolines. *Eur. J. Org. Chem.* 2020, 3997–4003. doi:10.1002/ejoc.202000536

Kang, G.-Q., Duan, W.-G., Lin, G.-S., Yu, Y.-P., Wang, X.-Y., and Lu, S.-Z. (2019). Synthesis of Bioactive Compounds from 3-Carene (II): Synthesis, Antifungal Activity and 3D-QSAR Study of (Z)- and (E)-3-Caren-5-One Oxime Sulfonates. *Molecules* 24 (3), 477. doi:10.3390/molecules24030477

Kanungo, M., and Joshi, J. (2014). Impact of Pyraclostrobin (F-500) on Crop Plants. *Plant Sci. Today.* 1, 174–178. doi:10.14719/pst.2014.1.3.60

Kasiotis, K. M., Tzanetou, E. N., and Haroutounian, S. A. (2014). Pyrazoles as Potential Anti-angiogenesis Agents: A Contemporary Overview. *Front. Chem.* 2, 78. doi:10.3389/fchem.2014.00078

Liu, T., Peng, F., Cao, X., Liu, F., Wang, Q., Liu, L., et al. (2021). Design, Synthesis, Antibacterial Activity, Antiviral Activity, and Mechanism of Myricetin Derivatives Containing a Quinazolinone Moiety. *ACS Omega* 6, 30826–30833. doi:10.1021/acsomega.1c05256

Mu, J.-X., Shi, Y.-X., Yang, M.-Y., Sun, Z.-H., Liu, X.-H., Li, B.-J., et al. (2016). Design, Synthesis, DFT Study and Antifungal Activity of Pyrazolecarboxamide Derivatives. *Molecules* 21 (1), 68. doi:10.3390/molecules21010068

Saleh, N. M., El-Gazzar, M. G., Aly, H. M., and Othman, R. A. (2020). Novel Anticancer Fused Pyrazole Derivatives as EGFR and VEGFR-2 Dual TK Inhibitors. *Front. Chem.* 7, 917. doi:10.3389/fchem.2019.00917

Si, W.-J., Wang, X.-B., Chen, M., Wang, M.-Q., Lu, A.-M., and Yang, C.-L. (2019). Design, Synthesis, Antifungal Activity and 3D-QSAR Study of Novel Pyrazole Carboxamide and Niacinamide Derivatives Containing Benzimidazole Moiety. *New J. Chem.* 43, 3000–3010. doi:10.1039/C8NJ05150J

Su, S., Zhou, Q., Tang, X., Peng, F., Liu, T., Liu, L., et al. (2021). Design, Synthesis, and Antibacterial Activity of Novel Myricetin Derivatives Containing Sulfonate. *Monatsh. Chem.* 152, 345–356. doi:10.1007/s00706-021-02739-1

Sun, J., and Zhou, Y. (2015). Synthesis and Antifungal Activity of the Derivatives of Novel Pyrazole Carboxamide and Isoxazolol Pyrazole Carboxylate. *Molecules* 20, 4383–4394. doi:10.3390/molecules20034383

Sun, R., Wang, Z., Li, Y., Xiong, L., Liu, Y., and Wang, Q. (2013). Design, Synthesis, and Insecticidal Evaluation of New Benzoylureas Containing Amide and Sulfonate Groups Based on the Sulfonylurea Receptor Protein Binding Site for Diflubenzuron and Glibenclamide. *J. Agric. Food Chem.* 61, 517–522. doi:10.1021/jf304468b

Wang, R., Zhi, X., Li, J., and Xu, H. (2015). Synthesis of Novel Oxime Sulfonate Derivatives of 2′(2′,6′)-(Di)chloropicropodophyllotoxins as Insecticidal Agents. *J. Agric. Food Chem.* 63, 6668–6674. doi:10.1021/acs.jafc.5b02036

Wang, X., Wang, A., Qiu, L., Chen, M., Lu, A., Li, G., et al. (2020). Expedient Discovery for Novel Antifungal Leads Targeting Succinate Dehydrogenase: Pyrazole-4-Formylhydrazide Derivatives Bearing a Diphenyl Ether Fragment. *J. Agric. Food Chem.* 68, 14426–14437. doi:10.1021/acs.jafc.0c03736

Wang, X., Wang, X., Zhou, B., Long, J., and Li, P. (2021). Design, Synthesis, and Evaluation of New 4(3 H)-quinazolinone Derivatives Containing a Pyrazole Carboxamide Moiety. *J. Heterocycl. Chem.* 58, 2109–2116. doi:10.1002/jhet.4334

Wei, C., Zhao, L., Sun, Z., Hu, D., and Song, B. (2020). Discovery of Novel Indole Derivatives Containing Dithioacetal as Potential Antiviral Agents for Plants. *Pestic. Biochem. Physiol.* 166, 104568. doi:10.1016/j.pestbp.2020.104568

Wu, J., Song, B.-A., Hu, D.-Y., Yue, M., and Yang, S. (2012). Design, Synthesis and Insecticidal Activities of Novel Pyrazole Amides Containing Hydrazone Substructures. *Pest. Manag. Sci.* 68 (5), 801–810. doi:10.1002/ps.2329

Xie, D., Shi, J., Zhang, A., Lei, Z., Zu, G., Fu, Y., et al. (2018). Syntheses, Antiviral Activities and Induced Resistance Mechanisms of Novel Quinazoline Derivatives Containing a Dithioacetal Moiety. *Bioorg. Chem.* 80, 433–443. doi:10.1016/j.bioorg.2018.06.026

Yan, Z., Liu, A., Huang, M., Liu, M., Pei, H., Huang, L., et al. (2018). Design, Synthesis, DFT Study and Antifungal Activity of the Derivatives of Pyrazolecarboxamide Containing Thiazole or Oxazole Ring. *Eur. J. Med. Chem.* 149, 170–181. doi:10.1016/j.ejmech.2018.02.036

Zeng, X.-W., Huang, N., Xu, H., Yang, W.-B., Yang, L.-M., Qu, H., et al. (2010). Anti Human Immunodeficiency Virus Type 1 (HIV-1) Agents 4. Discovery of 5,5'-(p-Phenylenebisazo)-8-Hydroxyquinoline Sulfonates as New HIV-1 Inhibitors In Vitro. *Chem. Pharm. Bull.* 58, 976–979. doi:10.1248/cpb.58.976

Zhang, A., Yue, Y., Yang, J., Shi, J., Tao, K., Jin, H., et al. (2019). Design, Synthesis, and Antifungal Activities of Novel Aromatic Carboxamides Containing a Diphenylamine Scaffold. *J. Agric. Food Chem.* 67, 5008–5016. doi:10.1021/acs.jafc.9b00151

Zhang, J., He, F., Chen, J., Wang, Y., Yang, Y., Hu, D., et al. (2021). Purine Nucleoside Derivatives Containing a Sulfa Ethylamine Moiety: Design, Synthesis, Antiviral Activity, and Mechanism. *J. Agric. Food Chem.* 69, 5575–5582. doi:10.1021/acs.jafc.0c06612

Zhou, Q., Tang, X., Chen, S., Zhan, W., Hu, D., Zhou, R., et al. (2022). Design, Synthesis, and Antifungal Activity of Novel Chalcone Derivatives Containing a Piperazine Fragment. *J. Agric. Food Chem.* 70, 1029–1036. doi:10.1021/acs.jafc.1c05933

Conflict of Interest: The authors declare that the research was conducted in the absence of any commercial or financial relationships that could be construed as a potential conflict of interest.

Publisher's Note: All claims expressed in this article are solely those of the authors and do not necessarily represent those of their affiliated organizations, or those of the publisher, the editors and the reviewers. Any product that may be evaluated in this article, or claim that may be made by its manufacturer, is not guaranteed or endorsed by the publisher.

frontiers | Frontiers in Chemistry

Laboratory Screening of Control Agents Against Isolated Fungal Pathogens Causing Postharvest Diseases of Pitaya in Guizhou, China

Yong Li[†], Haijiang Chen*[†], Lan Ma, Youshan An, Hui Wang and Wenneng Wu*

Food and Pharmaceutical Engineering Institute, Guiyang University, Guiyang, China

Pitaya, or dragon fruit, is a typical tropical fruit with an appealing taste and diverse health benefits to humans. The plantation of pitaya in Guizhou province in China has greatly boosted the income of local farmers and alleviated poverty. However, the frequent occurrence of postharvest diseases has brought large economic loss. To find a solution, we set out to identify the postharvest disease-causing agents of Guizhou pitaya. Several fungi were isolated from diseased pitaya and identified as species based on the ITS1 sequence similarity. Of them, *Penicillium spinulosum*, *Phoma herbarum*, *Nemania bipapillata*, and *Aspergillus oryzae* were, for the first time, found to cause dragon fruit disease. In consideration of their prevalence in postharvest fruit diseases, *Alternaria alternata* H8 and *Fusarium proliferatum* H4 were chosen as representative pathogens for the drug susceptibility test. Among the tested drugs and plant extracts, 430 g/L tebuconazole and 45% prochloraz were found to be the most potent fungicides against H8 and H4, respectively. The research provides insights into the mechanism and control of postharvest diseases of dragon fruits in Guizhou, China, and thus could be of economic and social significance to local farmers and the government.

Keywords: pitaya, postharvest disease, pathogen identification, drug sensitivity test, plant extracts

INTRODUCTION

Dragon fruit or pitaya (*Hylocereus species*) belongs to the family Cataceae, which is a typical tropical fruit. Since its introduction to Guizhou province in 2001 (Wang et al., 2018), the fruit has been shown to be quite adapted to the local climate and ecology. So far, three varieties, purple dragon, crystal red dragon, and pink dragon, have been introduced and cultivated in Guizhou, and the dragon fruit-planting area in Guizhou province has increased to be the third in China (Wang et al., 2018). With its renowned health benefits to consumers and appealing taste, the locally produced dragon fruit is widely accepted in the domestic market. Dragon fruit cultivation in Guizhou province has greatly boosted the local economy and been lifting local farmers out of poverty. With the planting history and area growing, the incidences of dragon fruit diseases are increasingly more frequent, especially the postharvest diseases, which lead to the decline of the yield and quality of marketable dragon fruits, affecting the economic benefits ultimately.

Due to the interruption of nutrient supply, the vitality of the postharvest dragon fruits was weakened, the disease resistance was reduced, and they could be infected easily by pathogenic microorganisms during storage and transportation, resulting in illness. At present, there are kinds of diseases caused by microorganisms such as anthracnose, soft rot, canker, black spot, and

wilts in dragon fruit after harvest (Balendres and Bengoa, 2019). Among them, fungal diseases are more common and serious. Dragon fruit anthracnose was usually caused by *Colletotrichum gloeosporioides* (Masyahit et al., 2009) and *C. truncatum* (Guo et al., 2014). The pathogens that cause black spot disease of dragon fruit were reported to be *Alternaria alternata* (Castro et al., 2017) and *Bipolaris cactivora* (Tarnowski et al., 2010; Ben-Ze Ev et al., 2011). Dragon fruit soft rot is found to be caused by *Neoscytalidium dimidiatum* (Pan et al., 2021) and *Gilbertella persicaria* (Guo et al., 2012). However, there are few reports focusing on causative agents and control methods for postharvest diseases of dragon fruits in the Guizhou area.

In order to investigate the microbial species causing postharvest diseases on dragon fruits in Guizhou, samples of diseased dragon fruits were collected from the Luodian County of Guizhou province in China. Microbes were isolated from diseased fruit tissue and reinoculated on healthy fruits to confirm pathogenicity according to Koch's rule. Pathogenic microorganisms were identified by rDNA-ITS sequence similarity analysis. Finally, a variety of prevention and control reagents were screened for inhibition efficacy against selected pathogens by an indoor experiment. This study provides a helpful understanding of the mechanism of postharvest diseases and control measures for dragon fruits in Guizhou province and the neighboring area.

MATERIALS AND METHODS

Sample Collection and Microbial Isolation

Samples of diseased dragon fruits were collected in Luodian County in Guizhou Province. Pathogenic microorganisms were isolated by conventional tissue isolation methods in the laboratory. The potato dextrose agar (PDA) plates were used for separation and purification. The isolated strains were stored at −20°C in 40% glycerol.

Pathogenicity Test

Healthy dragon fruits were selected and soaked in 75% alcohol for 1 min, followed by repeated washes in sterile water, and surface-dried. Mycelia "cakes" (blank agar "cakes" as control) were chopped aseptically from the culture plate and placed onto the surface (non-injury inoculation) and the stabbing wound (stab inoculation) of dragon fruits, which was then allowed to incubate at 28°C, and the status of infection was observed along during incubation.

Morphological Characterization of Pathogens

The pathogenic microorganisms were cultured on PDA and incubated at 28°C. The colony morphology was checked regularly, and the mycelia were observed under a Model EX30 inverted microscope (Ningbo Shunyu Tech. Co. Ltd., Zhejiang, China).

DNA Extraction and Molecular Identification

The fungus was cultured in potato dextrose broth (PDB) at 28°C for 3 days, and the mycelia were collected for genomic DNA (gDNA) extraction. Fungal gDNA was extracted according to the users' instruction of the fungal genomic DNA rapid extraction kit (Sangon). The rDNA-ITS1 fragment of the gDNA was PCR-amplified using universal ITS1 primers and subjected to nucleotide sequencing. All the obtained sequences were searched for similarity against the NCBI nucleotide collection (nr) database with default parameters (https://blast.ncbi.nlm.nih.gov/Blast.cgi?PROGRAM=blastn&PAGE_TYPE=BlastSearch&LINK_LOC=blasthome). The phylogenetic tree was constructed using the neighbor-joining method to determine the taxonomic status.

Preparation of Tested Fungicides and Plant Extracts

All tested fungicides are commercially available. The plant extracts were prepared as such: the plant was air-dried and milled to powder. For the procedure, 10 g of the powder was extracted with 95% ethanol and heated for 4 h with refluxing. The extract was filtered and evaporated under reduced pressure. The residue was re-dissolved with hot water, cooled, and adjusted to a concentration of 500 mg/mL as stock solution.

Indoor Screening for Control Agents

Tested fungicide or plant extracts (Tween 20 as control) with appropriate quantity was added to melted PDA and cooled to make plates. The plates were then inoculated by placing an inoculum (4 mm disc from cultures of *A. alternata* and *F. proliferatum*) at the center and incubated at the ambient temperature of 28°C. Each test was performed in triplicate. After 6 days of incubation, the colony diameter was recorded, and the inhibition rate was calculated using the following formula:

$$\text{Inhibition rate} = \frac{diameter\ of\ control - diameter\ of\ treatment}{diameter\ of\ control - 4\ mm} \times 100\%.$$

Furthermore, the efficacy for the tested control agent was expressed as the half-maximal effective concentration (EC$_{50}$, the concentration at which the tested fungicide reduced mycelial growth by 50%) determined by regression of the inhibition rate against the log10 values of the fungicide concentrations.

RESULTS

Isolation and Purification of Pathogenic Fungi

A number of fungal isolates were separated from diseased dragon fruit tissue, and seven fungal strains were preliminarily established based on colony and mycelium morphology and labeled as H1, H2, H4, H6, H7, H8, and H9. Colony and conidia morphology are shown in **Figure 1**. The appearance of
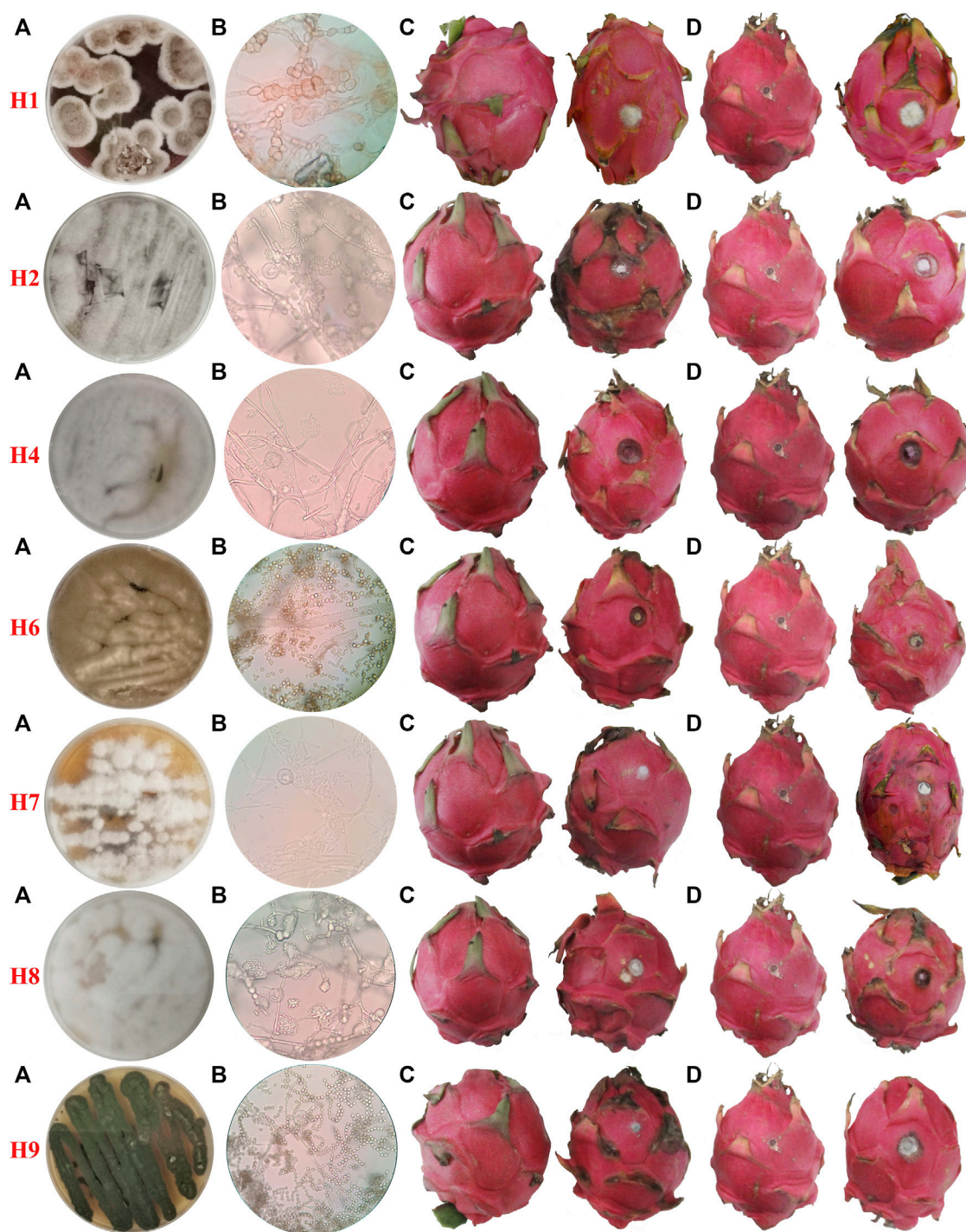
FIGURE 1 | Morphological characteristics of pathogens and pathogenicity confirmation. **(A)** Colony morphology on the PDA plate. **(B)** Microscopic image of conidia taken with ×400 magnification, **(C)** non-injury inoculation, and **(D)** injury inoculation; fruits on the right were inoculated with mycelia "cakes," and the ones on the left are blank controls.

the H1 colony on PDA is brown with white slowly growing edges. The spores are elliptical to round with varying sizes but connected in tandem to each other. The H2 colony is whitish gray and grows fast. Its spores are rod-shaped under the

microscope and distributed around the mycelia. The H4 strain colony exhibits a white appearance and grows fast with elliptical spores arranged in clusters around the top of the spore stalk. The colony of strain H6 is yellowish-brown

Strains	Taxonomy	Sequence similarity (%)	Top hit
H1	*Phoma herbarum*	99	MT367635.1
H2	*Colletotrichum nymphaeae*	100	MW217266.1
H4	*Alternaria alternata*	100	MN944587.1
H6	*Aspergillus oryzae*	99	MH345908.1
H7	*Penicillium spinulosum*	100	JQ639057.1
H8	*Fusarium proliferatum*	99	MG543763.1
H9	*Nemania bipapillata*	99	JQ341104.1

FIGURE 2 | Molecular phylogenetic tree based on the rDNA-ITS sequence similarity. Sequence alignment and tree building were performed by MEGA5.0 using the neighbor-joining method, and phylogeny was tested by 500 bootstrap replications. The numbers on branches were calculated as bootstrap values. Accession numbers of ITS1 sequences from isolated strains were, namely, ON514545.1 (H1), ON514546.1 (H2), ON514547.1 (H4), ON514548.1 (H6), ON514549.1 (H7), ON514550.1 (H8), and ON514551.1 (H9).

with dense hyphae, and the spores appear round when observed under a microscope. The H7 colony is white in appearance and grows slowly on PDA. The spores are irregularly rod-shaped. The H8 colony is white with dense mycelia. The spores are oval under the microscope and densely clustered around spore stalks. The H9 colony is dark green and grows fast; the spores are spherical and connected in tandem to each other to form long chains.

Pathogenicity of Isolated Microorganisms

The isolated strains were re-inoculated onto fruits in two ways, a non-injured inoculation and a stab-injured inoculation. As shown in **Figure 1**, all the seven strains can infect dragon fruits with or without an injury. Despite the presence of a stabbing wound, no observable infection occurred in control experiments where blank agar was used for 'inoculation'.

Taxonomic Identification

The ITS1 segments were PCR-amplified from corresponding genomic DNA extracted from the seven pathogenic fungi. Their nucleotide sequences were used as a query for blast searches, and top hits are listed in **Table 1**. According to the search results, the pathogenic strains were roughly assigned as *Phoma herbarum* H1, *Colletotrichum nymphaeae* H2, *Alternaria alternata* H4, *Aspergillus oryzae* H6, *Penicillium spinulosum* H7, *Fusarium proliferatum* H8, and *Nemania bipapillata* H9. Phylogenetic relationships based on the ITS1 sequence similarity between the strains and selected top hits are illustrated in **Figure 2**.

Preliminary Screening of Agro-Agents for Fungicides Against Representative Pathogenic Fungi

In consideration of the prevalence of *A. alternata* and *F. proliferatum* in fruit disease, the two strains H4 and H8 were chosen as representative pathogenic microorganisms of dragon fruit and tested their susceptibility to a series of agricultural agents. As shown in **Table 2**, a total of 20 agro-agents were screened for indoor toxicity at concentrations of 50 μg/ml and 10 μg/ml on *A. alternata* H4 and *F. proliferatum* H8. For *A. alternata* H4, at 50 μg/ml concentration, 10% difenoconazole, 430 g/L tebuconazole, and 3% zhongshengmycin showed the highest inhibition rate, while at 10 μg/ml concentration, 10% difenoconazole, 430 g/L tebuconazole, 50% iprodione were the three most potent candidates. For *F. proliferatum* H8, 3% benziothiazolinone, 430 g/L tebuconazole, and 45% prochloraz exhibited the highest toxicity at a concentration of 50 μg/ml, while at the 10 μg/ml level, 10% difenoconazole, 50% iprodione, and 45% prochloraz were the top three candidates. Notably, three microbial preparations were included in the screening; the insecticidal *Beauveria bassiana* showed the highest inhibition rate at 50 μg/ml concentration, and the fungicidal *Bacillus cereus* was the most potent at 10 μg/ml.

Inhibition Effect of 10 Edible and Medicinal Plant Extracts on the Tested Fungus

The ethanol extract was obtained from 10 edible and medicinal plants, namely, *Houttuynia cordata* Thunb, *Mentha haplocalyx*, *Zanthoxylum bungeanum* Maxim, *Lonicera japonica* Thunb, *Dendrobium officinale* Kimura et Migo, *Piper nigrum*, *Zingiber officinale* Roscoe, *Gastrodia elata*, *Schisandra chinensis*, and *Illicium verum*. Some of the plants are renowned for their microbe-inhibitory activity. The inhibition rate results in this

TABLE 2 | Inhibitory effects of 20 agro-agents at the concentrations of 50 µg/ml and 10 µg/ml on *A. alternata* H4 and *F. proliferatum* H8.

Agro-agents	Inhibition rate (%)			
	50 µg/ml		10 µg/ml	
	A. alternata H4	*F. proliferatum* H8	*A. alternata* H4	*F. proliferatum* H8
80% mancozeb	47.39 ± 1.72	33.52 ± 2.34	6.43 ± 1.93	17.96 ± 1.51
10% difenoconazole	92.46 ± 2.85	87.92 ± 3.60	80.76 ± 2.93	82.93 ± 3.37
2% wuyiencin	52.14 ± 2.40	56.36 ± 2.58	46.71 ± 2.91	38.08 ± 2.93
3% benziothiazolinone	73.68 ± 2.78	84.05 ± 3.56	54.44 ± 2.80	46.54 ± 1.38
50% chloroisobromine cyanuric acid	10.61 ± 2.33	12.49 ± 2.56	4.96 ± 2.80	6.01 ± 1.69
50% iprodione	70.25 ± 1.63	74.32 ± 2.79	56.37 ± 3.67	67.54 ± 2.79
50% benzylpenicillin	39.78 ± 1.61	56.12 ± 2.78	5.26 ± 2.70	16.51 ± 1.75
80% ethylicin	76.09 ± 2.85	82.54 ± 2.24	54.11 ± 2.00	61.54 ± 2.41
3% zhongshengmycin	82.90 ± 3.64	75.74 ± 2.54	29.91 ± 1.20	27.04 ± 2.01
75% chlorothalonil	54.32 ± 3.01	68.67 ± 1.89	48.44 ± 2.89	49.20 ± 2.07
50% sulfur·carbendazim	30.25 ± 1.46	19.27 ± 1.04	7.93 ± 2.44	3.58 ± 2.19
20% bismerthiazol	42.98 ± 1.42	52.10 ± 1.27	24.29 ± 2.21	35.12 ± 2.22
72% agricultural streptomycin sulfate	25.62 ± 2.81	18.96 ± 2.33	11.84 ± 2.77	8.49 ± 2.86
70% thiophanate methyl	13.10 ± 1.16	32.64 ± 2.64	5.35 ± 1.02	5.21 ± 2.57
50% kresoxim methyl	82.47 ± 1.92	68.79 ± 2.63	47.47 ± 1.39	64.79 ± 2.63
430 g/L tebuconazole	94.26 ± 301	95.46 ± 1.18	84.72 ± 3.61	75.46 ± 1.73
45% prochloraz	63.25 ± 2.51	98.79 ± 1.73	10.26 ± 1.85	84.26 ± 1.42
Bacillus cereus preparation (8*10^9 spores/g)	48.00 ± 2.06	42.61 ± 2.94	17.19 ± 2.83	20.69 ± 1.84
Beauveria bassiana preparation (2*10^{11} spores/g)	51.76 ± 2.99	78.96 ± 3.01	6.14 ± 2.28	3.73 ± 2.39
Verticillium chlamydosporium preparation (2.5 * 10^9 spores/g)	28.82 ± 1.70	17.13 ± 2.12	6.14 ± 2.64	12.25 ± 2.60

TABLE 3 | Determination of the inhibitory effect of 10 Chinese edible and medicinal plant extracts on *A. alternata* H4 and *F. proliferatum* H8.

Plant extract	Inhibition rate (%)		Plant extract	Inhibition rate (%)	
	A. alternata H4	*F. proliferatum* H8		*A. alternata* H4	*F. proliferatum* H8
Zanthoxylum bungeanum Maxim	68.75 ± 1.15	75.12 ± 2.38	*Mentha haplocalyx*	7.24 ± 1.03	32.48 ± 1.54
Lonicera japonica Thunb	11.27 ± 1.72	34.84 ± 1.69	*Dendrobium officinale* Kimura et Migo	37.94 ± 1.35	26.75 ± 1.82
Zingiber officinale Roscoe	70.14 ± 2.16	60.48 ± 1.37	*Piper nigrum*	69.84 ± 1.19	60.93 ± 1.79
Illicium verum	37.68 ± 1.27	52.48 ± 1.77	*Schisandra chinensis*	48.37 ± 2.42	35.17 ± 2.80
Houttuynia cordata Thunb	24.64 ± 1.93	45.11 ± 2.60	*Gastrodia elata*	15.24 ± 1.91	21.68 ± 2.54
80% ethylicin	100	100			

TABLE 4 | Determination of the efficacy of screened fungicides to *A. alternata* H4 and *F. proliferatum* H8.

Pathogenic strain	Control agent	Regression equation	Correlation coefficient	EC50 (µg/ml)
A. alternata H4	3% benziothiazolinone	y = 0.8324x+4.1566	0.9770	10.3089
	10% difenoconazole	y = 0.7454x+4.2309	0.9871	10.7595
	50% iprodione	y = 0.8428x+4.5227	0.9934	3.6840
	50% kresoxim-methyl	y = 0.5347x+4.3594	0.9813	15.7781
	80% ethylicin	y = 1.0551x+3.4653	0.9956	28.4809
	430 g/L tebuconazole	y = 0.2501x+5.4687	0.9254	0.0133
F. proliferatum H8	10% difenoconazole	y = 0.3704x+5.1064	0.9903	0.5161
	45% prochloraz	y = 0.8479x+6.6203	0.9013	0.0122
	50% iprodione	y = 0.9036x+4.2205	0.9953	7.2888
	50% kresoxim-methyl	y = 0.3352x+4.7836	0.9766	4.4216
	80% ethylicin	y = 0.9706x+3.8647	0.9959	14.7804
	430 g/L tebuconazole	y = 0.7926x+6.1988	0.9111	0.0307

study are shown in **Table 3**. All 10 ethanolic extracts prepared at a final concentration of 50 mg/ml showed an inhibitory effect on the two fungal pathogens, *A. alternata* H4 and *F. proliferatum* H8. In comparison, 50 mg/ml and 80% ethylicin was included in the test. The inhibition rates of *Zanthoxylum bungeanum* Maxim

against *A. alternata* H4 and *F. proliferatum* H8 were 68.75 and 75.12%, those of *Zingiber officinale* Roscoe were 70.14 and 60.48%, and those of *Piper nigrum* were 69.84 and 60.93%, respectively. The three extracts showed the highest inhibitory effect against both tested pathogens of dragon fruit. Notably, 80%

ethylicin at the same concentration exhibited a 100% inhibition rate in both strains.

Fungicidal Efficacy Test on Representative Fungi With Promising Candidates

Based on previousscreening results, several fungicides were selected for the efficacy test. As shown in **Table 4**, 430 g/L tebuconazole exhibited the smallest EC_{50} at 0.0133 μg/ml, suggesting the highest potency toward *A. alternata* H4, while 50% iprodione with EC_{50} at 3.6840 μg/ml showed the second highest potency. For the pathogen *F. proliferatum* H8, 45% prochloraz showed the smallest EC_{50} at 0.0122 μg/ml, and 430 g/L tebuconazole is the second smallest with EC_{50} at 0.0307 μg/ml. It is worth mentioning that the efficacy of the biological agent *Bacillus cereus* is also tested, which exhibited EC_{50} at 81.3915 μg/ml toward *F. proliferatum* H8.

DISCUSSION

This study described the isolation and identification of several pathogenic fungal strains from diseased dragon fruits suffering from soft rot, anthracnose, and black spot based on field observation. The capability of the pathogens to infect healthy dragon fruits was confirmed by re-inoculation. Based on the morphological and molecular characteristics, the isolates were roughly identified to be *P. herbarum* H1, *C. nymphaeae* H2, *A. alternata* H4, *A. oryzae* H6, *P. spinulosum* H7, *F. proliferatum* H8, and *N. bipapillata* H9. Previous studies have suggested that a variety of *Fusarium* can cause postharvest soft rot disease to dragon fruit (Oeurn et al., 2015), but few studies report on *F. proliferatum*, which is found for the first time in the study in Guizhou province, suggesting that *F. proliferatum* could be a regional pathogen. *C. gloeosporioides* (Bordoh et al., 2020) and *C. truncatum* (Guo et al., 2014; Vijaya et al., 2015) of *Colletotrichum* genera were recognized as the pathogenic microorganisms of pitaya anthracnose. *C. nymphaeae* was reported to cause anthrax in other fruits such as plum (Chang et al., 2018) and blueberry (Tomoo et al., 2015), and this is the first time found in diseased pitaya. *A. alternata* is the main pathogen causing postharvest disease, which can cause black spot disease in dragon fruit (Castro et al., 2017), pears (Tian et al., 2006), peaches (Inoue and Nasu, 2000), and other fruits (Prusky et al., 1997; Prusky et al., 1999; Zhao and Liu, 2012) in the post-harvest preservation. This study found first that *A. oryzae* can cause infection on dragon fruit. Since *A. oryzae* is a ubiquitous environmental fungus, the infection observed in this study could be opportunistic. This research reported for the first time several pathogenic microorganisms of dragon fruit in Guizhou, indicating that the distribution of pathogenic microorganisms in dragon fruit varies with a geographical environment which on the other hand signifies the importance of the geography-specific plan for prevention and control measures.

A. alternata and *F. proliferatum* are two typical postharvest pathogenic microorganisms that can cause postharvest diseases in a variety of fruits (Konstantinou et al., 2011; Abd Murad et al., 2017; Castro et al., 2017; Wang et al., 2021), so we selected these two to test their susceptibility to the control agents, respectively.

The results showed that *A. alternata* H4 exhibited the highest sensitivity to 430 g/L tebuconazole and the lowest sensitivity to 80% ethylicin, while *F. proliferatum* H8 showed the highest sensitivity to 45% prochloraz and the lowest sensitivity to *Bacillus cereus*. The results showed that 10% difenoconazole, 50% iprodione, 50% kresoxim-methyl, 80% ethylicin, and 430 g/L tebuconazole all had inhibitory effects on the two postharvest pathogenic microorganisms of pitaya to a certain degree. Natural antimicrobials obtained from plants can provide alternative materials instead of commonly used fungicides in a more sustainable and environment-friendly way (Romanazzi et al., 2012). This study demonstrated that the 10 edible and medicinal plant extracts all showed some inhibitory effects on the two representative pathogenic fungi, although they are much less potent than chemically synthesized fungicides. Chemical fungicides showing the most efficacy to tested pathogens can be good choices for field application; however, long-term single use of control agents will likely cause drug resistance of pathogenic microorganisms. Therefore, it is recommended to carry out field experiments using a combination of agents which would improve the control effect, but the study only conducted a sensitivity test indoors which may not represent the field effect.

Pathogenic microorganisms can infect fruits in many ways. For example, fungal spores can spread with the help of wind or insects to infect fruits. Therefore, cultivation and management should be strengthened at regular times, and attention should be paid to ventilation and light transmission to reduce the reproduction of fungi since the reproduction and accumulation of pathogenic microorganisms would cause more fruits to rot, aggravating microbial infections. At present, the postharvest preservation methods of dragon fruit mainly include low-temperature preservation, film preservation, chemical preservation, thermal treatments, and irradiation (Jalgaonkar et al., 2020). These preservation measures have problems such as being time-consuming and labor-intensive, high cost, chemical residues, environmental pollution, and food safety hazards. Plant extracts, especially those from edible or medicinal plants, with fungal inhibitory effects can find their use in postharvest disease prevention.

CONCLUSION

The study isolated seven strains from diseased dragon fruits, and their ability to infect healthy dragon fruits was confirmed. Of them, *Penicillium spinulosum*, *Phoma herbarum*, *Nemania bipapillata* and *Aspergillus oryzae* were for the first time found to cause dragon fruit disease. In consideration of their prevalence in postharvest fruit diseases, *A. alternata* H8 and *F. proliferatum* H4 were chosen as representative pathogens for the drug susceptibility test. Among the tested agro-agents and plant extracts, 430 g/L tebuconazole and 45% prochloraz were found to be the most potent fungicides against H8 and H4, respectively.

DATA AVAILABILITY STATEMENT

The datasets presented in this study can be found in online repositories. The names of the repository/repositories and

accession number(s) can be found in the article/supplementary material.

AUTHOR CONTRIBUTIONS

WW designed and devised the study, and YL and HC analyzed the data and prepared the original manuscript. HC supervised YA and LM for pathogen isolation and the drug sensitivity test. HW revised the manuscript. All authors discussed, edited, and approved the final version.

REFERENCES

Abd Murad, N. B., Mohamed Nor, N. M. I., Shohaimi, S., and Mohd Zainudin, N. A. I. (2017). Genetic Diversity and Pathogenicity of Fusarium Species Associated with Fruit Rot Disease in Banana across Peninsular Malaysia. *J. Appl. Microbiol.* 123, 1533–1546. doi:10.1111/jam.13582

Balendres, M. A., and Bengoa, J. C. (2019). Diseases of Dragon Fruit (Hylocereus Species): Etiology and Current Management Options. *Crop Prot.* 126, 104920. doi:10.1016/j.cropro.2019.104920

Ben-Ze Ev, I. S., Assouline, I., Levy, E., and Elkind, G. (2011). First Report of Bipolaris Cactivora Causing Fruit Blotch and Stem Rot of Dragon Fruit (Pitaya) in israel. *Phytoparasitica* 39, 195–197. doi:10.1007/s12600-011-0143-y

Bordoh, P. K., Ali, A., Dickinson, M., Siddiqui, Y., and Romanazzi, G. (2020). A Review on the Management of Postharvest Anthracnose in Dragon Fruits Caused by Colletotrichum Spp. *Crop Prot.* 130, 105067. doi:10.1016/j.cropro.2019.105067

Castro, J. C., Endo, E. H., de Souza, M. R., Zanqueta, E. B., Polonio, J. C., Pamphile, J. A., et al. (2017). Bioactivity of Essential Oils in the Control of *Alternaria alternata* in Dragon Fruit (Hylocereus Undatus Haw.). *Industrial Crops Prod.* 97, 101–109. doi:10.1016/j.indcrop.2016.12.007

Chang, T. H., Lee, Y. S., and Hassan, O. (2018). First Report of Anthracnose of Japanese Plum (Prunus Salicina) Caused by Colletotrichum Nymphaeae in Korea. *Plant Dis.* 102, 1461. doi:10.1094/PDIS-01-18-0018-PDN

Guo, L. W., Wu, Y. X., Ho, H. H., Su, Y. Y., Mao, Z. C., He, P. F., et al. (2014). First Report of Dragon Fruit (Hylocereus Undatus) Anthracnose Caused by Colletotrichum Truncatum in China. *J. Phytopathol.* 162, 272–275. doi:10.1111/jph.12183

Guo, L. W., Wu, Y. X., Mao, Z. C., Ho, H. H., and He, Y. Q. (2012). Storage Rot of Dragon Fruit Caused by Gilbertella Persicaria. *Plant Dis.* 96, 1826. doi:10.1094/PDIS-07-12-0635-PDN

Inoue, K., and Nasu, H. (2000). Black Spot of Peach Caused by Alternaria Alternata (fr.) Keissler. *J. Gen. Plant Pathol.* 66, 18–22. doi:10.1007/PL00012916

Jalgaonkar, K., Mahawar, M. K., Bibwe, B., and Kannaujia, P. (2020). Postharvest Profile, Processing and Waste Utilization of Dragon Fruit (Hylocereus spp.): A Review. *Food Rev. Int.* 1, 1–27. doi:10.1080/87559129.2020.1742152

Konstantinou, S., Karaoglanidis, G. S., Bardas, G. A., Minas, I. S., Doukas, E., and Markoglou, A. N. (2011). Postharvest Fruit Rots of Apple in greece: Pathogen Incidence and Relationships between Fruit Quality Parameters, Cultivar Susceptibility, and Patulin Production. *Plant Dis.* 95, 666–672. doi:10.1094/PDIS-11-10-0856

Masyahit, M., Sijam, K., Awang, Y., and Mohd Satar, M. G. (2009). The First Report of the Occurrence of Anthracnose Disease Caused by Colletotrichum Gloeosporioides (penz.) Penz. & Sacc. On Dragon Fruit (Hylocereus spp.) in Peninsular malaysia. *Am. J. Appl. Sci.* 6, 902–912. doi:10.3844/ajas.2009.902.912

Oeurn, S., Jitjak, W., and Sanoamuang, N. (2015). Fungi on Dragon Fruit in Loei Province, thailand and the Ability of Bipolaris Cactivora to Cause Post-harvest Fruit Rot. *Asia-Pacific J. Sci. Technol.* 20, 405–418. doi:10.14456/kkurj.2015.34

Pan, L., Zhang, R., Lu, F., Liu, C., and Fu, J. (2021). Comparative Proteomic Analysis of the Fungal Pathogen Neoscytalidium Dimidiatum Infection in the Pitaya. *Hortic. Environ. Biotechnol.* 62, 649–659. doi:10.1007/s13580-021-00341-2

Prusky, D., Fuchs, Y., Kobiler, I., Roth, I., Weksler, A., Shalom, Y., et al. (1999). Effect of Hot Water Brushing, Prochloraz Treatment and Waxing on the Incidence of Black Spot Decay Caused by Alternaria Alternata in Mango Fruits. *Postharvest Biol. Technol.* 15, 165–174. doi:10.1016/S0925-5214(98)00082-9

Prusky, D., Perez, A., Zutkhi, Y., and Ben-Arie, R. (1997). Effect of Modified Atmosphere for Control of Black Spot, Caused by Alternaria Alternata, on Stored Persimmon Fruits. *Phytopathology* 87, 203–208. doi:10.1094/PHYTO.1997.87.2.203

Romanazzi, G., Lichter, A., Gabler, F. M., and Smilanick, J. L. (2012). Recent Advances on the Use of Natural and Safe Alternatives to Conventional Methods to Control Postharvest Gray Mold of Table Grapes. *Postharvest Biol. Technol.* 63, 141–147. doi:10.1016/j.postharvbio.2011.06.013

Tarnowski, T. L. B., Palmateer, A. J., and Crane, J. H. (2010). First Report of Fruit Rot on Hylocereus Undatus Caused by Bipolaris Cactivora in South florida. *Plant Dis.* 94, 1506. doi:10.1094/PDIS-06-10-0406

Tian, S., Wan, Y., Qin, G., and Xu, Y. (2006). Induction of Defense Responses against Alternaria Rot by Different Elicitors in Harvested Pear Fruit. *Appl. Microbiol. Biotechnol.* 70, 729–734. doi:10.1007/s00253-005-0125-4

Tomoo, M., Harukuni, H., and Toyozo, S. (2015). First Occurrence of Blueberry Anthracnose Caused by Colletotrichum Nymphaeae (An Additional Pathogen) and Colletotrichum Fioriniae in Hokkaido. *Annu. Rep. Soc. Plant Prot. North Jpn.* 2015, 101–105. doi:10.11455/kitanihon.2015.66_101

Vijaya, S. I., Anuar, I. S. M., and Zakaria, L. (2015). Characterization and Pathogenicity ofColletotrichum truncatumCausing Stem Anthracnose of Red-Fleshed Dragon Fruit (Hylocereus Polyrhizus) in Malaysia. *J. Phytopathol.* 163, 67–71. doi:10.1111/jph.12261

Wang, C., Wang, Y., Wang, L., Li, X., Wang, M., and Wang, J. (2021). Fusarium Species Causing Postharvest Rot on Chinese Cherry in China. *Crop Prot.* 141, 105496. doi:10.1016/j.cropro.2020.105496

Wang, L., Zhang, X., Chen, W., Xiao, T., Zhao, X., Ma, Y., et al. (2018). Shading Reduced the Injury Caused by Winter Chill on Pitaya Plant. *Not. Bot. Horti Agrobo* 47, 470–477. doi:10.15835/nbha47111364

Zhao, Y. Z., and Liu, Z. H. (2012). First Report of Black Spot Disease Caused by Alternaria Alternata on Cherry Fruits in china. *Plant Dis.* 96, 1580. doi:10.1094/PDIS-04-12-0416-PDN

FUNDING

Preparation, Shelf, and Eating Quality of Ready-to-Eat "Guichang" Kiwifruit: Regulation by Ethylene and 1-MCP

Han Yan[1], Rui Wang[1]*, Ning Ji[1], Sen Cao[1], Chao Ma[1], Jiangkuo Li[2], Guoli Wang[3], Yaxin Huang[3], Jiqing Lei[1] and Liangjie Ba[1]

[1]College of Food and Pharmaceutical Engineering, Guiyang University, Guiyang, China, [2]Tianjin Key Laboratory of Postharvest Physiology and Storage of Agricultural Products, National Engineering and Technology Research Center for Preservation of Agricultural Produce, Tianjin, China, [3]Fruit Industry Development Service Centre for Xiuwen County, Guiyang, China

The acceptance of kiwifruit by consumers is significantly affected by its slow ripening and susceptibility to deterioration. Ready-to-eat "Guichang" kiwifruit and its preparation technology were studied by the regulation of ethylene and 1-MCP. Harvested kiwifruits were treated with 100–2000 $\mu l \, L^{-1}$ ethylene for 36 h (20°C) and then treatment with 0–0.5 $\mu l \, L^{-1}$ 1-MCP. The results showed that the preservation effect of 0.5 $\mu l \, L^{-1}$ 1-MCP is inefficient when the soluble solid content of kiwifruit exceeded 15%. The ethylene-treated fruits reached an "edible window" after 24 h, but a higher concentration of ethylene would not further improve ripening efficiency, while the optimal ethylene concentration was 250 $\mu l \, L^{-1}$. Moreover, after 250 $\mu l \, L^{-1}$ ethylene treatment, 0.5 $\mu l \, L^{-1}$ 1-MCP would effectively prolong the "edible window" of fruits by approximately 19 days. The volatile component variety and ester content of 0.5 $\mu l \, L^{-1}$ 1-MCP-treated fruits were not different from those of the CK group. Principal component analysis and hierarchical cluster analysis indicated that the eating quality of fruits treated with 0.5 $\mu l \, L^{-1}$ 1-MCP was similar to that of fruits treated with ethylene. Consequently, ready-to-eat "Guichang" kiwifruit preparation includes ripening with 250 $\mu l \, L^{-1}$ (20°C, 36 h) ethylene without exceeding the 1-MCP threshold and then treated with 0.5 $\mu l \, L^{-1}$ 1-MCP (20°C, 24 h). This study highlights the first development of a facile and low-cost preparation technology for ready-to-eat "Guichang" kiwifruit, which could reduce the time for harvested kiwifruit to reach the "edible window" and prolong the "edible window" of edible kiwifruit.

Keywords: instant kiwifruit, edible window, ethylene, 1-methylcyclopropene, regulation

1 INTRODUCTION

Kiwifruit production has experienced sustained growth globally, from 3.63 million tons in 2014 to 4.34 million tons in 2019. In addition, kiwifruit occupies an important position in the fruit market (Wang S. et al., 2021). Meanwhile, China is the largest kiwifruit producer in the world, with an annual output of 2.5 million tons and a planting area of 243,000 ha (Wang et al., 2021b). The Guizhou Province is located in southwest China and is one of the main production areas of kiwifruit, but also one of the world's three major karst landscape areas, the center of east Asia. This area is suitable for the growth of kiwifruit because of its unique geographical and climatic environment. "Guichang" kiwifruit is an independent breed, and its planting area reached over 40,000 hm^2 (Wang et al., 2021c)

in Guizhou Province. This variety is similar to "Hayward," with green flesh, sweet taste, and high vitamin C content, which is favored by consumers and commercialized.

Kiwifruit is a climacteric fruit, which indicates the characteristics of after-ripening. Hence, it is generally harvested at a physiologically mature stage—unripe and inedible. Consumers have to wait for 6–8 days to get the kiwifruit edible. Simultaneously, kiwifruit is sensitive to ethylene, and it produces a large amount of endogenous ethylene during the ripening stage; then, it rapidly softens and decays gradually as it reaches the "edible window" stage (Burdon et al., 2017; Tilahun et al., 2020; Wang H. et al., 2021; Huang et al., 2021). Therefore, this seriously affects the storage and consumption of kiwifruit. The aforementioned two factors affect the commodity value of kiwifruit along with reducing consumers' experience and the likelihood of repurchase. Accordingly, it is urgent and essential to develop a facile and low-cost preparation technology for ready-to-eat kiwifruit with a shorter softening time and a longer edible window time.

Ethylene is a natural gaseous plant hormone that plays a vital role in accelerating the softening and ripening of kiwifruit, thus reducing the waiting time to eat kiwifruit and promoting better flavor. Park et al. (2006) treated "Hayward" kiwifruit with $100 \, \mu g \, L^{-1}$ ethylene for 24 h at 20°C, and the firmness of the ethylene-treated fruit reached a minimum after 2 days, which was 8 days earlier than that of the untreated fruits. Lim et al. (2017) treated "Jecy" green kiwifruit with $200 \, \mu l \, L^{-1}$ ethylene for 12 h at 20°C and found that the firmness of the ethylene-treated fruit was reduced to 10 N at 2 days, which was 3 days earlier than CK. The fruit needs at least 2 days to reach the "edible window" throughout ethylene ripening. Moreover, there has been no report on the ripening efficiency of kiwifruit treated with a higher concentration of ethylene.

1-MCP is an ethylene receptor blocker, which can inhibit endogenous ethylene production and the physiological and biochemical reactions of fruit by irreversibly binding with the ethylene receptor (Gong et al., 2020). In previous studies, the 1-MCP treatment showed the effect of inhibited endogenous ethylene production, reduced respiratory rate, upregulated the expression of key enzyme genes in the ascorbic acid synthesis pathway, and promoted ascorbic acid metabolism in kiwifruit, thus enabling to delay the deterioration of fruit quality (Di Francesco et al., 2018; Huan et al., 2020; Zhang et al., 2021). However, the effect of 1-MCP on edible kiwifruit has not yet been reported.

In this study, the concept of ready-to-eat kiwifruit was proposed for the first time. The aim of the present study is to develop a kiwifruit post-harvest technology and innovate a ready-to-eat kiwifruit technology that includes 1) the threshold of 1-MCP on kiwifruit; 2) the effect of higher concentrations of ethylene (100, 250, 500, 1,000, and 2,000 $\mu l \, L^{-1}$) on the efficiency of kiwifruit ripening; 3) the preservation effect of 1-MCP on edible kiwifruit; 4) the flavor compounds of ready-to-eat kiwifruit; and 5) the eating quality of ready-to-eat kiwifruit is completely evaluated by HCA and PCA, including the Brix-acid ratio (BAR), pulp firmness, ascorbic acid (ASA), folic acid, color, and volatile components. These findings provide a technical basis

for reducing the post-harvest loss of kiwifruit and improving its commercial value.

2 MATERIALS AND METHODS

2.1 Materials

Kiwifruit (*Actinidia deliciosa* cv. "Guichang") was harvested in a kiwifruit garden, in Xiuwen County (106°40′14″ E, 26°57′35″ N) in 2020, and then immediately transported to a laboratory at Guiyang University. The average SSC of fruit was 7.0% ($n = 18$). On harvest day, all the fruits were placed at room temperature, and the callus lasted for 24 h before they were divided into three parts to study the following: 1) threshold of 1-MCP treatment; 2) effect of ethylene on fruit ripening; and 3) effect of 1-MCP on the ripe fruit. In order to simulate the kiwifruit market model in practice, a batch of fruits was stored in a controlled atmosphere container (Tianjin Lvyuan Jieneng Air Conditioning Fresh-keeping Equipment Co., LTD., LYQT-400, China) and ready to be prepared for ready-to-eat kiwifruit. The storage conditions were as follows: O_2: 2%; CO_2: 4.5%; 90% RH (Di Francesco et al., 2018).

2.2 Treatment and Assessments
2.2.1 Threshold of 1-MCP Treatment
To investigate the threshold of 1-MCP on kiwifruit with different maturities, 2,400 fruits were employed and divided into six groups. Logically, the kiwifruit maturity was increased with shelf time because the kiwifruit was attributable to climacteric fruit. Herein, six groups of fruit with different maturities were obtained every 3 days. Immediately, 400 fruits were treated by 1-MCP (0.5 μl L-1, 24 h), named F0, F3, F6, F9, and F12, respectively. In comparison, the group obtained at 0 day without 1-MCP treatment was called CK. After treatment, a shelf was carried out for 12 days at 20°C, and the detection was performed at 0, 3, 6, 9, and 12 days in turn.

2.2.2 Effect of Ethylene on Fruit Ripening
After 45 days of controlled atmosphere storage, 1,800 fruits were divided into six groups for the ethylene ripening experiment (300 fruits in each group). Ethylene-treated (ET) groups were placed in plastic boxes (60 L, 55*40*31.5 cm) and then injected with different volumes of ethylene (100, 250, 500, 1,000, and 2,000 $\mu l \, L^{-1}$), while the control group was not treated by ethylene. These groups were named E1, E2, E3, E4, E5, and CK, respectively. The O_2 and CO_2 concentrations in the box were monitored by a headspace analyzer (Check Point II, Dansensor, Denmark) every 3 h. Ripening was terminated when the O_2 concentration in any group was lower than 5%. After treatment, a shelf experiment was carried out for 9 days at 20°C, and the detection was performed at 1, 3, 5, 7, and 9 days. Therefore, the optimum ripening conditions were obtained.

2.2.3 Effect of Ethylene on Ripe Fruit
Based on the ethylene ripening experiment results, the ripe kiwifruits were divided into three groups (450 fruits in each

group) for ethylene ripening according to the optimum conditions. Then, all the groups were treated with 0, 0.25, or 0.5 μl L^{-1} 1-MCP for 24 h at 20°C. After the treatment, all fruits were stored at 4°C for 14 days and then shelved for 7 days at 20°C. Detection was performed for the fruit at 0 day, 14 days (4°C), 3 days (20°C), 5 days (20°C), and 7 days (20°C).

For GC-MS, the fruit was peeled and frozen in liquid nitrogen and stored at −80°C.

2.3 Physicochemical Analysis

Fruit quality was assessed for the ethylene production (EP) rate, respiration intensity (RI), decay percentage, pulp firmness, SSC, titratable acid (TA), Brix-acid ratio (BAR), h°, starch, ascorbic acid (ASA), and folic acid.

In the aforementioned three experiments, 27 fruits in each group were selected for the determination of EP and RI throughout the experiment. EP and RI were calculated for a constant nine fruits per replication. Nine fruits were placed in a 3.2 L sealed plastic box at 20°C for 2 h. A gas chromatograph was loaded with 2 ml of sample gas from the plastic box (GC-14C, Shimadzu, Tokyo, Japan). The GC condition was referred to in a previous study and was modified (Patil et al., 2019). The inlet temperature was 145°C, the cylinder temperature was 40°C, the detector temperature was 180°C, and the auxiliary heater was 235°C. The heating procedure was as follows: 40°C for 7 min, then increased to 100°C at a rate of 10°C min^{-1}–100°C and maintained for 3 min.

Decay percentage was measured by counting the number of fruits decayed in each group by the method of Choi et al. (2019). Pulp firmness ($n = 18$) was measured according to Burdon et al.'s (2017) report, which used a texture analyzer (TA. XT Plus, SMS, England) fitted with a 2 mm penetrometer probe. The SSC ($n = 18$) and TA content ($n = 3$) were determined according to previous studies (Sivakumaran et al., 2016; Burdon et al., 2017). Then, BAR was calculated by SSC and TA. Pulp color ($n = 18$) was measured by a grating spectrophotometer (YS3060, 3nh Science and Technology Ltd., China) according to Patil et al.'s (2019) report. Starch, ASA, and folic acid content ($n = 3$) measurements were conducted with frozen materials, which were determined by a method based on previous studies (Johansson et al., 2005; Tavarini et al., 2008).

2.4 Sensory Evaluation

Sensory evaluation of kiwifruit was conducted by using a 9-point hedonic scale discussed by Nirmal et al. (2020). All samples were labeled with a three-digit code. Observations regarding the appearance, color, aroma, taste, and overall acceptability of each sample were performed by ten well-trained consumers.

2.5 GC-MS Analysis

Extraction of GC-MS-based volatiles was performed as described in a previous study with some modifications (Du et al., 2019). A 10 μl L^{-1} 3-octanol internal standard was prepared with n-hexane as the solvent. An internal standard of 1 μl and kiwifruit pulp, as well as 2.0 g sodium chloride and a polypropylene cap, were sealed by a polytetrafluoroethylene/silicon septum for each sample (Agilent Technologies, United States). In addition, the

prepared samples were heated in a water bath at 40°C for 30 min and then loaded into an Agilent 7890B GC system (Agilent Technologies, United States) by an Agilent 76978 headspace sampler.

The GC conditions were as follows: HP-5ms Agilent quartz capillary column (30 m × 0.32 mm, 0.25 μm; Agilent Technologies, America); helium carrier gas (99.999%), 2 ml min^{-1}, no shunt; injector temperature of 250°C. The initial temperature was 35°C and maintained for 3 min, increased to 45°C at a rate of 3°C min^{-1}, increased to 120°C at a rate of 2°C min^{-1}, increased to 240°C at a rate of 6°C min^{-1}, and maintained for 6 min. The MS conditions were as follows: electron impact ionization source; electron energy: 70 eV; ionization temperature: 230°C; quadrupole temperature: 150°C; interface temperature: 280°C; and quantity scanning range: 30–500 amu.

The identification of the unknown volatile compounds was performed by the NIST 17 L library. The volatile content relative to the internal standard was calculated according to the comparison between the internal standard content and the chromatographic peak area of the volatile and the internal standard. The formula is as follows:

$$\omega_x = \frac{A_x n_{is} M_x}{m_n A_{is}} \times 10^9,$$

where ω_x is the concentration of the unknown volatile (μg kg^{-1}), n_{is} is the amount of the internal standard substance (g mol^{-1}), M_x is the molar mass of the internal standard substance, A_x is the peak area of the unknown compound, A_{is} is the peak area of the internal standard substance, and m_n is the sample amount (g).

2.6 Statistical Analysis

Data results were statistically processed by SPSS 21.0 software (SPSS Inc., United States), and the results were expressed as the mean ± sd. Duncan multiplicity comparison was used for significance analysis ($p < 0.05$), and Origin Pro 2017 software (Origin Lab Inc., United States) was used for plotting.

3 RESULT

3.1 Threshold of 1-MCP Treatment

In previous studies, kiwifruit entered the "edible window" with SSC of 14–20% and firmness of 3.1–14 N (Deng et al., 2015; Quillehauquy et al., 2020; Zhang et al., 2021). However, the fruit began to soften rapidly at this stage, so the "edible window" was shortened. Therefore, it was of great importance for ready-to-eat kiwifruit to find the preservation threshold of kiwifruit affected by 1-MCP. As shown in **Figure 1A**, the samples of the F0, F3, F6, and F9 groups did not decay during the shelf life. In **Figures 1B and C**, the fruit maturities of the CK, F0, F3, F6, F9, and F12 groups were different because they were treated separately every 3 days in turn. The CK group reached an "edible window" at 12 days (SSC: 15.11%, pulp firmness: 8.36 N). Meanwhile, the ranges of SSC and pulp firmness of F0, F3, and F6 were 12.46–13.15% and 30.12–16.55 N (**Figures 1B, C**), respectively. Obviously, the fruit was inedible at this stage. The F9 group was within its
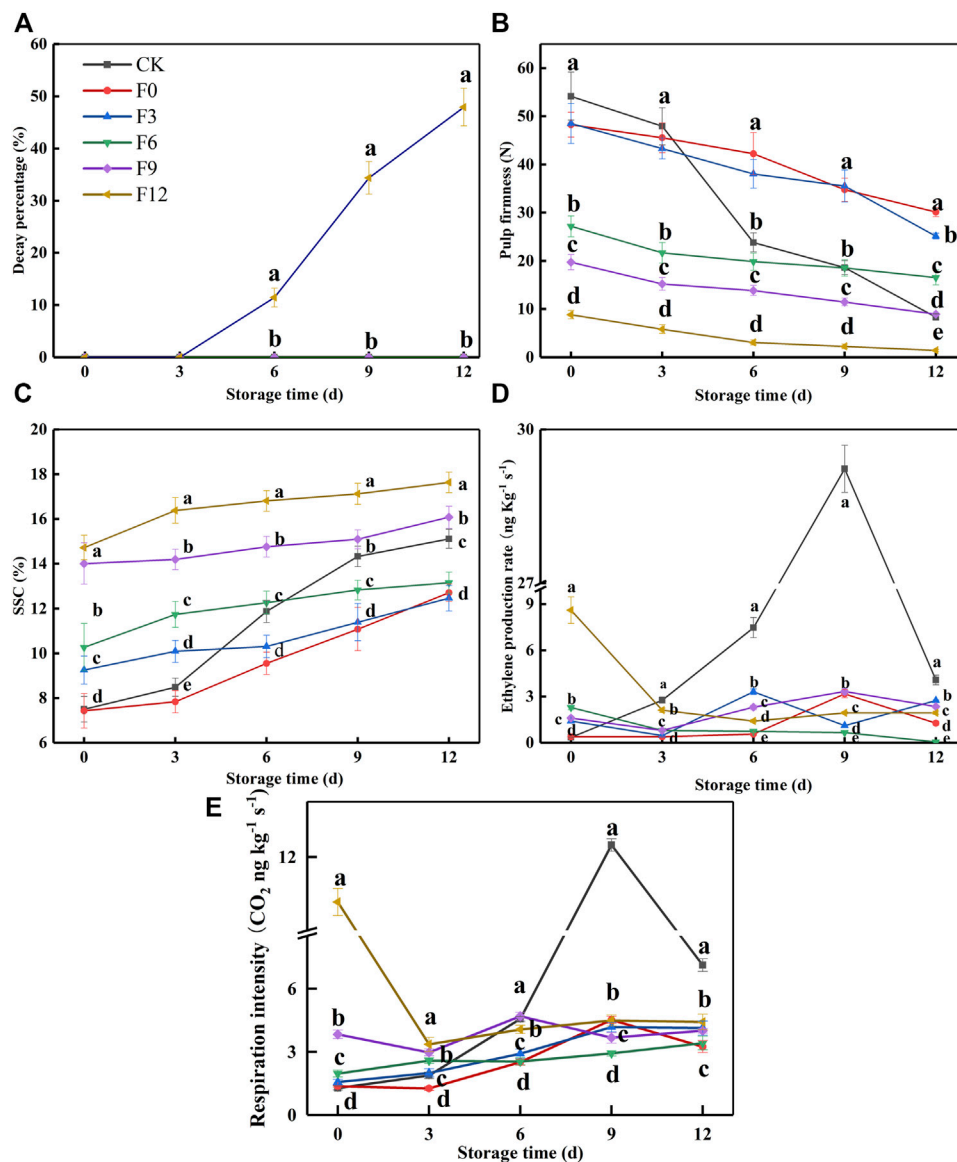
FIGURE 1 | Decay percentage **(A)**, pulp firmness **(B)**, SSC **(C)**, ethylene production rate **(D)**, and respiration intensity **(E)** variations during fruit storage in the 1-MCP threshold experiment. Data are the means of three replicates ± standard deviation (*n* = 18). According to Duncan's test, values with different letters are significantly different (*p* < 0.05).

"edible window" from 6 days (SSC: 14.76%, pulp firmness: 13.86 N) to 12 days (SSC: 16.08%, pulp firmness: 8.98 N), with a fruit quality similar to that of the CK group at 12 days (SSC: 15.11%, pulp firmness: 8.36 N) (*p* < 0.05). According to the aforementioned SSC, firmness, and decay percentage, 1-MCP provided an obvious preservation effect on F0, F3, F6, and F9 groups. Although the SSC of the F12 group was the highest, its decay percentage increased gradually from 11.45 to 47.91% until 12 days (**Figure 1A**). The previous results indicated that 1-MCP had a poor preservation effect on the F12 group.

The EP and RI of the CK group gradually increased to a maximum until 9 days and then sharply decreased to 4.09 ng kg^{-1} h^{-1} and 7.11 ng kg^{-1} s^{-1} at 12 days, respectively

(**Figures 1C, D**). In contrast, the highest EP and RI of the F0, F3, F6, and F9 groups were 2.28–3.32 ng kg^{-1} h^{-1} and 3.42–4.69 ng kg^{-1} s^{-1}, respectively, which were lower than those of the CK group (29.23 ng kg^{-1} h^{-1} and 12.32 ng kg^{-1} s^{-1}). The EP and RI of the F12 group decreased at first and then remained basically unchanged from 3 to 12 days. Because the climacteric of the CK group occurred at 9 days, the F12 group had undergone a climacteric before treatment with 1-MCP. In addition, the EP and RI of the F12 group at 0 day were higher than those of the CK group at 12 days, which indicated that 1-MCP was ineffective in the F12 group. Altogether, it was recommended that the threshold of 1-MCP on Guichang kiwifruit be SSC: 15%.
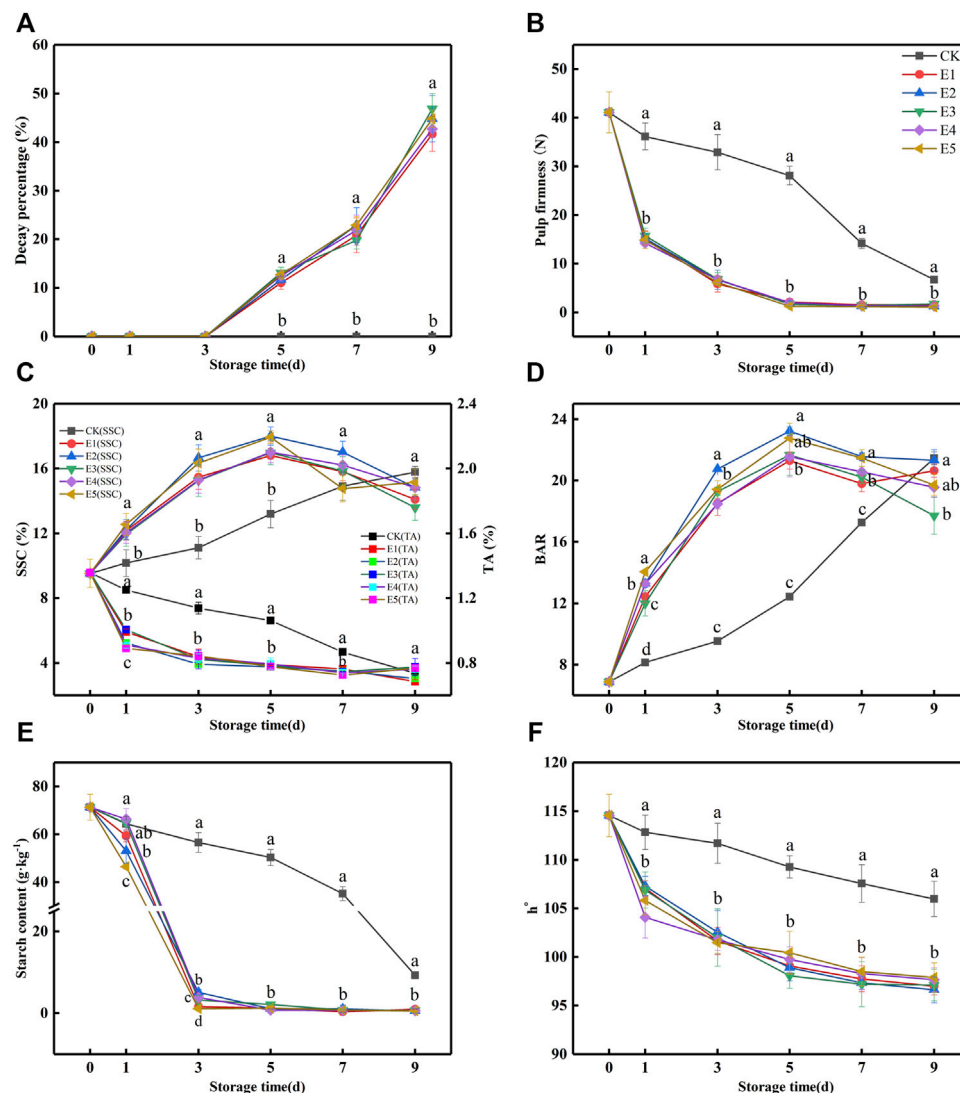
FIGURE 2 | Decay percentage **(A)**, pulp firmness **(B)**, SSC and TA **(C)**, BAR **(D)**, starch **(E)**, and h° **(F)** variations during fruit storage in the ethylene ripening experiment. (CK: 0 µl L^{-1}, E1: 100 µl L^{-1}, E2: 250 µl L^{-1}, E3: 500 µl L^{-1}, E4: 1,000 µl L^{-1}, and E5: 2,000 µl L^{-1}). Data are the means of three replicates ± standard deviation (n = 18). According to Duncan's test, values with different letters are significantly different ($p < 0.05$).

3.2 Effect of Ethylene on Fruit Ripening

From previous studies, kiwifruit needs 2–3 days to reach the "edible window" after treatment with 100 µl kg^{-1}, 100 µg L^{-1}, and 200 µl L^{-1} ethylene (Park et al., 2006; Lim et al., 2017; Tilahun et al., 2020). To improve ripening efficiency, we attempt to directly ripen kiwifruit to an edible window, thus higher concentrations of ethylene (100, 250, 500, 1,000, and 2,000 µl L^{-1}) and shorter ripening time were introduced. The concentrations of O_2 and CO_2 were monitored with a headspace analyzer every 3 h to prevent anaerobic respiration during ethylene ripening. Ripening was stopped at 36 h because the O_2 concentration in the ET groups was lower than 5% (**Supplementary Figure S1**). From **Figures 2B and C**, after 36 h of ripening, the SSC of fruit was increased from 9.53 to 12.4%, and the pulp firmness of fruit was decreased from 41.1 to

14.2 N. It was closest to the edible window (SSC: 14–21%; pulp firmness: 3.1–14 N).

After ripening, a shelf was performed under 20°C for 9 days. First, the decay percentage of all groups is presented in **Figure 2A**. At 5 days, the samples from ET groups began to decay. However, decay did not occur in the CK group. According to **Figure 2B**, the pulp firmness of ET rapidly decreased after ripening by ethylene to a nearly edible firmness at 1 day (14.2–15.7 N), while the pulp firmness of the CK group was 36.15 N at this time point. At 3 days, the pulp firmness of the ET groups (5.84–6.83 N) reached edible firmness, while the CK group was at 9 days. Although ethylene ripening accelerated fruit softening and decay, there was no difference among the ET fruits.

From **Figure 2C**, ethylene accelerated the increase in SSC in the ET groups, which was significantly higher than that in the CK
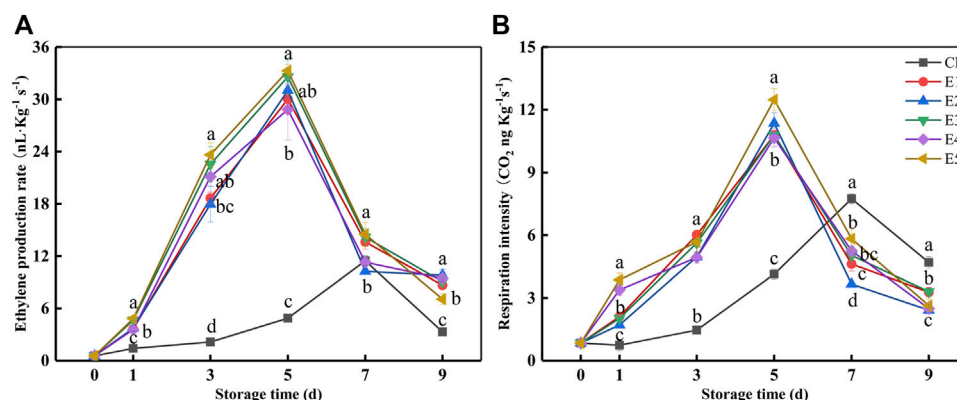
FIGURE 3 | Ethylene production rate **(A)** and respiration intensity **(B)** variations during fruit storage in the ethylene ripening experiment. Data are the means of three replicates ± standard deviation (*n* = 18). Values with different letters are significantly different according to Duncan's test (*p* < 0.05).

group at 1–5 days. The SSC of the ET groups reached the edible SSC (14–20%) at 3 days (15.26–16.66%) and increased to a maximum (16.81–18.01%) at 5 days. However, the SSC of the CK group reached a maximum (15.78%) at 9 days, which was lower than that of the ET groups. According to the SSC, decay percentage, and pulp firmness of the ET groups (**Figures 2A–C**), the samples reached the "edible window" at 3 days, but the decay percentage exceeded 10% at 5 days. Ethylene ripening promoted TA reduction in kiwifruit. As shown in **Figure 2C**, the TA of the ET groups decreased sharply at first and then slowed until 9 days. However, the reduction of CK was slower and lower than ET from 1 to 7 days. BAR, calculated by SSC and TA, was used to measure fruit taste, which was an important indicator of the taste of fruit (**Figure 2D**). From **Figures 2C and D**, the BAR of samples in all groups showed an increasing trend, followed by an increase in SSC and a decrease in TA. Clearly, the changes in SSC and TA in the ET groups were more rapid than those in the CK group. When the sample was in the "edible window" before decay, the highest BARs of the CK, E1, E2, E3, E4, and E5 groups were 21.44, 18.50, 20.74, 19.28, 18.48, and 19.42, respectively. At this stage, the highest BAR of the E2 group (3 days) was closest to that of the CK group (9 days) and higher than that of E1, E3, and E4, which indicated that the taste of fruit with 250 µl L^{-1} ethylene ripening was the most similar to that of the CK group.

Kiwifruit provides energy for its physiological and metabolic activities through the decomposition of starch, which is eventually converted into fructose and glucose to promote the rise of SSC (Lim et al., 2017). Therefore, the maturity of kiwifruit can be evaluated by the starch content. As shown in **Figure 2E**, the starch content of the CK and ET groups showed a downward trend during the shelf, and ET was faster than CK. At 3 days, the starch content of the ET groups was 1.11, 5.13, 3.26, 3.85, and 1.11 g kg^{-1}, respectively. The E2 group was higher than E1, E3, E4, and E5, which indicated that the quality of E1, E3, E4, and E5 was poorer than that of E2. Hence, the ripening effect of E2 was the best in the ET groups.

Fruit color always directly affects the shopping experience of the consumer (Xia et al., 2021). Patil et al. stated that when kiwifruit "Hort16A" was treated with 1 µl L^{-1} ethylene at 1.5°C for 3 weeks, the h° of the treated group was significantly lower than

that of CK (Patil et al., 2019). According to a prior report on kiwifruit (Deng et al., 2015), when h° was close to 90°, the sample seemed yellow, and as h° increased, the sample appeared greener. In this study, the h° of the ET groups was significantly lower than that of CK (**Figure 2F**). However, there were no differences between E1, E2, E3, E4, and E5. From **Figure 2F**, the h° of all ET groups at 1 day (104.08–107.30) was closest to that of CK at 9 days (105.98) before decay.

All the indicator results shown in **Figure 2** could be interpreted by EP and RI (**Figure 3**) after ripening. The EP and RI of the ET groups increased, and the maximum occurred at 5 days (28.83–33.28 ng kg^{-1} s^{-1} and 10.64–12.48 ng kg^{-1} s^{-1}). While the maximum of CK appeared at 7 days (11.46 µl kg^{-1} h^{-1} and 7.74 ng kg^{-1} s^{-1}), it was 60.24–65.56% and 27.25–37.98% lower than ET, respectively. In **Figures 2B–F** and **Figure 3**, the pulp firmness, SSC, TA, BAR, and h° of the ET groups changed rapidly within 1–5 days, which was consistent with the changing trend of EP and RI. In addition, when the SSC, EP, and RI (**Figures 2C, 3**) reached the maximum, the fruit from ET groups began to decay (**Figure 2A**), which indicated the fruit was in senescence. Taken together, there were no differences in pulp firmness, SSC, TA, or h° among the ET groups.

3.3 Effect of 1-MCP on the Ripe Fruit

After the 250 µl L^{-1} ethylene ripening, the SSC of fruits reached a high level (SSC: 14%), and it reached the edible window. Subsequently, the fruits will rapidly decay without any treatment. Therefore, we proposed to prepare ready-to-eat kiwifruit with a long edible window. In the present work, the ready-to-eat kiwifruit was prepared by ethylene ripening followed by 1-MCP preservation. Herein, 1,350 ripe fruits (SSC: 14.51%) were treated with 1-MCP. The effect of 1-MCP (0 µl L^{-1}; 0.25 µl L^{-1}; 0.5 µl L^{-1}) on the shelf life of edible kiwifruit was further investigated. In order to evaluate the shelf-life of ready-to-eat kiwifruit under the supermarket condition, a shelf-life experiment was performed at 4°C for 14 days and then at 20°C for 7 days.

From **Figure 4**, no decay occurred in any group during the 4°C shelves for 14 days. When samples were placed on 20°C shelves, the 0 µl L^{-1} 1-MCP group began to decay at 3 days, and the decay percentage was 11.87%. The 0.25 and 0.5 µl L^{-1} 1-MCP groups
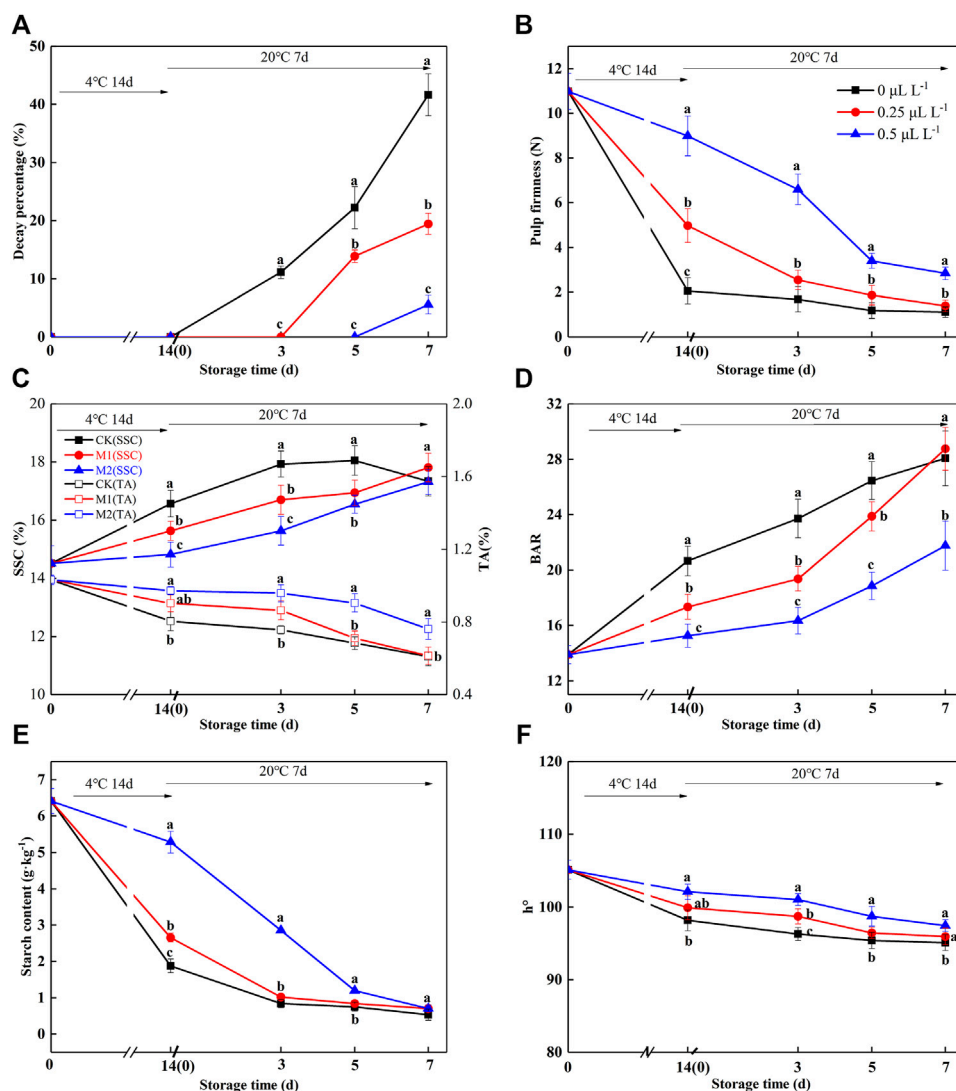
FIGURE 4 | Decay percentage **(A)**, pulp firmness **(B)**, SSC and TA **(C)**, BAR **(D)**, starch **(E)**, and h° **(F)** variations during shelf life in the 1-MCP preservation experiment. Data are the means of three replicates ± standard deviation (*n* = 18). According to Duncan's test, values with different letters are significantly different (*p* < 0.05).

began to decay at 5 days or 7 days, and the decay percentages were 11.88 and 14.58%, respectively.

To reduce the risk of a negative consumer experience, prior to decay, all groups underwent sensory evaluation, nutrition, and volatile component analysis. The sensory evaluation results (appearance, color, aroma, taste, overall) were presented in **Table 1**. With time, although the values of "color" and "appearance" decreased, "aroma" and "taste" increased, and there was no difference in the "overall" value before decay.

Before treatment with 1-MCP, the pulp firmness, SSC, TA, BAR, starch, and h° of ripe kiwifruit were 10.98 N, 14.5 1%, 1.03%, 13.89, 6.41 g kg^{-1}, and 105.13 (**Figures 4B–F**), respectively. As expected, the pulp firmness of the 1-MCP treatment showed a slowly decreasing trend during the shelf life, and the pulp firmness of the 0.5 μl L^{-1} 1-MCP group was higher than that of the other groups

from 14 days (4°C) to 7 days (20°C) (**Figure 4B**). The SSC of the 0 μl L^{-1} 1-MCP group increased rapidly until 5 days (20°C) and then decreased slowly, while the SSC of the 0.25 and 0.5 μl L^{-1} 1-MCP groups increased much slower than that of the 0 μl L^{-1} 1-MCP group (**Figure 4C**). The highest SSCs of the three groups were 16.57%, 16.70%, and 16.55% before decay (**Figure 4C**). For TA, there was no difference between the 0.25 and 0.5 μl L^{-1} 1-MCP groups at 14 days (4°C), but the TA of the 0.25 μl L^{-1} 1-MCP group was higher than that of the 0 and 0.5 μl L^{-1} 1-MCP groups at 20°C. The BAR of the 0.5 μl L^{-1} 1-MCP group was lower than that of the 0 and 0.25 μl L^{-1} 1-MCP groups until 5 days (20°C) due to the highest SSC and lowest TA (**Figure 4D**). Because of the increased SSC (**Figure 4C**), the BAR of the 0.5 μl L^{-1} 1-MCP group increased rapidly at 3 days (20°C) and reached the highest level (18.86%) at 5 days (20°C). According to the BAR and decay percentage, the quality of kiwifruit treated with

TABLE 1 | Sensory score of kiwifruits.

Shelf time	Treatment	Sensory Attribute				
		Appearance	Color	Aroma	Taste	Overall
0 d	0 µl L^{-1}	8.4 ± 0.6	7.5 ± 0.5	5.6 ± 0.6	5.2 ± 0.4	5.7 ± 0.5
4°C	0 µl L^{-1}	7.4 ± 0.6[a]	7.1 ± 0.5[a]	6.6 ± 0.6[a]	6.8 ± 0.4[a]	7.7 ± 0.4[a]
14 days	0.25 µl L^{-1}	8.1 ± 0.4[a]	7.2 ± 0.5[a]	5.7 ± 0.5[a]	5.9 ± 0.5[a]	6.3 ± 0.6[b]
	0.5 µL/L	8.2 ± 0.4[a]	7.2 ± 0.6[a]	5.7 ± 0.4[a]	5.5 ± 0.6[b]	6.2 ± 0.4[b]
20°C 3 days	0 µl L^{-1}	—	—	—	—	—
	0.25 µl L^{-1}	7.2 ± 0.5[a]	7.0 ± 0.5[a]	6.6 ± 0.5[a]	6.7 ± 0.5[a]	7.1 ± 0.5[a]
	0.5 µl L^{-1}	7.8 ± 0.7[a]	7.1 ± 0.6[a]	6.0 ± 0.5[a]	6.4 ± 0.6[a]	6.7 ± 0.5[a]
20°C 5 days	0 µl L^{-1}	—	—	—	—	—
	0.25 µl L^{-1}	—	—	—	—	—
	0.5 µl L^{-1}	7.3 ± 0.3	6.7 ± 0.5	6.2 ± 0.6	7.6 ± 0.5	7.3 ± 0.6

Data are the means of nine replicates ± standard deviation. In columns, different superscript letters at the same time indicate significant differences according to Duncan's test (p < 0.05).

FIGURE 5 | Ethylene production rate **(A)** and respiration intensity **(B)** variations during shelf life in the 1-MCP preservation experiment. Data are the means of three replicates ± standard deviation (*n* = 18). According to Duncan's test, values with different letters are significantly different (*p* < 0.05).
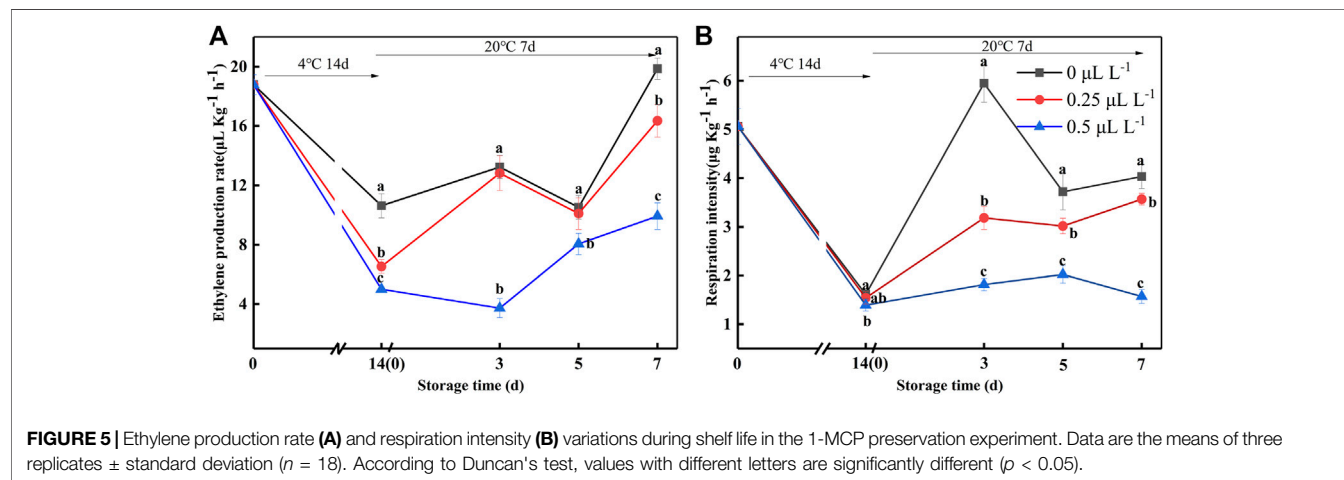
0.5 µl L^{-1} 1-MCP was better than that of the 0 and 0.25 µl L^{-1} 1-MCP groups.

In a previous study, the starch content was positively correlated with pulp firmness. The decreasing trend of starch content was similar to that of pulp firmness, as shown in **Figure 4E**, so the 0.5 µl L^{-1} 1-MCP group was slower than the groups of 0 and 0.25 µl L^{-1} 1-MCP from 0 to 5 days (20°C). In this study, there was a rapid decrease in starch content in the CK and M1 groups on the 4°C shelves. The starch contents of the 0, 0.25, and 0.5 0.5 µl L^{-1} 1-MCP groups were 0.83, 0.84, and 0.70 g kg^{-1} before decay, respectively. As a result, 0.5 µl L^{-1} 1-MCP treatment delayed the starch degradation of ripe kiwifruit.

According to a study on d'Anjou, 1-MCP treatment delayed the decrease in h° so that the peel color was greener than that of the control group (Guo et al., 2020). In this study, 1-MCP effectively delayed the h° decrease in ripening kiwifruit, which was higher than 0 µl L^{-1} 1-MCP group from 14 days (4°C) to 7 days (20°C) (**Figure 4F**). This suggested that 0.5 L L^{-1} 1-MCP could keep the pulp color of "Guichang" kiwifruit.

FIGURE 6 | ASA and folic acid variations during shelf life in the 1-MCP preservation experiment. Data are the means of three replicates ± standard deviation (*n* = 18). According to Duncan's test, values with different letters are significantly different (*p* < 0.05).

FIGURE 7 | Heatmap of volatile components.
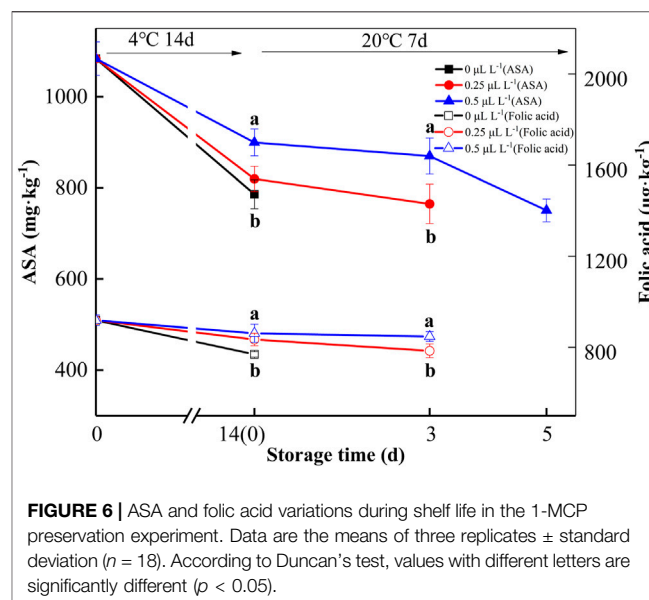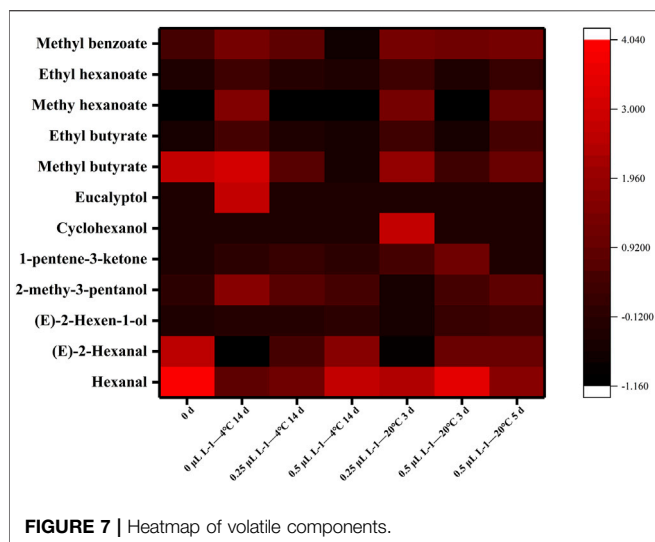
To verify the effectiveness of 1-MCP on ripening fruits, EP and RI were measured (**Figure 5**). The EP and RI were 6.57 ng kg^{-1} s^{-1} and 1.41 ng kg^{-1} s^{-1} at 0 day, respectively. The EP and RI of the 0, 0.25, and 0.5 μl L^{-1} 1-MCP groups showed a similar trend: they decreased at 14 days (4°C) but rapidly increased at 3 days (20°C). Throughout the 20°C shelf life, the EP and RI of the 0.5 μl L^{-1} 1-MCP group were lower than those of the 0 and 0.25 μl L^{-1} 1-MCP groups. Hence, the 1-MCP treatment effectively inhibited the increase in EP and RI at both 4 and 20°C.

ASA and folic acid are important nutrients, and 1-MCP can inhibit the metabolism of ASA and folic acid in kiwifruit (Xu et al., 2019). At 0 day, the ASA and folic acid contents of the sample were 1,083.8 mg kg^{-1} and 918.4 μg kg^{-1}, respectively, as shown in **Figure 6**. The ASA and folic acid contents gradually decreased over time. The ASA and folic acid contents of 0, 0.25, and 0.5 μl L^{-1} 1-MCP groups were 545.1, 637.6, 750.7 mg kg^{-1} and 606.1, 654.5, and 764.8 μg kg^{-1} at 7 days (20°C), respectively. Hence, 0.5 μl L^{-1} 1-MCP treatment effectively delayed the decline in ASA and folic acid in kiwifruit.

3.4 The Flavor Compounds of Ready-to-Eat Kiwifruit

Flavor is a fundamental field that includes volatiles and taste (sugars and acids), which are detected in the mouth and nose and affect the eating quality of kiwifruit (Civille and Oftedal, 2012; Zeng et al., 2020). Previous research finds that ethylene ripening improved kiwifruit flavor (sweetness and aroma) (Günther et al., 2015; Lim et al., 2017). However, the effect of 1-MCP on the flavor of "edible window" kiwifruit was not clear. There was no significant difference in BAR (**Figure 4D**) before decay, in this study, but the "fruit" aroma from the sensory evaluation (**Table 1**) was insufficient after 0.5 μl L^{-1} 1-MCP treatment. Thus, the current study compared the changes in volatile components between ready-to-eat kiwifruit and kiwifruit subjected to ethylene ripening.

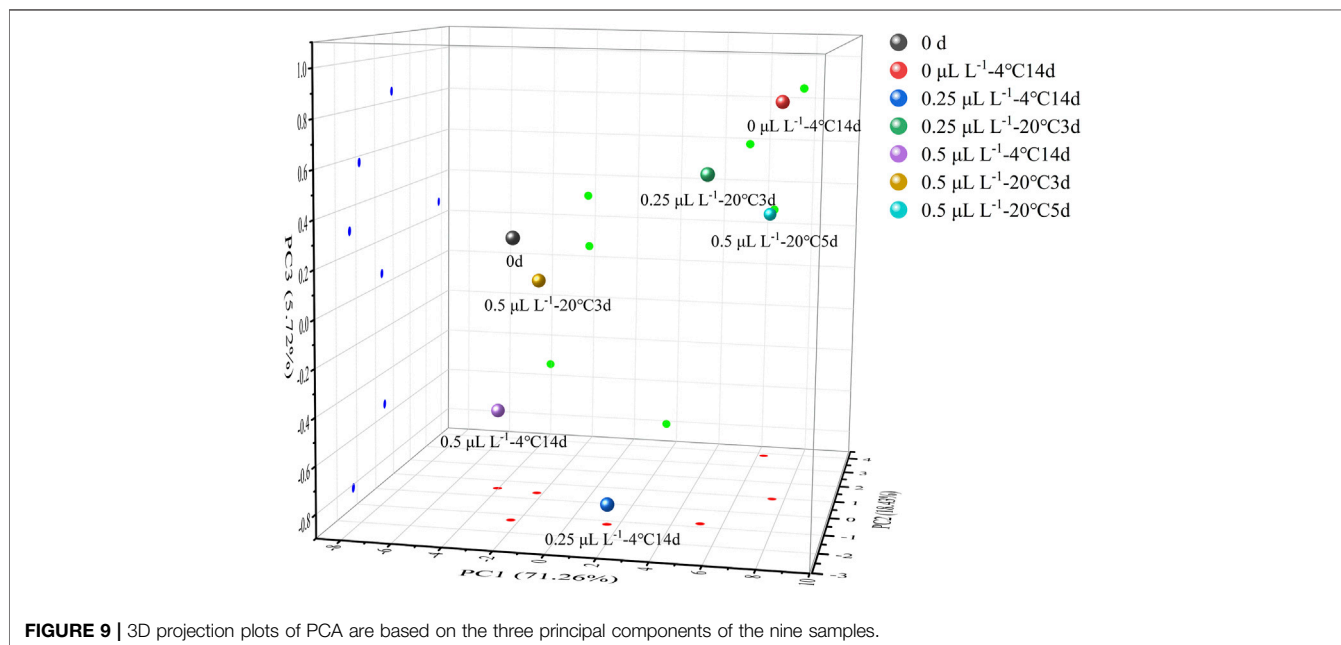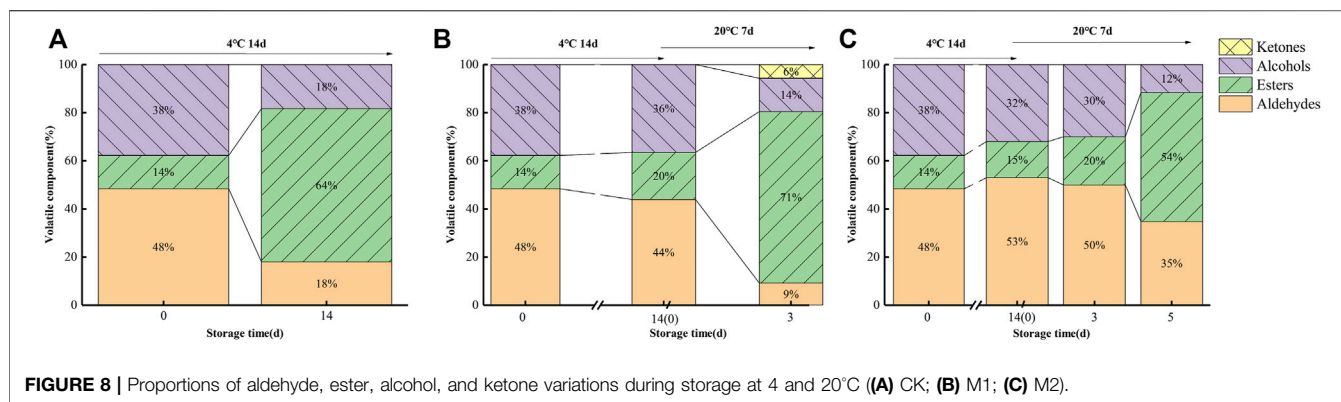**Figures 7** and **8** illustrate the differences in kiwifruit scent in each group. Chen et al. concluded that the volatile components of kiwifruit at lower maturity were mainly aldehydes. Then, esters were gradually

formed when the fruit ripened (Chen et al., 2020). Volatile chemicals are represented by colors in the heatmap (**Figure 7**); the redder the color, the higher the amount. The contents of hexanal and (E)-2-hexanal were the highest in sample 0 days. In contrast, they were lowest in sample 0 μl L^{-1} –4°C at 14 days and lower than samples 0.25 μl L^{-1} –20°C at 3 days and 0.5 μl L^{-1} –20°C at 5 days. The content of eucalyptol was the highest in sample 0 μl L^{-1} –4°C at 14 days. The contents of cyclohexanol and 1-pentene-3-ketone were the highest in the sample 0.25 μl L^{-1} –20°C at 3 days. At 14 days, sample 0 μl L^{-1} at –4°C included greater concentrations of methyl butyrate, ethyl butyrate, methyl hexanoate, methyl benzoate, and ethyl hexanoate. Consequently, the 1-MCP treatment effectively inhibited the production of these ester substances. Combined with the results from **Figures 7** and **8**, it is clear that the aldehyde concentration declined over time, but the ester content rose. In 14 days (4°C), the proportions of aldehydes, esters, and alcohols in the 0 μl L^{-1} 1-MCP group were 18, 64, and 18%, respectively. Meanwhile, there were 44%, 20%, and 36% in the 0.25 μl L^{-1} 1-MCP group and 56%, 8%, and 36% in the 0.5 μl L^{-1} 1-MCP group. This finding revealed that 1-MCP hindered the breakdown of aldehydes and alcohols or the creation of esters, which corroborated Zhang et al.'s (2009) report. On the other hand, the proportion of esters in the 0.5 μl L^{-1} 1-MCP group (20%) was lower than that in the 0.25 μl L^{-1} 1-MCP group (71%) at 20°C for 3 days. However, it increased to 54% at 20°C for 5 days. Hence, the inhibitory effect of 0.5 μl L^{-1} 1-MCP on the "fruit" aroma was more obvious. This outcome was consistent with the sensory evaluation results. The aroma value of the 0.5 μl L^{-1} 1-MCP group was lower than that of the 0 and 0.25 μl L^{-1} 1-MCP groups before 20°C for 5 days, but there was no difference before decay (**Table 1**). The exact composition of the volatile component is presented in **Supplementary Table S2**.

3.5 Multivariate Analysis for the Eating Quality of Ready-to-Eat Kiwifruit

To obtain a more comprehensive assessment of ready-to-eat kiwifruit eating quality, the indicators of BAR, pulp firmness, h°, "overall" of sensory evaluation, ASA, folic acid, hexanal, (E)-2-hexanal, methyl butyrate, and ethyl butyrate were selected and analyzed using PCA and HCA. Thus, the edible quality at different stages was clearly defined.

Figure 9 illustrates the PCA results. PC1, PC2, and PC3 contributed 71.26%, 18.43%, and 5.72%, respectively, to the variance, with the three principal components accounting for 95.41 percent. Color, aroma, taste, and nutrition are important sensory indicators for measuring food quality for consumers. From the results of the sensory evaluation, sample 0 μl L^{-1} –4°C at 14 days was used as a standard because it had the highest value of "overall" in **Table 1**. Clearly, sample 0.25 μl L^{-1} –20°C at 5 days was closest to sample 0 μl L^{-1} –4°C at 14 days. This indicated that the eating quality was comparable to sample 0 μl L^{-1} –4°C at 14 days. By contrast, sample 0 day was closer to sample 0.5 μl L^{-1} –4°C at 14 days and 0.5 μl L^{-1} –20°C at 3 days. This indicated that μl L^{-1} 1-MCP delayed the change in eating quality. However, prior to decay, the eating quality was similar between ethylene-ripening kiwifruit and 0.5 μl L^{-1} 1-MCP-treated kiwifruit. HCA was used to confirm the PCA results. All samples were divided into two clusters: samples

FIGURE 8 | Proportions of aldehyde, ester, alcohol, and ketone variations during storage at 4 and 20°C ((**A**) CK; (**B**) M1; (**C**) M2).

FIGURE 9 | 3D projection plots of PCA are based on the three principal components of the nine samples.

0 day, 0.25 µl L^{-1} −4°C at 14 days, 0.25 µl L^{-1} −20°C at 3 days, 20°C at 5 days, 0.5 µl L^{-1} −4°C at 14 days, 0.5 µl L^{-1} −20°C at 3 days, and 0.5 µl L^{-1} −20°C at 5 days in Cluster I and samples 0 µl L^{-1} −4°C at 14 days and 0.5 µl L^{-1} −20°C at 5 days in cluster II. Significantly, the Euclidean distance between 0 µl L^{-1} −4°C at 14 days and 0.5 µl L^{-1} −20°C at 5 days was minimal. The result was provided for PCA. Although the "overall" value of all groups showed no significant difference before decay (**Table 1**), the eating quality of 0.5 µl L^{-1} −20°C at 5 days was most similar to that of 0 µl L^{-1} −4°C at 14 days.

4 DISCUSSION

As a climacteric fruit, kiwifruit ripens slowly under natural conditions and begins to deteriorate rapidly when climacteric production occurs, greatly affecting fresh kiwifruit sales and exacerbating post-harvest fruit loss. This trial establishes that the sequential applications of ethylene and 1-MCP to inedible kiwifruit

could accelerate its after-ripening and maintain the "edible window." However, it is necessary to first determine the threshold of 1-MCP on kiwifruit. It is attempting to avert an adverse situation that occurs when excessive fruit maturity results in 1-MCP ineffectively. 1-MCP is an ethylene receptor blocker that protects the fruit from the interference of ethylene and delays the deterioration of fruit quality (Gong et al., 2020). In this study, 1-MCP was unable to inhibit the ethylene production rate and respiration intensity of kiwifruit when SSC exceeded 15%. Meanwhile, the firmness of the fruit rapidly decreased, and the decay percentage was over 47.91%. To further improve the ripening effectiveness, this study applied higher concentrations of ethylene (100–1,000 µl L^{-1}) to kiwifruit. As expected, the ethylene treatment had a noticeable effect. The ethylene production rate and respiration intensity of all ethylene-treated groups rapidly increased, with rapid changes in pulp firmness, SSC, BAR, h°, and starch content. However, the 1,000 and 2,000 µl L^{-1} ethylene treatments performed poorly in terms of ripening efficiency. When the EP and RI (**Figure 3**) reached the

maximum, the fruit of the ET groups began to decay (**Figure 2A**), which indicated that the fruit was in senescence. Taken together, there were no significant differences between the ET groups in terms of pulp firmness, SSC, TA, or h°. In a previous study, in which it took at least 2 days to reach edible hardness (Park et al., 2006; Lim et al., 2017), the fruit of the 250 µl L^{-1} ethylene-treatment group was close to edible firmness at 1 day. The BAR of the E2 group was the highest before decay in the ET groups (**Figures 2B–D**). Additionally, the starch content of E1, E3, E4, and E5 was lower than that of E2 after 3 days (**Figure 2E**), indicating that the quality of E1, E3, E4, and E5 was lower than that of E2, despite the fact that they were within the "edible window." As a result, it was recommended that "Guichang" kiwifruit should be treated with 250 µl L^{-1} ethylene. However, the edible kiwifruit must be consumed within 5 days (**Figure 3A**), which presents a challenge for both sellers and consumers. After ripening, it is necessary to preserve the "Guichang" kiwifruit.

After 1 day of 250 µl L^{-1} ethylene ripening, the maturity of the fruit did not exceed the 1-MCP threshold (SSC: 15%). In this case, 1-MCP could be used immediately to treat the fruit. As illustrated in **Figure 4**, 0.5 µl L^{-1} 1-MCP treatment inhibited the decay percentage. In addition, the changes in pulp firmness, SSC, BAR, starch, ASA, and folic acid content were suppressed. 1-MCP treatment had no effect on the overall pattern of pulp firmness reduction; however, it slowed the rate of pulp firmness reduction. In the present study, the pulp firmness of 0.5 µl L^{-1} 1-MCP-treated fruits was close to CK at 20°C for 7 days. Furthermore, the changes in SSC were the same.

While 1-MCP treatment is an effective way to delay the deterioration of fruit quality and extend its shelf life, its misuse will result in a loss of flavor (Huan et al., 2020). Flavor consists of BAR and volatile compounds. In this study, as the TA content of fruits in the 0.5 µl L^{-1} 1-MCP treatment group was effectively maintained, BAR was at the lowest level. However, a comprehensive decay percentage analysis revealed no difference in the maximum BAR of fruits before decay between any of the two groups. On the other hand, there was no difference in the highest score of "taste" among all groups. Aldehydes and esters are important volatile components in kiwifruit that contribute to a special aroma. In this study, the predominant aldehydes were *(E)*-2-hexenal and hexenal, which were characteristic volatile components of kiwifruit and contributed to its "grassy" aroma (Du et al., 2019; Lan et al., 2021). The "sweetness" and "fruit" aromas in kiwifruit were attributed to esters such as methyl butyrate, ethyl butyrate, and methyl hexanoate. In addition, the typical kiwifruit aroma was produced by ethyl butyrate (Zhao et al., 2021). During late ripening, the content of ester was increased. As shown in **Figure 7**, the content of ester of 1-MCP-treated fruit was significantly lower than that of CK. 1-MCP did not completely inhibit the production of esters. According to **Figures 7** and **8**, the changing trends of fruit ester content in all groups were the same, and the rate of the 1-MCP treatment group was lower than that of the CK group solely. The percentages of aldehydes and esters in the fruits of all groups were very similar before decay.

The edible quality of 0.5 µl L^{-1} 1-MCP-treated fruit was comparable to that of the CK group. Although the samples from the 0.5 µl L^{-1} 1-MCP group began to decay at 20°C for 7 days, the decay percentage was the lowest (5.56%). This meant that more fruits

with higher eating quality could maintain a longer "edible window" in the 0.5 µl L^{-1} 1-MCP group. The flavor and taste of 0.5 µl L^{-1} 1-MCP-treated fruits were worse than those of CK. However, due to the longer "edible window" of ready-to-eat kiwifruit, its flavor and taste would gradually improve. In summary, the optimal 1-MCP treatment concentration of ready-to-eat kiwifruit was 0.5 µl L^{-1}.

Recently, the kiwifruit industry has been severely impacted by the limiting factors of slow ripening and subsequent rapid deterioration. In previous studies, kiwifruit was always treated with ethylene or 1-MCP alone. Innovatively, ethylene ripening followed by 1-MCP preservation was employed in the present study. Finally, ready-to-eat kiwifruit was prepared by the regulation of ethylene and 1-MCP. A simple and low-cost strategy was attempted and confirmed to extend the "edible window." Ready-to-eat "Guichang" kiwifruit was prepared using 250 µl L^{-1} ethylene (20°C, 36 h), followed by 0.5 µl L^{-1} 1-MCP for 24 h (20°C), resulting in a longer shelf life (4°C for 14 days, 20°C for 5 days) than the CK group (4°C for 14 days). We hope that ready-to-eat kiwifruit will be a viable alternative to traditional marketing and production patterns of the climacteric fruit industry.

DATA AVAILABILITY STATEMENT

The original contributions presented in the study are included in the article/**Supplementary Material**; further inquiries can be directed to the corresponding author.

AUTHOR CONTRIBUTIONS

Conceptualization and methodology: HY, RW, JL, and GW; investigation: HY, RW, NJ, and JL; formal analysis: HY, YH, LB, SC, CM, RW, and JL; data curation: HY, LB, SC, CM, YH, NJ, RW, and JL; writing—original draft preparation: HY and RW; writing—review and editing: HY, RW, and NJ; all authors have read and agreed to the published version of the manuscript.

FUNDING

SUPPLEMENTARY MATERIAL

The Supplementary Material for this article can be found online at: https://www.frontiersin.org/articles/10.3389/fchem.2022.934032/full#supplementary-material.

REFERENCES

Burdon, J., Pidakala, P., Martin, P., and Billing, D. (2017). Softening of 'Hayward' Kiwifruit on the Vine and in Storage: The Effects of Temperature. *Sci. Hortic.* 220, 176–182. doi:10.1016/j.scienta.2017.04.004

Chen, Y., Feng, X., Ren, H., Yang, H., Liu, Y., Gao, Z., et al. (2020). Changes in Physicochemical Properties and Volatiles of Kiwifruit Pulp Beverage Treated with High Hydrostatic Pressure. *Foods* 9 (4), 485. doi:10.3390/foods9040485

Choi, H. R., Tilahun, S., Park, D. S., Lee, Y. M., Choi, J. H., Baek, M. W., et al. (2019). Harvest Time Affects Quality and Storability of Kiwifruit (Actinidia spp.) *Sci. Hortic.* 256, 108523. doi:10.1016/j.scienta.2019.05.050

Civille, G. V., and Oftedal, K. N. (2012). Sensory Evaluation Techniques - Make "good for You" Taste "good". *Physiology Behav.* 107 (4), 598–605. doi:10.1016/j.physbeh.2012.04.015

Deng, L., Jiang, C.-Z., Mu, W., and Wang, Q. (2015). Influence of 1-MCP Treatments on Eating Quality and Consumer Preferences of 'Qinmei' Kiwifruit during Shelf Life. *J. Food Sci. Technol.* 52 (1), 335–342. doi:10.1007/s13197-013-0986-y

Di Francesco, A., Mari, M., Ugolini, L., and Baraldi, E. (2018). Effect of Aureobasidium Pullulans Strains against Botrytis Cinerea on Kiwifruit during Storage and on Fruit Nutritional Composition. *Food Microbiol.* 72, 67–72. doi:10.1016/j.fm.2017.11.010

Du, D., Xu, M., Wang, J., Gu, S., Zhu, L., and Hong, X. (2019). Tracing Internal Quality and Aroma of a Red-Fleshed Kiwifruit during Ripening by Means of GC-MS and E-Nose. *RSC Adv.* 9 (37), 21164–21174. doi:10.1039/C9RA03506K

Gong, H. J., Fullerton, C., Billing, D., and Burdon, J. (2020). Retardation of 'Hayward' Kiwifruit Tissue Zone Softening during Storage by 1-methylcyclopropene. *Sci. Hortic.* 259, 108791. doi:10.1016/j.scienta.2019.108791

Günther, C. S., Marsh, K. B., Winz, R. A., Harker, R. F., Wohlers, M. W., White, A., et al. (2015). The Impact of Cold Storage and Ethylene on Volatile Ester Production and Aroma Perception in 'Hort16A' Kiwifruit. *Food Chem.* 169, 5–12. doi:10.1016/j.foodchem.2014.07.070

Guo, J., Wei, X., Lü, E., Wang, Y., and Deng, Z. (2020). Ripening Behavior and Quality of 1-MCP Treated d'Anjou Pears during Controlled Atmosphere Storage. *Food control.* 117, 107364. doi:10.1016/j.foodcont.2020.107364

Huan, C., Zhang, J., Jia, Y., Li, S. e., Jiang, T., Shen, S., et al. (2020). Effect of 1-methylcyclopropene Treatment on Quality, Volatile Production and Ethanol Metabolism in Kiwifruit during Storage at Room Temperature. *Sci. Hortic.* 265, 109266. doi:10.1016/j.scienta.2020.109266

Huang, W., Billing, D., Cooney, J., Wang, R., and Burdon, J. (2021). The Role of Ethylene and Abscisic Acid in Kiwifruit Ripening during Postharvest Dehydration. *Postharvest Biol. Technol.* 178, 111559. doi:10.1016/j.postharvbio.2021.111559

Johansson, M., Jastrebova, J., Grahn, A., and Jägerstad, M. (2005). Separation of Dietary Folates by Gradient Reversed-phase HPLC: Comparison of Alternative and Conventional Silica-Based Stationary Phases. *Chroma* 62 (1-2), 33–40. doi:10.1365/s10337-005-0571-2

Lan, T., Gao, C., Yuan, Q., Wang, J., Zhang, H., Sun, X., et al. (2021). Analysis of the Aroma Chemical Composition of Commonly Planted Kiwifruit Cultivars in China. *Foods* 10 (7), 1645. doi:10.3390/foods10071645

Lim, S., Lee, J. G., and Lee, E. J. (2017). Comparison of Fruit Quality and GC-MS-based Metabolite Profiling of Kiwifruit 'Jecy Green': Natural and Exogenous Ethylene-Induced Ripening. *Food Chem.* 234, 81–92. doi:10.1016/j.foodchem.2017.04.163

Nirmal, N. P., Mereddy, R., Webber, D., and Sultanbawa, Y. (2021). Biochemical, Antioxidant and Sensory Evaluation of *Davidsonia pruriens* and Davidsoina Jerseyana Fruit Infusion. *Food Chem.* 342, 128349. doi:10.1016/j.foodchem.2020.128349

Park, Y. S., Jung, S. T., and Gorinstein, S. (2006). Ethylene Treatment of 'Hayward' Kiwifruits (Actinidia Deliciosa) during Ripening and its Influence on Ethylene Biosynthesis and Antioxidant Activity. *Sci. Hortic.* 108 (1), 22–28. doi:10.1016/j.scienta.2006.01.001

Patil, A. S., Maurer, D., Feygenberg, O., and Alkan, N. (2019). Exploring Cold Quarantine to Mango Fruit against Fruit Fly Using Artificial Ripening. *Sci. Rep.* 9. doi:10.1038/s41598-019-38521-x

Quillehauquy, V., Fasciglione, M. G., Moreno, A. D., Monterubbianesi, M. G., Casanovas, E. M., Sánchez, E. E., et al. (2020). Effects of Cold Storage Duration

and 1-MCP Treatment on Ripening and 'eating Window' of 'Hayward' Kiwifruit. *Jbr* 10 (3), 419–435. doi:10.3233/JBR-190492

Sivakumaran, S., Huffman, L., Sivakumaran, S., and Drummond, L. (2018). The Nutritional Composition of Zespri SunGold Kiwifruit and Zespri Sweet Green Kiwifruit. *Food Chem.* 238, 195–202. doi:10.1016/j.foodchem.2016.08.118

Tavarini, S., Degl'Innocenti, E., Remorini, D., Massai, R., and Guidi, L. (2008). Antioxidant Capacity, Ascorbic Acid, Total Phenols and Carotenoids Changes during Harvest and after Storage of Hayward Kiwifruit. *Food Chem.* 107 (1), 282–288. doi:10.1016/j.foodchem.2007.08.015

Tilahun, S., Choi, H. R., Park, D. S., Lee, Y. M., Choi, J. H., Baek, M. W., et al. (2020). Ripening Quality of Kiwifruit Cultivars Is Affected by Harvest Time. *Sci. Hortic.* 261, 108936. doi:10.1016/j.scienta.2019.108936

Wang, H., Wang, J., Mujumdar, A. S., Jin, X., Liu, Z.-L., Zhang, Y., et al. (2021a). Effects of Postharvest Ripening on Physicochemical Properties, Microstructure, Cell Wall Polysaccharides Contents (Pectin, Hemicellulose, Cellulose) and Nanostructure of Kiwifruit (Actinidia Deliciosa). *Food Hydrocoll.* 118, 106808. doi:10.1016/j.foodhyd.2021.106808

Wang, Q., Zhang, C., Long, Y., Wu, X., Su, Y., Lei, Y., et al. (2021b). Bioactivity and Control Efficacy of the Novel Antibiotic Tetramycin against Various Kiwifruit Diseases. *Antibiotics* 10 (3), 289. doi:10.3390/antibiotics10030289

Wang, Q., Zhang, C., Wu, X., Long, Y., and Su, Y. (2021c). Chitosan Augments Tetramycin against Soft Rot in Kiwifruit and Enhances its Improvement for Kiwifruit Growth, Quality and Aroma. *Biomolecules* 11 (9), 1257. doi:10.3390/biom11091257

Wang, S., Qiu, Y., and Zhu, F. (2021d). Kiwifruit (Actinidia Spp.) A Review of Chemical Diversity and Biological Activities. *Food Chem.* 350, 128469. doi:10.1016/j.foodchem.2020.128469

Xia, H., Wang, X., Zhou, Y., Su, W., Jiang, L., Deng, H., et al. (2021). Biochemical and Molecular Factors Governing Flesh-Color Development in Two Yellow-Fleshed Kiwifruit Cultivars. *Sci. Hortic.* 280, 109929. doi:10.1016/j.scienta.2021.109929

Xu, F., Liu, S., Liu, Y., Xu, J., Liu, T., and Dong, S. (2019). Effectiveness of Lysozyme Coatings and 1-MCP Treatments on Storage and Preservation of Kiwifruit. *Food Chem.* 288, 201–207. doi:10.1016/j.foodchem.2019.03.024

Zeng, Y., Wang, M. Y., Hunter, D. C., Matich, A. J., McAtee, P. A., Knäbel, M., et al. (2020). Sensory-Directed Genetic and Biochemical Characterization of Volatile Terpene Production in Kiwifruit. *Plant Physiol.* 183 (1), 51–66. doi:10.1104/pp.20.00186

Zhang, B., Yin, X.-r., Li, X., Yang, S.-l., Ferguson, I. B., and Chen, K.-s. (2009). Lipoxygenase Gene Expression in Ripening Kiwifruit in Relation to Ethylene and Aroma Production. *J. Agric. Food Chem.* 57 (7), 2875–2881. doi:10.1021/jf9000378

Zhang, Y., Wang, K., Xiao, X., Cao, S., Chen, W., Yang, Z., et al. (2021). Effect of 1-MCP on the Regulation Processes Involved in Ascorbate Metabolism in Kiwifruit. *Postharvest Biol. Technol.* 179, 111563. doi:10.1016/j.postharvbio.2021.111563

Zhao, Y., Zhan, P., Tian, H.-L., Wang, P., Lu, C., Tian, P., et al. (2021). Insights into the Aroma Profile in Three Kiwifruit Varieties by HS-SPME-GC-MS and GC-IMS Coupled with DSA. *Food Anal. Methods* 14 (5), 1033–1042. doi:10.1007/s12161-020-01952-8

A Short Review of Anti-Rust Fungi Peptides: Diversity and Bioassays

Julie Lintz, Guillaume Dubrulle, Euan Cawston, Sébastien Duplessis and Benjamin Petre *

Université de Lorraine, INRAE, IAM, Nancy, France

Pucciniales are fungal pathogens of plants that cause devastating rust diseases in agriculture. Chemically-synthesized pesticides help farmers to control rust epidemics, but governing bodies aim at limiting their use over the next decade. Defense peptides with antimicrobial activities may help to innovate a next generation of phytosanitary products for sustainable crop protection. This review comprehensively inventories the proteins or peptides exhibiting a biochemically-demonstrated antifungal activity toward Pucciniales (*i.e.*, anti-rust proteins or peptides; hereafter 'ARPs'), and also analyses the bioassays used to characterize them. In total, the review scrutinizes sixteen publications, which collectively report 35 ARPs. These studies used either *in vitro* or *in planta* bioassays, or a combination of both, to characterize ARPs; mostly by evaluating their ability to inhibit the spore germination process *in vitro* or to inhibit fungal growth and rust disease development *in planta*. Also, the manuscript shows that almost no mode of action against rust fungi was elucidated, although some might be inferred from studies performed on other fungi. This short review may serve as a knowledge and methodological basis to inform future studies addressing ARPs.

Keywords: interaction, defense protein, recombinant protein, mechanism, antifungal

RUST FUNGI IMPOSE A HEAVY PESTICIDE TOLL ON AGRICULTURE

Rust fungi (Pucciniales) are fast-evolving plant pathogens that can infect key crops and threaten global food security (Aime et al., 2018; Figueroa et al., 2020; Duplessis et al., 2021). Farmers notably rely on the use of chemically-synthesized fungicides to control rust epidemics (Oliver and Hewitt, 2014; Cook et al., 2021). Due to the suspected or proven toxicity of those products, governing bodies aim at rapidly limiting their use in agriculture. For instance, the European Commission "Farm to Fork" (F2F) strategy aims at reducing by 50% the use of chemically-synthesized pesticides by 2030 (European Commission, 2020). Therefore, modern agriculture urgently seeks alternatives to chemically-synthesized pesticides. In this context, research and innovation actors aim at developing new tools and solutions for sustainable crop protection, notably by exploiting both our knowledge of the plant immune system and naturally-occurring antimicrobial molecules (Dangl et al., 2013; Moscou and van Esse, 2017; Schwinges et al., 2019; Chen et al., 2021).

DEFENSE PROTEINS AND PEPTIDES ARE EFFECTIVE MICROBE KILLERS

Some proteins or peptides can directly kill microbes; mostly thank to their cationic property which leads to an interaction with negatively charged membranes of microbes (Tam et al., 2015). For instance, plants possess large protein families referred to as 'pathogenesis-related' (PR), whose members exhibit consistent antimicrobial activities (Van Loon and Van Strien, 1999; Van Loon et al., 2006). Such proteins and peptides may provide innovators with molecular chassis to develop active substances for the next generation of biopharmaceuticals and phytosanitary products (Haney et al., 2019). In agriculture, optimized and vectorized anti-microbial proteins or peptides may assist the development of biological pesticides (aka biopesticides) (Montesinos et al., 2012; Schwinges et al., 2019; Li et al., 2021). Such amino acid-based biopesticides would have the advantage of being residue-free and less likely to display harmful effects towards consumers and ecosystems (Kumar et al., 2021). In such a context, we need to better understand the diversity of defense proteins and peptides and how they function.

This study aimed at building a knowledge and methodological basis to assist future studies addressing proteins or peptides that exhibit an antifungal activity against rust fungi (i.e., anti-rust peptides or proteins; hereafter ARPs). To this end, we first performed a systematic analysis of the literature to build a comprehensive list of ARPs. Importantly, this analysis considered only the studies that used the exogenous application of a purified ARP on a rust fungus in vitro or in planta to evaluate its anti-rust activity (i.e., direct anti-rust evidence); it thus disregarded the studies that used non-biochemical approaches (e.g., genetic approaches using protein over-expression in planta). Then, we analyzed the bioassays used to characterize ARPs, in order to build a portfolio of methods and approaches that could be used in future studies, and surveyed the limited information available about the ARP modes of action. The review ends by discussing key peptide features that should be considered in future studies.

A CATALOG OF 35 ARPS WITH NOTICEABLE PROPERTIES

To identify ARPs, we performed a systematic literature survey on the Web of Science by performing searches with combinations of key words such as "exogenous peptide", "antimicrobial activity", "Pucciniales", "rust", or "inhibition germination". This survey identified sixteen papers, published between 1996 and 2021 (**Table 1**). Collectively, these papers explicitly reported 35 different ARPs with an antimicrobial activity towards eleven Pucciniales species (**Table 1**; **Figure 1A**). Three rust species served as models in more than three papers: the Asian soybean rust fungus *Phakopsora pachyrhizi* (*Phakosporaceae*; five papers, twelve ARPs reported) (Fang et al., 2010; Vasconcelos et al., 2011; Brand et al., 2012; Lacerda et al., 2016; Schwinges et al., 2019), the white pine blister rust fungus *Cronartium ribicola*

(*Cronartiaceae*; three papers; six ARPs reported) (Jacobi et al., 2000; Zamany et al., 2011; Liu et al., 2021) and the wheat leaf rust fungus *Puccinia triticina* (*Pucciniaceae*; three papers; seven ARPs reported) (Barna et al., 2008; Alfred et al., 2013; Wang et al., 2020) (**Figure 1A**). The eight remaining rust species were addressed in less than two papers, and belong either to the *Pucciniaceae* or to the *Melampsoraceae* families (Corrêa et al., 1996; Mathivanan et al., 1998; Rauscher et al., 1999; Dracatos et al., 2014; Petre et al., 2016).

In total, 18 ARPs originate from plants, 10 derive from animals or fungi, and 7 are synthetic peptides (**Table 1**). Overall, the 35 ARPs grouped into two categories: small and large ARPs; comprising less or more than 50 amino acids, respectively (**Figure 1B**). ARPs globally display variable predicted isoelectric points, ranging from 4.95 to 12.6. The nine large ARPs carry an N-terminal signal peptide for secretion, and all but two belong to a well-defined plant pathogenesis related (PR) protein family (Van Loon and Van Strien, 1999). Small ARPs were obtained by chemical synthesis (performed in house or by a company to which the peptide was purchased), and large ARPs were obtained *via* the chromatographic purification of protein extracts from fungal, yeast, or bacterial cultures (**Figure 1B**).

Among the 35 ARPs, some present noticeable properties or activities that could be exploited for crop protection. For instance, RISP (Rust Induced Secreted Protein), a large ARP from poplar, showed a targeted activity that inhibits Pucciniales growth without affecting the growth of other fungi and bacteria (Petre et al., 2016). RISP could thus represent an active compound that controls rust epidemics without altering beneficial microbe communities, which may help achieve sustainable, integrated crop protection (Hacquard et al., 2017). Also, some ARPs display high stability that may be critical to withstand harsh field conditions (such as UV exposure, light and temperature variations, rain washing, and interaction with microflora and microbiota). Indeed, four ARPs are thermostable (PuroA; PuroB, RISP and chitinase EC 3.2.1.14); meaning that they remain stable and functional despite being exposed to high temperatures (Mathivanan et al., 1998; Alfred et al., 2013; Petre et al., 2016). Furthermore, some ARPs could effectively protect leaves from rust infection for weeks by stably remaining on the leaf surface (Petre et al., 2016; Schwinges et al., 2019).

ARP STUDIES COMBINE *IN VITRO* AND *IN PLANTA* APPROACHES

To better understand the approaches used to evaluate ARP properties and activities, we analyzed the material and method sections of the sixteen studies reported in the **Table 1**. The studies used two main approaches: in vitro or in planta (**Table 1**, **Figure 1C**). *In vitro* approaches mostly evaluate the ability of purified peptides to inhibit the spore germination process, as the obligate biotrophic nature of most *Pucciniales* prevents the use of in vitro growth inhibition assays commonly used with

TABLE 1 | An overview of plant anti-rust peptides (ARPs).

References	Number of ARP reported (ARP IDs)	ARPs belong to plant pathogenesis-related (PR) gene families	ARP originate from plants	Targeted rust species (rust disease)	Purified ARP obtention method	*In vitro* approach used [ARP concentration range]	*In planta* approach used [ARP concentration range]
Alfred et al., 2013	4 (PuroA*; Pina-R39G; PuroB*; GSP-5D)	no	yes (wheat; *Triticum aestivum*)	*Puccinia striiformis* f. sp. *tritici* (wheat yellow rust or wheat stripe rust); *Puccinia triticina* (wheat leaf rust)	chemical (solid-phase synthesis)	yes (1, 3) [0.01-1 mg/mL]	yes (4, 6) [0.01-1 mg/mL]
Barna et al., 2008	1 (PAF; *Penicillium* antifungal protein)	no	no (fungus *Penicillium chrysogenum*)	*Puccinia triticina* (wheat leaf rust)	cellular (chromatographic purification of *P. chrysogenum* culture extract)	yes (1; 2) [0.001-0.1 mg/mL]	yes (4, 6) [0.1-1 mg/mL]
Brand et al., 2012	7 (IAPs: P61458; A5LDU0; Gm0025x0067; Gm0026x00785; A3KLW0; Q7YRI0; Q9XEY7)	no	yes (soybean; *Glycine max*); no (various animals species)	*Phakopsora pachyrhizi* (asian soybean rust)	chemical (solid-phase synthesis) or commercial (purchased peptides)	no	yes (5) [0.001-1 mg/mL]
Corrêa et al., 1996	5 (RGD; GRGDGSPK; RGDSPC; RGDS; GRGD)	no	no (synthetic peptides)	*Uromyces appendiculatus* (bean rust)	NA	yes (1; 2; 3) [0.01-2 mM]	no
Dracatos et al., 2014	2 (NaD1 & NaD2; Class II & I defensins, respectively)	yes (PR-12)	yes (tobacco; *Nicotiana alata*)	*Puccinia coronata* f. sp. *avenae* (crown rust); *Puccinia sorghi* (maize common rust)	cellular (chromatographic purification following heterologous expression in the yeast *Pichia pastoris*)	yes (1; 2; 3) [0.0001-0.1 mg/mL]	yes (4) [0.1-1 mg/mL]
Fang et al., 2010	2 (Sp2 & Sp39; random 12-mer peptides)	no	yes (soybean; *Glycine max*)	*Phakopsora pachyrhizi* (asian soybean rust)	viral (phage-display)	yes (1; 2) [0.5- 1.5×10^{13} virions/mL]	yes (5) [1.5×10^{13} virions/mL]
Jacobi et al., 2000	4 (Cecropin B; (Ala[8,13,18])-magainin II amide; D2A21 & D4E1 synthetic membrane interactive peptides)	no	no (animal or synthetic peptides)	*Melampsora medusae* (conifer-aspen leaf rust); *Cronartium ribicola* (white pine blister rust)	commercial (purchased peptides)	yes (1) [0.0001-0.1 mg/mL]	no
Lacerda et al., 2016	1 (Drr230a; defensin)	yes (PR-12)	yes (pea; *Pisum sativum*)	*Phakopsora pachyrhizi* (asian soybean rust)	cellular (chromatographic purification following heterologous expression in the yeast *Pichia pastoris*)	yes (1) [1-10 mg/mL]	yes (5) [1-10 mg/mL]
Liu et al., 2021	1 (PmPR10-3.1; *Pinus monticola* pathogenesis-related protein 10-3.1)	yes (PR-10)	yes (white pine; *Pinus monticola*)	*Cronartium ribicola* (white pine blister rust)	cellular (chromatographic purification following heterologous expression in the bacteria *Escherichia coli*)	yes (2) [0.1-1 mg/mL]	no
Mathivanan et al., 1998	1 (EC 3.2.1.14; chitinase*)	no	no (fungus *Fusarium chlamydosporum*)	*Puccinia arachidis* (peanut rust)	cellular (chromatographic purification from *P. chrysogenum* culture extract)	yes (1) [0.1-1 mg/mL]	no
Petre et al., 2016	1 (RISP*; rust-induced secreted protein)	no	yes (poplar; *Populus trichocarpa*)	*Melampsora larici-populina* (poplar leaf rust)	cellular (chromatographic purification following heterologous expression in the bacteria *Escherichia coli*)	yes (1; 2) [0.1-1 mg/mL]	yes (5; 6) [0.1-1 mg/mL]
Rauscher et al., 1999	1 (Pr-1a; pathogenesis-related 1a)	yes (PR-1)	yes (broad bean; *Vicia faba*)	*Uromyces fabae* (broad bean rust)	cellular (chromatographic	yes (1) (unknown)	no

(Continued)

TABLE 1 | Continued

References	Number of ARP reported (ARP IDs)	ARPs belong to plant pathogenesis-related (PR) gene families	ARP originate from plants	Targeted rust species (rust disease)	Purified ARP obtention method	*In vitro* approach used [ARP concentration range]	*In planta* approach used [ARP concentration range]
Schwinges et al., 2019	1 (DS01*; dermaseptin 01)	no	no (frog *Phyllomedusa genus*)	*Phakopsora pachyrhizi* (asian soybean rust)	purification from bean leaf extracts) cellular (chromatographic purification following heterologous expression in the bacteria *Escherichia coli*)	yes (3) [0.01-0.1 mg/mL]	yes (4) [0.1-1 mg/mL]
Vasconcelos et al., 2011	1 (XIP; chitinase-like xylanase inhibitor protein)	yes (PR-8)	yes (coffee; *Coffea arabica*)	*Phakopsora pachyrhizi* (asian soybean rust)	cellular (chromatographic purification following heterologous expression in the yeast *Pichia pastoris*)	yes (1) [1-10 mg/mL]	no
Wang et al., 2020	2 (TaTLP1 & TaPR1; *Triticum aestivum* thaumatin-like protein 1 & *Triticum aestivum* pathogenesis-related protein 1, respectively)	yes (PR-1 & PR-5)	yes (wheat; *Triticum aestivum*)	*Puccinia triticina* (wheat leaf rust)	cellular (chromatographic purification following heterologous expression in the bacteria *Escherichia coli*)	yes (2) [1-10 mg/mL]	no
Zamany et al., 2011	1 (Pm-AMP1; *Pinus monticola* antimicrobial peptide 1)	no	yes (white pine; *Pinus monticola*)	*Cronartium ribicola* (white pine blister rust)	cellular (chromatographic purification following heterologous expression in the bacteria *Escherichia coli*)	yes (2; 3) [0.01-0.1 mg/mL]	no

(*) ARP with specific properties, which are detailed in the main text.
(1) the study evaluated the ARP-mediated inhibition of spore germination by calculating germination rates.
(2) the study evaluated ARP-mediated inhibition of the growth or differentiation of germ tube or hyphae assay by calculating elongation or branching reduction.
(3) the study measured ARP-mediated alteration of fungal structure morphology or infection structure development by microscopy.
(4) the study performed ARP treatment prior to rust inoculation.
(5) the study performed ARP treatment concomitant to rust inoculation.
(6) the study performed ARP treatment after rust inoculation.

cultivable fungi. *In planta* approaches evaluate the ability of peptide treatments to reduce the growth of the fungus on the host plant (most often on leaves). Amongst the sixteen publications, eight used only *in vitro* approaches, one used only an *in-planta* approach, and seven combined both (**Table 1**).

The most common *in vitro* assay (used in eleven studies) assesses the ability of a peptide to inhibit spore germination ('inhibition of germination assay'). In such an assay, the experimenter classically spreads spores onto an agar medium with peptides at a concentration usually ranging from 0.01 to 0.1 mg/mL, and evaluates afterward the germination rate. In addition, ten studies used *in vitro* assays to evaluate the inhibition of the elongation of germ tubes or hyphae, the development of infection structures (e.g., appressoria), or the altered morphology of fungal structures. *In planta* assays assess the ability of a peptide to inhibit fungal growth on a leaf ('infection assay'). In such an assay, the experimenter classically inoculates the rust fungus onto its host plant (or on detached leaves or leaf discs) before, during, or after treatment with purified peptides at a concentration usually ranging from 0.1 to 1 mg/mL, and evaluates afterward the appearance of disease

symptoms by using a visual scoring system. Such scoring classically evaluates uredinia size and distribution, necrosis, and chlorosis depending on each pathosystem (Roelfs and Martens, 1988; Godoy et al., 2006). Noteworthy, for both *in vitro* and *in planta* approaches, two papers used electron microscopy to assess the alteration of fungal cellular structures (Rauscher et al., 1999; Lacerda et al., 2016). Such an approach reveals in detail the structural outcome of ARP treatment, but is arduous and costly to implement, explaining its seldom use.

ARP MODES OF ACTIONS REMAIN MOSTLY UNKNOWN

To better understand how ARPs function, we screened the literature to identify reported modes of actions. This screen identified only two publications that reported information pertaining to the mode of action. Firstly, Fang and colleagues (2010) reported that Sp2 and Sp39 bind to a protein with an
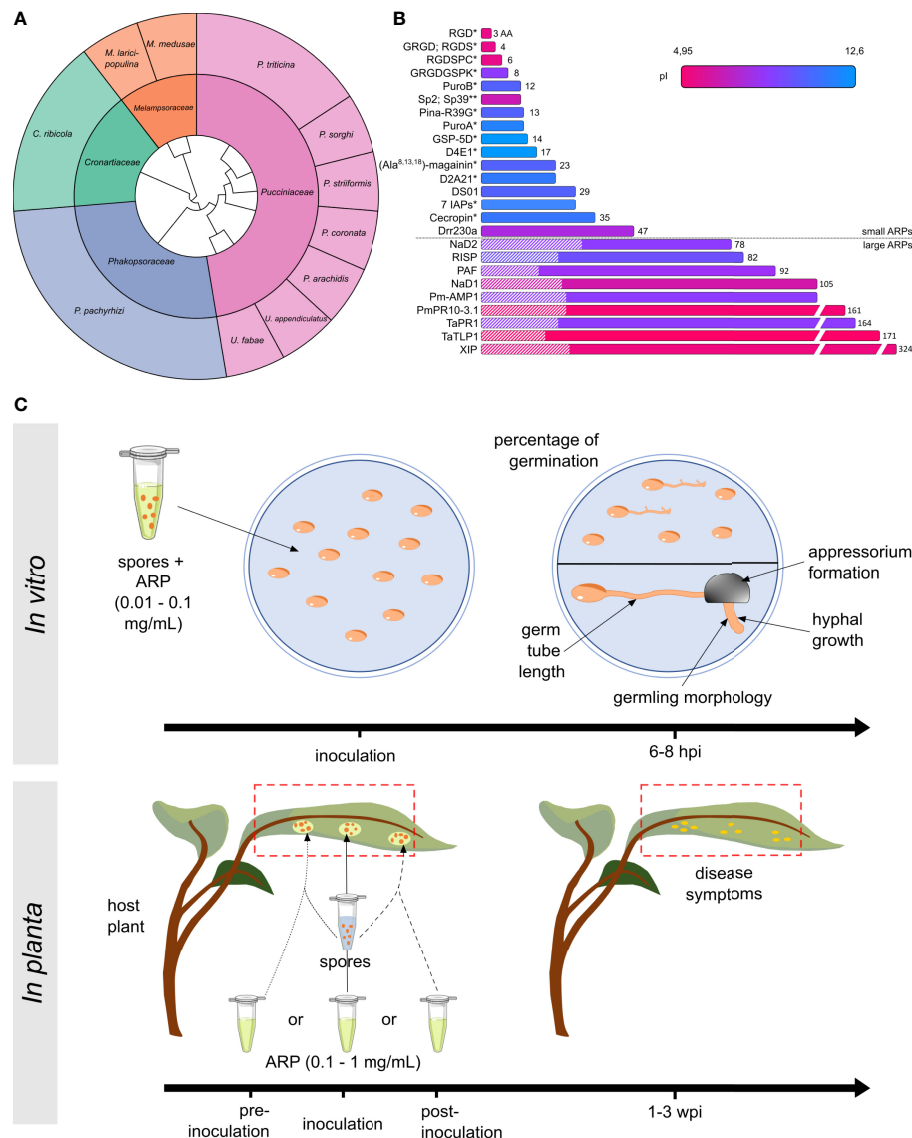
FIGURE 1 | Overview of known anti-rust peptides (ARPs) and bioassays. **(A)** Sunburst phylogenetic tree of Pucciniales taxa and species used to evaluate ARPs activities. The inner and outer circles indicate Pucciniales families and species, respectively. The genus names are *Phakopsora*, *Cronartium*, *Melampsora*, *Puccinia*, or *Uromyces*. **(B)** Classification of the ARP according to their length in amino acid (aa: linear scale). Predicted isoelectric points (pl: color gradient) and known signal peptides for secretion (hatched area) are indicated. ARPs were i) purified by chromatographic purification from proteinaceous cellular extracts, ii) chemically synthesized or purchased (*), or iii) phage-displayed (**). Amino acid sequences for EC 3.2.1.14 and Pr-1a were not indicated in the original publications. **(C)** For *in vitro* bioassays, spores are treated with 0.01 to 0.1 mg/mL purified ARP and spread onto water agar media, and the percentage of germination or the germling morphology and development is assessed 6 to 8 hours post inoculation (hpi) (see **Supplementary Figure S1** for more details). For *in planta* bioassays, host plant (whole plant, detached leaf, or leaf disc) are treated with 0.1 to 1 mg/mL purified ARP prior to inoculation (dotted line), concomitantly with inoculation (solid line), or after inoculation (dashed line). Disease symptoms are assessed using a visual scoring system 1 to 3 weeks post inoculation (wpi). Typically, the scoring system assessed uredinia size, uredinia distribution, necrosis, or chlorosis.

apparent size of 20 kDa from germinated urediniospores of *P. pachyrhizi*; though the paper did not evaluate the biological relevance of that observation (Fang et al., 2010). Secondly, Mathivanan and colleagues (1998) used light microscopy to show that treatment with a chitinase altered the cell wall appearance of *P. arachidis* urediniospores (Mathivanan et al., 1998). The purified peptide also displayed a chitinase activity,

suggesting that it exhibits its anti-rust activity by degrading polysaccharides on the spore surface. For all the other ARPs, the literature reports no known modes of action against rust fungi. However, for some ARPs, a mode of action was proposed, or could be inferred, based on assays performed with other phytopathogenic fungi that are not Pucciniales. For instance, NaD1 binds to the cell wall of *Fusarium oxysporum* hyphae and

permeabilizes the plasma membrane (Van Der Weerden et al., 2008; Van Der Weerden et al., 2010) (**Supplementary Figure S1**). To conclude, ARP modes of action remain vastly unknown, though knowledge gained *via* other fungi may be relevant.

CONCLUSION AND OUTLOOK: KEY THINGS TO CONSIDER FOR FUTURE ARP STUDIES

Overall, this short review inventoried sixteen papers that collectively reported 35 anti-rust peptides (ARPs) targeting in total 11 different rust species. It showed that the studies mainly used *in vitro* assays, sometimes complemented by *in planta* assays, to evaluate ARP properties and activities. The study also highlighted a clear knowledge gap regarding ARP modes of actions, since no explicit mode of action against rust fungi has been reported so far.

Defense proteins and peptides are growingly viewed as new active substances that can be leveraged to implement a next generation of sustainable biopesticides. In the case of ARPs, the research community crucially needs to better understand their mode of action in order to reach technology readiness levels aligned with phytosanitary implementation. Future studies could leverage the methods and technologies used in model fungi to decipher ARP modes of actions. Notably, assays that use fluorescent labels may help track ARPs and identify their binding sites on spores. Also, structure-function analyses that use truncated or site-directed mutagenized ARPs may help identify functional domains and residues important for anti-rust activity, stability, and specificity.

AUTHOR CONTRIBUTIONS

Conception and design of the study (JL, BP, SD); data acquisition, analysis, and interpretation (JL, GD, EC, BP); manuscript drafting (JL, GD, EC); manuscript revision and editing (JL, GD, EC, BP, SD). All authors contributed to the article and approved the submitted version.

SUPPLEMENTARY MATERIAL

The Supplementary Material for this article can be found online at: https://www.frontiersin.org/articles/10.3389/fagro.2022.966211/full#supplementary-material

Supplementary Figure 1 | Detailed effects of anti-rust peptides (ARPs). Effects of ARPs are shown on an urediniospore that germinates by differentiating a germ tube, an appressorium, and then infection hyphae. The rectangular insert on the bottom left indicates the proposed modes of actions discussed in the main text. (a) delay of *Cronartium ribicola* urediniospore germination; (b) particularly on chitin of nascent germ tube walls; (c) only against *Puccinia coronata* f. sp *avenae*; (d) only against *Puccinia sorghi*; (e) binding to a protein from *Phakopsora pachyrhizi* without a defined mode of action.

REFERENCES

Aime, M. C., Bell, C. D., and Wilson, A. W. (2018). Deconstructing the Evolutionary Complexity Between Rust Fungi (*Pucciniales*) and Their Plant Hosts. *Stud. Mycol.* 89, 143–152. doi: 10.1016/j.simyco.2018.02.002

Alfred, R. L., Palombo, E. A., Panozzo, J. F., Bariana, H., and Bhave, M. (2013). Stability of Puroindoline Peptides and Effects on Wheat Rust. *World J. Microbiol. Biotechnol.* 29, 1409–1419. doi: 10.1007/s11274-013-1304-6

Barna, B., Leiter, É., Hegedus, N., Bíró, T., and Pócsi, I. (2008). Effect of the *Penicillium Chrysogenum* Antifungal Protein (PAF) on Barley Powdery Mildew and Wheat Leaf Rust Pathogens. *J. Basic Microbiol.* 48, 516–520. doi: 10.1002/jobm.200800197

Brand, G. D., Magalhães, M. T. Q., Tinoco, M. L. P., Aragão, F. J. L., Nicoli, J., Kelly, S. M., et al. (2012). Probing Protein Sequences as Sources for Encrypted Antimicrobial Peptides. *PloS One* 7, e45848. doi: 10.1371/journal.pone.0045848

Chen, E. H. L., Weng, C. W., Li, Y. M., Wu, M. C., Yang, C. C., Lee, K. T., et al. (2021). *De Novo* Design of Antimicrobial Peptides With a Special Charge Pattern and Their Application in Combating Plant Pathogens. *Front. Plant Sci.* 12. doi: 10.3389/fpls.2021.753217

Cook, N. M., Chng, S., Woodman, T. L., Warren, R., Oliver, R. P., and Saunders, D. G. O. (2021). High Frequency of Fungicide Resistance-Associated Mutations in the Wheat Yellow Rust Pathogen *Puccinia Striiformis* F. Sp. *Tritici. Pest Manag. Sci.* 77, 3358–3371. doi: 10.1002/ps.6380

Corrêa, A., Staples, R. C., and Hoch, H. C. (1996). Inhibition of Thigmostimulated Cell Differentiation With RGD-Peptides in *Uromyces* Germlings. *Protoplasma* 194, 91–102. doi: 10.1007/bf01273171

Dangl, J. L., Horvath, D. M., and Staskawicz, B. J. (2013). Pivoting the Plant Immune System From Dissection to Deployment. *Science* 341, 746–751. doi: 10.1126/science.1236011

Dracatos, P. M., van der Weerden, N. L., Carroll, K. T., Johnson, E. D., Plummer, K. M., and Anderson, M. A. (2014). Inhibition of Cereal Rust Fungi by Both Class I and II Defensins Derived From the Flowers of *Nicotiana Alata. Mol. Plant Pathol.* 15, 67–79. doi: 10.1111/mpp.12066

Duplessis, S., Lorrain, C., Petre, B., Figueroa, M., Dodds, P. N., and Aime, M. C. (2021). Host Adaptation and Virulence in Heteroecious Rust Fungi. *Annu. Rev. Phytopathol.* 59, 403–422. doi: 10.1146/annurev-phyto-020620-121149

European Commission (2020) *A Farm to Fork Strategy for a Fair, Healthy and Environmentally-Friendly Food System* (Brussels: European Commission). Available at: https://www.eumonitor.eu/9353000/1/j4nvke1fm2yd1u0_j9vvik7m1c3gyxp/vl8tq28k4sxt/v=s7z/f=/com(2020)381_en.pdf (Accessed May 05, 2022).

Fang, Z. D., Marois, J. J., Stacey, G., Schoelz, J. E., English, J. T., and Schmidt, F. J. (2010). Combinatorially Selected Peptides for Protection of Soybean Against

Phakopsora Pachyrhizi. Phytopathology 100, 1111–1117. doi: 10.1094/PHYTO-12-09-0365

Figueroa, M., Dodds, P. N., and Henningsen, E. C. (2020). Evolution of Virulence in Rust Fungi - Multiple Solutions to One Problem. *Curr. Opin. Plant Biol.* 56, 20–27. doi: 10.1016/j.pbi.2020.02.007

Godoy, C. V., Koga, L. J., and Canteri, M. G. (2006). Diagrammatic Scale for Assessment of Soybean Rust Severity. *Fitopatol. Bras.* 31, 63–68. doi: 10.1590/S0100-41582006000100011

Hacquard, S., Spaepen, S., Garrido-Oter, R., and Schulze-Lefert, P. (2017). Interplay Between Innate Immunity and the Plant Microbiota. *Annu. Rev. Phytopathol.* 55, 565–589. doi: 10.1146/annurev-phyto-080516-035623

Haney, E. F., Straus, S. K., and Hancock, R. E. W. (2019). Reassessing the Host Defense Peptide Landscape. *Front. Chem.* 7. doi: 10.3389/fchem.2019.00043

Jacobi, V., Plourde, A., Charest, P. J., and Hamelin, R. C. (2000). *In Vitro* Toxicity of Natural and Designed Peptides to Tree Pathogens and Pollen. *Can. J. Bot.* 78, 455–461. doi: 10.1139/b00-025

Kumar, J., Ramlal, A., Mallick, D., and Mishra, V. (2021). An Overview of Some Biopesticides and Their Importance in Plant Protection for Commercial Acceptance. *Plants* 10, 1185. doi: 10.3390/plants10061185

Lacerda, A. F., Del Sarto, R. P., Silva, M. S., de Vasconcelos, E., Coelho, R. R., Dos Santos, V., et al. (2016). The Recombinant Pea Defensin Drr230a is Active Against Impacting Soybean and Cotton Pathogenic Fungi From the Genera *Fusarium, Colletotrichum* and *Phakopsora. 3 Biotech* 6 (1), 59. doi: 10.1007/s13205-015-0320-7

Li, J., Hu, S., Jian, W., Xie, C., and Yang, X. (2021). Plant Antimicrobial Peptides: Structures, Functions, and Applications. *Bot. Stud.* 62, 1–15. doi: 10.1186/s40529-021-00312-x

Liu, J. J., Fernandes, H., Zamany, A., Sikorski, M., Jaskolski, M., and Sniezko, R. A. (2021). In-Vitro Anti-Fungal Assay and Association Analysis Reveal a Role for the *Pinus Monticola* PR10 Gene (Pmpr10-3.1) in Quantitative Disease Resistance to White Pine Blister Rust. *Genome* 64, 693–704. doi: 10.1139/gen-2020-0080

Mathivanan, N., Kabilan, V., and Murugesan, K. (1998). Purification, Characterization, and Antifungal Activity of Chitinase From *Fusarium Chlamydosporum*, a Mycoparasite to Groundnut Rust, *Puccinia Arachidis. Can. J. Microbiol.* 44, 646–651. doi: 10.1139/w98-043

Montesinos, E., Badosa, E., Cabrefiga, J., Planas, M., Feliu, L., and Bardají, E. (2012). "Antimicrobial Peptides for Plant Disease Control. From Discovery to Application," in *ACS Symposium Series. (Washington, USA: American Chemical Society)*, 235–261. doi: 10.1021/bk-2012-1095.ch012

Moscou, M. J., and van Esse, H. P. (2017). The Quest for Durable Resistance. *Science* 358, 1541–1542. doi: 10.1126/science.aar4797

Oliver, R. P., and Hewitt, H. G. (2014). "Fungicides in Crop Protection," (Wallingford: Centre for Agriculture and Bioscience International publishing).

Petre, B., Hecker, A., Germain, H., Tsan, P., Sklenar, J., Pelletier, G., et al. (2016). The Poplar Rust-Induced Secreted Protein (RISP) Inhibits the Growth of the Leaf Rust Pathogen *Melampsora Larici-Populina* and Triggers Cell Culture Alkalinisation. *Front. Plant Sci.* 62. doi: 10.3389/fpls.2016.00097

Rauscher, M., Ádám, A. L., Wirtz, S., Guggenheim, R., Mendgen, K., and Deising, H. B. (1999). PR-1 Protein Inhibits the Differentiation of Rust Infection Hyphae in Leaves of Acquired Resistant Broad Bean. *Plant J.* 19, 625–633. doi: 10.1046/j.1365-313X.1999.00545.x

Roelfs, A. P., and Martens, J. W. (1988). An International System of Nomenclature for *Puccinia Graminis* F. Sp. *Tritici. Phytopathology* 78, 526–533. doi: 10.1094/PHYTO-78-526

Schwinges, P., Pariyar, S., Jakob, F., Rahimi, M., Apitius, L., Hunsche, M., et al. (2019). A Bifunctional Dermaseptin-Thanatin Dipeptide Functionalizes the Crop Surface for Sustainable Pest Management. *Green Chem.* 21, 2316–2325. doi: 10.1039/c9gc00457b

Tam, J. P., Wang, S., Wong, K. H., and Tan, W. L. (2015). Antimicrobial Peptides From Plants. *Pharmaceuticals* 8, 711–757. doi: 10.3390/ph8040711

Van Der Weerden, N. L., Hancock, R. E. W., and Anderson, M. A. (2010). Permeabilization of Fungal Hyphae by the Plant Defensin NaD1 Occurs Through a Cell Wall-Dependent Process. *J. Biol. Chem.* 285, 37513–37520. doi: 10.1074/jbc.M110.134882

Van Der Weerden, N. L., Lay, F. T., and Anderson, M. A. (2008). The Plant Defensin, NaD1, Enters the Cytoplasm of *Fusarium Oxysporum* Hyphae. *J. Biol. Chem.* 283, 14445–14452. doi: 10.1074/JBC.M709867200

Van Loon, L. C., Rep, M., and Pieterse, C. M. J. (2006). Significance of Inducible Defense-Related Proteins in Infected Plants. *Annu. Rev. Phytopathol.* 44, 135–162. doi: 10.1146/annurev.phyto.44.070505.143425

Van Loon, L. C., and Van Strien, E. A. (1999). The Families of Pathogenesis-Related Proteins, Their Activities, and Comparative Analysis of PR-1 Type Proteins. *Physiol. Mol. Plant Pathol.* 55, 85–97. doi: 10.1006/pmpp.1999.0213

Vasconcelos, E. A. R., Santana, C. G., Godoy, C. V., Seixas, C. D. S., Silva, M. S., Moreira, L. R. S., et al. (2011). A New Chitinase-Like Xylanase Inhibitor Protein (XIP) From Coffee (*Coffea Arabica*) Affects Soybean Asian Rust (*Phakopsora Pachyrhizi*) Spore Germination. *BMC Biotechnol.* 11, 11–14. doi: 10.1186/1472-6750-11-14

Wang, F., Yuan, S., Wu, W., Yang, Y., Cui, Z., Wang, H., et al. (2020). TaTLP1 Interacts With TaPR1 to Contribute to Wheat Defense Responses to Leaf Rust Fungus. *PloS Genet.* 16 (1–23), e10087. doi: 10.1371/journal.pgen.1008713

Zamany, A., Liu, J.-J., Ekramoddoullah, A., and Sniezko, R. (2011). Antifungal Activity of a *Pinus Monticola* Antimicrobial Peptide 1 (Pm-AMP1) and its Accumulation in Western White Pine Infected With *Cronartium Ribicola. Can. J. Microbiol.* 57, 667–679. doi: 10.1139/w11-046

Design, Synthesis, and Antifungal Activity of Novel 1,2,4-Triazolo[4,3-c] trifluoromethylpyrimidine Derivatives Bearing the Thioether Moiety

Chunyi Liu[†], Qiang Fei[†]*, Nianjuan Pan and Wenneng Wu

Food and Pharmaceutical Engineering Institute, Guiyang University, Guiyang, China

Crop disease caused by fungi seriously affected food security and economic development. Inspired by the utilization of fungicide containing 1,2,4-triazole and trifluoromethylpyrimidine, a novel series of 1,2,4-triazolo[4,3-c]trifluoromethylpyrimidine derivatives bearing the thioether moiety were synthesized. Meanwhile, the antifungal activities of the title compounds were evaluated and most compounds exhibited obvious antifungal activities against cucumber *Botrytis cinerea*, strawberry *Botrytis cinerea*, tobacco *Botrytis cinerea*, blueberry *Botrytis cinerea*, *Phytophthora infestans*, and *Pyricularia oryzae* Cav. Among the compounds, 4, 5h, 5o, and 5r showed significant antifungal activities against three of the four *Botrytis cinerea*, which indicated the potential to become the leading structures or candidates for resistance to *Botrytis cinerea*.

Keywords: pyrimidine, synthesis, fungicidal activity, 1, 2, 4-triazol, *Botrytis cinerea*

1 INTRODUCTION

Crop disease caused by fungi seriously affected food security and economic development (O'Brien, 2017; Yang et al., 2021). The application of existing antifungal agents was limited, due to the high resistance and security caused by fungicide abuse (Wei et al., 2021). It is increasingly urgent to develop new antimicrobial agents with high antimicrobial performances and good environmental friendliness.

Triazole fungicides are vital five-membered nitrogen-containing heterocycles, which are one of the largest categories of fungicides in the world, and they are widely used in agriculture field. The listed triazole fungicides include Cyproconazole, Epoxiconazole, and Prothioconazole (**Figure 1**). And there are also triazolopyrimidine fungicides ametoctradin. 1,2,4-Triazole derivatives have been extensively applied in antifungal (Sun et al., 2021), antitumor (Abdelrehim, 2021), antibacterial (Pathak et al., 2021), antiviral (Shao et al., 2021), herbicidal (Yang et al., 2022), and insecticidal (Fan et al., 2019) agents.

Pyrimidine is an essential part of DNA and RNA in living system (Kumar and Narasimhan, 2018). Pyrimidine derivatives exhibited diverse biological properties, such as antineoplastic (Kesari et al., 2021), anti-inflammatory (Abdel-Aziz et al., 2021), antiviral (Abu-Zaied et al., 2021), and antimicrobial (El-mahdy and Farouk, 2021) activities. In addition, fused pyrimidine systems, such as pyrrolo [3,2-d] pyrimidine and 1,2,4-triazolo[1,5-a]pyrimidine, also possess extensive biological activities (Cawrse et al., 2018; Wang et al., 2019; Baillache and Unciti-Broceta, 2020; Basyouni et al., 2021; Wang R.-X. et al., 2021; Fayed et al., 2022). For example, Abulkhair (El-Shershaby et al., 2021) developed a set of triazoloquinazoline derivatives and screened the most potential compound against four human cancer cell lines. Since the invention of ethirimol, a series of pyrimidine fungicides were commercialized including ethirimol, dimethirimol, azoxystrobin, and fenarimol (**Figure 1**).
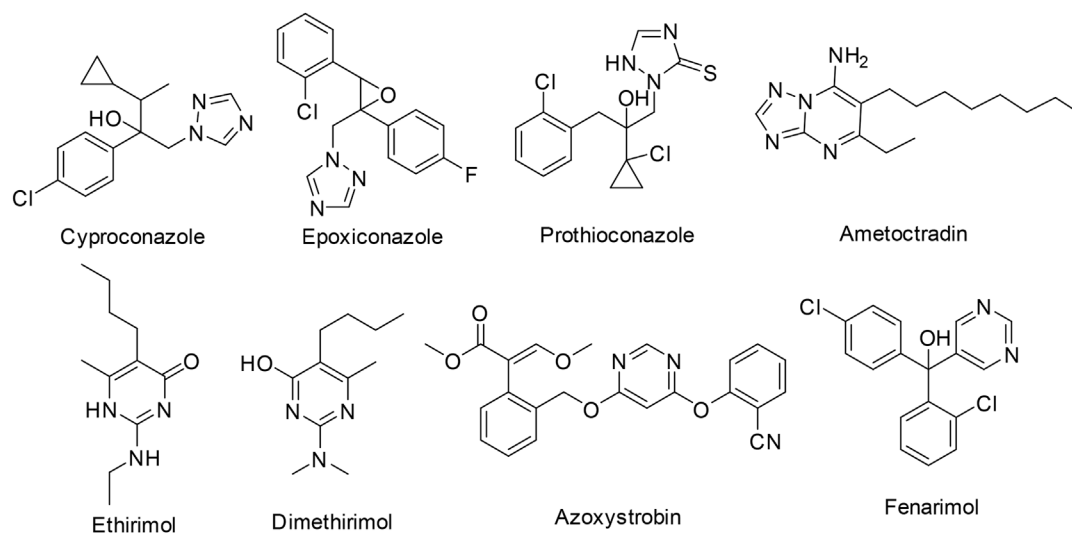
FIGURE 1 | The structure of the sterilizing agent and triamcinolone.
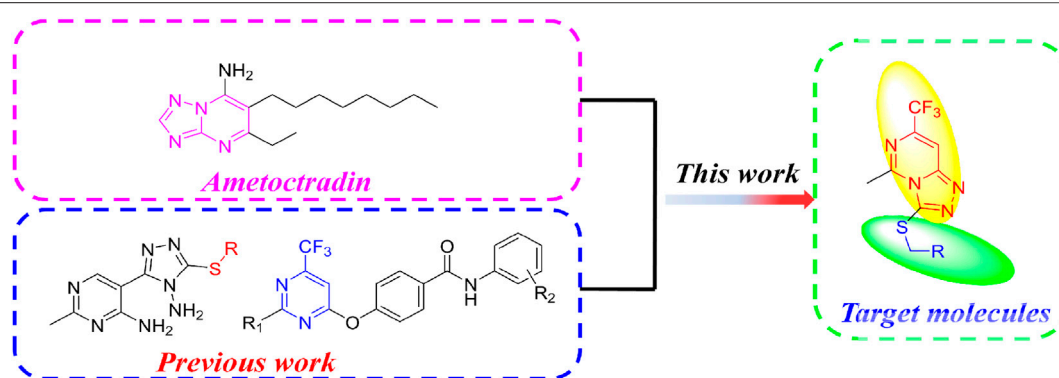
FIGURE 2 | Design of the target molecules.

Moreover thioether is generally recognized as a linking structure which is able to reduce the lipophilicity. Meanwhile, the linker is beneficial to enhance the drug likeness of bioactive molecules (Ding et al., 2021).

Based on the aforementioned consideration, we constructed a fused pyrimidine structure similar to ametoctradin. Furthermore, referring our previous works (Wu W. et al., 2019; Yu et al., 2021), trifluoromethyl was introduced into the pyrimidine scaffold and thioether linker was promoted. Finally we designed and synthesized a novel series of thio-1,2,4-triazolo[4,3-c]pyrimidine derivatives on account of the molecular hybridization strategy (**Figure 2**).

2 MATERIALS AND METHODS

2.1 Chemistry
All solvents were dried by standard methods in advance and distilled before use. The melting points of the products were determined on a XT-4 binocular microscope (Beijing Tech Instrument Co., China). ^{1}H NMR and ^{13}C NMR (solvent DMSO-d_6) spectral analyses were performed on a Bruker Avance NEO 600 NMR spectrometer (^{1}H, 600 MHz; ^{13}C, 150 MHz) at room temperature. TMS was used as an internal standard. Mass spectrometry (MS) data were obtained on a Thermo Scientific Q Exactive Focus instrument. The following abbreviations were used to label chemical shift multiplicities: s = singlet, d = doublet, t = triplet, and m = multiplet. Analytical TLC was performed on silica gel GF-254.

2.2 General Procedure for the Preparation of Intermediates 1–2
Intermediates 1 and 2 were synthesized by the methods of our previous work (Wu W.-N. et al., 2019).

2.3 General Procedure for the Preparation of Intermediates 3

2-Methyl-4-chloro-6-trifluoromethylpyrimidine (20 mmol) and absolute ethanol (50 ml) were weighed, added into a three-necked flask, and stirred under ice bath conditions, and hydrazine hydrate (30 mmol) was added dropwise slowly to the reaction system; after the addition was completed, the reaction was carried out in an ice bath, and the reaction was followed by TLC until the raw material was completed. Then water was added to obtain a yellow solid. The solid was purified by column chromatography, eluting with petroleum ether: ethyl acetate 20:1, which gave a pale yellow solid.

4-Hydrazinyl-2-methyl-6-(trifluoromethyl)pyrimidine (3): Pale yellow solid; yield 40.6%; m.p.113.4–114.8°C; ^{1}H NMR (600 MHz, DMSO-d_6) δ 8.45(s, 1H, pyrimidine-H), 7.14(s, 1H, pyrimidine-NH-), 4.60(s, 1H, -NH$_2$), 2.86(s, 3H, -CH$_3$).

2.4 General Procedure for the Preparation of Intermediates 4

Intermediate 3 (50 mmol) and triethylamine (75 mmol) were placed in a three-necked flask of 250 ml, anhydrous ethanol was added to dissolve. CS$_2$ (75 mmol) was slowly added dropwise, stirred for 30 min, and then heated to reflux for 3 h; the reaction was detected by TLC. After the reaction was completed, the solvent was rotary-evaporated and water was added to suction filtration to remove insoluble matter. The filtrate was adjusted to pH 3 with 10% hydrochloric acid, placed in a refrigerator, and left to stand overnight, suction-filtered, and dried to obtain intermediate 4.

5-Methyl-7-(trifluoromethyl)-[1,2,4]triazolo [4,3-c] pyrimidine-3-thiol (4) White solid; yield 53.4%; m.p.143.7–144.2°C; ^{1}H NMR (600 MHz, DMSO-d_6) δ 8.42(s, 1H, pyrimidine-H), 2.91 (s, 3H, CH$_3$-); ^{13}C NMR (150 MHz, DMSO-d_6) δ 165.31, 152.96, 152.82, 142.23(q, J = 35.1 Hz), 142.23(q, J = 272.25 Hz), 108.16, 20.11; MS (ESI) m/z: 233.1 ([M-H]$^-$).

2.5 General Procedure for the Preparation of the Target Compounds 5a-5s

Intermediate 4 (10 mmol) was added into a triethylamine (15 mmol) aqueous solution, and after stirring at room temperature for 0.5 h, benzyl chloride (11 mmol) with different substituent was added, the reaction was carried out at room temperature, and the reaction was detected by TLC. After completion, the system was filtered to obtain the solid mixture. The mixture was purified by column chromatography to obtain the target compounds 5a–5s.

3-[(2,4-dichlorobenzyl)thio]-5-methyl-7-(trifluoromethyl)-[1,2,4]triazolo[4,3-c]pyrimidine (5q): White solid; yield 69.49%; m.p.72.1–74.6°C; ^{1}H NMR (600 MHz, DMSO-d_6) δ 8.32(s, 1H, Pyrimidine), 7.69(d, 1H, J = 7.8 Hz), 7.67(d, 1H, J = 1.8 Hz), 7.34(dd, 1H, J_1 = 1.8 H, J_2 = 6.6 Hz), 4.64(s, 2H, SCH$_2$), 2.93(s, 3H, CH$_3$); ^{13}C NMR (150 MHz, DMSO-d_6) δ 167.00, 152.58, 152.23, 141.98 (q, J = 35.5 Hz), 134.81, 134.32, 133.62, 133.27, 129.44,

127.95, 122.44 (q, J = 271.5Hz), 109.41, 32.75, 20.11; MS (ESI) m/z: 393.0([M + H]$^+$), 415.0 ([M + Na]$^+$).

2.6 *In vitro* Antifungal Activity Test

The mycelial growth rates method (Du et al., 2021; Wang S. et al., 2021) was selected to evaluate the antifungal activities of the compounds 5a–5r against six phytopathogenic fungi, including cucumber *Botrytis cinerea*, tobacco *Botrytis cinerea*, blueberry *Botrytis cinerea*, *Phytophthora infestans*, strawberry *Botrytis cinerea*, and *Pyricularia oryzae* Cav. The tested compounds were dissolved in 0.5 ml dimethyl formamide (DMF) and then added 9.5 ml sterile water to prepare the test liquids. The test liquids were poured into 90 ml potato dextrose agar (PDA) to maintain the concentrations of the compounds, 50 μg/ml. Each treatment was replicated three times. The inoculated plates were fostered at 25 ± 1°C for 3–4 days. Tebuconazole and pyraclostrobin were acted as positive controls. The cross method was utilized to measure the diameter of the mycelium. The inhibition rate I (%) was calculated through the following formula, where C (cm) represents the average diameter of fungi growth on untreated PDA and T (cm) represents the average diameter of fungi on treated PDA.

$$I(\%) = [(C - T)/(C - 0.4)] \times 100$$

3 RESULTS AND DISCUSSION

3.1 Chemistry

The general synthetic route for the target compounds 5a–5s is depicted in **Scheme 1**. Acetamidine hydrochloride and ethyl trifluoroacetoacetate were used as raw materials. The target compounds 5a–5s were synthesized in five steps, including cyclization, chlorination, hydrazinolysis, cyclization, and thioetherification. The synthesized compounds were confirmed by ^{1}H NMR, ^{13}C NMR, and mass spectrometry.

In the ^{1}H NMR data of compound 5q, a singlet appeared at 8.32 ppm indicated the presence of CH proton of the 8-trifluoromethylpyrimidine. A dd peak presented at 7.34 ppm signified the presence of CH proton in 3-phenyl. A singlet appeared at 4.64 ppm indicated the presence of CH of -SCH$_2$- group. The singlet at 2.93 ppm indicated the CH$_3$ proton in pyrimidine ring. Meanwhile, in the ^{13}C NMR data of compound 5q, two quartets at 141.98 and 122.44 ppm indicated the presence of -CF$_3$ in the pyrimidine fragment. Signals at 32.75 and 20.11 ppm indicated the presence of carbon in the -SCH$_2$- and CH$_3$. In addition, compound 5q was further confirmed by MS data with the ([M + H]$^+$) and [M + Na]$^+$peaks.

3.2 Antifungal Activity Test *in vitro*

The antifungal activity of key intermediate 4 and target compounds 5a–5s was evaluated through the mycelial growth rates method. Most compounds exhibited some activity towards *Botrytis cinerea* (**Table 1**). As cucumber *Botrytis cinerea*, the inhibition rates of compounds 4, 5b, 5f,

SCHEME 1 | Synthetic route for 5a–5s.
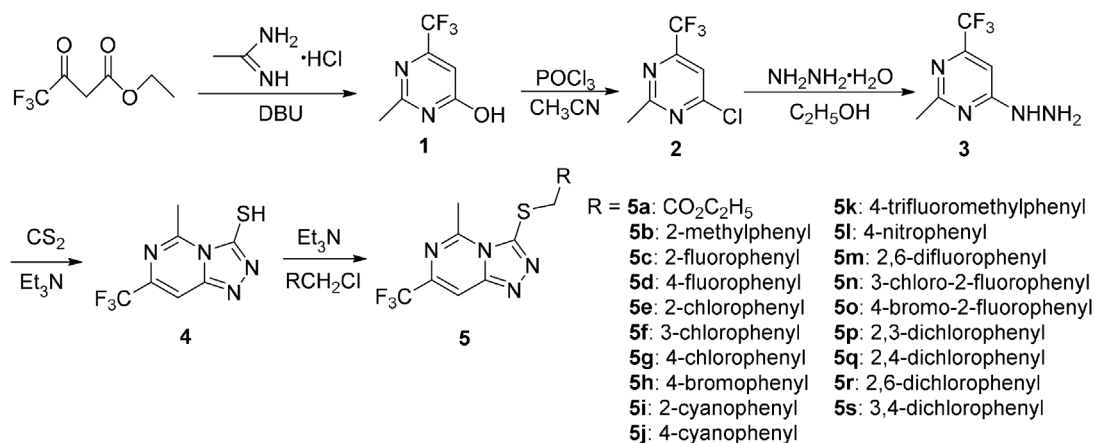
TABLE 1 | The antifungal activities of the compounds 4 and 5a–5s against plant pathogens of cucumber *Botrytis cinerea*, strawberry *Botrytis cinerea*, tobacco *Botrytis cinerea*, blueberry *Botrytis cinerea*, *Phytophthora infestans,* and *Pyricularia oryzae* Cav. *in vitro* at 50 μg/ml.

Compounds	Inhibition Rate (%)					
	Cucumber *Botrytis cinerea*	Tobacco *Botrytis cinerea*	Blueberry botrytis *cinerea*	*Phytophthora infestans*	Strawberry *Botrytis cinerea*	*Pyricularia oryzae* Cav.
4	75.86 ± 1.80	64.35 ± 2.31	58.68 ± 2.15	45.62 ± 1.12	82.68 ± 1.69	50.34 ± 1.26
5a	61.36 ± 1.56	36.66 ± 1.42	45.28 ± 2.61	16.27 ± 2.64	66.02 ± 1.27	26.85 ± 1.94
5b	77.78 ± 1.35	35.69 ± 1.73	57.65 ± 1.09	24.40 ± 1.17	65.05 ± 2.60	37.65 ± 1.36
5c	61.01 ± 2.47	23.79 ± 2.28	57.01 ± 1.69	15.96 ± 1.05	47.57 ± 1.19	33.65 ± 1.14
5d	55.80 ± 3.12	34.07 ± 1.80	43.33 ± 1.07	20.78 ± 3.38	63.75 ± 1.44	23.46 ± 2.26
5e	45.46 ± 2.59	35.37 ± 1.29	44.30 ± 2.67	13.25 ± 2.07	69.57 ± 1.13	25.61 ± 1.57
5f	71.97 ± 1.35	35.65 ± 1.16	54.72 ± 1.18	26.50 ± 1.18	60.53 ± 3.03	30.56 ± 1.63
5g	62.38 ± 3.05	48.54 ± 2.32	57.34 ± 2.68	17.46 ± 1.56	72.89 ± 1.04	26.24 ± 1.81
5h	72.31 ± 2.05	38.26 ± 1.34	60.23 ± 2.26	23.51 ± 2.13	74.37 ± 3.75	36.18 ± 3.80
5i	53.29 ± 1.84	24.75 ± 2.35	50.17 ± 1.08	12.94 ± 1.29	76.35 ± 3.16	32.41 ± 2.46
5j	65.15 ± 1.61	34.40 ± 1.25	56.68 ± 2.01	20.48 ± 1.08	77.85 ± 3.28	31.80 ± 3.08
5k	67.47 ± 1.64	38.26 ± 3.18	52.21 ± 1.64	15.96 ± 3.66	77.32 ± 3.46	25.93 ± 2.20
5l	53.03 ± 3.01	28.28 ± 2.25	47.24 ± 1.98	15.96 ± 2.51	76.66 ± 3.32	29.31 ± 2.71
5m	75.63 ± 2.17	30.85 ± 1.10	65.04 ± 1.15	21.62 ± 2.11	63.19 ± 2.65	34.37 ± 2.19
5n	76.58 ± 2.26	39.37 ± 1.90	59.70 ± 2.38	31.26 ± 1.24	68.71 ± 2.81	38.22 ± 3.07
5o	80.38 ± 2.41	46.93 ± 2.34	64.12 ± 1.10	38.60 ± 1.87	75.31 ± 1.78	46.97 ± 1.68
5p	53.03 ± 1.95	29.58 ± 1.17	42.35 ± 1.84	14.15 ± 1.39	70.60 ± 1.28	27.46 ± 2.49
5q	63.89 ± 1.15	72.99 ± 3.09	42.02 ± 1.20	19.26 ± 1.35	71.52 ± 1.69	26.54 ± 3.05
5r	73.57 ± 2.94	78.68 ± 2.31	46.12 ± 3.84	23.65 ± 3.12	79.85 ± 2.87	30.26 ± 2.18
5s	55.80 ± 1.68	33.11 ± 1.49	33.56 ± 3.37	17.46 ± 3.79	73.75 ± 1.34	27.46 ± 2.14
Tebuconazole	100.00 ± 1.37	100.00 ± 1.32	100.00 ± 2.23	100.00 ± 1.17	100.00 ± 1.06	81.25 ± 2.28
Pyraclostrobin	100.00 ± 1.13	100.00 ± 2.24	100.00 ± 1.12	100.00 ± 2.08	100.00 ± 2.26	83.34 ± 1.18

5h, 5m, 5n, 5o, and 5r were 75.86, 77.78, 71.97, 72.31, 75.63, 76.58, 80.38, and 73.57%, respectively. Moreover, compounds 4, 5g, 5h, 5i, 5j, 5k, 5l, 5o, 5p, 5q, 5r, and 5s showed good antifungal activities against strawberry *Botrytis cinerea* and, the inhibition rates were 82.68, 72.89, 74.37, 76.35, 77.85, 77.32, 76.66, 75.31, 70.60, 71.52, 79.85, and 73.75%, respectively. In particular, four compounds 4, 5h, 5o, and 5r presented obvious activity to three of the four *Botrytis cinerea*. This also indicated the potential of these four compounds as leading structures or candidates against *Botrytis cinerea*.

Further structure–activity relationship analysis signified that the introduction of halogen atom could improve the antifungal activities against *Botrytis cinerea*. Especially for strawberry *Botrytis cinerea*, it was more obvious. Moreover, the introduction of electron withdrawing group, such as -CN, -CF₃, and -NO₂, could increase the activity of compounds to a certain extent. For example, compounds 5i, 5j, 5k, and 5l appeared a good activity against strawberry *Botrytis cinerea*. In addition, most compounds represented ordinary activities towards *Phytophthora infestans and Pyricularia oryzae* Cav.,

which indicated these compounds were not favor to the inhibition of these two fungi.

4 CONCLUSION

In summary, a novel series of 1,2,4-triazolo[4,3-*c*] trifluoromethylpyrimidine derivatives bearing the thioether moiety were designed, synthesized, and characterized. The antifungal activities of the target compounds were also evaluated. Most compounds exhibited obvious antifungal activities against cucumber *Botrytis cinerea*, strawberry *Botrytis cinerea*, tobacco *Botrytis cinerea*, blueberry *Botrytis cinerea*, *Phytophthora infestans* and *Pyricularia oryzae* Cav. Notably, four compounds 4, 5h, 5o, and 5r were selected and showed significant antifungal activities against three of the four *Botrytis cinerea*. This indicated that these compounds are expected to become the leading structures or candidates for resistance to *Botrytis cinerea*.

DATA AVAILABILITY STATEMENT

The datasets presented in this study can be found in online repositories. The names of the repository/repositories and accession number(s) can be found below: Cambridge Crystallographic Data Centre, 2189490.

REFERENCES

Abdel-Aziz, S. A., Taher, E. S., Lan, P., Asaad, G. F., Gomaa, H. A. M., El-Koussi, N. A., et al. (2021). Design, Synthesis, and Biological Evaluation of New Pyrimidine-5-Carbonitrile Derivatives Bearing 1,3-thiazole Moiety as Novel Anti-inflammatory EGFR Inhibitors with Cardiac Safety Profile. *Bioorg. Chem.* 111, 104890. doi:10.1016/j.bioorg.2021.104890

Abdelrehim, E.-s. M. (2021). Synthesis and Screening of New [1,3,4]Oxadiazole, [1,2,4]Triazole, and [1,2,4]Triazolo[4,3-*B*][1,2,4]triazole Derivatives as Potential Antitumor Agents on the Colon Carcinoma Cell Line (HCT-116). *ACS Omega* 6 (2), 1687–1696. doi:10.1021/acsomega.0c05718

Abu-Zaied, M. A., Elgemeie, G. H., and Mahmoud, N. M. (2021). Anti-covid-19 Drug Analogues: Synthesis of Novel Pyrimidine Thioglycosides as Antiviral Agents against SARS-COV-2 and Avian Influenza H5N1 Viruses. *ACS Omega* 6 (26), 16890–16904. doi:10.1021/acsomega.1c01501

Baillache, D. J., and Unciti-Broceta, A. (2020). Recent Developments in Anticancer Kinase Inhibitors Based on the Pyrazolo[3,4-D]pyrimidine Scaffold. *RSC Med. Chem.* 11 (10), 1112–1135. doi:10.1039/D0MD00227E

Basyouni, W. M., Abbas, S. Y., El-Bayouki, K. A. M., Dawood, R. M., El Awady, M. K., and Abdelhafez, T. H. (2021). Synthesis and Antiviral Screening of 2-(propylthio)-7-substituted-thiazolo[5,4-d]pyrimidines as Anti-bovine Viral Diarrhea Virus Agents. *J. Heterocycl. Chem.* 58 (9), 1766–1774. doi:10.1002/jhet.4307

Cawrse, B. M., Lapidus, R. S., Cooper, B., Choi, E. Y., and Seley-Radtke, K. L. (2018). Anticancer Properties of Halogenated Pyrrolo[3,2-D]pyrimidines with Decreased Toxicity via N5 Substitution. *ChemMedChem* 13 (2), 178–185. doi:10.1002/cmdc.201700641

Ding, M., Wan, S., Wu, N., Yan, Y., Li, J., and Bao, X. (2021). Synthesis, Structural Characterization, and Antibacterial and Antifungal Activities of Novel 1,2,4-Triazole Thioether and Thiazolo[3,2-B]-1,2,4-Triazole Derivatives Bearing the 6-Fluoroquinazolinyl Moiety. *J. Agric. Food Chem.* 69 (50), 15084–15096. doi:10.1021/acs.jafc.1c02144

Du, S., Yuan, Q., Hu, X., Fu, W., Xu, Q., Wei, Z., et al. (2021). Synthesis and Biological Activity of Novel Antifungal Leads: 3, 5-Dichlorobenzyl Ester

AUTHOR CONTRIBUTIONS

CL and NP contributed to the synthesis, purification, and characterization of all compounds and the activity research and prepared the original manuscript. QF and WW designed and supervised the research and revised the manuscript. All authors have read and agreed to the published version of the manuscript.

FUNDING

SUPPLEMENTARY MATERIAL

The Supplementary Material for this article can be found online at: https://www.frontiersin.org/articles/10.3389/fchem.2022.939644/full#supplementary-material

Derivatives. *J. Agric. Food Chem.* 69 (51), 15521–15529. doi:10.1021/acs.jafc.1c04022

El-mahdy, K. M., and Farouk, O. (2021). Efficient Access to Some New Pyrimidine Derivatives and Their Antimicrobial Evaluation. *J. Heterocycl. Chem.* 58 (12), 2261–2269. doi:10.1002/jhet.4350

El-Shershaby, M. H., Ghiaty, A., Bayoumi, A. H., Ahmed, H. E. A., El-Zoghbi, M. S., El-Adl, K., et al. (2021). 1,2,4-Triazolo [4,3-c] Quinazolines: a Bioisosterism-Guided Approach towards the Development of Novel PCAF Inhibitors with Potential Anticancer Activity. *New J. Chem.* 45 (25), 11136–11152. doi:10.1039/D1NJ00710F

Fan, C. C., Jiao, S. L., Qin, M., and Zou, Z. H. (2019). 3, 5-Bis (2-Hydroxyphenyl)-1 H-1, 2, 4-Triazole Derivatives: Synthesis, Crystal Structure and Insecticidal Activity. *ChemistrySelect* 4 (29), 8593–8597. doi:10.1002/slct.201901706

Fayed, E. A., Nosseir, E. S., Atef, A., and El-Kalyoubi, S. A. (2022). *In Vitro* antimicrobial Evaluation and In Silico Studies of Coumarin Derivatives Tagged with Pyrano-Pyridine and Pyrano-Pyrimidine Moieties as DNA Gyrase Inhibitors. *Mol. Divers* 26 (1), 341–363. doi:10.1007/s11030-021-10224-4

Kesari, C., Rama, K. R., Sedighi, K., Stenvang, J., Björkling, F., Kankala, S., et al. (2021). Synthesis of Thiazole Linked Chalcones and Their Pyrimidine Analogues as Anticancer Agents. *Synth. Commun.* 51 (9), 1406–1416. doi:10.1080/00397911.2021.1884262

Kumar, S., and Narasimhan, B. (2018). Therapeutic Potential of Heterocyclic Pyrimidine Scaffolds. *Chem. Central J.* 12, 38. doi:10.1186/s13065-018-0406-5

O'Brien, P. A. (2017). Biological Control of Plant Diseases. *Australas. Plant Pathol.* 46, 293–304. doi:10.1007/s13313-017-0481-4

Pathak, P., Novak, J., Shukla, P. K., Grishina, M., Potemkin, V., and Verma, A. (2021). Design, Synthesis, Antibacterial Evaluation, and Computational Studies of Hybrid Oxothiazolidin-1,2,4-triazole Scaffolds. *Arch. Pharm.* 354 (6), 2000473. doi:10.1002/ardp.202000473

Shao, W.-B., Wang, P.-Y., Fang, Z.-M., Wang, J.-J., Guo, D.-X., Ji, J., et al. (2021). Synthesis and Biological Evaluation of 1,2,4-Triazole Thioethers as Both Potential Virulence Factor Inhibitors against Plant Bacterial Diseases and Agricultural Antiviral Agents against Tobacco Mosaic Virus Infections. *J. Agric. Food Chem.* 69 (50), 15108–15122. doi:10.1021/acs.jafc.1c05202

Sun, S.-X., Yan, J.-H., Zuo, J.-T., Wang, X.-B., Chen, M., Lu, A.-M., et al. (2021). Design, Synthesis, Antifungal Evaluation, and Molecular Docking of Novel 1,2,4-triazole Derivatives Containing Oxime Ether and Cyclopropyl Moieties as Potential Sterol Demethylase Inhibitors. *New J. Chem.* 45 (40), 18898–18907. doi:10.1039/D1NJ03578A

Wang, R.-X., Du, S.-S., Wang, J.-R., Chu, Q.-R., Tang, C., Zhang, Z.-J., et al. (2021). Design, Synthesis, and Antifungal Evaluation of Luotonin A Derivatives against Phytopathogenic Fungi. *J. Agric. Food Chem.* 69 (48), 14467–14477. doi:10.1021/acs.jafc.1c04242

Wang, S., Li, Z.-R., Suo, F.-Z., Yuan, X.-H., Yu, B., and Liu, H.-M. (2019). Synthesis, Structure-Activity Relationship Studies and Biological Characterization of New [1,2,4]triazolo[1,5-A]pyrimidine-Based LSD1/KDM1A Inhibitors. *Eur. J. Med. Chem.* 167, 388–401. doi:10.1016/j.ejmech.2019.02.039

Wang, S., Yuan, X.-H., Wang, S.-Q., Zhao, W., Chen, X.-B., and Yu, B. (2021). FDA-approved Pyrimidine-Fused Bicyclic Heterocycles for Cancer Therapy: Synthesis and Clinical Application. *Eur. J. Med. Chem.* 214, 113218. doi:10.1016/j.ejmech.2021.113218

Wei, L., Zhang, J., Tan, W., Wang, G., Li, Q., Dong, F., et al. (2021). Antifungal Activity of Double Schiff Bases of Chitosan Derivatives Bearing Active Halogeno-Benzenes. *Int. J. Biol. Macromol.* 179, 292–298. doi:10.1016/j.ijbiomac.2021.02.184

Wu, W.-N., Jiang, Y.-M., Fei, Q., and Du, H.-T. (2019). Synthesis and Fungicidal Activity of Novel 1,2,4-triazole Derivatives Containing a Pyrimidine Moiety. *Phosphorus, Sulfur, Silicon Relat. Elem.* 194 (12), 1171–1175. doi:10.1080/10426507.2019.1633321

Wu, W., Chen, M., Wang, R., Tu, H., Yang, M., and Ouyang, G. (2019). Novel Pyrimidine Derivatives Containing an Amide Moiety: Design, Synthesis, and Antifungal Activity. *Chem. Pap.* 73, 719–729. doi:10.1007/s11696-018-0583-7

Yang, L., Sun, Y., Lu, Z., Liang, J., Wang, T., and Luo, J. (2022). Synthesis and Herbicidal Activity of Pyrimidyl-1,2,4-triazole Derivatives Containing Aryl Sulfonyl Moiety. *J. Heterocycl. Chem* 59 (4), 704–719. doi:10.1002/jhet.4410

Yang, Z., Sun, Y., Liu, Q., Li, A., Wang, W., and Gu, W. (2021). Design, Synthesis, and Antifungal Activity of Novel Thiophene/Furan-1,3,4-Oxadiazole Carboxamides as Potent Succinate Dehydrogenase Inhibitors. *J. Agric. Food Chem.* 69 (45), 13373–13385. doi:10.1021/acs.jafc.1c03857

Yu, X., Lan, W., Chen, M., Xu, S., Luo, X., He, S., et al. (2021). Synthesis and Antifungal and Insecticidal Activities of Novel *N*-Phenylbenzamide Derivatives Bearing a Trifluoromethylpyrimidine Moiety. *J. Chem.* 2021, 1–8. doi:10.1155/2021/8370407

A briefly overview of the research progress for the abscisic acid analogues

Yaming Liu†, Shunhong Chen†, Panpan Wei, Shengxin Guo and Jian Wu*

State Key Laboratory Breeding Base of Green Pesticide and Agricultural Bioengineering, Key Laboratory of Green Pesticide and Agricultural Bioengineering, Ministry of Education, Center for R&D of Fine Chemicals of Guizhou University, Guiyang, China

Abscisic acid (ABA) is an important plant endogenous hormone that participates in the regulation of various physiological processes in plants, including the occurrence and development of somatic embryos, seeddevelopment and dormancy. ABA is called "plant stress resistance factor", while with the limitation of the rapid metabolic inactivation and photoisomerization inactivation of ABA for its large-scale use. Understanding the function and role of ABA in plants is of great significance to promote its application. For decades, scientists have conducted in-depth research on its mechanism of action and signaling pathways, a series of progress were achieved, and hundreds of ABA analogues (similar in structure or function) have been synthesized to develop highly active plant growth regulators and tools to elucidate ABA perception. In this review, we summarize a variety of ABA analogues, especially the ABA receptor analogues, and explore the mechanisms of ABA action and catabolism, which will facilitate the development of novel ABA analogues with high biological activities.

Introduction

The environment that plants depend on for survival is constantly changing, and some adverse conditions, such as extreme temperature, drought, salinization and other abiotic stresses, can seriously affect the growth and development of plants (Young, 2007). Future climate change will lead to a gradual increase in the frequency (Guo et al., 2021). Therefore, it is important to improve the adaptability of plants to these abiotic stresses, especially drought.

Plant hormones play an important role in regulating plant adaptation to abiotic stresses (Waadt et al., 2022). Abscisic acid (ABA) synthesis is one of the fastest responses to stresses in plants (Zhao et al., 2018). ABA is a phytohormone which is named for its function in inhibiting plant growth and promoting leaf shedding. Subsequently, more and more studies show that ABA is also involved in regulating
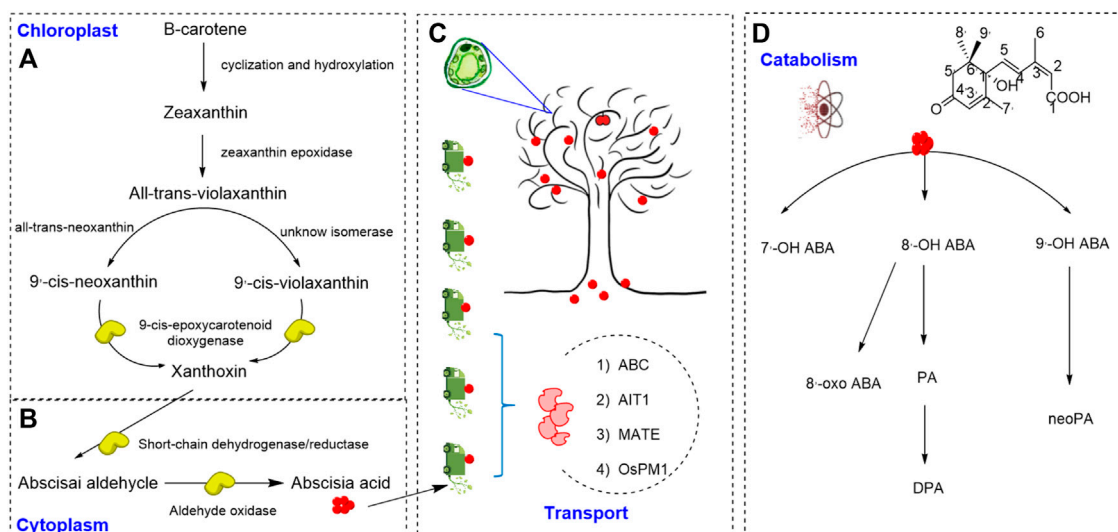
FIGURE 1
ABA biosynthesis, transport and catabolism **(A,B)**. Biosynthetic pathway of abscisic acid (Izquierdo-Bueno et al., 2018; Takino et al., 2018). **(C)** Transport form of abscisic acid (Kuromori et al., 2010; Kang et al., 2015). **(D)** The catabolic pathway of abscisic acid (Nambara and Marion-Poll, 2005).

other growth and development processes of plants, such as seed germination, dormancy and stomatal closure. Moreover, ABA has been reported to control the expression of many stress-responsive genes and involve in many kinds of stress responses in plants (Hoth et al., 2002; Seki et al., 2002; Nemhauser et al., 2006).

The studies on the function and application for ABA have made remarkable achievements in the past 20 years. The synthesis, perception and transduction of ABA signals have been summarized (Young, 2007; Fidler et al., 2015; Zhang, et al., 2015), Asghar, Ma and co-workers had surveyed the advances from the functions of ABA (such as the effects on osmotic stress or on the seed dormancy, germination, and plant resistance to transpiration), respectively (Ma et al., 2018; Asghar et al., 2019). However, few summaries for ABA derivatives and structural analogues (especially studies after 2014), biosynthesis, transport and catabolism have not been made. Therefore, this article summarizes the research overview for the ABA based on the following aspects: Firstly, the discovery of ABA receptor structure and signal transduction mechanism, as well as the regulation of ABA on plants under abiotic stress is introduced. Secondly, the current discovery of ABA analogues and their functions are summarized. Finally, the existing challenges are discussed. This brief article gives an overview on the progress for the ABA analogues in the past decades and introduces the latest progress. The aim for this briefly article provides readers with a convenient route to touch this topic, and hopefully serve some educational purpose for graduate students and assist further research in related fields.

ABA biosynthesis, transport and catabolism

As shown in Figures 1A,B, ABA is a sesquiterpenoid phytohormone containing 15 carbon atoms. ABA is synthesized in plants mainly using the C_{40} indirect pathway (also known as the carotenoid pathway), which is initiated from the cleavage of a C_{40} precursor known as β-carotene (Izquierdo-Bueno et al., 2018.; Takino el al., 2018). After cyclization and hydroxylation, β-carotene is converted to zeaxanthin (C_{40}), which is catalyzed by zeaxanthin epoxidase (ZEP) to form all-trans-violaxanthin (C_{40}). This pathway then bifurcates into two pathways. All-trans-violaxanthin can be further converted to 9′-cis-neoxanthin (C_{40}) through all-trans-neoxanthin (C_{40}), or it is converted to 9′-cis-violaxanthin (C_{40}) directly by an unknown isomerase (North et al., 2007). Then, 9′-cis-violaxanthin and 9′-cis-neoxanthin both can be catalyzed by 9-cis-epoxycarotenoid dioxygenase (NCED) to produce xanthoxin (the C_{15} precursor of ABA), which can also act as a growth inhibitor (Anstis et al., 1975; Schwartz et al., 1997). Xanthoxin is presumed to migrate from the plastid to the cytosol (Nambara and Marion-Poll, 2005), where it is converted to abscisic aldehyde. Then abscisic aldehyde is eventually oxidized to ABA by abscisic aldehyde oxidase (AAO3) (Bittner et al., 2001; Cheng et al., 2002).

Recent studies showed that stress-induced ABA biosynthesis primarily occurs in vascular tissues and leaves, but ABA functions in various cells (Kuromori et al., 2010; Zhang et al., 2018). Therefore, it is important for ABA to transport among different organs, especially in the systemic stress responses of the whole plant. The active transport of ABA is mediated by many

factors, such as ATP-binding cassette (ABC) transporters (Kuromori et al., 2010; Kang et al., 2015), ABA-IMPORTING TRANSPORTER1 (AIT1, which is also known as low-affinity nitrate transporter NRT1.2) (Kanno et al., 2012), DTX type/ multidrug and toxic compound extrusion (MATE) transporters (Yu et al., 2014), and AWPM 19 family proteins (OsPM1) (Yao et al., 2018). These ABA transporters have been increasingly shown to be involved in stress responses, which are shown in the Figure 1C.

The catabolism of ABA in plant is controlled via two pathways: hydroxylation and conjugation, as shown in Figure 1D (Nambara and Marion-Poll, 2005). ABA can be hydroxylated via oxidation at three positions of the ring structure, C-7′, C-8′, and C-9′, triggering further inactivation steps, of which C-8′ is the primary site in plants (Cutler and Krochko, 1994). The unstable 8′-hydroxy ABA is converted to phaseic acid (PA) (Kushiro et al., 2004; Nambara and Marion-Poll, 2005), and PA has been reported to selectively activate a subset of ABA receptor PYLs (Weng et al., 2016). PA is then converted to dihydrophaseic acid (DPA), which is further catalyzed to DPA-4-O-β-D-glucoside (DPAG) (Weng et al., 2016). ABA conjugation is another pathway to regulate cellular ABA amounts under both normal and dehydration conditions (Lee et al., 2006; Xu et al., 2012). ABA and hydroxy ABA are conjugated with glucose for inactivation, forming different conjugates. The ABA-glucose ester (ABA-GE) is the predominant form of these conjugates and stored in vacuoles and the apoplast (Dietz et al., 2000; Liu et al., 2015). When the environment changes such as dehydration, ABA-GE is rapidly transformed to active ABA by β-glucosidases (Lee et al., 2006; Xu et al., 2012). The conjugation/ deconjug-ation cycle enables plants to phenotypically adapt to their environment through ABA-mediated responses by activating and inactivating ABA rapidly (Chen et al., 2020).

ABA signal transduction and the role of ABA pathways in stress signaling

The ABA signaling pathway has been studied for several decades, and the core ABA signaling components including three protein classes: ABA receptors, negative regulators and positive regulators (Danquah et al., 2014). ABA functions in plants through cellular recognition by the intracellular receptor. Many ABA receptors have been reported so far, such as H subunit of Chloroplast Mg^{2+}-chelatase, G-protein coupled Receptor 2, GPCR-type G protein, and Pyracbactin Resistance/Pyracbactin resistance-like/Regulatory Component of ABA Receptor (PYR/PYL/RCAR) (Guo et al., 2011).

PYR/PYL/RCARs are the most important among these receptors, the discovery of which basically elucidates the ABA signaling pathway (Ma et al., 2009; Park et al., 2009). Most plants encode more than one PYR/PYL/RCAR proteins, and they are differentially expressed in multiple organs, cells during different growth stages (Antoni et al., 2013; Dittrich et al., 2018). Genetic

evidences showed that a high level of functional redundancy exists in this gene family, but they are essential for ABA perception, signal transduction and response to stress in plants. PYR/PYL/RCAR mutants displayed impaired ABA responses (Miao et al., 2018; Zhao et al., 2018), while overexpression of PYR/PYL/RCARs enhanced ABA responses to impact abiotic stress tolerance (Santiago et al., 2009; Mega et al., 2019).

As shown in Figure 2A, Protein Phosphatase 2Cs (PP2Cs) and SNF1-related protein kinase 2s (SnRKs) are major negative regulators and positive regulators of ABA signaling, respectively. PYR/PYL/RCARs show conformational change upon binding of ABA, which exposes the interaction surface allowing for favorable binding of some PP2Cs (Cutler et al., 2010). Consequently, the activities of PPC2s are inhibited, allowing activation of SnRK2s. Then SnRK2s activate downstream target proteins, including basic-domain leucine zipper (bZIP) transcription factors, anion channels and NADPH oxidases, to induce ABA responses. In the absence of ABA, PP2Cs are unable to bind to PYR/PYL/RCARs and they inactivate SnRKs by dephosphorylation (Soon et al., 2012). ABA is commonly known as the "stress hormone" that responds to variety of environmental stresses, especially for abiotic stresses (Kanchan et al., 2017). When plants encounter various abiotic stresses, such as salinity, extreme temperature, heavy metal, drought, UV-B, water stresses, endogenous ABA levels increase rapidly due to the increase of ABA biosynthesis and inhibition of ABA degradation. Then the downstream specific signaling pathways are activated and gene expression levels are modified (Kanchan et al., 2017).

As shown in Figure 2B, osmotic stress caused by environmental stresses, such as high salinity, drought and cold, results in dehydration and inhibition of water uptake in plants. ABA accumulates under osmotic stress conditions and plays an important role in the stress responses and tolerance of plants (Shinozaki and Yamaguchi-Shinozaki 2000; Finkelstein et al., 2002). ABA promotes short-term responses like stomatal closure to maintain water balance (Agurla et al., 2018). For example, under salt stress, ABA is accumulated in plant roots and transported to the leaves, which leads to the decrease of leaf expansion rate and stomatal closure. As a result, the reduced transpiration rate and increased salt transportation in the root cap alleviate the damage causing by salt stress. ABA also stimulates longer-term growth responses through regulation of stress-responsive genes, the products of which may function in dehydration tolerance. Silva-Ortega et al., reported that ABA can regulate the expression of P5CS, which promotes the production and accumulation of osmotic adjustment substances like proline, betaine, and soluble sugar (Silva-Ortega et al., 2008).

Excepting mediating stomatal closure and osmotic regulation, ABA also involves in the balance of ion concentration under abiotic stresses. ABA participates in the modification of ATPase in plasma membrane and vacuolar membrane to provide more driving force for Na^+/H^+ antiporter, which strengthens Na^+ efflux and ion

FIGURE 2
ABA signal transduction and the role of ABA pathways in stress signaling **(A)** The working model of ABA-dependent recognition and inhibition of PP2Cs by PYLs (Cutler et al., 2010; Soon et al., 2012). **(B)** The role of abscisic acid pathways in stress signaling (Shinozaki and Yamaguchi-Shinozaki, 2000; Finkelstein et al., 2002).
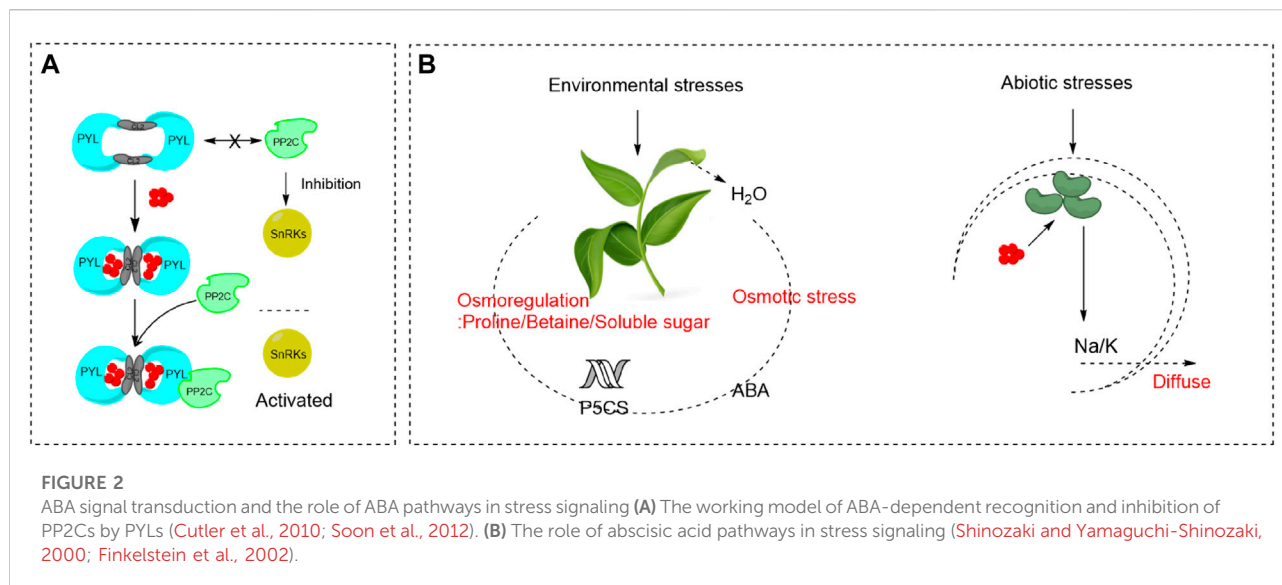
regionalization to alleviate the damage of salt and alkaline stress (Janicka-Russak and Kłobus, 2007; Khadri et al., 2007). Three major pathways involved in the heavy metal detoxification can be triggered by ABA, inhibiting the uptake, altering the translocation from root to shoot, and promoting the conjugation with chelators (Hu et al., 2020). In addition, the decrease of photosynthesis caused by salt, heavy metal, alkaline and cold stress can be effectively relieved by ABA (Saradhi et al., 2010). The addition of exogenous ABA can accelerate the recovery of plant photosystem II, restore the photosynthetic inactivation state of the core complex to normal, maintain the stability of photosynthetic organs, and enhance the photosynthetic efficiency of leaf light capture and conversion (Saradhi et al., 2010). Moreover, ABA can interact with other stress resistance elements, such as antioxidant defense system and the MAPK cascades, to help plants resist environmental stresses (Danquah et al., 2014; Shu et al., 2016; Yang and Guo, 2018).

Chemical manipulation of ABA signaling structural analogues

Considering the importance of ABA signaling in many processes, including stress tolerance, seed germination, root growth and development, and senescence, small molecule chemicals can manipulate ABA signaling showing potential applications in agricultural production. Among them, the most extensively studied are the analogues of ABA receptor (Bari and Jones, 2009). Up to date, many compounds have been identified as significant ABA-agonist/antagonist and can be employed to reverse the excessive/moderate ABA action, which is shown in Figure 3.

In 1997, Rose synthesized compounds **1** and **2** (Rose et al., 1997), and carried out a series of anti-stress experiments, officially started the research on the application of ABA analogues in plants. They found that both compounds **1** and **2** could stimulate the radial conduction of water in maize roots just like ABA. In subsequent studies, analogues **1** and **2** were found to reduce chloride ion concentration and ethylene content in plants. More importantly, they can delay the consumption of CO_2 assimilation under adverse conditions. The activity of compound **2** was better than that of abscisic acid, as the activity of compound **1** was similar to that of ABA. Oxidative hydroxylation of 8′- and 9′-methyl is the key to the metabolic inactivation of abscisic acid in plants. Therefore, modification of 8′- and 9′- methyl groups to obtain more stable ABA analogues has become the research direction of many scientists.

Nicholas M. Irvine et al. synthesized an anthracenone analogue of ABA (**3**) (Irvine et al., 2000), and Takahiro Inoue synthesized new ABA analogues (**4** and **5**) (Inoue and Oritani, 2000) by regioselective hydrocyanation and possessed a cyano or methoxycarbonyl group at the 6′α-position. Bioactivity tests were performed separately, and the results show that all the compounds were less than ABA, but raised the possibility of structural modification at the 6′α-position. In the same year, Cutler found that compounds (+)-8′-acetylen-ABA (**1**) and (+)-9′ -propargyl-ABA (**6**) (Cutler et al., 2000) showed better activity than ABA in inhibiting arabidopsis seed germination. Among them (+)-8′-acetylene-ABA (**1**) can inhibit not only arabidopsis seed germination, but also maize cell growth and wheat embryo germination.

Ueno found that compounds **7** and **8** (Ueno et al., 2005) had no inhibitory effect on cytochrome P450 monooxidase, which might be caused by the fact that the C-8 group was too large to
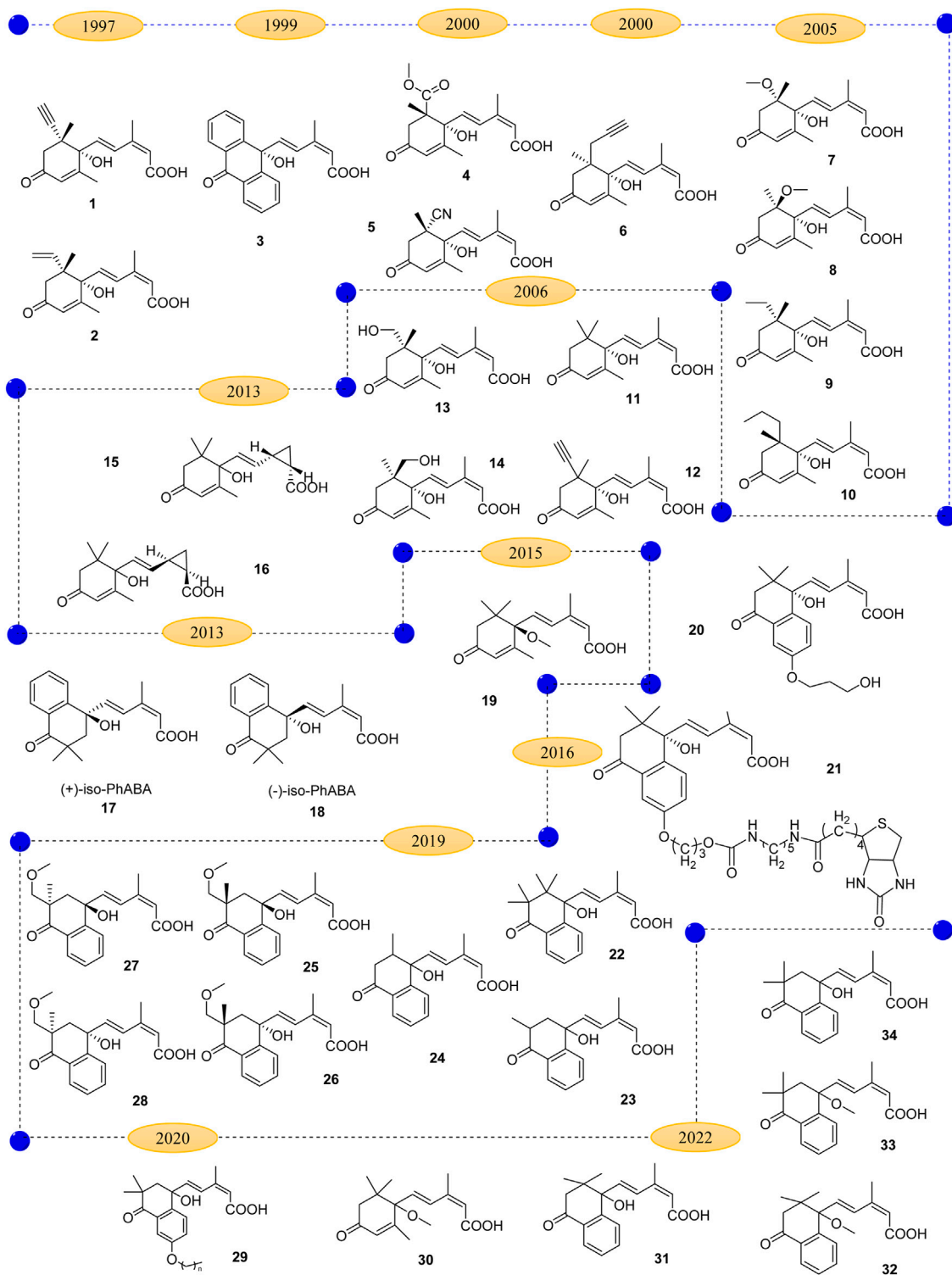
FIGURE 3
The development of abscisic acid structural analogues.

bind with 8' -hydroxylase. When C-8′ methyl hydrogen is replaced by methyl and ethyl groups, 8' -methyl abscisic acid (**9**) and 8' -ethyl abscisic acid (**10**) were obtained (Ueno et al., 2005). The results showed that compound **9** was a competitive inhibitor of 8' -hydroxylase, while compound **10** had no inhibitory activity. This may be due to the fact that methoxyl and ethyl have similar stereoscopic sizes and are similarly unable to bind to the active site, so it is thought that methyl group may be the largest group tolerated by the active binding site.

Nyangulu and co-workers (Nyangulu et al., 2006) synthesized tetrahydronaphthone ABA analogue **11** by substituting benzene ring of aromatic hydrocarbon for planar propylene group structure on six rings. When the concentration was 0.33 μmol/L, the inhibition rate of ABA was about 40%, while the inhibition rate of compound **11** was less than 10%. The R configuration of compound **11** was similar to that of S configuration. Compound **12** showed a highly activity in inhibiting germination of *Arabidopsis thaliana* seeds (Nyangulu et al., 2006). Compounds **13** and **14** were synthesized on the basis of improved compounds **1** and **2** (Nyangulu et al., 2006). They suggested that when the 8' -hydroxylase oxidizes **11** to **13**, it inhibited further cyclization of compound **13** to PA analogue due to instability. Suspension culture of maize cells showed that the metabolic rate of compound **11** was similar to ABA. Compounds **13** and **14** exhibited similar activity to ABA at high concentrations. The biggest defect of ABA in practical application is poor photostability.

In order to obtain more stable ABA analogues, Liu has synthesized a photostable *cis*-2, 3-cyclopropanated abscisic acid analogue. They described the effect of ABA analogue isomers on activity. The photoisomerization study showed that compounds **15** and **16** (Liu et al., 2013) reached *cis* and inverse equilibrium in 44 and 36 h, respectively under 254 nm UV light, which was much longer than ABA (12 h) and thus had better photostability. The biological activities of compounds **15** and **16** under two modes of seed germination and seedling growth were tested. The results showed that at high concentrations (3 μmol/L and 5 μmol/L), both compounds had better inhibitory effects on seed germination than ABA did. But its inhibitory effect was lower than ABA at low concentration. The inhibitory effect of the two target compounds on the growth of *Arabidopsis thaliana* seedlings was lower than that of ABA at each concentration. Overall, compound **15** showed higher activity than compound **16**. However, in most cases, the biological activity of the *cis* structure is lower than that of the trans structure, and the difference of the results provides an important basis for further study of the structure-activity relationship of ABA.

Han et al. developed a new ABA analogue named (+) 2′,3′-*iso*-PhABA (**17** and **18**) in order to overcome its oxidative inactivation. *In vivo* experiments, the activity of (+) - *iso* -PhABA (**17**) was significantly higher than that of (+)-ABA,

including inhibition of lettuce and *Arabidopsis* seed germination (the inhibitory activity on arabidopsis thaliana seed germination is about 14 times of (+)-ABA), wheat embryo germination and rice seedling elongation. Protein phosphatase 2C (PP2C) activity showed that (+) - *iso* - PhABA (**23**) was an effective and selective ABA receptor agonist, which could better bind to PYL10 (Tan et al., 2013).

With the discovery of ABA receptor proteins and the application of chemical genetics in agriculture, Chantel L. Benson synthesized a series of ABA analogues as chemical probes to understand functional redundancy in the ABA receptor family (Benson et al., 2015). In PBI 352 (**19**), the substitution of hydrogen on C-10 by methyl group for OH induced stomatal closure, but did not affect the selectivity of analogues in *Arabidopsis* seedling germination or root growth. This selectivity has potential utility in practical applications where temporary drought protection can be provided to plants without reducing concomitant root growth. For all tested RCARs, the analogue PBI 352 (**19**) significantly reduced its receptor-binding activity compared with (*S*)-ABA (**1**), and PBI 352 (**19**) binds RCAR8 to inhibit ABI2.

Rajagopalan et al., developed a library of ABA analogues containing 240 compounds that are structural variants of the basic molecule S-(+)-ABA. These molecules were synthesized primarily for specific structural activity studies, and one antagonist PBI686 (**20**), was identified to be active on both RCAR receptors (Rajagopalan et al., 2016). Analogues PBI686 (**20**) and PBI664 (**21**) have no agonist activity by themselves, but are effective antagonists of ABA receptors blocking phosphatase binding to receptors.

In 2019, Wan et al., designed and synthesized five analogues of an earlier 2′,3′-*iso*-PhABA (Wan et al., 2019). Bioassay results showed that the number and position of methyl groups and the substitution of hydrogen atoms on methyl groups have great influence on the activity. Compared with 2′,3′-*iso*-PhABA, dimethyl-PhABA (**22**) showed slightly decreased inhibitory activity on seed germination and seedling growth of rice. However, it significantly reduced the ability to inhibit wheat embryo germination. Both demethyl-*iso*-PhABA (**23**) and demethyl- PhABA (**24**) showed weak inhibitory activity, and 11′-methoxy- PhABA (**25/26**) were more potent than their isomers **30/31** in all bioassays. These results suggested that the preservation of quaternary carbon at the 2′ or 3′ position is necessary for the maintenance of ABA-like biological activity, and the demethylation at the 3′ position is more significant. Among them, **25/26** showed good inhibitory activity and different binding selectivity to ABA receptor PYR1 and PYL2/PYL5.

Che et al., described a class of ABA agonist/antagonist probes, APAn (**29**) that regulate either agonist or antagonist activity according to the length of the 6′-alkoxy chain (Che et al., 2020). With the extension of alkoxy chain, the receptor binding potential increased gradually, and the inhibitory

FIGURE 4
Modification sites of abscisic acid structural analogues.
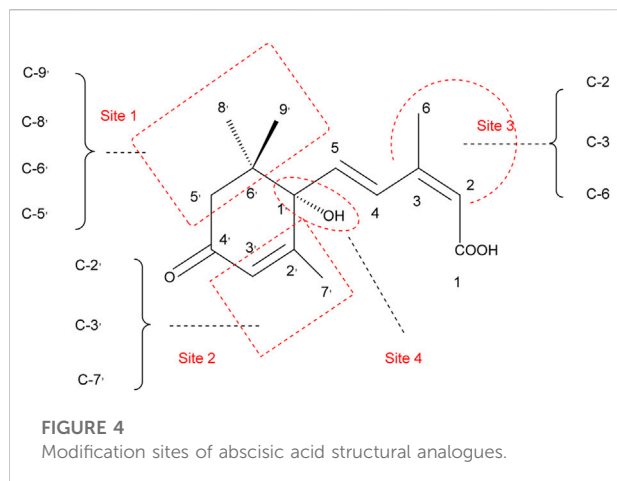
activity of HAB1 decreased. Theoretical analysis based on molecular docking and molecular dynamics simulations showed that some factors outside the ligand binding pocket in the receptor also affected ligand binding to the receptor. Van der Waals interaction between alkyl chains in APAn made the ligand binding to the ABA receptor tighter. This enhanced binding makes it an antagonist rather than a weakened agonist.

Recently, Wan et al., synthesized a series of ABA analogues and tested their activities (Wan et al., 2022). The results showed that the hydroxyl group of $1'$-OH is an important functional group for seed germination and development. Therefore, compound **31** and **33** can inhibit seed germination, but which is not related to stomatal movement and response to drought stress regulated by ABA and its analogues. Methylation of $1'$-OH significantly reduced their ability to bind to single receptor PYL5 and slightly enhanced their ability to bind to dimer receptor PYL2. The decreased inhibitory activities of **30**, **32**, and **34** on seed germination may be related to the decreased affinity of PYL5, which is caused by the destruction of hydrogen bond network. This suggests that PYL5 is a selective receptor closely related to plant growth.

The above section summarized **34** representative ABA analogues, and some have regulatory activity and some have inhibitory activity of P450 oxidase in the decomposition process, which can be used to study the molecular mechanism of ABA action and catabolism. Through the analysis of the activity or enzyme inhibitory activity of different analogues, it is known that there is a certain difference between the ABA active group and the structure inhibited by ABA $8'$-hydroxylase, and this difference will help the development of new ABA analogues (An ideal enzyme inhibitor should have the ABA structural features required for substrate specificity, but not the structural features required to activate the ABA signaling

pathway). Overall, the modification of site 1 (Figure 4), the spatial size and saturation will directly affect the binding ability of the compound to the target. The difference of the groups on site 2 (Figure 4) may block the binding ability of the downstream phosphatase to the receptor. The modification of site 3 (Figure 4) is to improve the high stability provides a new design idea. The modification (methylation) of site 4 (Figure 4) changes the binding ability of the analogue to the receptor by changing the hydrogen bond network.

ABA function analogues

In recent years, scientists have screened many ABA functional analogues (Figure 5) using chemical genetic methods, their structures are very different from the structure of ABA. Among which, the most representative structures are sulfonamides and amide derivatives.

Pyrabactin, a naphthalene-sulfonamide derivative, is the first synthetic ABA mimic (Park et al., 2009). Pyrabactin displayed several ABA-like activities, such as inhibition of seed germination (Park et al., 2009), induced stomatal closure (Puli and Raghavendra, 2012) and enhanced root hydraulic conductivity (Fan et al., 2015). It could be used to improve the drought tolerance of crop plants. Several structural analogues of pyrabactin have been screened and the structure-activity relationship revealed that pyridyl nitrogen is important for binding affinity biological activity (Helander et al., 2016). Studies also discovered that pyrabactin exhibits distinct responses towards PYL-subtypes. It strongly activates PYR1/PYL1 but acts as an antagonist for PYL2 and PYL3 (Melcher et al., 2010; Miyakawa and Tanokura, 2011).

Okamoto et al., identified sulfonamide AM1 (also named as quinabactin), through a yeast two-hybrid screen (Okamoto et al., 2013). Quinabactin showed a broader spectrum of PYL activity with enhanced bioactivity as compared to pyrabactin. Quinabactin treatments inhibited seed germination, prevented leaf water loss, and promoted drought resistance (Cao et al., 2013). Cao et al. developed a series of AM1 fluorine derivatives (AMFs) by progressively substituting fluorine atoms on the benzyl ring. The fluorine atoms in AMFs increase the plasma membrane permeability and hydrogen bonding network. Among these derivatives, AMF4 was proved to be a better agonist than AM1 or ABA (Cao et al., 2017). Overtveldt et al. designed phosphonamide analogues of pyrabactin, which given a different physiological response by selectively stimulating ABA-signaling pathways (Van Overtveldt et al., 2015). Further efforts exploited the structure of cyanabactin, which has a nitrile and isopropyl substituted monocyclic ring system instead of the bicyclic ring system in pyrabactin and quinabactin (Park et al., 2009; Cao et al., 2013). Using a wheat cell free-based drug screening approach, Nemoto et al. identified two novel ABA receptor
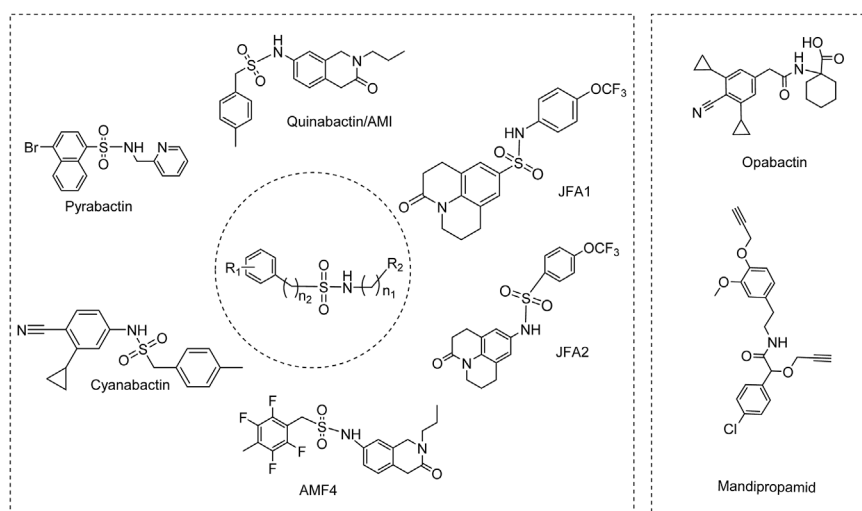
FIGURE 5
Abscisic acid functional analogues

agonists with bioactivity, in which JFA1 and JFA2. JFA2 was demonstrated to induce drought tolerance without affecting root growth (Nemoto et al., 2018). Cyanabactin has superior ABA-like activity in vegetative tissues and is highly effective to control plant water use (Vaidya et al., 2017). Recently, Vaidya et al. developed opabactin by a combination of virtual screening, x-ray crystallography, and structure-guided design. Opabactin is the most potent ABA agonist developed, which showed approximately sevenfold increase in receptor affinity relative to ABA and up to 10-fold greater activity *in vivo* (Vaidya et al., 2019).

As a known fungicide, mandipropamid (Figure 5) was reported to interact with a hextuple PYR1 mutant (PYR1^MANDI) and induced stomatal closure and inhibited seed germination in transgenic plants with PYR1^MANDI (Park et al., 2015).

Conclusion and outlooks

In this brief review, the research progress of ABA analogues including mechanism of action, signaling pathways, and ABA functional analogs is reviewed. the representative 34 structural analogs and 8 functional analogs are summarized, and the differences in biological activity and catabolism of ABA analogues are systematically analyzed. we conclude that the C-5', C-6', C-8', C-9' space size (functional group size) and saturations could directly affect the binding ability of the compound to the target, methyl may

be the largest group that can be accepted. Differences in groups on C-2', C-3', C-7' may block the ability of downstream phosphatases to bind to receptors. The improved photostability of C-2, C-3, C-6 provides a new design idea (cyclopropyl). Methylation of C-1' alters the binding capacity of the analogues to the receptor by altering the hydrogen bonding network. Activity analysis of sulfonamide-based ABA functional analogues revealed that pyrabactin exhibits distinct responses towards PYL-subtypes. It strongly activates PYR1/PYL1 but acts as an antagonist for PYL2 and PYL3, and AM1 showed a broader spectrum of PYL activity with higher bioactivity compared to pyrabactin. Opabactin, the most potential ABA agonist to date, showed an approximately sevenfold increase in receptor affinity relative to ABA and up to 10-fold greater activity *in vivo*.

Currently, studies have revealed that PYLs can be divided into dimer receptors (PYR1, PYL1 to PYL3) and monomeric receptors (PYL4 to PYL13). However, the specific functional differences between them in the ABA signaling pathway are unclear. Utilizing chemical genetics to clarify these differences is an important means for understanding the function of PYLs proteins and an important measure to discover novel ABA functional analogues. Furthermore, on the basis of the predecessors, the in-depth research on the structure-activity relationship of ABA analogues are expected to discover ABA analogues with novel structure, higher activity and better selectivity. Foreseeably, novel ABA functional analogues will play an important role in agriculture.

Author contributions

All authors have read and agreed to the published version of the manuscript. YL, SC, and PW collected and analyzed the refences. YL completed pictures and spreadsheets, conceived and wrote the draft of the manuscript. SG and JW revised and the paper.

Funding

Conflict of interest

The authors declare that the research was conducted in the absence of any commercial or financial relationships that could be construed as a potential conflict of interest.

Publisher's note

All claims expressed in this article are solely those of the authors and do not necessarily represent those of their affiliated organizations, or those of the publisher, the editors and the reviewers. Any product that may be evaluated in this article, or claim that may be made by its manufacturer, is not guaranteed or endorsed by the publisher.

References

Agurla, S., Gahir, S., Munemasa, S., Murata, Y., and Raghavendra, A. S. (2018). Mechanism of stomatal closure in plants exposed to drought and cold stress. *Adv. Exp. Med. Biol.* 1081, 215–232. doi:10.1007/978-981-13-1244-1_12

Anstis, P. J. P., Friend, J., and Gardner, D. C. J. (1975). The role of xanthoxin in the inhibition of pea seedling growth by red light. *Phytochemistry* 14 (1), 31–35. doi:10.1016/0031-9422(75)85002-3

Antoni, R., Gonzalez-Guzman, M., Rodriguez, L., Peirats-Llobet, M., Pizzio, G. A., Fernandez, M. A., et al. (2013). PYRABACTIN RESISTANCE1-LIKE8 plays an important role for the regulation of abscisic acid signaling in root. *Plant Physiol.* 161 (2), 931–941. doi:10.1104/pp.112.208678

Asghar, M. A., Li, Y., Jiang, H., Sun, X., Ahmad, B., Imran, S., et al. (2019). Crosstalk between abscisic acid and auxin under osmotic stress. *Agron. J.* 111 (5), 2157–2162. doi:10.2134/agronj2018.10.0633

Bari, R., and Jones, J. D. G. (2009). Role of plant hormones in plant defence responses. *Plant Mol. Biol.* 69 (4), 473–488. doi:10.1007/s11103-008-9435-0

Benson, C. L., Kepka, M., Wunschel, C., Rajagopalan, N., Nelson, K. M., Christmann, A., et al. (2015). Abscisic acid analogs as chemical probes for dissection of abscisic acid responses in *Arabidopsis thaliana*. *Phytochemistry* 113, 96–107. doi:10.1016/j.phytochem.2014.03.017

Bittner, F., Oreb, M., and Mendel, R. R. (2001). ABA3 is a molybdenum cofactor sulfurase required for activation of aldehyde oxidase and xanthine dehydrogenase in *Arabidopsis thaliana*. *J. Biol. Chem.* 276 (44), 40381–40384. doi:10.1074/jbc.C100472200

Cao, M.-J., Zhang, Y.-L., Liu, X., Huang, H., Zhou, X. E., Wang, W.-L., et al. (2017). Combining chemical and genetic approaches to increase drought resistance in plants. *Nat. Commun.* 8 (1), 1183. doi:10.1038/s41467-017-01239-3

Cao, M., Liu, X., Zhang, Y., Xue, X., Zhou, X. E., Melcher, K., et al. (2013). An ABA-mimicking ligand that reduces water loss and promotes drought resistance in plants. *Cell Res.* 23 (8), 1043–1054. doi:10.1038/cr.2013.95

Che, C., Zeng, Y., Xu, Y., Lu, H., Xu, Y., Zhang, X., et al. (2020). APAn, a class of ABA receptor agonism/antagonism switching probes. *J. Agric. Food Chem.* 68 (32), 8524–8534. doi:10.1021/acs.jafc.0c02154

Chen, K., Li, G. J., Bressan, R. A., Song, C. P., Zhu, J. K., and Zhao, Y. (2020). Abscisic acid dynamics, signaling, and functions in plants. *J. Integr. Plant Biol.* 62 (1), 25–54. doi:10.1111/jipb.12899

Cheng, W.-H., Endo, A., Zhou, L., Penney, J., Chen, H.-C., Arroyo, A., et al. (2002). A unique short-chain dehydrogenase/reductase in Arabidopsis glucose signaling and abscisic acid biosynthesis and functions. *Plant Cell* 14 (11), 2723–2743. doi:10.1105/tpc.006494

Cutler, A. J., and Krochko, J. E. (1994). Formation and breakdown of ABA. *Trends Plant Sci.* 4 (12), 472–478. doi:10.1016/S1360-1385(99)01497-1

Cutler, A. J., Rose, P. A., Squires, T. M., Loewen, M. K., Shaw, A. C., Quail, J. W., et al. (2000). Inhibitors of abscisic acid 8'-hydroxylase. *Biochemistry* 39, 13614–13624. doi:10.1021/bi0014453

Cutler, S. R., Rodriguez, P. L., Finkelstein, R. R., and Abrams, S. R. (2010). Abscisic acid: Emergence of a core signaling network. *Annu. Rev. Plant Biol.* 61, 651–679. doi:10.1146/annurev-arplant-042809-112122

Danquah, A., de Zelicourt, A., Colcombet, J., and Hirt, H. (2014). The role of ABA and MAPK signaling pathways in plant abiotic stress responses. *Biotechnol. Adv.* 32 (1), 40–52. doi:10.1016/j.biotechadv.2013.09.006

Dietz, K. J., Sauter, A., Wichert, K., Messdaghi, D., and Hartung, W. (2000). Extracellular β-glucosidase activity in barley involved in the hydrolysis of ABA glucose conjugate in leaves. *J. Exp. Bot.* 51 (346), 937–944. doi:10.1093/jexbot/51.346.937

Dittrich, M., Mueller, H. M., Bauer, H., Peirats-Llobet, M., Rodriguez, P. L., Geilfus, C.-M., et al. (2019). The role of Arabidopsis ABA receptors from the PYR/PYL/RCAR family in stomatal acclimation and closure signal integration. *Nat. Plants* 5 (9), 1002–1011. doi:10.1038/s41477-019-0490-0

Fan, W., Li, J., Jia, J., Wang, F., Cao, C., Hu, J., et al. (2015). Pyrabactin regulates root hydraulic properties in maize seedlings by affecting PIP aquaporins in a phosphorylation-dependent manner. *Plant Physiology Biochem.* 94, 28–34. doi:10.1016/j.plaphy.2015.05.005

Fidler, J., Zdunek-Zastocka, E., and Bielawski, W. (2015). Regulation of abscisic acid metabolism in relation to the dormancy and germination of cereal grains. *Acta Soc. Bot. Pol.* 84 (1), 3–11. doi:10.5586/asbp.2015.004

Finkelstein, R. R., Gampala, S. S., and Rock, C. D. (2002). Abscisic acid signaling in seeds and seedlings. *PlantCell* 14 (Suppl. l), S15–S45. doi:10.1105/tpc.010441

Guo, J., Yang, X., Weston, D. J., and Chen, J.-G. (2011). Abscisic acid receptors: Past, present and FutureF. *J. Integr. Plant Biol.* 53 (6), 469–479. doi:10.1111/j.1744-7909.2011.01044.x

Guo, S., He, F., Song, B., and Wu, J. (2021). Future direction of agrochemical development for plant disease in China. *Food Energy Secur* 10 (4), e293. doi:10.1002/fes3.293

Helander, J. D. M., Vaidya, A. S., and Cutler, S. R. (2016). Chemical manipulation of plant water use. *Bioorg. Med. Chem.* 24 (3), 493–500. doi:10.1016/j.bmc.2015.11.010

Hoth, S., Morgante, M., Sanchez, J.-P., Hanafey, M. K., Tingey, S. V., and Chua, N.-H. (2002). Genome-wide gene expression profiling in Arabidopsis thaliana reveals new targets of abscisic acid and largely impaired gene regulation in theabi1-1mutant. *J. Cell Sci.* 115 (Pt 24), 4891–4900. doi:10.1242/jcs.00175

Hu, B., Deng, F., Chen, G., Chen, X., Gao, W., Long, L., et al. (2020). Evolution of abscisic acid signaling for stress responses to toxic metals and metalloids. *Front. Plant Sci.* 11, 909. doi:10.3389/fpls.2020.00909

Inoue, T., and Oritani, T. (2000). Syntheses of (±)-Methyl 6'α-Demethyl-6'α-cyanoabscisate and (±)-Methyl 6'α-Demethyl-6'α-methoxycarbonylabscisate. *Biosci. Biotechnol. Biochem.* 64 (5), 1071–1074. doi:10.1271/bbb.64.1071

Irvine, N. M., Rose, P. A., Cutler, A. J., Squires, T. M., and Abrams, S. R. (2000). Anthracenone ABA analogue as a potential photoaffinity reagent for ABA-binding proteins. *Phytochemistry* 53 (3), 349–355. doi:10.1016/S0031-9422(99)00482-3

Izquierdo-Bueno, I., González-Rodríguez, V. E., Simon, A., Dalmais, B., Pradier, J. M., Le Pêcheur, P., et al. (2018). Biosynthesis of abscisic acid in fungi: Identification of a sesquiterpene cyclase as the key enzyme inBotrytis cinerea. *Environ. Microbiol.* 20 (7), 2469–2482. doi:10.1111/1462-2920.14258

Janicka-Russak, M., and Kłobus, G. (2007). Modification of plasma membrane and vacuolar H+-ATPases in response to NaCL and ABA. *J. Plant Physiology* 164 (3), 295–302. doi:10.1016/j.jplph.2006.01.014

Kang, J., Yim, S., Choi, H., Kim, A., Lee, K. P., Lopez-Molina, L., et al. (2015). Abscisic acid transporters cooperate to control seed germination. *Nat. Commun.* 6, 8113. doi:10.1038/ncomms9113

Kanno, Y., Hanada, A., Chiba, Y., Ichikawa, T., Nakazawa, M., Matsui, M., et al. (2012). Identification of an abscisic acid transporter by functional screening using the receptor complex as a sensor. *Proc. Natl. Acad. Sci. U.S.A.* 109 (24), 9653–9658. doi:10.1073/pnas.1203567109

Khadri, M., Tejera, N. A., and Lluch, C. (2007). Sodium chloride-ABA interaction in two common bean (Phaseolus vulgaris) cultivars differing in salinity tolerance. *Environ. Exp. Bot.* 60 (2), 211–218. doi:10.1016/j.envexpbot.2006.10.008

Kim, S. Y. (2007). Recent advances in ABA signaling. *J. Plant Biol.* 50 (2), 117–121. doi:10.1007/BF03030619

Kuromori, T., Miyaji, T., Yabuuchi, H., Shimizu, H., Sugimoto, E., Kamiya, A., et al. (2010). ABC transporter AtABCG25 is involved in abscisic acid transport and responses. *Proc. Natl. Acad. Sci. U.S.A.* 107 (5), 2361–2366. doi:10.1073/pnas.0912516107

Kushiro, T., Okamoto, M., Nakabayashi, K., Yamagishi, K., Kitamura, S., Asami, T., et al. (2004). The arabidopsis cytochrome P450 CYP707A encodes ABA $8'$-hydroxylases: Key enzymes in ABA catabolism. *Embo J.* 23 (7), 1647–1656. doi:10.1038/sj.emboj.7600121

Lee, K. H., Piao, H. L., Kim, H.-Y., Choi, S. M., Jiang, F., Hartung, W., et al. (2006). Activation of glucosidase via stress-induced polymerization rapidly increases active pools of abscisic acid. *Cell* 126 (6), 1109–1120. doi:10.1016/j.cell.2006.07.034

Liu, Z., Yan, J.-P., Li, D.-K., Luo, Q., Yan, Q., Liu, Z.-B., et al. (2015). UDP-Glucosyltransferase71C5, a major glucosyltransferase, mediates abscisic acid homeostasis in arabidopsis. *Plant Physiol.* 167 (4), 1659–1670. doi:10.1104/pp.15.00053

Ma, Y., Cao, J., He, J., Chen, Q., Li, X., and Yang, Y. (2018). Molecular mechanism for the regulation of ABA homeostasis during plant development and stress responses. *Ijms* 19 (11), 3643. doi:10.3390/ijms19113643

Ma, Y., Szostkiewicz, I., Korte, A., Moes, D., Yang, Y., Christmann, A., et al. (2009). Regulators of PP2C phosphatase activity function as abscisic acid sensors. *Science* 324 (5930), 1064–1068. doi:10.1126/science.1172408

Mega, R., Abe, F., Kim, J.-S., Tsuboi, Y., Tanaka, K., Kobayashi, H., et al. (2019). Tuning water-use efficiency and drought tolerance in wheat using abscisic acid receptors. *Nat. Plants* 5 (2), 153–159. doi:10.1038/s41477-019-0361-8

Melcher, K., Xu, Y., Ng, L.-M., Zhou, X. E., Soon, F.-F., Chinnusamy, V., et al. (2010). Identification and mechanism of ABA receptor antagonism. *Nat. Struct. Mol. Biol.* 17 (9), 1102–1108. doi:10.1038/nsmb.1887

Miao, C., Xiao, L., Hua, K., Zou, C., Zhao, Y., Bressan, R. A., et al. (2018). Mutations in a subfamily of abscisic acid receptor genes promote rice growth and productivity. *Proc. Natl. Acad. Sci. U.S.A.* 115 (23), 6058–6063. doi:10.1073/pnas.1804774115

Miyakawa, T., and Tanokura, M. (2011). Regulatory mechanism of abscisic acid signaling. *Biophysics* 7, 123–128. doi:10.2142/biophysics.7.123

Nambara, E., and Marion-Poll, A. (2005). Abscisic acid biosynthesis and catabolism. *Annu. Rev. Plant Biol.* 56, 165–185. doi:10.1146/annurev.arplant.56.032604.144046

Nemhauser, J. L., Hong, F., and Chory, J. (2006). Different plant hormones regulate similar processes through largely nonoverlapping transcriptional responses. *Cell* 126 (3), 467–475. doi:10.1016/j.cell.2006.05.050

Nemoto, K., Kagawa, M., Nozawa, A., Hasegawa, Y., Hayashi, M., Imai, K., et al. (2018). Identification of new abscisic acid receptor agonists using a wheat cell-free based drug screening system. *Sci. Rep.* 8 (1), 4268. doi:10.1038/s41598-018-22538-9

North, H. M., Almeida, A. D., Boutin, J.-P., Frey, A., To, A., Botran, L., et al. (2007). The Arabidopsis ABA-deficient mutant aba4 demonstrates that the major route for stress-induced ABA accumulation is via neoxanthin isomers. *Plant J. Cell Mol. Biol.* 50 (5), 810–824. doi:10.1111/j.1365-313X.2007.03094.x

Nyangulu, J. M., Nelson, K. M., Rose, P. A., Gai, Y., Loewen, M., Lougheed, B., et al. (2006). Synthesis and biological activity of tetralone abscisic acid analogues. *Org. Biomol. Chem.* 4 (7), 1400–1412. doi:10.1039/b509193d

Okamoto, M., Peterson, F. C., Defries, A., Park, S.-Y., Endo, A., Nambara, E., et al. (2013). Activation of dimeric ABA receptors elicits guard cell closure, ABA-regulated gene expression, and drought tolerance. *Proc. Natl. Acad. Sci. U.S.A.* 110 (29), 12132–12137. doi:10.1073/pnas.1305919110

Park, S.-Y., Fung, P., Nishimura, N., Jensen, D. R., Fujii, H., Zhao, Y., et al. (2009). Abscisic acid inhibits type 2C protein phosphatases via the PYR/PYL family of START proteins. *Science* 324 (5930), 1068–1071. doi:10.1126/science.1173041

Park, S.-Y., Peterson, F. C., Mosquna, A., Yao, J., Volkman, B. F., and Cutler, S. R. (2015). Agrochemical control of plant water use using engineered abscisic acid receptors. *Nature* 520 (7548), 545–548. doi:10.1038/nature14123

Puli, M. R., and Raghavendra, A. S. (2012). Pyrabactin, an ABA agonist, induced stomatal closure and changes in signalling components of guard cells in abaxial epidermis of Pisum sativum. *J. Exp. Bot.* 63 (3), 1349–1356. doi:10.1093/jxb/err364

Rajagopalan, N., Nelson, K. M., Douglas, A. F., Jheengut, V., Alarcon, I. Q., McKenna, S. A., et al. (2016). Abscisic acid analogues that act as universal or selective antagonists of phytohormone receptors. *Biochemistry* 55, 5155–5164. doi:10.1021/acs.biochem.6b00605

Rose, P. A., Cutler, A. J., Irvine, N. M., Shaw, A. C., Squires, T. M., Loewen, M. K., et al. (1997). 8'-Acetylene ABA: An irreversible inhibitor of ABA 8'-hydroxylase. *Bioorg. Med. Chem. Lett.* 7 (19), 2543–2546. doi:10.1016/S0960-894X(97)10015-4

Santiago, J., Rodrigues, A., Saez, A., Rubio, S., Antoni, R., Dupeux, F., et al. (2009). Modulation of drought resistance by the abscisic acid receptor PYL5 through inhibition of clade A PP2Cs. *Plant J. Cell Mol. Biol.* 60 (4), 575–588. doi:10.1111/j.1365-313X.2009.03981.x

Saradhi, P. P., Suzuki, I., Katoh, A., Sakamoto, A., Sharmila, P., Shi, D.-J., et al. (2000). Protection against the photo-induced inactivation of the photosystem II complex by abscisic acid. *Plant Cell Environ.* 23 (7), 711–718. doi:10.1046/j.1365-3040.2000.00579.x

Schwartz, S. H., Tan, B. C., Gage, D. A., Zeevaart, J. A. D., and McCarty, D. R. (1997). Specific oxidative cleavage of carotenoids by VP14 of maize. *Science* 276 (5320), 1872–1874. doi:10.1126/science.276.5320.1872

Seki, M., Ishida, J., Narusaka, M., Fujita, M., Nanjo, T., Umezawa, T., et al. (2002). Monitoring the expression pattern of around 7,000 Arabidopsis genes under ABA treatments using a full-length cDNA microarray. *Funct. Integr. Genomics* 2 (6), 282–291. doi:10.1007/s10142-002-0070-6

Shinozaki, K., and Yamaguchi-Shinozaki, K. (2000). Molecular responses to dehydration and low temperature: Differences and cross-talk between two stress signaling pathways. *Curr. Opin. Plant Biol.* 3 (3), 217–223. doi:10.1016/s1369-5266(00)80068-0

Shu, S., Gao, P., Li, L., Yuan, Y., Sun, J., and Guo, S. (2016). Abscisic acid-induced H2O2 accumulation enhances antioxidant capacity in pumpkin-grafted cucumber leaves under Ca(NO3)2 stress. *Front. Plant Sci.* 7, 1489. doi:10.3389/fpls.2016.01489

Silva-Ortega, C. O., Ochoa-Alfaro, A. E., Reyes-Agüero, J. A., Aguado-Santacruz, G. A., and Jiménez-Bremont, J. F. (2008). Salt stress increases the expression of p5cs gene and induces proline accumulation in cactus pear. *Plant Physiology Biochem.* 46 (1), 82–92. doi:10.1016/j.plaphy.2007.10.011

Soon, F.-F., Ng, L.-M., Zhou, X. E., West, G. M., Kovach, A., Tan, M. H. E., et al. (2012). Molecular mimicry regulates ABA signaling by SnRK2 kinases and PP2C phosphatases. *Science* 335 (6064), 85–88. doi:10.1126/science.1215106

Takino, J., Kozaki, T., Sato, Y., Liu, C., Ozaki, T., Minami, A., et al. (2018). Unveiling biosynthesis of the phytohormone abscisic acid in fungi: Unprecedented mechanism of core scaffold formation catalyzed by an unusual sesquiterpene synthase. *J. Am. Chem. Soc.* 140 (39), 12392–12395. doi:10.1021/jacs.8b08925

Tan, Z. H., Han, X. Q., Wan, C., and Xiao, Y. (2013). High-activity benzoiso abscisic acid analogue and preparation method thereof. CN. Patent No 103,435,472. Beijing: China National Intellectual Property Administration.

Ueno, K., Yoneyama, H., Saito, S., Mizutani, M., Sakata, K., Hirai, N., et al. (2005). A lead compound for the development of ABA $8'$-hydroxylase inhibitors. *Bioorg. Med. Chem. Lett.* 15 (23), 5226–5229. doi:10.1016/j.bmcl.2005.08.042

Vaidya, A. S., Helander, J. D. M., Peterson, F. C., Elzinga, D., Dejonghe, W., Kaundal, A., et al. (2019). Dynamic control of plant water use using designed ABA receptor agonists. *Science* 366 (6464), eaaw8848. doi:10.1126/science.aaw8848

Vaidya, A. S., Peterson, F. C., Yarmolinsky, D., Merilo, E., Verstraeten, I., Park, S.-Y., et al. (2017). A rationally designed agonist defines subfamily IIIA abscisic acid receptors as critical targets for manipulating transpiration. *ACS Chem. Biol.* 12 (11), 2842–2848. doi:10.1021/acschembio.7b00650

Van Overtveldt, M., Heugebaert, T. S. A., Verstraeten, I., Geelen, D., and Stevens, C. V. (2015). Phosphonamide pyrabactin analogues as abscisic acid agonists. *Org. Biomol. Chem.* 13 (18), 5260–5264. doi:10.1039/c5ob00137d

Vishwakarma, K., Upadhyay, N., Kumar, N., Yadav, G., Singh, J., Mishra, R. K., et al. (2017). Abscisic acid signaling and abiotic stress tolerance in plants: A review on current knowledge and future prospects. *Front. Plant Sci.* 08, 161. doi:10.3389/fpls.2017.00161

Waadt, R., Seller, C. A., Hsu, P.-K., Takahashi, Y., Munemasa, S., and Schroeder, J. I. (2022). Plant hormone regulation of abiotic stress responses. *Nat. Rev. Mol. Cell Biol.* doi:10.1038/s41580-022-00479-6

Wan, C., Hong, Q., Zhang, X., Zeng, Y., Yang, D., Che, C., et al. (2019). Role of the ring methyl groups in 2′,3′-benzoabscisic acid analogues. *J. Agric. Food Chem.* 67 (17), 4995–5007. doi:10.1021/acs.jafc.8b07068

Wan, C., Yang, D., Liu, R., Lu, H., Che, C., Xu, Y., et al. (2022). 1′-OH of ABA and its analogs is a crucial functional group correspondence to seed germination and development of plants. *J. Mol. Struct.* 1249, 131650. doi:10.1016/j.molstruc.2021.131650

Weng, J.-K., Ye, M., Li, B., and Noel, J. P. (2016). Co-Evolution of hormone metabolism and signaling networks expands plant adaptive plasticity. *Cell* 166 (4), 881–893. doi:10.1016/j.cell.2016.06.027

Wenjian, L., Xiaoqiang, H., Yumei, X., Jinlong, F., Yuanzhi, Z., Huizhe, L., et al. (2013). Synthesis, photostability and bioactivity of 2,3-cyclopropanated abscisic acid. *Phytochemistry* 96, 72–80. doi:10.1016/j.phytochem.2013.09.029

Xu, Z.-Y., Lee, K. H., Dong, T., Jeong, J. C., Jin, J. B., Kanno, Y., et al. (2012). A vacuolar β-glucosidase homolog that possesses glucose-conjugated abscisic acid hydrolyzing activity plays an important role in osmotic stress responses in arabidopsis. *Plant Cell* 24 (5), 2184–2199. doi:10.1105/tpc.112.095935

Yang, Y., and Guo, Y. (2018). Unraveling salt stress signaling in plants. *J. Integr. Plant Biol.* 60 (9), 796–804. doi:10.1111/jipb.12689

Yao, L., Cheng, X., Gu, Z., Huang, W., Li, S., Wang, L., et al. (2018). The AWPM-19 family protein OsPM1 mediates abscisic acid influx and drought response in rice. *Plant Cell* 30 (6), 1258–1276. doi:10.1105/tpc.17.00770

Yu, X.-Z., Wang, D.-Q., and Zhang, X.-H. (2014). Chelator-induced phytoextraction of zinc and copper by rice seedlings. *Ecotoxicology* 23 (4), 749–756. doi:10.1007/s10646-014-1188-8

Zhang, F.-P., Sussmilch, F., Nichols, D. S., Cardoso, A. A., Brodribb, T. J., and McAdam, S. A. M. (2018). Leaves, not roots or floral tissue, are the main site of rapid, external pressure-induced ABA biosynthesis in angiosperms. *J. Exp. Bot.* 69 (5), 1261–1267. doi:10.1093/jxb/erx480

Zhang, X. L., Jiang, L., Xin, Q., Liu, Y., Tan, J. X., and Chen, Z. Z. (2015). Structural basis and functions of abscisic acid receptors PYLs. *Front. Plant Sci.* 6. doi:10.3389/fpls.2015.00088

Zhao, Y., Zhang, Z., Gao, J., Wang, P., Hu, T., Wang, Z., et al. (2018). Arabidopsis duodecuple mutant of PYL ABA receptors reveals PYL repression of ABA-independent SnRK2 activity. *Cell Rep.* 23 (11), 3340–3351. e5. doi:10.1016/j.celrep.2018.05.044

Melatonin Enhances the Postharvest Disease Resistance of Blueberries Fruit by Modulating the Jasmonic Acid Signaling Pathway and Phenylpropanoid Metabolites

Guangfan Qu, Wenneng Wu, Liangjie Ba, Chao Ma, Ning Ji and Sen Cao*

Food and Pharmaceutical Engineering Institute, Guiyang University, Guiyang, China

In this study, to investigate the physiological and molecular mechanisms of melatonin inhibiting the postharvest rot of blueberry fruits, blueberry fruits were dipped in 0.3 mmol L^{-1} melatonin solution for 3 min and stored at 0°C for 80 days. The results indicated that melatonin did not significantly ($p > 0.05$) inhibit the mycelial growth or spore germination of *Alternaria alternata*, *Botrytis cinerea*, and *Colletotrichum gloeosporioides*. In addition, an *in vivo* study revealed that melatonin treatment increased the enzymatic activities of phenylalanine ammonia lyase (PAL), cinnamate 4-hydroxylase (C4H), 4-coumarate-CoA ligase (4CL), cinnamyl alcohol dehydrogenase (CAD), polyphenol oxidase (PPO), and peroxidase (POD) in fruits. Furthermore, genes related to jasmonic acid synthesis were upregulated (*VaLOX*, *VaAOS*, and *VaAOC*), as were those related to pathogenesis-related proteins (*VaGLU* and *VaCHT*) and phenylpropane metabolism (*VaPAL*, *VaC4H*, *Va4CL*, *VaCAD*, *VaPPO*, and *VaPOD*), which promoted the accumulation of total phenols, flavonoids, anthocyanins, and lignin in the fruits. These results suggest that melatonin enhances the postharvest disease resistance of blueberry fruits by mediating the jasmonic acid signaling pathway and the phenylpropane pathway.

Keywords: blueberry, melatonin, jasmonic acid signaling pathway, phenylpropanoid metabolites, disease resistance

INTRODUCTION

Blueberries (*Vaccinium* sp. in the Ericaceae family) produce small fruits that are rich in nutritional and health-promoting components such as anthocyanins, flavanols, and polyphenols, which have been suggested to have antiaging, immune-enhancing, and memory-improving functions (Gong et al., 2014; Ji N. et al., 2021.). However, blueberries are susceptible to microbial pathogens during storage and sale because of their thin skins and high moisture contents. Infestation by microbial pathogens causes rapid fruit softening, water loss, rot, and nutrient loss (Wang et al., 2010), which severely reduce the commercial value of the fruit. A wide range of microbial pathogens can cause the postharvest rot of blueberries, mainly *Alternaria alternata*, *Botrytis cinerea*, and *Colletotrichum gloeosporioides* (Wang et al., 2010). Recently, it has been reported that exogenous substances such as ethanol (Ji Y. et al., 2021), natamycin (Saito et al., 2022), sodium nitroprusside (Ge et al., 2019), and jasmonic acid methyl ester (Wang et al., 2020a) can minimize the postharvest rot of blueberries. The effects of these substances are mainly attributed to the inhibition of the growth of microbial pathogens *via* their action as fungicides or to the induction of disease resistance in fruits *via* their action as exogenous inducers.

Jasmonic acid (JA) is an important phytohormone that regulates plant growth and development and induces resistance to biotic and abiotic stresses (Liu et al., 2019). In plant defense responses, plants can not only activate the JA signaling pathway by transmitting the systemic proteins produced by pathogenic microorganisms as signal molecules to adjacent parts through apoplast and phloem but also activate JA signaling by using exogenous inducers and transmit the corresponding signal molecules to adjacent parts for defense response (Truman et al., 2007). In addition, the secondary metabolites of phenylpropane, such as total phenols, flavonoids, and lignans, are closely related to plant defense functions, and the synthesis and accumulation of these metabolites are regulated by phenylalanine ammonia lyase (PAL), cinnamate 4-hydroxylase (C4H), 4-coumarate-CoA ligase (4CL), cinnamyl alcohol dehydrogenase (CAD), polyphenol oxidase (PPO), peroxidase (POD), and other key enzymes (Ren et al., 2020; Ji N. et al., 2021.). However, on the ripening and senescence of the fruit, the activity of these enzymes gradually decreases, and the accumulation of phenylpropane metabolites slowly decreases, resulting in the loss of fruit defenses against biotic and abiotic stresses (Bennett and Wallsgrove, 1994). However, the treatment of fruits with exogenous inducers, such as salicylic acid (Zhang H. et al., 2021), terpinen-4-ol (Li et al., 2020), and sodium nitroprusside (Ge et al., 2019), can effectively regulate the enzymatic activities of phenylpropane metabolism in fruits and promote the accumulation of the secondary metabolites of phenylpropane, thus improving the postharvest disease resistance.

Melatonin (MT) is an endogenous bioactive molecule with multiple regulatory functions involved in various physiological processes, such as ripening, aging, and defense in fruits and vegetables (Li et al., 2017). In recent years, MT has been shown to not only improve the postharvest fruit quality but also enhance fruit resistance to pathogenic microorganisms (Moustafa-Farag et al., 2020). Shang et al. (2021) found that MT induction promoted the accumulation of total phenols, flavonoids, and anthocyanins in blueberry fruits and enhanced the antioxidant capacity of fruits. It was also found that the accumulation of polyphenols, flavonoids, and anthocyanins could effectively enhance the antioxidant capacity of fruits and delay the softening and senescence of fruits (Lin et al., 2018; Lin et al., 2020.). In addition, MT treatment has been shown to induce the enhanced postharvest disease resistance in jujube fruit (*Ziziphus jujuba*) (Zhang et al., 2022), cherry tomatoes (Liu et al., 2019), and grapes (Gao et al., 2020), and this is mainly attributed to the role of MT in scavenging reactive oxygen radicals, improving the antioxidant capacity, maintaining the metabolic energy balance, and promoting the accumulation of secondary metabolites of phenylpropane. MT can also mediate disease-resistance signaling pathways, such as those involving JA, NO, and salicylic acid, to improve the fruit disease resistance (Shi et al., 2015.; Liu et al., 2019.; Bhardwaj et al., 2022). However, the physiological and molecular mechanisms by which MT enhances the postharvest disease resistance in blueberries remain unclear.

Therefore, we investigated the potential physiological and molecular mechanisms by which MT maintains the blueberry quality and reduces the postharvest rot, focusing on 1) the effect of MT on the postharvest pathogenic microorganisms (*B. cinerea*, *A. alternata*, and *C. gloeosporioides*) in blueberries, 2) the effect of MT on the fruit JA signaling pathway, and 3) the effect of MT on the metabolites of phenylpropane.

MATERIALS AND METHODS

Fruits and Treatments

Rabbiteye blueberry (*Vaccinium ashei* cv. Powder blue) fruits were harvested in July 2021 from a blueberry plantation in Majiang, China. Fully ripe fruits were selected and picked by hand. Fruits were placed in plastic boxes and immediately returned to the laboratory of the Guizhou fruit processing engineering technology research center. Next, fruits of uniform size that were free from mechanical damage, plant diseases, and insect pests were selected for the experiment. First, the blueberries were treated with 0, 0.1, 0.3, and 0.5 mmol L^{-1} MT and stored at $0 \pm 0.5°C$ for 80 days. The preliminary test results showed that 0.3 mmol L^{-1} MT treatment significantly inhibited blueberry rot. Therefore, 0.3 mmol L^{-1} MT was used for further study. The fruits were randomly divided into two groups, 150 boxes of fruits in each group, immersed in MT solution (0.3 mmol L^{-1}) or distilled water (control) for 3min. Subsequently, the fruits were removed and allowed to dry naturally at room temperature. Finally, all the blueberries were packed in plastic boxes (120 fruits per box), in polyethylene (PE20) bags, and precooled at $0 \pm 0.5°C$ for 48 h and, then, the bag was tied. Every 20 days, some of the fruits were removed from storage at $0 \pm 0.5°C$, cut into small pieces, frozen in liquid nitrogen, and immediately stored at -80°C. The enzyme activity, gene expression, and phenylpropane metabolites in the fruits were subsequently analyzed.

Preparation of Spore Suspensions and Determination of Mycelial Growth and Spore Germination

A. alternata, *B. cinerea*, and *C. gloeosporioides* were isolated from the diseased blueberries. The purified pathogenic fungi were inoculated into potato dextrose agar (PDA) medium and incubated at 25°C for 7 days. Then, 10 ml (containing 0.01% Tween 80) of sterile water was added to the Petri dishes, and the spore solution was diluted with sterile water by light scraping with a sterilized applicator, followed by the filtration of the solution through four layers of sterile gauze. The spore suspension was adjusted to 1×10^6 spores/mL by using a hemocytometer.

The inhibitory effect of MT on the mycelia of *A. alternata*, *B. cinerea*, and *C. gloeosporioides* was determined using the method reported by Pan et al. (2022). MT was dissolved in a small volume of ethanol and mixed with sterile water. The colonies of *A. alternata*, *B. cinerea*, and *C. gloeosporioides* were punched with a sterile punch (5-mm diameter) from the edge of the colonies cultured for 5 days and placed in the center of the medium containing 0 (blank control) or 0.3 mmol L^{-1}MT in PDA (containing 0.05% ethanol by volume). The colonies were incubated at 25°C for 6 days, and the colony diameters were measured every 3 days. Each treatment was repeated three times.

The spore germination assay was slightly modified from the method described by Olmedo et al. (2017). Sterilized slides were placed in PDA medium containing 0 or 0.3 mmol L^{-1} MT, and after the medium had solidified, 5 µL of *A. alternata*, *B. cinerea*, and *C. gloeosporioides* spore solutions were placed in the center of the slides. The slides were placed in sterile Petri dishes and incubated at 25°C with 80–85% relative humidity (RH) for 8 h. Spore germination was observed at different times (after 4 and 8 h) using a CX21 light microscope (Olympus Co., Ltd., Tokyo, Japan), and each treatment was repeated three times. The spores were considered to have germinated when the length of the spore germination tube was greater than the diameter of the spore itself, and 100 spores were observed for each treatment to calculate the germination rate. The germination rate was given by the number of germinated spores divided by the total number of spores.

Determination of PAL, C4H, 4CL, CAD, PPO, and POD activities.

The PAL activity in the blueberries was determined using the method described by Zhang W. et al. (2021) with appropriate modifications. Briefly, 0.5 ml enzyme solution, 0.5 ml of 20 mmol/L L-phenylalanine solution, and 3.0 ml of 50 mmol L^{-1} borate buffer (pH 8.8, containing 5 mmol L^{-1} β-mercaptoethanol, 2 mmol L^{-1} of ethylenediaminetetraacetic acid (EDTA), and 40 g L^{-1} polyvinylpyrrolidone (PVP)) were added to the reaction tubes. After placing the reaction tube in a water bath heated to 37°C for 60 min, 0.1 ml of 6 mol L^{-1} HCl was added to terminate the reaction, and the absorbance value of the reaction solution was measured at 290 nm. A change in the optical density (OD, 0.01 h^{-1}) was taken as a unit of the enzyme activity, which is expressed in U g^{-1}, where U = $0.01\Delta OD_{290}$ h^{-1}.

The C4H and 4CL activities in the blueberries were determined using the method described by Li et al. (2019) with appropriate modifications. For C4H, 50 µL of enzyme solution, 100 µL of 0.5 mmol L^{-1} D-glucose-6-phosphate disodium salt, 1 ml of 2 mmol L^{-1} *trans*-cinnamic acid, 100 µL of 0.5 mmol L^{-1} oxidized disodium coenzyme II, and 2 ml of 50 mmol L^{-1} extraction buffer (pH 7.5, containing 2 mmol L^{-1} of β-mercaptoethanol) were added to the reaction tube. After heating the reaction tube in a water bath at 37°C for 1 h, the reaction was terminated by adding 200 µL of 6 mol L^{-1} HCL, and the absorbance of the reaction solution was measured at 340 nm. The change in the OD value (0.01 min^{-1}) was used as a unit of enzyme activity, which was expressed in U g^{-1}, where U = $0.01\Delta OD_{340}$ min^{-1}.

For 4CL, the reaction system was 0.1 ml of enzyme solution, 0.3 ml of 50 µmol L^{-1} adenosine triphosphate (ATP), 0.3 ml of 5 µmol L^{-1} coenzyme A (CoA), and 0.15 ml of 0.3 µmol L^{-1} *p*-coumaric acid. The reaction solution was heated in a water bath at 40°C for 10 min, and the absorbance of the reaction solution was measured at 333 nm. The change in the OD value (0.01 min^{-1}) was used as a unit of the enzyme activity, which is expressed in U g^{-1}, where U = $0.01\Delta OD_{333}$ min^{-1}.

The CAD activity in the blueberries was determined by using the method of Li et al. (2017) with appropriate modifications. Briefly, 0.5 ml of enzyme solution, 1.4 ml of 1 mol L^{-1} *trans*-cinnamic acid, and 1 ml of 2 mmol L^{-1} nicotinamide adenine dinucleotide phosphate (NADPH) were added to the reaction tube. The reaction tube was kept in a water bath at 37°C for 1 h, and then,

the reaction was terminated by adding 0.2 ml of 1 mol L^{-1} HCl. The absorbance of the reaction solution was measured at a wavelength of 340 nm. The change in the OD value (0.01 min^{-1}) was used as a unit of the enzyme activity, which is expressed in U g^{-1}.

The method of Lin et al. (2013) with slight modifications was used to determine the PPO activity in the blueberries. First, 3 ml of the enzyme extract was added to 3.9 ml of the 0.05 mol L^{-1} sodium phosphate buffer solution and 1 ml of 0.1 mol L^{-1} catechol solution. The reaction solution was kept in a water bath at 37°C for 10 min, and 2 ml of 20% trichloroacetic acid was then added to terminate the reaction. The absorbance of the reaction solution was recorded at a wavelength of 420 nm. One unit of the PPO activity was defined as the amount of enzyme required to increase the OD value by 0.01 min^{-1}, and the results are expressed in U g^{-1}.

The POD activity in the blueberries was determined using the method of Wang et al. (2021). Briefly, 0.5 ml of the enzyme extract was added to 3.0 ml of a mixture of 25 mmol L^{-1} guaiacol and 200 µL of 0.5 mol L^{-1} H_2O_2, and the change in absorbance at 470 nm was immediately recorded. The change in the OD value (1 min^{-1}) was used as a unit of the enzyme activity, which is expressed in U g^{-1}.

Determination of the Contents of Phenylpropanol Metabolites

The total phenolic content of the blueberries was determined using the forintanol method (Liu et al., 2018). Briefly, a sample (2 g) was homogenized with 70% ethanol, centrifuged at 4°C and 10,000 rpm for 15 min, and the supernatant was collected. The supernatant (1 ml) and 3 ml of 0.25 mol L^{-1} of Folin phenol were added to a 25-ml volumetric flask and shaken. After allowing it to stand for 30 s, 6 ml of 12% sodium carbonate solution was added, and distilled water was added to make the solution up to the scale line. It was then left for 1 h. Then, the absorbance was measured at 765 nm. The total phenol content is expressed as milligrams per gram.

The flavonoid content of the blueberries was determined using the method of Wang et al. (2020b). Fruit pulp (1 g) was homogenized with the precooled 1% HCI–methanol solution and transferred to a 20-ml graduated tube to ensure a constant volume. The filtrate was stored at 4°C for 20 min, filtered, and collected. The absorbance was measured at 325 nm, and the flavonoid content is expressed as milligrams per gram.

The anthocyanin content in the blueberries was determined according to the method reported by Chen et al. (2017) with slight modifications. Each sample (2 g) was homogenized by grinding with a small amount of 60% ethanol and made up to 50 ml with 60% ethanol. After incubation in a water bath at 50°C for 60 min, the solution was filtered, and the filtrate was collected. Two test tubes were taken, one of which is added with 1 ml of filtrate and 9 ml of pH KCl buffer solution, and the other is added with 1 ml of the filtrate and 9 ml of pH 4.5 sodium acetate (NaAc) buffer solution. The absorbance values were measured at 510 and 700 nm after standing for 40 min. The anthocyanin content is expressed as milligrams/100 g of the fruit.

The method described by Zhang et al. (2020) with slight modifications was used to determine the lignin content of the blueberries. A sample of 1 g was homogenized by grinding with

Gene	Forward primer (5'→3')	Reverse primer (5'→3')
VaMET	ACCCTGACATGAGCTTCTCG	ACCCAAATCTCTGCTTGCTG
VaPAL	AGTCATCCGATCATCGACAAAG	TTGTCCATCGAGACTCCAATG
VaC4H	GCCGTTTCTCAGAGGGTATTTG	CATTTCAGACTGTTGTTGTCCATC
Va4CL	TCTTACTCCGACAAACCCGC	TGATACCCAGTTGGTTGATGAAG
VaCAD	AGGGATAAACTTGGAGGGTTTG	TTGAAGCCTTGAGCATTGGAAC
VaPPO	GCCATTCTGGAACTGGGACTC	GGTTGCTGTTTATTCGTGCCTT
VaPOD	GACCTGAAGTCCCATTCCATC	ATCCAGAACGCTCCTTGTGG
VaGLU	GCCGTTGGGAATGAAGTGAAT	GGAATGGGTTGCTTACGAGTG
VaCHT	GGTAGCAACTGACCCAACCATT	GATCCCACCGTTGATTATGTTAGT
VaLOX	GGAAAGCCACAGTGGAAGCA	AGAGTCGTGAGCGAGGACATG
VaAOS	GATCAAGCCGCGTTCAATT	CGGAGGGATACGGAAGGTGT
VaAOC	ACTCAGAGCCATCTCCTCCG	TTCTGTTGGGGTGCTCTGG

5 ml of 95% ethanol, and the precipitate was collected by centrifugation at 4°C and 1,000*g* for 15 min. The precipitate was washed three times with ethanol and hexane (1:2, v/v) and collected. Subsequently, the precipitate was dried in an oven at 60°C. Then, 1 ml of a 25% acetyl bromide–glacial acetic acid solution was added to the dried precipitate, and this mixture was held in a water bath at 70°C for 30 min. Afterward, 1 ml of $2 \, \text{mol} \, L^{-1}$ NAOH was added to terminate the reaction. Then, 2 ml of glacial acetic acid and 0.1 ml of $7.5 \, \text{mol} \, L^{-1}$ hydroxylamine hydrochloride were added to the reaction solution, which was centrifuged again to collect the supernatant. The absorbance was measured at 280 nm. The lignin content is expressed as $OD_{280} \, g^{-1}$ fresh weight (FW).

Quantitative Real-Time Polymerase Chain Reaction (qRT-PCR) Analysis

Blueberry memory RNA (mRNA) was extracted using a Total Plant RNA Extraction Kit (TIANGEN Biotech Co., Ltd., Beijing, China). The mRNA concentration and purity were determined using a NanoDrop2000 ultra-micro spectrophotometer (Thermo Scientific, United States), and its integrity was examined by 1% agarose gel electrophoresis. Copy DNA (cDNA) was generated by the reverse transcription of RNA using the Servicebio® RT First Strand cDNA Synthesis Kit (Servicebio, United States) and subjected to fluorescent qRT-PCR. The primer sequences used are listed in **Table 1**, and *VaMET* was used as the internal reference gene (Wang et al., 2021). The relative gene expression was calculated using the $2^{-\Delta \Delta Ct}$ method (Naik et al., 2007).

Statistical Analysis

All the experiments were repeated three times, and the data are expressed as the mean ± standard deviation (SD). Duncan's multiple range test was used for the analysis, and significance was set at $p < 0.05$. Origin 2018 was used to plot the data.

RESULTS

Effects of melatonin treatment on growth inhibition and spore germination of *A. alternata*, *B. cinerea*, and *C. gloeosporioides in vitro*.

As shown in **Figures 1A,B**, there was no significant difference ($p > 0.05$) in the diameters of the colonies of *A. alternata*, *B. cinerea*, and *C. gloeosporioides* after MT treatment compared to the control group after 3 and 6 days. Furthermore, the spore germination rates of the three fungi after MT treatment were not significantly different ($p > 0.05$) from those of the control group. In addition, there was no significant difference in the spore germination rates of the three fungi after MT treatment compared to the control group after 4 and 8 h ($p > 0.05$) (**Figure 1C**). As shown previously, MT showed no inhibitory activity against *A. alternata*, *B. cinerea*, and *C. gloeosporioides*.

Effect of melatonin treatment on gene expression related to the JA signaling pathway.

As shown in **Figures 2A,B**, the relative expression of key genes related to JA synthesis, *VaLOX*, and *VaAOS* (which are related to lipoxygenase (LOX) and allene oxide synthase (AOS)) in the MT-treated fruits first increased and then decreased, reaching the highest relative expression after 60 days ($p < 0.05$), and these were 2.65 and 3.69 times higher than those of the control group, respectively. The relative expression of *VaAOC* in the control fruit was relatively stable in the first 60 days but increased rapidly after 60 days. The relative expression of *VaAOC* (related to allene oxide cyclase (AOC)) in the MT-treated fruit increased gradually from 0 to 80 days and was significantly higher than that in the control group at 40, 60, and 80 days ($p < 0.05$).

Effect of Melatonin Treatment on the Activities of Defense Enzymes

As shown in **Figures 3A,C,E,F**, the activities of PAL, 4CL, PPO, and POD in the MT-treated fruits increased and then decreased from 0 to 80 days. The PAL and 4CL activities were the highest after 60 days ($p < 0.05$), being 1.14 and 1.26 times higher than those of the control group, respectively. The activities of PPO and POD were the highest after 40 days ($p < 0.05$), being 1.30 and 1.16 times higher than those of the control group, respectively.

As shown in **Figure 3B**, the C4H activity decreased slightly during the first 20 days. After 40 and 60 days, the C4H activity in the MT-treated group was significantly higher than that in the control group
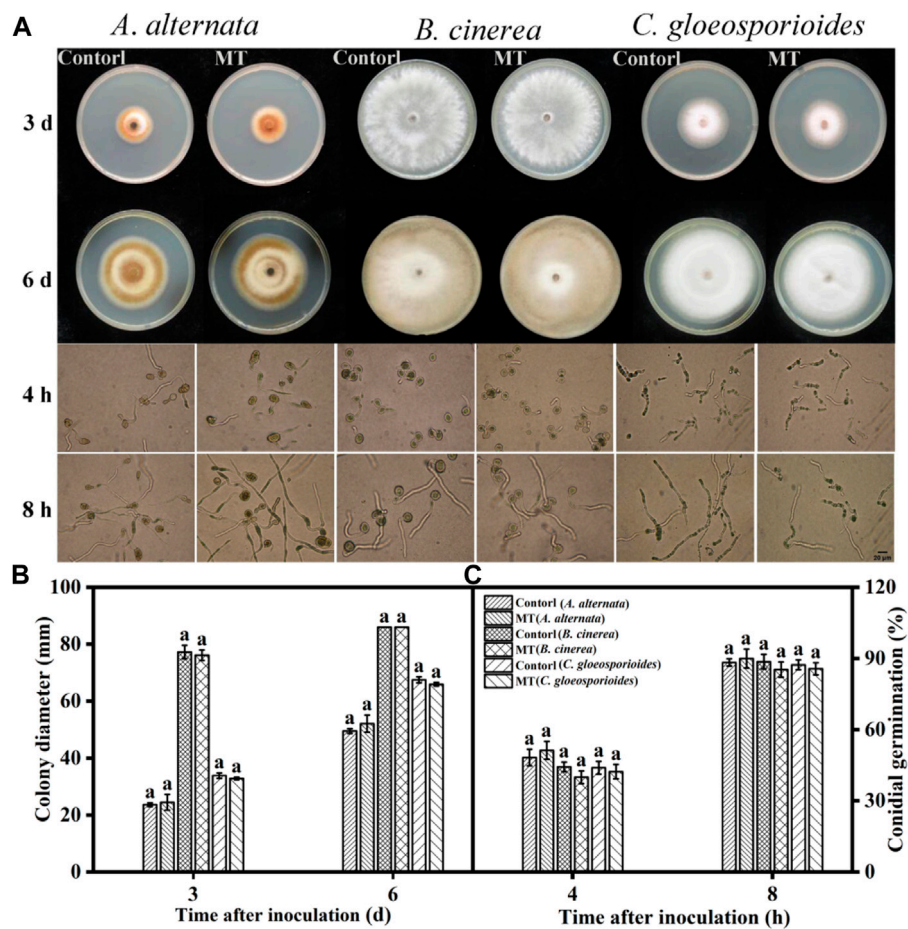
FIGURE 1 | Effects of MT on *in vitro* growth inhibition and spore germination of *A. alternata*, *B. cinerea*, and *C. gloeosporoides*: **(A)** Photographs of cultures, **(B)** colony diameters, and **(C)** spore germination rates. Significant differences between the MT-treated and control groups were compared for the same strain. Different letters represent significant differences ($p < 0.05$). Data are presented as the mean ± SD.
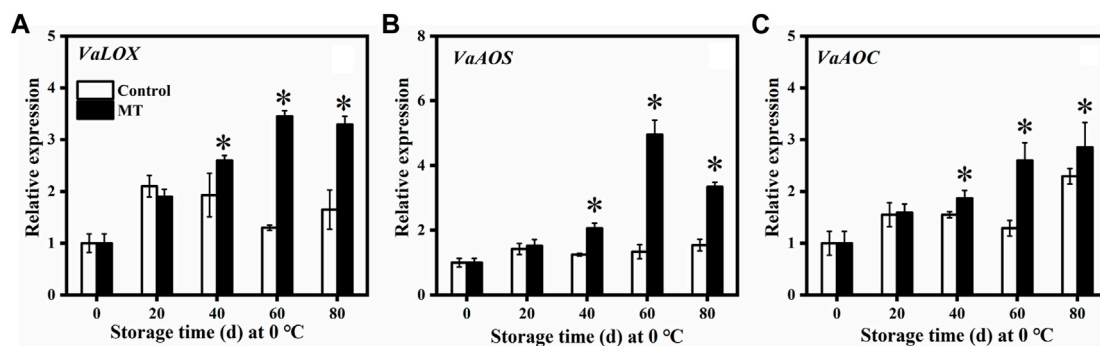
FIGURE 2 | Effects of MT treatment on the gene expressions of *VaLOX***(A)**, *VaAOS***(B)**, and *VaAOC* **(C)** of blueberry fruits during the postharvest storage at 0°C. Here, symbol * indicates significant differences ($p < 0.05$). Data are presented as the mean ± SD.

($p < 0.05$), being 1.10 and 1.11 times higher than that in the control group, respectively. The CAD activity of both the MT-treated and control fruits gradually increased from 0 to 80 days (**Figure 3D**). In particular, MT treatment significantly increased the CAD activity after 40, 60, and 80 days ($p < 0.05$), and these values are 1.25, 1.40, and 1.14 times higher than those of the control group, respectively.
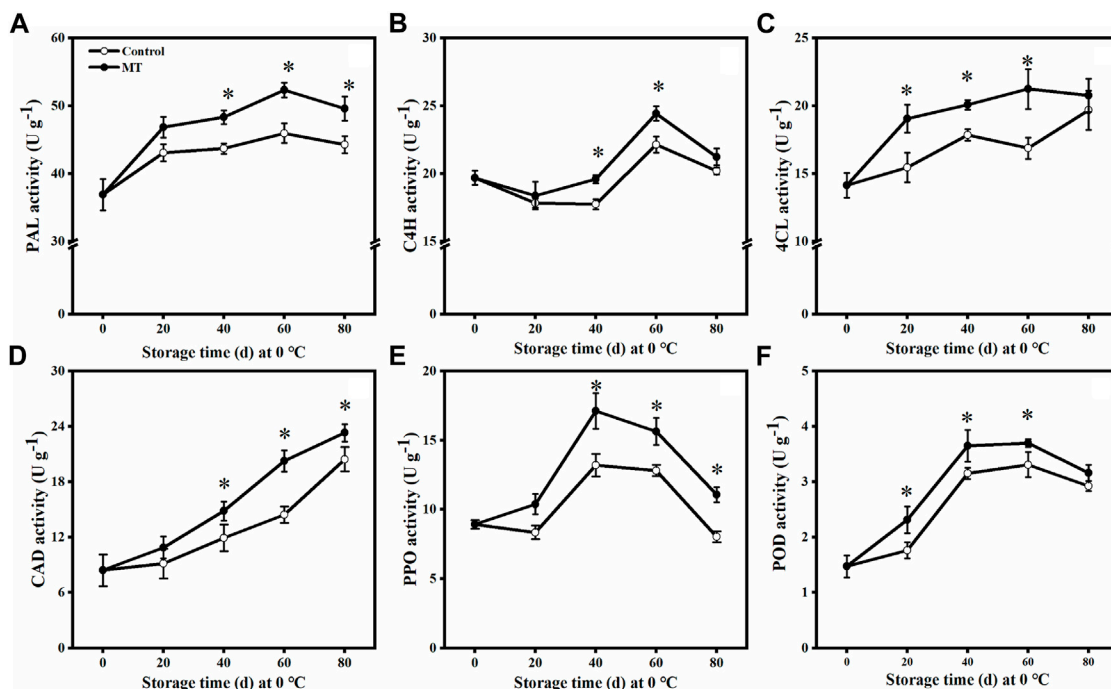
FIGURE 3 | Effects of MT treatment on PAL **(A)**, C4H **(B)**, 4CL **(C)**, CAD **(D)**, PPO **(E)**, and POD **(F)** activities of blueberry fruits during the postharvest storage at 0°C. Here, symbol * indicates significant differences ($p < 0.05$). Data are presented as the mean ± SD.
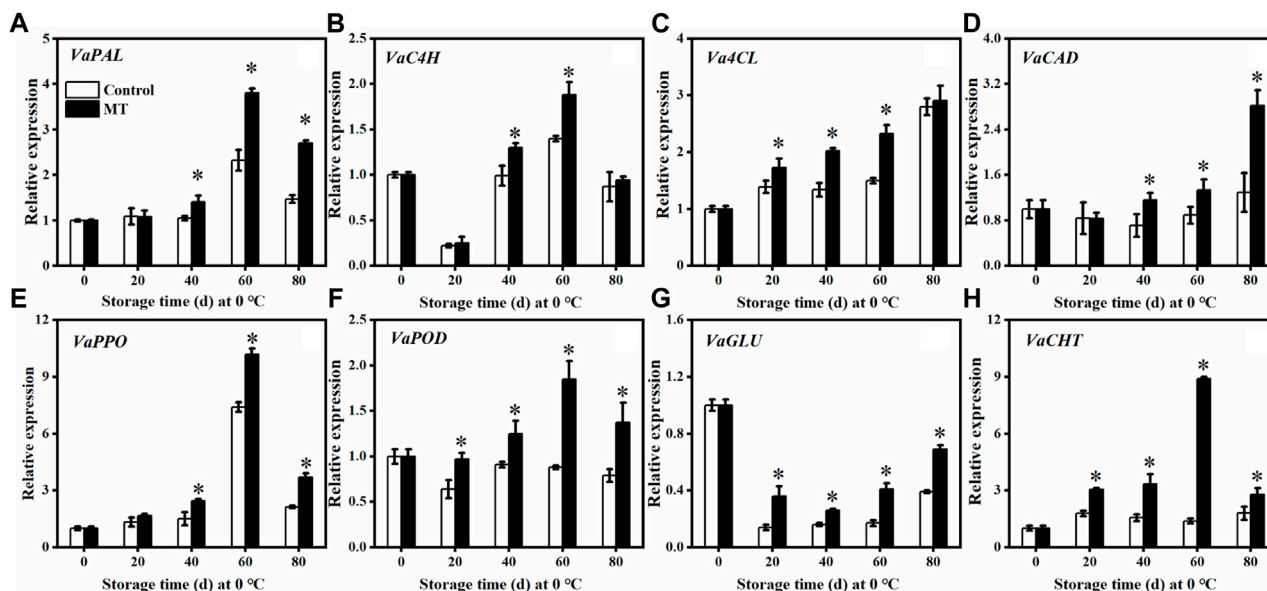
FIGURE 4 | Effects of MT treatment on the gene expressions of *VaPAL* **(A)**, *VaC4H* **(B)**, *Va4CL* **(C)**, *VaCAD* **(D)**, *VaPPO* **(E)**, *VaPOD* **(F)**, *VaGLU* **(G)**, and *VaCHT* **(H)** during the postharvest storage at 0°C. Here, symbol * indicates significant differences ($p < 0.05$). Data are presented as the mean ± SD.

Effect of Melatonin Treatment on the Expression of Genes Related to Defense Enzymes

As shown in **Figures 4A–D**, the relative expressions of *VaPAL* and *VaC4H* in the MT-treated fruits were not significantly different from those of the control group during the first 20 days ($p > 0.05$). After 60 days of storage, the relative expressions of *VaPAL* and *VaC4H* reached the highest levels ($p < 0.05$), which are 1.70 and 1.34 times higher than those of the control group, respectively. In contrast, the relative expressions of *Va4CL* and *VaCAD* in the MT-treated fruits reached the highest level after 80 days: 1.04 and 2.19 times higher than that of the control group, respectively. Compared with the control group, the relative expression of *Va4CL* in the MT-treated fruits was significantly higher ($p < 0.05$) after 20, 40, and 60 days, whereas the relative expression of *VaCAD* was significantly higher ($p < 0.05$) after 40 days. In contrast, the relative expressions of *VaPPO* (**Figure 4E**) and *VaPOD* (**Figure 4F**) in the MT-treated fruits increased and then decreased. After 40 days of storage, both *VaPPO* and *VaPOD* expressions were significantly upregulated after MT treatment ($p < 0.05$).

Concerning the pathogenesis-related proteins, the relative expression of *VaGLU* in the MT-treated group and the control group decreased and then increased during storage (**Figure 4G**). Overall, the relative expression of *VaGLU* was low but was significantly increased after MT treatment ($p < 0.05$). Throughout the storage period, the relative expression of *VaCHT* in the MT-treated fruits was significantly ($p < 0.05$) higher than that in the control (**Figure 4H**), specifically, 1.71, 2.13, 6.40, and 1.56 times higher than that in the control group after 0, 20, 40, 60, and 80 days, respectively.

Effects of Melatonin Treatment on the Total Phenol, Flavonoid, Anthocyanin, and Lignin Contents in the Blueberry Fruit

As shown in **Figure 5**, MT treatment promoted the accumulation of total phenols, flavonoids, anthocyanins, and lignin in the blueberries. After 60 days of storage, the total phenolic content of the MT-treated fruits reached the highest level ($p < 0.05$), which is 1.34 times higher than that of the control group (**Figure 5A**). The initial flavonoid content of the fruit was 1.16 mg g^{-1}, which gradually increased from 0 to 60 days and slightly decreased after 80 days of storage. The flavonoid content of the MT-treated fruit was significantly higher than that of the control group after 60 and 80 days of storage ($p < 0.05$) (**Figure 5B**). Throughout the storage period, the anthocyanin and lignin contents increased and then decreased, and after 20 days of storage, the anthocyanin content of the MT-treated fruits was significantly higher than that of the control group ($p < 0.05$): 1.04, 1.05, 1.02, and 1.09 times higher than that of the control group (**Figure 5C**), respectively. The lignin content of the MT-treated fruits reached the highest level after 40 days ($p < 0.05$), and this was 10.00% higher than that of the control group, decreasing to a lower level after 80 days. Therefore, MT treatment promoted the accumulation of polyphenols, flavonoids, anthocyanins, and lignin in the fruit and delayed their decay in the late storage period, suggesting improvement in the disease resistance of the blueberries.

DISCUSSION

JA is a signaling molecule that activates plant defenses to counter pathogen infestation and is synthesized in plants mainly through the octadecenoic acid pathway (Ruan et al., 2019). In this pathway, LOX are the key enzymes that convert linolenic acid to 13(*S*)-hydroxylinolenic acid, which is further converted by AOS and AOC to 12-oxo-phytodienoic acid. This product is then reduced and *β*-oxidized to produce JA (Ruan et al., 2019). It has been shown that JA enhances the defenses of peaches against *Penicillium expansum* by inducing NO production and, thus increasing the PAL, GLU, and CHT enzyme activities (Yu et al., 2012). In addition, JA induces the upregulation of *PAL* and *CHT* gene expressions and promotes phenolic product accumulation in tobacco plants (Keinnen et al., 2001). The results of this study showed that MT treatment upregulated *VaLOX*, *VaAOS*, and *VaAOC* gene expressions (**Figure 2**) and promoted JA synthesis, which in turn induced the accumulation of disease resistance–inducing substances in the blueberry fruits (**Figure 5**). This result is consistent with the study of Liu et al. (2019), who applied exogenous MT to induce improved resistance to *B. cinerea* in tomatoes.

When plants are exposed to biotic or abiotic stresses, a series of defense reactions are initiated. Phenylpropane metabolism is an important defense response pathway in the plant body (Wei et al., 2017). PAL is a key rate-limiting enzyme in the metabolism of phenylpropane and catalyzes the formation of cinnamic acid from phenylpropane, which is further converted to *p*-coumaric acid by C4H (Hu et al., 2014). POD and CAD are involved in lignin synthesis, whereas PPO is closely associated with plant resistance to pathogenic microbial invasion, specifically by catalyzing the oxidation of phenolic substances to produce antimicrobial substances (Hu et al., 2019). Li et al. (2019) found that MT treatment increased the activities of enzymes related to phenylpropane metabolism and enhanced the resistance of tomato fruits to *B. cinerea*. Zhang H. et al. (2021) demonstrated that salicylic acid induces the elevated expression of genes for enzymes related to phenylpropane metabolism, promotes the accumulation of phenylpropane secondary metabolites, and reduces the postharvest rot in *Lycium barbarum* fruit. Liu et al. (2022) showed that methionine treatment promotes lignin accumulation and enhances the resistance of jujube to *A. alternata*. In this study, MT treatment increased the activities of enzymes related to phenylpropane metabolism (PAL, C4H, 4CL, CAD, PPO, and POD) (**Figure 3**), the expressions of related genes (*VaPAL*, *VaC4H*, *Va4CL*, *VaCAD*, *VaPPO*, and *VaPOD*) (**Figure 4**), and the accumulation of polyphenols, flavonoids, anthocyanins, and lignin (**Figure 5**), thereby improving the postharvest disease resistance in blueberries.

GLU and CHT are pathogenesis-related proteins in plant tissues that can induce resistance to further invasion by pathogenic bacteria, disrupt the cell walls of fungi, and reduce fungal viability, thereby enhancing disease resistance (Hu et al., 2019). Huang et al. (2021) found that MT treatment upregulated *GLU* and *CHT* gene expressions and enhanced the resistance of ginger rootstocks to *Fusarium oxysporum* and *Penicillium compactum*. In our study, we found that MT treatment upregulated the expression of the pathogenesis-related proteins, *VaGLU* and *VaCHT* (**Figures 4G,H**), which is consistent with the abovementioned results. In addition, we found that MT did not significantly inhibit the colony diameter or spore
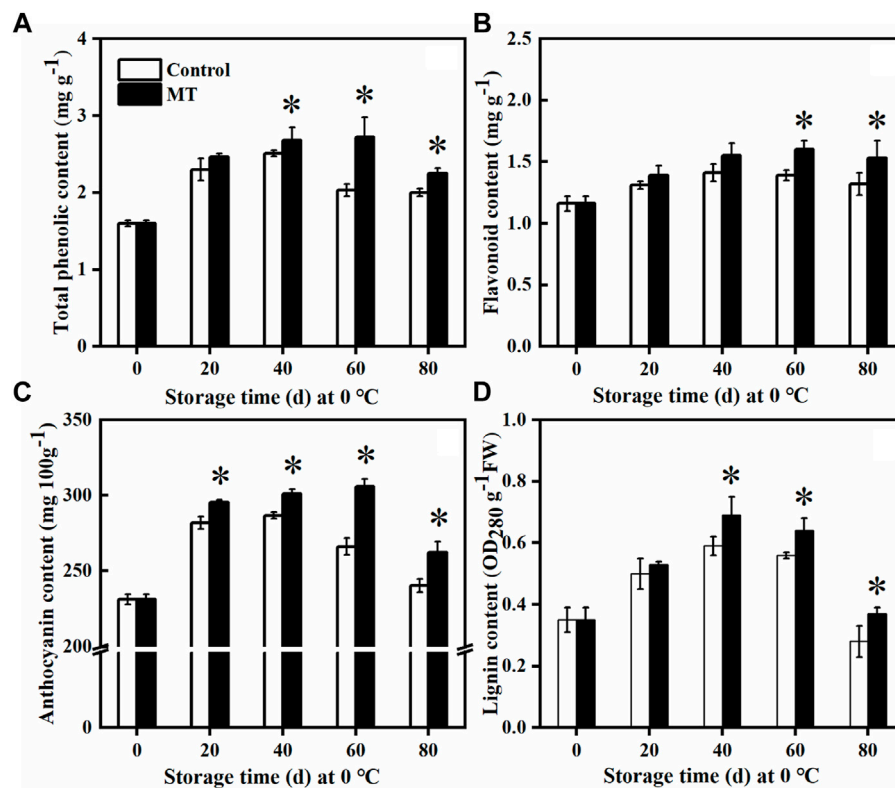
FIGURE 5 | Effects of MT treatment on the total phenol **(A)**, flavonoid **(B)**, anthocyanin **(C)**, and lignin **(D)** contents of blueberry fruits during postharvest storage at 0°C. Here, symbol * indicates significant differences ($p < 0.05$). Data are presented as the mean ± SD.

germination of *A. alternata*, *B. cinerea*, and *C. gloeosporioides* (**Figure 1**). This result is consistent with the results of Li et al. (2019), who used MT treatment to induce resistance to *B. cinerea* in tomatoes, and Zhang et al. (2022), who applied MT treatment to induce resistance to *A. alternata* in jujube fruit. In summary, MT had no inhibitory activity against *A. alternata*, *B. cinerea*, and *C. gloeosporioides*, suggesting that it reduced the postharvest rot of blueberries by inducing the activation of the JA signaling pathway and regulating the accumulation of phenylpropane metabolites.

CONCLUSION

In summary, the results of this study showed that MT treatment promoted the accumulation of polyphenols, flavonoids, anthocyanins, and lignans. In addition, MT treatment increased the enzymatic activities of PAL, C4H, 4CL, CAD, PPO, and POD and upregulated the expression of genes related to JA synthesis (*VaLOX*, *VaAOS*, and *VaAOC*), pathogenesis-related proteins (*VaGLU* and *VaCHT*), and genes related to phenylpropane metabolism (*VaPAL*, *VaC4H*, *Va4CL*, *VaCAD*, *VaPPO*, and *VaPOD*). These results suggest that MT treatment of blueberries may induce the activation of JA signaling and phenylpropane pathways as defense responses, thus effectively controlling blueberry rot during storage. Therefore, the application of MT could be an effective strategy for preserving blueberries after harvest.

DATA AVAILABILITY STATEMENT

The authors acknowledge that the data presented in this study must be deposited and made publicly available in an acceptable repository, prior to publication. Frontiers cannot accept an article that does not adhere to our open data policies.

AUTHOR CONTRIBUTIONS

GQ contributed to manuscript preparation, figure and table preparation, and manuscript editing and revision. WW, LB, and CM contributed to manuscript revision. WW and NJ helped during experiments and data analysis. SC designed and supervised the research and revised the manuscript. All authors discussed, edited, and approved the final version.

FUNDING

REFERENCES

Bennett, R. N., and Wallsgrove, R. M. (1994). Secondary Metabolites in Plant Defence Mechanisms. *New Phytol.* 127, 617–633. doi:10.1111/j.1469-8137.1994.tb02968.x

Bhardwaj, R., Pareek, S., Saravanan, C., and Yahia, E. M. (2022). Contribution of Pre-storage Melatonin Application to Chilling Tolerance of Some Mango Fruit Cultivars and Relationship with Polyamines Metabolism and γ-aminobutyric Acid Shunt Pathway. *Environ. Exp. Bot.* 194, 104691. doi:10.1016/j.envexpbot.2021.104691

Chen, Y., Hung, Y.-C., Chen, M., and Lin, H. (2017). Effects of Acidic Electrolyzed Oxidizing Water on Retarding Cell Wall Degradation and Delaying Softening of Blueberries during Postharvest Storage. *Lwt* 84, 650–657. doi:10.1016/j.lwt.2017.06.011

Gao, S., Ma, W., Lyu, X., Cao, X., and Yao, Y. (2020). Melatonin May Increase Disease Resistance and Flavonoid Biosynthesis through Effects on DNA Methylation and Gene Expression in Grape Berries. *BMC Plant Biol.* 20 (1), 231. doi:10.1186/s12870-020-02445-w

Ge, Y., Li, X., Li, C., Tang, Q., Duan, B., Cheng, Y., et al. (2019). Effect of Sodium Nitroprusside on Antioxidative Enzymes and the Phenylpropanoid Pathway in Blueberry Fruit. *Food Chem.* 295, 607–612. doi:10.1016/j.foodchem.2019.05.160

Gong, P., Chen, F.-x., Wang, L., Wang, J., Jin, S., and Ma, Y.-m. (2014). Protective Effects of Blueberries (Vaccinium Corymbosum L.) Extract against Cadmium-Induced Hepatotoxicity in Mice. *Environ. Toxicol. Pharmacol.* 37, 1015–1027. doi:10.1016/j.etap.2014.03.017

Hu, M., Yang, D., Huber, D. J., Jiang, Y., Li, M., Gao, Z., et al. (2014). Reduction of Postharvest Anthracnose and Enhancement of Disease Resistance in Ripening Mango Fruit by Nitric Oxide Treatment. *Postharvest Biol. Technol.* 97, 115–122. doi:10.1016/j.postharvbio.2014.06.013

Hu, M., Zhu, Y., Liu, G., Gao, Z., Li, M., Su, Z., et al. (2019). Inhibition on Anthracnose and Induction of Defense Response by Nitric Oxide in Pitaya Fruit. *Sci. Hortic.* 245, 224–230. doi:10.1016/j.scienta.2018.10.030

Huang, K., Sui, Y., Miao, C., Chang, C., Wang, L., Cao, S., et al. (2021). Melatonin Enhances the Resistance of Ginger Rhizomes to Postharvest Fungal Decay. *Postharvest Biol. Technol.* 182, 111706. doi:10.1016/j.postharvbio.2021.111706

Ji, N., Wang, J., Li, Y., Li, M., Jin, P., and Zheng, Y. (2021a). Involvement of PpWRKY70 in the Methyl Jasmonate Primed Disease Resistance against Rhizopus Stolonifer of Peaches via Activating Phenylpropanoid Pathway. *Postharvest Biol. Technol.* 174, 111466. doi:10.1016/j.postharvbio.2021.111466

Ji, Y., Hu, W., Liao, Z., Jiang, A., Yang, X., Guan, Y., et al. (2021b). Effect of Ethanol Vapor Treatment on the Growth of *Alternaria alternata* and *Botrytis Cinerea* and Defense-Related Enzymes of Fungi-Inoculated Blueberry during Storage. *Front. Microbiol.* 12, 618252. doi:10.3389/fmicb.2021.618252

Keinnen, M., Oldham, N. J., and Baldwin, I. T. (2001). Rapid HPLC Screening of Jasmonate-Induced Increases in Tobacco Alkaloids, Phenolics, and Diterpene Glycosides in Nicotiana Attenuata. *J. Agric. Food Chem.* 49 (8), 3553–3558. doi:10.1021/jf01020010.1021/jf010200+

Li, H., Suo, J., Han, Y., Liang, C., Jin, M., Zhang, Z., et al. (2017). The Effect of 1-methylcyclopropene, Methyl Jasmonate and Methyl Salicylate on Lignin Accumulation and Gene Expression in Postharvest 'Xuxiang' Kiwifruit during Cold Storage. *Postharvest Biol. Technol.* 124, 107–118. doi:10.1016/j.postharvbio.2016.10.003

Li, S., Xu, Y., Bi, Y., Zhang, B., Shen, S., Jiang, T., et al. (2019). Melatonin Treatment Inhibits Gray Mold and Induces Disease Resistance in Cherry Tomato Fruit during Postharvest. *Postharvest Biol. Technol.* 157 (C), 110962. doi:10.1016/j.postharvbio.2019.110962

Li, Z., Wang, N., Wei, Y., Zou, X., Jiang, S., Xu, F., et al. (2020). Terpinen-4-ol Enhances Disease Resistance of Postharvest Strawberry Fruit More Effectively Than Tea Tree Oil by Activating the Phenylpropanoid Metabolism Pathway. *J. Agric. Food Chem.* 68, 6739–6747. doi:10.1021/acs.jafc.0c01840

Lin, Y.-F., Hu, Y.-H., Lin, H.-T., Liu, X., Chen, Y.-H., Zhang, S., et al. (2013). Inhibitory Effects of Propyl Gallate on Tyrosinase and its Application in Controlling Pericarp Browning of Harvested Longan Fruits. *J. Agric. Food Chem.* 61, 2889–2895. doi:10.1021/jf305481h

Lin, Y., Huang, G., Zhang, Q., Wang, Y., Dia, V. P., and Meng, X. (2020). Ripening Affects the Physicochemical Properties, Phytochemicals and Antioxidant Capacities of Two Blueberry Cultivars. *Postharvest Biol. Technol.* 162, 111097. doi:10.1016/j.postharvbio.2019.111097

Lin, Y., Wang, Y., Li, B., Tan, H., Li, D., Li, L., et al. (2018). Comparative Transcriptome Analysis of Genes Involved in Anthocyanin Synthesis in Blueberry. *Plant Physiology Biochem.* 127, 561–572. doi:10.1016/j.plaphy.2018.04.034

Liu, C., Chen, L., Zhao, R., Li, R., Zhang, S., Yu, W., et al. (2019). Melatonin Induces Disease Resistance to *Botrytis Cinerea* in Tomato Fruit by Activating Jasmonic Acid Signaling Pathway. *J. Agric. Food Chem.* 67 (22), 6116–6124. doi:10.1021/acs.jafc.9b00058

Liu, C., Zheng, H., Sheng, K., Liu, W., and Zheng, L. (2018). Effects of Postharvest UV-C Irradiation on Phenolic Acids, Flavonoids, and Key Phenylpropanoid Pathway Genes in Tomato Fruit. *Sci. Hortic.* 241, 107–114. doi:10.1016/j.scienta.2018.06.075

Liu, Y., Lei, X., Deng, B., Chen, O., Deng, L., and Zeng, K. (2022). Methionine Enhances Disease Resistance of Jujube Fruit against Postharvest Black Spot Rot by Activating Lignin Biosynthesis. *Postharvest Biol. Technol.* 190, 111935. doi:10.1016/j.postharvbio.2022.111935

Moustafa-Farag, M., Almoneafy, A., Mahmoud, A., Elkelish, A., Arnao, M., Li, L., et al. (2020). Melatonin and its Protective Role against Biotic Stress Impacts on Plants. *Biomolecules* 10, 54. doi:10.3390/biom10010054

Naik, D., Dhanaraj, A. L., Arora, R., and Rowland, L. J. (2007). Identification of Genes Associated with Cold Acclimation in Blueberry (Vaccinium Corymbosum L.) Using a Subtractive Hybridization Approach. *Plant Sci.* 173, 213–222. doi:10.1016/j.plantsci.2007.05.003

Olmedo, G. M., Cerioni, L., González, M. M., Cabrerizo, F. M., Rapisarda, V. A., and Volentini, S. I. (2017). Antifungal Activity of β-carbolines on Penicillium digitatum and Botrytis Cinerea. *Food Microbiol.* 62, 9–14. doi:10.1016/j.fm.2016.09.011

Pan, L., Chen, X., Xu, W., Fan, S., Wan, T., Zhang, J., et al. (2022). Methyl Jasmonate Induces Postharvest Disease Resistance to Decay Caused by *Alternaria alternata* in Sweet Cherry Fruit. *Sci. Hortic.* 292, 110624. doi:10.1016/j.scienta.2021.110624

Ren, Y., Xue, Y., Tian, D., Zhang, L., Xiao, G., and He, J. (2020). Improvement of Postharvest Anthracnose Resistance in Mango Fruit by Nitric Oxide and the Possible Mechanisms Involved. *J. Agric. Food Chem.* 68 (52), 15460–15467. doi:10.1021/acs.jafc.0c04270

Ruan, J., Zhou, Y., Zhou, M., Yan, J., Khurshid, M., Weng, W., et al. (2019). Jasmonic Acid Signaling Pathway in Plants. *Ijms* 20 (10), 2479. doi:10.3390/ijms20102479

Saito, S., Wang, F., and Xiao, C.-L. (2022). Natamycin as a Postharvest Treatment to Control Gray Mold on Stored Blueberry Fruit Caused by Multi-Fungicide Resistant *Botrytis Cinerea*. *Postharvest Biol. Technol.* 187, 111862. doi:10.1016/j.postharvbio.2022.111862

Shang, F., Liu, R., Wu, W., Han, Y., Fang, X., Chen, H., et al. (2021). Effects of Melatonin on the Components, Quality and Antioxidant Activities of Blueberry Fruits. *Lwt* 147 (5), 111582. doi:10.1016/j.lwt.2021.111582

Shi, H., Chen, Y., Tan, D.-X., Reiter, R. J., Chan, Z., and He, C. (2015). Melatonin Induces Nitric Oxide and the Potential Mechanisms Relate to Innate Immunity against Bacterial Pathogen Infection in Arabidopsis. *J. Pineal Res.* 59 (1), 102–108. doi:10.1111/jpi.12244

Truman, W., Bennett, M. H., Kubigsteltig, I., Turnbull, C., and Grant, M. (2007). Arabidopsis Systemic Immunity Uses Conserved Defense Signaling Pathways and Is Mediated by Jasmonates. *Proc. Natl. Acad. Sci. U.S.A.* 104 (3), 1075–1080. doi:10.1073/pnas.0605423104

Wang, H., Chen, Y., Lin, H., Lin, M., Chen, Y., and Lin, Y. (2020b). 1-Methylcyclopropene Containing-Papers Suppress the Disassembly of Cell Wall Polysaccharides in Anxi Persimmon Fruit during Storage. *Int. J. Biol. Macromol.* 151, 723–729. doi:10.1016/j.ijbiomac.2020.02.146

Wang, H., Cheng, X., Wu, C., Fan, G., Li, T., and Dong, C. (2021). Retardation of Postharvest Softening of Blueberry Fruit by Methyl Jasmonate Is Correlated with Altered Cell Wall Modification and Energy Metabolism. *Sci. Hortic.* 276, 109752. doi:10.1016/j.scienta.2020.109752

Wang, H., Kou, X., Wu, C., Fan, G., and Li, T. (2020a). Methyl Jasmonate Induces the Resistance of Postharvest Blueberry to Gray Mold Caused by Botrytis Cinerea. *J. Sci. Food Agric.* 100 (11), 4272–4281. doi:10.1002/jsfa.10469

Wang, S. Y., Chen, C.-T., and Yin, J.-J. (2010). Effect of Allyl Isothiocyanate on Antioxidants and Fruit Decay of Blueberries. *Food Chem.* 120, 199–204. doi:10.1016/j.foodchem.2009.10.007

Wei, Y., Zhou, D., Peng, J., Pan, L., and Tu, K. (2017). Hot Air Treatment Induces Disease Resistance through Activating the Phenylpropanoid Metabolism in Cherry Tomato Fruit. *J. Agric. Food Chem.* 65 (36), 8003–8010. doi:10.1021/acs.jafc.7b02599

Yu, Q., Chen, Q., Chen, Z., Xu, H., Fu, M., Li, S., et al. (2012). Activating Defense Responses and Reducing Postharvest Blue Mold Decay Caused by Penicillium expansum in Peach Fruit by Yeast Saccharide. *Postharvest Biol. Technol.* 74, 100–107. doi:10.1016/j.postharvbio.2012.07.005

Zhang, H., Liu, F., Wang, J., Yang, Q., Wang, P., Zhao, H., et al. (2021a). Salicylic Acid Inhibits the Postharvest Decay of Goji Berry (Lycium Barbarum l.) by Modulating the Antioxidant System and Phenylpropanoid Metabolites. *Postharvest Biol. Technol.* 178, 111558. doi:10.1016/j.postharvbio.2021.111558

Zhang, L. L., Yu, Y. W., Chang, L. L., Wang, X. J., and Zhang, S. Y. (2022). Melatonin Enhanced the Disease Resistance by Regulating Reactive Oxygen Species Metabolism in Postharvest Jujube Fruit. *J. Food Process. Preserv.* 46 (3), e16363. doi:10.1111/jfpp.16363

Zhang, W., Jiang, H., Cao, J., and Jiang, W. (2021b). UV-C Treatment Controls Brown Rot in Postharvest Nectarine by Regulating ROS Metabolism and Anthocyanin Synthesis. *Postharvest Biol. Technol.* 180, 111613. doi:10.1016/j.postharvbio.2021.111613

Zhang, X., Zong, Y., Li, Z., Yang, R., Li, Z., Bi, Y., et al. (2020). Postharvest Pichia Guilliermondii Treatment Promotes Wound Healing of Apple Fruits. *Postharvest Biol. Technol.* 167, 111228. doi:10.1016/j.postharvbio.2020.111228

Conflict of Interest: The authors declare that the research was conducted in the absence of any commercial or financial relationships that could be construed as a potential conflict of interest.

The handling editor HL declared a past co-authorship with the author RW.

Publisher's Note: All claims expressed in this article are solely those of the authors and do not necessarily represent those of their affiliated organizations, or those of the publisher, the editors, and the reviewers. Any product that may be evaluated in this article, or claim that may be made by its manufacturer, is not guaranteed or endorsed by the publisher.

Design, Synthesis, and Biological Activity of Novel Chalcone Derivatives Containing an 1,2,4-Oxadiazole Moiety

Ling Luo[1], Dan Liu[1], Shichao Lan[1,2] and Xiuhai Gan[1]*

[1]State Key Laboratory Breeding Base of Green Pesticide and Agricultural Bioengineering, Key Laboratory of Green Pesticide and Agricultural Bioengineering, Ministry of Education, Guizhou University, Guiyang, China, [2]School of Biological Sciences, Guizhou Education University, Guiyang, China

To discover a lead compound for agricultural use, 34 novel chalcone derivatives containing an 1,2,4-oxadiazole moiety were designed and synthesized. Their nematocidal activities against *Bursaphelenchus xylophilus*, *Aphelenchoides besseyi*, and *Ditylenchus dipsaci* and their antiviral activities against tobacco mosaic virus (TMV), pepper mild mottle virus (PMMoV), and tomato spotted wilt virus (TSWV) were evaluated. Biological assay results indicate that compounds **A13** and **A14** showed good nematocidal activities against *B. xylophilus*, *A. besseyi*, and *D. dipsaci*, with LC_{50} values of 35.5, 44.7, and 30.2 μg/ml and 31.8, 47.4, and 36.5 μg/ml, respectively, which are better than tioxazafen, fosthiazate, and abamectin. Furthermore, compound **A16** demonstrated excellent protective activity against TMV, PMMoV, and TSWV, with EC_{50} values of 210.4, 156.2, and 178.2 μg/ml, respectively, which are superior to ningnanmycin (242.6, 218.4, and 180.5 μg/ml).

Keywords: plant-parasitic nematodes, chalcone, 1, 2, 4-oxadiazole, nematocidal activity, antiviral activity

INTRODUCTION

Plant-parasitic nematodes (PPNs) are a very important group of pests that include more than 60 regulated species. These pests are extremely difficult to prevent and cause annual global agricultural losses of roughly $157 billion (Abad, et al., 2008; Bernard, et al., 2017; Abd-Elgawad, 2020; Kantor, et al., 2022). At present, the application of chemical nematicides is the most reliable and effective method to control PPNs. However, these treatments are mainly based on highly toxic organophosphorus and carbamate nematocides, such as fosthiazate, cadusafos, fenamiphos, dazomet, aldicarb, oxamyl, and so on. The long-term use, overuse, and misuse of these nematicides have not only led to poor control effect and serious resistance but have also seriously harmed the environment (Ntalli and Caboni, 2012; Chen, et al., 2020). Meanwhile, plant virus disease, as a "plant cancer," can lead to considerable crop loss (Chen, et al., 2016). Although Ribavirin is widely used to prevent plant virus disease, its inhibitory effect to a virus is less than 50% at 500 mg/L (Wang, et al., 2012). To date, we still lack effective and low toxicity nematicides and antiviral agents for use in agricultural production. In addition, a combined infection of PPNs and viruses will significantly increase the loss of agricultural production. Hence, the discovery of new, environmentally friendly, and efficient nematicides and antiviral agents is key to controlling plant nematode and virus diseases.

Natural products have often been the source of new drug discovery and have the benefits of low toxicity, easy decomposition, and are environmentally friendly (Leonard and Stephen, 2007; Qian, et al., 2010; Chen, et al., 2020). As one of the most important natural products, chalcone is widely found in plants (Du, et al., 2013) and has various biological activities, including anticancer (Kim,

FIGURE 1 | Design of the target compounds.
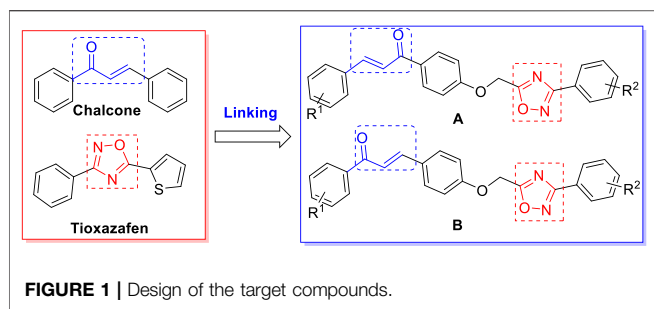
et al., 2013; Wang, et al., 2015), antibacterial (Wei, et al., 2016), antifungal (Lahtchev, et al., 2008) and antiviral (Park, et al., 2011) effects in medicine. In addition, chalcone and its derivatives have insecticidal (Thirunarayanan, et al., 2010), nematicidal (Attar, et al., 2011; Nunes, et al., 2013; Caboni, et al., 2016), antiviral (Du, et al., 2013), and other agricultural activities. In our previous work, we reported that chalcone derivatives containing 1,3,4-oxadiazole/thiadiazole, purine, and ferulic acid moieties have excellent antiviral activities (Gan, et al., 2017a; Gan, et al., 2017b).

As an important heterocyclic compound, 1,2,4-oxadiazole has been widely studied by pesticide scientists with a wide range of biological activities, such as herbicidal (Hang, et al., 2014), antibacterial (Karad, et al., 2017), antifungal (Yang, et al., 2021), and insecticidal activities (Fernandes, et al., 2020), among others. Tioxazafen, which is one of the 1,2,4-oxadiazole compounds, was designed by Monsanto as a new type of seed treatment agent to control nematodes in soybean, corn, and cotton (Slomczynska, et al., 2015). However, Tioxazafen has not formally been used on a large scale in agricultural production. To enhance the flexibility of the structure of Tioxazafen and discover the high activity 1,2,4-oxadiazole compound, some 1,2,4-oxadiazole derivatives containing 1,3,4-oxadiazole/thiadiazole and amide moieties with good nematocidal, antibacterial, and antifungal activities have been synthesized (Zhu, et al., 2020; Liu, et al., 2022).

Based on the biological activity of chalcone and 1,2,4-oxadiazole derivatives, the current study aims to further improve the nematocidal activity, and to extend the biological activity of chalcone and 1,2,4-oxadiazole moieties. In particular, a 1,2,4-oxadiazole fragment is introduced to the chalcone skeleton to obtain 34 novel chalcone derivatives containing 1,2,4-oxadiazole moiety (**Figure 1**). Their nematocidal activities against *Bursaphelenchus xylophilu*s, *Aphelenchoides besseyi,* and *Ditylenchus dipsaci* and their antiviral activities to tobacco mosaic virus (TMV), pepper mild mottle virus (PMMoV), and tomato spotted wilt virus (TSWV) were then evaluated.

MATERIALS AND METHODS

General Information
The melting points of the compounds were determined on an X-4B microscope melting point apparatus and were uncorrected (Shanghai Electrophysics Optical Instrument Co., Ltd., Shanghai, China). The ^{1}H NMR and ^{13}C NMR spectra data of the

compounds were recorded on a Bruker DPX-400 spectrometer (Bruker, Billerica, MA, United States), using DMSO-d_6 as solvents and tetramethylsilane as an internal standard. The high-resolution mass spectrometer (HRMS) data of the compounds were obtained with a Thermo Scientific Q-Exactive (Thermo Scientific, Missouri, MOThermo, United States). Reactions were detected by thin-layer chromatography (TLC) and visualized under UV light at 254 nm. Chromatography was conducted on silica gel 200–300 mesh.

Synthesis
Preparation Procedure for Intermediates 2 and 6
As shown in **Schemes 1** and **2**, the chalcone intermediates **2** and **6** were obtained according to our previously reported methods (Gan, et al., 2017c). First, 0.2 M aqueous sodium hydroxide solution (22 mmol) was added to a solution of 4-hydroxyacetophenone or 4-hydroxybenzaldehyde (20 mmol) and various substituted benzaldehyde or acetophenone (20 mmol) in 20 ml ethanol, and then stirred at room temperature for 12 h. Second, upon reaction completion (monitored by TLC), the mixture was poured into ice-water and acidified to a pH value of 2–3 by dropwise addition of aqueous HCl, filtered, washed, and dried to obtain intermediates **2** and **6**.

Preparation Procedure for Intermediate 4
An aqueous solution of sodium hydroxide (50 mmol) was added to a solution of hydroxylamine hydrochloride (50 mmol) in 30 ml ethanol and stirred at room temperature. Various benzonitriles (50 mmol) were then added to the mixture. The mixture was heated to reflux and monitored with TLC. After completion of the reaction, the precipitated product was filtrated and the filtrate was concentrated under reduced pressure. The residue was dissolved with toluene and chloroacetyl chloride (50 mmol) was added dropwise into the mixture in an ice bath, and then refluxed for 10 h. The solvent was removed and the residue was dissolved with dichloromethane and washed with brine. The organic layer was then dried and further purified by column chromatography to afford intermediate **4**.

Preparation Procedure for the Target Compounds A1–A21 and B1–B13
A solution of intermediate **4** (2.0 mmol) in 5 ml DMF was added to a solution of intermediate **2** or **6** (2.0 mmol), K$_2$CO$_3$ (2.2 mmol) in 5 ml *N*,*N*-dimethylformamide (DMF) and warmed to 40°C for 4 h. Upon completion of reaction, the mixture was poured into ice-water, filtered, and recrystallized from methanol to give the pure target compounds **A1–A21** and **B1–B13**. The physical properties, ^{1}HNMR, ^{13}CNMR, and HRMS for title compounds are reported in the **Supplementary Data**. The spectral data of **A1** and **B1** are shown below.

(E)-3-(2,4-dichlorophenyl)-1-(4-((3-phenyl-1,2,4-oxadiazol-5-yl)methoxy)phenyl)prop-2-en-1-one (**A1**). White powder; m.p. 154–155°C; yield 89%; ^{1}H NMR (400 MHz, DMSO-d_6): δ 8.02 (d, *J* = 6.4 Hz, 2H), 7.79 (d, *J* = 8.8 Hz, 2H), 7.77 (d, *J* = 1.6 Hz, 1H), 7.59–7.58 (m, 5H), 7.40 (d, *J* = 16.0 Hz, 1H), 7.17

SCHEME 1 | Synthetic process and the experimental method of the target compounds **A1–A21**.

SCHEME 2 | Synthetic process and the experimental method of the target compounds **B1–B13**.
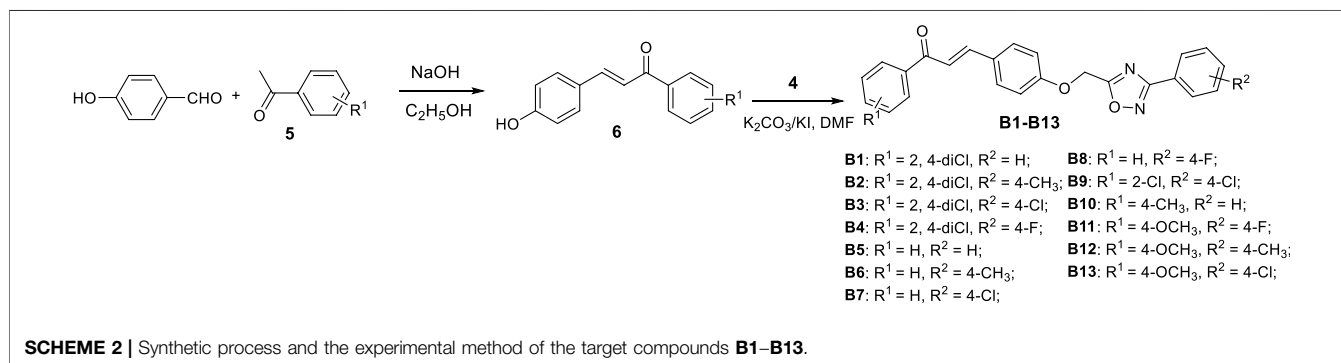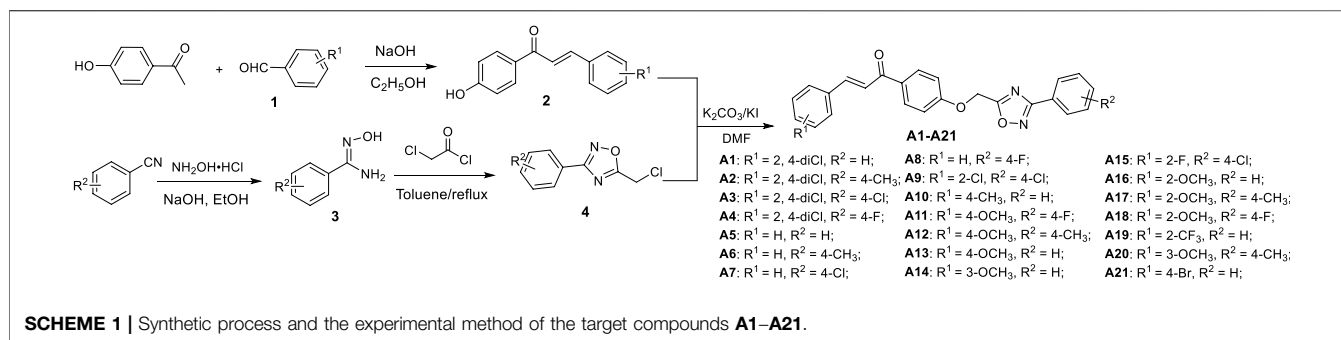
(d, J = 9.2 Hz, 2H), 7.16 (d, J = 15.6 Hz, 1H), 5.70 (s, 2H); ^{13}C NMR (101 MHz, DMSO-d_6): δ 192.83, 175.99, 168.85, 160.07, 147.02, 138.07, 135.90, 132.31, 131.63, 131.50, 131.50, 131.10, 130.12, 129.84, 129.84, 128.38, 128.10, 127.56, 127.56, 126.20, 124.95, 115.80, 115.80, 61.39. HRMS (ESI) m/z for $C_{24}H_{17}O_3N_2Cl_2$ $[M+H]^+$ calcd: 451.06107, found: 451.05978.

(E)-1-(2,4-dichlorophenyl)-3-(4-((3-phenyl-1,2,4-oxadiazol-5-yl)methoxy)phenyl)prop-2-en-1-one (**B1**). Faint yellow powder; m.p. 126–127°C; yield 56%; ^{1}H NMR (400 MHz, DMSO-d_6): δ 8.33–8.27 (m, 3H), 8.12–7.98 (m, 4H), 7.79 (d, J = 1.6 Hz, 1H), 7.67–7.59 (m, 4H), 7.33 (d, J = 8.8 Hz, 2H), 5.82 (s, 2H); ^{13}C NMR (101 MHz, DMSO-d_6): δ 187.54, 175.87, 168.27, 161.79, 137.19, 135.98, 135.57, 132.31, 131.92, 131.67, 131.67, 131.65, 130.30, 129.95, 129.84, 129.84, 128.39, 127.57, 127.57, 126.20, 125.72, 115.39, 115.39, 61.51. HRMS (ESI) m/z for $C_{24}H_{17}O_3N_2Cl_2$ $[M+H]^+$ calcd: 451.06107, found: 451.05972.

Nematocidal Activity Test

B. xylophilus, *A. besseyi,* and *D. dipsaci* were bred with potato dextrose agar–*Botrytis cinerea* provided from the Fine Chemical Research and Development Center of Guizhou University (Guizhou, China). The nematocidal bioassays of these target compounds was tested based on the previous reported methods with minor modification (Wei, et al., 2021). The compound was dissolved with 50 μl DMF, and was then diluted with 1% Tween-80 to obtain 50 and 10 μg/ml concentrations. Meanwhile, fosthiazate and tioxazafen were used as positive controls at the same concentrations and without compounds solution as a negative control

group. Then, 10 μl of nematode suspension with 50 nematodes and 300 μl of the solution were added to the corresponding hole of 48-well plates, each treatment was repeated three times, and they were then placed in a biochemical incubator at 27°C for dark light culture. After 48 h, the dead nematodes were counted and the corrected mortality was calculated with the following formula:

Corrected mortality %
= [(mortality of treatment % − mortality of negative control %)/
(1 − mortality of negative control %)] × 100

Antiviral Activity Test

Nicotiana tabacum cv. K326, *Nicotiana benthamiana*, and *Nicotiana glutinosa* L. plants were cultivated in a greenhouse. *N. tabacum* cv. K326 was used to determine systemic TMV infection, and *N. benthamiana* was used to determine systemic PMMoV and TSWV infection. *N. glutinosa* L. was used as a local lesion host to evaluate the antiviral activity against TMV, PMMoV, and TSWV when the plants grew to 5–6 leaf stages. TMV, PMMoV, and TSWV were purified by the Gooding method (Gooding and Hebert, 1967) and the curative, protective activities of compounds were performed with the reported methods at 500 μg/ml (Song, et al., 2005; Zan, et al., 2021; Shi, et al., 2022). The EC_{50} values of the antiviral activity at concentrations of 500, 250, 125, 62.5, and 31.25 μg/ml were then calculated. The positive controls included ribavirin and ningnanmycin. Measurements were performed in triplicates.

RESULTS AND DISCUSSION

Chemistry

The influence of the catalyst, temperature, and solvent for preparation compound **A1** was tested and evaluated to obtain the facile, high efficiency, and yield synthetic method of the target compound; the results are given in **Table 1**. The results indicate that the yield of compound **A1** was affected by the catalyst, solvent, and temperature. The optimum synthesis condition is catalyst as K_2CO_3/KI, DMF as solvent, and reaction for 6 h at 80°C. Under this condition, the yield of compound **A1** achieved 89%. The other compounds were then prepared with the same condition. The structures of all of the

TABLE 1 | The reaction conditions for compound **A1** were optimized.

Entry	Catalyst	Solvent	Temperature/°C	Yield[a] (%)
1	K_2CO_3	CH_3CN	r.t	32
2	Na_2CO_3	CH_3CN	r.t	15
3	NaOH	CH_3CN	r.t	21
3	K_2CO_3/KI	CH_3CN	r.t	38
4	K_2CO_3/KI	CH_3CN	80	71
5	K_2CO_3	DMF	r.t	39
6	K_2CO_3/KI	DMF	r.t	56
7	K_2CO_3	DMF	60	85
8	K_2CO_3	$(CH_3)_2CO$	56	48
9	K_2CO_3	DMF	80	83
10	K_2CO_3/KI	DMF	60	89

[a]Isolated yield.

TABLE 2 | Nematicidal activity of compounds **A1**–**A21** and **B1**–**B13**.[a]

Compd.	Corrected mortality ±SD (%)[b]					
	B. xylophilus		*A. besseyi*		*D. dipsaci*	
	50 µg/ml	10 µg/ml	50 µg/ml	10 µg/ml	50 µg/ml	10 µg/ml
A1	26.6 ± 3.8	—	32.0 ± 6.5	—	—	—
A2	—	—	—	—	22.4 ± 2.9	—
A3	—	—	—	—	—	—
A4	37.7 ± 3.9	—	—	—	—	—
A5	38.8 ± 4.9	—	32.0 ± 6.5	—	23.1 ± 1.3	—
A6	30.6 ± 5.8	—	21.2 ± 2.4	—	20.6 ± 5.2	—
A7	—	—	24.6 ± 5.3	20.5 ± 2.2	24.7 ± 0.4	—
A8	—	—	21.5 ± 2.3	—	22.6 ± 8.0	—
A9	48.9 ± 7.4	26.9 ± 5.7	—	—	30.7 ± 3.5	24.2 ± 5.9
A10	26.9 ± 5.2	—	—	—	30.7 ± 5.3	—
A11	20.7 ± 4.7	—	24.1 ± 8.6	—	22.0 ± 2.8	—
A12	41.0 ± 6.9	23.5 ± 4.1	—	—	27.7 ± 8.2	—
A13	100	25.8 ± 4.9	100	25.8 ± 5.9	100	25.8 ± 1.9
A14	100	25.1 ± 5.6	100	—	100	24.1 ± 1.6
A15	47.9 ± 5.7	32.1 ± 7.7	—	—	—	—
A16	21.5 ± 1.5	—	—	—	—	—
A17	—	—	—	—	—	—
A18	36.5 ± 9.5	25.4 ± 1.0	—	—	25.4 ± 1.0	—
A19	44.9 ± 6.1	23.3 ± 6.7	—	—	—	—
A20	25.5 ± 5.5	—	—	—	—	—
A21	23.0 ± 4.5	—	—	—	23.4 ± 6.2	—
B1	29.9 ± 6.5	—	25.2 ± 7.1	—	22.4 ± 6.0	—
B2	37.7 ± 6.7	—	21.8 ± 3.3	—	28.8 ± 1.2	—
B3	51.8 ± 5.8	—	25.6 ± 4.0	—	25.5 ± 3.8	—
B4	28.1 ± 7.8	—	25.0 ± 3.3	—	24.9 ± 9.0	—
B5	31.1 ± 5.8	—	29.5 ± 2.8	20.8 ± 7.3	33.2 ± 1.5	23.3 ± 2.7
B6	37.0 ± 1.1	—	70.8 ± 1.8	—	29.9 ± 6.2	20.7 ± 6.6
B7	27.8 ± 6.3	—	—	—	21.6 ± 4.4	—
B8	—	—	—	—	25.3 ± 5.9	—
B9	—	—	—	—	29.3 ± 3.4	—
B10	—	—	22.9 ± 2.8	—	22.4 ± 4.7	—
B11	—	—	31.5 ± 4.3	—	41.0 ± 7.4	22.2 ± 4.1
B12	—	—	59.6 ± 9.2	—	—	—
B13	25.1 ± 1.1	—	35.8 ± 1.7	—	33.0 ± 6.5	—
Tioxazafen[b]	34.3 ± 7.7	—	40.0 ± 6.1	20.1 ± 2.5	29.0 ± 3.7	—
Fosthiazate[b]	43.9 ± 5.2	23.2 ± 9.8	—	—	33.3 ± 1.6	—
Abamectin[b]	49.4 ± 6.3	31.9 ± 4.2	42.3 ± 2.0	22.2 ± 3.2	33.6 ± 1.3	20.2 ± 3.3

[a]Average of three replicates.
[b]The commercial antiviral agents tioxazafen, fosthiazate, and abamectin were used for comparison of activity.
"—" No activity or corrected mortality <20%.

TABLE 3 | The LC$_{50}$ values of nematicidal activity of compounds.

Compd.	LC$_{50}$ (µg/ml)[a]		
	B. xylophilus	A. besseyi	B. cinerea
A13	35.5 ± 3.5	44.7 ± 5.4	30.2 ± 2.0
A14	31.8 ± 0.9	47.4 ± 2.5	36.5 ± 0.7
Tioxazafen[b]	>200	>200	>200
Fosthiazate[b]	>200	>200	>200
Abamectin[b]	103.8 ± 1.5	>200	106.2 ± 2.1

[a]Average of three replicates.
[b]The commercial antiviral agents tioxazafen, fosthiazate, and abamectin were used for comparison of activity.

compounds were identified with ^{1}H NMR, ^{13}C NMR, and HRMS. Two doublets appear in the ^{1}H NMR data of compound **A1**, 7.40 (J = 16.0 Hz) ppm and 7.16 (J = 15.6 Hz) ppm, which indicate the presence of the HC=CH group. The proton of CH$_2$ appears as a singlet at 5.70 ppm. Meanwhile, the 192.83 ppm peak of the ^{13}C NMR data indicates the presence of the C=O group, and the 170.32 and 167.66 ppm peaks indicate the presence of C proton in the 1,2,4-oxadiazol group. The 61.39 ppm peak indicates the presence of the C proton of the CH$_2$ group. Furthermore, compound **A1** was confirmed correctly with HRMS data of the [M+H]$^+$ as 451.05978, the calculated value was 451.06107.

Nematocidal Activity Test

The results of nematocidal activities of compounds are given in **Table 2**. As shown in **Table 2**, compounds **A13**, **A14**, and **B3** exhibited higher nematocidal activity against *B. xylophilus* at 50 µg/ml, the corrected mortalities were 100%, 100%, and 51.8%, respectively, which are superior to those of tioxazafen (34.3%), fosthiazate (43.9%), and abamectin (49.4%). Meanwhile, compounds **A13**, **A14**, **B6**, and **B12** showed good nematocidal activity against *A. besseyi* at 50 µg/ml, with corrected mortalities of 100%, 100%, 70.8%, and 59.6%, which are better than tioxazafen (40.0%) and abamectin (42.3%). In addition, compounds **A13**, **A14**, and **B11** possessed desired nematocidal activity against *D. dipsaci*, with corrected mortalities of 100%, 100%, and 41.0%, respectively, which are superior to tioxazafen (29.0%), fosthiazate (33.3%), and abamectin (33.6%). However, there was dissatisfactory nematocidal activity of all compounds against *B. xylophilus*, *A. besseyi*, and *D. dipsaci* at 10 µg/ml.

To further confirm their nematicidal activities of compounds **A13** and **A14**, the LC$_{50}$ values of compounds **A13** and **A14** against *B. xylophilus*, *A. besseyi*, and *D. dipsaci* were evaluated as tioxazafen, fosthiazate, and abamectin for positive controls; the results are given in **Table 3**. As shown in **Table 3**, compounds **A13** and **A14** had LC$_{50}$ values of 35.5, 44.7, and 30.2 µg/ml and 31.8, 47.4, and 36.5 µg/ml against *B. xylophilus*, *A. besseyi*, and *D. dipsaci*, respectively, which are superior to tioxazafen, fosthiazate, and abamectin. In addition, the results indicate that **A** series

compounds have better nematocidal activity than the **B** series compound. However, there is no obvious regularity between activity and structure.

Antiviral Activity Test

The antiviral activities of the target compounds were performed with the half leaf blight spot method and the results are given in **Tables 4** and **5**. As shown in **Table 4**, compounds **A4**, **A11**, **A16**, **A18**, and **A20** exhibited better curative activity against TMV at 500 µg/ml, with values of 49.8%, 53.6%, 57.2%, 52.3%, and 51.2%, respectively, which are superior than those of ribavirin (39.9%) and ningnanmycin (49.8%). These compounds also showed good protective activity to TMV, the inhibitory was 64.5%, 67.9%, 68.6%, 65.2%, and 67.1%, respectively, which are better than those of ribavirin (51.2%) and ningnanmycin (61.3%). Meanwhile, compounds **A4**, **A11**, **A16**, **A18**, and **B11** showed desirable curative action against PMMoV, the values were 52.3%, 53.6%, 56.5%, 55.6%, and 52.9%, which are better than those of ribavirin (31.6%) and ningnanmycin (51.8%). Furthermore, compounds **A4**, **A11**, **A16**, **A18**, **A20,** and **B11** showed excellent protective activity against PMMoV, with values of 67.1%, 65.6%, 71.8%, 70.2%, 68.1%, and 63.7%, respectively, which are superior to ribavirin (48.8%) and ningnanmycin (63.3%). Unfortunately, the curative effect of compounds to TSWV was dissatisfactory. However, compounds **A16** (69.5%) and **A18** (65.6%) showed better protective activity against TSWV than ribavirin (46.2%) and ningnanmycin (65.1%). The results of the EC$_{50}$ values (**Table 5**) indicate that compounds **A16** and **A18** showed excellent curative and protective activities against TMV and PMMoV, with EC$_{50}$ values of 368.7 and 210.4 µg/ml, 310.8 and 156.2 µg/ml, 410.5 and 251.2 µg/ml, and 345.6 and178.2 µg/ml, respectively, which are superior to ningnanmycin (420.5 and 242.6 µg/ml, and 415.8 and 218.4 µg/ml, respectively). In addition, compound **A16** (178.9 µg/ml) showed better protective activity against TSWV than ningnanmycin (180.5 µg/ml).

Structure-activity relationship analysis based on protective activity against three viruses indicates that **A** series compounds have better antiviral activity than **B** series compounds, which is consistent with the trend of nematicidal activity. Further structure-activity relationship analysis demonstrated that the compound with R$_1$ as OCH$_3$ showed better antiviral activity than that of the compounds with other groups, such as **A13** (R^1 = 4-OCH$_3$, R^2 = H) > **A21** (R^1 = 4-Br, R^2 = H), **A10** (R^1 = 4-CH$_3$, R^2 = H), **A5** (R^1 = H, R^2 = H), and **A1** (R^1 = 2,4-diCl, R^2 = H). In particular, the compound with 2-OCH$_3$ of R^1 had the best antiviral activity; for example, **A16** (R^1 = 2-OCH$_3$, R^2 = H) > **A13** (R^1 = 4-OCH$_3$, R^2 = H) > **A14** (R^1 = 3-OCH$_3$, R^2 = H). Compared with the electron-donating group (CH$_3$), the introduction of strong electron withdraw group (F) into R$_2$ can favor antiviral activity, such as **A18** (R^1 = 2-OCH$_3$, R^2 = 4-F) > **A17** (R^1 = 2-OCH$_3$, R^2 = 4-CH$_3$) and **A11** (R^1 = 4-OCH$_3$, R^2 = 4-F) > **A12**

TABLE 4 | Antiviral activities of compounds **A1**–**A21** and **B1**–**B13** at 500 µg/ml.[a]

Compd.	TMV		PMMoV		TSWV	
	Curative activity (%)	Protective activity (%)	Curative activity (%)	Protective activity (%)	Curative activity (%)	Protective activity (%)
A1	45.6 ± 1.9	60.3 ± 2.5	39.5 ± 1.1	56.1 ± 1.8	27.8 ± 3.0	46.5 ± 2.2
A2	38.9 ± 2.9	49.8 ± 1.1	45.3 ± 2.5	57.2 ± 1.4	35.7 ± 1.0	45.6 ± 2.3
A3	36.1 ± 2.3	47.2 ± 2.6	40.6 ± 1.7	49.3 ± 1.8	32.9 ± 2.7	48.0 ± 1.9
A4	49.8 ± 1.1	64.5 ± 3.4	52.3 ± 2.5	67.1 ± 2.3	46.7 ± 1.9	63.1 ± 2.8
A5	23.6 ± 2.6	54.2 ± 1.9	39.8 ± 1.9	60.2 ± 2.2	31.2 ± 1.3	54.8 ± 2.9
A6	37.8 ± 2.1	54.1 ± 2.9	43.8 ± 3.1	59.2 ± 3.1	33.3 ± 1.7	51.2 ± 2.5
A7	30.6 ± 1.8	49.5 ± 2.5	36.3 ± 1.2	50.6 ± 1.9	29.8 ± 1.1	55.6 ± 1.9
A8	31.8 ± 2.6	51.6 ± 1.8	35.6 ± 1.2	48.9 ± 1.3	30.3 ± 2.9	45.9 ± 1.7
A9	40.8 ± 2.3	59.2 ± 1.9	45.2 ± 1.8	61.4 ± 2.5	37.9 ± 1.1	54.8 ± 1.9
A10	38.9 ± 1.2	54.9 ± 3.1	43.3 ± 2.4	57.2 ± 1.9	35.6 ± 2.0	51.7 ± 2.2
A11	53.6 ± 2.6	67.9 ± 1.8	53.6 ± 3.1	65.6 ± 2.5	47.2 ± 2.7	63.8 ± 1.9
A12	34.8 ± 2.8	49.7 ± 1.1	30.9 ± 2.1	56.5 ± 1.8	33.1 ± 1.4	43.9 ± 1.3
A13	38.9 ± 1.5	62.1 ± 2.5	40.8 ± 1.6	57.6 ± 2.3	36.5 ± 2.4	56.5 ± 2.1
A14	33.8 ± 1.8	43.7 ± 1.7	31.3 ± 2.8	46.5 ± 0.9	33.7 ± 2.0	40.0 ± 0.8
A15	43.3 ± 2.1	51.9 ± 2.8	40.1 ± 2.2	63.1 ± 3.3	33.0 ± 1.1	43.6 ± 1.9
A16	57.2 ± 2.4	68.2 ± 1.6	56.5 ± 1.9	71.8 ± 2.9	48.3 ± 1.6	69.5 ± 2.8
A17	39.3 ± 1.9	61.2 ± 2.2	41.2 ± 2.1	60.5 ± 3.1	33.9 ± 2.7	54.2 ± 1.9
A18	52.3 ± 2.6	65.2 ± 1.9	55.6 ± 1.2	70.2 ± 2.9	47.9 ± 1.1	65.6 ± 2.5
A19	36.8 ± 1.7	53.1 ± 2.4	31.9 ± 1.0	51.8 ± 1.7	29.0 ± 1.5	43.7 ± 1.9
A20	51.3 ± 2.7	67.1 ± 2.3	51.1 ± 2.4	68.1 ± 2.6	48.7 ± 1.9	62.8 ± 1.3
A21	47.3 ± 2.2	60.0 ± 1.9	50.3 ± 3.0	61.7 ± 1.3	45.3 ± 2.8	55.2 ± 2.6
B1	31.5 ± 1.8	45.3 ± 2.1	28.6 ± 1.3	46.2 ± 2.5	27.3 ± 1.9	37.5 ± 2.1
B2	30.4 ± 2.5	48.9 ± 2.3	29.3 ± 1.8	43.5 ± 0.9	31.1 ± 1.5	41.8 ± 1.2
B3	32.8 ± 1.9	46.7 ± 1.3	35.6 ± 3.2	45.1 ± 1.7	33.9 ± 2.4	44.6 ± 1.8
B4	36.7 ± 2.3	52.1 ± 2.6	38.5 ± 1.9	58.4 ± 2.2	32.8 ± 1.4	46.9 ± 3.1
B5	40.8 ± 1.7	43.4 ± 3.9	36.3 ± 2.1	50.6 ± 3.3	33.0 ± 1.6	42.6 ± 1.8
B6	26.4 ± 1.9	41.9 ± 2.3	28.1 ± 1.7	43.5 ± 2.2	23.9 ± 2.8	43.0 ± 2.1
B7	42.9 ± 1.2	43.1 ± 1.2	41.2 ± 0.9	50.1 ± 1.8	36.6 ± 1.2	52.9 ± 2.4
B8	29.5 ± 2.6	46.7 ± 2.7	38.1 ± 1.4	43.6 ± 3.1	28.9 ± 2.1	39.6 ± 1.1
B9	42.4 ± 1.9	54.1 ± 3.1	45.1 ± 1.5	58.8 ± 2.8	38.0 ± 1.8	52.1 ± 3.4
B10	40.6 ± 2.5	51.4 ± 3.2	38.5 ± 2.2	41.8 ± 1.1	30.3 ± 1.7	43.9 ± 1.6
B11	43.6 ± 1.0	58.9 ± 1.9	52.9 ± 3.7	63.7 ± 1.9	42.8 ± 2.0	60.5 ± 1.3
B12	29.8 ± 1.4	46.8 ± 2.5	35.2 ± 1.2	49.1 ± 2.0	32.8 ± 1.7	41.9 ± 2.2
B13	40.1 ± 2.6	51.9 ± 1.1	30.5 ± 1.6	55.4 ± 2.1	36.1 ± 2.8	48.1 ± 2.9
Ribavirin[b]	39.9 ± 2.3	51.2 ± 1.2	35.6 ± 1.6	48.8 ± 1.9	37.8 ± 1.0	46.2 ± 2.1
Ningnanmycin[b]	49.8 ± 1.8	62.3 ± 2.5	51.8 ± 3.1	63.3 ± 1.7	49.1 ± 2.8	65.2 ± 1.7

[a]Average of three replicates.
[b]The commercial antiviral agents ribavirin and ningnanmycin were used for comparison of activity.

TABLE 5 | The EC_{50} values of the compounds against TMV, PMMoV, and TSWV[a].

Compd.	TMV		PMMoV		TSWV	
	Curative activity	Protective activity	Curative activity	Protective activity	Curative activity	Protective activity
A4	501.4 ± 6.3	289.5 ± 4.8	482.7 ± 7.9	196.5 ± 5.8	601.4 ± 9.5	312.1 ± 8.4
A11	489.5 ± 9.0	225.8 ± 9.1	491.3 ± 5.8	219.6 ± 4.9	585.3 ± 7.4	354.2 ± 9.0
A16	368.7 ± 3.3	210.4 ± 8.8	310.8 ± 9.1	156.2 ± 8.1	576.9 ± 3.7	178.9 ± 3.1
A18	410.5 ± 5.9	251.2 ± 7.1	345.6 ± 3.4	178.2 ± 3.6	610.4 ± 3.8	215.2 ± 6.2
A20	490.2 ± 8.5	301.5 ± 6.2	411.9 ± 5.7	270.3 ± 4.7	595.2 ± 5.2	380.5 ± 9.1
B11	560.2 ± 4.9	318.9 ± 6.6	426.3 ± 9.1	280.5 ± 3.6	610.4 ± 5.8	368.1 ± 4.6
Ribavirin[b]	690.5 ± 7.5	505.1 ± 4.6	780.5 ± 8.6	568.6 ± 5.6	810.7 ± 9.2	650.2 ± 4.5
Ningnanmycin[b]	420.5 ± 6.5	242.6 ± 7.7	415.8 ± 4.9	218.4 ± 6.3	408.8 ± 8.1	180.5 ± 3.9

[a]Average of three replicates.
[b]The commercial antiviral agents ribavirin and ningnanmycin were used for comparison of activity.

(R^1 = 4-OCH$_3$, R^2 = 4-CH$_3$), **A4** (R^1 = 2,4-diCl, R^2 = 4-F) > **A2** (R^1 = 2,4-diCl, R^2 = 4-CH$_3$).

CONCLUSION

In the present work, 34 novel chalcone derivatives containing an 1,2,4-oxadiazole moiety were synthesized and assessed for the nematocidal and antiviral activities of all of the compounds. The results show that compounds **A13** and **A14** have excellent nematocidal activities against *B. xylophilus*, *A. besseyi*, and *D. dipsaci* and are superior to tioxazafen, fosthiazate, and abamectin. Furthermore, compound **A16** has better protective activity against TMV, PMMoV, and TSWV than that of ribavirin and ningnanmycin. Therefore, chalcone derivatives containing an 1,2,4-oxadiazole moiety can be considered as candidate leading structures for the development of new pesticides.

DATA AVAILABILITY STATEMENT

The datasets presented in this study can be found in online repositories. The names of the repository/repositories and accession number(s) can be found in the article/ **Supplementary Material**.

AUTHOR CONTRIBUTIONS

LL and DL contributed to the synthesis, characterization, and activity research of all compounds. LL prepared the original manuscript. LL and SL analyzed the data. XG designed and supervised the research and revised the manuscript. All authors discussed, edited, and approved the final version.

FUNDING

SUPPLEMENTARY MATERIAL

The Supplementary Material for this article can be found online at: https://www.frontiersin.org/articles/10.3389/fchem.2022.943062/ full#supplementary-material

REFERENCES

Abad, P., Gouzy, J., Aury, J.-M., Castagnone-Sereno, P., Danchin, E. G. J., and Deleury, E. (2008). Genome Sequence of the Metazoan Plant-Parasitic Nematode *Meloidogyne incognita*. *Nat. Biotechnol.* 26, 909–915. doi:10.1038/nbt.1482

Abd-Elgawad, M. M. M. (2020). Biological Control Agents in the Integrated Nematode Management of Pepper in Egypt. *Egypt. J. Biol. Pest Co.* 30, 1–10. doi:10.1186/s41938-020-00273-6

Attar, S., O'Brien, Z., Alhaddad, H., Golden, M. L., and Calderón-Urrea, A. (2011). Ferrocenyl Chalcones versus Organic Chalcones: A Comparative Study of Their Nematocidal Activity. *Bioorg. Med. Chem.* 19, 2055–2073. doi:10.1016/j.bmc.2011.01.048

Bernard, G. C., Egnin, M., and Bonsi, C. (2017). The Impact of Plant-Parasitic Nematodes on Agriculture and Methods of Control. *Nematology* 7, 122–151. doi:10.5772/intechopen.68958

Caboni, P., Aissani, N., Demurtas, M., Ntalli, N., and Onnis, V. (2016). Nematicidal Activity of Acetophenones and Chalcones against *Meloidogyne incognita* and Structure–Activity Considerations. *Pest Manag. Sci.* 72, 125–130. doi:10.1002/ps.3978

Chen, J. X., Li, Q. X., and Song, B. A. (2020). Chemical Nematicides: Recent Research Progress and Outlook. *J. Agric. Food Chem.* 68, 12175–12188. doi:10.1021/acs.jafc.0c02871

Chen, M. H., Li, P., Hu, D. Y., Zeng, S., Li, T. X., Jin, L., et al. (2016). Synthesis, Antiviral Activity, 3D-QSAR, and Interaction Mechanisms Study of Novel Malonate Derivatives Containing Quinazolin-4(3*h*)-One Moiety. *Bioorg. Med. Chem. Lett.* 26, 168–173. doi:10.1021/jf301337610.1016/j.bmcl.2015.11.006

Du, G., Han, J. M., Kong, W. S., Zhao, W., Yang, H. Y., Yang, G. Y., et al. (2013). Chalcones from the Flowers of Rosa Rugosa and Their Anti-tobacco Mosaic Virus Activities. *Kor. Chem. Soc.* 34, 1263–1265. doi:10.5012/bkcs.2013.34.4.1263

Fernandes, F. S., Santos, H., Lima, S. R., Conti, C., Rodrigues, M. T., Zeoly, L. A., et al. (2020). Discovery of Highly Potent and Selective Antiparasitic New Oxadiazole and Hydroxy-Oxindole Small Molecule Hybrids. *Eur. J. Med. Chem.* 201, 112418. doi:10.1016/j.ejmech.2020.112418

Gan, X. H., Hu, D. Y., Chen, Z., Wang, Y. J., and Song, B. A. (2017a). Synthesis and Antiviral Evaluation of Novel 1,3,4-Oxadiazole/Thiadiazole-Chalcone Conjugates. *Bioorg. Med. Chem.* 27, 4298–4301. doi:10.1016/j.bmcl.2017.08.038

Gan, X. H., Hu, D. Y., Wang, Y. J., Yu, L., and Song, B. (2017b). A. Novel Trans-ferulic Acid Derivatives Containing a Chalcone Moiety as Potential Activator for Plant Resistance Induction. *J. Agric. Food Chem.* 65, 4367–4377. doi:10.1021/acs.jafc.7b00958

Gan, X. H., Wang, Y. J., Hu, D. Y., and Song, B, A. (2017c). Design, Synthesis, and Antiviral Activity of Novel Chalcone Derivatives Containing a Purine Moiety. *Chin. J. Chem.* 35, 665–672. doi:10.1002/cjoc.201600568

Gooding, G. V. J., and Hebert, T. T. (1967). A Simple Technique for Purification of Tobacco Mosaic Virus in Large Quantities. *Phytopathology* 57, 1285–1287. doi:10.1098/rstl.1767.0047

Hang, T. H., Chen, H., Chen, J., and Zhang, A. D. (2014). Syntheses, Crystal Structures, and Biological Activities of Two 5-Pyrimidinyl-1,2,4-Oxadiazoles. *Chin. J. Struc. Chem.* 10, 1455–1459. doi:10.14102/j.cnki.0254-5861.2014.10.029

Kantor, M., Handoo, Z., Kantor, C., and Carta, L. (2022). Top Ten Most Important U.S.-Regulated and Emerging Plant-Parasitic Nematodes. *Horticulturae* 8, 208. doi:10.3390/horticulturae8030208

Karad, S. C., Purohit, V. B., Thummar, R. P., Vaghasiya, B. K., Kamani, R. D., Thakor, P., et al. (2017). Synthesis and Biological Screening of Novel 2-Morpholinoquinoline Nucleus Clubbed with 1,2,4-Oxadiazole Motifs. *Eur. J. Med. Chem.* 126, 894–909. doi:10.1016/j.ejmech.2016.12.016

Kim, S. H., Lee, E., Baek, K. H., Kwon, H. B., Woo, H., Lee, E. S., et al. (2013). Chalcones, Inhibitors for Topoisomerase I and Cathepsin B and L, as Potential Anti-cancer Agents. *Bioorg. Med. Chem. Lett.* 23, 3320–3324. doi:10.1016/j.bmcl.2013.03.106

Lahtchev, K. V., Batovska, D. I., Parushev, S. P., Ubiyvovk, V. M., and Sibirny, A. A. (2008). Antifungal Activity of Chalcones: A Mechanistic Study Using Various Yeast Strains. *Eur. J. Med. Chem.* 43, 2220–2228. doi:10.1016/j.ejmech.2007.12.027

Leonard, G. C., and Stephen, O. D. (2007). Natural Products that Have Been Used Commercially as Crop Protection Agents. *Pest Manag. Sci.* 63, 524–554. doi:10.1002/ps.1378

Liu, D., Luo, L., Wang, Z. X., Ma, X. Y., and Gan, X. H. (2022). Design, Synthesis and Antifungal/Nematicidal Activity of Novel 1,2,4-Oxadiazole Derivatives Containing Amide Fragments. *Int. J. Mol. Sci.* 23, 1596. doi:10.3390/ijms23031596

Ntalli, N. G., and Caboni, P. (2012). Botanical Nematicides: A Review. *J. Agric. Food Chem.* 60, 9929–9940. doi:10.1021/jf303107j

Nunes, A. S., Campos, V. P., Mascarello, A., Stumpf, T. R., Chiaradia-Delatorre, L. D., Machado, M. A. T., et al. (2013). Activity of Chalcones Derived from 2,4,5-Trimethoxybenzaldehyde against *Meloidogyne Exigua* and *In Silico* Interaction of One Chalcone with a Putative Caffeic Acid 3-*O*-Methyltransferase from *Meloidogyne Incognita*. *Exp. Parasitol.* 135, 661–668. doi:10.1016/j.exppara.2013.10.003

Park, J. Y., Jeong, H. J., Kim, Y. M., Park, S. J., Rho, M. C., Park, K. H., et al. (2011). Characteristic of Alkylated Chalcones from *Angelica Keiskei* on Influenza Virus Neuraminidase Inhibition. *Bioorg. Med. Chem. Lett.* 21, 5602–5604. doi:10.1016/j.bmcl.2011.06.130

Qian, X. H., Lee, P. W., and Cao, S. (2010). China: Forward to the Green Pesticides via a Basic Research Program. *J. Agric. Food Chem.* 58, 2613–2623. doi:10.1021/jf904098w

Shi, J., He, H. F., Hu, D. Y., and Song, B. A. (2022). Defense Mechanism of *Capsicum Annuum* L. Infected with Pepper Mild Mottle Virus Induced by Vanisulfane. *J. Agric. Food. Chem.* 70, 3618–3632. doi:10.1021/acs.jafc.2c00659

Slomczynska, U., South, M. S., Bunkers, G. J., Edgecomb, D., Wyse-Pester, D., Selness, S., et al. (2015). Tioxazafen: A New Broad-Spectrum Seed Treatment Nematicide. *J. Am. Chem. Soc.* 10, 129–147. doi:10.1021/bk-2015-1204.ch010

Song, B. A., Zhang, H. P., Wang, H., Yang, S., Jin, L. H., Hu, D. Y., et al. (2005). Synthesis and Antiviral Activity of Novel Chiral Cyanoacrylate Derivatives. *J. Agric. Food. Chem.* 53, 7886–7891. doi:10.1021/jf051050w

Thirunarayanan, G., Surya, S., Srinivasan, S., Vanangamudi, G., and Sathiyendiran, V. (2010). Synthesis and Insect Antifeedant Activities of Some Substituted Styryl 3, 4-Dichlorophenyl Ketones. *Spectrochim. Acta A.* 75, 152–156. doi:10.1016/j.saa.2009.10.003

Wang, H. M., Zhang, L., Liu, J., Yang, Z. L., Zhao, H. Y., Yang, Y., et al. (2015). Synthesis and Anti-cancer Activity Evaluation of Novel Prenylated and Geranylated Chalcone Natural Products and Their Analogs. *Eur. J. Med. Chem.* 92, 439–448. doi:10.1016/j.ejmech.2015.01.007

Wang, Z. W., Wang, L., Ma, S., Liu, Y. X., Wang, L. Z., and Wang, Q. M. (2012). Design, Synthesis, Antiviral Activity, and SARs of 1,4-Aminophenanthroindolizidines. *J. Agric. Food Chem.* 60, 5825–5831. doi:10.1021/jf3013376

Wei, C. Q., Huang, J. J., Luo, Y. Q., Wang, S. B., Wu, S. K., Xing, Z. F., et al. (2021). Novel Amide Derivatives Containing an Imidazo [1,2-*α*] Pyridine Moiety: Design, Synthesis as Potential Nematicidal and Antibacterial Agents. *Pestic. Biochem. Physiol.* 175, 104857. doi:10.1016/j.pestbp.2021.104857

Wei, Z. Y., Chi, K. Q., Yu, Z. K., Liu, H. Y., Sun, L. P., Zheng, C. J., et al. (2016). Synthesis and Biological Evaluation of Chalcone Derivatives Containing Aminoguanidine or Acylhydrazone Moieties. *Bioorg. Med. Chem. Lett.* 26, 5920–5925. doi:10.1016/j.bmcl.2016.11.001

Yang, S., Ren, C. L., Ma, T. Y., Zou, W. Q., Dai, L., Tian, X. Y., et al. (2021). 1,2,4-Oxadiazole-Based Bio-Isosteres of Benzamides: Synthesis, Biological Activity and Toxicity to *Zebrafish Embryo*. *Int. J. Mol. Sci.* 22, 2367. doi:10.3390/ijms22052367

Zan, N. N., Li, J., He, H. F., Hu, D. Y., and Song, B. A. (2021). Discovery of Novel Chromone Derivatives as Potential Anti-TSWV Agents. *J. Agric. Food. Chem.* 69, 10819–10829. doi:10.1021/acs.jafc.1c03626

Zhu, L. Z., Zeng, H. N., Liu, D., Fu, Y., Wu, Q., Song, B. A., et al. (2020). Design, Synthesis, and Biological Activity of Novel 1,2,4-Oxadiazole Derivatives. *BMC Chem.* 14, 68. doi:10.1186/s13065-020-00722-1

Design, synthesis, and insecticidal activity evaluation of piperine derivatives

Chiying Zhang[1†], Qingqiang Tian[1†] and Yahui Li[1,2]*

[1]Key Laboratory of Agri-Food Safety of Anhui Province, School of Resources and Environment, Anhui Agricultural University, Hefei, China, [2]State Key Laboratory Breeding Base of Green Pesticide and Agricultural Bioengineering, Key Laboratory of Green Pesticide and Agricultural Bio-engineering, Ministry of Education, Guizhou University, Guiyang, China

Structural optimization of natural products has become one of the most effective ways to develop novel pesticides. In this study, 30 novel pesticide derivatives containing a linear bisamide were synthesized. Then, their insecticidal activities against *P. xylostella* were evaluated. Results indicate that different bisamide substitutes show different larvicidal structure−activity relationships. At the same time, 2-trifluoroethyl is the most efficient substituent. The bioactivity results showed that most of the desired compounds exhibited better insecticidal activity against *P. xylostella* than piperine. Among them, **compound D28** resulted in 90% mortality at 1 mg/ml concentration. This study provides a novel protocol for the discovery of new insecticides. The molecular docking results indicated that compound D28 could act on *γ*-aminobutyric acid receptors.

KEYWORDS

piperine derivatives, insecticidal activity, linear bisamide, *Plutella xylostella*, Lepidoptera

1 Introduction

Plutella xylostella, also known as "dangling silkworm" or "diamondback moth," is a pest commonly found on vegetables, causing damage by larvae feeding on the leaves of cruciferous vegetables. In recent years, the damage of *Plutella xylostella* has become increasingly serious, with significant adverse effects on the yield and quality of cruciferous vegetables (Wang et al., 2011; Zhao et al., 2022). The primary commercial agents used to control *Plutella xylostella* are traditional insecticides such as emamectin. However, long-term use of these insecticides results in moderate to high resistance (Lima Neto et al., 2021; Shen et al., 2017). Consequently, developing novel insecticides is an important endeavor (He et al., 2016; Liu et al., 2020; Xia et al., 2022). During the past few decades, natural product structural optimization has been a promising way to develop high-efficiency pesticides (Swain, 1977; Sun et al., 2013). In agricultural pest prevention, natural products have unique advantages (Tang et al., 2012; Roman, 2016; Liu et al., 2018), such as 1) it is relatively safe for higher mammals and natural enemies of pests; 2) it is environmentally friendly (Tong et al., 2018); 3) it has a new insecticidal mode of action (Gaur and Bao, 2021); and 4) it reduces pesticide resistance (Chen et al.,

FIGURE 1
Overall design idea of this work.
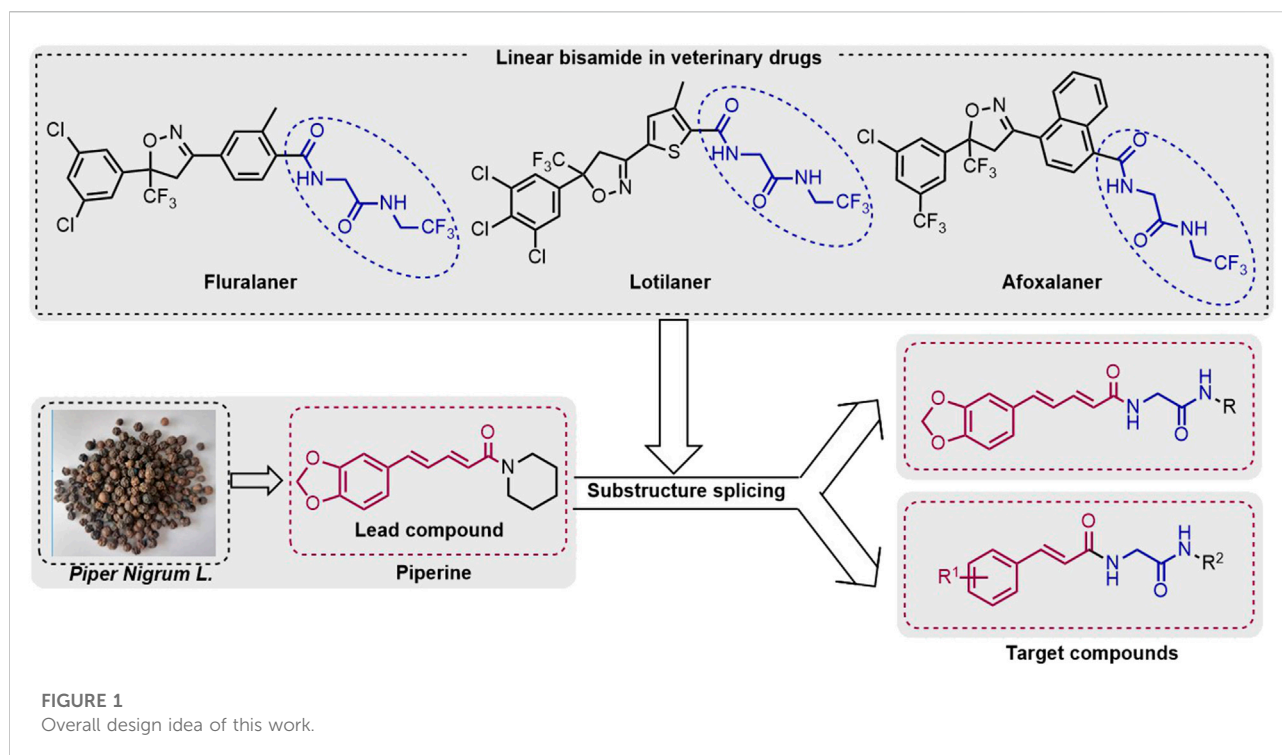
2017). For example, Neemaceae showed broad-spectrum insecticidal activity against many plant pests. Euonymus has been successfully commercialized to control rice pests, stored grain pests, and tree pests (Wu et al., 2001; Tang et al., 2004).

Piperine, as a cinnamon amide alkaloid (Parmar et al., 1997), shows a broad range of bioactivities such as antiobesity (Sunila and Kuttan, 2004), antiparasitic (Ribeiro et al., 2004.; Franklim et al., 2013), and lipid-lowering effects (Kimura et al., 2006; Park et al., 2012). In addition, piperine and its derivatives exhibit effective insecticidal properties against various agricultural pests. For example, Barbosa et al. reported a series of piperine derivatives by modifying the piperidine ring of piperine, which showed effective insecticidal activity against *Ascia monuste orseis* (Paula et al., 2000). Ribero et al. (2004) designed a series of piperine derivatives with effective insecticidal activity against *Trypanosoma cruzi*. Xu and Yang, (2017) found that piperine derivatives show stomach toxicity activity against agricultural pests with effects comparable to the commercial botanical pesticide toosendanin (CN107892685A). Han et al. (2021) designed a series of compounds that combined the benzo [*d*][1,3]dioxole moiety of piperine, which showed effective insecticidal activity against *Ostrinia furnacalis*.

Bisamide compounds show effective biological activities for agricultural pest control. However, the use of linear bisamides in the development of insecticides is still in its infancy. In contrast, linear bisamides are significant structural motifs in some veterinary drugs (for example, fluralaner, lotilaner, and

afoxolaner) (Figure 1). Due to the novel action mechanism and viable activity of linear bisamides and the piperine skeleton, this study designed and synthesized a variety of piperine bisamide derivatives. The target compounds' insecticidal activities against *P. xylostella* were systematically investigated.

2 Materials and methods

2.1 Chemical part

2.1.1 General information

Most of the chemicals were purchased from Aladdin, energy-chemical, TCI, or Alfa Aesar. NMR spectra were recorded on Bruker Avance 600 spectrometers. Chemical shifts (ppm) were given relative to the solvent. Melting points of the target molecules were determined using a Shanghai Yice WRX-4 melting point meter. High-resolution mass spectrometry data were determined on a Thermo Scientific (UHPLC-Q-Orbitrap).

2.1.2 Preparation of compound A

A solution of 20% KOH–EtOH (44 ml) was added to 5.7 g (20.0 mmol) of piperine at room temperature. The mixture was stirred at 80 C for 20 h. Then, 10% hydrochloric acid was added to adjust the pH of the mixture to 3. The mixture was filtered

under reduced pressure, washed with water, and recrystallized in ethanol to obtain intermediate A in 81% yield (3.5 g).

(2E,4E)-5-(Benzo[d][1,3]dioxol-5-yl)penta-2,4-dienoic (A): brown solid, 3.5g, yield 81%, mp: 163.4–166.5°C, ^{1}H NMR (600 MHz, DMSO-d_6) δ = 7.32–7.23 (m, 1H, Ar-H), 7.19 (s, 1H, Ar-H), 7.03–6.83 (m, 4H, -CH = CH-), 6.01 (s, 2H, -CH$_2$), 5.90 (d, J = 15.1 Hz, 1H, Ar-H). ^{13}C NMR (151 MHz, DMSO-d_6) δ = 168.02, 148.52, 148.40, 144.97, 140.15, 130.96, 125.27, 123.42, 121.58, 108.91, 106.20, 101.77. HRMS (ESI) calcd for $C_{12}H_{11}O_4$ [M + H]$^+$: 219.06519, found 219.06514.

2.1.3 General procedure for preparing compound C

A mixture of intermediate **A** (10.0 mmol, 2.18 g), glycine methyl ester hydrochloride (9.0 mmol, 1.13 g), HOBt (10.0 mmol, 1.35 g), DIEPA (10.0 mmol, 1.29 g), and 20 ml of DCM was stirred at 0°C for 15 min. Then, EDCI (10 mmol, 1.92 g) was added. The reaction was stirred at 25°C for 18 h. After the reaction was completed, the solvent was removed under reduced pressure, and the crude product was purified by column chromatography to obtain intermediate **B**. Then, a mixture of intermediate **B** (10.0 mmol, 2.88 g) and KOH (20.0 mmol, 1.12 g) was added in 30 ml of H$_2$O/CH$_3$OH/THF(v:v:v = 1:1:1) and stirred at room temperature for 12 h. Then, 10% of HCl solution was added until the solid no longer formed, and the crude product was purified by column chromatography to obtain intermediate **C**.

((2E,4E)-5-(Benzo[d][1,3]dioxol-5-yl)penta-2,4-dienoyl) glycine (C): brown solid, 2.56 g, yield 93%, mp: 214.5–216.7°C, ^{1}H NMR (600 MHz, DMSO-d_6) δ = 8.35 (s, 1H, -NH), 7.26–7.09 (m, 2H, Ar-H), 6.96 (d, J = 7.8 Hz, 1H, Ar-H), 6.92–6.65 (m, 3H, -CH = CH-), 6.13 (d, J = 15.0 Hz, 1H, -CH = CH-), 5.99 (s, 2H, -CH$_2$), 3.82 (d, J = 5.5 Hz, 2H, -CH$_2$). ^{13}C NMR (151 MHz, DMSO-d_6) δ = 171.72, 166.21, 148.33, 148.19, 140.49, 138.70, 131.18, 125.53, 124.22, 123.06, 108.88, 106.13, 101.67, 41.21. HRMS (ESI) calcd for $C_{14}H_{14}O_5N$ [M + H]$^+$: 276.08665, found 276.08572.

2.1.4 Preparation of target compounds D1–D28

A mixture of intermediate **C** (1.0 mmol, 275 mg), amine (1.2 mmol), HOBt (1.2 mol, 162.14 mg), DIEPA (1.2 mol, 155.1 mg), and 10 ml of DCM was stirred at 0°C for 15 min. Then, EDCI (1.2 mol, 230.0 mg) was added, and the reaction mixture was stirred at 25°C for 18 h. After the reaction was completed, the solvent was removed under reduced pressure to give the crude product, and the target compounds were obtained *via* recrystallization using ethyl acetate and petroleum ether as the solvent.

(2E,4E)-5-(Benzo[d][1,3]dioxol-5-yl)-N-(2-oxo-2-(Phenylamino)ethyl)penta-2,4-dienamide (D1): brown solid, 81.2 mg, yield 23.2%, mp: >250.0°C, ^{1}H NMR (600 MHz, DMSO-d_6) δ = 9.99 (s, 1H, NH), 8.39 (t, J = 5.8 Hz, 1H, -NH), 7.57 (d, J = 7.8 Hz, 2H, Ar-H), 7.28 (t, J = 7.9 Hz, 2H,

Ar-H), 7.24 (d, J = 1.1 Hz, 1H, Ar-H), 7.19–7.15 (m, 1H, Ar-H), 7.02 (t, J = 7.4 Hz, 1H, Ar-H), 6.98–6.83 (m, 4H, Ar-H and -CH = CH-), 6.19 (d, J = 15.0 Hz, 1H, -CH = CH-), 6.02 (s, 2H, -CH$_2$), 3.96 (d, J = 5.9 Hz, 2H, -CH$_2$). ^{13}C NMR (151 MHz, DMSO-d_6) δ = 168.24, 166.12, 148.37, 148.19, 140.24, 139.33, 138.57, 131.28, 129.14, 125.66, 124.56, 123.66, 123.06, 119.61, 108.86, 106.15, 101.68, 43.33. HRMS (ESI) calcd for $C_{20}H_{19}O_4N_2$ [M + H]$^+$: 351.13393, found 351.13257.

(2E,4E)-5-(Benzo[d][1,3]dioxol-5-yl)-N-(2-oxo-2-(o-tolylamino) ethyl)penta-2,4-dienamide (D2): red solid, 88.0 mg, yield 24.1%, mp: >250.0°C, ^{1}H NMR (600 MHz, DMSO-d_6) δ = 9.32 (s, 1H, -NH), 8.43 (s, 1H, -NH), 7.40 (d, J = 7.4 Hz, 1H, Ar-H), 7.25–7.11 (m, 4H, Ar-H), 7.05 (d, J = 6.9 Hz, 1H, Ar-H), 6.98–6.84 (m, 4H, Ar-H and -CH = CH-), 6.19 (d, J = 15.0 Hz, 1H, -CH = CH-), 6.01 (s, 2H, -CH$_2$), 4.00 (d, J = 4.5 Hz, 2H, -CH$_2$), 2.17 (s, 3H, -CH$_3$). ^{13}C NMR (151 MHz, DMSO-d_6) δ = 168.32, 166.25, 148.37, 148.20, 140.32, 138.63, 136.51, 131.83, 131.26, 130.71, 126.39, 125.64, 125.53, 125.00, 124.50, 123.07, 108.86, 106.15, 101.68, 43.24, 18.13. HRMS (ESI) calcd for $C_{21}H_{21}O_4N_2$ [M + H]$^+$: 365.14958, found 365.14801.

(2E,4E)-5-(Benzo[d][1,3]dioxol-5-yl)-N-(2-oxo-2-(m-tolylamino) ethyl)penta-2,4-dienamide (D3): red solid, 148.1 mg, yield 40.6%, mp: 225.6–226.1°C, ^{1}H NMR (600 MHz, DMSO-d_6) δ = 9.90 (s, 1H, -NH), 8.37 (s, 1H, -NH), 7.42–7.32 (m, 2H, Ar-H), 7.24 (s, 1H, Ar-H), 7.18–7.14 (m, 2H, Ar-H), 6.97 (d, J = 7.9 Hz, 1H, Ar-H), 6.95–6.82 (m, 4H, Ar-H and -CH = CH-), 6.18 (d, J = 15.0 Hz, 1H, -CH = CH-), 6.01 (s, 2H, -CH$_2$), 3.94 (d, J = 5.1 Hz, 2H, -CH$_2$), 2.24 (s, 3H, -CH$_3$). ^{13}C NMR (151 MHz, DMSO-d_6) δ = 168.17, 166.13, 148.36, 148.19, 140.26, 139.23, 138.60, 138.32, 131.26, 128.99, 125.64, 124.53, 124.38, 123.09, 120.13, 116.80, 108.87, 106.12, 101.68, 43.32, 21.60. HRMS (ESI) calcd for $C_{21}H_{21}O_4N_2$ [M + H]$^+$: 365.14958, found 365.14841.

(2E,4E)-5-(Benzo[d][1,3]dioxol-5-yl)-N-(2-oxo-2-(p-tolylamino) ethyl)penta-2,4-dienamide (D4): red solid, 116 mg, yield 31.5%, mp: 178.8–180.7°C, ^{1}H NMR (600 MHz, DMSO-d_6) δ = 9.90 (s, 1H, -NH), 8.37 (t, J = 5.5 Hz, 1H, -NH), 7.44 (d, J = 8.2 Hz, 2H, Ar-H), 7.24 (s, 1H, Ar-H), 7.16 (m, 1H, Ar-H), 7.08 (d, J = 8.1 Hz, 2H, Ar-H), 6.99–6.81 (m, 4H, Ar-H and -CH = CH-), 6.18 (d, J = 15.0 Hz, 1H, -CH = CH-), 6.02 (s, 2H, -CH$_2$), 3.94 (d, J = 5.7 Hz, 2H, -CH$_2$), 2.22 (s, 3H, -CH$_3$). ^{13}C NMR (151 MHz, DMSO-d_6) δ = 167.98, 166.09, 148.37, 148.19, 140.21, 138.55, 136.81, 132.58, 131.28, 129.51, 125.66, 124.59, 123.06, 119.64, 108.86, 106.15, 101.68, 43.28, 20.84. HRMS (ESI) calcd for $C_{21}H_{21}O_4N_2$ [M + H]$^+$: 365.14958, found 365.14871.

(2E,4E)-5-(Benzo[d][1,3]dioxol-5-yl)-N-(2-((4-(tert-butyl) phenyl)amino)-2-oxoethyl)penta-2,4-dienamide (D5): red solid, 198.3 mg, yield 48.7%, mp: 124.4–125.1°C, ^{1}H NMR (600 MHz, DMSO-d_6) δ = 9.92 (s, 1H, NH), 8.38 (t, J = 5.3 Hz, 1H, -NH), 7.47 (d, J = 8.3 Hz, 2H, Ar-H), 7.29 (d, J = 8.4 Hz, 2H, Ar-H), 7.23 (s, 1H, Ar-H), 7.17 (m, 1H, Ar-H), 7.00–6.84 (m, 4H, Ar-H and -CH = CH-), 6.19 (d, J = 15.0 Hz, 1H, -CH = CH-), 6.01 (s, 2H, -CH = CH-), 3.95 (d, J = 5.6 Hz, 2H, -CH$_2$), 1.22 (s, 9H, -CH$_3$). ^{13}C NMR (151 MHz, DMSO-d_6) δ = 168.01, 166.13, 148.36, 148.19, 146.06, 140.24, 138.57, 136.71, 131.27, 125.72, 124.57, 123.05, 119.45, 114.17, 108.86, 106.15,

101.67, 43.24, 34.41, 31.62. HRMS (ESI) calcd for $C_{24}H_{27}O_4N_2$ [M + H]$^+$: 407.19653, found 407.19501.

(2E,4E)-5-(Benzo[d][1,3]dioxol-5-yl)-N-(2-((3,5-dimethylphenyl)amino)-2-oxoethyl)penta-2,4-dienamide (**D6**): yellow solid, 73.4 mg, yield 19.4%, mp: >250.0°C ^{1}H NMR (600 MHz, DMSO-d_6) δ = 9.81 (s, 1H, -NH), 8.36 (t, J = 5.5 Hz, 1H, -NH), 7.24 (s, 1H, Ar-H), 7.21–7.12 (m, 3H, Ar-H), 6.98–6.83 (m, 4H, Ar-H and -CH = CH-), 6.66 (s, 1H, Ar-H), 6.18 (d, J = 15.0 Hz, 1H, -CH = CH-), 6.01 (s, 2H, -CH$_2$), 3.92 (d, J = 5.7 Hz, 2H, -CH$_2$), 2.20 (s, 6H, -CH$_3$).^{13}C NMR (151 MHz, DMSO-d_6) δ = 168.08, 166.13, 148.37, 148.19, 140.22, 139.15, 138.57, 138.09, 131.27, 125.65, 125.22, 124.56, 123.06, 117.43, 108.86, 106.14, 101.68, 43.37, 21.51. HRMS (ESI) calcd for $C_{22}H_{23}O_4N_2$ [M + H]$^+$: 379.16523, found 379.16409.

(2E,4E)-5-(Benzo[d][1,3]dioxol-5-yl)-N-(2-((3-ethynylphenyl)amino)-2-oxoethyl)penta-2,4-dienamide (**D7**): red solid, 59.8 mg, yield 15.9%, mp: 203.5–205.5°C, ^{1}H NMR (600 MHz, DMSO-d_6) δ = 10.10 (s, 1H, -NH), 8.40 (t, J = 5.5 Hz, 1H, -NH), 7.76 (s, 1H, Ar-H), 7.55 (d, J = 8.2 Hz, 1H, Ar-H), 7.30 (t, J = 7.9 Hz, 1H, Ar-H), 7.24 (s, 1H, Ar-H), 7.19–7.12 (m, 2H, Ar-H), 6.99–6.96 (m, 1H, Ar-H), 6.94–6.90 (m, 1H, -CH = CH-), 6.89–6.86 (m, 2H, -CH = CH-), 6.18 (d, J = 15.0 Hz, 1H, -CH = CH-), 6.02 (s, 2H, -CH$_2$), 4.13 (s, 1H, CH≡), 3.96 (d, J = 5.8 Hz, 2H, -CH$_2$). ^{13}C NMR (151 MHz, DMSO-d_6) δ = 168.58, 166.15, 148.37, 148.20, 140.28, 139.54, 138.61, 131.28, 129.63, 126.92, 125.65, 124.50, 123.08, 122.47, 122.44, 120.19, 108.86, 106.15, 101.68, 83.79, 80.90, 43.37. HRMS (ESI) calcd for $C_{22}H_{19}O_4N_2$ [M + H]$^+$: 375.13393, found 375.13269.

(2E,4E)-5-(Benzo[d][1,3]dioxol-5-yl)-N-(2-oxo-2-((3,4,5-trimethoxyphenyl)amino)ethyl) penta-2,4-dienamide (**D8**): red solid, 183.3 mg, yield 41.6%, mp: 189.3–192.9°C, ^{1}H NMR (600 MHz, DMSO-d_6) δ = 9.92 (s, 1H, -NH), 8.36 (t, J = 5.7 Hz, 1H, -NH), 7.24 (s, 1H, Ar-H), 7.18–7.14 (m, 1H, Ar-H), 6.99–6.94 (m, 3H, Ar-H), 6.93–6.84 (m, 3H, -CH = CH-), 6.18 (d, J = 15.0 Hz, 1H, -CH = CH-), 6.01 (s, 2H, -CH$_2$), 3.92 (d, J = 5.8 Hz, 2H, -CH$_2$), 3.70 (s, 6H, -CH$_3$), 3.59 (s, 3H, -CH$_3$). ^{13}C NMR (151 MHz, DMSO-d_6) δ = 168.08, 166.14, 153.15, 148.36, 148.19, 140.28, 138.61, 135.43, 131.25, 125.62, 124.50, 123.09, 108.87, 106.13, 101.68, 97.52, 60.54, 56.17, 43.32. HRMS (ESI) calcd for $C_{23}H_{25}O_7N_2$ [M + H]$^+$: 441.16563, found 441.16418.

(2E,4E)-5-(Benzo[d][1,3]dioxol-5-yl)-N-(2-((2-fluorophenyl)amino)-2-oxoethyl)penta-2,4-dien-amide (**D9**): white solid, 122.4 mg, yield 33%, mp: 185.5–188.9°C, ^{1}H NMR (600 MHz, DMSO-d_6) δ = 9.77 (s, 1H, -NH), 8.41 (t, J = 5.7 Hz, 1H, -NH), 7.85 (d, J = 6.6 Hz, 1H, Ar-H), 7.32–7.06 (m, 5H, Ar-H), 6.99–6.82 (m, 4H, Ar-H and -CH = CH-), 6.18 (d, J = 15.0 Hz, 1H, -CH = CH-), 6.02 (s, 2H, -CH$_2$), 4.03 (d, J = 5.8 Hz, 2H, -CH$_2$). ^{13}C NMR (151 MHz, DMSO-d_6) δ = 168.74, 166.19, 154.01 (d, $^1J_{C-F}$ = 246.1 Hz), 148.37, 148.21, 140.36, 138.64, 131.27, 126.36 (d, $^2J_{C-F}$ = 12.1 Hz), 125.64, 124.78, 124.76, 124.44, 123.08, 115.95, 115.82, 108.86, 106.15, 101.68, 43.16.^{19}F NMR (564 MHz, DMSO) δ = -124.94. HRMS (ESI) calcd for $C_{20}H_{18}O_4N_2F$ [M + H]$^+$: 369.12451, found 369.12305.

(2E,4E)-5-(Benzo[d][1,3]dioxol-5-yl)-N-(2-((3-fluorophenyl)amino)-2-oxoethyl)penta-2,4-dien-amide (**D10**): red solid, 67.1 mg, yield 18.2%, mp: 226.0–227.5°C, ^{1}H NMR (600 MHz, DMSO-d_6) δ = 10.22 (s, 1H, -NH), 8.41 (s, 1H, -NH), 7.56 (d, J = 11.6 Hz, 1H, Ar-H), 7.30 (dt, J = 17.2, 7.9 Hz, 2H, Ar-H), 7.24 (s, 1H, Ar-H), 7.18–7.14 (m, 1H, Ar-H), 6.97–6.83 (m, 5H, Ar-H and -CH = CH-), 6.18 (d, J = 15.0 Hz, 1H, -CH = CH-), 6.01 (s, 2H, -CH$_2$), 3.96 (d, J = 5.6 Hz, 2H, -CH$_2$). ^{13}C NMR (151 MHz, DMSO-d_6) δ = 168.66, 166.19, 162.57 (d, $^1J_{C-F}$ = 241.6 Hz), 148.37, 148.20, 141.04 (d, $^2J_{C-F}$ = 12.1 Hz), 140.34, 138.64, 131.26, 130.8 (d, $^3J_{C-F}$ = 9.1 Hz), 125.63, 124.43, 123.08, 115.31, 110.12 (d, $^2J_{C-F}$ = 21.2 Hz), 108.87, 106.37 (d, $^2J_{C-F}$ = 27.2 Hz), 106.15, 101.68, 43.36.^{19}F NMR (564 MHz, DMSO) δ = -112.05. HRMS (ESI) calcd for $C_{20}H_{18}O_4N_2F$ [M + H]$^+$: 369.12451, found 369.12344.

(2E,4E)-5-(Benzo[d][1,3]dioxol-5-yl)-N-(2-((4-fluorophenyl)amino)-2-oxoethyl)penta-2,4-dien- amide (**D11**): white solid, 120.0 mg, yield 32.6%. mp: 251.8–253.6°C ^{1}H NMR (600 MHz, DMSO-d_6) δ = 10.05 (s, 1H, -NH), 8.40 (t, J = 5.8 Hz, 1H, -NH), 7.59–7.57 (m, 2H, Ar-H), 7.24 (d, J = 1.2 Hz, 1H, Ar-H), 7.14 (dt, J = 17.7, 9.8 Hz, 3H, Ar-H), 6.98–6.84 (m, 4H, Ar-H and -CH = CH-), 6.18 (d, J = 15.0 Hz, 1H, -CH = CH-), 6.02 (s, 2H, -CH$_2$), 3.94 (d, J = 5.8 Hz, 2H, -CH$_2$). ^{13}C NMR (151 MHz, DMSO-d_6) δ = 168.19, 166.11, 159.43 (d, $^1J_{C-F}$ = 240.1 Hz), 148.28 (d, $^2J_{C-F}$ = 27.3 Hz), 140.25, 138.59, 135.71, 131.27, 125.65, 124.53, 123.07, 121.38, 115.70 (d, $^2J_{C-F}$ = 22.7 Hz), 109.99, 108.86, 106.14, 101.68, 43.25.^{19}F NMR (564 MHz, DMSO) δ = -119.48. HRMS (ESI) calcd for $C_{20}H_{18}O_4N_2F$ [M + H]$^+$: 369.12451, found 369.12338.

(2E,4E)-5-(Benzo[d][1,3]dioxol-5-yl)-N-(2-((3-chlorophenyl)amino)-2-oxoethyl)penta-2,4-dien-amide (**D12**): yellow solid, 82.5 mg, yield 21.5% mp: 223.8–225.7°C, ^{1}H NMR (600 MHz, DMSO-d_6) δ = 10.19 (s, 1H, -NH), 8.41 (t, J = 5.7 Hz, 1H, -NH), 7.77 (s, 1H, Ar-H), 7.43 (d, J = 8.2 Hz, 1H, Ar-H), 7.31 (t, J = 8.1 Hz, 1H, Ar-H), 7.24 (s, 1H, Ar-H), 7.18–7.14 (m, 1H, Ar-H), 7.08 (d, J = 8.0 Hz, 1H, Ar-H), 6.98–6.83 (m, 4H, Ar-H and -CH = CH-), 6.18 (d, J = 15.1 Hz, 1H, -CH = CH-), 6.02 (s, 2H, -CH$_2$), 3.95 (d, J = 5.8 Hz, 2H, -CH$_2$). ^{13}C NMR (151 MHz, CDCl$_3$) δ = 173.45, 170.92, 153.12, 152.95, 145.52, 145.07, 143.39, 138.25, 136.02, 135.62, 130.39, 129.19, 128.14, 127.84, 123.80, 122.72, 113.62, 110.90, 106.43, 48.12. HRMS (ESI) calcd for $C_{20}H_{18}O_4N_2Cl$ [M + H]$^+$: 385.09496, found 385.09415.

(2E,4E)-N-(2-((3-Acetylphenyl)amino)-2-oxoethyl)-5-(benzo[d][1,3]dioxol-5-yl)penta-2,4-dien-amide (**D13**): brown solid, 137 mg, yield 35.0%, mp: >250.0°C, ^{1}H NMR (600 MHz, DMSO-d_6) δ = 10.20 (s, 1H, -NH), 8.40 (s, 1H, -NH), 8.15 (s, 1H, Ar-H), 7.83 (d, J = 7.6 Hz, 1H, Ar-H), 7.64 (d, J = 7.4 Hz, 1H, Ar-H), 7.45 (t, J = 7.8 Hz, 1H, Ar-H), 7.24 (s, 1H, Ar-H), 6.97 (d, J = 7.4 Hz, 2H, Ar-H), 6.90–6.83 (m, 3H, Ar-H and -CH = CH-), 6.19 (d, J = 15.0 Hz, 1H, -CH = CH-), 6.02 (s, 2H, -CH$_2$), 3.98 (d, J = 5.3 Hz, 2H, -CH$_2$), 2.53 (s, 3H, -CH$_3$).^{13}C NMR (151 MHz, DMSO-d_6) δ = 198.01, 168.62, 166.16, 148.37, 148.20, 140.29, 139.70, 138.62, 137.82, 131.27, 129.60, 125.64, 124.50, 124.09, 123.72, 123.08, 118.84, 108.86, 106.15, 101.68, 43.37, 27.11.

HRMS (ESI) calcd for $C_{22}H_{21}O_5N_2$ [M + H]$^+$: 393.14450, found 393.14301.

(2E,4E)-5-(Benzo[d][1,3]dioxol-5-yl)-N-(2-((4-(methylthio)phenyl)amino)-2-oxoethyl)penta-2,4-dienamide (D14): brown solid, 54.5 mg, yield 13.7%, mp: 208.9–211.3°C, ^{1}H NMR (600 MHz, DMSO-d_6) δ = 10.01 (s, 1H, -NH), 8.39 (t, J = 5.7 Hz, 1H, -NH), 7.53 (d, J = 8.6 Hz, 2H, Ar-H), 7.23 (s, 1H, Ar-H), 7.22–7.18 (m, 2H, Ar-H), 7.17–7.10 (m, 1H, Ar-H), 6.99–6.95 (m, 1H, Ar-H), 6.89 (m, 3H, -CH = CH-), 6.18 (d, J = 15.0 Hz, 1H, -CH = CH-), 6.01 (s, 2H, -CH$_2$), 3.95 (d, J = 5.8 Hz, 2H, -CH$_2$), 2.41 (s, 3H, -CH$_3$). ^{13}C NMR (151 MHz, DMSO-d_6) δ = 168.16, 166.14, 148.37, 148.19, 140.26, 138.58, 136.87, 132.24, 131.27, 127.67, 125.64, 124.54, 123.05, 120.33, 108.86, 106.15, 101.68, 43.31, 16.05. HRMS (ESI) calcd for $C_{21}H_{21}O_4N_2S$ [M + H]$^+$: 397.12165, found 397.12054.

(2E,4E)-5-(benzo[d][1,3]dioxol-5-yl)-N-(2-((3-(benzyloxy)phenyl)amino)-2-oxoethyl)penta-2,4-dienamide (D15): red solid, 99.2 mg, yield 21.7%, mp: 191.0–192.0°C, ^{1}H NMR (600 MHz, DMSO) δ = 9.97 (s, 1H, -NH), 8.37 (t, J = 5.5 Hz, 1H, -NH), 7.41 (d, J = 7.6 Hz, 2H, Ar-H), 7.36 (t, J = 6.8 Hz, 3H, Ar-H), 7.30 (t, J = 6.8 Hz, 1H, Ar-H), 7.24 (s, 1H, Ar-H), 7.17 (dt, J = 15.2, 9.2 Hz, 2H, Ar-H), 7.10 (d, J = 7.9 Hz, 1H, Ar-H), 6.97 (d, J = 8.1 Hz, 1H, Ar-H), 6.95–6.78 (m, 4H, Ar-H and -CH = CH-), 6.69 (d, J = 8.0 Hz, 1H, -CH = CH-), 6.18 (d, J = 15.0 Hz, 1H, Ar-H), 6.02 (s, 2H, -CH$_2$), 5.04 (s, 2H, -CH$_2$), 3.95 (d, J = 5.8 Hz, 2H, -CH$_2$). ^{13}C NMR (151 MHz, DMSO-d_6) δ = 168.31, 166.10, 159.06, 148.37, 148.19, 140.53, 140.25, 138.59, 137.49, 131.28, 129.97, 128.84, 128.21, 128.01, 125.65, 124.53, 123.09, 112.15, 109.97, 108.87, 106.38, 106.13, 101.68, 69.60, 43.34. HRMS (ESI) calcd for $C_{27}H_{25}O_5N_2$ [M + H]$^+$: 457.17580, found 457.17459.

(2E,4E)-5-(Benzo[d][1,3]dioxol-5-yl)-N-(2-((4-(benzyloxy)phenyl)amino)-2-oxoethyl)penta-2,4-dienamide (D16): yellow solid, 97.6 mg, yield 21.3%, mp: 231.4–233.5°C, ^{1}H NMR (600 MHz, DMSO) δ = 9.86 (s, 1H, -NH), 8.37 (t, J = 5.6 Hz, 1H, -NH), 7.47 (d, J = 8.9 Hz, 2H, Ar-H), 7.41 (d, J = 7.4 Hz, 2H, Ar-H), 7.35 (dt, J = 7.1, 5.0 Hz, 3H, Ar-H), 7.29 (t, J = 7.1 Hz, 1H, Ar-H), 7.24 (s, 1H, Ar-H), 6.97 (d, J = 7.7 Hz, 1H, Ar-H), 6.95–6.85 (m, 5H, Ar-H and -CH = CH-), 6.18 (d, J = 15.0 Hz, 1H, -CH = CH-), 6.01 (s, 2H, -CH = CH-), 5.03 (s, 2H, -CH$_2$), 3.92 (d, J = 5.8 Hz, 2H, -CH$_2$). ^{13}C NMR (151 MHz, DMSO-d_6) δ = 167.76, 166.11, 154.75, 148.36, 148.19, 140.21, 138.55, 137.63, 132.69, 131.27, 128.81, 128.06, 125.65, 124.60, 123.05, 121.16, 116.24, 115.35, 108.87, 106.15, 101.68, 69.89, 43.21. HRMS (ESI) calcd for $C_{27}H_{25}O_5N_2$ [M + H]$^+$: 457.17580, found 457.17438.

(2E,4E)-5-(Benzo[d][1,3]dioxol-5-yl)-N-(2-((4-((2,6-difluorobenzyl)oxy)phenyl)amino)-2-oxoethyl)penta-2,4-dienamide (D17): yellow solid, 89.7 mg, yield 18.2%, mp: 203.9–206.5°C, ^{1}H NMR (600 MHz, DMSO-d_6) δ = 9.89 (s, 1H, -NH), 8.38 (s, 1H, -NH), 7.49 (d, J = 8.9 Hz, 3H, Ar-H), 7.24 (s, 1H, Ar-H), 7.17–7.13 (m, 3H, Ar-H), 6.97 (t, J = 7.9 Hz, 3H, Ar-H), 6.92–6.84 (m, 3H, -CH = CH-), 6.19 (d, J = 15.0 Hz, 1H, -CH = CH-), 6.02 (s, 2H, -CH$_2$), 5.04 (s, 2H,

-CH$_2$), 3.94 (d, J = 5.7 Hz, 2H, -CH$_2$). ^{13}C NMR (151 MHz, DMSO-d_6) δ = 167.83, 166.08, 162.49, 160.84, 154.46, 148.28 (d, $^2J_{C-F}$ = 28.3 Hz), 140.21, 138.56, 133.17, 132.05, 131.28, 125.66, 124.59, 123.09, 121.10, 115.92 (d, $^1J_{C-F}$ = 199.3 Hz), 115.42, 112.18 (dd, J = 21.2, 4.5 Hz), 108.86, 106.13, 101.68, 58.38, 43.21. ^{19}F NMR (564 MHz, DMSO) δ = -115.17. HRMS (ESI) calcd for $C_{27}H_{23}O_5N_2F_2$ [M + H]$^+$: 493.15695, found 493.15533.

(2E,4E)-5-(Benzo[d][1,3]dioxol-5-yl)-N-(2-oxo-2-((4-((4-(trifluoromethyl)benzyl)oxy)phenyl)-amino) ethyl) penta-2,4-dienamide (D18): brown solid, 118.5 mg, yield 22.5%, mp: 200.6–202.7°C, ^{1}H NMR (600 MHz, DMSO-d_6) δ = 9.90 (s, 1H, -NH), 8.39 (s, 1H, -NH), 7.72 (d, J = 7.4 Hz, 2H, Ar-H), 7.63 (d, J = 7.5 Hz, 2H, Ar-H), 7.50–7.46 (m, 2H, Ar-H), 7.24 (s, 1H, Ar-H), 7.19–7.13 (m, 1H, Ar-H), 6.96 (t, J = 8.7 Hz, 3H, Ar-H), 6.91–6.83 (m, 3H, -CH = CH-), 6.19 (d, J = 15.0 Hz, 1H, -CH = CH-), 6.02 (s, 2H, -CH$_2$), 5.16 (s, 2H, -CH$_2$), 3.94 (d, J = 5.6 Hz, 2H, -CH$_2$). ^{13}C NMR (151 MHz, DMSO-d_6) δ = 167.81, 166.09, 154.39, 148.37, 148.19, 142.54, 140.21, 138.56, 132.96, 131.27, 128.38, 125.68 (t, $^4J_{C-F}$ = 4.53 Hz), 124.59, 123.08, 121.15, 115.37, 108.85, 106.12, 101.68, 68.96, 43.21. ^{19}F NMR (564 MHz, DMSO) δ = -60.97. HRMS (ESI) calcd for $C_{28}H_{24}O_5N_2F_3$ [M + H]$^+$: 525.16318, found 525.16119.

(2E,4E)-5-(Benzo[d][1,3]dioxol-5-yl)-N-(2-oxo-2-((4-(pyridin-2-ylmethoxy)phenyl)amino)ethyl)-penta-2,4-dienamide (D19): brown solid, 95.2 mg, yield 20.8%, mp: 211.2–214.5°C ^{1}H NMR (600 MHz, DMSO-d_6) δ = 9.86 (s, 1H, -NH), 8.54 (d, J = 4.1 Hz, 1H, -NH), 8.36 (t, J = 5.5 Hz, 1H, Ar-H), 7.80 (td, J = 7.7, 1.7 Hz, 1H, Ar-H), 7.48 (d, J = 8.9 Hz, 3H, Ar-H), 7.33–7.29 (m, 1H, Ar-H), 7.24 (d, J = 1.2 Hz, 1H, Ar-H), 7.18–7.14 (m, 1H, Ar-H), 7.00–6.79 (m, 7H, Ar-H and -CH = CH-), 6.18 (d, J = 15.0 Hz, 1H, -CH = CH-), 6.02 (s, 2H, -CH$_2$), 5.11 (s, 2H, -CH$_2$), 3.93 (d, J = 5.8 Hz, 2H, -CH$_2$). ^{13}C NMR (151 MHz, DMSO-d_6) δ = 167.79, 166.07, 157.25, 154.51, 149.49, 148.37, 148.18, 140.20, 138.56, 137.34, 132.88, 131.28, 125.66, 124.60, 123.32, 123.08, 122.05, 121.17, 115.30, 108.86, 106.13, 101.68, 70.95, 43.20. HRMS (ESI) calcd for $C_{26}H_{24}O_5N_3$ [M + H]$^+$: 458.17105, found 458.16992.

(2E,4E)-5-(Benzo[d][1,3]dioxol-5-yl)-N-(2-((3-(benzyloxy)phenyl)amino)-2-oxoethyl)penta-2,4-dienamide (D20): brown solid, 110.4 mg, yield 24.8%, mp: 182.9–185.0°C ^{1}H NMR (600 MHz, DMSO-d_6) δ = 10.02 (s, 1H, -NH), 8.39 (t, J = 5.6 Hz, 1H, -NH), 7.58 (d, J = 8.8 Hz, 2H, Ar-H), 7.33 (t, J = 7.9 Hz, 2H, Ar-H), 7.24 (s, 1H, Ar-H), 7.18–7.14 (m, 1H, Ar-H), 7.07 (t, J = 7.3 Hz, 1H, Ar-H), 7.02–6.82 (m, 8H, Ar-H and -CH = CH-), 6.19 (d, J = 15.0 Hz, 1H, -CH = CH-), 6.02 (s, 2H, -CH$_2$), 3.95 (d, J = 5.7 Hz, 2H, -CH$_2$). ^{13}C NMR (151 MHz, DMSO-d_6) δ = 168.08, 166.12, 157.78, 152.22, 148.37, 148.19, 140.24, 138.58, 135.24, 131.28, 130.36, 125.66, 124.56, 123.40, 123.06, 121.31, 119.85, 118.32, 108.86, 106.15, 101.68, 43.28. HRMS (ESI) calcd for $C_{26}H_{23}O_5N_2$ [M + H]$^+$: 443.16015, found 443.15891.

(2E,4E)-5-(Benzo[d][1,3]dioxol-5-yl)-N-(2-(benzylamino)-2-oxoethyl)penta-2,4-dienamide (D21): red solid, 62.2 mg, yield

17.1%, mp: 173.6–175.8°C, ^{1}H NMR (600 MHz, DMSO-d_6) δ = 8.38 (t, J = 5.3 Hz, 1H, -NH), 8.33 (t, J = 5.6 Hz, 1H, -NH), 7.29 (t, J = 7.4 Hz, 2H, Ar-H), 7.26–7.07 (m, 5H, Ar-H), 6.97 (d, J = 7.9 Hz, 1H, Ar-H), 6.94–6.82 (m, 3H, -CH = CH-), 6.15 (d, J = 15.0 Hz, 1H, -CH = CH-), 6.01 (s, 2H, -CH$_2$), 4.27 (d, J = 5.8 Hz, 2H, -CH$_2$), 3.81 (d, J = 5.7 Hz, 2H, -CH$_2$). ^{13}C NMR (151 MHz, DMSO-d_6) δ = 169.42, 166.04, 148.37, 148.18, 140.10, 139.80, 138.50, 131.28, 128.64, 127.63, 127.15, 125.66, 124.73, 123.04, 108.86, 106.13, 101.68, 42.72, 42.52. HRMS (ESI) calcd for C$_{21}$H$_{21}$O$_4$N$_2$ [M + H]$^+$: 365.14958, found 365.14828.

(2E,4E)-5-(Benzo[d][1,3]dioxol-5-yl)-N-(2-((2-chlorobenzyl) amino)-2-oxoethyl)penta-2,4-dienamide **(D22)**: red solid, 182 mg, yield 45.6%, mp: 180.1–183.0°C, ^{1}H NMR (600 MHz, DMSO-d_6) δ = 8.40 (s, 1H, -NH), 8.36 (t, J = 5.4 Hz, 1H, -NH), 7.40 (d, J = 7.6 Hz, 1H, Ar-H), 7.35–7.21 (m, 4H, Ar-H), 7.18–7.14 (m, 1H, Ar-H), 6.97 (d, J = 8.0 Hz, 1H, Ar-H), 6.95–6.79 (m, 3H, -CH = CH-), 6.15 (d, J = 15.0 Hz, 1H, -CH = CH-), 6.01 (s, 2H, -CH$_2$), 4.32 (d, J = 5.7 Hz, 2H, -CH$_2$), 3.84 (d, J = 5.8 Hz, 2H, -CH$_2$). ^{13}C NMR (151 MHz, DMSO-d_6) δ = 169.72, 166.10, 148.37, 148.18, 140.14, 138.54, 136.66, 132.36, 131.27, 129.46, 129.18, 128.98, 127.53, 125.65, 124.67, 123.08, 108.86, 106.12, 101.68, 42.72, 40.43. HRMS (ESI) calcd for C$_{21}$H$_{20}$O$_4$N$_2$Cl [M + H]$^+$: 399.11061, found 399.10913.

(2E,4E)-5-(Benzo[d][1,3]dioxol-5-yl)-N-(2-oxo-2-(phenethylamino)ethyl)penta-2,4-dienamide **(D23)**:white solid, 147.5 mg, yield 38.9%, mp: 166.5–168.4°C, ^{1}H NMR (600 MHz, DMSO-d_6) δ = 8.26 (t, J = 5.4 Hz, 1H, -NH), 7.93 (s, 1H, -NH), 7.27–7.23 (m, 3H, Ar-H), 7.21–7.09 (m, 4H, Ar-H), 7.00–6.82 (m, 4H, Ar-H and -CH = CH-), 6.15 (d, J = 15.0 Hz, 1H, -CH = CH-), 6.01 (s, 2H, -CH$_2$), 3.73 (d, J = 5.8 Hz, 2H, -CH$_2$), 3.29–3.25 (m, 2H, -CH$_2$), 2.69 (t, J = 7.3 Hz, 2H, -CH$_2$). ^{13}C NMR (151 MHz, DMSO-d_6) δ = 169.23, 165.96, 148.37, 148.18, 140.11, 139.83, 138.51, 131.28, 129.03, 128.75, 126.50, 125.65, 124.69, 123.07, 108.86, 106.12, 101.68, 42.69, 40.66, 35.62. HRMS (ESI) calcd for C$_{22}$H$_{23}$O$_4$N$_2$ [M + H]$^+$: 379.16523, found 379.16385.

(2E,4E)-5-(Benzo[d][1,3]dioxol-5-yl)-N-(2-oxo-2-((3-phenylpropyl)amino)ethyl)penta-2,4-dienamide **(D24)**: white solid, 161.9 mg, yield 44.6%, mp: 166.5–168.4°C, ^{1}H NMR (600 MHz, DMSO-d_6) δ = 8.29 (t, J = 5.5 Hz, 1H, -NH), 7.90 (d, J = 4.9 Hz, 1H, -NH), 7.30–7.22 (m, 3H, Ar-H), 7.20–7.09 (m, 4H, Ar-H), 6.98–6.94 (m, 1H, Ar-H), 6.94–6.77 (m, 3H, -CH = CH-), 6.16 (d, J = 15.0 Hz, 1H, -CH = CH-), 6.01 (s, 2H, -CH$_2$), 3.74 (d, J = 5.8 Hz, 2H, -CH$_2$), 3.08–3.04 (m, 2H, -CH$_2$), 2.57–2.51 (m, 2H, -CH$_2$), 1.73–1.63 (m, 2H, -CH$_2$). ^{13}C NMR (151 MHz, DMSO-d_6) δ = 169.20, 165.95, 148.36, 148.17, 142.15, 140.05, 138.47, 131.28, 128.70, 128.68, 126.12, 125.66, 124.75, 123.05, 108.86, 106.12, 101.68, 42.71, 38.60, 32.89, 31.30. HRMS (ESI) calcd for C$_{23}$H$_{25}$O$_4$N$_2$ [M + H]$^+$: 393.18088, found 393.17938.

(2E,4E)-5-(Benzo[d][1,3]dioxol-5-yl)-N-(2-(naphthalen-2-ylamino)-2-oxoethyl)penta-2,4-dienamide **(D25)**: brown solid, 93.3 mg, yield 23.31%, mp: 141.9–144.2°C ^{1}H NMR (600 MHz, DMSO-d_6) δ = 10.01 (s, 1H, -NH), 8.50 (s, 1H, -NH), 8.07 (d, J = 6.8 Hz, 1H, Ar-H), 7.91 (d, J = 6.7 Hz, 1H, Ar-H), 7.75 (d, J = 7.5 Hz, 1H, Ar-H), 7.58–7.46 (m, 3H, Ar-H), 7.24 (s, 1H, Ar-H), 6.92 (dt, J = 37.5, 12.0 Hz, 6H, Ar-H and -CH = CH-), 6.23 (d, J = 14.8 Hz, 1H, -CH = CH-), 6.01 (s, 2H, -CH$_2$), 4.15 (s, 2H, -CH$_2$). ^{13}C NMR (151 MHz, DMSO-d_6) δ = 169.14, 166.35, 148.37, 148.20, 140.32, 138.62, 134.15, 133.80, 131.27, 128.52, 128.21, 126.46, 125.98, 125.66, 124.59, 124.05, 123.17, 123.07, 115.91, 108.87, 107.96, 106.15, 101.69, 43.37. HRMS (ESI) calcd for C$_{24}$H$_{21}$O$_4$N$_2$ [M + H]$^+$: 401.14958, found 401.14816.

(2E,4E)-5-(Benzo[d][1,3]dioxol-5-yl)-N-(2-(benzo[d][1,3]dioxol-5-ylamino)-2-oxoethyl)penta-2,4-dienamide **(D26)**: black solid, 110.4 mg, yield 27.9%, mp: 198.5–201.9°C ^{1}H NMR (600 MHz, DMSO-d_6) δ = 9.91 (s, 1H, -NH), 8.37 (s, 1H, -NH), 7.28–7.21 (m, 2H, Ar-H), 7.18–7.14 (m, 1H, Ar-H), 6.99–6.91 (m, 3H, Ar-H), 6.90–6.86 (m, 2H, -CH = CH-), 6.83 (t, J = 5.8 Hz, 1H, -CH = CH-), 6.18 (d, J = 15.1 Hz, 1H, -CH = CH-), 6.02 (s, 2H, -CH$_2$), 5.95 (s, 2H, -CH$_2$), 3.92 (d, J = 5.7 Hz, 2H, -CH$_2$). ^{13}C NMR (151 MHz, DMSO-d_6) δ = 167.88, 166.08, 148.37, 148.19, 147.47, 143.33, 140.22, 138.56, 133.74, 131.28, 125.65, 124.57, 123.06, 112.44, 108.86, 108.44, 106.14, 101.82, 101.68, 101.37, 43.24. HRMS (ESI) calcd for C$_{21}$H$_{19}$O$_6$N$_2$ [M + H]$^+$: 395.12376, found 395.12210.

(2E,4E)-5-(Benzo[d][1,3]dioxol-5-yl)-N-(2-((1-methyl-1H-indol-5-yl)amino)-2-oxoethyl)penta-2,4-dienamide **(D27)**: yellow solid, 142.8 mg, yield 35.4%, mp: 218.4–221.1°C, ^{1}H NMR (600 MHz, DMSO-d_6) δ = 9.81 (s, 1H, -NH), 8.38 (t, J = 5.6 Hz, 1H, -NH), 7.84 (s, 1H, Ar-H), 7.33 (d, J = 8.8 Hz, 1H, Ar-H), 7.28–7.22 (m, 2H, Ar-H), 7.19–7.15 (m, 1H, Ar-H), 7.00–6.82 (m, 4H, Ar-H and -CH = CH-), 6.34 (d, J = 2.8 Hz, 1H, -CH = CH-), 6.20 (d, J = 15.0 Hz, 1H, -CH = CH-), 6.02 (s, 2H, -CH$_2$), 3.97 (d, J = 5.8 Hz, 2H, -CH$_2$), 3.73 (s, 3H, -CH$_3$). ^{13}C NMR (151 MHz, DMSO-d_6) δ = 167.62, 166.07, 148.37, 148.18, 140.15, 138.52, 133.78, 131.47, 131.30, 130.56, 128.26, 125.69, 124.70, 123.06, 115.24, 111.42, 109.87, 108.86, 106.14, 101.68, 100.65, 43.33, 32.92. HRMS (ESI) calcd for C$_{23}$H$_{22}$O$_4$N$_3$ [M + H]$^+$: 404.16048, found 404.15900.

(2E,4E)-5-(Benzo[d][1,3]dioxol-5-yl)-N-(2-oxo-2-((2,2,2-trifluoroethyl)amino)ethyl)penta-2,4-dienamide **(D28)**: yellow solid, 70.5 mg, yield 19.7%, mp: 154.2–156.1°C ^{1}H NMR (600 MHz, DMSO-d_6) δ = 8.52 (t, J = 5.9 Hz, 1H, -NH), 8.32 (t, J = 5.6 Hz, 1H, -NH), 7.23 (s, 1H, Ar-H), 7.17–7.13 (m, 1H, Ar-H), 6.97 (d, J = 7.9 Hz, 1H, Ar-H), 6.91–6.87 (m, 3H, -CH = CH-), 6.14 (d, J = 15.0 Hz, 1H, -CH = CH-), 6.01 (s, 2H, -CH$_2$), 3.90–3.86 (m, 2H, -CH$_2$), 3.83 (d, J = 5.8 Hz, 2H, -CH$_2$). ^{13}C NMR (151 MHz, DMSO-d_6) δ = 170.38, 166.05, 148.37, 148.19, 140.25, 138.59, 131.26, 125.62, 124.52, 123.07, 108.86, 106.13, 101.68, 42.33. ^{19}F NMR (564 MHz, DMSO) δ = -70.71. HRMS (ESI) calcd for C$_{16}$H$_{16}$O$_4$N$_2$F$_3$ [M + H]$^+$: 357.10567, found 357.10431.
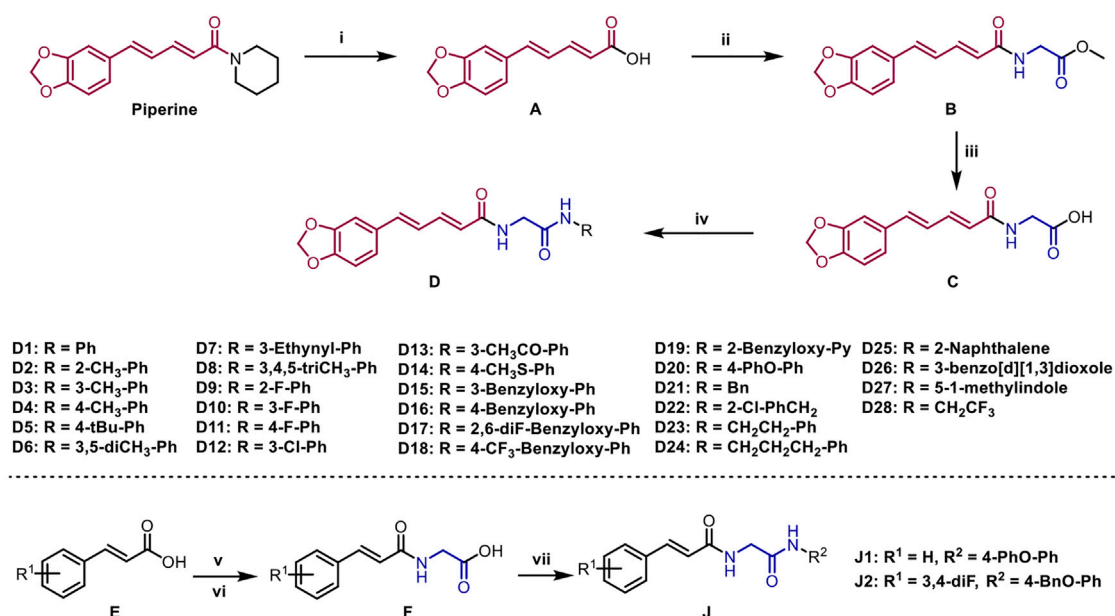
Reaction conditions: (i) NaOH, EtOH, 85 °C, 12 h; (ii) HOBt, DIEPA, EDCI, Glycine methyl ester hydrochloride, DCM, 0-25 °C, 18 h; (iii) NaOH, EtOH, 85 °C, 12 h; (iv) Amine, HOBt, DIEPA, EDCI, DCM, 0-25 °C; (v) HOBt, DIEPA, EDCI, Glycine methyl ester hydrochloride, DCM, 0-25 °C, 18 h; (vi) NaOH, EtOH, 85 °C, 12 h; (vii) Amine, HOBt, DIEPA, EDCI, DCM, 0-25 °C.

FIGURE 2
Synthesis route of the target compounds. Reaction conditions: (i) NaOH and EtOH, 85°C, 12 h; (ii) HOBt, DIEPA, EDCI, glycine methyl ester hydrochloride, and DCM, 0–25°C, 18 h; (iii) NaOH and EtOH, 85°C, 12 h; (iv) amine, HOBt, DIEPA, EDCI, and DCM, 0–25°C; (v) HOBt, DIEPA, EDCI, glycine methyl ester hydrochloride, and DCM, 0–25°C, 18 h; (vi) NaOH and EtOH, 85°C, 12 h; (vii) amine, HOBt, DIEPA, EDCI, and DCM, 0–25°C.

2.1.5 Preparation of intermediates F1 and F2

A mixture of intermediate **E** (10.0 mmol), glycine methyl ester hydrochloride (9.0 mmol, 1.13 g), HOBt (10.0 mmol, 1.35 g), DIEPA (10.0 mmol, 1.29 g), and 20 ml of DCM was stirred at 0°C for 15 min. Then, EDCI (10 mol, 1.92 g) was added, and the mixture was stirred at 25°C for 18 h. After the reaction was completed, the solvent was removed under reduced pressure. Then, a mixture of KOH (20.0 mmol, 1.12 g) and 30 ml of H_2O/ CH_3OH/THF ($v:v:v$ = 1:1:1) was added to the crude products, and the reaction mixture was stirred at room temperature for 12 h. Then, 10% of HCl solution was added until a solid precipitate formed. The solvent was removed under reduced pressure, and the crude product was purified by column chromatography to obtain intermediates **F1** and **F2.**

***Cinnamoylglycine* (F1)**: white solid, 1.75 g, yield 85%, mp: 198.4–201.5°C, ^{1}H NMR (600 MHz, DMSO-d_6) δ = 8.42 (s, 1H, -NH), 7.55 (d, J = 7.4 Hz, 2H, Ar-H), 7.47–7.28 (m, 4H, Ar-H and -CH = CH-), 6.71 (d, J = 15.8 Hz, 1H, -CH = CH-), 3.87 (d, J = 5.1 Hz, 2H, -CH$_2$). ^{13}C NMR (151 MHz, DMSO-d_6) δ = 171.64, 165.77, 139.63, 135.25, 129.95, 129.35, 127.99, 122.17, 41.30. HRMS (ESI) calcd for $C_{11}H_{12}O_3N$ [M + H]$^+$: 206.08117, found 206.08066.

***(E)*-(3-(3,4-Difluorophenyl)*acryloyl*)*glycine* (F2)**: white solid, 1.98 g, yield 82%, mp: 210.0–213.1°C, ^{1}H NMR (600 MHz, DMSO-d_6) δ = 8.38 (s, 1H, -NH), 7.72–7.62 (m, 1H, Ar-H), 7.49–7.27 (m, 3H, Ar-H and -CH = CH-), 6.68 (d, J = 15.6 Hz, 1H, -CH = CH-), 3.87 (d, J = 3.0 Hz, 2H, -CH$_2$). ^{13}C NMR (151 MHz, DMSO-d_6) δ = 171.58, 165.39, 151.07 (dd, J = 46.8, 12.1 Hz), 149.47 (dd, J = 45.3, 12.1 Hz), 137.52, 133.21 (dd, J = 6.0, 4.5 Hz), 125.19 (dd, J = 7.6, 4.5 Hz), 123.52, 118.42 (d, $^3J_{C-F}$ = 18.1 Hz), 116.69 (d, $^3J_{C-F}$ = 16.6 Hz), 41.31. ^{19}F NMR (564 MHz, DMSO) δ = -136.97, -138.11. HRMS (ESI) calcd for $C_{11}H_{10}O_3NF_2$ [M + H]$^+$: 242.06233, found 242.06166.

2.1.6 Preparation of target compounds J1 and J2

A mixture of intermediate **F** (1.0 mmol), amine (1.2 mmol), HOBt (1.2 mol, 162.14 mg), DIEPA (1.2 mol, 155.1 mg), and 10 ml of DCM was stirred at 0°C for 15 min. Then, EDCI (1.2 mol, 230.0 mg) was added, and the reaction mixture was stirred at 25°C for 18 h. After the reaction was completed, the solvent was removed under reduced pressure to give the crude product. Then, the target compounds **J1** and **J2** were obtained *via* recrystallization using ethyl acetate and petroleum ether as the solvent.

TABLE 1 Insecticidal activity of piperine and target compounds against *P. xylostella* on larvae (mortality (%) ± SD) (48 h).

Compound	Insecticidal activity against *Plutella xylostella*[a]
	0.2 mg/ml (%)
Piperine[b]	0
D1	13.8[a]± 1.9
D2	3.5 ± 1.9
D3	17.2 ± 3.3
D4	3.5 ± 3.9
D5	3.6 ± 0
D6	6.9 ± 0
D7	0
D8	13.3 ± 3.9
D9	13.3 ± 1.9
D10	20 ± 0
D11	6.9 ± 3.3
D12	26.7 ± 1.9
D13	3.5 ± 1.9
D14	3.5 ± 1.9
D15	3.3 ± 1.9
D16	3.6 ± 0
D17	20.7 ± 1.9
D18	20.7 ± 1.9
D19	20.0 ± 0
D20	3.5 ± 1.9
D21	10.3 ± 1.9
D22	3.3 ± 1.9
D23	26.7 ± 1.9
D24	3.5 ± 1.9
D25	6.9 ± 3.3
D26	6.9 ± 3.3
D27	6.9 ± 3.3
D28	43.3 ± 1.9
J1	3.5 ± 1.9
J2	13.8 ± 1.9

[a]Average of three replicates.
[b]Piperine was used as control.

TABLE 2 Insecticidal activity of piperine and D28 against *P. xylostella* at 1 mg/ml on larvae (mortality (%) ± SD) (48 h).

Compound	Insecticidal activity against *Plutella xylostella*[a]
	1 mg/ml (%)
Piperine[a]	0
D28	90.0 ± 0

[a]Average of three replicates.

***N*-(2-oxo-2-((4-Phenoxyphenyl)amino)ethyl) cinnamamide (J1)**: white solid, 58.2 mg, yield 15.6%, mp: 213.4–217.5°C, ^{1}H NMR (600 MHz, DMSO-d_6) δ = 10.07 (s, 1H, -NH), 8.45 (t, *J* = 5.5 Hz, 1H, -NH), 7.59–7.55 (m, 4H, Ar-H), 7.47–7.30 (m, 6H, Ar-H), 7.07 (t, *J* = 7.4 Hz, 1H, Ar-H), 6.97–6.93 (m, 4H, Ar-H), 6.76 (d, *J* = 15.8 Hz, 1H, -CH = CH-), 4.01 (d, *J* = 5.8 Hz, 2H, -CH$_2$). ^{13}C NMR (151 MHz, DMSO-d_6) δ = 167.96, 165.88, 157.76, 152.24, 139.54, 135.28, 135.19, 130.37, 129.95, 129.37, 128.00, 123.42, 122.31, 121.34, 119.87, 118.32, 43.31. HRMS (ESI) calcd for $C_{23}H_{21}O_3N_2$ [M + H][+]: 373.15467, found 373.15344.

(E)-*N*-(2-((4-(benzyloxy)phenyl)amino)-2-oxo-ethyl)-3-(3,4-difluorophenyl)acrylamide (J2): white solid, 49.5 mg, yield 11.7%, mp: 246.2–248.3°C, ^{1}H NMR (600 MHz, DMSO-d_6) δ = 9.90 (s, 1H, -NH), 8.39 (t, *J* = 5.6 Hz, 1H, Ar-H), 7.69–7.65 (m, 1H, Ar-H), 7.51–7.39 (m, 7H, Ar-H), 7.35 (t, *J* = 7.5 Hz, 2H, Ar-H), 7.29 (t, *J* = 7.2 Hz, 1H, Ar-H), 6.94 (d, *J* = 8.9 Hz, 2H, Ar-H), 6.75 (d, *J* = 15.8 Hz, 1H, -CH = CH-), 5.03 (s, 2H, -CH$_2$), 3.98 (d, *J* = 5.6 Hz, 2H, -CH$_2$). ^{13}C NMR (151 MHz, DMSO-d_6) δ = 167.53, 165.45, 154.77, 151.12 (dd, *J* = 43.8, 12.1 Hz), 149.48 (dd, *J* = 40.8, 13.6 Hz), 137.48 (d, $^2J_{C-F}$ = 39.3 Hz), 133.29 (dd, *J* = 6.0, 3.0 Hz), 132.64, 128.81, 128.32 (d, $^1J_{C-F}$ = 117.8 Hz), 128.18, 128.06, 125.15 (dd, *J* = 6.0, 3.0 Hz), 123.77, 121.16, 118.45 (d, $^2J_{C-F}$ = 18.1 Hz), 116.68 (d, $^2J_{C-F}$ = 18.1 Hz), 115.35, 69.87, 43.25.^{19}F NMR (564 MHz, DMSO) δ = -137.01, -138.10.

2.2 Bioactivity assay against *P. xylostella*

The biological activity was evaluated using the leaf dipping method. The stock solution of insecticides was diluted using an aqueous solution of 0.05% Triton X-80. Cabbage leaf discs were dipped in solutions with the insecticide concentration (0.2 mg/ml) for 15 s and allowed to dry for 2 h. Control discs were treated with a 0.05% Triton X-80 solution. All the dipped leaf discs were dried at room temperature before being placed in Petri dishes (10 cm in diameter). Each set of concentrations was replicated three times. Next, 10 s-instar larvae were transferred to each Petri dish. The dishes were then stored in an incubator at 25 ± 2°C, 70 ± 20% RH (relative humidity) and kept under a 14:10 h light/dark photoperiod. Larvae mortality was recorded at 48 h.

2.3 Docking

A bioinformatics analysis for the molecular docking of **D28** with GABA$_A$ receptor was conducted according to the method used by Sun et al. (2021). A homology model of GABA$_A$ was constructed using the online server SWISS-MODEL (https://swissmodel.expasy.org/). Molecular docking of **D28** with GABA$_A$ receptor was performed using Autodock software
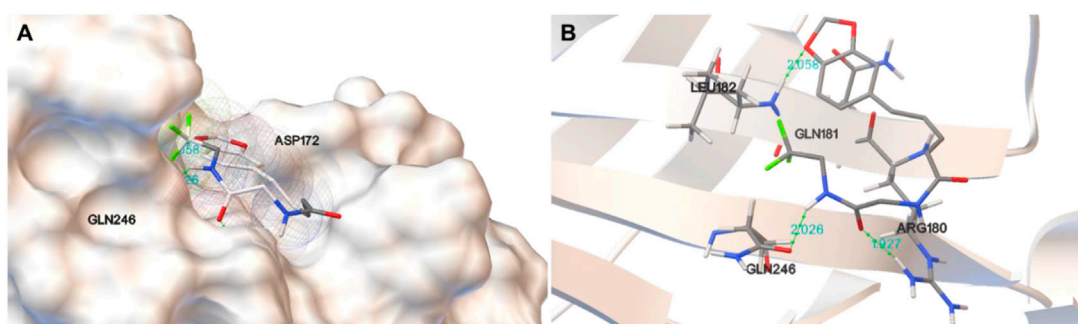
FIGURE 3
Molecular docking results of D28 with GABA$_A$ receptor analyzed using PyMOL software. **(A)** Protein surface view for docking of D28 with GABA$_A$ receptor with the interaction of a hydrogen bond; **(B)** picture of the docking of D28 with GABA$_A$ receptor, with binding sites at ARG180, GLN246, and LEU182.

(version 4.2) (Bajaj et al., 1996). The energetically minimized three-dimensional structure of AITC was constructed using Chem 3D ultra 2010. The pdb files of **D28** and GABA$_A$ receptor were set as the ligand and the receptor, respectively, followed by sequenced procedures using Autogrid and Autodock. Docking results with minimized reaction energy were selected, and binding sites were analyzed with PyMOL software (Seeliger and de Groot, 2010).

3 Results and discussion

3.1 Chemistry

The synthetic routes of compounds **D1**–**D28**, **J1**, and **J2** are outlined in Figure 2. The pathway started from the reaction of piperine and NaOH in EtOH under 85°C for 12 h, which produced intermediate **A**. Then, intermediate **A** reacted with methyl glycinate to produce intermediate **B** in the presence of HOBt, DIPEA, and EDCI using CH$_2$Cl$_2$ as the solvent. Next, intermediate **B** reacted with KOH in H$_2$O/CH$_3$OH/THF (*v:v:v* = 1:1:1) to produce intermediate **C**. The target compounds **D1**–**D28** were obtained *via* a condensation reaction between intermediate **C** and different amines. The compounds **J1** and **J2** were prepared using **E1** and **E2** as the starting materials that was followed by two condensation reactions to form the target compounds **J1** and **J2**. All desired products were confirmed by ^{1}H-NMR, ^{13}C-NMR, ^{19}F-NMR, and HRMS.

3.2 Insecticidal biological activity

The results of the insecticidal activity against *P. xylostella* are shown in Table 1. These compounds showed better insecticidal activities against *P. xylostella* than piperine,

although most of the target compounds had low insecticidal activities with a mortality rate of less than 20% at a concentration of 0.2 mg/ml. Compounds **D12**, **D23**, and **D28** showed the highest activity among these compounds, with a mortality rate of 26.7, 26.7, and 43.3% at 48h, respectively. To further compare the difference in insecticidal activities of compound **D28** and piperine, the mortality rates of these two compounds were tested at 1 mg/ml (Table 2), and compound **D28** showed 90% mortality. From the structure–activity relationship, R showed significant effects on the insecticidal activities of the target compounds. When R was trifluoroethyl, compound **D28** showed the best insecticidal activities, followed by arenethyl. When chlorine was substituted at the 3-position of the benzene ring, compound **D12** showed higher insecticidal activity. When the substituent R was CH$_3$, compounds with CH$_3$ at the meta-position showed higher activity, for instance, **D3** (3-CH$_3$) > **D2** (2-CH$_3$) ≈ **D4** (4-CH$_3$). Meanwhile, when R was benzyloxy-substituted phenyl, it seemed to have higher activity than alkyl-substituted phenyl. For instance, **D18** (4-CF$_3$-Benzyloxy-Ph) > **D8** (3,4,5-triCH$_3$-Ph) > **D21** (Bn).

3.3 Molecular docking of compound D28 with GABA$_A$ receptor

To identify the binding affinity of **D28** and GABA$_A$ receptor, we determined the molecular docking of **D28** and GABA$_A$ receptor using Autodock software (Figure 3). Figure 3A and b indicate that **D28** binds at ARG180, GLN246, and LEU182 within the GABA$_A$ receptor by hydrogen bonds, of which distances were 1.927, 2.026, and 2.058 Å, respectively. The molecular docking results indicated that compound D28 could act on the GABA$_A$ receptor.

4 Conclusion

In summary, 30 novel piperine derivatives containing linear bisamide were designed and synthesized. The structures of these compounds were confirmed *via* ^{1}H-NMR, ^{13}C-NMR, and HRMS. The insecticidal activities of these compounds were evaluated, and all of them have better insecticidal activities against *P. xylostella* than piperine. In addition, compound **D28** displayed good insecticidal activity. The insecticidal mechanism of compound **D28** was studied using molecular docking, and the results indicated that compound 34 may act on $GABA_A$ receptors. These findings indicated that these piperine derivatives have the potential to be a promising lead compound for further study.

Data availability statement

The original contributions presented in the study are included in the article/Supplementary Material; further inquiries can be directed to the corresponding author.

Author contributions

YL designed the experiments. CZ and QT performed the experiments and analyzed the data. YL wrote the manuscript.

Conflict of interest

The authors declare that the research was conducted in the absence of any commercial or financial relationships that could be construed as a potential conflict of interest.

Publisher's note

All claims expressed in this article are solely those of the authors and do not necessarily represent those of their affiliated organizations, or those of the publisher, the editors, and the reviewers. Any product that may be evaluated in this article, or claim that may be made by its manufacturer, is not guaranteed or endorsed by the publisher.

Supplementary material

The Supplementary Material for this article can be found online at: https://www.frontiersin.org/articles/10.3389/fchem.2022.973630/full#supplementary-material

References

Bajaj, C. L., Pascucci, V., and Schikore, D. R. (1996). "Fast isocontouring for improved Interactivity," in Proceedings of 1996 Symposium on Volume Visualization, San Francisco, CA, USA, 29-29 Oct. 1996, 39–46.

Chen, Y., Wu, J., Wang, A., Qi, Z., Jiang, T., Chen, C., et al. (2017). Discovery of N-(5-((5-Chloro-4-((2-(isopropylsulfonyl)phenyl)amino)pyrimidin-2-yl) amino)-4-methoxy-2-(4-methyl-1,   4   -diazepan-1-yl)phenyl)acrylamide (CHMFL-ALK/EGFR-050) as a potent ALK/EGFR dual kinase inhibitor capable of overcoming a variety of ALK/EGFR associated drug resistant mutants in NSCLC. Eur. J. Med. Chem. 139, 674–697. doi:10.1016/j.ejmech.2017.08.035

Franklim, T. N., Freire-de-Lima, L., Diniz, J. D. N. S., Previato, J. O., Castro, R. N., Mendonça-Previato, L., et al. (2013). Design, synthesis and trypanocidal evaluation of novel 1, 2, 4-Triazoles-3-thiones derived from natural piperine. Molecules 18, 6366–6382. doi:10.3390/molecules18066366

Gaur, R., and Bao, G.-H. (2021). Chemistry and pharmacology of natural catechins from camellia sinensis as anti-MRSA agents. Curr. Top. Med. Chem. 21, 1519–1537. doi:10.2174/1568026621666210524100632

Han, Q., Wu, N., Li, H.-L., Zhang, J.-Y., Li, X., Deng, M.-F., et al. (2021). A piperine-based scaffold as a novel starting point to develop inhibitors against the potent molecular target OfChtI. J. Agric. Food Chem. 69, 7534–7544. doi:10.1021/acs.jafc.0c08119

He, F., Li, B., Ai, G., Kange, A. M., Zhao, Y., Zhang, X., et al. (2016). Transcriptomics analysis of the Chinese pear pathotype of Alternaria alternata gives insights into novel mechanisms of HSAF antifungal activities. Int. J. Mol. Sci. 19, 1841. doi:10.3390/ijms19071841

Kimura, K., Yamaoka, M., and Kamisaka, Y. (2006). Inhibition of lipid accumulation and lipid body formation in oleaginous yeast by effective components in spices, carvacrol, eugenol, thymol, and piperine. J. Agric. Food. Chem. 54, 3528–3534. doi:10.1021/jf0531149

Lima Neto, J. E., da Solidade Ribeiro, L. M., and de Siqueira, H. Á. A. (2021). Inheritance and fitness of Plutella xylostella (Lepidoptera: Plutellidae) resistance to chlorfenapyr. J. Econ. Entomol. 114, 875–884. doi:10.1093/jee/toaa299

Liu, H., Ren, Z.-L., Wang, W., Gong, J.-X., Chu, M.-J., Ma, Q.-W., et al. (2018). Novel coumarin-pyrazole carboxamide derivatives as potential topoisomerase II inhibitors: Design, synthesis and antibacterial activity. Eur. J. Med. Chem. 157, 81–87. doi:10.1016/j.ejmech.2018.07.059

Liu, Z., Li, Q., and Song, B. (2020). Recent research progress in and perspectives of mesoionic insecticides: Nicotinic acetylcholine receptor inhibitors. J. Agric. Food Chem. 68, 11039–11053. doi:10.1021/acs.jafc.0c02376

Park, U. H., Jeong, H. S., Jo, E. Y., Park, T., Yoon, S. K., Kim, E.-J., et al. (2012). Piperine, a component of black pepper, inhibits adipogenesis by antagonizing

PPARγ activity in 3T3-L1 cells. *J. Agric. Food Chem.* 60, 3853–3860. doi:10.1021/jf204514a

Parmar, V. S., Jain, S. C., Bisht, K. S., Jain, R., Taneja, P., Jha, A., et al. (1997). Phytochemistry of the genus piper. *Phytochemistry* 46, 597–673. doi:10.1016/S0031-9422(97)00328-2

Paula, V. F. d., Barbosa, L. C. d. A., Demuner, A. J., Piló-Veloso, D., and Picanço, M. C. (2000). Synthesis and insecticidal activity of new amide derivatives of piperine. *Pest Manag. Sci.* 56, 168–174. doi:10.1002/(sici)1526-4998(200002)56:2<168:aid-ps110>3.0.co;2-h

Ribeiro, T. S., Freire-de-Lima, Le., Previato, J. O., Previato, L. M., Heise, N., Freire de Lima, M. E., et al. (2004). Toxic effects of natural piperine and its derivatives on epimastigotes and amastigotes of trypanosoma cruzi. *Bioorg. Med. Chem. Lett.* 14, 3555–3558. doi:10.1016/j.bmcl.2004.04.019

Roman, P. (2016). History, presence and perspective of using plant extracts as commercial botanical insecticides and farm products for protection against insects – A review. *Plant Prot. Sci.* 52, 229–241. doi:10.17221/31/2016-PPS

Seeliger, D., and de Groot, B. L. (2010). Ligand docking and binding site analysis with PyMOL and autodock/vina. *J. Comput. Aided. Mol. Des.* 24, 417–422. doi:10.1007/s10822-010-9352-6

Shen, J., Li, D., Zhang, S., Zhu, X., Wan, H., Li, J., et al. (2017). Fitness and inheritance of metaflumizone resistance in *Plutella xylostella*. *Pestic. Biochem. Physiol.* 139, 53–59. doi:10.1016/j.pestbp.2017.04.010

Sun, J., Lv, X.-H., Qiu, H.-Y., Wang, Y.-T., Du, Q.-R., Li, D.-D., et al. (2013). Synthesis, biological evaluation and molecular docking studies of pyrazole derivatives coupling with a thiourea moiety as novel CDKs inhibitors. *Eur. J. Med. Chem.* 68, 1–9. doi:10.1016/j.ejmech.2013.07.003

Sun, Y., Jiang, Y., Wu, H., Xu, N., Ma, Z., Zhang, C., et al. (2021). Function of four mitochondrial genes in fumigation lethal mechanisms of allyl isothiocyanate against *Sitophilus zeamais* adults. *Pestic. Biochem. Physiol.* 179, 104947. doi:10.1016/j.pestbp.2021.104947

Sunila, E. S., and Kuttan, G. (2004). Immunomodulatory and antitumor activity of piper longum linn and piperine. *J. Ethnopharmacol.* 90, 339–346. doi:10.1016/j.jep.2003.10.016

Swain, T. (1977). Secondary compounds as protective agents. *Annu. Rev. Plant Physiol.* 28, 479–501. doi:10.1146/annurev.pp.28.060177.002403

Tang, J.-F., Lv, X.-H., Wang, X.-L., Sun, J., Zhang, Y.-B., Yang, Y.-S., et al. (2012). Design, synthesis, biological evaluation and molecular modeling of novel 1, 3, 4-oxadiazole derivatives based on vanillic acid as potential immunosuppressive agents. *Bioorg. Med. Chem.* 20, 4226–4236. doi:10.1016/j.bmc.2012.05.055

Tang, M., Wang, Z., and Shi, Y. (2004). Involvement of cytochrome c release and caspase activation in toosendanin-induced PC12 cell apoptosis. *Toxicology* 201, 31–38. doi:10.1016/j.tox.2004.03.023

Tong, Z., Duan, J., Wu, Y., Liu, Q., He, Q., Shi, Y., et al. (2018). Evaluation of highly detectable pesticides sprayed in Brassica napus L.: Degradation behavior and risk assessment for honeybees. *Molecules* 23, 2482. doi:10.3390/molecules23102482

Wang, H., Yang, Z., Fan, Z., Wu, Q., Zhang, Y., Mi, N., et al. (2011). Synthesis and insecticidal activity of *N*-tert-Butyl-*N, N'*-diacylhydrazines containing 1, 2, 3-thiadiazoles. *J. Agric. Food Chem.* 59, 628–634. doi:10.1021/jf104004q

Wu, W.-J., Wang, M.-A., Zhu, J.-B., Zhou, W., Hu, Z., Ji, Z., et al. (2001). Five new insecticidal sesquiterpenoids from *Celastrus angulatus*. *J. Nat. Prod.* 64, 364–367. doi:10.1021/np0004193

Xia, D., Liu, H., Cheng, X., Maraswami, M., Chen, Y., Lv, X., et al. (2022). Recent developments of coumarin-based hybrids in drug discovery. *Curr. Top. Med. Chem.* 22, 269–283. doi:10.2174/1568026622666220105105450

Xu, H., and Yang, R. (2017). *Piperine derivatives, preparation method and application of preparation of botanical insecticides*. Xi'an, Shanxi Province: Northwest A&F University. CN 107892685 A.

Zhao, Z., Xu, Q., Chen, W., Wang, S., Yang, Q., Dong, Y., et al. (2022). Rational design, synthesis, and biological investigations of *N*-methylcarbamoylguanidinyl azamacrolides as a novel chitinase inhibitor. *J. Agric. Food Chem.* 70, 4889–4898. doi:10.1021/acs.jafc.2c00016

Check for updates

Combined analysis of the transcriptome and proteome of *Eucommia ulmoides* Oliv. (Duzhong) in response to *Fusarium oxysporum*

Yingxia Lu[1†], Xuan Dong[1,2]*[†], Xiaozhen Huang[1,2],
De-gang Zhao[2,3], Yichen Zhao[1,2]* and Lei Peng[1]

[1]College of Tea Sciences, Guizhou University, Guiyang, China, [2]The Key Laboratory of Plant Resources Conservation and Germplasm Innovation in Mountainous Region (Ministry of Education), Guiyang, China, [3]Guizhou Academy of Agricultural Science, Guiyang, China

Eucommia ulmoides Oliv. (Duzhong), a valued traditional herbal medicine in China, is rich in antibacterial proteins and is effective against a variety of plant pathogens. *Fusarium oxysporum* is a pathogenic fungus that infects plant roots, resulting in the death of the plant. In this study, transcriptomic and proteomic analyses were used to explore the molecular mechanism of *E. ulmoides* counteracts *F. oxysporum* infection. Transcriptomic analysis at 24, 48, 72, and 96 h after inoculation identified 17, 591, 1,205, and 625 differentially expressed genes (DEGs), while proteomics identified were 66, 138, 148, 234 differentially expressed proteins (DEPs). Meanwhile, GO and KEGG enrichment analyses of the DEGs and DEPs showed that they were mainly associated with endoplasmic reticulum (ER), fructose and mannose metabolism, protein processing in the ER, type II diabetes mellitus, the ribosome, antigen processing and presentation, and the phagosome. In addition, proteome and transcriptome association analysis and RT-qPCR showed that the response of *E. ulmoides* to *F. oxysporum* was likely related to the unfolded protein response (UPR) of the ER pathway. In conclusion, our study provided a theoretical basis for the control of *F. oxysporum*.

Introduction

Eucommia ulmoides Oliv. (Duzhong) is a traditional Chinese herbal medicine and is recorded in the ancient pharmacy classics, Shen Nong's Herbal Classic and Compendium of Materia Medical (Anderson, 1982). It is the only existing species of the family Eucommiaceae (Tokumoto et al., 2016). The leaves and bark of *E. ulmoides* have been listed in the Chinese Pharmacopoeia (Qian et al., 2010), and its medicinal components have attracted extensive attention. It has been used to treat hypertension,

hyperlipidemia, obesity, diabetes, inflammation, and other conditions. In addition, it also has antiviral, antibacterial, antioxidant, antitumor, and other activities (Qian et al., 2010; Fujiwara et al., 2016; Hussain et al., 2017; Cho et al., 2018; Lee et al., 2018).

Fusarium oxysporum is a widespread plant pathogenic fungus, belonging to the imperfect fungi. It is a soil-borne parasite and produces large numbers of sickle-shaped conidia through asexual reproduction after infecting the plant (Gordon and Martyn, 1997; Michielse and Rep, 2010). It infects the plant roots and causes deterioration of the vascular bundles, damages the functioning of the ducts, and may cause the death of the plant through damage at all stages of the plant growth (Pietro et al., 2010). *Fusarium* infection affects a large number of crops with important economic value, such as the Musaceae, Rosaceae, Cucurbitaceae, Brassicaceae, Solanaceae, and Fabaceae (Gordon and Martyn, 1997; Edel-Hermann and Lecomte, 2019), which has brought serious losses to agricultural production. Our laboratory's previous research found that the total protein extracted from *E. ulmoides* had a significant inhibitory effect on *F. oxysporum* (Liu et al., 2007). However, the molecular mechanism of *E. ulmoides* counteracts *F. oxysporum* infection was not clear yet.

With the development of high-throughput sequencing technologies, "omics" analyses have been widely applied to the study of plant-microbe interactions, especially in the study of plant responses to pathogen stress. The transcriptome represents the sum of all transcripts produced by a particular tissue or cell of a species at a specific time (Guo et al., 2021). Transcriptome sequencing can determine the expression of all genes during a particular period, which provides an important reference for gene transcription (Wilhelm and Landry, 2009). Transcriptome sequencing has been used extensively to study biotic and abiotic stresses in plants, and the technology can provide a comprehensive picture of gene expression in target biological tissues under specific stress conditions. Comparative transcriptome analysis can identify changes in the expression of genes associated with specific physiological or pathological conditions (Shi et al., 2020). Proteomics is used to identify and quantify the overall protein content of cells, tissues, or organisms. It is an effective complement to other omics analyses, such as genomics and transcriptomics. It provides a useful basis for elucidating the structure and function of proteins, resolving cellular signaling pathways (Wasinger et al., 1995; Mann et al., 2001; Monti et al., 2005), and understanding pathogenic mechanisms (Saleh et al., 2019).

With the development of biological information, in this study, we explore to study the molecular mechanism of *E. ulmoides* in response to *F. oxysporum* using transcriptome and proteome methods. This study will provide a theoretical basis for the control of *F. oxysporum*.

Materials and methods

Materials

The seeds of *E. ulmoides* were collected from *E. ulmoides* trees that had been established for over 10 years in the Key Laboratory of Mountain Plant Resource Protection and Germplasm Innovation, Institute of Agricultural Bioengineering, Guizhou University. *F. oxysporum* was isolated from *Passiflora edulis* Sims according to the method of Sarwar et al. (2005) showing characteristic symptoms of wilt and identified by the Tea Biotechnology Laboratory of Tea College of Guizhou University. Plants of *P. edulis* Sims showing characteristic symptoms of wilt were collected with fibrous tertiary roots on the basis of visual observations and brought in the laboratory for isolation of *F. oxysporum*.

Sample preparation

The peels of the mature seeds of *E. ulmoides* were removed and the seeds surfaces were thoroughly cleaned using sterile water. Then the seeds were soaked in sterile water for 12 h and rinsed with tap water. After disinfection with 75% alcohol for 60 s, the seeds were washed several times with sterile water, followed by soaking in NaClO solution with 10% available chlorine for 15 min. After several further washes with sterile water, the seeds were dried on sterile water-absorbing paper. The seed coat was then cut using a scalpel and inoculated on solid Murashige and Skoog (MS) basal medium with vitamins (cultured in a glass incubator containing 50 ml MS medium with a diameter of 5.5 cm and a height of 12 cm) and cultured under a light/dark cycle of 16/8 h at 25°C. After 15–20 days when the cotyledons were fully expanded, the roots of *E. ulmoides* seedlings with 2-4 true leaves were inoculated with *F. ulmoides*. The inoculated seedlings were cultured in dark at 25°C. After inoculation for 0, 24, 48, 72, and 96 h, the naked eye fungal infection and necrotic part were removed and the samples for subsequent experiments were collected from the tissue 1 cm above the removed tissue. Then, the collected samples were snap-frozen in liquid nitrogen and stored at -80°C.

RNA extraction and transcriptome sequencing

The collected samples (100 mg) were ground with liquid nitrogen. Total RNA was extracted using the Plant RNA Extraction Kit (ComWin Biotech Co., Ltd., Beijing, China) according to the supplied method, and three replicates were prepared for each treatment. Poly-A tailed mRNA was enriched using Oligo dT magnetic beads. The RNA was then fragmented and reverse-transcribed using random N6 primers. After

synthesis of double-stranded DNA, the ends were flattened and phosphorylated at the 5′ end, while the 3′ end had a protruding "A" sticky end. The ligated product was amplified by PCR with specific primers (forward primer: 5′-GAACGACATGGCTAC GA-3′ and reverse primer: 5′-TGTGAGCCAAGGAGTTG-3′), the PCR product was heat-denatured to single-stranded DNA and then cyclized with a bridge primer to obtain a single-stranded circular DNA library and sequenced using DNBSEQ platform.

The raw sequencing data contains reads with low quality, splice contamination, and high contents of unknown base N. These reads need to be removed before data analysis to ensure the reliability of the results. The filtering software SOAPnuke version 1.4.0 was used for analysis and filtering was performed using Trimmomatic v0.36 to remove the reads containing the connector, those with unknown base N contents greater than 5%, and low-quality reads with mass values of less than 10 accounting for more than 20% of the total base number of the reads. The clean reads were then used for subsequent analysis and were mapped to the Eucommia reference genome (https://www.ncbi.nlm.nih.gov/bioproject/?term=PRJNA357336) (Chen et al., 2022) using HISAT 2.1.0 (Kim et al., 2015). The clean reads were also compared with reference gene sequences using Bowtie 22.2.5 (Langmead and Salzberg, 2012) and RSEM 1.2.8 (Li and Dewey, 2011) was used to calculate the expression levels of the genes and transcripts. All the programs were used with default parameters. The data that support the findings of this study have been deposited into CNGB Sequence Archive (CNSA) of China National GeneBank DataBase (CNGBdb) with accession number of CNP0003469.

Protein extraction and mass spectrometry analysis

The total protein of *E. ulmoides* was extracted according to the method of Yu et al. (2018) and analyzed by Nano LC-1DTM plus system (Eksigent, Dublin, CA, United States) combined with Triple TOF5600 MS (Foster City, CA, United States).

Max Quant version 1.5.2.8 (Cox et al., 2011) was used for processing the LC-MS/MS data. The *E. ulmoides* protein database downloaded from NCBI was used for MS/MS identification. The results of the Max Quant analysis, including the initial search for the precursor mass with a tolerance of 20 μl/ml, were used for mass recalibration (Cox and Mann, 2008). The false discovery rate (FDR) for peptide and protein identification was set at 0.01. Label-free quantification with a minimum of two ratio counts was used for normalization and the sum of two ratio counts was used to determine the normalized protein levels for comparison between samples (Cox and Mann, 2008). The IBAQ algorithm was used to calculate the absolute abundance of different proteins in a single sample (Luber et al., 2010), and the proteins were

filtered to eliminate common contaminants and the interference of opposite databases. The data that support the findings of this study have been deposited into CNGB Sequence Archive (CNSA) of China National GeneBank DataBase (CNGBdb) with accession number of CNP0003469.

Functional annotation and enrichment analysis

To annotate unigenes which were assembled by Stringtie, sequences were searched by BLASTx against the NCBI non-redundant protein (nr) database and other databases, including the Swiss-Prot protein database, the Kyoto Encyclopedia of Genes and Genomes (KEGG) and the Gene Ontology (GO) databases. KEGG enrichment scatter plots and GO enrichment bar plots were constructed using the OmicStudio tools at https://www.omicstudio.cn/tool.

Identification of differentially expressed genes and differentially expressed proteins

The DESeq2 R package (https://genomebiology.biomedcentral.com/articles/10.1186/s13059-014-0550-8, accessed on November 2020) was used to analyses the differential expression between groups; it uses a model based on the negative binomial distribution to provide statistical routines for determining differential expressions in digital gene expression data. The resulting p-values were adjusted by using Benjamini and Hochberg's approach to control the false discovery rate (FDR < 0.01). Genes with an adjusted p value < 0.01 by DESeq2 were assigned as differentially expressed genes (DEGs). The protein differences between two groups were analyzed by t-tests. Proteins with p values ≤ 0.01 were considered to be differentially expressed proteins (DEPs).

Protein-mRNA correlation analysis

To correlate transcript and protein expression profiles, accession numbers from the proteome were extracted and compared with the annotated RNA-Seq libraries. A protein-mRNA correlation analysis was performed using the regularized-logarithm transformation (rlog) value of the spectral counts and the normalized log2 probe intensity for mRNAs. Briefly, we calculated the global Spearman correlation coefficient, rho, for protein-mRNA pairs within all DEPs and DEGs, similar regulatory patterns of DEPs and DEGs and opposite regulatory patterns of DEPs and DEGs, respectively. Adjusted p values based on the analysis of DEPs

TABLE 1 List of primers used in this study.

No.	Gene ID	Annotation names	Forward primer (5'-3')	Reverse primers (5'-3')
1	GWHTAAAL010245	Elongation factor-1 alpha	TGATTGAGAGGTCCACAAACC	CCAATCTTGTAGACATCCTGGAG
2	GWHGAAAL008628	Translation initiation factor eIF-2B subunit alpha	CAACGTGTTGCTCGGAAAAG	GGTGAACCTTCATTCGTGGG
3	GWHGAAAL012002	BCL2-associated athanogene 1	AGGAAATGGGAATAAGGTGGC	AGCATGTGATTCTCCATCGG
4	GWHPAAAL009648	Endoplasmic reticulum chaperone BiP	GGTCACATTTGAAGTCGATGC	TCAATCTCCTCTTGGCTCAAC
5	GWHGAAAL005471	HSP20 family protein	TTCCCTCTCCTATCCTCTTCC	CTGCCTCTGTCCTGATTATGAG
6	GWHGAAAL020098	Heat shock 70 kDa protein 1/2/6/8	AGCAGAGAAATACAAGTCAGAGG	TGGCCTGATCAATAGCATCC
7	GWHGAAAL010874	Hypoxia up-regulated 1	GGTTGAATTCTACTGGGCTCC	CAGATGTAGGTATTGAAGACGAGG
8	GWHPAAAL013860	Hsp70-Hsp90	AGAAACCAGAGCGGCAAC	CTTTGGTATAATGCTGAATCGCTG
9	GWHPAAAL019641	Protein disulfide-isomerase A6	GTCCTAGTGGAATTCTATGCTCC	GTGTCGGCATCAACATTGG
10	GWHPAAAL025197	Calnexin	AAAAGACGATTCCCGACCC	GCATCCTCATCCCAGTCATC
11	GWHPAAAL008473	Calreticulin	GAAGAGGATGGAATATGGAGAGC	CTTCAACACATAGAGGTCGGG
12	GWHGAAAL023146	Ubiquitin-conjugating enzyme E2	ATGGCTCCGAGAAAATACGTC	CATACACCAATCGCCAAGTTG
13	GWHGAAAL022038	F-box and WD-40 domain protein 1/11	ATCCGACAGCAAGAACATCC	AACACGAACCTTACCATCCTG

and DEGs were computed by the Benjamini-Hochberg procedure (Benjamini and Hochberg, 1995). The KEGG enrichment analysis and Advanced Heatmap Plots were performed using the OmicStudio tools by R version 3.6.3 (https://www.omicstudio.cn).

Analysis of the relative gene expression

Total RNA was extracted from powdered *E. ulmoides* samples using the Plant RNA Extraction Kit (ComWin Biotech Co., Ltd., Beijing, China). The RNA was reverse-transcribed using a Goldenstar™ RT6 cDNA Synthesis Kit (Tsingke Biotechnology, Beijing, China) according to the manufacturer's instructions. Real-time quantitative polymerase chain reaction (RT-qPCR) was performed using the reaction sample (10 μl) with SoFast EvaGreen® Supermix (Bio-Rad, Hercules, CA, United States) and the RT-PCR assay was completed using the CFX ConnectTM Real-Time PCR System (Bio-Rad, Hercules, CA, United States), each sample was run in triplicate with appropriate negative controls, under the same condition used in previous studies: 95°C for 3 min, then 39 cycles of 95°C for 10 s, 65°C for 20 s, and 72°C for 10 s. Fluorescence data were collected at the end of the second step and, following cycling, the melting curve was determined in the range of 65–95°C with an increment of 0.05°C/s. Gene expression was normalized using elongation factor-1 alpha as an internal control. The specific primers used in RT-qPCR were designed by the RNA Folding Form (http://www.unafold.org/mfold/applications/rna-folding-form.php) and Primer Quest™ Tool (https://sg.idtdna.com/pages/tools/primerquest) and listed in Table 1. The $2^{-\Delta\Delta Ct}$ method was used to calculate the relative expression levels. Each treatment was analyzed for three times.

Results

Morphological observations

The roots morphology of *E. ulmoides* seedlings inoculated with *F. oxysporum* was observed. As shown in Figure 1, after 24 h of inoculation, no mycelia were observed on the MS basal medium and the roots of *E. ulmoides* seedlings, while small numbers of new mycelia of *F. oxysporum* were visible after 48 h; no obvious lesions or necrosis were seen on the roots at either time. After 72 h of inoculation, large numbers of new mycelia of *F. oxysporum* were apparent, although there was no evidence of lesions or necrosis. After 96 h of inoculation, the root of *E. ulmoides* was eroded by *F. oxysporum*, with clear signs of necrosis and finger sheath-like detachments.

RNA-Seq data analysis

A total of 15 samples (label as ck-1, ck-2, ck-3, 24h-1, 24h-2, 24h-3, 48h-1, 48h-2, 48h-3, 72h-1, 72h-2, 72h-3, 96h-1, 96h-2, 96h-3) were tested using the DNBSEQ platform. The quality indicators of the filtered reads are shown in Supplementary Table S1. The results showed that a total of 95.99 GB high-quality reads were obtained from the RNA-Seq transcriptome sequencing. Each sample had three independent biological replicates and each sample produced an average of 6.40 GB of data. The Q20 and Q30 of each sample were over 96.04% and 87.42%, respectively. The block diagram of the FPKM values for each sample was shown in Supplementary Figure S1, which showed that the data are accurate and could be used directly for further analysis. The average comparison rate between the samples and the genome was 68.49%. A total of 5177 new genes were predicted and the expression of 28,604 genes was detected, of
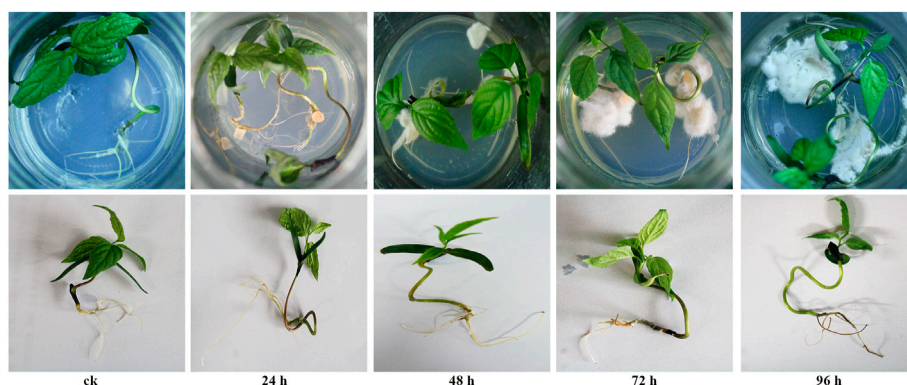
FIGURE 1
The roots morphology of *E. ulmoides* seedlings after 0, 24, 48, 72, and 96 h of inoculation with *F. oxysporum*.
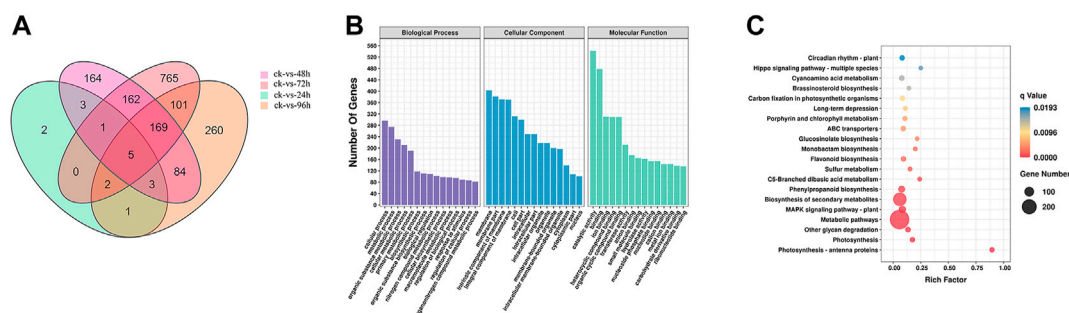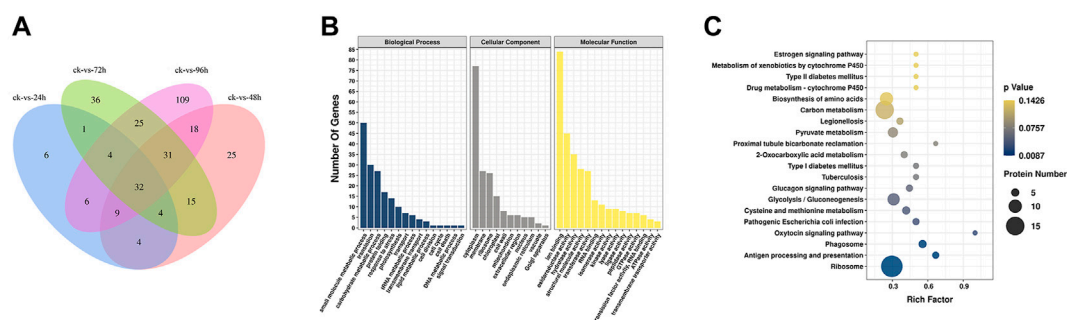

FIGURE 2
(A) Venn diagram of DEGs in *E. ulmoides* compared before (ck) with 24, 48, 72, and 96 h of inoculation with *F. oxysporum*, respectively. **(B)** GO analysis of DEGs in *E. ulmoides* between 0 and 72 h of inoculation with *F. oxysporum*. **(C)** KEGG enrichment analysis of DEGs in *E. ulmoides* between 0 and 72 h of inoculation with *F. oxysporum*.

which 23,478 were known genes and 5,126 were possibly new genes. A total of 57,545 new transcripts were detected, of which 15,439 belonged to new variable splicing subtypes of known protein-coding genes, 5,177 were transcripts of new protein-coding genes, and the remaining 36,929 were long non-coding RNAs.

Bioinformatic analysis of differentially expressed genes

After 72 h of inoculation with *F. oxysporum*, the Venn diagram (Figure 2A) showed that the greatest number (1205) of DEGs in *E. ulmoides* were present, and the DEGs are visually represented in the volcano plot (Supplementary Figure S2) with the numbers of up- and downregulated genes being 292 and 913, respectively. Meanwhile, after 72 h of inoculation, the annotation of genes using the GO database indicated that the total number of

genes (TB) and the significantly DEGs between the inoculated and uninoculated treatments (TS) with *F. oxysporum* were 23,802 and 1,013, respectively. The top four DEGs annotations in the biological process (BP) category were found to be cellular process, metabolic process, organic substance metabolic process, and cellular metabolic process, with the numbers of S genes (the number of significantly DEGs annotated in the designated database) were 296, 274, 231, and 211, respectively. In the cellular components (CC) category, DEGs were enriched in the membrane, membrane part, intrinsic component of membrane, and integral component of membrane categories, with S gene numbers of 403, 382, 371, and 370, respectively. The CC categories of cell, cell part, intracellular, intracellular part, intracellular organelle, and organelle were also enriched, and the numbers of S genes were 312, 300, 249, 249, 218, and 218, respectively. In the molecular functions (MF) category, the DEGs were enriched in catalytic activity, binding, ion binding, heterocyclic compound binding,

FIGURE 3
(A) Venn diagram of DEPs in *E. ulmoides* compared before (ck) with 24, 48, 72, and 96 h of inoculation with *F. oxysporum*, respectively. **(B)** GO analysis of DEPs in *E. ulmoides* between 0 and 72 h of inoculation with *F. oxysporum*. **(C)** KEGG enrichment analysis of DEPs in *E. ulmoides* between 0 and 72 h of inoculation with *F. oxysporum*.

organic cyclic compound binding, and transferase activity. The numbers of genes were 542, 478, 310, 309, 309, 212, and 212, respectively (Figure 2B; Supplementary Figure S3). KEGG pathway enrichment (Figure 2C; Supplementary Figure S4) showed that there were 12,550 TB genes and 600 TS genes. DEGs were significantly enriched in metabolic pathways, biosynthesis of secondary metabolites, plant-pathogen interaction, MAPK signaling pathway-plant, fructose and mannose metabolism, phosphatidylinositol signaling system, and protein processing in ER, with the gene numbers of 288, 174, 56, 55, 12, 10, and 9, respectively.

Proteome annotation analysis

After the component analysis (Supplementary Figure S5) and cluster analysis (Supplementary Figure S6) of the DEPs, the data from three biological replicates obtained after 0, 24, 48, 72, and 96 h of inoculation with *F. oxysporum* were analyzed, indicating that both the samples and the data were reliable and could be further analyzed. A total of 1,595 peptides were obtained by searching and analyzing the peptides in the total proteomic library of *E. ulmoides* obtained before and after inoculation with *F. oxysporum*. Overall, 1397, 1268, 1206, 1220, and 1166 peptides were obtained after 0, 24, 48, 72, and 96 h of inoculation, respectively.

The Venn diagram (Figure 3A) showed that the number of DEPs was highest at 96 h after inoculation with *F. oxysporum*. The DEPs were visualized using a volcano plot (Supplementary Figure S7), indicating that eight proteins were up-regulated and 226 were downregulated after 96 h of inoculation compared with their expression before inoculation. The GO database indicated that the significant DEPs were enriched in small-molecule metabolic process, translation, carbohydrate metabolic process, protein folding, response to stress, and other BP. The number of

DEPs in these categories were 50, 30, 27, 17, and 14, respectively. In the CC category, DEPs were enriched in cytoplasm, membrane, ribosome, chloroplast, and chloroplast, with 77, 27, 26, and 15 proteins in the respective categories. In terms of MF, the numbers of DEPs enriched in ion binding, oxidoreductase activity, hydrolase activity, structural molecule activity were 84, 45, 35, 28, and 27, respectively (Figure 3B; Supplementary Figure S8). KEGG pathway analysis (Figure 3C; Supplementary Figure S9) showed the most significant enrichment in the ribosome, carbon metabolism, biosynthesis of amino acids, glycolysis/gluconeogenesis, pyruvate metabolism, protein processing in ER, phagosome, antigen processing and presentation, and type II diabetes categories. The number of DEPs in each of these pathways was 18, 15, 10, 9, 7, 6, 5, 4, and 2, respectively.

Analysis of the association between the proteomic and transcriptomic data

To correlate the transcript and protein expression profiles, the DEPs from the proteomic analysis were compared with the annotated RNA-Seq library. The results showed that 153 of the 326 proteins were expressed in the same pattern as their mRNAs, indicating that the expression of almost half of the proteins was regulated directly at the transcriptional level. Cluster analysis on these 326 DEGs and DEPs (Supplementary Figure S10) indicated that both DEGs and DEPs were reliable and could be further analyzed. Figure 4 showed 153 and 158 genes with similar and opposite regulatory patterns at the transcriptional and protein levels were analyzed for correlations, obtaining the pearson correlation coefficients (r) of 0.718 and -0.677, respectively. The red boxes in the KEGG pathways (Figure 5) highlight the pathways in which both DEPs and DEGs were common enriched in transcription, translation, and folding, sorting and degradation.
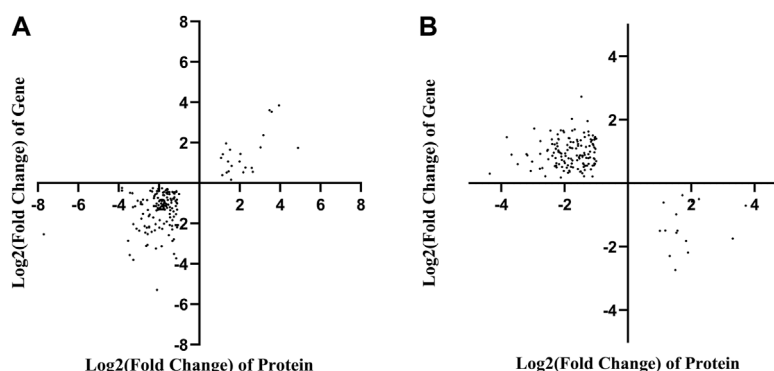
FIGURE 4
Correlation analysis based on the proteomics and transcriptomics. **(A)** Correlation analysis of differentially expressed proteins and genes with the same tendency of change. **(B)** The correlation analysis of significant differential expression of proteins and genes with opposite trends.

RT-qPCR results

The relative expression level of the DEPs and DEGs enriched in the ER pathway (ID: ko04141) were further analyzed using RT-qPCR method. The results showed that the relative expression level of translation initiation factor eIF-2B subunit alpha after 24, 48, 72, and 96 h of inoculation with *F. oxysporum* was 0.05, 0.15, 0.61, and 0.24 times lower than that of ck group (Figure 6A). The relative expression level of BCL2-associated athanogene 1 was 5.75 and 16.53 times higher at 48 and 72 h after inoculation, respectively, than ck group (Figure 6B). The ER contains at least three types of molecular chaperones of protein folding. The first of these includes the heat shock molecular chaperones such as HSP20, HSP70, and HSP90, the second includes the lectin molecular chaperones calcium-linked protein and calcium network protein, while the last category comprises enzymes related to protein processing and Ca^{2+} homeostasis, such as protein disulfide isomerase (PDI). The results of this study (Figures 6C–J) showed that, except for calreticulin, whose expression was suppressed after inoculation with *F. oxysporum*, the expression of all other molecular chaperones, including ER chaperone BiP, HSP20 family protein, heat shock 70 kDa protein 1/2/6/8, heat shock protein hsp70-hsp90, PDI A6, and calnexin, increased significantly at 72 h after inoculation, with the relative expression of hypoxia upregulated 1 increased 65.53 times more than before inoculation. During ER stress, the ER-associated degradation (ERAD) is activated at the transcriptional level to remove misfolded proteins, increasing their degradation by the ubiquitin-proteasome system. Figures 6K-L showed that the expression of the ubiquitin-binding enzyme E2 and ubiquitin-ligase F-box increased significantly at 72 h after inoculation, which were 10.07 and 75.26 times higher than those before inoculation, respectively.

Discussion

F. oxysporum is an important pathogenic fungus, which can cause skin and eye lesions in mammals through infection of breaks in the skin, and also causes fusarium wilt in many crops through soil transmission, leading to serious economic losses in agricultural production. The control of *F. oxysporum* in agricultural production relies mainly on chemical fungicides which pose a major risk to the environment and food safety (Mukhtar, 2007; Jahanshir and Dzhalilov, 2010; Swarupa et al., 2014). It is, thus, important to investigate the antimicrobial mechanisms of traditional Chinese herbal medicine for the development of plant immune inducer (Dewen et al., 2017) and antimicrobial drugs with high efficacy and low toxicity. *E. ulmoides* is a traditional Chinese medicinal plant, recorded in The Classic of Herbal Medicine, that has proven antifungal property against *Botrytis cinerea* in our previous study (Liu et al., 2008).

In our present study, transcriptomic and proteomic analyses results showed that the KEGG pathway mainly concentrated in protein processing in ER, fructose and mannose metabolism, phosphatidylinositol signaling system, ribosome, protein processing in ER, phagosome, and antigen processing and presentation. Some previous studies (Malhotra and Kaufman, 2007; Wen and Wei, 2015; Ma, 2019; Zhang and Wei, 1997) had demonstrated that these pathways were related to the ER and ER misfolding. Therefore, our results demonstrated that *E. ulmoides* responds to *F. oxysporum* infection by mechanisms related to ER. The ER is an important organelle in the secretion pathway of eukaryotes and participates in the coordination of a variety of cellular activities such as protein processing and calcium homeostasis. It is also one of the important hubs for plant responses to various stresses (Martinez and Chrispeels, 2003; Helenius and Aebi, 2004; Kamauchi et al., 2005; Chen and Brandizzi, 2013; Doblas et al., 2013; Howell, 2013; Mishiba
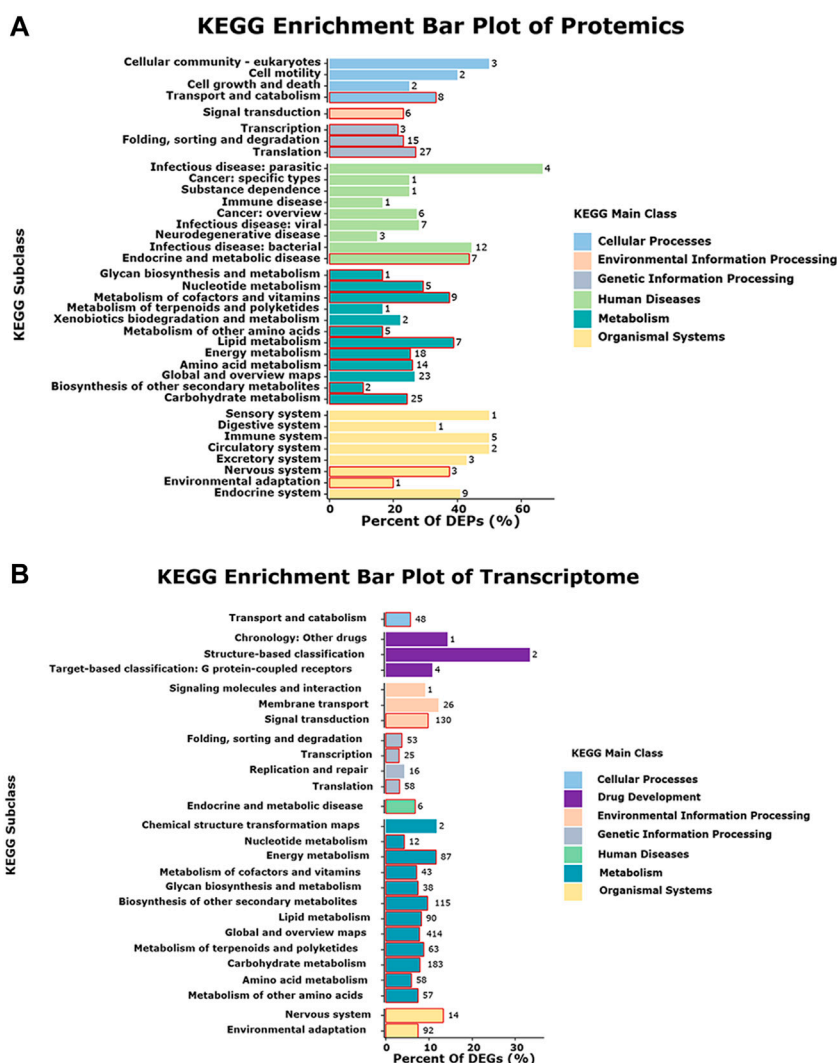
FIGURE 5
Pathway enriched in both the proteome and transcriptome. The red boxes represent in the pathways that are enriched in both protein and mRNA. **(A)** KEGG enrichment bar plot of Protemics. **(B)** KEGG enrichment bar plot of Transcriptome.

et al., 2013; Pollier et al., 2013; Cai et al., 2014; Williams et al., 2014). When plants are stressed by pathogenic infections, there is an accumulation of large numbers of unfolded or misfolded proteins in the ER lumen, leading to ER stress and adversely affecting the normal functioning of the organelle (Howell, 2013). If the protein accumulation exceeds the ER capacity, the cell responds by upregulating specific ER-associated genes and enzymes to restore homeostasis. This process is termed the ER stress response (Howell, 2013; Jing and Wang, 2020). Plant ER stress sensors can recognize ER stress and trigger the ER stress response, also called the unfolded protein response (UPR). The UPR has been shown to play an important role in interactions between plants and microorganisms (Wan and Jiang, 2016). The ER stress

signaling pathway is closely related to plant immunity and represents an important part of the plant's resistance to pathogen infection (Zhang et al., 2016; Qiang et al., 2021; Zhou et al., 2021). However, there is a lack of information on how plants respond to pathogen infection and activate ER stress-mediated immunity (ERSI).

The RT-qPCR results showed that the gene relative expression of ER chaperone protein BiP was significantly up-regulated after 48 and 72 h of inoculation with *F. oxysporum*. Upregulated expression of BiP is often considered to be a marker for ERS and UPR activation (Pobre et al., 2019). Meanwhile, the gene relative expression of translation initiation factor eIF-2B subunit alpha was inhibited after inoculation with *F. oxysporum*. It is possible that this could be the result of incorrect folding or
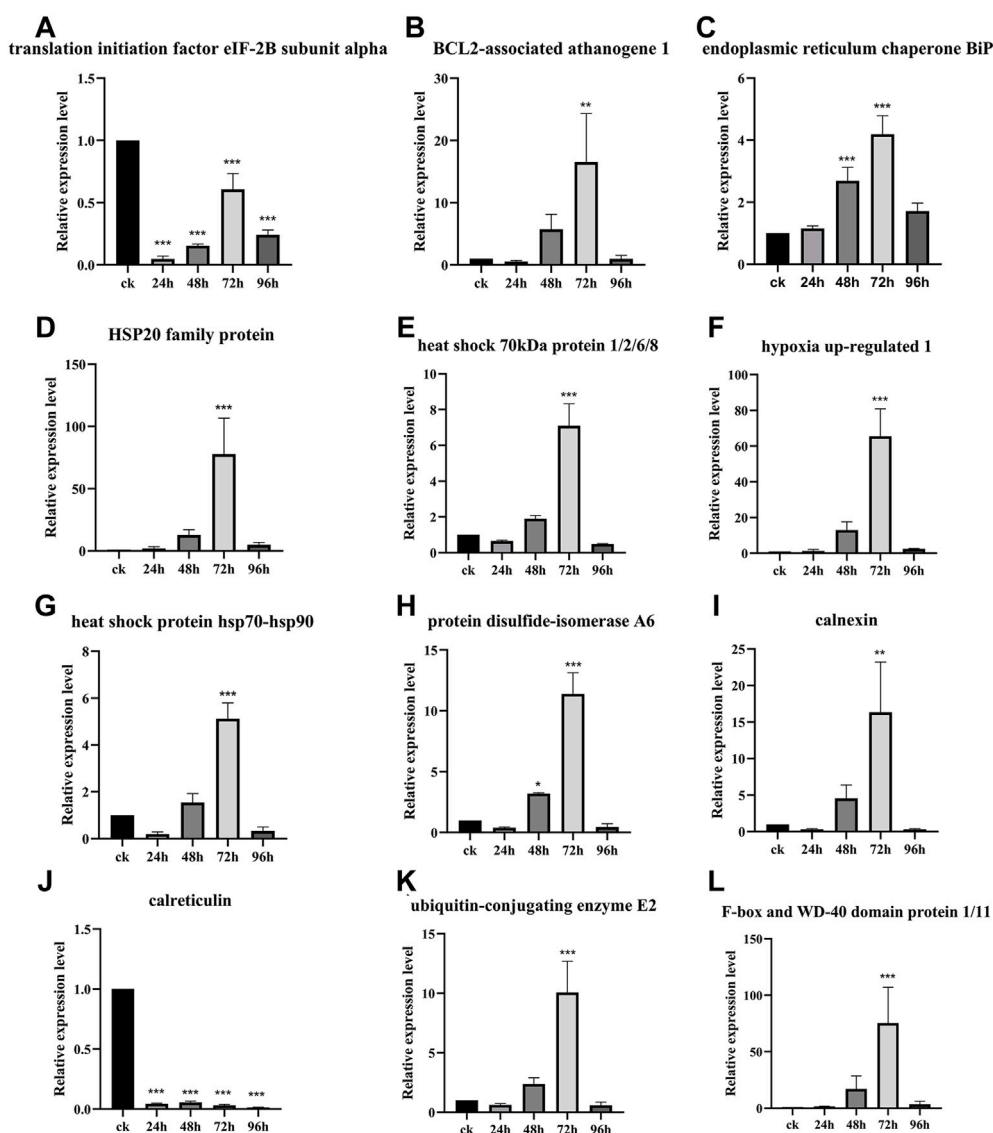
FIGURE 6

Gene relative expression analysis of the ER pathway-related genes. Data are shown as the mean of three biological replicates $\pm$ SD. The * represents significant difference (**$p < 0.01$, ***$p < 0.001$, Student's t-test). **(A)** Translation initiation factor eIF-2B subunit alpha. **(B)** BCL2-associated athanogene 1. **(C)** Endoplasmic reticulum chaperone BiP. **(D)** HSP20 family protein. **(E)** Heat shock 70 kDa protein 1/2/6/8. **(F)** Hypoxia upregulated 1. **(G)** Heat shock protein hsp70-hsp-90. **(H)** Protein disulfide-isomerase A6. **(I)** Calnexin. **(J)** Calreticulin. **(K)** Ubiquitin-conjugating enzyme E2. **(L)** F-box and WD-40 domain protein 1/11.

wrong assembly of the protein, leading to binding by BiP to retain its unfolded state and prevent further misfolding. These reactions can lead to the phosphorylation of protein kinase R (PKR)-like ER kinase (PERK) protein dimer and cytoplasmic domain and eIF2. Phosphorylation of the latter at serine 51 blocks the binding of eIF2 to ATP and reduces the translation of its downstream mRNA (Harding et al., 2002; Ni et al., 2009). These reactions reduce the translation and synthesis of proteins, reduce the influx of new proteins to the ER, and thus prevent further increases in the numbers of unfolded proteins, thus lowering ERS (Harding

et al., 2002; Ni et al., 2009). Combining the results of the analysis of BiP and eIF2α in this study with reported results, we speculate that the activation of the UPR in the *E. ulmoides* response to *F. oxysporum* is likely to be *via* the PERK/ATF4 of the ER pathway. This would prolong ERS and prevent the restoration of intracellular homeostasis and apoptosis would be induced by activation of the apoptosis regulator B lymphocyte 2 gene family (Marciniak et al., 2004). In this study, we also observed a significant increase in the expression of the BCL2-associated athanogene, further suggesting that the PERK/ATF4 of the ER
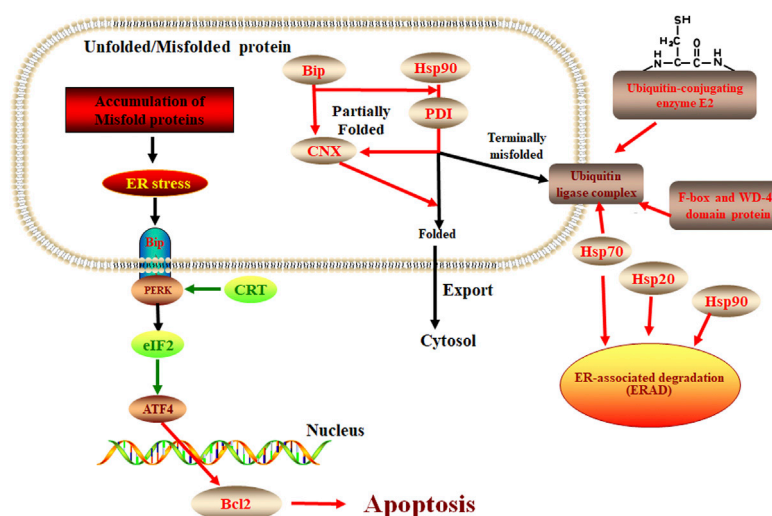
FIGURE 7
The protein processing in the ER pathway in *E. ulmoide* response to *F. oxysporum*. Red color represents up-accumulated genes or proteins in this pathway, while the green color represents down-accumulated.

pathway may play an important role in *E. ulmoides* response to *F. oxysporum*. At present, most of the studies on the UPR in plants have focused on IRE1-X box binding protein, transcriptional activator 6, and site-2 proteases (S2P) (Celli and Tsolis, 2015). However, the PERK/ATF4 of the ER pathway has only been studied in animals and has not been reported in plants (Zhang et al., 2021). Both the proteomic and transcriptomic association analysis and RT-qPCR verification indicated that the response of *E. ulmoides* to *F. oxysporum* is likely to be associated with the PERK/ATF4 of the ER pathway.

The UPR can coordinate transcriptional and translational changes in cells, up-regulate the expression of molecular chaperones involved in folding and stabilizing the proteins in the ER lumen, and induce the expression of stress proteins in the ER. In this study, the expression of ER molecular chaperones such as HSP20, HSP70, HSP90, protein disulfide isomerase (PDI), and calnexin (CNX) was significantly increased at 72 h after inoculation. It has been reported that HSP chaperones such as BIP and HSP90 can recognize misfolded proteins (Park and Seo, 2015; Usman et al., 2017; Ul Haq et al., 2019). The lectin molecular chaperones calnexin (CNX), calreticulin (CRT), and CRT are proteins related to protein processing and Ca²⁺ homeostasis, including PDI, CNX, and CRT, which could help localize unfolded proteins in the ER lumen to prevent unfolded/misfolded proteins from being exported. In ERS, the ERAD is activated at the transcriptional level to remove and degrade misfolded proteins. This process restores protein homeostasis (Harding et al., 1999; Balch et al., 2008). In addition, CNX links misfolded proteins through transmembrane domain interactions, activating protein

degradation by the ubiquitin-proteasome system and signal transduction associated with phagocytosis, thus accomplishing the degradation of unfolded or misfolded proteins. The role of protein ubiquitination in plant growth and development and stress response has been widely recognized (Belknap and Garbarino, 1996). In this study E2 and F-box protein were significantly increased at 72 h after inoculation. These results suggest that molecular chaperones in the ER pathway (ko04141) are also involved in the response of *E. ulmoides* to *F. oxysporum*.

ER stress response plays an important role in plant response to pathogen infection and other stresses, extensive evidence shows that the ER pathway contributes to plant immunity in various ways (Li et al., 2009; Nekrasov et al., 2009; Saijo et al., 2009). There is also evidence that the ER pathway is manipulated by microbes to lead to successful colonization. For example, the symbiotic fungus *Piriformospora indica* establishes successful symbiosis by inducing plant ER stress but inhibiting the adaptive UPR, which eventually results in ER-PCD mediated by vacuolar processing enzymes (VPEs) (Qiang et al., 2012). In our study, we found the response of *E. ulmoides* to *F. oxysporum* was likely related to the unfolded protein response of the ER pathway. Some studies have shown that the process of apoptosis is contrary to the expression of CRT (Xu et al., 2014). Our study showed that when *E. ulmoides* was infected by *F. oxysporum*, the increased expression of ER chaperone proteins makes the protein fold correctly and causes ubiquitination and ERAD reaction, while the inhibition of CRT and EIF2 expression increases the expression of BCL2 and causes apoptosis, so as to protect plants

(Figure 7). In addition, we also observed that the relative expression of the hypoxia upregulated 1 gene of the HSP70 family and the F-box and WD-40 domain protein 1/11 gene of the ERAD were highest at 72 h after inoculation, being 65.53 and 75.26 times greater, respectively, than before inoculation. It is speculated that these two genes may be key to the *E. ulmoides* infection response in the activation of ER pathway.

Conclusion

In this study, proteome and transcriptome association analysis and RT-qPCR results showed that the response of *E. ulmoides* to *F. oxysporum* was likely related to the ER pathway. In the future, we will study the genes functions in the ER pathway through model plant transgenic technology to further explore the role of these genes in the response of *E. ulmoides* to *F. oxysporum*.

Data availability statement

The datasets presented in this study can be found in online repositories. The names of the repository/repositories and accession number(s) can be found below: https://db.cngb.org/-CNP0003469.

Author contributions

D-gZ and YZ designed the study. YL analyzed the data and wrote the article. XD performed the research. LP and XH edited the manuscript. All authors have read and agreed to the published version of the manuscript.

Conflict of interest

The authors declare that the research was conducted in the absence of any commercial or financial relationships that could be construed as a potential conflict of interest.

Publisher's note

All claims expressed in this article are solely those of the authors and do not necessarily represent those of their affiliated organizations, or those of the publisher, the editors and the reviewers. Any product that may be evaluated in this article, or claim that may be made by its manufacturer, is not guaranteed or endorsed by the publisher.

Supplementary material

The Supplementary Material for this article can be found online at: https://www.frontiersin.org/articles/10.3389/fchem.2022.1053227/full#supplementary-material

References

Anderson, W. R., and Cronquist, A. (1982). An integrated system of classification of flowering plants. *Brittonia* 34, 268–270. doi:10.2307/2806386

Balch, W. E., Morimoto, R. I., Dillin, A., and Kelly, J. W. (2008). Adapting proteostasis for disease intervention. *Science* 319, 916–919. doi:10.1126/science.1141448

Belknap, W. R., and Garbarino, J. E. (1996). The role of ubiquitin in plant senescence and stress responses. *Trends Plant Sci.* 1, 331–335. doi:10.1016/s1360-1385(96)82593-0

Benjamini, Y., and Hochberg, Y. (1995). Controlling the false discovery rate: A practical and powerful approach to multiple testing. *J. R. Stat. Soc. Ser. B Methodol.* 57, 289–300. doi:10.1111/j.2517-6161.1995.tb02031.x

Cai, Y. M., Yu, J., and Gallois, P. (2014). Endoplasmic reticulum stress-induced PCD and caspase-like activities involved. *Front. Plant Sci.* 5, 41. doi:10.3389/fpls.2014.00041

Celli, J., and Tsolis, R. M. (2015). Bacteria, the endoplasmic reticulum and the unfolded protein response: Friends or foes? *Nat. Rev. Microbiol.* 13, 71–82. doi:10.1038/nrmicro3393

Chen, M. J., Zhai, J. H., Zhang, J. J., Li, H., Niu, X. J., Liu, Y. X., et al. (2022). Transcriptomic and physiological analyses of pigment accumulation in Eucommia ulmoides 'hongye. *Phyt. B. Aires.* 91, 1027–1044. doi:10.32604/phyton.2022.019106

Chen, Y., and Brandizzi, F. (2013). IRE1: ER stress sensor and cell fate executor. *Trends Cell Biol.* 23, 547–555. doi:10.1016/j.tcb.2013.06.005

Cho, S., Hong, R., Yim, P., Yeom, M., Lee, B., Yang, W. M., et al. (2018). An herbal formula consisting of Schisandra chinensis (Turcz.) Baill, Lycium chinense Mill and Eucommia ulmoides Oliv alleviates disuse muscle atrophy in rats. *J. Ethnopharmacol.* 213, 328–339. doi:10.1016/j.jep.2017.10.008

Cox, J., and Mann, M. (2008). MaxQuant enables high peptide identification rates, individualized p.p.b.-range mass accuracies and proteome-wide protein quantification. *Nat. Biotechnol.* 26, 1367–1372. doi:10.1038/nbt.1511

Cox, J., Neuhauser, N., Michalski, A., Scheltema, R. A., Olsen, J. V., and Mann, M. (2011). Andromeda: A peptide search engine integrated into the MaxQuant environment. *J. Proteome Res.* 10, 1794–1805. doi:10.1021/pr101065j

Dewen, Q., Yijie, D., Yi, Z., Shupeng, L., and Fachao, S. (2017). Plant immunity inducer development and application. *Mol. Plant. Microbe. Interact.* 30, 355–360. doi:10.1094/MPMI-11-16-0231-CR

Doblas, V. G., Amorim-Silva, V., Pose, D., Rosado, A., Esteban, A., Arro, M., et al. (2013). The SUD1 gene encodes a putative E3 ubiquitin ligase and is a positive regulator of 3-hydroxy-3-methylglutaryl coenzyme a reductase activity in Arabidopsis. *Plant Cell* 25, 728–743. doi:10.1105/tpc.112.108696

Edel-Hermann, V., and Lecomte, C. (2019). Current status of Fusarium oxysporum formae speciales and races. *Phytopathology* 109, 512–530. doi:10.1094/PHYTO-08-18-0320-RVW

Fujiwara, A., Nishi, M., Yoshida, S., Hasegawa, M., Yasuma, C., Ryo, A., et al. (2016). Eucommicin A, a beta-truxinate lignan from Eucommia ulmoides, is a selective inhibitor of cancer stem cells. *Phytochemistry* 122, 139–145. doi:10.1016/j.phytochem.2015.11.017

Gordon, T. R., and Martyn, R. D. (1997). The evolutionary biology of Fusarium oxysporum. *Annu. Rev. Phytopathol.* 35, 111–128. doi:10.1146/annurev.phyto.35.1.111

Guo, P., Tang, h., Liu, C., Wei, S., and Huang, J. (2021). Differential Expression Analysis of Genes Related to Flesh Color in <i>Hylocereu polyrhizus</i> and <i>Hylocereu undatus</i>. *Mol. Plant Breed.* 19, 4311–4326. doi:10.5376/mpb.2021.12.0006

Harding, H. P., Calfon, M., Urano, F., Novoa, I., and Ron, D. (2002). Transcriptional and translational control in the Mammalian unfolded protein response. *Annu. Rev. Cell Dev. Biol.* 18, 575–599. doi:10.1146/annurev.cellbio.18.011402.160624

Harding, H. P., Zhang, Y., and Ron, D. (1999). Protein translation and folding are coupled by an endoplasmic-reticulum-resident kinase. *Nature* 397 (6716), 271–274. doi:10.1038/16729

Helenius, A., and Aebi, M. (2004). Roles of N-linked glycans in the endoplasmic reticulum. *Annu. Rev. Biochem.* 73, 1019–1049. doi:10.1146/annurev.biochem.73.011303.073752

Howell, S. H. (2013). Endoplasmic reticulum stress responses in plants. *Annu. Rev. Plant Biol.* 64, 477–499. doi:10.1146/annurev-arplant-050312-120053

Hussain, T., Tan, B., Rahu, N., Hussain Kalhoro, D., Dad, R., and Yin, Y. (2017). Protective mechanism of Eucommia ulmoids flavone (EUF) on enterocyte damage induced by LPS. *Free Radic. Biol. Med.* 108, S40. doi:10.1016/j.freeradbiomed.2017.04.152

Jahanshir, A., and Dzhalilov, S. (2010). The effects of fungicides on Fusarium oxysporum F. SP. Lycopersici associated with Fusarium wilt of tomato. *J. Plant Prot. Res.* 50, 172–178. doi:10.2478/v10045-010-0029-x

Jing, M. F., and Wang, Y. C. (2020). Plant pathogens utilize effectors to hijack the host endoplasmic reticulum as part of their infection strategy. *Engineering* 6 (5), 500–504. doi:10.1016/j.eng.2020.03.003

Kamauchi, S., Nakatani, H., Nakano, C., and Urade, R. (2005). Gene expression in response to endoplasmic reticulum stress in *Arabidopsis thaliana*. *FEBS J.* 272, 3461–3476. doi:10.1111/j.1742-4658.2005.04770.x

Kim, D., Langmead, B., and Salzberg, S. L. (2015). Hisat: A fast spliced aligner with low memory requirements. *Nat. Methods* 12, 357–360. doi:10.1038/nmeth.3317

Langmead, B., and Salzberg, S. L. (2012). Fast gapped-read alignment with Bowtie 2. *Nat. Methods* 9, 357–359. doi:10.1038/nmeth.1923

Lee, G. H., Lee, H. Y., Choi, M. K., Choi, A. H., Shin, T. S., and Chae, H. J. (2018). Eucommia ulmoides leaf (EUL) extract enhances NO production in ox-LDL-treated human endothelial cells. *Biomed. Pharmacother.* 97, 1164–1172. doi:10.1016/j.biopha.2017.11.035

Li, B., and Dewey, C. N. (2011). Rsem: Accurate transcript quantification from RNA-seq data with or without a reference genome. *BMC Bioinforma.* 12, 323. doi:10.1186/1471-2105-12-323

Li, J., Zhao-Hui, C., Batoux, M., Nekrasov, V., Roux, M., Chinchilla, D., et al. (2009). Specific ER quality control components required for biogenesis of the plant innate immune receptor EFR. *Proc. Natl. Acad. Sci. U. S. A.* 106, 15973–15978. doi:10.1073/pnas.0905532106

Liu, S. H., Zhao, D. G., and Song, B. A. (2007). Effect of Eucommia bark protein against plant pathogenic fungi. *Agrochemicals* 46, 848–850. doi:10.16820/j.cnki.1006-0413.2007.12.020

Liu, S. H., Zhao, D. G., and Song, B. A. J. A. (2008). Study on inhibition activity of Eucommia ulmoides antifungal protein to Botrytis cinerea. *Agrochemicals* 11, 836–838. doi:10.16820/j.cnki.1006-0413.2008.11.021

Luber, C. A., Cox, J., Lauterbach, H., Fancke, B., Selbach, M., Tschopp, J., et al. (2010). Quantitative proteomics reveals subset-specific viral recognition in dendritic cells. *Immunity* 32, 279–289. doi:10.1016/j.immuni.2010.01.013

Ma, S. (2019). Study on mannose regulating ER stress and alleviating islet inflammation in early stage of type I diabetes. *Third Military Medical University.* doi:10.27001/d.cnki.gtjyu.2019.000451

Malhotra, J. D., and Kaufman, R. J. (2007). The endoplasmic reticulum and the unfolded protein response. *Semin. Cell Dev. Biol.* 18, 716–31. doi:10.1016/j.semcdb.2007.09.003

Mann, M., Hendrickson, R. C., and Pandey, A. (2001). Analysis of proteins and proteomes by mass spectrometry. *Annu. Rev. Biochem.* 70, 437–473. doi:10.1146/annurev.biochem.70.1.437

Marciniak, S. J., Yun, C. Y., Oyadomari, S., Novoa, I., Zhang, Y., Jungreis, R., et al. (2004). CHOP induces death by promoting protein synthesis and oxidation in the stressed endoplasmic reticulum. *Genes Dev.* 18, 3066–3077. doi:10.1101/gad.1250704

Martinez, I. M., and Chrispeels, M. J. (2003). Genomic analysis of the unfolded protein response in arabidopsis shows its connection to important cellular processes [W]. *Plant Cell* 15 (2), 561–576. doi:10.1105/tpc.007609

Michielse, C. B., and Rep, M. (2010). Pathogen profile update: Fusarium oxysporum. *Mol. Plant Pathol.* 10, 311–324. doi:10.1111/j.1364-3703.2009.00538.x

Mishiba, K., Nagashima, Y., Suzuki, E., Hayashi, N., Ogata, Y., Shimada, Y., et al. (2013). Defects in IRE1 enhance cell death and fail to degrade mRNAs encoding secretory pathway proteins in the Arabidopsis unfolded protein response. *Proc. Natl. Acad. Sci. U. S. A.* 110, 5713–5718. doi:10.1073/pnas.1219047110

Monti, M., Orru, S., Pagnozzi, D., and Pucci, P. (2005). Functional proteomics. *Clin. Chim. Acta* 357 (2), 140–150. doi:10.1016/j.cccn.2005.03.019

Mukhtar, I. (2007). Comparison of phytochemical and chemical control of Fusarium oxysporium f. sp. ciceri. *Mycopath* 5, 107–110.

Nekrasov, V., Li, J., Batoux, M., Roux, M., Chu, Z. H., Lacombe, S., et al. (2009). Control of the pattern-recognition receptor EFR by an ER protein complex in plant immunity. *EMBO J.* 28, 3428–3438. doi:10.1038/emboj.2009.262

Ni, M., Zhou, H., Wey, S., Baumeister, P., and Lee, A. S. (2009). Regulation of PERK signaling and leukemic cell survival by a novel cytosolic isoform of the UPR regulator GRP78/BiP. *PLoS One* 4 (8), e6868. doi:10.1371/journal.pone.0006868

Park, C. J., and Seo, Y. S. (2015). Heat shock proteins: A review of the molecular chaperones for plant immunity. *Plant Pathol. J.* 31, 323–333. doi:10.5423/PPJ.RW.08.2015.0150

Pietro, A. D., Madrid, M. P., Caracuel, Z., Delgado-Jarana, J., and Roncero, M. I. G. (2010). Fusarium oxysporum: Exploring the molecular arsenal of a vascular wilt fungus. *Mol. Plant Pathol.* 4, 315–325. doi:10.1046/j.1364-3703.2003.00180.x

Pobre, K. F. R., Poet, G. J., and Hendershot, L. M. (2019). The endoplasmic reticulum (ER) chaperone BiP is a master regulator of ER functions: Getting by with a little help from ERdj friends. *J. Biol. Chem.* 294, 2098–2108. doi:10.1074/jbc.REV118.002804

Pollier, J., Moses, T., Gonzalez-Guzman, M., De Geyter, N., Lippens, S., Vanden Bossche, R., et al. (2013). The protein quality control system manages plant defence compound synthesis. *Nature* 504 (7478), 148–152. doi:10.1038/nature12685

Qian, Z. Z., Yang, D., Liu, Y. Z., and Peng, Y. (2010). Pharmacopoeia of the people's Republic of China (2010 edition):a milestone in development of China's healthcare. *Chin. Herb. Med.* 2, 157–160.

Qiang, X., Liu, X., Wang, X., Zheng, Q., Kang, L., Gao, X., et al. (2021). Susceptibility factor RTP1 negatively regulates Phytophthora parasitica resistance via modulating UPR regulators bZIP60 and bZIP28. *Plant Physiol.* 186, 1269–1287. doi:10.1093/plphys/kiab126

Qiang, X., Zechmann, B., Reitz, M. U., Kogel, K. H., and Schafer, P. (2012). The mutualistic fungus Piriformospora indica colonizes Arabidopsis roots by inducing an endoplasmic reticulum stress-triggered caspase-dependent cell death. *Plant Cell* 24, 794–809. doi:10.1105/tpc.111.093260

Saijo, Y., Tintor, N., Lu, X. L., Rauf, P., Pajerowska-Mukhtar, K., Haweker, H., et al. (2009). Receptor quality control in the endoplasmic reticulum for plant innate immunity. *EMBO J.* 28, 3439–3449. doi:10.1038/emboj.2009.263

Saleh, S., Staes, A., Deborggraeve, S., and Gevaert, K. (2019). Targeted proteomics for studying pathogenic bacteria. *Proteomics* 19, e1800435. doi:10.1002/pmic.201800435

Sarwar, N., Zahid, C. M., Haq, I., and Jamil, F. F. (2005). Induction of systemic resistance in chickpea against Fusarium wilt by seed treatment with Salicylic acid and Bion. *Pak J. Bot.* 37, 989–995. doi:10.1378/chest.10732

Shi, W., Zhao, S. L., Liu, K., Sun, Y. B., Ni, Z. B., Zhang, G. Y., et al. (2020). Comparison of leaf transcriptome in response to Rhizoctonia solani infection between resistant and susceptible rice cultivars. *BMC Genomics* 21, 245. doi:10.1186/s12864-020-6645-6

Swarupa, V., Ravishankar, K. V., and Rekha, A. (2014). Plant defense response against Fusarium oxysporum and strategies to develop tolerant genotypes in banana. *Planta* 239, 735–751. doi:10.1007/s00425-013-2024-8

Tokumoto, Y., Kajiura, H., Takeno, S., Harada, Y., Suzuki, N., Hosaka, T., et al. (2016). Induction of tetraploid hardy rubber tree, <i>Eucommia ulmoides</i>, and phenotypic differences from diploid. *Plant Biotechnol. (Tokyo).* 33, 51–57. doi:10.5511/plantbiotechnology.15.1219a

Ul Haq, S., Khan, A., Ali, M., Khattak, A. M., Gai, W. X., Zhang, H. X., et al. (2019). Heat shock proteins: Dynamic biomolecules to counter plant biotic and abiotic stresses. *Int. J. Mol. Sci.* 20, 5321. doi:10.3390/ijms20215321

Usman, M. G., Rafii, M. Y., Martini, M. Y., Yusuff, O. A., Ismail, M. R., and Miah, G. (2017). Molecular analysis of Hsp70 mechanisms in plants and their function in response to stress. *Biotechnol. Genet. Eng. Rev.* 33, 26–39. doi:10.1080/02648725. 2017.1340546

Wan, S., and Jiang, L. (2016). Endoplasmic reticulum (ER) stress and the unfolded protein response (UPR) in plants. *Protoplasma* 253, 753–764. doi:10.1007/s00709-015-0842-1

Wasinger, V. C., Cordwell, S. J., Cerpa-Poljak, A., Yan, J. X., Gooley, A. A., Wilkins, M. R., et al. (1995). Progress with gene-product mapping of the Mollicutes: Mycoplasma genitalium. *Electrophoresis* 16, 1090–1094. doi:10.1002/elps. 11501601185

Wen, Q., and Wei, S. (2015). Research progress on the role of endoplasmic reticulum stress in glucose and lipid metabolism. Editors Zhong Guo, Xu Mu, Shou Yi, and Wen Zhai 31, 52–53. (in chinese). Available at: https://kns.cnki.net/ kcms/detail/detail.aspx?FileName=ZXWA201510048&DbName=CJFQ2015.

Wilhelm, B. T., and Landry, J. R. (2009). RNA-Seq-quantitative measurement of expression through massively parallel RNA-sequencing. *Methods* 48, 249–257. doi:10.1016/j.ymeth.2009.03.016

Williams, B., Verchot, J., and Dickman, M. B. (2014). When supply does not meet demand-ER stress and plant programmed cell death. *Front. Plant Sci.* 5, 211. doi:10. 3389/fpls.2014.00211

Xu, M., Wang, T., Yu, L., Wang, W., Zeng, S., Chen, Z., et al. (2014). Endoplasmic reticulum stress response and related molecular chaperones*Prog. Anatomical Sci. Biochem. Physiol*, 20147, 38120–38426. doi:10.16695/j.cnki.1006-2947.2014.04. 00210.1016/j.pestbp.2017.06.005

Yu, L., Wang, W., Zeng, S., Chen, Z., Yang, A., Shi, J., et al. (2018). Label-free quantitative proteomics analysis of Cytosinpeptidemycin responses in southern rice black-streaked dwarf virus-infected rice. *Pestic. Biochem. Physiol.* 147, 20–26. doi:10.1016/j.pestbp.2017.06.005

Zhang, H., Wang, D., and Zhang, Z. (2016). Progress and prospects in the research on wheat drought response and resistance mechanisms using transcriptomic and proteomic approaches. *J. Triticeae Crops* 36, 878–887. doi:10.7606/j.issn.1009-1041.2016.07.08

Zhang, R., Sun, Y., Su, J., Wang, S., Liu, Y., Tong, H., et al. (2021). Advances in endoplasmic reticulum stress in plants. *Curr. Biotechnol.* 11, 289–296. doi:10.19586/ j.2095-2341.2020.0147

Zhang, X., and Wei, H. (1997). Advances in antigen processing and presentation. *Foreign Medicine (Immunology)* 1, 1–5. (in chinese). Available at: https://kns.cnki. net/kcms/detail/detail.aspx?FileName=GYMF199701000&DbName=CJFQ1997.

Zhou, Y., Yang, K., Cheng, M., Cheng, Y., Li, Y., Ai, G., et al. (2021). Double-faced role of Bcl-2-associated athanogene 7 in plant–Phytophthora interaction. *J. Exp. Bot.* 72, 5751–5765. doi:10.1093/jxb/erab252

Advantages of publishing in Frontiers

OPEN ACCESS
Articles are free to read
for greatest visibility
and readership

FAST PUBLICATION
Around 90 days
from submission
to decision

HIGH QUALITY PEER-REVIEW
Rigorous, collaborative,
and constructive
peer-review

TRANSPARENT PEER-REVIEW
Editors and reviewers
acknowledged by name
on published articles

Frontiers
Avenue du Tribunal-Fédéral 34
1005 Lausanne | Switzerland

Visit us: www.frontiersin.org
Contact us: frontiersin.org/about/contact

**REPRODUCIBILITY OF
RESEARCH**
Support open data
and methods to enhance
research reproducibility

DIGITAL PUBLISHING
Articles designed
for optimal readership
across devices

FOLLOW US
@frontiersin

IMPACT METRICS
Advanced article metrics
track visibility across
digital media

EXTENSIVE PROMOTION
Marketing
and promotion
of impactful research

LOOP RESEARCH NETWORK
Our network
increases your
article's readership